UNIVERSITÀ DELLA CALABRIA

Dipartimento di Biologia, Ecologia e Scienze della Terra

Dottorato di Ricerca in

Life Science and Technology

CICLO

XXXVI

Identification of epigenetic mechanisms involved in seed coat development.

Settore Scientifico Disciplinare: BIO/01 (Botanica Generale)

Coordinatore: Ch.mo Prof. Tommaso Angelone

Tommaso Angelone
11.04.2024 11:54:36
GMT+01:00

Supervisore: Ch.mo Prof. Leonardo Bruno

BRUNO LEONARDO
09.04.2024 13:53:29
GMT+01:00

Supervisore: Ch.ma Prof.ssa Adriana Chiappetta

CHIAPPETTA ADRIANA ADA
09.04.2024 12:45:05
GMT+00:00

Dottoranda: Dott.ssa Emanuela Talarico

EMANUELA TALARICO
09.04.2024 13:26:13
GMT+01:00

RIASSUNTO

L'evoluzione del seme è un affascinante aspetto della storia dell'evoluzione e della botanica. I semi si sono evoluti nel corso di milioni di anni e sono considerati un significativo adattamento, che ha contribuito al successo delle Spermatofite. I semi forniscono protezione e garanzia di dispersione, permettendo alle piante di riprodursi con successo in una vasta gamma di condizioni. Questa storia evolutiva ha portato alla ricchezza di biodiversità che possiamo vedere oggi sulla Terra. Inoltre, i semi mostrano notevoli adattamenti per sopravvivere a lunghi viaggi, tra cui diverse forme, dimensioni e meccanismi di dispersione. Ma tutto questo non sarebbe stato possibile senza l'evoluzione dell'ovulo, all'interno del quale avviene la riproduzione sessuale. L'ovulo è, infatti, la struttura in cui avviene la formazione del gametofito femminile, la fecondazione, l'embriogenesi e lo sviluppo del seme dopo la fecondazione.

In tale contesto, lo scopo del mio progetto di dottorato è stato quello di identificare, a livello evolutivo, i meccanismi molecolari ed epigenetici coinvolti nello *switch* da ovulo a seme, in piante di *Ginkgo biloba*. In particolare, l'attenzione è stata focalizzata solo all'evento di impollinazione, che, in tale sistema, è separato da un lungo intervallo temporale (quattro/cinque mesi) dalla fecondazione. Inoltre, *Ginkgo biloba*, appartenente alle Gimnosperme e unica specie superstite dell'ordine Ginkgoales, è stato utilizzato come modello sperimentale, dal momento che è considerato un fossile vivente, grazie alle sue antiche origini risalenti al Permiano, periodo conclusivo del Paleozoico, momento evolutivo in cui per la prima volta si è avuto lo sviluppo di un tegumento a coprire il megasporangio. Un'interessante caratteristica di *Ginkgo*, che lo rende particolarmente adatto allo scopo della ricerca, è la produzione di strutture definite "*fleshy-fruit like*", attrattive per gli animali. Infatti, dopo la fecondazione, il tegumento assume una consistenza simile a quella del mesocarpo dei frutti carnosi, sebbene non possano essere identificati come tali, dal momento che le Gimnosperme sono sprovviste di ovario.

Diversi approcci, che includono sequenziamento di RNA, ibridazione *in situ* di acidi nucleici, localizzazione di ormoni vegetali e immunoprecipitazione della cromatina accoppiata a sequenziamento (ChIP-seq), sono stati condotti su ovuli a diversi stadi di sviluppo, al fine di identificare i *pathways* chiave e i geni epigeneticamente regolati, coinvolti nello *switch* da ovulo a seme. In particolare, al

fine di identificare anche i principali *pathways* modulati dal cruciale evento dell'impollinazione, sono stati utilizzati tre stadi di sviluppo dell'ovulo di *Ginkgo*, raccolti immediatamente dopo la finestra temporale in cui avviene l'emissione della goccia pollinica. In tale contesto, l'emissione della goccia pollinica costituisce un aspetto interessante, dal momento che, in molte Gimnosperme, identifica il momento di possibile ricezione del polline. I campioni sono stati, quindi, raccolti da due diversi campi sperimentali, il primo caratterizzato dalla presenza di piante sia maschili che femminili, il secondo in cui sono presenti solo piante femminili. I due campi sperimentali sono geograficamente distanti, motivo per il quale le piante del secondo sito sono impossibilitate a ricevere il polline e quindi utili per comprendere come prosegue lo sviluppo dell'ovulo in assenza del processo di impollinazione.

Inoltre, questa tesi di dottorato è stata parte di un progetto più ampio, che ha previsto la collaborazione con i gruppi di ricerca coordinati dalla Professoressa Barbara Baldan, dell'Università di Padova, e dalla Professoressa Lucia Colombo, dell'Università di Milano, contribuendo a produrre una grande mole di dati su *Ginkgo*, ma anche su *Arabidopsis*, che da sempre rappresenta la specie modello in biologia vegetale.

Con il contributo anche dei risultati da noi prodotti, è stato possibile comparare le due specie e descrivere alcuni dei geni chiave coinvolti nello sviluppo dell'ovulo in *Ginkgo*.

Infine, la maggior parte delle analisi bioinformatiche relative all'esperimento di ChIP-seq riportate in questa tesi sono state ottenute in collaborazione con il Professore Ernesto Picardi dell'Università degli Studi di Bari Aldo Moro e con la Dottoressa Antonella Muto, post-doc nel mio gruppo di ricerca all'Università della Calabria.

ABSTRACT

The evolution of seeds is a fascinating aspect of evolutionary history and plant biology. Seeds have evolved over millions of years and are considered a significant adaptation that has contributed to the success of land plants. Seeds provide protection and a means of dispersal, enabling plants to reproduce successfully in a wide range of conditions. This evolutionary history has led to the rich diversity of plant species we see on Earth today. Seeds show remarkable adaptations to survive long journeys, including different shapes, sizes and mechanisms for dispersal. But none of these features would have been possible without the evolution of the ovule, within which sexual reproduction occurs. Indeed, ovule is the structure in which take place the formation of female gametophyte, fertilisation, embryogenesis and seed development upon fertilisation.

In this scenario, the aim of this Ph. D. project was to identify, at evolutionary level, the molecular and epigenetic mechanisms involved in the ovule-to-seed switch in *Ginkgo biloba* plants. In particular, the focus was only on the pollination event, which in such a system is separated from fertilisation by a long time interval (i.e. four/five months). Indeed, *Ginkgo biloba*, a member of the gymnosperms and the only extant species of the order Ginkgoales, was used as experimental model because it is considered a living fossil due to its very ancient origins, dating back to the Permian period, the last period of the Palaeozoic, when an integument developed for the first time to cover the megasporangium. An interesting characteristic of *Ginkgo*, which makes it suitable for this purpose, is the production of fleshy fruit-like structures that are attractive to animals. Indeed, already after pollination, the integument takes on a consistency similar to that of mesocarp of fleshy fruit, leading to the hypothesis that it may represent a precursor to the fruit, although it cannot be identified as such because gymnosperms lack an ovary.

Various approaches, including RNA sequencing, *in situ* gene expression, hormones localization and chromatin immunoprecipitation following by sequencing (ChIP-seq), on ovules at different stages were performed in order to identify the key pathways and the epigenetically regulated genes involved in ovule-seed switch. In order to identify the main pathways modulated by the crucial pollination event, three developmental stages of the *Ginkgo* ovule, collected immediately after the time frame

in which pollination drop emission occurs, were used. In this context, pollination drop emission is an interesting aspect because, in many gymnosperms, it identifies the time point of possible pollen reception. Therefore, samples were collected from two different experimental fields, the first characterised by the presence of both male and female plants, and the second where only female plants are present. The two experimental fields are geographically distant from each other, which means that the plants in the second field are unable to receive pollen, so they are useful for understanding how ovule development proceeds in the absence of the pollination event.

Moreover, this Ph. D. thesis was part of a larger project, which involved collaboration with the research groups coordinated by Professor Barbara Baldan, University of Padua, and Professor Lucia Colombo, University of Milan, helping to produce a large amount of data on *Ginkgo*, but also on *Arabidopsis*, which has always been the model species in plant biology. With the contribution also of the results we produced, it was possible to compare the two species and describe some of the key genes involved in ovule development in *Ginkgo*.

Finally, most of the bioinformatic analyses related to the ChIP-seq experiment reported in this thesis were performed in collaboration with Professor Ernesto Picardi of the University of Bari Aldo Moro and Dr. Antonella Muto, post-doc in my research group at the University of Calabria.

PREMISE

The present thesis describes the research work performed during my doctorate. In particular, the thesis is divided in different parts: a first introductory chapter (chapter I), three successive chapters (chapters II, III, IV) describing the experimental approaches and the obtained results, and the final one (chapter V) illustrating conclusions and future perspectives.

In detail:

- In Chapter I were illustrated the subjects of the thesis, considering the molecular networks involved in ovule and seed development and the epigenetics mechanisms which regulate these processes known in the experimental model plant *Arabidopsis thaliana* and the state of art in non-model plants such gymnosperms and in particular *Ginkgo biloba*;
- In Chapter II, key genes modulated in the ovules of *Ginkgo* at various developmental stages were investigated, and genes influenced by epigenetic regulatory mechanisms before and after pollination were identified;
- In Chapter III, the crucial role of the pollination event was investigated using ovules collected from both female plants that received pollen and unpollinated female plants, through transcriptomic and *in situ* approaches;
- In Chapter IV were identified the cyto-histological localisation domains of plant hormones known in literature to be mainly involved in ovule development (i.e. auxin and cytokinin) in pollinated and unpollinated ovules.

Taken together, the results obtained help to fill some of the knowledge gaps that still exist in the study of the developmental biology of non-model species that are still elusive.

CHAPTER I

Introduction to the molecular networks involved in ovule and seed development and the evolutionary history of seeds.

The developmental predecessor of the seed: the ovule

The evolution of seeds is one of the most important evolutionary innovations in the history of plant and human civilisation, as human diets strongly depend on them (Bai *et al.*, 2022).

In plants, seed represented a dynamic structure that allowed the colonisation of a variety of previously inaccessible habitats (Rudall, 2021). It contains a new, genetically different individual and the reserve substances, stored within the endosperm tissue, necessary in the early stages of life. The seed also has numerous structures to improve its dispersal capacity and allows germination only when environmental conditions are suitable to grow (Taylor *et al.*, 2009). This quiescent state in which the seeds remain until germination is imposed by the seed coat, which is entirely of maternal origin, since it is nothing more than the integuments of the ovule transformed into a seed coat. Indeed, in Spermatophytes, which include gymnosperms and angiosperms, the seed originates from a fertilized ovule, in which megasporogenesis and megagametogenesis occurred (Guo and Zheng, 2013). Ovules originate by a protrusion of placental tissue and differentiate three different regions: the most apical portion, the nucellus, the median portion, the chalaza, and the basal portion, the funiculus, which connects ovule to placenta and drives nutrients in the ovule during its development. From the chalaza originate one or more sterile envelopes, the integuments. They are initiated as annular outgrowths and progressively enveloping the nucellus, leaving an opening known as a micropyle (Rudall, 2021). At the same time, at the tip of the nucellus, a single cell, the archeospore, differentiates into a megasporocyte, the Megaspore Mother Cell (MMC), which undergoes in meiosis, originating four megaspores. Three of these degenerate and only one, the Functional Megaspore (FM) remains (Ceccato *et al.*, 2013).

In gymnosperms, the surviving megaspore is enclosed in the megasporangium, which in turn is surrounded by one integument open to the micropyle. The megaspore

undergoes mitotic divisions to form the female gametophyte, which at maturity is composed of the primary endosperm and two or more archegonia, sac-like structures arranged at the micropylar pole, inside which the egg cell is located (Nepi *et al.*, 2009). Frequently, in gymnosperms plants a pollination drop is ejected from the micropyle, which has the function of retaining and transporting the pollen grains inside the nucellus (Prior *et al.*, 2019). After this event, the micropyle closes, allowing the sperm to fertilize the egg cell and form the zygote, which then develops into an embryo.

In angiosperms, FM undergoes to three mitotic divisions, arising an eight-nucleated structure. In most angiosperms, these nuclei migrate and arrange themselves in a precise order. Three of them migrate at chalaza region, three at micropylar zone and two at the central zone. Subsequently, this structure undergoes to cellularisation, producing seven cells, respectively the antipodal cells, the two synergids with the egg cell at the centre and the binucleated larger central cell (Larsson *et al.*, 2017). This structure represents the embryo sac, also named female gametophyte.

In angiosperms, the typical process of double fertilisation occurs after interaction with the pollen tube, which releases the sperm nuclei. One nucleus fertilises the egg cell, giving rise to the embryo, and another fertilises the central cell, giving rise to the triploid endosperm (Larsson *et al.*, 2017). The ovules are connected to the placenta in the chalaza through the funiculus, which has the function of conduction and support (Endress, 2011), and they are enclosed within the pistil, formed by the fusion of two or more carpels (Gasser and Robinson-Beers, 1993).

The differences in ovule morphology between gymnosperms and angiosperms are also reflected in the final structure of the seed. In particular, gymnosperms seeds are often defined “naked”. Indeed, gymnosperms have no ovary to enclose ovules, and the seeds are often found naked on the scales of cones at the maturity stage. In gymnosperms seeds, the embryo is enveloped by both a haploid maternal tissue, the primary endosperm, which constitutes the main source of nutrition, and a diploid integument of maternal origin, which differentiates in seed coat. On the contrary, in angiosperms ovules are enclosed in the ovary, which, after fertilization, develops to give rise to the fruit. Therefore, the fruit encloses one or more seeds, and for this reason they are named covered (Linkies *et al.*, 2010).

Insight into the molecular mechanisms involved in ovule development in the angiosperm model species *Arabidopsis thaliana* (L.) Heynh

Ovule development and its subsequent transformation into seed is controlled by an intricate molecular network involving the coordinated action of many genes, transcription factors and phytohormones. Almost all information on this topic was obtained through the study of the model organism *Arabidopsis thaliana*. Many genes are involved in polarity establishment, meristem maintenance, floral organ determination, ovule identity, and structure specification (Shi and Yang, 2011).

Crucially, *APETALA2* (*AP2*), *AINTEGUMENTA* (*ANT*) and genes belonging to the MADS-box group, such as *SEEDSTICK* (*STK*), *AGAMOUS* (*AG*) and *SHATTERPROOF* (*SHP*), contribute to ovule primordium initiation (Coito *et al.*, 2018; Zumajo-Cardona and Ambrose, 2020). On the other hand, also the homeobox gene *WUSCHEL* (*WUS*) is essential (Groß-Hardt *et al.*, 2002). *WUS* is known to work in the maintenance of the stem cells niche presents in the Shoot Apical Meristem (SAM) (Dodsworth, 2009). However, in ovules, although its expression domain is in the tip of the nucellus, it was discovered that *WUS* is really important for integument formation. According to several studies (Baker *et al.*, 1997; Elliott *et al.*, 1996; Klucher *et al.*, 1996; Schneitz *et al.*, 1997; Groß-Hardt *et al.*, 2002), the ovules of *wus* mutants remain radially symmetrical and do not develop integuments, thus recalling the phenotype of *aintegumenta* (*ant*) ovules. Ectopic structures at the funiculus' sides are observed when *WUS* is expressed ectopically in the chalaza under the *ANT* promoter control. These structures morphologically similar to integuments suggest that *WUS* is sufficient to induce integument development in cells close to the *WUS* expression area (Groß-Hardt *et al.*, 2002). In addition, integuments initiation involves *BELL1* (*BEL1*), which belongs to the BELL-like homeodomain group, *AINTEGUMENTA* (*ANT*) and *INNER NO OUTER* (*INO*), which belong to the *YABBY* group and are specific for the outer integument (Shigyo, 2006; Pagnussat, 2007). In particular, on the abaxial side of the ovule primordium, *INO* polar expression induces the formation of the outer integument (Balasubramanian and Schneitz, 2000; Meister *et al.*, 2002; Villanueva *et al.*, 1999). *INO* is regulated through a positive feedback loop by *NOZZLE/SPOROCYTELESS* (*NZZ/SPL*), which encodes a putative transcription factor, and also by *AINTEGUMENTA* (*ANT*), which encodes an AP2 family

transcription factor (Elliott *et al.*, 1996; Klucher *et al.*, 1996; Nole-Wilson and Krizek, 2000; Balasubramanian and Schneitz, 2002; Meister *et al.*, 2002). In particular, *NZZ* and *ANT* function in a temporal manner to inhibit and activate *INO*, respectively (Balasubramanian and Schneitz, 2000, 2002). Indeed, *ant* mutant ovules express *INO* too late, whereas *nzz* mutant ovules express *INO* too early. Due to this aspect, *nzz* mutants ovules show an impairment of the proximal-distal development, smaller nucellus and hyperplastic funiculus, highlighting that the control of *NZZ* on *INO* expression is crucial to prevent it from expressing itself too early, allowing time for the development of the proximal-distal axis to complete (Shi and Yang, 2011).

Also, *SUPERMAN* (*SUP*) acts as an *INO* regulator. It encodes a zinc finger transcription factor (Sakai *et al.*, 1995) and can interferes with the maintenance of *INO* feedback control on the adaxial side of the ovule primordium, acting as a *INO* spatial repressor (Meister *et al.*, 2002; **Fig. 1**). Interestingly, in *sup* mutants' ovules, *INO* expression is present throughout the chalaza, and the outer integument develops equally on the adaxial and abaxial sides of the primordium (Gaiser *et al.*, 1995; Balasubramanian and Schneitz, 2002; Meister *et al.*, 2002). In *Arabidopsis*, the expression of *INO* in the adaxial chalaza is also prevented by *ABERRANT TESTA SHAPE* (*ATS*, also known as *KANADI4, KAN4*) which belongs to the *GARP* gene family and control integuments development and separation. *ATS* is expressed in a little cluster of cells between the two integuments and *ats* mutants produce a single integument (McAbee *et al.*, 2006; **Fig. 1**). Four *KANADI*s have been identified in *Arabidopsis*, two of which, *KAN1* and *KAN2*, are involved in the development of the ovule integuments, in particular in determining the polarity of the outer integument. Phylogenetic analyses have shown that genes homologous to *ATS* are present in all vascular plants, but the origin of the *ATS* clade has not yet been clarified (Zumajo-Cardona and Ambrose, 2020). In turn, *ATS* activity is repressed by *UNICORN* (*UCN*), which encodes a kinase involved in the maintenance of planar tegument growth. Also, *PHABULOSA* (*PHB*), *PHAVOLUTA* (*PHV*), and *CORONA* (*CNA*), three Class III homeodomain leucine zipper transcription factors (HD-ZIP III), contribute to limit the spatial expression of *WUS* and control the development of integuments and the inner integument adaxial identity (Kelley and Gasser, 2009; Yamada *et al.*, 2016). In particular, the development of adaxial cell types on abaxial sites and radialised lateral

organs, following semidominant gain-of-function mutations in *PHB*, suggests that *PHB* promotes adaxial cell fate in *Arabidopsis*. All floral organs generated by homozygous *phb-1d* mutants are entirely radialised, and ovules do not develop, resulting in their extreme tiny size and sterility (McConnell and Barton, 1998). All three of these transcription factors, *PHB*, *PHV* and *CNA*, have as their expression domain exclusively the inner integument, while another HD-ZIP III transcription factor, *REVOLUTA*, is expressed in both outer and inner integuments (Sieber *et al.*, 2004; Kelley *et al.*, 2009; **Fig. 1**). Lastly, *SHORT INTEGUMENTS1* (*SIN1*), also identified as *DICER LIKE-1*, is one of the genes involved in integument elongation processes, once its identity has been established, as well as in general plant growth processes (Zumajo-Cardona and Ambrose, 2020).

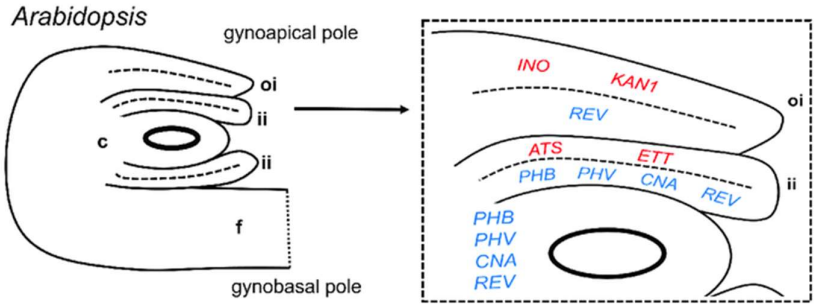

Fig. 1. Image from Arnault *et al.* (2018). Schematic representation of expression patterns of ovule integument regulators in *Arabidopsis thaliana*. Abaxial-promoting genes are shown in red and adaxial-promoting ones in blue. c, chalaza; f, funiculus; ii, inner integument; oi, outer integument.

In this intricate molecular network, phytohormones such as auxins, cytokinins (CKs), brassinosteroids (BRs) and gibberellins (GAs) are particularly involved (Barro-Trastoy *et al.*, 2020). Auxins are widely recognized for controlling cell division, elongation, and differentiation in the majority of growth and developmental processes (Weijers *et al.*, 2018). One of their key roles is to encourage the development of organ primordia in both shoots and roots (Overvoorde *et al.*, 2010; Wang and Jiao, 2018). Both local auxin biosynthesis (Brumos *et al.*, 2018) and polar auxin transport (Okada *et al.*, 1991; van Berkel *et al.*, 2013), which is primarily supported by the auxin efflux carriers known as PIN-FORMED (PIN) family (Zhou and Luo, 2018), contribute to

the auxin accumulation in the organ initiation sites. Indeed, several studies suggest that auxin maxima identify the sites of emerging ovule primordia. Auxin signalling, highlighted via *pDR5::GFP* reporter system, was found at the tip of ovule primordia (Benková *et al.*, 2003; Ceccato *et al.*, 2013). In addition, MMC and the epidermis of ovule primordia exhibit high levels of *TRYPTOPHAN AMINOTRANSFERASE OF ARABIDOPSIS1* (*TAA1*) expression (Nole-Wilson *et al.*, 2010). Some components of the auxin signalling system, such as AUXIN RESPONSE TRANSCRIPTION FACTOR (ARFs) can also participate to ovule initiation. For example, in *Arabidopsis*, the ovule primordia include a widespread localization of MONOPTEROS (ARF5/MP). Among the PIN proteins, PIN1 and PIN3 are specifically detected in ovules (Ceccato *et al.*, 2013). More in details, PIN1 was shown to be positioned in the outer cell layer of ovule primordia, particularly at the primordium tip (Benkova *et al.* 2003; Ceccato *et al.*, 2013), also PIN3 exhibits a similar expression pattern in ovule primordia, although the signal is weaker than PIN1 (Ceccato *et al.*, 2013). The strong loss-of-function allele of *PIN1* cause the development of abnormal pistils, characterised by defective style and stigma and without ovules (Benkova *et al.*, 2003). In addition, *PIN1* expression in ovule primordia is under the *CUC1* and *CUC2* control, which in turn are positively regulated by MP (Galbiati *et al.*, 2013). On the other hand, MP binds the *ANT* promoter inducing the gene expression (Galbiati *et al.*, 2013; Yamaguchi *et al.*, 2013), which seems to have a role in auxin homeostasis in young pistils. Indeed, *TRYPTOPHAN AMINOTRANSFERASE OF ARABIDOPSIS 1* (*TAA1*), involved in auxin biosynthesis, is directly activated by *ANT* in floral buds (Krizek *et al.*, 2020). These data suggest that ovule initiation is strongly related to pattern of synthesis and distribution of auxin.

Together with auxins, also cytokinins (CKs) play a key role during ovule development. Indeed, through GUS assay it was found that in *Arabidopsis* three *ARABIDOPSIS HISTIDINE PROTEIN KINASES* (*AHKs*), which act as two component sensors of cytokinins, were expressed in carpel and developing ovules (Nishimura *et al.*, 2004; Bencivenga *et al.*, 2012). Moreover, numerous experiments show that CKs are strongly related to the quantity of ovules formed. Indeed, the *cre1-12 ahk2-2 ahk3* triple receptor mutant with impaired CK sensing exhibits a decrease in the quantity of ovules per pistil, compared to the wild-type (Yuan and Kessler,

2019). On the other hand, an increase in the quantity of ovules is observed when the CK catabolism is inhibited (Bartrina *et al.*, 2011). Interestingly, CUC1 and CUC2 were identified as regulators of CKs homeostasis in ovule primordia. Cucinotta and collaborators (2018) showed that the two-component system signalling sensor (TCS), which reflects the CK response, can promote the expression of the LUCIFERASE (LUC) reporter gene under the direction of *CUC1* and *CUC2*. In addition, during ovule initiation, also polar auxin transport is related to CKs. Indeed, *PIN1* expression was reduced in the CKs insensitive mutant *crf2 crf3 crf6* and was not rescued by the treatments with the exogenous synthetic cytokinin 6-benzylaminopurine (BAP) (Cucinotta *et al.*, 2016). In the *PIN1* promoter there is a cis-regulatory sequence named PIN CYTOKININ RESPONSE ELEMENT (PCRE) and Cytokinin Response Factors (CRFs) can bind them, acting as direct transcriptional regulators (Simaskova *et al.*, 2015). All these evidences demonstrate that ovule initiation is a process finely regulated by a cross-talk between auxin and cytokinin hormones.

No less important are auxin and CKs in ovule patterning, not only in ovule initiation, as previously reported. *pin1-5* mutant produces ovules as finger-like structures but they fail to reach maturity (Bencivenga *et al.*, 2012). In line with this evidence, PIN1 activity is seen in the developing funiculus, in the inner integument cell membranes, and in the outer cell layer of the elongated ovule primordia surrounding the nucellus. These cells are most likely delivering auxins to the tip of the primordia, where a DR5 signal is still discernible (Benková *et al.*, 2003; Ceccato *et al.*, 2013). *spl-1* mutant presents ovules with PIN1 and DR5 signals reduced in the nucellus, inner integument, and funiculus, suggesting that SPL is a positive regulator of PIN1 and auxin response (Bencivenga *et al.*, 2012). On the contrary, *bel1* mutant results in the ectopic expression of *PIN1* in the integument primordia and in the epidermal layer of funiculus, suggesting that BEL1 is crucial for PIN1's proper localization in the chalaza (Bencivenga *et al.*, 2012). Similarly to *pin1-5* mutant, the *cre1-12 ahk2-2 ahk3-3* mutant shows finger-like ovules unable to develop (Bencivenga *et al.*, 2012). The link between auxin and cytokinin in ovule patterning is highlighted by other observations: PIN1 signal was not observed in *cre1-12 ahk2-2 ahk3-3* mutant and *pin1-5* mutant is insensitive to BAP (Bencivenga *et al.*, 2012). Lastly, CKs can modulate the expression in nucellus and chalaza of *SPL* and *BEL1*

respectively, which in turn control *PIN1* expression in the same sites (Barro-Trastoy *et al.*, 2020).

However, other hormones, such as gibberellins (GAs) and brassinosteroids (BRs) are also involved in ovule morphogenesis, although auxin and CKs appear to be the main players. For example, by interacting with *ATS*, auxin can control the space between the ovule integuments. On the other hand, *ATS* can modulate GA levels, since *della* mutants show abnormalities in integument development, probably due to the lack of interaction of DELLA proteins with *ATS*. As for BRs, they are involved in the development of the outer integument by regulating the expression of *INO* (Barro-Trastoy *et al.*, 2020).

In this context, programmed cell death (PCD) events that affect the nucellar tissues to make way for the developing gametophyte also play a specific role (Wang *et al.*, 2021a). In the developing gametophyte up to the time of fertilisation, the action of auxin influx and efflux carriers is crucial, as it has been observed that nucellar degeneration processes correlate with precise spatio-temporal localisation of auxin, mediated by the family of PIN-FORMED transporters (Wang *et al.*, 2021a). Specifically, in *Arabidopsis*, PIN1 transports auxin of maternal origin within the nucellus, whereas PIN3, PIN4 and PIN7 transport it to the degenerating nucellar cells and also controls the expansion of the central vacuole of the gametophyte (Wang *et al.*, 2021a; **Fig. 2**). Indeed, it is known from the literature that nucellar degeneration processes involve three basic steps: vacuolization, cell death and elimination, the first of which also corresponds to a strong accumulation of auxin (Lituiev *et al.*, 2013).

Furthermore, in *Arabidopsis*, expression of the gene encoding cysteine endopeptidase (*CEP1*), the initiator of nucellar PCD, was found in nucellar cells undergoing vacuolization during the last mitotic divisions leading to gametophyte development until fertilisation (Zhou *et al.*, 2016). This finding again highlights not only the strong link between high auxin levels and vacuolization, leading to cell death, but also the pivotal role of auxin in these processes.

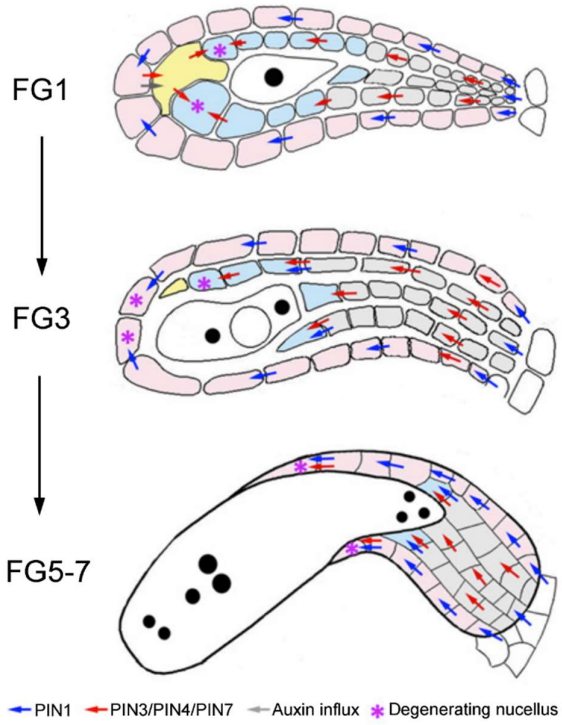

Fig. 2. Image from Wang *et al.* (2021). In *Arabidopsis* nucellar degeneration is strongly related to auxin efflux. During the mitotic divisions leading to the formation of the complete embryo sac, PIN1 transports auxin in the micropylar region through the Ncap from distal maternal tissue. Together with the auxin synthesised there, it moves by simultaneous efflux and influx into the degenerating megaspores. Here the auxin is redistributed by PIN3/PIN4/PIN7 in the Npad, leading its degeneration. Auxin homeostasis allow cell vacuolation and degeneration, which result in expansion of FG central vacuole. Ncap: outer layer of the nucellus (pink); Npad: cells which surround FG (blue); Nbase: the region near the chalaza (grey); degenerating megaspores: yellow.

The importance of pollination event in angiosperms

The decisive event that determines the switch from ovule to seed development is fertilisation. However, in *Arabidopsis*, there are only a few hours between pollination and fertilisation, and pollination alone appears to play a crucial role in activating/deactivating some mechanisms (Zhong *et al.*, 2017). This is even more evident considering *drop1* and *drop2* mutants, which produce pollen tubes devoid of sperm cells. In these *Arabidospis* mutants, even the mere interaction between the pollen tube and the ovule is sufficient to trigger the signalling that allows the ovule to increase in size, often referred to as the starting point for seed development (Zhong *et al.*, 2017). In addition, it has been shown that, in unpollinated *Arabidopsis* pistils, stigmas go through PCD process. Specifically, transcriptional profiling demonstrated

that in unpollinated pistils, the NAC transcription factors KIRA1 (KIR1) and ORESARA1 (ORE1) are activated in the senescence program (Gao *et al.*, 2018). In addition, recent finding in *Arabidopsis* showed that unpollinated ovules undergo senescence processes, involving first the sporophytic tissues, then the integuments, and finally the gametophyte, under the control of some NAC transcription factors. In particular, a combined mutation of NAP/ANAC029, SHYG/ANAC047, and ORE1/ANAC092, the three most up-regulated NAC (NAM, ATAF1/2, and CUC2) transcription factors, resulted in a significant delay in ovule senescence and an extension of fertility (Van Durme *et al.*, 2023). Taken together, these results suggest that ovules longevity and receptivity during pollination timeframe are finely regulated by a molecular network imposed by maternal (sporophytic) tissues, in which other transcription factors are probably also involved (Van Durme *et al.*, 2023). This aspect is particularly interesting and deserves further investigation.

Epigenetic mechanisms underlying the switch from ovule to seed

Seed development involves the co-development of three distinct structures: the embryo, the endosperm and the seed coat (Figueiredo and Köhler, 2018). Specifically, the embryo has a diploid set of chromosomes, half male and half female; in angiosperms, the endosperm has a triploid set of chromosomes, one third male and two thirds female; the seed coat has a diploid set of chromosomes, all female (Ingram, 2010). The initiation of seed development is negatively controlled by a proteins family, belonging to the Polycomb Group (PcG), which are responsible for cell differentiation during the development, acting through epigenetic regulatory mechanisms (Golbabapour *et al.*, 2013). PcG proteins tend to form multimeric complexes, including the Polycomb Repressive Complex 1 and Polycomb Repressive Complex 2 (PRC1 and PRC2) (Roszak and Köhler, 2011). PRC2 is capable of inducing histone modifications by catalysing, via histone methyltransferase, the trimethylation of lysine 27 on histone H3 (H3K27me3) (Kar *et al.*, 2017), while the monoubiquitination of histone H2A at lysine 119 (H2AK119ub), which is catalysed by PRC1, further compacts the chromatin and stabilizes the repressed state (Bemer and Grossniklaus, 2012).

Methylation is the main hallmark of PcG-mediated gene silencing. In particular, trimethylation of histone H3 causes repression of the expression of genes responsible for development (Golbabapour *et al.*, 2013). After fertilisation, a molecular signalling, still not yet fully elucidated, initiates from the endosperm and migrates to the integuments of the ovule, removing the repression of PcG genes at specific loci, enabling the initiation of seed development (Roszak and Köhler, 2011). Different PRC2 complexes have been characterized in *Arabidopsis*, based on their homology with the complexes identified initially in *Drosophyla melanogaster*. Indeed, in both plants and animals, PcG complexes are crucial for phase transitions and determining cell fate (Bemer and Grossniklaus, 2012). However, in *Drosophila*, a single gene encodes the respective subunits (Wang *et al.*, 2006; Margueron and Reinberg, 2011), while in *Arabidopsis* small gene families encode PRC2 core subunits. More in details, the homologs of *E(z)* are *SWINGER* (*SWN*), *CURLY LEAF* (*CLF*) and *MEDEA* (*MEA*), the homologs of *Nurf55* are *MULTICOPY SUPPRESSOR OF IRA1-5* (*MSI1-5*), the *Esc* homolog is *FERTILISATION INDEPENDENT ENDOSPERM* (*FIE*) and lastly *Su(z)12* are *EMBRYONIC FLOWER2* (*EMF2*), *VERNALIZATION2* (*VRN2*) and *FERTILISATION INDEPENDENT SEED2* (*FIS2*). The combination of all subunits can form three different PRC2 (Bemer and Grossniklaus, 2012; **Fig. 3**). EMF-PRC2 and VRN-PRC2 activities are mainly involved in sporophytic development, while FIS-PRC2 in gametophytic development (Derkacheva and Henning, 2014). Indeed, EMF-PRC2, formed by SWN/CLF, EMF2, FIE and MSI1, acts silencing genes known as floral regulators, i.e. *FLOWERING LOCUS T* (*FT*), *AGAMOUS* (*AG*) and *APETALA3* (*AP3*), while VRN-PRC2, which includes SWN/CLF, VRN2, FIE and MSI1, after vernalisation, encourages flowering by repressing *FLOWERING LOCUS C* (*FLC*) (Gendall *et al.*, 2001; Chanvivattana *et al.*, 2004).

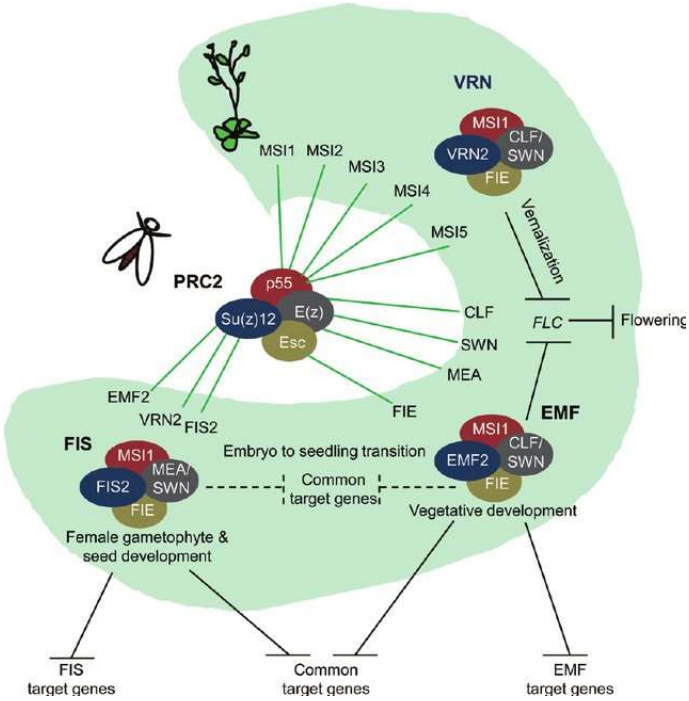

Fig. 3. Image from Derkacheva and Hennig (2014). PRC2 subunits in *Arabidopsis* and respective homologues in *Drosophila*. All complexes are required in several processes in plant development.

FIS-PRC2, which is the first PRC2 identified in *Arabidopsis*, consisting of MEA, FIS2, FIE and MSI1, play a key role in FG and seed development. Indeed, endosperm formation is inhibited by FIS-PRC2 in the absence of fertilisation, such that *fis* mutants mimic apomictic plants and are able to initiate endosperm development even in the absence of fertilisation (Köhler *et al.*, 2003). EMF and VRN-PRC2 complexes are also involved in seed development, but they act on seed coat formation (Pankaj *et al.*, 2023). Importantly, initiation of seed coat development occurs only after fertilisation. However, even in absence of fertilisation, mutants for PcG proteins active in sporophytic tissues can form seed coat (Roszak and Köhler 2011), suggesting that EMF and VRN-PRC2 complexes inhibit genes involved in seed coat development before fertilisation. Indeed, genes encoding EMF and VRN-PRC2 components are severely suppressed after fertilisation (Figueiredo *et al.* 2016).

The evolution of the seed

The production of seed is an expensive strategy in terms of energy, but ensures great success not only on land dispersion but also to plant embryo survive, thanks to the protection and nourishment offered to it. What distinguishes this important innovation and consequently land plants is the alternation of two different generations. First, the gametophyte, male or female, represents the haploid entity capable to differentiate gametes; the fusion of the gametes gives rise to the zygote, with a diploid set of chromosomes, which represents the sporophyte. Finally, through meiosis, the sporophyte gives rise to the haploid spore, thus restarting the cycle (Pires, 2014). The first land plants that evolved the sporophyte enclosed in gametophytic tissue had a great competitive advantage in reproduction; indeed, many different morphologies of sporophytes subsequently evolved, culminating in the dominance of land plants in the Devonian period (Bateman *et al.*, 1998). However, land plants encompass bryophytes, lycophytes, ferns, gymnosperms, and angiosperms, and among them differences in alternation of generation can be observed. In the most primitive clades, the haploid gametophyte is the prevalent generation, whereas in vascular plants the diploid sporophyte is dominant (Pandey *et al.*, 2022), according to the relative period of the developmental process that each phase occupies (Bowman *et al.*, 2016).

Throughout evolutionary history, sporophytes have gradually increased in size, in contrast to gametophytes, which have become gradually smaller (Pires, 2014). The first fossils attesting the presence of specialised ovule integuments and then seeds are dated from around 365 million years ago (Linkies *et al.*, 2010). One of the most important advantages of seeds are the resistance and the ability to remain dormant and be transported over long distances before germination, during which are essential the nutritional reserves accumulated in the endosperm. The dominance of gymnosperms on the global flora for most of the last 300 million years demonstrates the success achieved by seed plants (Willis and McElwain, 2014). Today gymnosperms include four clades (Cycadales, Ginkgoales, Pinales and Gnetales) and approximately 800 living species, whereas angiosperms represent the largest group, with approximately 250,000 species (Donoghue and Doyle, 2000).

The transition from the progymnosperms to the seed plants required three different evolutionary innovation: the transition to heterospory from homospory, hence the production of specialised male and female spores, the innovations of the integuments and the evolution of specialised structures used for pollen reception (Niklas, 1997; Doyle, 2006). Taken together, these innovations had the task to promote the enfranchisement from dependence on the presence of water during fertilisation (Linkies *et al.*, 2010; Pires, 2014). More in details, this independence has not been totally achieved in all clades. Indeed, all angiosperms and most gymnosperms pollen grains produce, after pollination, a pollen tube, which carries the non-motile sperms until the egg cell, whose fertilisation gives rise to the diploid embryo. This is called siphonogamy and it is a process completely water independent. However, cycads and *Ginkgo*, the oldest clades among gymnosperms, are an exception because they have multiflagellated sperms. These, at the time of fertilisation, swim to the archegonia, which bear the egg cells (Linkies *et al.*, 2010).

In the late Devonian, a paraphyletic group of progymnosperms conquered the land. They shared vegetative structures that would be shown by future seed plants, but the reproductive strategies were similar to those of the Pteridophytes. Many fossil seeds of different progymnosperms species present a stratification of the seed coat. The inner layer is thin and membranous, the outer is sclerenchymatous, however, both layers do not close the micropylar canal (Linkies *et al.*, 2010). Initially, progymnosperms showed homospory, but there are fossils attesting to the presence of heterosporous progymnosperms even in the Carboniferous and Permian, where they probably coexisted with gymnosperms, since the origins of angiosperms do not date back before the Cretaceous period (Wang *et al.*, 2021b). The layering of the seed coat is an interesting feature because some of these layers have taken on particular morphologies during evolution in order to increase the seed's ability to disperse.

The experimental model selected: *Ginkgo biloba* L.

Ginkgo biloba L. is a species of particular interest for studies aimed to better understanding the diversity among existing plants, because it is the only extant species of the division Ginkgophytes (Douglas *et al.*, 2007). Fossils show that Ginkgophytes were already present in the early Mesozoic, although some finds date back to the last period of the Palaeozoic, the Permian. Only one class and order are included in the Ginkgophytes, Ginkgopsida and Ginkgoales respectively. However, five families are included, four of which (Karkeniaceae, Umaltolepidiaceae, Yimaiaceae and Schmeissneriaceae) are extinct, while Ginkgoaceae represents the more recent family. Of the genera, nine are extinct and only the genus *Ginkgo* survives. Of the eleven species that once existed, only *Ginkgo biloba* is still alive. Based on this evidence, it is often referred to *Ginkgo biloba* as a "living fossil" (Stanković, 2016). *Ginkgo* was originally widespread in both the southern and northern hemispheres. Later, however, its distribution areal declined significantly and reduced to a few populations in what is now China, where it survived the Pleistocene (Singh *et al.*, 2008; Jin *et al.*, 2012; Stanković, 2016). In line with these evidences, *Ginkgo* presents some primitive traits, such as dichotomously veined leaves, reproduction, single but three-layered ovule integument, coenocytic female gametophyte, multiflagellated motile spermatozoids, lack of dormancy (Douglas *et al.*, 2007; Wang *et al.*, 2011; Stanković, 2016). It's a dioecious plant, so it carries male and female organs from different individuals, which reached the full maturity after 20-30 years (Christianson and Jernstedt, 2009). Male and female reproductive organs, known as micro- and macrostrobiles respectively, grow from short shoots at the same time as leaves (**Fig. 4A, C**) and are extruded by buds named brachyblasts. Concerning microstrobiles, they have pollen-bearing cones, which are constitute by microsporophylls (**Fig. 4A**), that, in turn, bears elongate, pendulous microsporangia (**Fig. 4B**). As *Ginkgo* is an anemophilous species, the pollen grains are carried by the wind when microsporangia are open. These, in turn, fall to the ground once the pollen grains have been released (Stanković, 2016).

On the contrary, the macrostrobiles are essentially stalk-like peduncles with ovules at the top, often in pairs (**Fig. 4C**). Upon pollination, the *Ginkgo* ovule has a characteristic organisation: a single integument, the nucellus and the pollen chamber. The integument surrounds the nucellus, keeping the micropylar canal open, which is

particularly tapered and ends in the pollen chamber, below which, in the nucellus, the micropylar parietal tissue, the *tapetum*, the gametophyte and the chalazal parietal tissue are progressively distinguished (Douglas *et al.*, 2007; **Fig. 4D;** for more details see **Fig. 5A, B**). When the ovules are ready to be pollinated, they release a pollination drop composed mainly of sugars (sucrose, glucose and fructose) to catch the pollen grains carried by the wind (Jin *et al.*, 2012). The droplet then dries and retracts, pulling the pollen grains into the pollen chamber. However, fertilisation does not occur until about four to five months after pollination (Douglas *et al.*, 2007). During this time, the development of the male and female gametophytes continues slowly.

Concerning the female gametophyte, it is in a coenocytic stage and comprises about 1000 free nuclei enclosed by tapetal cells, which progressively degenerate allowing cellularisation (Lee, 1955; D'Apice *et al.*, 2021). During gametophyte cellularisation two groups of cells get together at the gametophyte micropilar pole and a single cell for each group enlarges, representing the archegonial initial cell (Wang *et al.*, 2014; D'Apice *et al.*, 2021). Egg cells reside inside the archegonia, specialised structures for fluid-base reproduction (Li *et al.*, 2007; Von Aderkas *et al.*, 2018). In turn, the archegonia are enclosed by archegonial jacket, cell layers involved in the transfer of protein granules and starch in the archegonium during its development (Lee, 1955; Cionini, 1971). During these processes, the integument also undergoes changes. Immediately after pollination, three different integument layers begin to be distinguished. Proceeding from outside to inside the first layer is the *sarcotesta*, characterized by the presence of mucilaginous canals and isodiametric cells; the second layer is the *sclerotesta*, recognizable thanks to the smaller but thick walled cells; and the third layer is the *endotesta*, which presents elongated cells. After pollination the *sarcotesta* will take on a fleshy appearance, similar to what happens to the pericarp of the fleshy fruits of angiosperms (D'Apice *et al.*, 2021).

At the same time, the male gametophyte also continues its development in the nucellus. In fact, about a week after pollination, the pollen germinates, producing an haustorial pollen tube (Friedman, 1987). The pollen tube penetrates in nucellar tissues, where it draws nourishment and ramifies considerably (Offer *et al.*, 2023).

Although two archegonia and thus two egg cells are present, two multiflagellated motile spermatozoids are released, but usually only one of which is able to fertilise the

egg cell and only one embryo is generated (Lee, 1955; Stanković, 2016; **Fig. 4E, F**). Following fertilisation, the seed may still remain attached to the branch or fall to the ground. In both cases, the embryo will continue its development (Stanković, 2016). The seed coat reflects the three layers that had already been observed in the ovule tegument, although it is even more evident. The outer layer (the *sarcotesta*) is soft and fleshy, similar to an apricot in shape and colour, the middle layer (the *sclerotesta*) is highly lignified, the inner layer (the *endotesta*) is thin and paper-like (D'Apice *et al.*, 2021; Stanković, 2016). The seeds have a rather unpleasant smell, because *sarcotesta* presents some volatile compounds such as butyric acid. However, they are dispersed by the animals, according to a zoocory strategy, which is why the presence of a fleshy *sarcotesta* is extremely important for successful dispersal but also for germination (Stanković, 2016). Mammals usually eat *Ginkgo* seeds because of their juicy and nutrient-dense *sarcotesta*, contributing to the dispersal. In addition, although the lack of fossilized *Ginkgo* seeds, there are many theories about what animals may have distributed seeds during the plant's lengthy evolutionary history. According to some evidence, it might be a kind of dinosaur, the ancestors of birds, or some species of rodent, like *Multituberculata* (Stanković, 2016; Nigris *et al.*, 2021).

Nowadays depending on the latitude, the events described so far occur at different times. In warm climates, the pollination happens in April, the fertilisation in September and the seed germination in March of the next year. In cold climates they have shifted by about one or two months: the pollination occurs in May, the fertilisation in October and the seed germination in June of the following year (Stanković, 2016).

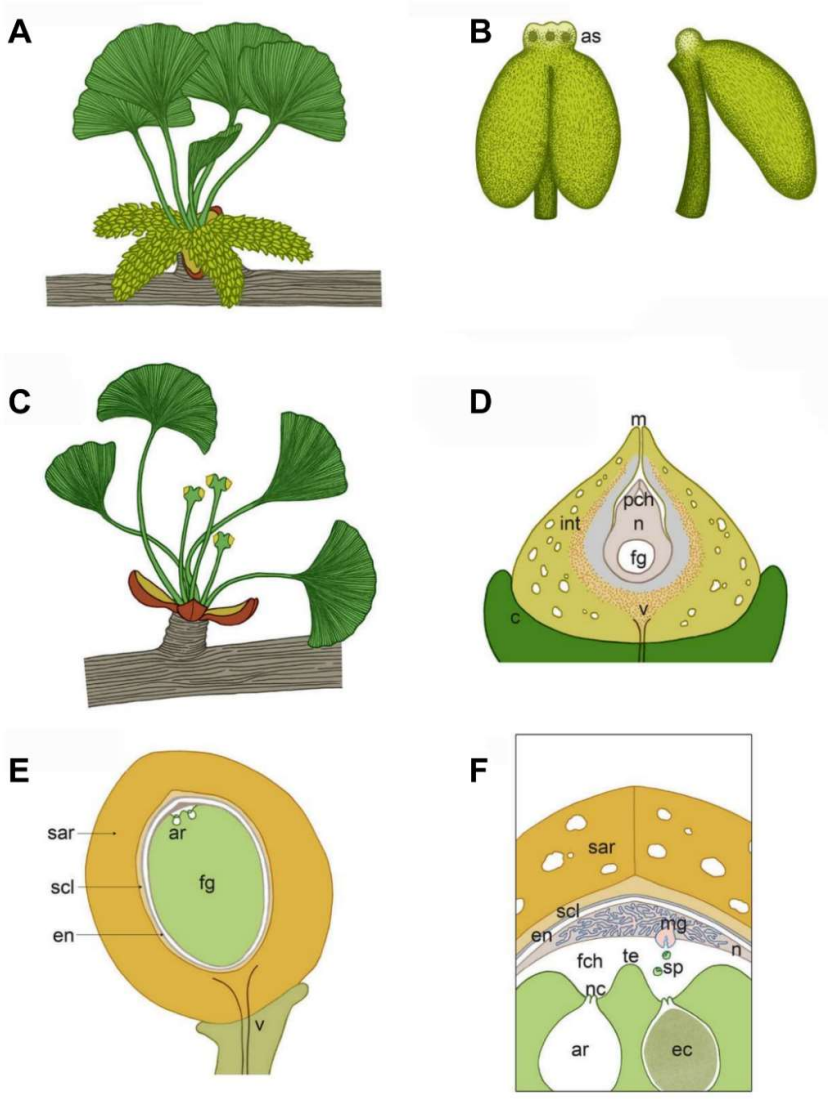

Fig. 4. Image modified from Offer *et al.* (2023). Schematic representation of the male (A-B) and female (C-F) reproductive structures of *Ginkgo biloba* at different developmental stages. (A) Male brachyblast with pendulous cones, which comprises several microsporophylls. (B) Magnification of a single microsporophyll seen from the front and the side. Are visible the air sacs (as) and the microscorangia. (C) Female brachyblast with ovules located at the end of stalks. (D) Longitudinal section of ovule during pollination timeframe. Visible is the single three-layered integument (int), which leaves the micropylar channel (m) open and below which is the pollen chamber (pch). In the nucellus (n), female gametophyte (fg) is developing. The vasculature (v) is mainly localized in stalk and collar (c). (E) Longitudinal section of ovule during fertilisation timeframe. The integument has completed the differentiation of the three layers (sarcotesta, sar; sclerotesta, scl; endotesta, en). The female gametophyte (fg) has completed its development, enlarging at the expense of the nucellar tissues and cellularising, and the archegonia (ar) have formed. (F) Close up of fertilisation. The multiflagellated sperm cells (sp) are released and swim up to the archegonia (ar). The characteristic tentpole (te) in the fertilisation chamber (fch) separating the archegonia (ar) is visible. Of the two sperm cells only one will pass through the neck cells (nc) and fertilise the egg cell (eg). ar: archegonia; as: air sac; c: collar; ec: egg cell; en: endotesta; fch: fertilisation chamber; fg: female gametophyte; m: micropyle; mg: macrogametophyte; n: nucellus; nc: neck cells; p: pollen; pch: pollen chamber; sar: sarcotesta; scl: sclerotesta; sp: sperm cells; te: tentpole; v: vasculature.

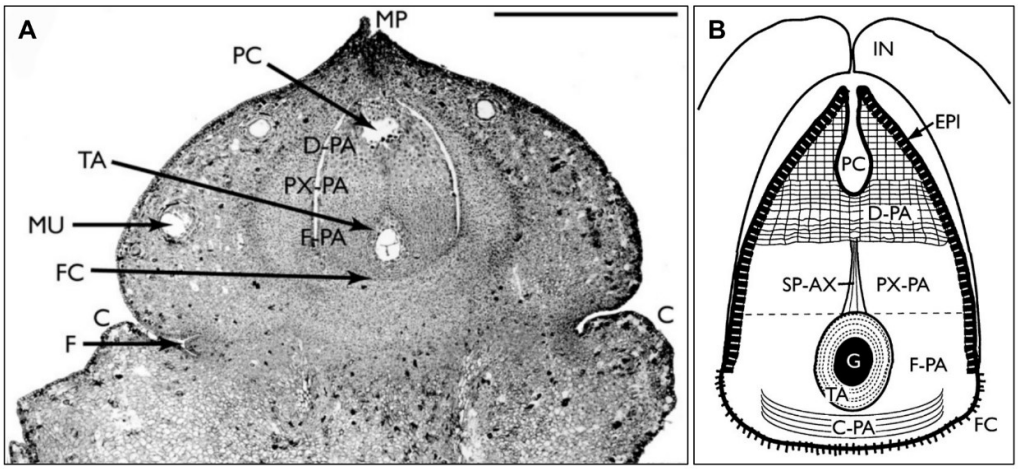

Fig. 5. Images modified from Douglas *et al.* (2007). Longitudinal section (A) and respective schematic model (B) of *G. biloba* ovule immediately after pollination, with emphasis to the different regions of nucellus. C: collar; C-PA: chalazal parietal tissue; D-PA: distal micropylar parietal tissue; EPI: epidermis; FC: flattened-cells layer; F-PA: flanking parietal tissue; G: female gametophyte; IN: integument; PC: pollen chamber; PX-PA: proximal micropylar parietal tissue; SP-AX: sporangial axial column of cells; TA: *tapetum*. (A) Scale bar = 1 mm

Aim of the projects

The development of seed and its developmental predecessor, the ovule, are widely studied in angiosperms, especially in model species *Arabidopsis thaliana*, but they are poorly explored in gymnosperms (Rudall, 2021). In this scenario, we focused the studies on *Ginkgo*, whose ovules present interesting and primitive characteristics and has been extensively described. In *Ginkgo*, pollination and fertilisation events are separated by a long interval (i.e. 4-5 months), in which ovule continues to grow and female gametophyte differentiation occurs, suggesting that pollination event could trigger the signal for ovule transformation in seed. The use of such an ancient and at the same time so interesting species is excellent for an *evo-devo* approach, as a topic from developmental biology is studied with an evolutionary point of view. Indeed, sometimes, it is necessary to investigate the past in depth in order to better understand the present and appreciate the biodiversity that surrounds us.

In the context of this research, the reproductive biology of *Ginkgo* was studied, with a focus on the molecular networks underlying its ovule development.

For this purpose, the expression profiles of genes belonging to pathways of interest, the localisation domains of some of the main phytohormones, auxin and

cytokinin, and some of the epigenetically controlled key genes involved in the ovule-to-seed transition were investigated. Since it has been documented in the literature that female *Ginkgo* plants that are geographically separated from male plants have aborted all of their ovules after the emission of the pollination drop (Friedman, 1987), many of these aspects have also been studied in absence of pollination. Indeed, for several approaches pollinated (PO) and unpollinated ovules (UO), the last ones collected from female plants geographically isolated from male plants, were used. For both condition, three different stages were used: 1, 6 and 8 days after the end of pollination drop emission.

While remembering how distant the species are, the vast amount of information available concerning the model organism *Arabidopsis thaliana* was the starting point for this research, aimed at adding a small piece of knowledge in the great evolutionary story of the past, which still continues to fascinate today.

In particular, the goals of my research were three:

- Epigenetics, which plays a key role in gene expression thanks to the post-translational histone modifications;
- Role of pollination event, widely studied in angiosperms, in which, however, it is extremely close to fertilisation, imposing a clear distinction between the molecular signalling triggered by the two events, but still elusive in gymnosperms;
- Role of hormones, extremely involved in all processes that occur in the life of plant organisms, but with particular attention on auxin and cytokinin, which assume a pivotal role during sexual organs development.

The results obtained during my Ph. D. project contribute to an overview of the reproductive biology of *Ginkgo*.

REFERENCES

Arnault, G., Vialette, A. C., Andres-Robin, A., Fogliani, B., Gâteblé, G., and Scutt, C. P. (2018). Evidence for the extensive conservation of mechanisms of ovule integument development since the most recent common ancestor of living angiosperms. *Frontiers in Plant Science*, *9*, 1352.

Bai, S. N., Rao, G. Y., and Yang, J. (2022). Origins of the seed: The "golden-trio hypothesis". *Frontiers in Plant Science*, *13*, 965000.

Baker, S. C., Robinson-Beers, K., Villanueva, J. M., Gaiser, J. C., and Gasser, C. S. (1997). Interactions among genes regulating ovule development in *Arabidopsis thaliana*. *Genetics*, *145*(4), 1109-1124.

Balasubramanian, S., and Schneitz, K. (2000). *NOZZLE* regulates proximal-distal pattern formation, cell proliferation and early sporogenesis during ovule development in *Arabidopsis thaliana*. *Development*, *127*(19), 4227-4238.

Balasubramanian, S., and Schneitz, K. (2002). *NOZZLE* links proximal-distal and adaxial-abaxial pattern formation during ovule development in *Arabidopsis thaliana*. *Development*, *127*(19), 4227–4238.

Barro-Trastoy, D., Dolores Gomez, M., Tornero, P., and Perez-Amador, M. A. (2020). On the way to ovules: the hormonal regulation of ovule development. *Critical Reviews in Plant Sciences*, *39*(5), 431-456.

Bartrina, I., Otto, E., Strnad, M., Werner, T., and Schmülling, T. (2011). Cytokinin regulates the activity of reproductive meristems, flower organ size, ovule formation, and thus seed yield in *Arabidopsis thaliana*. *The Plant Cell*, *23*(1), 69-80.

Bateman, R. M., Crane, P. R., DiMichele, W. A., Kenrick, P. R., Rowe, N. P., Speck, T., and Stein, W. E. (1998). Early evolution of land plants: phylogeny, physiology, and ecology of the primary terrestrial radiation. *Annual Review of Ecology and Systematics*, *29*(1), 263-292.

Bemer, M., and Grossniklaus, U. (2012). Dynamic regulation of Polycomb group activity during plant development. *Current opinion in plant biology*, *15*(5), 523-529.

Bencivenga, S., Simonini, S., Benková, E., and Colombo, L. (2012). The transcription factors BEL1 and SPL are required for cytokinin and auxin signaling during ovule development in *Arabidopsis*. *The Plant Cell*, *24*(7), 2886-2897.

Benková, E., Michniewicz, M., Sauer, M., Teichmann, T., Seifertová, D., Jürgens, G., and Friml, J. (2003). Local, efflux-dependent auxin gradients as a common module for plant organ formation. *Cell*, *115*(5), 591-602.

Bowman, J. L., Sakakibara, K., Furumizu, C., and Dierschke, T. (2016). Evolution in the cycles of life. *Annual review of genetics*, *50*, 133-154.

Brumos, J., Robles, L. M., Yun, J., Vu, T. C., Jackson, S., Alonso, J. M., and Stepanova, A. N. (2018). Local auxin biosynthesis is a key regulator of plant development. *Developmental cell*, *47*(3), 306-318.

Ceccato, L., Masiero, S., Roy, D. S., Bencivenga, S., Roig-Villanova, I., Ditengou, F. A., Palme, K., Simon, R., and Colombo, L. (2013). Maternal control of PIN1 is required for female gametophyte development in *Arabidopsis*. *PloS one*, *8*, e66148.

Chanvivattana, Y., Bishopp, A., Schubert, D., Stock, C., Moon, Y. H., Sung, Z. R., and Goodrich, J. (2004). Interaction of Polycomb-group proteins controlling flowering in *Arabidopsis*. *Development 131*(21), 5263–5276.

Christianson, M. L., and Jernstedt, J. A. (2009). Reproductive short-shoots of *Ginkgo biloba*: A quantitative analysis of the disposition of axillary structures. *American Journal of Botany*, *96*(11), 1957-1966.

Cionini, P. G. (1971). A DNA cytophotometric study on cell nuclei of the archegonial jacket in the female gametophyte of *Ginkgo biloba*. *Caryologia*, *24*(4), 493-500.

Coito, J. L., Silva, H., Ramos, M. J., Montez, M., Cunha, J., Amâncio, S., Costa, M. M. R., and Rocheta, M. (2018). *Vitis* flower sex specification acts downstream and independently of the ABCDE model genes. *Frontiers in Plant Science*, *9*, 1029.

Cucinotta, M., Manrique, S., Cuesta, C., Benková, E., Novak, O., and Colombo, L. (2018). CUP-SHAPED COTYLEDON1 (CUC1) and CUC2 regulate cytokinin homeostasis to determine ovule number in *Arabidopsis*. *Journal of experimental botany*, *69*(21), 5169-5176.

Cucinotta, M., Manrique, S., Guazzotti, A., Quadrelli, N. E., Mendes, M. A., Benková, E., and Colombo, L. (2016). Cytokinin response factors integrate auxin and cytokinin pathways for female reproductive organ development. *Development*, *143*(23), 4419-4424.

D'Apice, G., Moschin, S., Araniti, F., Nigris, S., Di Marzo, M., Muto, A., Banfi, C., Bruno, L., Colombo, L., and Baldan, B. (2021). The role of pollination in controlling *Ginkgo biloba* ovule development. *New Phytologist*, *232*(6), 2353-2368.

Derkacheva, M., and Hennig, L. (2014). Variations on a theme: Polycomb group proteins in plants. *Journal of experimental botany*, *65*(10), 2769-2784.

Dodsworth, S. (2009). A diverse and intricate signalling network regulates stem cell fate in the shoot apical meristem. *Developmental Biology*, *336*(1), 1-9.

Donoghue, M. J., and Doyle, J. A. (2000). Seed plant phylogeny: demise of the anthophyte hypothesis?. *Current Biology*, *10*(3), R106-R109.

Douglas, A. W., Stevenson, D. W., and Little, D. P. (2007). Ovule development in *Ginkgo biloba* L., with emphasis on the collar and nucellus. *International Journal of Plant Sciences*, *168*(9), 1207-1236.

Doyle, J. A. (2006). Seed ferns and the origin of angiosperms. *The Journal of the Torrey Botanical Society*, *133*(1), 169-209.

Elliott, R. C., Betzner, A. S., Huttner, E., Oakes, M. P., Tucker, W. Q., Gerentes, D., Perez, P., and Smyth, D. R. (1996). *AINTEGUMENTA*, an *APETALA2*-like gene of *Arabidopsis* with pleiotropic roles in ovule development and floral organ growth. *The Plant Cell*, *8*(2), 155-168.

Endress, P. K. (2011). Angiosperm ovules: diversity, development, evolution. *Annals of Botany*, *107*(9), 1465-1489.

Figueiredo, D. D., and Köhler, C. (2018). Auxin: a molecular trigger of seed development. *Genes and development*, *32*(7-8), 479-490.

Figueiredo, D. D., Batista, R. A., Roszak, P. J., Hennig, L., and Köhler, C. (2016). Auxin production in the endosperm drives seed coat development in Arabidopsis. *Elife*, *5*, e20542.

Friedman, W. E. (1987). Growth and development of the male gametophyte of *Ginkgo biloba* within the ovule (in vivo). *American Journal of Botany*, *74*(12), 1797-1815.

Gaiser, J. C., Robinson-Beers, K., and Gasser, C. S. (1995). The *Arabidopsis SUPERMAN* gene mediates asymmetric growth of the outer integument of ovules. *The Plant Cell*, *7*(3), 333-345.

Galbiati, F., Sinha Roy, D., Simonini, S., Cucinotta, M., Ceccato, L., Cuesta, C., Simaskova, M., Benková, E., Kamiuchi, Y., Aida, M., Weijers, D., Simon, R., Masiero S., and Colombo, L. (2013). An integrative model of the control of ovule primordia formation. *The Plant Journal*, *76*(3), 446-455.

Gao, Z., Daneva, A., Salanenka, Y., Van Durme, M., Huysmans, M., Lin, Z., De Winter, F., Vanneste, S., Karimi, M., Van de Velde, J., Vadepoele, K., Van de Walle, D., Dewettinck, K., Lambrecht, B. N., and Nowack, M. K. (2018). KIRA1 and ORESARA1 terminate flower receptivity by promoting cell death in the stigma of *Arabidopsis*. *Nature plants*, *4*(6), 365-375.

Gasser, C. S., and Robinson-Beers, K. (1993). Pistil development. *The Plant Cell*, *5*(10), 1231.

Gendall, A. R., Levy, Y. Y., Wilson, A., and Dean, C. (2001). The *VERNALIZATION 2* gene mediates the epigenetic regulation of vernalization in *Arabidopsis*. *Cell*, *107*(4), 525-535.

Golbabapour, S., Majid, N. A., Hassandarvish, P., Hajrezaie, M., Abdulla, M. A., and Hadi, A. H. A. (2013). Gene silencing and Polycomb group proteins: an overview of their structure, mechanisms and phylogenetics. *Omics: a journal of integrative biology*, *17*(6), 283-296.

Groß-Hardt, R., Lenhard, M., and Laux, T. (2002). *WUSCHEL* signaling functions in interregional communication during *Arabidopsis* ovule development. *Genes and Development*, *16*(9), 1129-1138.

Guo, A., and Zheng, C. X. (2013). Female gametophyte development. *Journal of Plant Biology, 56*, 345-356.

Ingram, G. C. (2010). Family life at close quarters: communication and constraint in angiosperm seed development. *Protoplasma*, *247*(3-4), 195-214.

Jin, B., Zhang, L., Lu, Y., Wang, D., Jiang, X. X., Zhang, M., and Wang, L. (2012). The mechanism of pollination drop withdrawal in *Ginkgo biloba* L. *BMC Plant Biology*, *12*(1), 1-9.

Kar, G., Kim, J. K., Kolodziejczyk, A. A., Natarajan, K. N., Torlai Triglia, E., Mifsud, B., Elderkin, S., Marioni, J. C., Pombo, A., and Teichmann, S. A. (2017). Flipping between Polycomb repressed and active transcriptional states introduces noise in gene expression. *Nature communications*, *8*(1), 36.

Kelley, D. R., and Gasser, C. S. (2009). Ovule development: genetic trends and evolutionary considerations. *Sexual plant reproduction*, *22*, 229-234.

Kelley, D. R., Skinner, D. J., and Gasser, C. S. (2009). Roles of polarity determinants in ovule development. *The Plant Journal*, *57*(6), 1054-1064.

Klucher, K. M., Chow, H., Reiser, L., and Fischer, R. L. (1996). The *AINTEGUMENTA* gene of *Arabidopsis* required for ovule and female gametophyte development is related to the floral homeotic gene *APETALA2*. *The Plant Cell*, *8*(2), 137-153.

Köhler, C., Hennig, L., Spillane, C., Pien, S., Gruissem, W., and Grossniklaus, U. (2003). The Polycomb-group protein MEDEA regulates seed development by controlling expression of the MADS-box gene *PHERES1*. *Genes and development*, *17*(12), 1540-1553.

Krizek, B. A., Blakley, I. C., Ho, Y. Y., Freese, N., and Loraine, A. E. (2020). The *Arabidopsis* transcription factor AINTEGUMENTA orchestrates patterning genes and auxin signaling in the establishment of floral growth and form. *The Plant Journal*, *103*(2), 752-768.

Larsson, E., Vivian-Smith, A., Offringa, R., and Sundberg, E. (2017). Auxin homeostasis in *Arabidopsis* ovules is anther-dependent at maturation and changes dynamically upon fertilisation. *Frontiers in Plant Science*, *8*, 1735.

Lee, C. L. (1955). Fertilisation in *Ginkgo biloba*. *Botanical Gazette*, *117*(2), 79-100.

Li, D. H., Yang, X., and Cui, K. M. (2007). Formation of archegonium chamber is associated with nucellar-cell programmed cell death in *Ginkgo biloba*. *Protoplasma*, *231*, 173-181.

Linkies, A., Graeber, K., Knight, C., and Leubner-Metzger, G. (2010). The evolution of seeds. *New Phytologist*, *186*(4), 817-831.

Lituiev, D. S., Krohn, N. G., Müller, B., Jackson, D., Hellriegel, B., Dresselhaus, T., and Grossniklaus, U. (2013). Theoretical and experimental evidence indicates that there is no detectable auxin gradient in the angiosperm female gametophyte. *Development*, *140*(22), 4544-4553.

Margueron, R., and Reinberg, D. (2011). The Polycomb complex PRC2 and its mark in life. *Nature*, *469*(7330), 343-349.

McAbee, J. M., Hill, T. A., Skinner, D. J., Izhaki, A., Hauser, B. A., Meister, R. J., Venugopala Reddy, G., Meyerowitz, E.M., Bowman, J.L., and Gasser, C. S. (2006). *ABERRANT TESTA SHAPE* encodes a KANADI family member, linking polarity determination to separation and growth of *Arabidopsis* ovule integuments. *The Plant Journal*, *46*(3), 522-531.

McConnell, J. R., and Barton, M. K. (1998). Leaf polarity and meristem formation in Arabidopsis. *Development*, *125*(15), 2935-2942.

Meister, R. J., Kotow, L. M., and Gasser, C. S. (2002). SUPERMAN attenuates positive *INNER NO OUTER* autoregulation to maintain polar development of *Arabidopsis* ovule outer integuments. *Development, 129*(18), 4281–4289

Nepi, M., von Aderkas, P., Wagner, R., Mugnaini, S., Coulter, A., and Pacini, E. (2009). Nectar and pollination drops: how different are they?. *Annals of Botany, 104*(2), 205-219.

Nigris, S., D'Apice, G., Moschin, S., Ciarle, R., and Baldan, B. (2021). Fleshy structures associated with ovule protection and seed dispersal in gymnosperms: a systematic and evolutionary overview. *Critical Reviews in Plant Sciences*, *40*(4), 285-302.

Niklas, K. J. (1997). *The evolutionary biology of plants*. University of Chicago Press.

Nishimura, C., Ohashi, Y., Sato, S., Kato, T., Tabata, S., and Ueguchi, C. (2004). Histidine kinase homologs that act as cytokinin receptors possess overlapping functions in the regulation of shoot and root growth in *Arabidopsis*. *The Plant Cell*, *16*(6), 1365-1377.

Nole-Wilson, S., and Krizek, B. A. (2000). DNA binding properties of the *Arabidopsis* floral development protein AINTEGUMENTA. *Nucleic Acids Research*, *28*(21), 4076-4082.

Nole-Wilson, S., Azhakanandam, S., and Franks, R. G. (2010). Polar auxin transport together with *AINTEGUMENTA* and *REVOLUTA* coordinate early *Arabidopsis* gynoecium development. *Developmental biology*, *346*(2), 181-195.

Offer, E., Moschin, S., Nigris, S., and Baldan, B. (2023). Reproductive mechanisms in *Ginkgo* and *Cycas*: sisters but not twins. *Critical Reviews in Plant Sciences*, *42*(5), 283-299.

Okada, K., Ueda, J., Komaki, M. K., Bell, C. J., and Shimura, Y. (1991). Requirement of the auxin polar transport system in early stages of *Arabidopsis* floral bud formation. *The Plant Cell*, *3*(7), 677-684.

Overvoorde, P., Fukaki, H., and Beeckman, T. (2010). Auxin control of root development. *Cold Spring Harbor perspectives in biology*, *2*(6), a001537.

Pagnussat, G. C., Yu, H. J., and Sundaresan, V. (2007). Cell-fate switch of synergid to egg cell in *Arabidopsis eostre* mutant embryo sacs arises from misexpression of the BEL1-like homeodomain gene BLH1. *The Plant Cell*, *19*(11), 3578-3592.

Pandey, S., Moradi, A. B., Dovzhenko, O., Touraev, A., Palme, K., and Welsch, R. (2022). Molecular control of sporophyte-gametophyte ontogeny and transition in plants. *Frontiers in Plant Science*, *12*, 789789.

Pankaj, R., Lima, R. B., Luo, G. Y., Ehlert, S., Finger, P., Sato, H., and Figueiredo, D. D. (2023). Seed coat formation in *Arabidopsis* requires a concerted action of JUMONJI histone H3K27me3 demethylases and Brassinosteroid signaling. *bioRxiv*, 2023-12.

Pires, N. D. (2014). Seed evolution: parental conflicts in a multi-generational household. *Biomolecular concepts*, *5*(1), 71-86.

Prior, N., Little, S. A., Boyes, I., Griffith, P., Husby, C., Pirone-Davies, C., Stevenson, D. W., Tomlinson, P. B., and von Aderkas, P. (2019). Complex reproductive secretions occur in all extant gymnosperm lineages: a proteomic survey of gymnosperm pollination drops. *Plant reproduction*, *32*, 153-166.

Roszak, P., and Köhler, C. (2011). Polycomb group proteins are required to couple seed coat initiation to fertilisation. *Proceedings of the National Academy of Sciences*, *108*(51), 20826-20831.

Rudall, P. J. (2021). Evolution and patterning of the ovule in seed plants. *Biological Reviews*, *96*(3), 943-960.

Sakai, H., Medrano, L. J., and Meyerowitz, E. M. (1995). Role of *SUPERMAN* in maintaining *Arabidopsis* floral whorl boundaries. *Nature*, *378*(6553), 199-203.

Schneitz, K., Hülskamp, M., Kopczak, S. D., and Pruitt, R. E. (1997). Dissection of sexual organ ontogenesis: a genetic analysis of ovule development in *Arabidopsis thaliana*. *Development*, *124*(7), 1367-1376.

Shi, D. Q., and Yang, W. C. (2011). Ovule development in *Arabidopsis*: progress and challenge. *Current opinion in plant biology*, *14*(1), 74-80.

Shigyo, M., Hasebe, M., and Ito, M. (2006). Molecular evolution of the AP2 subfamily. *Gene*, *366*(2), 256-265.

Sieber, P., Gheyselinck, J., Gross-Hardt, R., Laux, T., Grossniklaus, U., and Schneitz, K. (2004). Pattern formation during early ovule development in *Arabidopsis thaliana*. *Developmental biology*, *273*(2), 321-334.

Šimášková, M., O'Brien, J. A., Khan, M., Van Noorden, G., Ötvös, K., Vieten, A., De Clercq, I., Van Haperen, J. M. A., Cuesta, C., Hoyerová, K., Vanneste, S., Marhavý, P., Wabnik, K., Van Breusegem, F., Nowack, M., Murphy, A., Friml, J., Weijers, D., Beeckman, T., and Benková, E. (2015). Cytokinin response factors regulate PIN-FORMED auxin transporters. *Nature communications*, *6*(1), 8717.

Singh, B., Kaur, P., Singh, R. D., and Ahuja, P. S. (2008). Biology and chemistry of *Ginkgo biloba*. *Fitoterapia*, *79*(6), 401-418.

Stanković, M. (2016). Biology and ecology of *Ginkgo biloba* L.(Ginkgoaceae). *Ginkgo biloba*, L.

Taylor, E. L., Taylor, T. N., and Krings, M. (2009). *Paleobotany: the biology and evolution of fossil plants. Academic Press.*

Van Berkel, K., de Boer, R. J., Scheres, B., and ten Tusscher, K. (2013). Polar auxin transport: models and mechanisms. *Development*, *140*(11), 2253-2268.

Van Durme, M., Olvera-Carrillo, Y., Pfeiffer, M. L., Doll, N. M., De Winter, F., Lin, Z., and Nowack, M. K. (2023). Fertility loss in senescing *Arabidopsis* ovules is controlled by the maternal sporophyte via a NAC transcription factor triad. *Proceedings of the National Academy of Sciences*, *120*(25), e2219868120.

Villanueva, J. M. (1999). *Genetic analysis of ovule outer integument mutants and the positional cloning of the INNER NO OUTER gene in Arabidopsis thaliana*. University of California, Davis.

Von Aderkas, P., Prior, N. A., and Little, S. A. (2018). The evolution of sexual fluids in gymnosperms from pollination drops to nectar. *Frontiers in Plant Science*, *9*, 1844.

Wang, D., Lu, Y., Zhang, M., Lu, Z., Luo, K., Cheng, F., and Wang, L. (2014). Structure and function of the neck cell during fertilisation in *Ginkgo biloba* L. *Trees*, *28*, 995-1005.

Wang, D., Tyson, M. D., Jackson, S. S., and Yadegari, R. (2006). Partially redundant functions of two SET-domain polycomb-group proteins in controlling initiation of seed development in Arabidopsis. *Proceedings of the National Academy of Sciences*, *103*(35), 13244-13249.

Wang, J., Guo, X., Xiao, Q., Zhu, J., Cheung, A. Y., Yuan, L., Vierling, E., and Xu, S. (2021a). Auxin efflux controls orderly nucellar degeneration and expansion of the female gametophyte in *Arabidopsis*. *New Phytologist*, *230*(6), 2261-2274.

Wang, J., Hilton, J., Pfefferkorn, H. W., Wang, S., Zhang, Y., Bek, J., Pšenička, J., Seyfullah, L. J., and Dilcher, D. (2021b). Ancient noeggerathialean reveals the seed plant sister group diversified alongside the primary seed plant radiation. *Proceedings of the National Academy of Sciences*, *118*(11), e2013442118.

Wang, L., Wang, D., LIN, M. M., Lu, Y., JIANG, X. X., and Jin, B. (2011). An embryological study and systematic significance of the primitive gymnosperm *Ginkgo biloba*. *Journal of Systematics and Evolution*, *49*(4), 353-361.

Wang, Y., and Jiao, Y. (2018). Auxin and above-ground meristems. *Journal of experimental botany*, *69*(2), 147-154.

Weijers, D., Nemhauser, J., and Yang, Z. (2018). Auxin: small molecule, big impact. *Journal of Experimental Botany*, *69*(2), 133-136.

Willis, K., and McElwain, J. (2014). *The evolution of plants*. Oxford University Press, USA.

Yamada, T., Sasaki, Y., Hashimoto, K., Nakajima, K., and Gasser, C. S. (2016). *CORONA*, *PHABULOSA* and *PHAVOLUTA* collaborate with *BELL1* to confine *WUSCHEL* expression to the nucellus in *Arabidopsis* ovules. *Development*, *143*(3), 422-426.

Yamaguchi, N., Wu, M. F., Winter, C. M., Berns, M. C., Nole-Wilson, S., Yamaguchi, A., Coupland, G., Krizek, B. A., and Wagner, D. (2013). A molecular framework for auxin-mediated initiation of flower primordia. *Developmental cell*, *24*(3), 271-282.

Yuan, J., and Kessler, S. A. (2019). A genome-wide association study reveals a novel regulator of ovule number and fertility in *Arabidopsis thaliana*. *PLoS genetics*, *15*(2), e1007934.

Zhong, S., Zhang, J., and Qu, L. J. (2017). The signals to trigger the initiation of ovule enlargement are from the pollen tubes: The direct evidence. *Journal of integrative plant biology*, *59*(9), 600-603.

Zhou, J. J., and Luo, J. (2018). The PIN-FORMED auxin efflux carriers in plants. *International journal of molecular sciences*, *19*(9), 2759.

Zhou, L. Z., Höwing, T., Müller, B., Hammes, U. Z., Gietl, C., and Dresselhaus, T. (2016). Expression analysis of KDEL-CysEPs programmed cell death markers during reproduction in *Arabidopsis*. *Plant reproduction*, *29*, 265-272.

Zumajo-Cardona, C., and Ambrose, B. A. (2020). Phylogenetic analyses of key developmental genes provide insight into the complex evolution of seeds. *Molecular phylogenetics and evolution, 147,* 106778.

CHAPTER II

Unravelling the epigenetic mechanisms involved in seed coat development

ABSTRACT

Epigenetic modifications of DNA histones play a crucial role in the regulation of gene expression in plants. Trimethylation of lysine residues on histone 3 (H3K27me3) has been extensively studied in recent years. This epigenetic mark, typically associated with transcriptionally silenced regions, is linked to the activity of Polycomb Repressive Complex 2 (PRC2). These complexes modulate the transition from ovule to seed in *Arabidopsis thaliana*. Specifically, PRC2 controls the transition by preventing central cell proliferation and suppressing autonomous seed coat development in the absence of fertilisation (Derkacheva and Henning, 2014).

In *Arabidopsis*, and in angiosperms in general, the signal that determines the removal of PRC2-mediated gene silencing is attributed to fertilisation, which occurs a few hours after pollination, making it impossible to distinguish between the two events.

Otherwise, in *Ginkgo*, as in other gymnosperms, pollination and fertilisation are separated in time by a few months, and it has been observed that the mere arrival of pollen before fertilisation triggers a series of molecular events that lead to the proper development of the ovule integument (D'Apice *et al*., 2021) and inhibit abortion (Friedman, 1987).

To better understand the molecular mechanism triggered by the pollination event in relation to the epigenetic repression exerted by PRC2 in *Ginkgo biloba*, Chromatin Immunoprecipitation coupled with sequencing (ChIP-seq) was performed on pools of ovules collected during the pollination period (from March to April 2020), by using specific antibody against H3K27me3. Four stages were considered according to D'Apice *et al.* (2021): the pre-pollination stage (Stage 7), the pollination drop emission stage (Stage 8.1), and two post-pollination drop emission stages, occurring 6 and 8 days after the emission of the pollination drop respectively (Stage 8.3 and Stage 8.4).

In particular ChIP-seq results were compared with RNA-seq dataset BioProject ID code PRJNA700482 (D'Apice *et al.*, 2021) to identify the differentially expressed genes modulated by the pollination event and regulated by histone modifications.

Overall, the obtained results suggest that the arrival of pollen into the pollen chamber epigenetically regulates a limited number of pathways essential for the proper development of the ovule, like plant hormone pathway, phenylpropanoids biosynthesis and also some transcription factors (TFs) belonging to MADS-box and AP2 (APETALA2)/EREBP (Ethylene Responsive Element Binding Protein) families.

All the results reported here are part of a larger investigation, carried out mainly by our collaborators at the University of Padua and within the PRIN 2017 project (20175R447S). A manuscript presenting the comprehensive results is in progress. Therefore, I have provided a summary of the analyses performed. The 18 genes discussed here were selected based on their significance in both datasets, RNA-seq and ChIP-seq.

INTRODUCTION

Basic concepts of epigenetics

Epigenetics, derived from the Greek "epi" (upon, above, beyond) and "genetic" (DNA sequence), refers to an additional layer of information beyond that encoded in the DNA sequence. Indeed, epigenetics is the study of heritable changes in gene expression or cellular phenotype that occur without alterations to the underlying DNA sequence (Casadesús and Noyer-Weidner, 2013). Therefore, although the DNA complement is basically identical in all somatic cells of an organism, the expression patterns of genes exhibit considerable variations among distinct cell types and can be clonally inherited (Felsenfeld, 2014). The regulation of gene expression by epigenetics mainly involves DNA methylation, histone modification including methylation, acetylation and ubiquitination of histone N-tails, and post-transcriptional silencing facilitated by small non-coding RNAs (Cyr and Domann, 2011). In the model plant *Arabidopsis*, more than 130 genes are known to be under epigenetic regulation (Brukhin and Albertini, 2021).

In plants, DNA methylation primarily targets 5-cytosine. Methylation occurs in three different contexts: symmetric CH, CHG, and asymmetric CHH, where H represents any nucleotide except G (Lucibelli *et al.*, 2022). In symmetric contexts, CG or CHG repetitive motifs, known as CG islands, are frequently methylated (Gouil and Baulcombe, 2016). Methylation of CG during replication is mediated by methyltransferase 1 (MET1) in a semi-conserved manner, whereas chromomethylase 3 (CMT3) methyltransferase aids in CHG methylation (Brukhin and Albertini, 2021). Asymmetrically methylated CHH sites require *de novo* methylation after each replication cycle, catalysed by domain-rearranged methyltransferase 2 (DRM2), which is involved in RNA-directed DNA methylation (RdDM). In addition, CHH methylation can occur independently of RdDM, facilitated by chromomethylase 2 (CMT2), homologous to CMT3. The enzyme DNA methylation 1 (DDM1) remodels chromatin by eliminating the histone H1 linker in compact heterochromatic regions, allowing access to DNA to methyltransferases. DRM2-mediated methylation predominantly targets euchromatic regions, including short and long transposable elements (TE) and pericentromeric sites (Law and Jacobsen, 2010). Polymerase IV and polymerase V, both plant homologues of polymerase II, play critical roles in the biogenesis of small interfering RNAs (siRNAs) required for RNA-directed DNA methylation (RdDM). Polymerase IV is responsible for the synthesis of single-stranded RNA (ssRNA) at various silencing targets, including retrotransposons, viruses, transgenes and repetitive genes. RNA-dependent RNA polymerase 2 (RDR2) then facilitates the conversion of ssRNA into double-stranded RNA (dsRNA). The dsRNA is then processed by dicer-like 3 (DCL3) into 24- and 23-nucleotide small interfering RNAs (siRNAs). One strand of the siRNA duplex is placed on Argonaute (AGO4). The siRNAs loaded to AGO4 complement the transcripts of polymerase V and engage DRM2, triggering the initiation of *de novo* methylation at genomic sites in all contexts (Matzke and Mosher, 2014; Zhou and Law, 2015).

On the other hand, enzymes involved in DNA demethylation are DNA glycosylase repressor of silencing 1 (ROS1), demeter (DME), demeter-like 2 (DML2), and DML3. Their action mechanism comprises the elimination of methylated cytosine, replaced with a non-methylated cytosine. In all plant reproduction processes and

during ontogenesis, DNA methylation and demethylation represent dynamic mechanisms of genetic control, ensuring proper development (Li *et al*., 2018).

In addition, the regulation of gene expression also encompasses post-translational histones modifications (PTM). Histones are basic proteins abundant in lysine and arginine, which easily bind DNA molecules (Cabej, 2019). Their role is to package DNA strands in the nucleus and to regulate transcription and replication through epigenetic mechanisms. Indeed, chromatin is a complex of DNA packed on proteins, forming chromosomes. Five types of histones were identified: H1, H2A, H2B, H3 and H4 (Kornberg and Lorch, 1999). Each nucleosome, the single unit of the chromatin, contains a central particle, the core, made up of 146 base pairs of supercoiled DNA that wraps around nearly twice a disc-shaped complex formed by two molecules of histones H2A, H2B, H3 and H4 assembled in an octamer. Histone H1 is positioned outside the core and represents the connecting histone to the next nucleosome (Kornberg and Lorch, 1999). Chromatin remodelling comprises an alteration of its structure, due primarily to histone modifications, which alter the accessibility of DNA to TFs and polymerases, controlling in this way the gene expression and participating in the phenotypic variability (Brukhin and Albertini, 2021).

Similar to DNA methylation, chromatin remodelling is closely linked to plant development and reproduction. However, the main epigenetic marks of interest are the methylation of specific lysines of histone H3. Indeed, histone acetylation (Tekel and Haynes, 2017) and trimethylation at lysine 3 and 4 of histone H3 (indicated as H3K4me3 and H3K3me3, respectively) determines an accessible state of chromatin, defined as "active", which enables gene expression. Conversely, dimethylation at lysine 9 and trimethylation at lysine 27 (indicated as H3K9me2 and H3K27me3, respectively) induce gene silencing due to a repressive state of chromatin, which inhibits the transcriptional activity of genes (Brukhin and Albertini, 2021).

These processes often recruit the activity of PRC2, which suppresses specific target genes through the application of H3K27me3 (Kradolfer *et al.*, 2013). PRC2 is evolutionarily conserved and governs several developmental and reproductive processes and the early stage of seed development in plants (Brukhin and Albertini, 2021).

Changes in histone modifications after fertilisation

Differentially methylated regions (DMRs) are more present in the paternal respect to the maternal genome (Zhang *et al.*, 2014). This is related to a phenomenon known as imprinting, which determines, based on parental gene expression, the presence of DMRs (Gehring *et al.*, 2009; Rodrigues *et al.*, 2013; Zhang *et al.*, 2014). Genomic imprinting leads to differentially expression of genetically identical alleles after fertilisation. In flowering plants, genomic imprinting is primarily observed in the endosperm (Jahnke and Scholten, 2009; Luo *et al.*, 2011; Nodine and Bartel, 2012; Pignatta *et al.*, 2014). The link between paternally-expressed imprinted genes (PEGs) and DMRs suggests that the maternally hypomethylated regions are also involved in the repression of neighboring genes (Hsieh *et al.*, 2011; Rodrigues *et al.*, 2013; Zhang *et al.*, 2014). Interestingly, PRC2 targets DMRs in proximity of the silenced maternal alleles of PEGs (Zhang *et al.*, 2014; Moreno-Romero *et al.*, 2016). It has been observed that in *Arabidopsis* and *Zea mays* H3K27me3 is applied also at hypomethylated regions in the maternal genome, inducing the imprinted expression of PEGs (Makarevitch *et al.*, 2013; Zhang *et al.*, 2014). PRC2 activity and DNA methylation are usually considered to be mutually exclusive (Weinhofer *et al.*, 2010; Deleris *et al.*, 2012; Reddington *et al.*, 2013). However, in *Arabidopsis* endosperm, the presence of H3K27me3 has been frequently observed in highly methylated pericentromeric DNA regions. This observation suggests that the two phenomena are not always mutually exclusive (Moreno-Romero *et al.*, 2016).

More in details, paternal pericentromeric regions seem to be the main target of H3K27me3 compared to maternal ones. Conversely, heterochromatic marks like H3K9me2 and H3K27me1 are more present in maternal pericentromeric regions respect to paternal ones (Moreno-Romero *et al.*, 2016). In addition, maternal and paternal chromatin have two different histone H3 variants during the first nuclei divisions in early *Arabidopsis* endosperm, due to replication-coupled exchange of paternal histone from H3.1 to H3.3 (Ingouff *et al.*, 2007). The inability of the histone variant H3.3 to be targeted by enzymatic mechanisms via H3K27me1 could explain the delay in the formation of heterochromatin in the paternal endosperm genome (Jacob *et al.*, 2014). However, immediately after fertilisation, in zygote nucleus are

removed maternal and paternal H3 variants, deleting all the histone-mediated parental-specific information (Ingouff *et al.*, 2010).

PRC2 are widely studied in numerous taxa, as they are responsible for cell differentiation during developmental processes. In plants, they have been firstly characterized in *Arabidopsis*, based on the homology with Su(z)12 in the *Drosophyla* complexes (Bemer and Grossniklaus, 2012). More in details, have been characterised three different PRC2, including EMF-PRC2, VRN-PRC2, and FIS-PRC2 complexes, which act in several stages of plant development. The first two mainly act in sporophytic generation, the latter one in gametophytic generation (Derkacheva and Henning, 2014). Concerning seed development, EMF and VRN-PRC2 act in seed coat formation, repressing genes involved in seed coat development before fertilisation, whereas FIS-PRC2 is crucial to initiate endosperm development (Figueiredo *et al.* 2016). In *Arabidopsis*, FIS-PRC2 is formed by FERTILISATION INDEPENDENT SEED2 (FIS2), FERTILISATION INDEPENDENT ENDOSPERM (FIE), MEDEA (MEA), and MULTICOPY SUPPRESSOR OF IRA1 (MSI1) (Mozgova and Hennig, 2015). H3K27me FIS-PRC2-mediated on maternal PEG alleles is necessary for imprinted expression. Indeed, the lack of FIS-PRC2 function results in a failure of repression of the maternal alleles of PEGs (Hsieh *et al.*, 2011; Wolff *et al.*, 2011). Interestingly, in the endosperm *MEA* and *FIS2* gene are entirely maternally expressed (Rodrigues and Zilberman, 2015), while *msi1* mutants produces seeds with a high lethality rate, highlighting the need for FIS-PRC2 activity in the female gametophyte (FG) to allow proper seed development after fertilisation (Leroy *et al.*, 2007). Orthologs of *FIS2* and *MEA* have not been found in any plants other than Brassicaceae (Luo *et al.*, 2009). However, in rice and maize, the PRC2 that acts in the endosperm has been characterised and shows homology with the proteins belonging to the sporophytic PRC2 of *Arabidopsis* (Tonosaki and Kinoshita, 2015). Maternally expressed PRC2 genes are also found in the endosperm of rice and maize, suggesting that independent evolution of imprinted expression of PRC2 has occurred in monocots and dicots (Danilevskaya *et al.*, 2003; Luo *et al.*, 2009).

Genes target of PRC2 before and after fertilisation

It has been observed that in *Arabidopsis*, FIS-PRC2 induces the repression of genes involved in auxin biosynthesis before fertilisation occurs, such as *YUCCA* and *TRYPTOPHAN AMINOTRANSFERASE*, in the central cell. Contextually, EMF and VRN-PRC2 inhibits the expression of genes strongly related in seed coat differentiation, involved in gibberellin and in phenylpropanoids biosynthesis, such as *TRANSPARENT TESTA* (also known as *DIHYDROFLAVONOL 4-REDUCTASE*) (Figueiredo and Köhler, 2018). Fertilisation triggers the removal of this repression and shifts PRC2 activity to other target genes, such as *MADS-box* (Zhang *et al*., 2018), whose activity is required during the ovule. Indeed, many TFs, belonging to MADS-box family and AP2/EREBP are involved in the ovule, which represent the structure in which sexual reproduction occurs in spermatophytes (Favaro *et al*., 2003; Shigyo *et al*., 2006; Guo and Zheng, 2013). Indeed, in *Arabidopsis* has been identified different MADS-box genes, including *SEEDSTICK* (*STK*), *AGAMOUS* (*AG*), *SHATTERPROOF1* (*SHP1*) and *SHP2*, which control ovule development (Yadegari and Drews, 2004). *AINTEGUMENTA* (*ANT*), an *APETALA2*-like gene of *Arabidopsis* is also required for integuments initiation from the chalaza (Cucinotta *et al.*, 2020).

In angiosperms, the molecular signalling that determines PRC2 activity is attributed to the fertilisation event, since fertilisation and pollination are often very close in time (in *Arabidopsis* around 12 hours). On the other hand, in gymnosperms such as *Ginkgo*, where the two events are separated by a long time interval (i.e. four/five months), it is interesting to study whether the triggering event is pollination or fertilisation. Given *Ginkgo*'s phylogenetic position of singular interest, it is important to investigate whether PRC2's mechanism of action, involving H3K27me3, is conserved.

Here, for the first time, this aspect was addressed and some of the PRC2 target genes, closely linked to the ovule-to-seed switch, were identified.

MATERIAL AND METHODS

Plant material

Pools of ovules were collected in the pollination period (March and April 2020), from 10 female plants at the Botanical Garden of the University of Calabria, Rende (CS), Italy (39° 17′ 43″ N, 16° 15′ 13″ E). Four stages were considered, as described in D'Apice *et al.* (2021): stage 7 (the pre-pollination stage); stage 8.1 (the pollination drop emission stage); and stages 8.3 and 8.4 (post-pollination drop stages respectively 6 and 8 days after the emission of the pollination drop).

For RNA extraction, thirty ovules for each stage analysed were collected, immediately frozen in liquid nitrogen and stored at -80 °C until use.

Chromatin Immunoprecipitation (ChIP)

At least of fifty ovules for each stage analysed were collected and immediately subjected to cross-linking, to make a "bridge" between DNA and histones. In particular, samples were fixed in 1% formaldehyde for 10 minutes and then rinsed in 0.125 M glycine for 5 minutes under vacuum infiltrations at room temperature. Ovules were washed in cold sterile water, frozen in liquid nitrogen and stored at -80 °C until use.

ChIP experiments were performed according to Bowler *et al*. (2004) protocol, with some modifications. A total of 2 g of ground ovules for each stage were used and nuclei were isolated and lysed in the presence of protease inhibitors. The isolated chromatin underwent sonication 18 times for 30 seconds using a SONICS Vibra-cell sonicator. For immunoprecipitation, a specific antibody against H3K27me3 (ref. C15410069-50UG) from Diagenode was employed. Immunoprecipitated DNA was purified using the MINelute PCR Product Purification Kit (Qiagen) following the manufacturer's protocol and supplemented with RNase A.

The DNA integrity was checked on 1% agarose gel, while DNA concentration of each sample was evaluated by Invitrogen Qubit 3.0 Fluorometer (Thermo Fisher Scientific, USA).

DNA sequencing and bioinformatic analysis

Libraries were sequenced on the NextSeq 500 (Illumina, San Diego, CA) platform by IGA Technology Services in Udine (Italy). Up to ~65 reads million sequencing reads were generated for each replicate representing >30-fold coverage of the *Ginkgo* genome. For each time point two biological replicates were used.

Biofiormatic analyses were conducted by Professor Ernesto Picardi (University of Bari Aldo Moro). Reads were mapped to the *Ginkgo* genome (version released on 04 June 2019, downloaded from http://gigadb.org/dataset/100613) using Bowtie2. To assess differential H3K27me3 levels, a comparison of read abundances on the epic2 lists of peaks was performed using MAnorm (MA) according the pipeline described in Payá-Milans *et al.* (2019). The threshold for Differentially Methylated Genes (DMGs) was set to a fold-change of 0.5 (indicated as M value) and a P- value adjusted ≤ 0.05.

RNA-seq dataset

For the transcriptomic analysis were used raw reads deposited with the BioProject ID code PRJNA700482 (D'Apice *et al.*, 2021). Differentially Expressed Genes (DEGs) were then calculated by DESeq2 package in R. The threshold for DEGs was set to a fold-change of 0.5 and a P- value adjusted ≤ 0.05.

The overlap between ChIP-seq dataset (DMGs list) and RNA-seq dataset (DEGs list) was performed to identify genes modulated during ovule development and regulated through epigenetic mechanisms.

RNA isolation and quantitative Real Time-PCR (RT-qPCR)

Ovules of *Ginkgo* collected at different developmental stages were used to isolate total RNA using Agilent Total RNA Isolation Mini Kit (Agilent Technologies, Santa Clara, CA, USA) according to manufacturer's protocol. cDNA was obtained retrotranscribing 3 µg of RNA by SuperScript III Reverse Transcriptase (Invitrogen, Milan, Italy). RT-qPCR was performed according to D'Apice *et al.* (2021). The specific primers were listed in **Table 1**. As normalization control, the housekeeping

gene *EF2* (*Gb_02896*) was used (D'Apice *et al*., 2021). The results were analysed using the $2^{-\Delta Ct}$ method. Mean values (± standard error) reported were the result of three independent biological replicates. Statistical analyses were performed, first testing the homogeneity (Leven Median test), and then analysed by ANOVA and Tukey's rank test ($P < 0.05$).

Table 1. Primers used in RT-qPCR for libraries results validation.

RT-qPCR primers			
GENE	**ID**	**Type of primer**	**SEQUENCE 5'-3'**
EF2	*Gb_02896*	forward	TCCATCTTCCTTCTCCATCC (D'Apice *et al*., 2021)
EF2	*Gb_02896*	reverse	CTTACCTTCATACCTGTTGCC (D'Apice *et al*., 2021)
PIN1	*Gb_06199*	forward	GCACGTCATGACCAAGCATA
PIN1	*Gb_06199*	reverse	GCCCTTCTTTGTCCAGTGGA
ANT	*Gb_07049*	forward	TCTCTCGTCACTACAGCCAC
ANT	*Gb_07049*	reverse	GAGAGATTGGGCCTTGCATG
DFR	*Gb_26470*	forward	ACATCATCTGCCGGAACTGT
DFR	*Gb_26470*	reverse	CCGCCTGTTCTGCTAATGTC
ANR	*Gb_10030*	forward	AAATCTGTGCAGGGCCGATA
ANR	*Gb_10030*	reverse	CTTCCATGCCGCACTGAAAT

RESULTS

Identification of differentially expressed and trimethylated genes during ovule development following the pollination event in Ginkgo biloba

As a first approach, as mentioned above, we used RNA-seq dataset obtained from *Ginkgo* ovules at different stages of development through to the pollination period. Globally, were found 4838 DEGs (**Figure 1A**). In detail, in the first comparison (stage 8.1/stage 7) were identified 2911 DEGs (2530 upregulated, 381 downregulated), in the second comparison (stage 8.3/stage 8.1) 1092 (57 upregulated, 1034 downregulated) and in the last comparison 1473 (205 upregulated, 1268

downregulated), highlighting the gradual increase of downregulated genes among the stages, probably triggered by pollination event (**Figure 1A**).

In parallel, to identify genes marked by H3K27me3 throughout the pollination event, chromatin immunoprecipitation followed by sequencing (ChIP-seq) was performed on ovules collected at the same stages: pre-pollination stage (stage 7), at the pollination drop sub-stage (stage 8.1) and at two post-pollination drop sub-stages (stages 8.3 and 8.4), according to D'Apice *et al*. (2021). A total of 4307 DMGs was identified among the adjacent stages (**Figure 1B**). In particular, in the first comparison (stage 8.1/stage 7) were found 1724 DMGs (634 hypertrimethylated, 1090 ipotrimethylated), in the second comparison (stage 8.3/stage 8.1) 2027 (448 hypertrimethylated, 1579 ipotrimethylated) and in the last comparison 2724 (2225 hypertrimethylated, 499 ipotrimethylated) (**Figure 1B**). In general, we observed an increase in hyper-trimethylation of gene loci, associated with an increase in the fraction of downregulated genes in the ovules at post-pollination stages. In order to identify among the DEGs those targeted by H3K27me3, we then performed an overlap between the two datasets. This revealed only 547 genes in common between DEGs and DMGs datasets (**Figure 1C**).

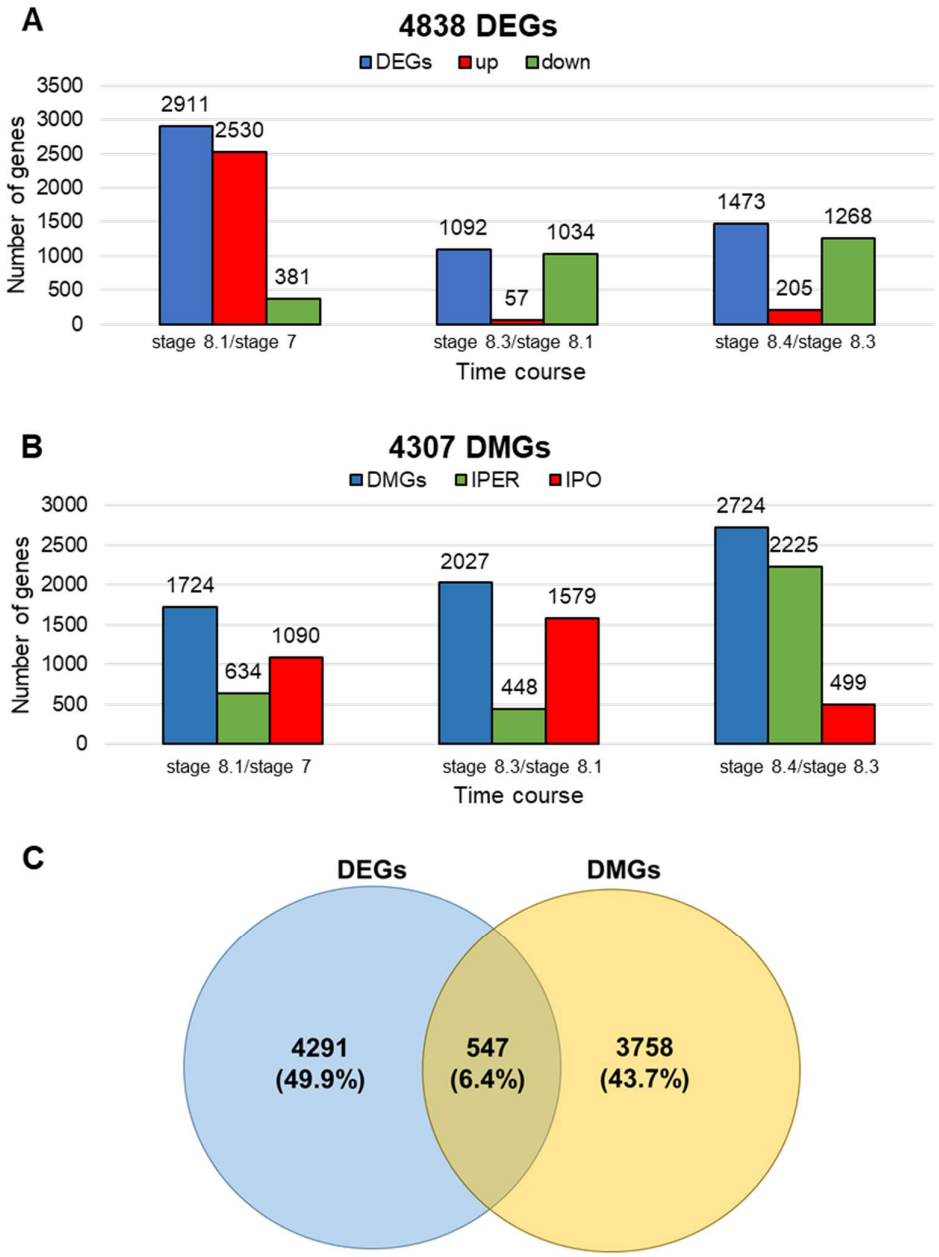

Figure 1. RNA-seq and ChIP-seq profiles. **(A)** Differentially expressed genes (DEGs) considering the comparison between adjacent time points (stage 8.1/stage 7, stage 8.3/stage 8.1, stage 8.4/stage 8.3, respectively). Gene expression level values were normalised by the DESEQ2 software (pvalue corrected < 0.05 and log2FC |0.5|). **(B)** Differentially trimethylated genes (DMGs) considering the comparison between adjacent time points (stage 8.1/stage 7, stage 8.3/stage 8.1, stage 8.4/stage 8.3, respectively). Trimethylation level values were evaluated by MA plot methods to normalize read density levels on provided peaks and calculate P-values (pvalue corrected < 0.05 and log2FC |0.5|). **(C)** Venn diagrams describing an overlapping of DEGs and DMGs sets.

Plant hormone pathway is regulated by epigenetic mechanisms during ovule development in Ginkgo biloba

Based on the comparison between the two datasets (RNA-seq and ChIP-seq), the most significant pathway observed was the hormonal pathway.

It's well known that hormones play a key role in all developmental processes, including ovule and seed formation (Barro-Trastoy *et al.*, 2020). For this reason, we firstly focused our attention on this specific pathway.

Indeed, 108 DEGs were involved in biosynthesis, transport and signalling of six different phytohormones (**Figure 2A**). Most of DEGs belonged to ethylene (34) and auxin (23) metabolism, followed by brassinosteroids (18) and cytokinins (17) (**Figure 2A**). All DEGs involved in the metabolism of the different hormones showed a global upregulation, except for ethylene, for which several genes were downregulated.

Among these genes, were found 28 DMGs (25.9% of total), almost half of which are involved in the ethylene pathway (13) (**Figure 2B**).

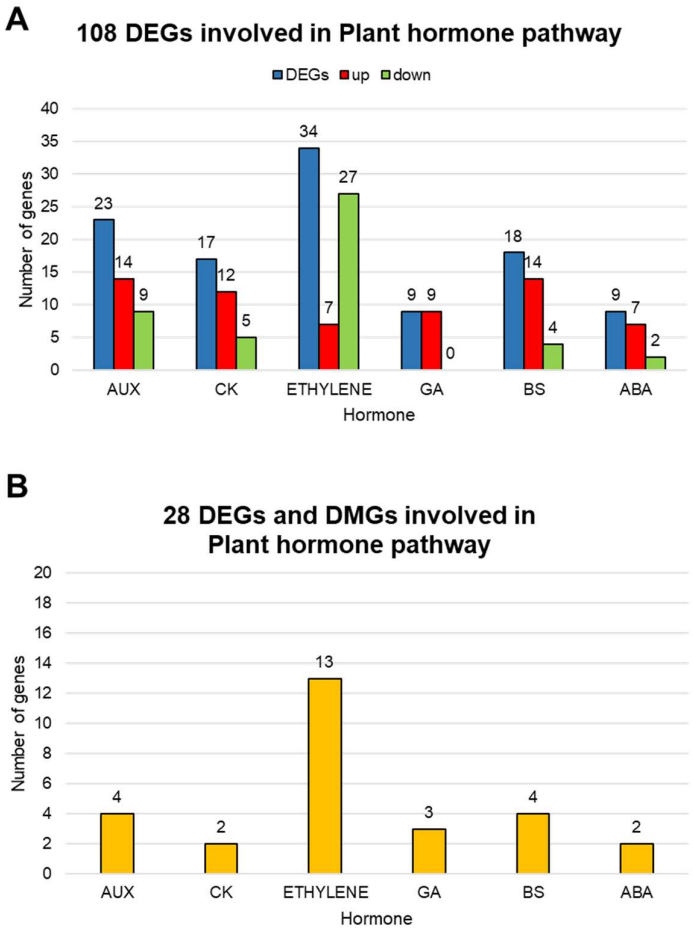

Figure 2. RNA-seq and ChIP-seq analysis related to genes belonging to plant hormone pathway **(A)** Differentially expressed genes (DEGs) considering the comparison between adjacent time points (stage 8.1/stage 7, stage 8.3/stage 8.1, stage 8.4/stage 8.3, respectively) involved in plant hormone pathway. Gene expression level values were normalised by the DESEQ2 software (pvalue corrected < 0.05 and log2FC |0.5|). **(B)** Differentially trimethylated genes (DMGs) and DEGs considering the comparison between adjacent time points (stage 8.1/stage 7, stage 8.3/stage 8.1, stage 8.4/stage 8.3, respectively) involved in plant hormone pathway.

Later, we focused our attention exclusively on genes that showed an anticorrelation between the Fold Change and MA values (hypertrimethylation - downregulation; hypotrimethylation - upregulation), as reported in **Table 2**.

Among the 8 genes analysed, 6 genes at the last comparison (stage 8.4/stage 8.3) showed an hypertrimethylation and downregulation. Only 2 genes (*GbGH3* and *GbGA3ox*) showed hypotrimethylation and upregulation in the first comparison (stage 8.1/stage 7). In addition, almost all of the genes are involved in hormone signal

transduction, with the exception of *GbPIN1* and *GbGA3ox*, which are involved in polar auxin transport and gibberellin biosynthesis, respectively.

This result suggests that the pollination may induce a general silencing of the hormone signalling in the days immediately following this event.

Table 2. Genes differentially expressed (DEGs) and differentially trimethylated (DMGs) along the hormone pathway. For each comparison (stage 8.1/stage 7; stage 8.3/stage 8.1; stage 8.4/stage 8.3), the log2FoldChange and M value were used to assign the colour: green indicates hypertrimetilation accompanied by downregulation, orange indicates hypotrimethylation accompanied by upregulation.

Hormone	**Comparisons**			**Function (source: UNIPROT, https://www.uniprot.org)**
	Stage 8.1/ Stage 7	**Stage 8.3/ Stage 8.1**	**Stage 8.4/ Stage 8.3**	
Auxins			*PIN1 (Gb_06199)*	Acts as a component of the auxin efflux carrier.
	GH3 (Gb_36596)			Catalyzes the synthesis of indole-3-acetic acid (IAA)-amino acid conjugates, providing a mechanism for the plant to cope with the presence of excess auxin.
Cytokinins			*LOG (Gb_32702)*	Cytokinin-activating enzyme working in the direct activation pathway.
			AHP (Gb_35949)	Functions as two-component phosphorelay mediators between cytokinin sensor histidine kinases and response regulators (B-type ARRs). Plays an important role in propagating cytokinin signal transduction through the multistep His-to-Asp phosphorelay.
Gibberellins	*GA3ox (Gb_34640)*			Converts the inactive gibberellin (GA) precursors in the bioactives gibberellins. Involved in the production of bioactive GA for vegetative growth and development, but not for the 3-beta-hydroxylation of GA in developing seeds.
Abscissic Acid			*PYL (Gb_39601)*	Receptor for abscisic acid (ABA) required for ABA-mediated responses such as stomatal closure and germination inhibition.

Ethylene			*ERF (Gb_12965)*	Probably acts as a transcriptional activator. Binds to the GCC-box pathogenesis-related promoter element. May be involved in the regulation of gene expression by stress factors and by components of stress signal transduction pathways (By similarity).
			CTR1 (Gb_05762)	Negative regulator in the ethylene response pathway.

Histograms showing the specific correlation between FC and M value for each gene are presented in **Figure 3**.

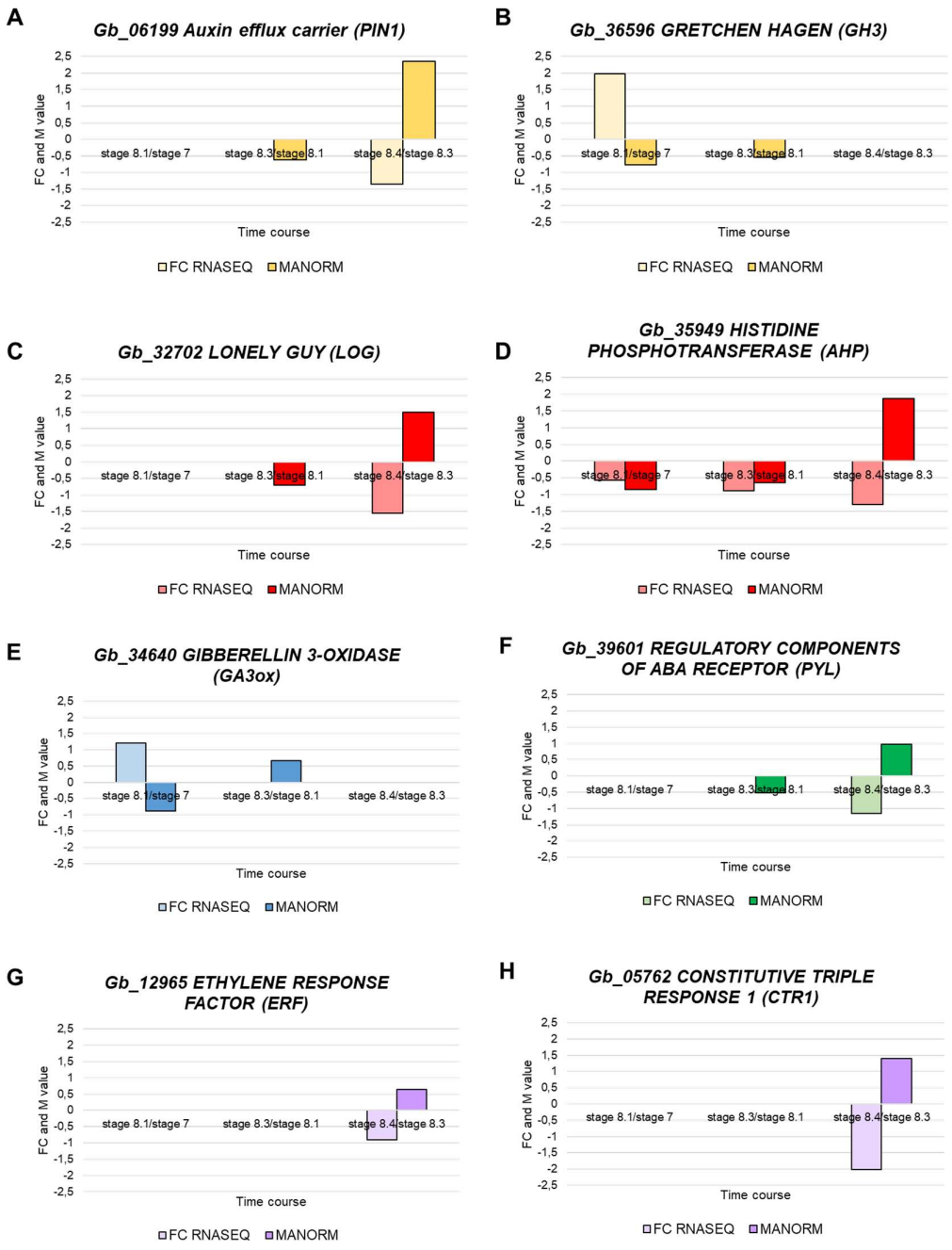

Figure 3. Anticorrelation between trimethylation and gene expression in plant hormone pathway. The graph shows the FC (RNA-seq) and MAnorm value (ChIP-seq) (pvalue corrected < 0.05 and log2FC |0.5|) of selected genes involved in **(A-B)** auxin (yellow), **(C-D)** cytokinins (red), **(E)** gibberellin (blue), **(F)** abscissic acid (green), **(G-H)** ethylene metabolism (violet). Light colours indicate FC, dark colours indicate MA value.

Key genes involved in ovule/seed development are modulated and marked by H3K27me3 after pollination event

In *Arabidopsis* is well characterized the role of several genes involved in all the processes which underlie the ovule and seed development. Among these, genes encoding TFs of the MADS-box family are essential for ovule development, but their activity is not required after fertilisation (Zhang *et al*., 2018). Conversely, phenylpropanoids biosynthesis is required after fertilisation because seed coat formation necessitates strong flavonoid deposition (Lepiniec *et al*., 2006).

We therefore focused our attention on them, and among the TFs, we looked at genes encoding the MADS-box and members of the AP2/EREBP family, among which we found *ANT*, already known for its role in ovule development in *Arabidopsis* (Losa *et al*., 2010).

All these retrieved genes are listed in **Table 3**. More specifically, of the 10 genes analysed, 1 showed hypotrimethylation and upregulation in the first comparison (stage 8.1/stage 7), and another 1 in the second (stage 8.3/stage 8.1). The majority of genes (8) displayed hypertrimethylation and downregulation. In particular, only 1 of them was hypertrimethylated and downregulated in the second comparison (stage 8.3/stage 8.1) and 7 in the last comparison (stage 8.4/stage 8.3).

Concerning TFs, we investigated genes encoding MADS-box and members of AP2/EREBP family, among which we found *ANT*, already known for its role in ovule development in *Arabidopsis* (Losa *et al*., 2010). All these genes showed hypertrimethylation and downregulation in the last comparison (stage 8.4/stage 8.3). Genes encoding enzymes involved in phenylpropanoid biosynthesis also showed a general downregulation in the last comparison (stage 8.4/stage 8.3).

Table 3. Genes differentially expressed (DEGs) and differentially trimethylated (DMGs) encoding transcription factors and enzyme involved in phenylpropanoids biosynthesis. For each comparison (stage 8.1/stage 7; stage 8.3/stage 8.1; stage 8.4/stage 8.3), the log2FoldChange and M value were used to assign the colour: green indicates hypertrimetilation accompanied by downregulation, orange indicates hypotrimethylation accompanied by upregulation.

Pathway	Comparisons			Function (source: UNIPROT, https://www.uniprot.org)
	Stage 8.1/ Stage 7	Stage 8.3/ Stage 8.1	Stage 8.4/ Stage 8.3	
Transcription Factors			*ANT (Gb_07049)*	Probably acts as a transcriptional activator. Binds to the GCC-box pathogenesis-related promoter element. May be involved in the regulation of gene expression by stress factors and by components of stress signal transduction pathways (By similarity).
			AGL6 (Gb_41549)	Probable transcription factor involved in flower development.
			MADS-box 22 (Gb_05128)	Probable transcription factor required for flowe development.
			MADS-box 6 (Gb_39109)	Probable transcription factor. Regulates floral organ identity and floral meristem determinacy. May be involved in the control of flowering time.
Phenylpropanoids biosynthesis		*PAL (Gb_16672)*		This is a key enzyme of plant metabolism catalyzing the first reaction in the biosynthesis from L-phenylalanine of a wide variety of natural products based on the phenylpropane skeleton.
			DFR (Gb_26470)	Bifunctional enzyme involved in flavonoid metabolism.
	ANR (Gb_22280)			Secondary metabolite biosynthesis; flavonoid biosynthesis.

		FLS (Gb_14024)		Catalyzes the formation of flavonols from dihydroflavonols. It can act on dihydrokaempferol to produce kaempferol, on dihydroquercetin to produce quercitin and on dihydromyricetin to produce myricetin (By similarity).
			UGT (Gb_30234)	Iridoid glucosyltransferase acting exclusively on 7-deoxyloganetin. No activity with 7-deoxyloganetic acid.
			UGT (Gb_09277)	

Histograms showing the specific correlation between FC and M value for each gene are presented below. In particular, genes encoding TFs are listed in **Figure 4**, and genes related to phenylpropanoid biosynthesis in **Figure 5**.

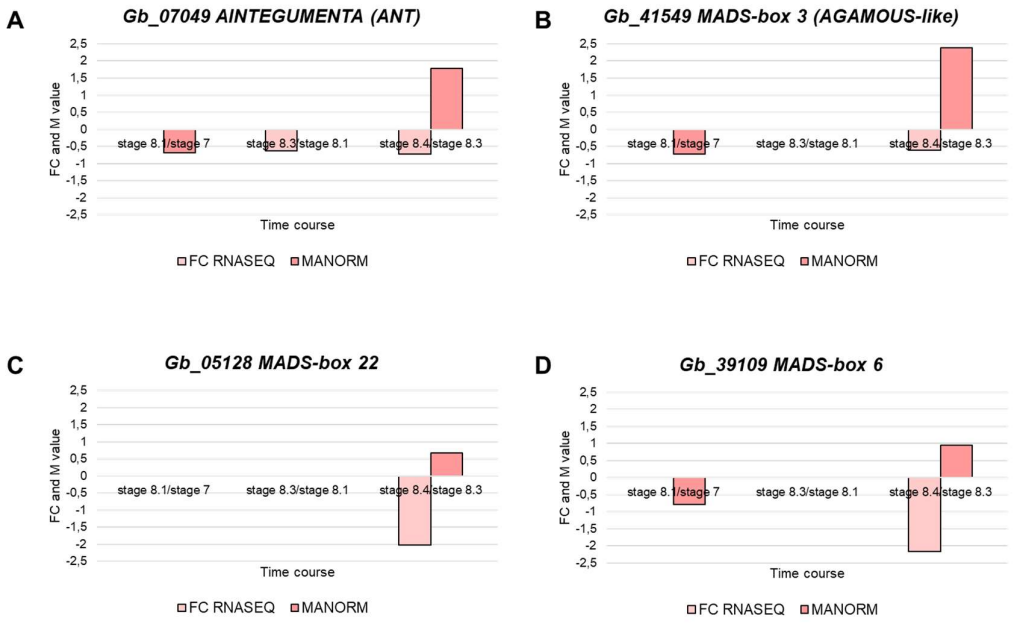

Figure 4. Anticorrelation between trimethylation and gene expression in plant hormone pathway. The graph shows the FC (RNA-seq) and MAnorm value (ChIP-seq) (pvalue corrected < 0.05 and log2FC |0.5|) of selected genes involved in ovule development, encoding genes belonging to **(A)** AP2/EREBP and **(B-D)** MADS-box families. Light colour indicates FC, dark colour indicates MA value.

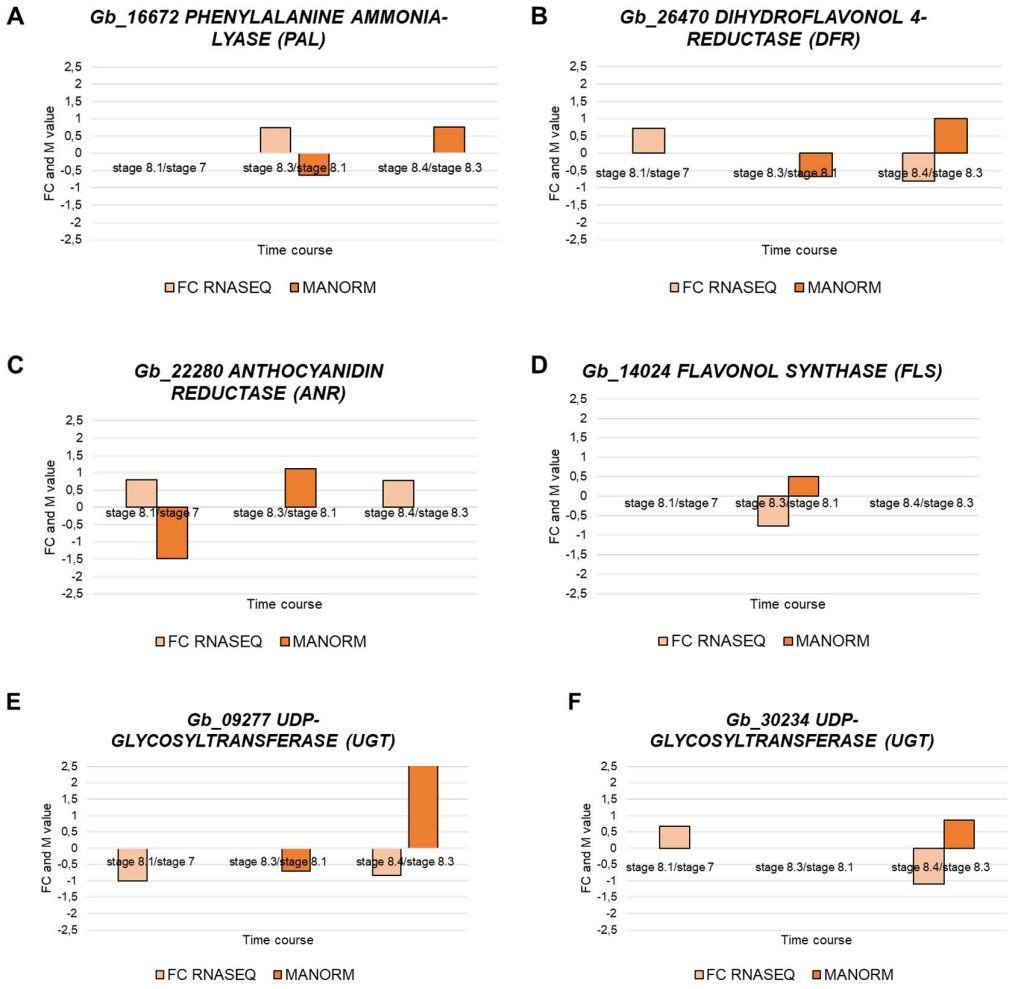

Figure 5. Anticorrelation between trimethylation and gene expression in plant hormone pathway. The graph shows the FC (RNA-seq) and MAnorm value (ChIP-seq) (pvalue corrected < 0.05 and log2FC |0.5|) of selected genes involved in phenylpropanoids biosynthesis **(A-F)**. Light colour indicates FC, dark colour indicates MA value.

Finally, RT-qPCR analyses, performed on selected genes, validated the reliability of the RNA-Seq analysis (**Figure 6**).

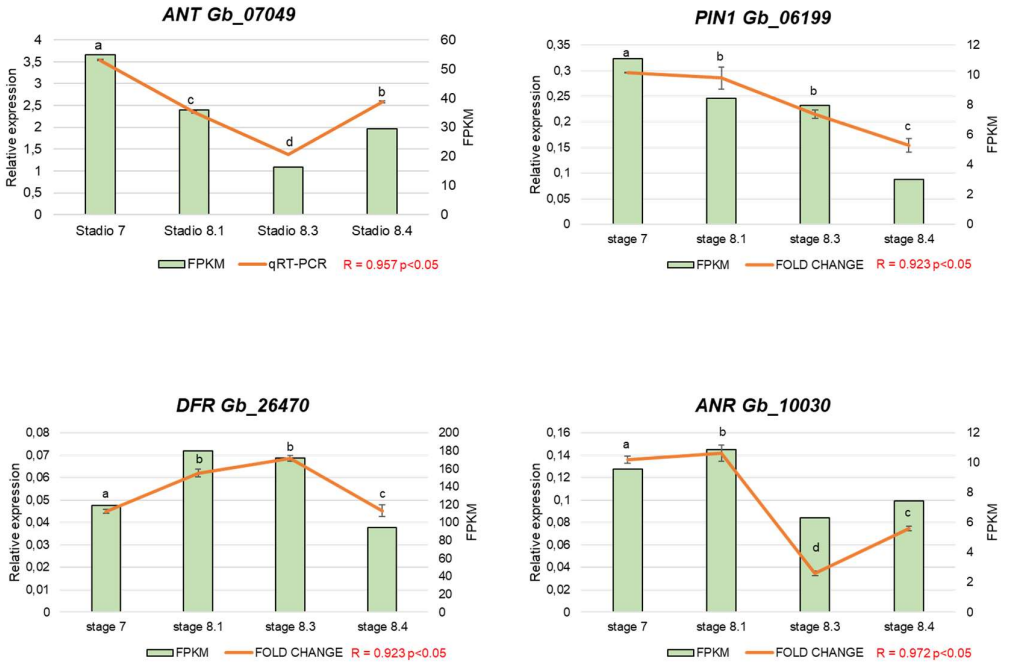

Figure 6. Relative expression by RT-qPCR of selected genes in primary ovules at different developmental stages of *Ginkgo biloba.* The expression level ($2^{\wedge-\Delta Ct}$) was reported in orange in the left y-axis and the FPKM value in the right y-axis; the x-axis indicates the developmental stages. Data present the mean ± SE of three independent experiments. Statistical analyses were performed on by ANOVA and a Tukey's rank test ($P < 0.05$) on ΔCt values. Letters on graphs indicate significant differences. As RNA-sequencing (FPKM) and RT-qPCR produce relative gene expression measures, to evaluate concordance in gene expression, Pearson correlation coefficient calculation was used for each pair of gene selected.

DISCUSSION

The involvement of PcG proteins in H3K27me3-mediated gene silencing has been implicated in several developmental processes in *Arabidopsis*, including leaf differentiation and the cessation of *WUSCHEL* (*WUS*) expression during floral meristem arrest (Lafos *et al.*, 2011; Liu *et al.*, 2011; Sun *et al.*, 2019). It was also demonstrated in *Arabidopsis* that PRC2 is involved in the epigenetic regulation of key flowering time genes such as *FLOWERING LOCUS C* (*FLC*), controlling the plant transitions phase (vegetative to the reproductive) (Derkacheva and Hennig, 2014). Instead, genes involved in seed coat differentiation are silenced before fertilisation by PcG proteins, which operate in maternal tissues surrounding the FG, the ovule

integuments (Roszak and Köhler, 2011). Indeed, although ovule integuments don't participate to double fertilisation, the transformation into seed coat starts immediately after it, highlighting the control that gametophyte exerts on the maternal tissues (Roszak and Köhler, 2011). In this context, the fertilisation represents the key event which determines the switch of the PRC2 activity. As a result, some previously silenced genes are freed from H3K27me3, allowing them to be expressed; other previously expressed genes are marked and silenced because their activity is no longer required (Roszak and Köhler, 2011; Derkacheva and Hennig, 2014; Figueiredo *et al*., 2016).

However, the extent to which H3K27me3 levels contribute to gene silencing during ovule development remains largely unexplored in gymnosperms, in which pollination and fertilisation are separated by a long interval. In this study, we aimed to characterise the pathways controlled by epigenetic mechanisms dependent on pollen arrival, using pre-pollination and post-pollination stages. In this context, we focused our attention on the activity of PRC2, whose mechanism of action is represented by H3K27me3 (Derkacheva and Henning, 2014).

In general, epigenetics can modulate gene expression, activating or inhibiting specific mechanisms based on developmental stage or external stimuli (Lin *et al.*, 2005). One of the most extensively studied epigenetic-type regulations is that mediated by PRC2. Indeed, H3K27me3 is integral to the epigenetic regulation of tissue-specific expression patterns in multicellular eukaryotes, including plants. It acts to silence direct targets while indirectly promoting gene expression by repressing miRNA genes (Lafos *et al*., 2011; Shivram *et al*., 2019). While there are indications that PcG proteins may indirectly activate their own expression during seed development, but the molecular mechanism is not full elucidate (Baroux *et al.*, 2006).

It has been observed in *Arabidopsis* that proteins belonging to the PRC2 induce the repression of genes involved in the development of seed integuments prior to fertilisation (Derkacheva and Hennig, 2014). Since in *Arabidopsis* the events of pollination and fertilisation are so close in time that they are difficult to distinguish, it is traditionally attributed to fertilisation the signalling determinant for the removal of PRC2-induced gene silencing on genes specifically involved in seed coat development (Figueiredo *et al*., 2016).

Here, we investigated if similar mechanisms can be induced after only pollination event in an ancient gymnosperm, by exploiting the long interval between pollination and fertilisation in *Ginkgo* (i.e. four/five months). ChIP-seq approach, with specific antibody against H3K27me3, which represents the characteristic mechanism of action of PRC2, was used to evaluate the level of trimethylation on specific genes. methylation peaks were analysed by according the pipeline described in Payá-Milans *et al.* (2019). The analysis allowed us to assign a MA value, to each target gene with H3K27me3 marks, which can be understood as the equivalent of the FC used in conventional transcriptomic analyses. This permitted us not only to attribute a binary characteristic of presence/absence of the trimethylation peak at the selected stages, but also to quantify trimethylation levels between adjacent stages, distinguishing genes as hypo- or hypertrimethylated.

Subsequently, we performed and overlap between RNA-seq (retrieved by D'Apice *et al.*, 2021) and ChIP-seq datasets performed at the same developmental stages (stage 7, the pre-pollination stage; stage 8.1, the pollination drop emission stage; and stages 8.3 and 8.4, post-pollination drop stages respectively 6 and 8 days after the emission of the pollination drop; according to D'Apice *et al.*, 2021). This overlap showed 547 common genes. Given the large number of results, pathways and genes known to be involved in the ovule-to-seed switch were specifically investigated.

Among these, several genes involved in hormone metabolism were investigated, given the key role of plant hormones in the ovule-to-seed switch. It's known from literature that before fertilisation, PRC2 inhibits the expression of target genes in specific tissues. Indeed, in the central cell, it represses the expression of genes involved in auxin biosynthesis, whereas in the ovule integuments represses genes encoding enzymes involved in gibberellin and flavonoids biosynthesis (Figueiredo and Köhler 2018). The fertilisation of the egg cell and central cell induces in the early endosperm the biosynthesis of auxin under control of paternally expressed imprinted genes. The auxin synthesised here migrates into the maternal sporophytic tissues (the integuments), where it acts as a signal molecule for the removal of PRC2, allowing the expression of genes involved in gibberellin biosynthesis and seed coat differentiation (such as *TRANSPARENT TESTA*, involved in flavonoids biosynthesis), until that moment silenced (Figueiredo and Köhler 2018).

Here, we found two genes involved in auxin metabolism that are targets of PRC2: *GbPIN1* and *GbGH3*. The first was down-regulated during the developmental stages, and silenced via H3K27me3 after the pollination event (comparison stage 8.4/stage 8.3). The second showed strong up-regulation in the earliest stages (comparison stage 8.1/stage 7) and was subsequently switched off. Taken together, these results suggest that around a week (stage 8.4) after the pollination, there is less activity in auxin metabolism This developmental stage is crucial, because, as described in Chapter III, the pollination drop secreted by the sporophytic tissue of the nucellus, has the task to capture pollen grain transported by wind. Drying and retracting drags it into the pollen chamber, where it can germinate after about a week (Friedman, 1987). Almost all of the results will be discussed in this thesis present the main changes in this specific stage, suggesting the determinant role of male gametophyte germination.

In addition, it's known that in *Arabidospsis* PIN1 activity is required in early stages of ovule development (Ceccato *et al.*, 2013). In particular, *pin1* mutants show arrest of gametogenesis and embryo sacs with only one or two nuclei (Ceccato *et al.*, 2013). After fertilisation, PIN proteins mainly act to establish the polarity of the embryo (Prasad and Dhonukshe, 2013). Although it is not clear what role PRC2 plays in silencing *PIN* genes in reproductive organs, it has been observed that EMF2-PRC2 inhibits lateral root formation by applying H3K27me3 to *PIN1*, thereby repressing the accumulation of auxin maxima (Gu *et al*., 2014).

Consistent with this finding, the lack of expression in later stages of *GH3*, which is known to be involved in the synthesis of auxin conjugates that mark auxin molecules for inactivation or degradation, could be due to the reduced auxin metabolism. In fact, conjugation to amino acids is a mechanism to reduce the bioavailability of free auxin, but until endosperm development there will be no intense auxin biosynthesis activities (Terol *et al.*, 2006; Figueiredo and Köhler 2018).

In other hormonal pathways, an increase in trimethylation levels has also been found in genes involved in signal transduction in the last stage (stage 8.4), probably due to the moment of stasis that the ovule undergoes, during which genetic reprogramming occurs with a view to the subsequent changes that it will undergo. The knowledge concerning the role PRC2 plays in the signal transduction of other hormones, such as cytokinins and ethylene, is still fragmentary (reviewed by

Yamamuro *et al*., 2016; Smolikova *et al*., 2021). However, it's reported in literature that PRC2 attenuates ABA-induced senescence in *Arabidopsis* by repressing ABA-induced senescence-associated genes (*SAGs*) (Liu *et al*., 2019). Indeed, in *clf-50 swn-1* double *SAGs* are not repressed, resulting in an early senescence (Liu *et al*., 2019). Based on this evidence, it is possible to assume that repression of genes involved in senescence is required in developing ovule. This aspect will be further explored in Chapter III, where the transcriptomic profiles of pollinated and unpollinated stages collected at three different time points after the end of pollination drop emission were compared. In particular, the results discussed below suggest that pollen inhibits senescence-related genes by preventing programmed cell death (PCD) in pollinated ovules. On the contrary, unpollinated ovules show early PCD, culminating in abortion.

Concerning gibberellins, the only gene found to be DEG and DMG is involved in their biosynthesis. More specifically, it showed hypotrimethylation in the first comparison (stage 8.1/stage 7) and hypertrimethylation in the second (stage 8.3/stage 8.1). Subsequently (stage 8.4/stage 8.3), it did not show significant changes in its trimethylation status, but it was always silenced. Interestingly, in *Arabidopsis*, gibberellins are crucial for seed coat differentiation, and genes involved in their biosynthesis are silenced by PRC2 before fertilisation in ovule integument (Figueiredo and Köhler 2018). After fertilisation, a signal starts from the newly fertilised central cell (future endosperm) and migrates into the integument of the ovule, where it causes the removal of PRC2 and allows the expression of these genes (Figueiredo and Köhler 2018).

In *Ginkgo*, following pollination it is possible to begin to distinguish the three layers that will later characterise the seed coat: *sarcotesta*, *sclerotesta* and *endotesta* (D'Apice *et al*., 2021). The differentiation of these three layers continues as the gametophyte develops, before fertilisation takes place, but it will be complete around two months after pollination (D'Apice *et al*., 2021). However, shortly after pollination, they can be distinguished mainly by the characteristics of their cells: isodiametric in *sarcotesta*, smaller and thick walled in *sclerotesta*, and elongated in *endotesta* (D'Apice *et al*., 2021). At the stages analysed, all three layers are still fleshy, and the complete lignification of the *sclerotesta* did not occur. Indeed, GC–MS-driven metabolomic analysis performed in D'Apice *et al*. (2021), showed a strong

accumulation of secondary metabolites involved in lignin biosynthesis such as quinic acid, sinapinic acid, sinapic acid, pantothenate, and phenylalanine in the post-pollination stages. This result suggests that pollination triggers metabolomics pathway involved in seed coat differentiation, initiating a process that will slowly lead to the complete lignification of the *sclerotesta* over the next two months.

The earliness of the stages analysed could explain the general silencing that has been observed in genes encoding enzymes involved in flavonoid biosynthesis, since their accumulation is likely to occur during the process of lignification of the intermediate layer (*sclerotesta*). Interestingly, among them, was also found *DFR*, which in *Arabidopsis* is also known as *TRANSPARENT TESTA 3*, which, as mentioned above, is known to be target of PRC2 in the ovule integument before fertilisation (Figueiredo and Köhler 2018). In *Arabidopsis*, *TT* is a small family of genes whose mutants have a phenotype that affects seed coat colour due to defects in different steps of the flavonoid biosynthesis pathway (Appelhagen *et al.*, 2013). In particular *tt3* mutants have yellow seeds, due to a mutation in the gene encoding DFR, which is downstream of the flavonoid biosynthetic pathway, so that the final derivatives that give the seed coat its characteristic brownish colour are not produced, but there is an accumulation of quercetin and kaempferol, which determine the yellow colour of the seeds (Appelhagen *et al.*, 2014).

Based on these assumptions, we can hypothesise that *DFR* in *Ginkgo* may play the same role and be regulated by a similar epigenetic mechanism as in *Arabidopsis*. However, given the early differentiation of the integument layers with respect to fertilisation, we can assume that the removal of H3K27me3 activity occurs after pollination, but at later stages than those analysed here.

Lastly, genes known in literature to be involved in ovule development were identified among DEGs and DMGs. Interestingly, all four genes were found to be hypertrimethylated and down-regulated in the last stage (comparison stage 8.4/stage 8.3). The transcripts of *Gb_07049* (*ANT*) and *Gb_41549* (*AGL6*) were localized by *in situ* hybridisation in D'Apice *et al*. (2022) in two different stages, in ovule primordia and during the emission of pollination drop (named stage 8). Considering only the second stage, corresponding to stage 8.1 used in D'Apice *et al*. (2022) and selected in this context, the results showed the presence of *ANT* transcripts in the ovule flap, which

represents the joining zone between ovule and stalk (D'Apice *et al*., 2022). On the contrary, *AGL6* expression was visible in integument, nucellus and *tapetum* (D'Apice *et al*., 2022). The expression of these genes in sporophytic tissues at earlier stages, suggest that they play a role in initiating the development of the ovule, accompanying it in a process of rapid growth until it reaches full maturity, as evidenced by the emission of the pollination drop, which marks the receptive phase. After this stage, their activity is no longer required, according to the RNA-seq results, given the new developmental stage that the ovule is undergoing. In particular, the initiation and development of ovule primordia in *Arabidopsis* needs the two-AP2domain-containing transcription factor encoded by *ANT*, which therefore carries out its activity in the earliest stages (Barro-Trastoy *et al.*, 2020). Considering other gymnosperms, *in situ* hybridisation on the early developmental stage of ovules of *Gnetum parvifolium* (Yamada *et al.*, 2008) and *Pinus thunbergia* (Shigyo and Ito, 2004) showed similar results, highlighting the importance which *ANT* has in ovule development.

In addition, after fertilisation, in *Arabidopsis* FIS-PRC2 induce the repression of target *MADS-box* genes, allowing the endosperm development (Zhang *et al*., 2018). Indeed, FIS-PRC2 mutants show up-regulation of several *MADS-box* genes and alteration in endosperm cellularisation, highlighting how crucial the silencing of these genes is in regulation of coenocytic endosperm development (Day *et al.*, 2008; Bemer *et al*., 2010; Gehring and Satyaki, 2017). Furthermore, *agl62* mutants are able to initiate embryo and endosperm development, but are unable to form the seed coat, suggesting the important role that *AGL62* expression has on its formation (Roszak and Köhler, 2011).

Taken together, the results presented here represent a starting point for discovering the molecular mechanisms underlying epigenetic control in very ancient plants. This work, as described above, is part of a research project involving other research groups to study these aspects by comparing *Ginkgo* and *Arabidopsis*. *Ginkgo* was chosen because it represents a very important resource for understanding the evolution of these aspects over thousands of years, whereas *Arabidopsis* as model plant species. Although preliminary, the results show for the first time that the regulatory mechanism mediated by PRC2 is present in a very ancient plant and allows the

identification of many of the target genes, some of which are also common in *Arabidopsis*.

REFERENCES

Appelhagen, I., Thiedig, K., Nordholt, N., Schmidt, N., Huep, G., Sagasser, M., and Weisshaar, B. (2014). Update on *transparent testa* mutants from *Arabidopsis thaliana*: characterisation of new alleles from an isogenic collection. *Planta*, *240*, 955-970.

Baroux, C., Gagliardini, V., Page, D. R., and Grossniklaus, U. (2006). Dynamic regulatory interactions of *Polycomb* group genes: *MEDEA* autoregulation is required for imprinted gene expression in *Arabidopsis*. *Genes and development*, *20*(9), 1081.

Barro-Trastoy, D., Dolores Gomez, M., Tornero, P., and Perez-Amador, M. A. (2020). On the way to ovules: the hormonal regulation of ovule development. *Critical Reviews in Plant Sciences*, *39*(5), 431-456.

Bemer, M., and Grossniklaus, U. (2012). Dynamic regulation of *Polycomb* group activity during plant development. *Current opinion in plant biology*, *15*(5), 523-529.

Bemer, M., Heijmans, K., Airoldi, C., Davies, B., and Angenent, G. C. (2010). An atlas of type I *MADS box* gene expression during female gametophyte and seed development in *Arabidopsis*. *Plant physiology*, *154*(1), 287-300.

Bowler, C., Benvenuto, G., Laflamme, P., Molino, D., Probst, A. V., Tariq, M., and Paszkowski, J. (2004). Chromatin techniques for plant cells. *The Plant Journal*, *39*(5), 776-789.

Brukhin, V., and Albertini, E. (2021). Epigenetic modifications in plant development and reproduction. *Epigenomes*, *5*(4), 25.

Cabej, N. R. (2019). *Epigenetic mechanisms of the cambrian explosion*. Academic Press.

Casadesús J., Noyer-Weidner M. Epigenetics. In: Maloy, S., and Hughes, K. (Eds.). (2013). *Brenner's encyclopedia of genetics*. Academic Press, 500-503.

Ceccato, L., Masiero, S., Roy, D. S., Bencivenga, S., Roig-Villanova, I., Ditengou, F. A., Palme, K., Simon, R., and Colombo, L. (2013). Maternal control of PIN1 is required for female gametophyte development in *Arabidopsis*. *PloS one*, *8*, e66148.

Cucinotta, M., Di Marzo, M., Guazzotti, A., de Folter, S., Kater, M. M., and Colombo, L. (2020). Gynoecium size and ovule number are interconnected traits that impact seed yield. *Journal of Experimental Botany*, *71*(9), 2479-2489.

Cyr, A. R., and Domann, F. E. (2011). The redox basis of epigenetic modifications: from mechanisms to functional consequences. *Antioxidants & redox signaling*, *15*(2), 551-589.

D'Apice, G., Moschin, S., Araniti, F., Nigris, S., Di Marzo, M., Muto, A., Banfi, C., Bruno, L., Colombo, L., and Baldan, B. (2021). The role of pollination in controlling *Ginkgo biloba* ovule development. *New Phytologist*, *232*(6), 2353-2368.

D'Apice, G., Moschin, S., Nigris, S., Ciarle, R., Muto, A., Bruno, L., and Baldan, B. (2022). Identification of key regulatory genes involved in the sporophyte and gametophyte development in *Ginkgo biloba* ovules revealed by in situ expression analyses. *American Journal of Botany*, *109*(6), 887-898.

Danilevskaya, O. N., Hermon, P., Hantke, S., Muszynski, M. G., Kollipara, K., and Ananiev, E. V. (2003). Duplicated fie genes in maize: expression pattern and imprinting suggest distinct functions. *The Plant Cell*, *15*(2), 425-438.

Day, R. C., Herridge, R. P., Ambrose, B. A., and Macknight, R. C. (2008). Transcriptome analysis of proliferating *Arabidopsis* endosperm reveals biological implications for the control of syncytial division, cytokinin signaling, and gene expression regulation. *Plant Physiology*, *148*(4), 1964-1984.

Deleris, A., Stroud, H., Bernatavichute, Y., Johnson, E., Klein, G., Schubert, D., and Jacobsen, S. E. (2012). Loss of the DNA methyltransferase MET1 Induces H3K9 hypermethylation at PcG target genes and redistribution of H3K27 trimethylation to transposons in *Arabidopsis thaliana*. *PLoS genetics*, *8*(11), e1003062.

Derkacheva, M., and Hennig, L. (2014). Variations on a theme: Polycomb group proteins in plants. *Journal of experimental botany*, *65*(10), 2769-2784.

Favaro, R., Pinyopich, A., Battaglia, R., Kooiker, M., Borghi, L., Ditta, G., Yanofsky, M. F., Kater, M. M., and Colombo, L. (2003). MADS-box protein complexes control carpel and ovule development in *Arabidopsis*. *The Plant Cell*, *15*(11), 2603-2611.

Felsenfeld, G. (2014). A brief history of epigenetics. *Cold Spring Harbor perspectives in biology*, *6*(1), a018200.

Figueiredo, D. D., and Köhler, C. (2018). Auxin: a molecular trigger of seed development. *Genes and development*, *32*(7-8), 479-490.

Figueiredo, D. D., Batista, R. A., Roszak, P. J., Hennig, L., and Köhler, C. (2016). Auxin production in the endosperm drives seed coat development in *Arabidopsis*. *Elife*, *5*, e20542.

Friedman, W. E. (1987). Growth and development of the male gametophyte of *Ginkgo biloba* within the ovule (in vivo). *American Journal of Botany*, *74*(12), 1797-1815.

Gehring, M., and Satyaki, P. R. (2017). Endosperm and imprinting, inextricably linked. *Plant physiology*, *173*(1), 143-154.

Gehring, M., Bubb, K. L., and Henikoff, S. (2009). Extensive demethylation of repetitive elements during seed development underlies gene imprinting. *Science*, *324*(5933), 1447-1451.

Gouil, Q., and Baulcombe, D. C. (2016). DNA methylation signatures of the plant chromomethyltransferases. *PLoS genetics*, *12*(12), e1006526.

Gu, X., Xu, T., and He, Y. (2014). A histone H3 lysine-27 methyltransferase complex represses lateral root formation in *Arabidopsis thaliana*. *Molecular Plant*, *7*(6), 977-988.

Guo, A., and Zheng, C. X. (2013). Female gametophyte development. *Journal of Plant Biology*, *56*, 345-356.

Hsieh, T. F., Shin, J., Uzawa, R., Silva, P., Cohen, S., Bauer, M. J., Hashimoto, M., Kirkbride, R. C., Harada, J. J., Zilberman, D. and Fischer, R. L. (2011). Regulation of imprinted gene expression in *Arabidopsis* endosperm. *Proceedings of the National Academy of Sciences*, *108*(5), 1755-1762.

Ingouff, M., Rademacher, S., Holec, S., Šoljić, L., Xin, N., Readshaw, A., Foo, S. H., Lahouze, B., Sprunck, S., and Berger, F. (2010). Zygotic resetting of the HISTONE 3

variant repertoire participates in epigenetic reprogramming in *Arabidopsis*. *Current Biology*, *20*(23), 2137-2143.

Jacob, Y., Bergamin, E., Donoghue, M. T., Mongeon, V., LeBlanc, C., Voigt, P., Underwood, C. J., Brunzelle, J. S., Michaels, S. D., Reinberg, D., Couture, J. F., and Martienssen, R. A. (2014). Selective methylation of histone H3 variant H3. 1 regulates heterochromatin replication. *Science*, *343*(6176), 1249-1253.

Jahnke, S., and Scholten, S. (2009). Epigenetic resetting of a gene imprinted in plant embryos. *Current Biology*, *19*(19), 1677-1681.

Kornberg, R. D., and Lorch, Y. (1999). Twenty-five years of the nucleosome, fundamental particle of the eukaryote chromosome. *Cell*, *98*(3), 285-294.

Kradolfer, D., Hennig, L., and Köhler, C. (2013). Increased maternal genome dosage bypasses the requirement of the FIS polycomb repressive complex 2 in *Arabidopsis* seed development. *PLoS genetics*, *9*(1), e1003163.

Lafos, M., Kroll, P., Hohenstatt, M. L., Thorpe, F. L., Clarenz, O., and Schubert, D. (2011). Dynamic regulation of H3K27 trimethylation during *Arabidopsis* differentiation. *PLoS genetics*, *7*(4), e1002040.

Law, J. A., and Jacobsen, S. E. (2010). Establishing, maintaining and modifying DNA methylation patterns in plants and animals. *Nature Reviews Genetics*, *11*(3), 204-220.

Lepiniec, L., Debeaujon, I., Routaboul, J. M., Baudry, A., Pourcel, L., Nesi, N., and Caboche, M. (2006). Genetics and biochemistry of seed flavonoids. *Annu. Rev. Plant Biol.*, *57*, 405-430.

Leroy, O., Hennig, L., Breuninger, H., Laux, T., and Köhler, C. (2007). Polycomb group proteins function in the female gametophyte to determine seed development in plants.

Li, Y., Kumar, S., and Qian, W. (2018). Active DNA demethylation: mechanism and role in plant development. *Plant cell reports*, *37*, 77-85.

Lin, K. T., Yeh, S. H., Chen, D. S., Chen, P. J., and Jou, Y. S. (2005). Epigenetic activation of α4, β2 and β6 integrins involved in cell migration in trichostatin A-treated Hep3B cells. *Journal of biomedical science*, *12*, 803-813.

Liu, C., Cheng, J., Zhuang, Y., Ye, L., Li, Z., Wang, Y., Qi, M., Xu, L., and Zhang, Y. (2019). Polycomb repressive complex 2 attenuates ABA-induced senescence in *Arabidopsis*. *The Plant Journal*, *97*(2), 368-377.

Liu, X., Kim, Y. J., Müller, R., Yumul, R. E., Liu, C., Pan, Y., Cao, Y., Goodrich, J., and Chen, X. (2011). *AGAMOUS* terminates floral stem cell maintenance in *Arabidopsis* by directly repressing *WUSCHEL* through recruitment of Polycomb Group proteins. *The Plant Cell*, *23*(10), 3654-3670.

Losa, A., Colombo, M., Brambilla, V., and Colombo, L. (2010). Genetic interaction between *AINTEGUMENTA* (*ANT*) and the ovule identity genes *SEEDSTICK* (*STK*), *SHATTERPROOF1* (*SHP1*) and *SHATTERPROOF2* (*SHP2*). *Sexual plant reproduction*, *23*, 115-121.

Lucibelli, F., Valoroso, M. C., and Aceto, S. (2022). Plant DNA methylation: An epigenetic mark in development, environmental interactions, and evolution. *International Journal of Molecular Sciences*, *23*(15), 8299.

Luo, M., Platten, D., Chaudhury, A., Peacock, W. J., and Dennis, E. S. (2009). Expression, imprinting, and evolution of rice homologs of the polycomb group genes. *Molecular plant*, *2*(4), 711-723.

Luo, M., Taylor, J. M., Spriggs, A., Zhang, H., Wu, X., Russell, S., Singh, M., and Koltunow, A. (2011). A genome-wide survey of imprinted genes in rice seeds reveals imprinting primarily occurs in the endosperm. *PLoS genetics*, *7*(6), e1002125.

Makarevitch, I., Eichten, S. R., Briskine, R., Waters, A. J., Danilevskaya, O. N., Meeley, R. B., Myers, C. L., Vaughn, M. W., and Springer, N. M. (2013). Genomic distribution of maize facultative heterochromatin marked by trimethylation of H3K27. *The Plant Cell*, *25*(3), 780-793.

Matzke, M. A., and Mosher, R. A. (2014). RNA-directed DNA methylation: an epigenetic pathway of increasing complexity. *Nature Reviews Genetics*, *15*(6), 394-408.

Moreno-Romero, J., Jiang, H., Santos-González, J., and Köhler, C. (2016). Parental epigenetic asymmetry of PRC 2-mediated histone modifications in the *Arabidopsis* endosperm. *The EMBO journal*, *35*(12), 1298-1311.

Mozgova, I., and Hennig, L. (2015). The polycomb group protein regulatory network. *Annual review of plant biology*, *66*, 269-296.

Nodine, M. D., and Bartel, D. P. (2012). Maternal and paternal genomes contribute equally to the transcriptome of early plant embryos. *Nature*, *482*(7383), 94-97.

Payá-Milans, M., Poza-Viejo, L., Martín-Uriz, P. S., Lara-Astiaso, D., Wilkinson, M. D., and Crevillén, P. (2019). Genome-wide analysis of the H3K27me3 epigenome and transcriptome in *Brassica rapa*. *GigaScience*, *8*(12), giz147.

Pignatta, D., Erdmann, R. M., Scheer, E., Picard, C. L., Bell, G. W., and Gehring, M. (2014). Natural epigenetic polymorphisms lead to intraspecific variation in *Arabidopsis* gene imprinting. *Elife*, *3*, e03198.

Prasad, K., and Dhonukshe, P. (2013). Polar auxin transport: cell polarity to patterning. In *Polar auxin transport* (pp. 25-44). Berlin, Heidelberg: Springer Berlin Heidelberg.

Reddington, J. P., Perricone, S. M., Nestor, C. E., Reichmann, J., Youngson, N. A., Suzuki, M., Reinhardt, D., Dunican, D. S., Prendergast, J. G., Mjoseng, H., Ramsahoye, B., Whitelaw, E., Greally, J. M., Adams, I. R., Bickmore, W., and Meehan, R. R. (2013). Redistribution of H3K27me3 upon DNA hypomethylation results in de-repression of Polycomb target genes. *Genome biology*, *14*, 1-17.

Rodrigues, J. A., and Zilberman, D. (2015). Evolution and function of genomic imprinting in plants. *Genes and development*, *29*(24), 2517-2531.

Rodrigues, J. A., Ruan, R., Nishimura, T., Sharma, M. K., Sharma, R., Ronald, P. C., Fischer, R. L., and Zilberman, D. (2013). Imprinted expression of genes and small RNA is associated with localized hypomethylation of the maternal genome in rice endosperm. *Proceedings of the National Academy of Sciences*, *110*(19), 7934-7939.

Roszak, P., and Köhler, C. (2011). Polycomb group proteins are required to couple seed coat initiation to fertilisation. *Proceedings of the National Academy of Sciences*, *108*(51), 20826-20831.

Shigyo, M., and Ito, M. (2004). Analysis of gymnosperm two-AP2-domain-containing genes. *Development Genes and Evolution*, *214*, 105-114.

Shigyo, M., Hasebe, M., and Ito, M. (2006). Molecular evolution of the AP2 subfamily. *Gene*, *366*(2), 256-265.

Shivram, H., Le, S. V., and Iyer, V. R. (2019). MicroRNAs reinforce repression of PRC2 transcriptional targets independently and through a feed-forward regulatory network. *Genome Research*, *29*(2), 184-192.

Smolikova, G., Strygina, K., Krylova, E., Leonova, T., Frolov, A., Khlestkina, E., and Medvedev, S. (2021). Transition from seeds to seedlings: Hormonal and epigenetic aspects. *Plants*, *10*(9), 1884.

Sun, B., Zhou, Y., Cai, J., Shang, E., Yamaguchi, N., Xiao, J., Looi, L. S., Wee, W. Y, Gao, X., Wagner, D., and Ito, T. (2019). Integration of transcriptional repression and polycomb-mediated silencing of *WUSCHEL* in floral meristems. *The Plant Cell*, *31*(7), 1488-1505.

Tekel, S. J., and Haynes, K. A. (2017). Molecular structures guide the engineering of chromatin. *Nucleic acids research*, *45*(13), 7555-7570.

Terol, J., Domingo, C., and Talón, M. (2006). The GH3 family in plants: genome wide analysis in rice and evolutionary history based on EST analysis. *Gene*, *371*(2), 279-290.

Tonosaki, K., and Kinoshita, T. (2015). Possible roles for polycomb repressive complex 2 in cereal endosperm. *Frontiers in plant science*, *6*, 144.

Weinhofer, I., Hehenberger, E., Roszak, P., Hennig, L., and Köhler, C. (2010). H3K27me3 profiling of the endosperm implies exclusion of polycomb group protein targeting by DNA methylation. *PLoS genetics*, *6*(10), e1001152.

Wolff, P., Weinhofer, I., Seguin, J., Roszak, P., Beisel, C., Donoghue, M. T., Spillane, C., Nordborg, M., Rehmsmeier, M., and Köhler, C. (2011). High-resolution analysis of parent-of-origin allelic expression in the *Arabidopsis* endosperm. *PLoS genetics*, *7*(6), e1002126.

Yadegari, R., and Drews, G. N. (2004). Female gametophyte development. *The Plant Cell*, *16*(suppl_1), S133-S141.

Yamada, T., Hirayama, Y., Imaichi, R., and Kato, M. (2008). *AINTEGUMENTA* homolog expression in *Gnetum* (gymnosperms) and implications for the evolution of ovulate axes in seed plants. *Evolution and development*, *10*(3), 280-287.

Yamamuro, C., Zhu, J. K., and Yang, Z. (2016). Epigenetic modifications and plant hormone action. *Molecular plant*, *9*(1), 57-70.

Zhang, M., Xie, S., Dong, X., Zhao, X., Zeng, B., Chen, J., Li, H., Yang, W., Zhao, H., Wang, G., Chen, Z., Sun, S., Hauck, A., Jin, W., and Lai, J. (2014). Genome-wide high resolution parental-specific DNA and histone methylation maps uncover patterns of imprinting regulation in maize. *Genome research*, *24*(1), 167-176.

Zhang, S., Wang, D., Zhang, H., Skaggs, M. I., Lloyd, A., Ran, D., An., L., Schumaker, K. S., Drews, G. N., and Yadegari, R. (2018). FERTILISATION-INDEPENDENT SEED-Polycomb Repressive Complex 2 plays a dual role in regulating type I MADS-box genes in early endosperm development. *Plant physiology*, *177*(1), 285-299.

Zhou, M., and Law, J. A. (2015). RNA Pol IV and V in gene silencing: Rebel polymerases evolving away from Pol II's rules. *Current opinion in plant biology*, *27*, 154-164.

CHAPTER III

Comparative transcriptomic profiling of pollinated and unpollinated ovules of *Ginkgo biloba* reveals specific pathways induced by pollen

ABSTRACT

In a gymnosperm such *Ginkgo biloba*, ovule development and female gametophyte differentiation are induced by the pollen, which triggers the transformation of the ovule integuments into seed coat, before fertilisation takes place. In line with this observation, in *Ginkgo*, female plants isolated from male plants experienced abortion of all their ovules after the emission of pollination drops, which marks the ovule's receptive phase to pollen grains. To investigate the molecular signal induced by pollination, we compared the transcriptomic profiles of pollinated and unpollinated ovules at three different stages followind the end of pollination drop emission. Transcriptomic analysis, combined with *in situ* expression analysis, revealed novel key pathways related to ovule development and pollination event, such as hormone metabolism, senescence and apoptosis, DNA replication, cell cycle regulation and mitosis. Here, we provided evidence that the pollen signal inhibits the programmed cell death pathway in the ovule, while promoting both the cell cycle and DNA replication pathways.

INTRODUCTION

The ovule development is an intricate process conserved in both angiosperms and gymnosperms in the early stages, from the sporangium formation to the functional megaspore differentiation (Yadegari and Drews, 2004). The ovule structure consists of a megasporangium, named nucellus, protected by one or two sterile outer envelopes, the integuments. They differentiate starting from annular outgrowths and progressively surround the nucellus to delimit an apical opening, named micropyle, which allows the male gametophyte, the pollen, which carries one or more male gametes, to enter inside the Female Gametophyte (FG) (Rudall, 2021). The FG is formed in the nucellus by a multistep process encompassing two phases:

megasporogenesis followed by megagametogenesis (Yadegari and Drews, 2004). In gymnosperms, multiple free nuclei originate the functional megaspore through nuclear divisions (free nuclear mitosis of the megagametophyte, FNMM). Then, cellularization takes place to generate a cellularised FG that differentiates two archegonia, each bearing one egg cell (Zhang and Zheng, 2016; Yang *et al.*, 2016). Based on this scenario, it is clear that ovules encompass multiple tissues that perform various roles within a highly constrained space, requiring a complex cascade of genes that generates localized cell proliferation, specific cell commitment and differentiation, as well Programmed Cell Death (PCD) during different developmental stages. In correlation, it has been demonstrated in *Arabidopsis* that a proper auxin influx and efflux deputed to PIN transporters is necessary for PCD processes which occurs in the nucellus (Wang *et al.*, 2021). More in details, PIN1 transports maternal auxin in the peripheral regions of nucellus, while PIN3, PIN4 and PIN7 redistribute it in the inner tissues, generating an auxin gradient which controls the degeneration of specific cells and the expansion of the gametophyte (Wang *et al.*, 2021).

However, the molecular networks regulating ovule development have been widely studied in angiosperms, using model species such as *Arabidopsis thaliana* (Drews and Koltunow, 2011; Cucinotta *et al.*, 2014, 2020), although recent works addressed the largely unexplored topic of ovule development in gymnosperms (Shigyo *et al.*, 2006; Yamada *et al.*, 2008; Chen *et al.*, 2017; Zumajo-Cardona *et al.*, 2021).

The differentiation of ovule integuments into seed coats, in *Arabidopsis*, is driven by double fertilisation, which is temporally close to the pollination event (Figueiredo *et al.*, 2016; Figueiredo and Köhler, 2018). On the contrary, in *Ginkgo*, where pollination is separated by fertilisation through a long time (i.e. four/five months), such as other gymnosperms, pollen arrival represents the signal which triggers ovule development, FG differentiation and the distinction of three distinguishable layers in the ovule integument, which will differentiate in seed coats long before fertilisation takes place (D'Apice *et al.*, 2021; 2022). Accordingly, *Ginkgo* female plants isolated from male plants aborted all their ovules following the emission of the pollination drop, which in this species characterizes the ovule receptive phase to pollination (Friedman, 1987). It has been demonstrated that the senescing unpollinated stigma tissue in *Arabidopsis* undergoes a PCD process. In particular,

transcriptional profiling revealed the NAC Transcription factors (TFs) *ORESARA1* (ORE1) and *KIRA1* (*KIR1*) activate senescence program in unpollinated pistils (Gao *et al.*, 2018). Moreover, in *Arabidopsis* ovules, the combined triple mutation of *NAC-LIKE ACTIVATED BY AP3/PI* (*NAP/ANAC029*), *SPEEDY HYPONASTIC GROWTH* (*SHYG*) and *ORESARA1* (*ORE1*) genes, which are the most expressed NAC at 4 days after emasculation, caused a delay in ovule senescence and an extension of fertility interval (Van Durme *et al.*, 2023).

In the present work, we aimed to study the pollen-triggered signalling mechanism in *Ginkgo* that influences the response of the ovule and represses the senescence process.

For this purpose, we performed a transcriptomic analysis on ovules collected immediately after the pollination period from both female plants that received pollen and unpollinated geographically isolated female plants. The characteristic feature of *Ginkgo*, shared with many gymnosperms, of secreting a drop from the ovule through the micropylar canal facilitated the identification of the pollination time. This drop is responsible for capturing pollen and transporting it into the ovule for germination (Prior *et al.*, 2019). Thus, the pollination drop emission timeframe was monitored and the pollinated (PO) and unpollinated (UO) ovules were collected from both sites at 1, 6 and 8 Days After the end of Drop emission (DAD).

The rationale was to identify the switch genes activated/deactivated by pollination event. We found several novel key pathways related to ovule development, such hormone metabolism, senescence and apoptosis, DNA replication, cell cycle regulation and mitosis.

We have analysed the expression domains of genes of interest by in situ hybridisation during ovule development, providing new insights into the molecular mechanisms regulating FG development in this species.

Taken together, a model can be drawn in which the pollen triggers the initiation of ovule enlargement and further differentiation, by inhibiting specific genes related to the senescence and apoptosis pathway, modulating the transcripts of genes involved in auxin transport, such as *PINs*, and ensuring proper expression of genes related to DNA replication and cell cycle regulation, allowing ovule development.

MATERIAL AND METHODS

Ovules collection

During pollination timeframe, comprised from March and April 2021, pools of PO and UO were collected. Specifically, PO were collected from ten female plants located at the Botanical Garden of the University of Calabria, Rende (CS), UO were collected from female isolated plants, located in Montalto Uffugo (CS). Sampling were conducted considering the stages described in D'Apice *et al.* (2021): before pollination were collected ovules at stages 6, 7 (stages before the emission of pollination drop), and stage 8.1 (during the emission of pollination drop). After the end of the drop emission (DAD), were selected three stages: 1 (UO_1, PO_1), 6 (UO_6, PO_6), and 8 days (UO_8, PO_8) respectively.

Ovule growth kinetics analysis

At least thirty ovules for each stage were measured considering the diameter at the widest part, using image processing and analysis program ImageJ (Schneider *et al.*, 2012). Statistical analyses were performed on diameters values, first testing the homogeneity (Leven Median test), and then analysed by ANOVA and Tukey's rank test ($P < 0.05$).

Paraffin embedding and cyto-istological analysis of ovules

Ginkgo ovules (twenty-five) for each analysed stage, respectively UO_1, UO_6, UO_8, PO_1, PO_6, PO_8 were processed as reported in D'Apice *et al.* (2021). Chemical fixation was performed by using 4% (w/v) paraformaldehyde in Phosphate Buffer Saline (PBS) (10XPBS: 1.3M NaCl, 70 mM Na_2HPO_4, 30mM NaH_2PO_4; pH 7.4) with vacuum infiltration and then sample were left overnight in fixative at 4°C. On the following day, the samples underwent dehydration through an ethanol series (30%, 50%, 70%, 85%, 95% in distilled sterile water, with each step lasting 1 hour), followed by the replacement of ethanol with a xylene series (25%, 50%, 75%, and 100%, with each step lasting 1 hour). Finally, a gradual substitution of xylene with

Paraplast Plus (Fisher Scientific) was performed, with daily replacements. The embedded ovules were preserved at 4°C until processing, and 10 μm sections were cut using the Leica RM2125RT microtome. Subsequently, slides were deparaffinised, rehydrated, and stained with 0.05% (w/v) toluidine blue. Histological sections were examined using the Leica DRMB microscope, and images were captured with the Leica DFC 320 digital camera (Leica, Milan, Italy).

RNA extraction and sequencing

Individual total RNA extractions were conducted for each of the 18 samples (comprising three biological replicates from a pool of ovules for each of the three stages analysed for PO and UO). The extraction needed 100 mg of ovule powder and was performed following the manufacturer's guidelines for the Agilent Total RNA Isolation Mini Kit (Agilent Technologies, Santa Clara, CA, USA). The cDNAs underwent library preparation by NOVOGENE Services. This process generated paired-end reads of 150 bp for each fragment. Strand-specific libraries were generated from mRNA extracted from both UO and PO at 1, 6, and 8 DAD. DESeq2 was subsequently employed to pinpoint noteworthy changes in gene expression associated with pollination in ovule samples. Differentially Expressed Genes (DEGs) meeting the criteria of a p-adjusted value < 0.05 and $|\log2 (\text{ratio})| > 1.5$ were identified through pairwise comparisons between libraries at corresponding time points (UO_1/PO_1; UO_6/PO_6; UO_8/PO_8). The raw data has been deposited under the code Bioproject PRJNA700482 at the Sequence Read Archive (SRA).

Real-Time Quantitative PCR (RT-qPCR) analysis

Quantitative real time were performed as according to D'Apice *et al.* (2021). The specific primers were reported in **Table 1**. As normalization control, the housekeeping gene *EF2* (*Gb_02896*) was used (D'Apice *et al*., 2021). The results were analysed using the $2^{-\Delta Ct}$ method. Mean values reported were the result of three independent biological replicates. As RNA-sequencing (FPKM) and RT-qPCR produce relative gene expression measures, to evaluate concordance in gene

expression, Pearson correlation coefficient calculation was used for each pair of gene selected. Statistical analyses were performed, first testing the homogeneity (Leven Median test), and then analysed by ANOVA and Tukey's rank test ($P < 0.05$).

Probe synthesis and in situ hybridisation

Chemical fixation and tissue processing for RNA *in situ* hybridisation followed the procedures outlined by D'Apice *et al.* (2022) and the details mentioned earlier, using a minimum of thirty PO and UO from each analysed stage. The sequences of the probes can be found in **Table 1**. Target sequences were amplified using primers containing the T7 sequence at the 5' end of the forward primer (sense) and the 5' end of the reverse primer (antisense) from cDNA obtained through retrotranscription of total RNA using the Invitrogen SuperScript III kit (Invitrogen, Waltham, Massachusetts, USA). Subsequently, the PCR products were employed for *in vitro* transcription using DIG-11-UTP, following the guidelines in the DIG RNA labeling kit (Roche Diagnostics GmbH, Mannheim, Germany), and stored at −20 °C until the hybridisation process. Tissue treatments, pre-hybridisation, post-hybridisation washes, and antibody treatment were carried out following the protocol reported in Ambrose *et al.* (2000). Detection was developed overnight using the NBT/BCIP detection solution (Roche Diagnostics GmbH, Mannheim, Germany). Slides were washed in stop buffer (100 mM Tris-HCl, pH 8.0; 1 mM EDTA), dehydrated, and mounted with Canada balsam (CARLO ERBA Reagents). Image capture was performed using a Leica DFC 320 digital camera (Leica, Milan, Italy).

Table 1. Primers used in RT-qPCR for libraries results validation and *in situ* hybridisations.

	RT-qPCR primers			
	GENE	**ID**	**Type of primer**	**SEQUENCE 5'-3'**
	EF2	*Gb_02896*	forward	TCCATCTTCCTTCTCCATCC (D'Apice *et al.*, 2021)
	EF2	*Gb_02896*	reverse	CTTACCTTCATACCTGTTGCC (D'Apice *et al.*, 2021)
	PIN1	*Gb_06199*	forward	GCACGTCATGACCAAGCATA
	PIN1	*Gb_06199*	reverse	GCCCTTCTTTGTCCAGTGGA
	RNS1	*Gb_27893*	forward	TACGAGTGGAGAGGGCAATC
	RNS1	*Gb_27893*	reverse	TCGTTTCTTCCTCGTCACCA

	CYSP1	*Gb_13610*	forward	GCTTGTGGCGCTAGGAATC
	CYSP1	*Gb_13610*	reverse	GCCTCTGCGTTTAGAAGGG
	CEP1	*Gb_10444*	forward	AGGCAGCACTCTTGGTTCTC
	CEP1	*Gb_10444*	reverse	CCCATCACCGTCTCTTGGAG
	MSH	*Gb_07613*	forward	TGGGTAGGTTAAAGCGAGCA
	MSH	*Gb_07613*	reverse	CCGGGTCACTTCTTCTGTCT
	cdkb	*Gb_38629*	forward	CCTGTCCTCTGTCACCCAAA
	cdkb	*Gb_38629*	reverse	CAAGCCCCAGATCTGCAATC
	CLV	*Gb_06318*	forward	TAAGGGTTGCTCTGCTATGC
	CLV	*Gb_06318*	reverse	TGGGTCTGAAAGCACTTGGA
	CAF	*Gb_06025*	forward	TACCGAAAGCAGCTCTCCAA
	CAF	*Gb_06025*	reverse	AGACAAGGACACAGGTGAGC
	MET1	*Gb_24436*	forward	AGTGCAGGAAATGGGATGGT
	MET1	*Gb_24436*	reverse	TCTTCCTGGAGCAATCTGGC
	CMT	*Gb_13672*	forward	AGTCTGGAAAGGTGGCTCTG
	CMT	*Gb_13672*	reverse	CTGCCATTTCCCGTTCACAA
***In situ* hybridisations primers**				
PROBE	**GENE**	**ID**	**Type of primer**	**SEQUENCE 5'-3'**
sense	*CYSP1*	*Gb_13610*	forward	TAATACGACTCACTATAGGGGCTTGTGGCGCTAGGAATC
	CYSP1	*Gb_13610*	reverse	TGAAGAGGCGATGAG
antisense	*CYSP1*	*Gb_13610*	forward	GCTTGTGGCGCTAGGAATC
	CYSP1	*Gb_13610*	reverse	TAATACGACTCACTATAGGGTGAAGATGAAGAGGCGATGAG
sense	*PIN1*	*Gb_06199*	forward	TAATACGACTCACTATAGGGACAGATCACAGTGCCAAGGA
	PIN1	*Gb_06199*	reverse	TCATGACACTTGCAGGAGG
antisense	*PIN1*	*Gb_06199*	forward	ACAGATCACAGTGCCAAGGA
	PIN1	*Gb_06199*	reverse	TAATACGACTCACTATAGGGTCATGACACTTGCAGGAGG
T7 RNA polymerase				TAATACGACTCACTATAGGG

Immuno-fluorescence detection of apoptosis by TUNEL assay

Fifteen *Ginkgo* ovules corresponding to each analysed stage (UO_1-8, PO_1-8) were fixed overnight at 4 °C in 4% (w/v) paraformaldehyde in 1XPBS. Subsequently, the samples underwent dehydration using an ethanol series, as previously described, and were embedded in Paraplast Plus (Sigma-Aldrich). Sections of 10 µm thickness were cut and mounted on poly-L-lysine-coated slides. Slides were then dewaxed through a xylene series and rehydrated. Following the manufacturer's instructions, the TUNEL assay was conducted using the "Click-iTTM Plus TUNEL Assay" (Thermo Fisher Scientific). Confocal images of median longitudinal sections

were captured using a Leica inverted TCS SP8 confocal scanning laser microscope. The detection of green fluorescence from incorporated EdUTP-Alexa FluorTM 488 was obtained with excitation peak centered at 495 nm and emission peak wavelength of 519 nm, and DAPI staining (1 g/ml) was observed with excitation peak centered at 358 nm and emission peak wavelength of 461 nm.

RESULTS

Loss of pollination triggers significant alterations in both the size and cyto-histological organisation of the ovule

To elucidate the role of pollination on ovule development, we established growth kinetics by measuring the diameter of PO and UO from the opening of the buds (stage 6 described in D'Apice *et al*., 2021) until 10 days after the end of pollination drop emission. Notably, we noticed that the pollination drop emission took place around mid-April in both sites. However, in isolated female plants unable to receive pollen, we observed a prolongation of this stage. Specifically, the pollination drop emission lasted approximately one week in plants where pollination occurred, while it extended to about two weeks in isolated female plants (**Figure 1A**).

Regarding ovule size, no significant differences were observed between the two sites until the emission of the pollination drop (stage 8.1). Following the pollination drop emission, PO exhibited rapid growth, whereas UO decreased in size, initiating a senescence process that ultimately led to ovule abortion in mid-May (**Figure 1A**). Drawing from this evidence, we selected three different time-points for the experiments: PO_1, PO_6, PO_8, UO_1, UO_6, UO_8, at 1, 6 and 8 DAD respectively.

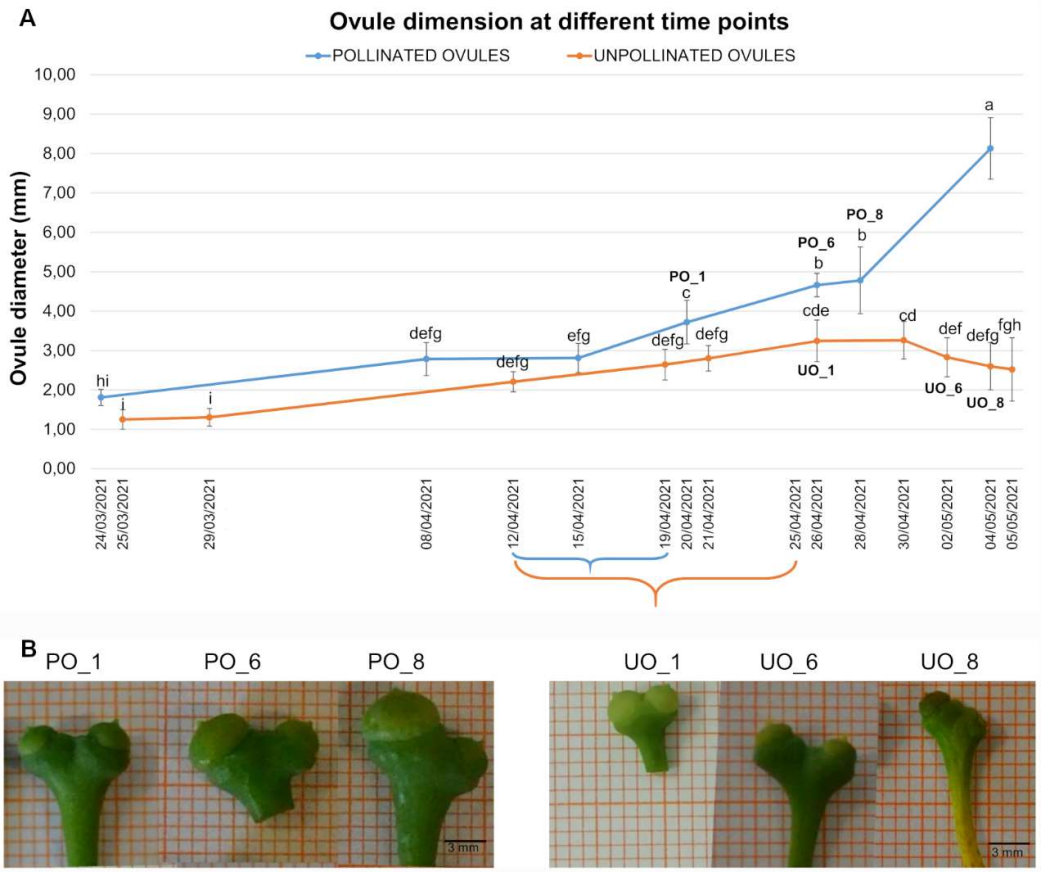

Figure 1. Ovule size in *Ginkgo biloba* over time (from April to May). (A) Growth kinetics of pollinated (PO) and unpollinated ovules (UO), considering the diameter of the ovule. Data present the mean ± SD. The brackets, blue for the PO and orange for the UO, indicates the timeframe of drop emission. Statistical significance of differences among values is indicated with different letters ($P<0.05$, ANOVA). **(B)** Macroscopic pictures of ovules at the three selected timepoint, PO_1-6 and UO_1-8 respectively. Scale bars: 3 mm.

First of all, we conducted histological analysis on ovules collected at the following stages: PO_1, PO_6, PO_8, UO_1, UO_6, UO_8 (**Figure 2**).

At both PO_1 and UO_1 stages, there were no discernible differences at the cyto-histological level. Notably, the integument formation, characteristic teardrop-shaped micropyle, and the coenocytic stage of development of the FG were observed (**Figure 2A, D**). However, between PO_6 and UO_6 several changes occurred. During the PO_6 stage, ovules exhibited a reduced opening of the micropyle, with the cells surrounding the pollen chamber collapsing inward, thereby narrowing the opening.

Additionally, the FG exhibited the presence of free nuclei confined within a single cell, a distinctive stage arising from nuclear divisions that occurred independently of cytokinesis, known as coenocytic stage (**Figure 2B**). In UO_6, no free nuclei were observed, suggesting that the FG is probably no longer in a coenocytic stage and is slowly progressing towards degeneration (**Figure 2E**). In addition, a tissues laceration was observed in the flattened-cells layer (**Figure 2E**). In the final stage, PO_8, the FG was increasing in size, the *tapetum* was undergoing degeneration, and all three layers of the integument were fully distinguishable (**Figure 1C**). Instead, in UO_8, the morphology was completely altered, the nucellus appeared disorganized and the laceration tissue in the flattened-cells layer was more extended when compared to UO_6 (**Figure 1F**).

Globally, we concluded that non-arrival pollen induces the cyto-histological disorganisation and allows ovule abortion.

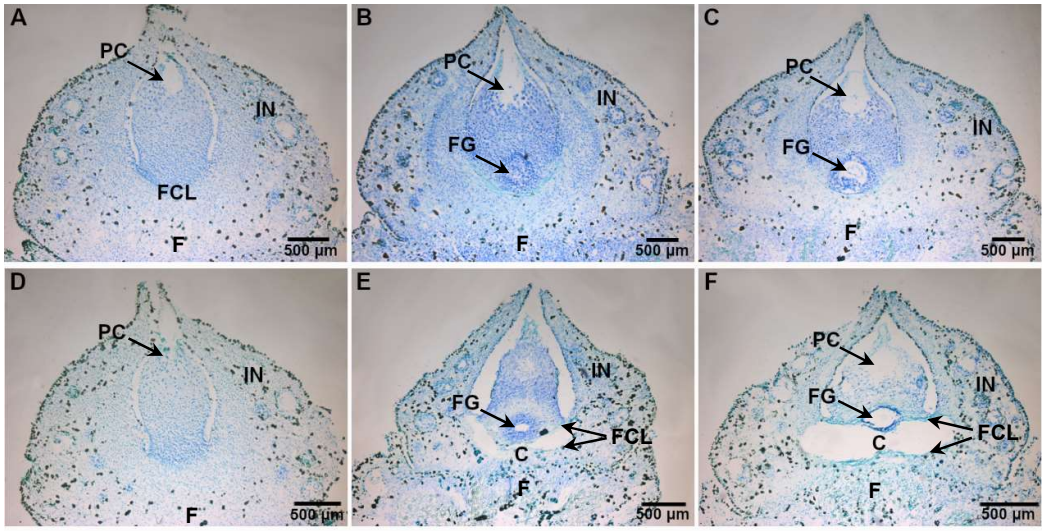

Figure 2. Cyto-histological analysis of the *Ginkgo biloba* ovules over time (from April to May). Microscopic observations at 1 **(A, D)**, 6 **(B, E)**, and 8 **(C, F)** DAD in both PO **(A-C)** and UO **(D-F)** ovules. Longitudinal histological sections were stained with blue toluidine. C, cavity; F, flap; FCL, flattened-cells layer; FG, female gametophyte; IN, integument; PC, pollen chamber; **(A-F)** Scale bars: 500 µm.

Pollination strongly modulates transcriptomic profiles of ovules

mRNA from both UO and PO collected at 1, 6, and 8 DAD was used to construct strand-specific libraries.

DESeq2 was subsequently employed to detect noteworthy changes in gene expression associated with pollination in ovule samples. Differentially Expressed Genes (DEGs), meeting the criteria of a p-adjusted value < 0.05 and |log2 (ratio)| > 1.5, were identified through pairwise comparisons between libraries at corresponding time points (UO_1/PO_1; UO_6/PO_6; UO_8/PO_8). A total of 6394 DEGs associated with pollination was identified through these pairwise comparisons (**Figure 3A**). Specifically, the UO_1/PO_1 comparison revealed 1274 DEGs with 651 upregulated and 623 downregulated genes. For UO_6/PO_6, there were 4471 DEGs (2383 upregulated and 2088 downregulated), and UO_8/PO_8 exhibited 3400 DEGs (1177 upregulated and 2223 downregulated) (**Figure 3A**). Furthermore, we identified both conserved and stage-specific DEGs between adjacent developmental stages, employing a Venn diagram (**Figure 3B**). The largest number of stage-specific DEGs, totalling 2139 (33.5% of the total), was identified in the UO_6/PO_6 comparison, followed by UO_8/PO_8 with 1276 (20%). Conversely, the UO_1/PO_1 comparison exhibited the smallest number of stage-specific DEGs, totalling 530 (8.3% of the total). This observation further implies that numerous biological processes underwent substantial changes in ovules from 1 DAD to 6 DAD. Additionally, we identified 300 (4.7%) conserved DEGs present in all three comparisons analysed (**Figure 3B**).

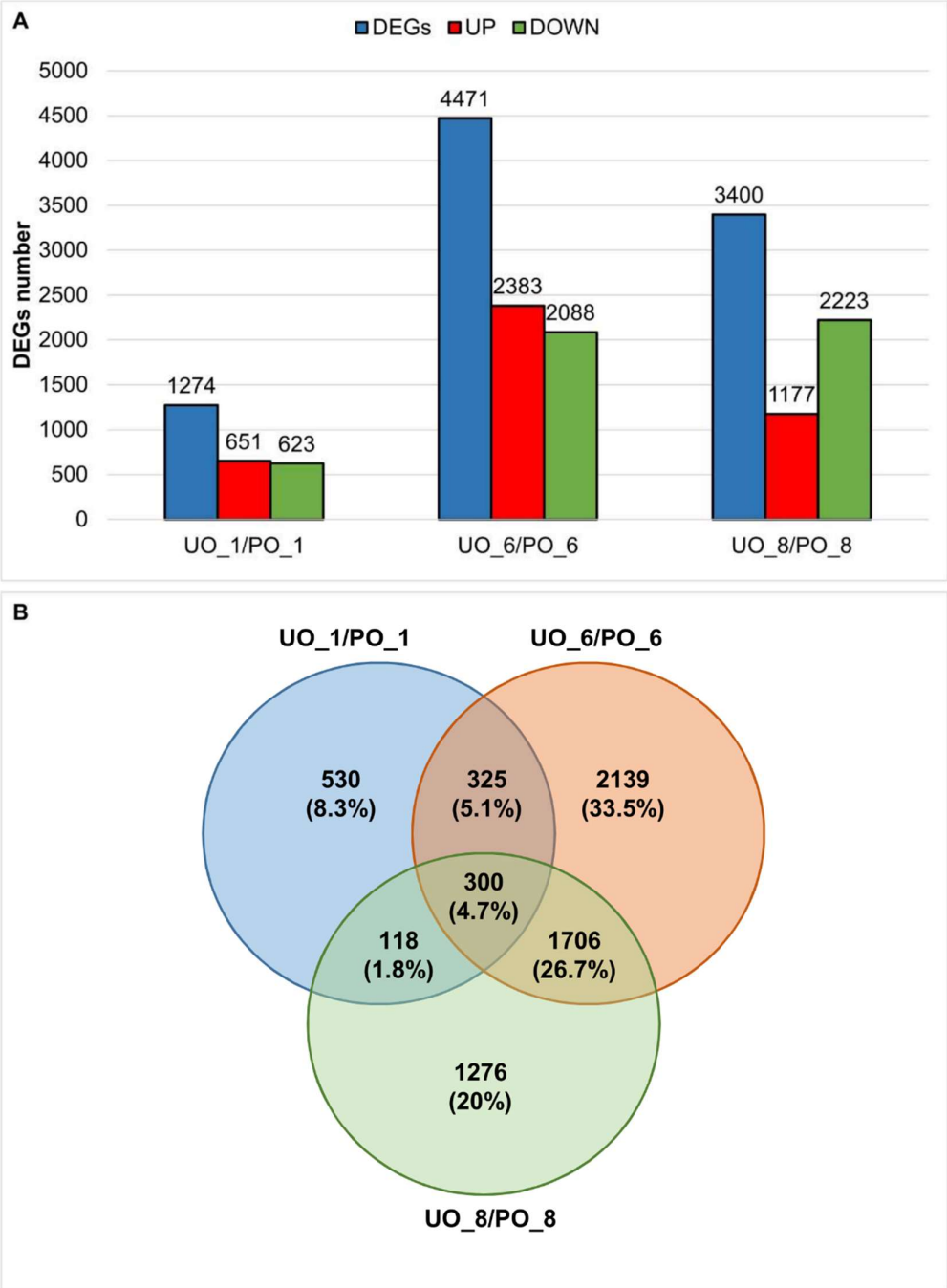

Figure 3. Transcriptomic analysis changes considering libraries at 1, 6, and 8 days after pollination. (A) Differentially expressed genes (DEGs) were determined by comparing unpollinated/pollinated ovules across the three time points (UO_1/PO_1, UO_6/PO_6, and UO_8/PO_8, respectively). Gene expression levels were normalized using the DESeq2 software (p-value corrected < 0.05 and log2FC |1.5|). **(B)** Venn diagrams illustrate the overlap of DEG sets from pairwise comparisons of pollinated and unpollinated ovules (UO_1 vs. PO_1, UO_6 vs. PO_6, UO_8 vs. PO_8).

Gene Ontology (GO) enrichment analysis conducted on DEGs in both UO and PO revealed a predominant enrichment in pathways related to response regulation. Notably, various categories within abiotic and biotic stress responses, including defence against fungi, defence against bacteria, and wounding, exhibited significant enrichment. Moreover, GO terms associated with stimuli and hormones, specifically ethylene and auxin-activated signalling pathways, regulation of transcription DNA-templated, methylation, and lipid catabolic processes, were also markedly impacted.

In this context, we prioritized genes from pathways significantly influenced by pollination signals, based on existing literature, like hormone metabolism, senescence and apoptosis, cell cycle regulation and mitosis, and DNA replication and damage repair. (**Figure 4**).

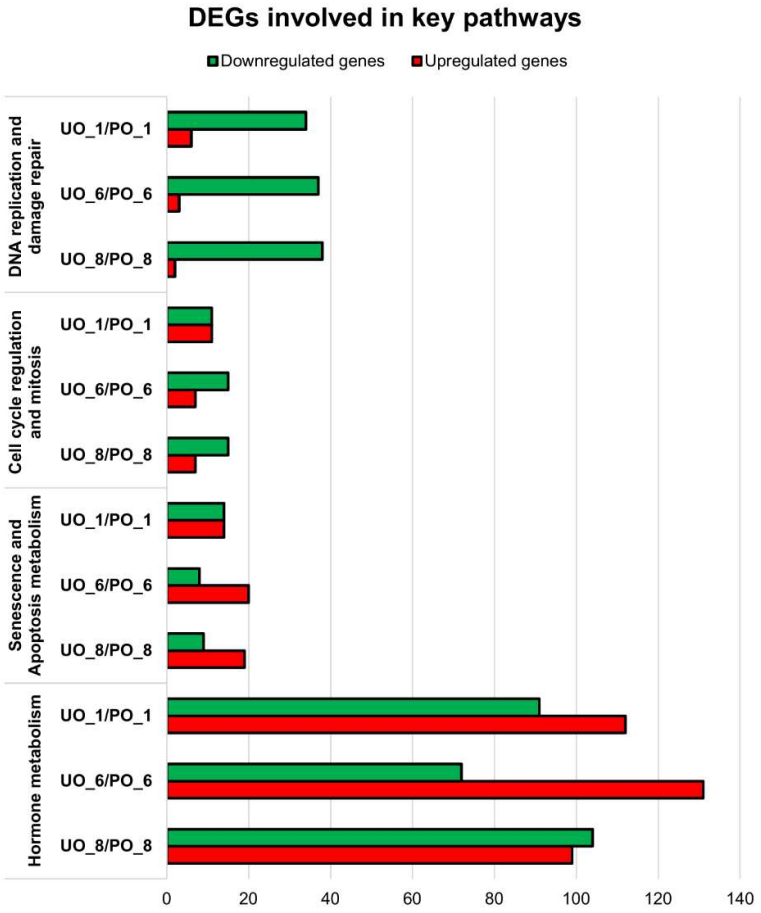

Figure 4. Diagram of the main pathways impacted resulted from RNA-seq experiment performed on *G. biloba* at the three time points. The bar length shows the number of up- and down-regulated genes (red and green respectively) belonging to the respective pathway.

In our study, histological analysis showed an abnormal FG development in UO, suggesting an anomaly in the karyokinesis and an indication of misregulation in the cell cycle, which were strongly modulated according to bioinformatic analysis. More in details, genes involved in cell cycle regulation and mitosis and DNA replication and damage repair are down-regulated in all UO stages, but especially in the last two, suggesting abnormalities in nucleic acid synthesis processes, which in turn affect the proper progression of the cell cycle. In addition, also genes encoding enzymes involved in senescence and apoptosis metabolism, such as metacaspases, ribonucleases, cysteine proteinases and autophagy-related protein, are strongly up-regulated in UO_6 and UO_8, compared to PO_6 and PO_8 respectively.

To verify the expression of selected genes, identified based on Illumina RNA-seq results, these were analysed by RT-qPCR using gene-specific primers (**Table 1**). The RT-qPCR (**Figure 5**) support the reliability of the RNA-seq analysis.

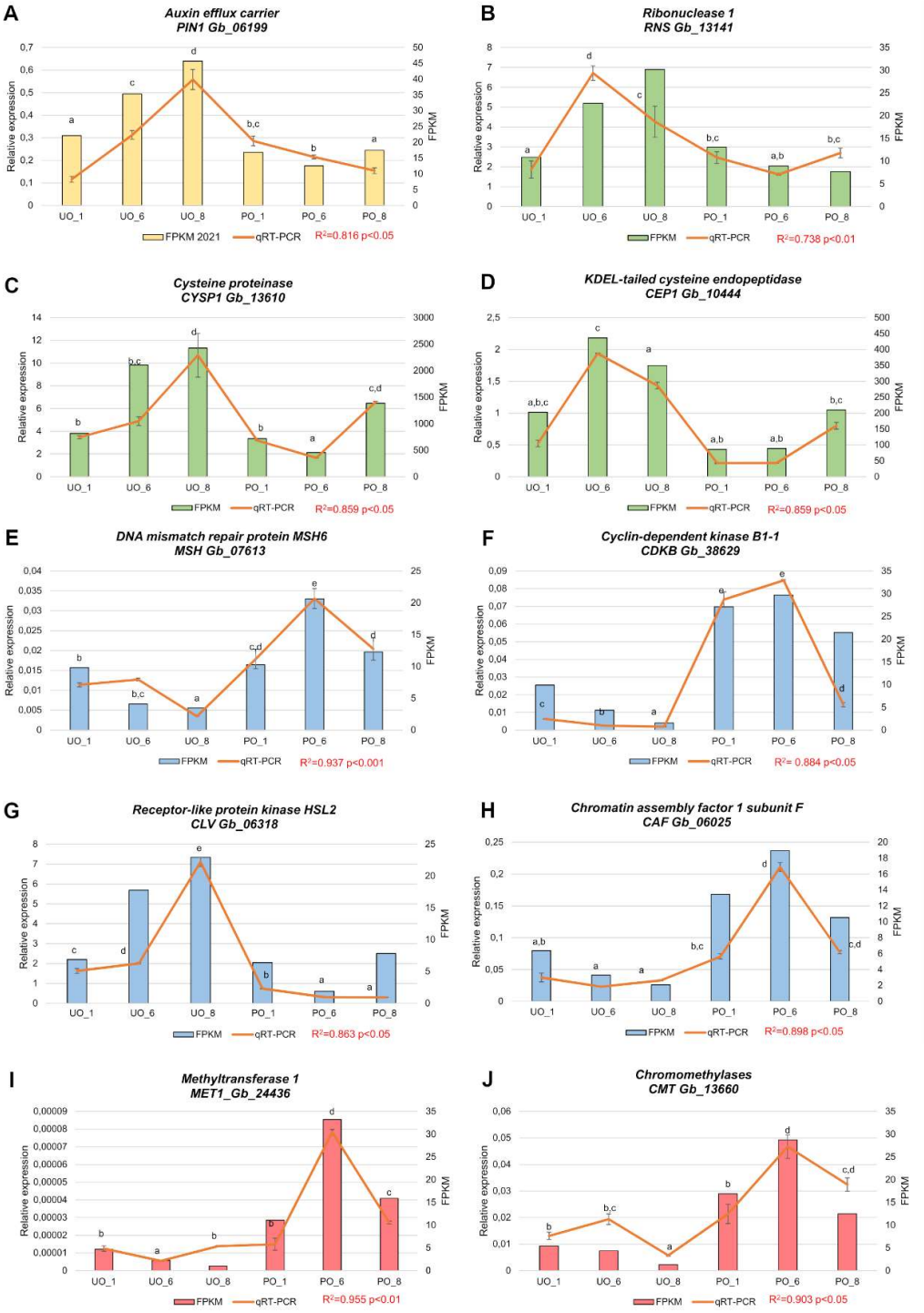

Figure 5. Validation of the expression patterns of 10 DEGs related to auxin (yellow), senescence and apoptosis (green), cell cycle (blue) and DNA replication (pink) pathways selected from the RNA-Seq analysis by RT-qPCR. The expression level ($2^{\wedge-\Delta Ct}$) was reported in orange in the left y-axis and the FPKM value in the right y-axis; the x-axis indicates days after pollination in both conditions, unpollinated (UO) and pollinated (PO) ovules. Data present the mean ± SE of three independent experiments. Statistical analyses were performed on by ANOVA and a Tukey's rank test ($P < 0.05$) on ΔCt values. Letters on graphs indicate significant differences. As RNA-sequencing (FPKM) and RT-qPCR produce relative gene expression measures, to evaluate concordance in gene expression, Pearson correlation coefficient calculation was used for each pair of gene selected.

Polar auxin transporters are differentially regulated before and after pollination

The majority of DEGs were related to hormone biosynthesis and signalling of ethylene (67 genes) and auxin (56 genes) (**Figure 6**).

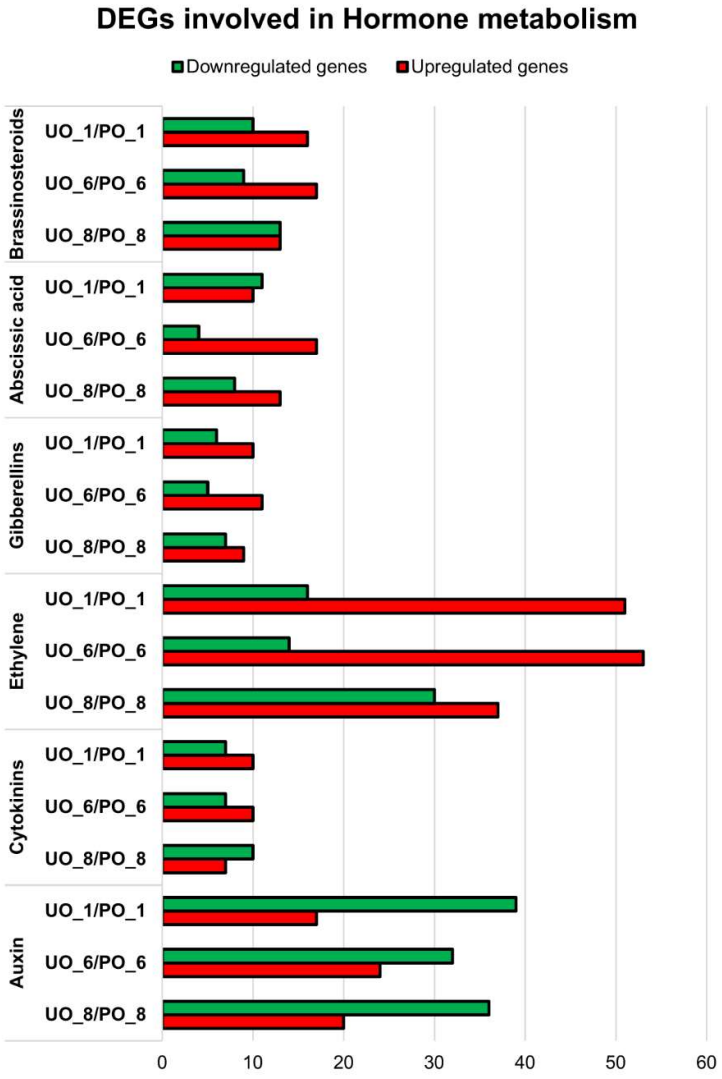

Figure 6. Diagram of the DEGs involved in hormone metabolism resulted from RNA-seq experiment performed on *Ginkgo biloba* at the three time points. The bar length shows the number of up- and down-regulated genes (red and green respectively) belonging to the respective pathway.

Notably, as reported above, auxin efflux carriers (PINs) play a key role in ovule auxin accumulation. Given the known role of PIN1 in the ovule development (Ceccato

et al., 2013), we decided to investigate by *in situ* hybridisation the cyto-histological localisation of the transcripts of the gene encoding the auxin efflux carrier *PIN1* (*Gb_06199*) (**Figure 7**), which, as reported in Chapter I, was identified as a target of PRC2 in the post-pollination stages. The expression level showed an up-regulation in UO (**Figure 5)**.

In PO_1 and UO_1 we observed the same signal localisation, the transcript was mainly localised in the flap, although a widespread slight signal was detected in the other tissues (**Figure 7A**). In PO_6 we observed a strong signal in the flap, in the innermost layer of the integument and lastly around the FG (**Figure 7B**). At the last stage PO_8, a little cluster of cells around FG showed an intense signal (**Figure 7C**). Considering UO, in the second stage, *Gb_06199* was expressed in the flap and in the nucellus (**Figure 7D**), whereas in UO_8 the signal slightly affected the whole structure, but specifically a cluster of labelled cells was observed in the pollen chamber and around the FG (**Figure 7E**).

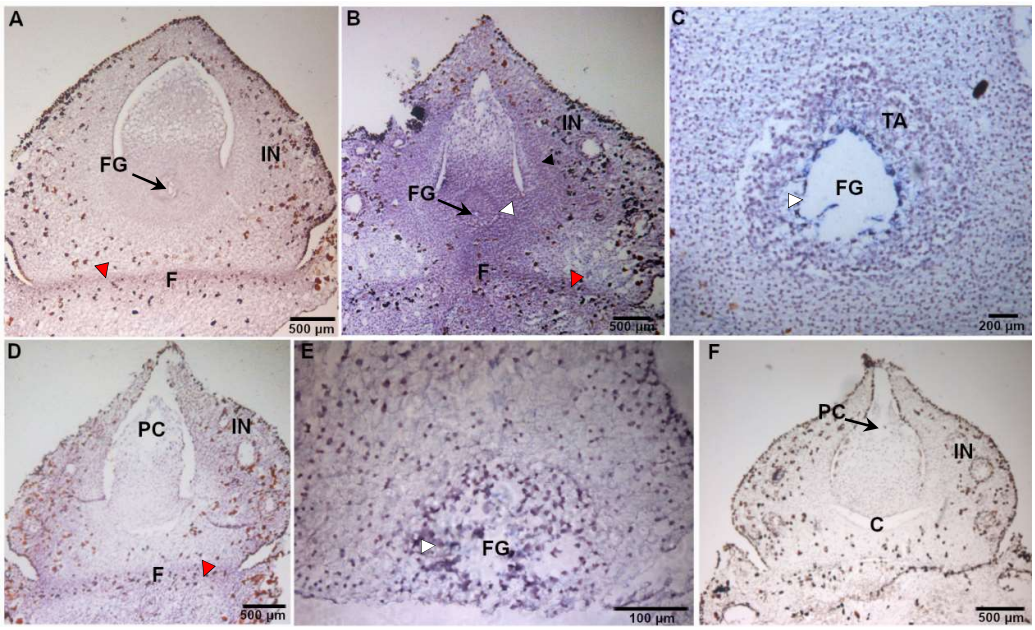

Figure 7. *In situ* hybridisation of *PIN1* (*Gb_06199*) with dig-labelled antisense probe (A-E). Longitudinal histological sections of pollinated (PO) **(A-C)** and unpollinated ovules (UO) **(D-E)** at stages 1 **(A)**, 6 **(B, D)** and 8 **(C, E)**. Signal is evidenced by purple staining **(A-E).** Longitudinal histological section of UO hybridised with *PIN1* sense probe **(F)**. C, cavity; F, flap; FG, female gametophyte; IN, integument; PC, pollen chamber. Red arrow heads indicate the signal in the flap; white arrow heads indicate the signal in female gametophyte and *tapetum*; black arrow head indicates the signal in the innermost layer of integument. **(A, B, D, F)** Scale bars: 500 µm; **(C)** Scale bar: 200 µm; **(E)** Scale bar: 100 µm.

Lack of pollination determines different expression pattern of the senescence-associated cysteine proteinase CYSP1.

As shown in **Figure 3**, considering both senescence and apoptosis metabolism, almost all gene presented a higher expression in the UO compared to the PO, particularly at the last stages. Within plants, the majority of enzymes involved in PCD are members of the cysteine protease (CYSP) family (Van Doorn and Woltering, 2008). Thus, we decided to investigate *CYSP1* (*Gb_13610*) by *in situ* hybridisation (**Figure 8**).

In PO_1, *CYSP1* expression was distributed throughout the ovules, with a heightened signal observed in the nucellus and flap (**Figure 8A**). In PO_6, a similar pattern of localization was noted, but the signal was notably intense in the *tapetum* (**Figure 8B**). By PO_8, *CYSP1* expression became restricted to the nucellus and the vicinity of the female gametophyte (FG) (**Figure 8C, G**). Regarding UO_1, no discernible differences were observed when compared to PO_1 (**Figure 8D**). In both UO_6 and UO_8, *CYSP1* was expressed across all ovule tissues, with a pronounced localization around the FG. (**Figure 8E, F, H**).

These results suggest that *CYSP1* is involved in the proper degeneration of nucellar tissues to support FG expansion in PO, whereas in UO it is correlated with the overall PCD process affecting the entire ovule.

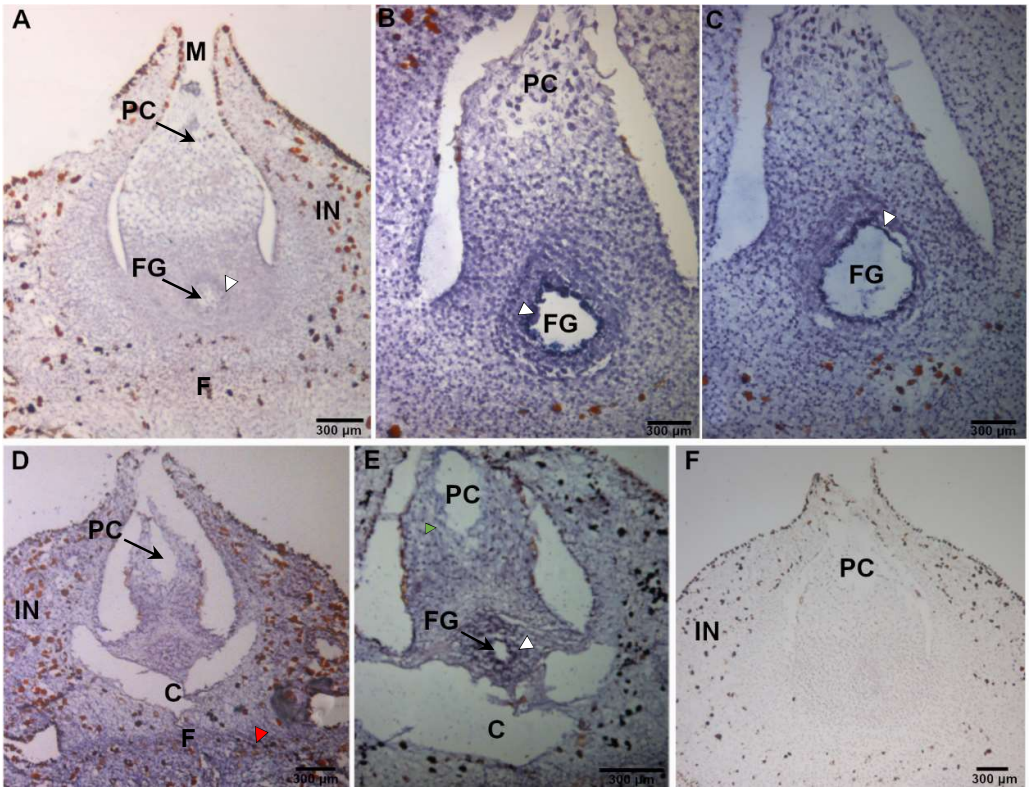

Figure 8. *In situ* hybridisation of *CYSP1* (*Gb_06199*) with dig-labelled antisense probe (A-E). Longitudinal histological sections of pollinated (PO) **(A-C)** and unpollinated ovules (UO) **(D-E)** at stages 1 **(A)**, 6 **(B, D)** and 8 **(C, E)**. Signal is evidenced by purple staining **(A-E).** Longitudinal histological section of PO hybridised with *CYSP1* sense probe **(F)**. C, cavity; F, flap; FG, female gametophyte; IN, integument; PC, pollen chamber. White arrow heads indicate the signal in the female gametophyte; red arrow head indicates the signal in the flap; green arrow head indicates the signal in the pollen chamber. **(A-F)** Scale bars: 300 µm.

Loss of pollination induces DNA degradation in nuclei

Transcriptomic and cyto-histological results suggested cell degeneration in UO. To better investigate the early target tissues of PCD processes, TUNEL assay was perfomed in longitudinal sections of UO (**Figure 9**) and PO (**Figure 10**). Interestingly, already in UO, apoptotic cells were observed in the basal portion of nucellus, the same zone in which the cavity was evident in later stages (**Figure 9A-C**). In UO_6 and UO_8 DNA fragmentation was detected in several nuclei, especially in pollen chamber, nucellus and integument (**Figure 9D-I**).

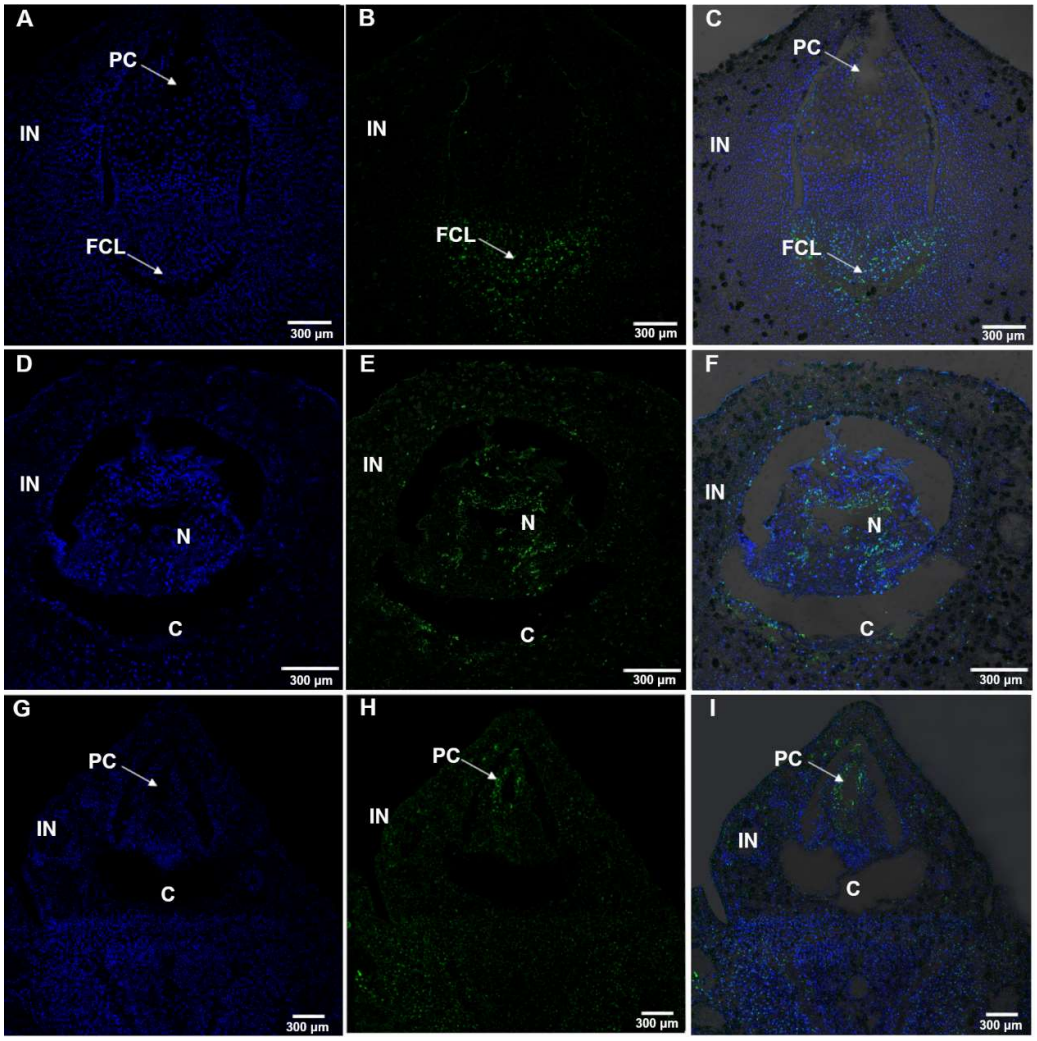

Figure 9. Confocal images of *Ginkgo biloba* unpollinated ovules show several TUNEL positive cells. *In situ* visualisation of nuclear DNA fragmentation was conducted through TUNEL staining on longitudinal histological sections in unpollinated ovules (UO) at stages 1 **(A-C),** 6 **(D-F)** and 8 **(G-I)**. TUNEL positive (apoptotic) cells are reported in green colour, while nuclei were counterstained with DAPI and reported in blue. From left to right: channel 1 image; channel 2 image; merged image (channel 1-2 and transmission. C, cavity; FCL, flattened-cells layer; IN, integument; N, nucellus; PC, pollen chamber. **(A-F)** Scale bars: 300 µm.

On the contrary, in PO, few spots of signal were identified in the integument (**Figure 10**), confirming the hypothesis that, in UO, immediately after pollination fail PCD events occur. Overall, the results evidence that pollination event inhibits PCD program and prevents cyto-histological disorganisation.

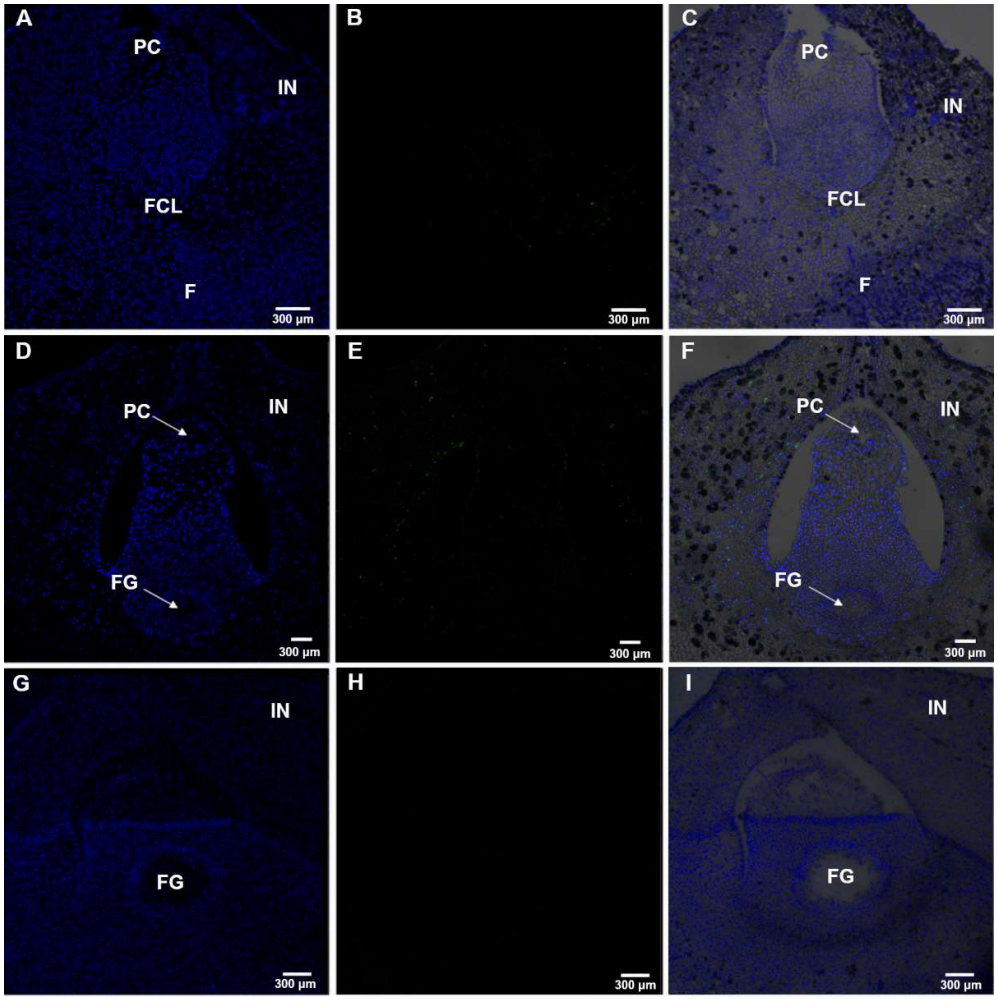

Figure 10. Confocal images of *Ginkgo biloba* pollinated ovules show the absence of TUNEL positive cells. *In situ* visualisation of nuclear DNA fragmentation was conducted through TUNEL staining on longitudinal histological sections in pollinated ovules (PO) at stages 1 **(A-C),** 6 **(D-F)** and 8 **(G-I)**. TUNEL positive (apoptotic) cells are reported in green colour, while nuclei were counterstained with DAPI and reported in blue. From left to right: channel 1 image; channel 2 image; merged image (channel 1-2 and transmission. F, flap; FCL, flattened-cells layer; FG, female gametophyte; IN, integument; PC, pollen chamber. **(A- F)** Scale bars: 300µm.

DISCUSSION

Cyto-histological features of pollinated and abortive ovules

Previous works showed that the pollen could act as the signal for subsequent ovule development and FG differentiation, initiating the differentiation of three distinct layers in the unique ovule integument, leading the transformation of the

integument into seed coats long before fertilisation occurs. (D'Apice *et al.*, 2021, 2022).

In this study, we illustrate the critical role of pollen arrival, as evidenced by the observation that *Ginkgo* female plants, isolated from male plants (and thus deprived of pollen arrival), experienced ovule abortion following the pollination drop timeframe, as also documented by Friedman (1987). Interestingly, also in plants bearing fleshy fruit, the ovary typically does not develop into the fruit without pollination (Shinozaki *et al.*, 2018).

Hence, the aim of this study was to investigate the potential mechanism behind ovule abortion by integrating anatomical observations, a transcriptomic approach, and *in situ* hybridisation analysis on *Ginkgo*.

Ovule development is the result of a successful pollination, implying a precise communication between the ovule integument, the FG, and the developing male gametophyte. In our investigations, the *Ginkgo* pollinated plants emitted the pollination drop lasting approximately 7 days, whereas unpollinated conditions led to an extended period of pollination drop production (approximately an extra week). Consistent with Jin *et al.* (2012), these findings suggest that plants allocate energy to continuously and repeatedly secrete abundant pollination drops during the pollination period. This active secretion serves to counteract the evaporative effects of wind and sunlight, enhancing the likelihood of ovules capturing pollen from the air. Moreover, the microstructures of pollinated and abortive ovules showed substantial differences. After 6 DAD, PO exhibited significantly enlarged sizes compared to UO, which instead showed a large cavity under the nucellus and then underwent a severe cell death process.

These results are in accordance with the findings of Wetzstein and collaborators (2013), in which, the abortive ovules of *Punica granatum* presented a gap between the inner and outer integuments. Also in *Cucumis sativus* (Li *et al.*, 2014), the aborted ovaries, due to no pollination event, showed atrophy or apoptosis of the cells that formed larger cavities between the inner epidermises. In *Camellia oleifera* although the integument of aborted ovules still increased in size, as does that of normal ovules, a large hollow cavity was not formed in the centre. There was little space for these sterile ovules to develop, especially in the late stage when the embryo sac was

solid. In general, this appeared to be the result of the nucellus failing to develop normally and being aborted before the embryo sac had matured (Gao *et al.*, 2017).

Sun and collaborators (2016) studied the causes of abortion during ovule development in *Prunus mume* Sieb. et Zucc. and found that in the abortive ovules, approximately half of the embryo sac did not differentiate or disintegrated when the plant was pollinated and fertilized, while in the other half the megaspore mother cells were stagnated at various stages in meiosis.

Pollination event induces differential expression of several ovule-related genes

The RNA-seq approach was employed to gain a deeper understanding of the genetic pathways associated with ovule abortion in *Ginkgo* in the absence of pollination. Consequently, the gene expression variations between UO and PO at three developmental stages were investigated. The data presented in this study reveal distinct alterations in transcriptomic profiles when comparing the two analysed conditions. Indeed 6394 DEGs (FC |1.5|) were found during the time course, with a prevalence of a slightly negative fraction, 53.95% (46.05% of the positive fraction), in the UO compared to the PO. Moreover, most of the DEGs were found in the comparison UO_6/PO_6, indicating that most responses to the pollination occurred about one week later its arrival, in concomitance with the germination of the male gametophyte (Friedman, 1987), suggesting that this process also plays a crucial role in determining large expression changes. This finding is consistent with Yao *et al.* (2018) results. Indeed, these studiy unveiled significant alterations in the transcriptome of *Pinus tabulaeformis* during the free nuclear mitosis of megagametophyte (FNMM), between the Fertile Line (FL) and Sterile line (SL). Specifically, they identified 7174 DEGs at the three developmental stages designated as FNM1, FNM2, and FNM3, selected in accordance with prior research (Pengjun *et al.*, 2003). The investigation revealed that the most significant differences at the transcriptional level occurred during FNM2, as evidenced by the highest number of DEGs.

Our functional classification of the DEGs has revealed that the largest number of genes fell into the biological processes categories of hormones, senescence, cell cycle, stress and defence response genes, etc. These data were also supported by results

obtained by Zhang *et al.* (2020), which performed similar study, investigating the transcriptomic data of natural ovule abortion mutants (female sterile line, SL) and the wild type (female fertile line, FL) of *Pinus tabuliformis* Carr.

Coordination between auxin transport and PCD is necessary for ovule development in Ginkgo biloba

Auxin transport was investigated not only because of its crucial role in FG development, as indicated by Wang *et al.* (2021), but also because is one of the pathways significantly affected. The nucellus, a transitory tissue within the developing ovule, provides support for gametophyte, and embryo/endosperm development in the early stages of seed development. It undergoes PCD during the formation of the FG (Domínguez *et al.*, 2001). In *Arabidopsis*, a part of the nucellus undergoes degeneration before fertilisation, while the remaining portion persists until after fertilisation (Xu *et al.*, 2016). However, Wang *et al.* (2021) reported that nucellar degeneration degeneration is initiated in cells adjacent to the developing FG, in a process involving auxin influx and efflux is implicated (Wang *et al.*, 2021). Auxin efflux under the control of PIN proteins is essential to achieve appropriate auxin maxima not only in *Arabidopsis* but also in maize (McSteen and Hake, 2001; Carraro *et al.*, 2006; Gallavotti *et al.*, 2008; Křeček *et al.*, 2009; Forestan *et al.*, 2012).

The bioinformatic analysis performed has showed that six genes encoding auxin efflux carriers, identified as *Gb_23207, Gb_03217, Gb_29191, Gb_03225, Gb_02144* and *Gb_37787*, presented a higher upregulation in the PO across the time. Interestingly, only the transcript *PIN1 Gb_06199* showed a strong reduction as soon as the pollen was received, suggesting a possible post regulation mechanism. For example, MP directly targets *CUC1* and *CUC2* to control *PIN1* expression and localization during the formation of ovule primordia (Galbiati *et al.*, 2013). Moreover, results reported in Chapter I evidenced the presence of H3K27me3 mark approximately one week after pollination, allowing us to identify an interesting gene regulated by both pollination event and epigenetic mechanism. Accordingly with its expression levels, *in situ* hybridisation of *PIN1 Gb_06199* transcripts revealed its

expression pattern in PO precisely localized in all epidermal nucellus layers surrounding the FG, while in the UO not a defined signal could be identified.
The current literature reports that auxin efflux carrier PIN1 transports auxin into the nucellus, while PIN3, PIN4 and PIN7 further deliver auxin to degenerating nucellar cells and concurrently controls FG central vacuole expansion (Wang *et al.*, 2021). We hypothesize that the pollination is required to regulate *GbPIN1*, to maintain a proper and controlled auxin flow. In fact, in the *Arabidopsis*, the *pin1* mutant displays inhibited degeneration of nucellar cells, while in a *pin3/4/7* triple mutant, nucellus cell death was accelerated, but with a reduced vacuolation suggesting that nucellar auxin accumulation might promote PCD (Wang *et al.*, 2021).

The expression of senescence/PCD genes in the nucellus of PO is not surprising because at this stage the nucellus rapidly degenerates owing to the FG enlargement, and to the male gametophyte growth. The haustorial male gametophyte indeed grows and deprives of nutrients the nucellar tissue that progressively degenerates (D'Apice *et al.*, 2021). Indeed, the transcriptomic approach has showed also the presence of two senescence key genes, *Gb_13610* and *Gb_10444,* strongly upregulated in UO, codifying for cysteine proteinase and KDEL- cysteine endopeptidase (KDEL CysEP) respectively, which are notoriously to be involved in PCD (Beers *et al.*, 2000, 2004; Schaller, 2004). We deeply investigated *CYSP1 Gb_13610*, whose transcript was predominantly identified in the nucellus under both conditions. Additionally, it was observed in the flap and integument in UO. The presence of *CYSP1* in tissues undergoing PCD, especially in cells destined to collapse, is unsurprising. Indeed, this observation is in concordance with many evidences in various plant tissues, including unpollinated ovaries of *Pisum sativum* (Cercós *et al.*, 1999), the outer integument transforming into the seed coat of *Phalaenopsis* (Nadeau *et al*., 1996), and the inner integument of ovule in *Brassica napus* after fertilisation (Wan *et al.*, 2002).

Loss of cell cycle and DNA replication and damage repair regulation might be involved in PCD in unpollinated ovules

As mentioned above, when the FG is in a coenocytic stage, it undergoes the FNM process, which corresponds to continuous karyokinesis (Yao *et al.*, 2018; Zhang

et al., 2020). Thus, the observed abnormal FG development in UO samples implies a disruption in the cell cycle and regulation, leading to ovule abortion. Among the DEGs involved in cell cycle regulation we found *CDKB*, which showed a down-regulation in UO, in line with the role reported in literature. Indeed, the DNA damage signals are transmitted via several proteins, suppressing the activity of cyclin-dependent kinase to arrest the cell cycle. Expression of CDKBs is under cell-cycle control, particularly CDKB1 is expressed from late S to M phase (Sancar *et al.*, 2004) while CDKB2 is expressed from G_2 to M phase, as confirmed in experiments in rice (*Oryza sativa*) (Umeda *et al.*, 1999) tobacco (*Nicotiana tabacum*) and *Arabidopsis* (Porceddu *et al.*, 2001).

Moreover, DNA replication and damage repair-related genes showed a strong up-regulation in PO. Among them, were present several genes encoding enzyme such as primases, polymerases and methyltransferases, which were inhibited in UO. These results are in strong agreement with those found in *Pinus tabuliformis* by Zhang *et al.* (2020). In fact, integrated transcriptomic and proteomic analyses on *Pinus tabuliformis* ovules from sterile and fertile lines identified the same pathways as the most affected, with a very high similarity of the genes involved to those obtained in that study. The hypothesis proposed by Zhang *et al.* (2020) is that in the sterile line there is a greater inefficiency of DNA replication and damage repair mechanisms, leading to an accumulation of DNA damage, which is reflected in an alteration of the cell cycle and ultimately in the abortion of the ovule. The results here obtained suggest a similar mechanism.

To better investigate these processes, we detected *in situ* the fragmentation sites through TUNEL assay. Indeed, during PCD, caspases act the DNA fragmentation, which represents one of the first signs of cellular disruption (Kuthanova *et al*., 2008). In this study, we demonstrated that DNA fragmentation initiated at the basal portion of the nucellus during the UO_1 stage, preceding the visibility of the cavity, suggesting that this represents one of the principal targets of early PCD. In UO_6 and UO_8, a progressive increase of the number of apoptotic cells was found in other tissues, such as nucellus, pollen chamber and integument.

Taken together, the results support the hypothesis that pollen is crucial for ovule development in *Ginkgo*, by preventing cyto-histological disorganisation and inhibiting PCD-related genes.

The results presented here are part of a research paper currently accepted for the publication in the Journal of Experimental Botany. The title of this manuscript is "Development of pollinated and unpollinated ovules in *Ginkgo biloba*: unravelling pollen's role in ovule tissue maturation", listed in Appendix as Manuscript n. 1.

REFERENCES

Ambrose, B. A., Lerner, D. R., Ciceri, P., Padilla, C. M., Yanofsky, M. F., and Schmidt, R. J. (2000). Molecular and genetic analyses of the *silky1* gene reveal conservation in floral organ specification between eudicots and monocots. *Molecular cell*, *5*(3), 569-579.

Beers, E. P., Jones, A. M., and Dickerman, A. W. (2004). The S8 serine, C1A cysteine and A1 aspartic protease families in *Arabidopsis*. *Phytochemistry*, *65*(1), 43-58.

Beers, E. P., Woffenden, B. J., and Zhao, C. (2000). Plant proteolytic enzymes: possible roles during programmed cell death. *Programmed cell death in higher plants*, 155-171.

Carraro, N., Forestan, C., Canova, S., Traas, J., and Varotto, S. (2006). *ZmPIN1a* and *ZmPIN1b* encode two novel putative candidates for polar auxin transport and plant architecture determination of maize. *Plant physiology*, *142*(1), 254-264.

Ceccato, L., Masiero, S., Roy, D. S., Bencivenga, S., Roig-Villanova, I., Ditengou, F. A., Palme, K., Simon, R., and Colombo, L. (2013). Maternal control of PIN1 is required for female gametophyte development in *Arabidopsis*. *PloS one*, *8*, e66148.

Cercós, M., Santamarıa, S., and Carbonell, J. (1999). Cloning and characterization of *TPE4A*, a thiol-protease gene induced during ovary senescence and seed germination in pea. *Plant Physiology*, *119*(4), 1341-1348.

Chen, F., Zhang, X., Liu, X., and Zhang, L. (2017). Evolutionary analysis of MIKCc-type MADS-box genes in gymnosperms and angiosperms. *Frontiers in Plant Science*, *8*, 895.

Cucinotta, M., Colombo, L., and Roig-Villanova, I. (2014). Ovule development, a new model for lateral organ formation. *Frontiers in Plant Science*, *5*, 117.

Cucinotta, M., Di Marzo, M., Guazzotti, A., de Folter, S., Kater, M. M., and Colombo, L. (2020). Gynoecium size and ovule number are interconnected traits that impact seed yield. *Journal of Experimental Botany*, *71*(9), 2479-2489.

D'Apice, G., Moschin, S., Araniti, F., Nigris, S., Di Marzo, M., Muto, A., Banfi, C., Bruno, L., Colombo, L., and Baldan, B. (2021). The role of pollination in controlling *Ginkgo biloba* ovule development. *New Phytologist*, *232*(6), 2353-2368.

D'Apice, G., Moschin, S., Nigris, S., Ciarle, R., Muto, A., Bruno, L., and Baldan, B. (2022). Identification of key regulatory genes involved in the sporophyte and gametophyte development in *Ginkgo biloba* ovules revealed by in situ expression analyses. *American Journal of Botany*, *109*(6), 887-898.

Dominguez, F., Moreno, J., and Cejudo, F. J. (2001). The nucellus degenerates by a process of programmed cell death during the early stages of wheat grain development. *Planta*, *213*(3).

Drews, G. N., and Koltunow, A. M. (2011). The female gametophyte. *The Arabidopsis book/American Society of Plant Biologists*, *9*.

Figueiredo, D. D., Batista, R. A., Roszak, P. J., Hennig, L., and Köhler, C. (2016). Auxin production in the endosperm drives seed coat development in *Arabidopsis*. *Elife*, *5*, e20542.

Figueiredo, D. D., and Köhler, C. (2018). Auxin: a molecular trigger of seed development. *Genes and development*, *32*(7-8), 479-490.

Forestan, C., Farinati, S., and Varotto, S. (2012). The maize *PIN* gene family of auxin transporters. *Frontiers in plant science*, *3*, 16.

Friedman, W. E. (1987). Growth and development of the male gametophyte of *Ginkgo biloba* within the ovule (in vivo). *American Journal of Botany*, *74*(12), 1797-1815.

Galbiati, F., Sinha Roy, D., Simonini, S., Cucinotta, M., Ceccato, L., Cuesta, C., Simaskova, M., Benkova, E., Kamiuchi, Y., Aida, M., Weijers, D., Simon, R., Masiero, S. and Colombo, L. (2013). An integrative model of the control of ovule primordia formation. *The Plant Journal*, *76*(3), 446-455.

Gallavotti, A., Yang, Y., Schmidt, R. J., and Jackson, D. (2008). The relationship between auxin transport and maize branching. *Plant physiology*, *147*(4), 1913-1923.

Gao, Z., Daneva, A., Salanenka, Y., Van Durme, M., Huysmans, M., Lin, Z., De Winter, F., Vanneste, S., Karimi, M., Van de Velde, J., Vadepoele, K., Van de Walle, D., Dewettinck, K., Lambrecht, B. N., and Nowack, M. K. (2018). KIRA1 and ORESARA1 terminate flower receptivity by promoting cell death in the stigma of *Arabidopsis*. *Nature plants*, *4*(6), 365-375.

Gao, C., Yang, R., and Yuan, D. (2017). Characteristics of developmental differences between fertile and aborted ovules in *Camellia oleifera*. *Journal of the American Society for Horticultural Science*, *142*(5), 330-336.

Jin, B., Wang, D., Lu, Y., Jiang, X. X., Zhang, M., Zhang, L., and Wang, L. (2012). Female short shoot and ovule development in *Ginkgo biloba* L. with emphasis on structures associated with wind pollination. *International Scholarly Research Notices*, *2012*.

Křeček, P., Skůpa, P., Libus, J., Naramoto, S., Tejos, R., Friml, J., and Zažímalová, E. (2009). The PIN-FORMED (PIN) protein family of auxin transporters. *Genome biology*, *10*(12), 1-11.

Kuthanova, A., Opatrny, Z., and Fischer, L. (2008). Is internucleosomal DNA fragmentation an indicator of programmed death in plant cells?. *Journal of experimental botany*, *59*(8), 2233-2240.

Li, J., Wu, Z., Cui, L., Zhang, T., Guo, Q., Xu, J., Jia, L., Lou, Q., Huang, S., Li, Z., and Chen, J. (2014). Transcriptome comparison of global distinctive features between pollination and parthenocarpic fruit set reveals transcriptional phytohormone cross-talk in cucumber (*Cucumis sativus* L.). *Plant and Cell Physiology*, *55*(7), 1325-1342.

McSteen, P., and Hake, S. (2001). *barren inflorescence2* regulates axillary meristem development in the maize inflorescence. *Development*, *128*(15), 2881–2891.

Nadeau, J. A., Zhang, X. S., Li, J., and O'Neill, S. D. (1996). Ovule development: identification of stage-specific and tissue-specific cDNAs. *The Plant Cell*, *8*(2), 213-239.

Pengjun, C., Fenglan, L., and Caixia, Z. (2003). Anatomic study of female sterility of *Pinus tabulaeformis* Carr. *Forest Ecosystems*, *5*(1), 13-19.

Porceddu, A., Stals, H., Reichheld, J. P., Segers, G., De Veylder, L., de Pinho Barrôco, R., Casteels, P., Montagu, M. V., Inzé, D., and Mironov, V. (2001). A plant-specific cyclin-dependent kinase is involved in the control of G2/M progression in plants. *Journal of Biological Chemistry*, *276*(39), 36354-36360.

Prior, N., Little, S. A., Boyes, I., Griffith, P., Husby, C., Pirone-Davies, C., Stevenson, D. W., Tomlinson, P. B., and von Aderkas, P. (2019). Complex reproductive secretions occur in all extant gymnosperm lineages: a proteomic survey of gymnosperm pollination drops. *Plant reproduction*, *32*, 153-166.

Rudall, P. J. (2021). Evolution and patterning of the ovule in seed plants. *Biological Reviews*, *96*(3), 943-960.

Sancar, A., Lindsey-Boltz, L. A., Ünsal-Kaçmaz, K., and Linn, S. (2004). Molecular mechanisms of mammalian DNA repair and the DNA damage checkpoints. *Annual review of biochemistry*, *73*(1), 39-85.

Schaller, A. (2004). A cut above the rest: the regulatory function of plant proteases. *Planta*, *220*, 183-197.

Schneider, C. A., Rasband, W. S., and Eliceiri, K. W. (2012). NIH Image to ImageJ: 25 years of image analysis. *Nature methods*, *9*(7), 671-675.

Shinozaki, Y., Ezura, H., and Ariizumi, T. (2018). The role of ethylene in the regulation of ovary senescence and fruit set in tomato (*Solanum lycopersicum*). *Plant signaling and behavior*, *13*(4), e1146844.

Shigyo, M., Hasebe, M., and Ito, M. (2006). Molecular evolution of the AP2 subfamily. *Gene*, *366*(2), 256-265.

Sun, H., Shi, T., Song, J., Xu, Y., Gao, Z., Song, X., Ni, Z. and Cai, B. (2016). Pistil abortion in Japanese apricot (*Prunus mume* Sieb. et Zucc.): isolation and functional analysis of *PmCCoAOMT* gene. *Acta Physiologiae Plantarum*, *38*, 1-11.

Umeda, M., Umeda-Hara, C., Yamaguchi, M., Hashimoto, J., and Uchimiya, H. (1999). Differential expression of genes for cyclin-dependent protein kinases in rice plants. *Plant Physiology*, *119*(1), 31-40.

Van Doorn, W. G., and Woltering, E. J. (2008). Physiology and molecular biology of petal senescence. *Journal of experimental botany*, *59*(3), 453-480.

Van Durme, M., Olvera-Carrillo, Y., Pfeiffer, M. L., Doll, N. M., De Winter, F., Lin, Z., and Nowack, M. K. (2023). Fertility loss in senescing *Arabidopsis* ovules is controlled by the maternal sporophyte via a NAC transcription factor triad. *Proceedings of the National Academy of Sciences*, *120*(25), e2219868120.

Wan, L., Xia, Q., Qiu, X., and Selvaraj, G. (2002). Early stages of seed development in *Brassica napus*: a seed coat-specific cysteine proteinase associated with programmed cell death of the inner integument. *The Plant Journal*, *30*(1), 1-10.

Wang, J., Guo, X., Xiao, Q., Zhu, J., Cheung, A. Y., Yuan, L., Vierling, E., and Xu, S. (2021). Auxin efflux controls orderly nucellar degeneration and expansion of the female gametophyte in *Arabidopsis*. *New Phytologist*, *230*(6), 2261-2274.

Wetzstein, H. Y., Yi, W., Porter, J. A., and Ravid, N. (2013). Flower position and size impact ovule number per flower, fruitset, and fruit size in pomegranate. *Journal of the American Society for Horticultural Science*, *138*(3), 159-166.

Xu, W., Fiume, E., Coen, O., Pechoux, C., Lepiniec, L., and Magnani, E. (2016). Endosperm and nucellus develop antagonistically in *Arabidopsis* seeds. *The Plant Cell*, *28*(6), 1343-1360.

Yadegari, R., and Drews, G. N. (2004). Female gametophyte development. *The Plant Cell*, *16*(suppl_1), S133-S141.

Yamada, T., Hirayama, Y., Imaichi, R., and Kato, M. (2008). *AINTEGUMENTA* homolog expression in *Gnetum* (gymnosperms) and implications for the evolution of ovulate axes in seed plants. *Evolution and development*, *10*(3), 280-287.

Yang, L., Wu, Y., Yu, M., Mao, B., Zhao, B., and Wang, J. (2016). Genome-wide transcriptome analysis of female-sterile rice ovule shed light on its abortive mechanism. *Planta*, *244*, 1011-1028.

Yao, Y., Han, R., Gong, Z., Zheng, C., and Zhao, Y. (2018). RNA-seq analysis reveals gene expression profiling of female fertile and sterile ovules of *Pinus tabulaeformis*

Carr. during free nuclear mitosis of the female gametophyte. *International Journal of Molecular Sciences*, *19*(8), 2246.

Zhang, M., Li, W., Feng, J., Gong, Z., Yao, Y., and Zheng, C. (2020). Integrative transcriptomics and proteomics analysis constructs a new molecular model for ovule abortion in the female-sterile line of *Pinus tabuliformis* Carr. *Plant Science*, *294*, 110462.

Zhang, M., and Zheng, C. X. (2016). Archegonium and fertilisation in Coniferopsida. *Trees*, *30*, 75-86.

Zumajo-Cardona, C., Little, D. P., Stevenson, D., and Ambrose, B. A. (2021). Expression analyses in *Ginkgo biloba* provide new insights into the evolution and development of the seed. *Scientific Reports*, *11*(1), 21995.

CHAPTER IV

Pollination event affects auxin and cytokinin accumulation and distribution in *Ginkgo biloba* ovule

ABSTRACT

Female gametophyte development is controlled by an intricate molecular network, in which plant hormones play a key role. In particular, auxin and cytokinin hormones are crucial during ovule development and after fertilisation for its transformation into seed. All these mechanisms are widely studied in angiosperms, especially in model species *Arabidopsis thaliana*, but they are poorly explored in gymnosperms. In this scenario, we extended the studies on *Ginkgo biloba*, whose ovules present interesting and primitive characteristics and has been extensively described. In *Ginkgo*, pollination and fertilisation events are separated by a long interval (i.e. 4-5 months), in which ovule continues to grow and female gametophyte differentiation occurs, suggesting that pollination event could trigger the signal for ovule transformation in seed. In this context, pollinated and unpollinated ovules, the last ones collected from female plants geographically isolated from male plants, were used. For both condition, three different stages were used: 1, 6 and 8 days after the end of pollination drop emission. Previous transcriptomic results showed that hormone metabolism pathway is strongly modulated by pollination event. Here we focused our attention on auxin and cytokinin metabolism, given their important involvement in female gametophyte development. Immunolocalisations of indol-3-acetic acid and *trans*-zeatin riboside were performed in both pollinated and unpollinated ovules, in order to evaluate if pollen arrival could affect their accumulation and distribution. The obtained results highlighted a strictly relation between auxin and cytokinin distribution and pollination event before the fertilisation in *Ginkgo*.

INTRODUCTION

Auxins and cytokinins (CKs) are plant hormones essential in almost every process of plant development (Paque and Weijers, 2016; Terceros *et al.*, 2020), for this reason they are widely studied in the field of developmental biology.

For example, auxin controls plant reproduction and the development of female and male reproductive organs in *Arabidopsis thaliana* (Larsson *et al.*, 2017). This evidence becomes even clearer when considering the genes involved in biosynthesis, transport and signalling that are expressed at early and late stages of ovule development. In particular, during the early stages of female gametophyte (FG) formation, the expression of *TRYPTOPHAN AMINOTRANSFERASE OF ARABIDOPSIS 1* (*TAA1*), whose enzyme is involved in the biosynthesis of free IAA^- through a tryptophan-dependent pathway, is reported in the chalazal region, together with the expression of genes encoding PIN-FORMED proteins (PINs), the polar auxin transporters (Pagnussat *et al.*, 2009; Nole-Wilson *et al.*, 2010; Ceccato *et al.*, 2013; Serbes *et al*., 2019), suggesting a central role for auxin in the initiation of integuments. *PINs* and *YUCCA* (*YUC*), which converts the indole-3-pyruvic acid (IPA) in indole-3-acetic acid, are expressed along the nucellus (Pagnussat *et al.*, 2009; Bencivenga *et al.*, 2011; Ceccato *et al.*, 2013), where was found also the activity of *DR5pro::GUS* auxin reporter gene (Pagnussat *et al.*, 2009; Bencivenga *et al.*, 2011), highlighting once again the involvement of auxin in ovule development (**Fig. 1**). In addition, an auxin gradient inside the FG allows the differentiation and specification of the cells that make up the embryo sac. The maximum auxin signal was detected in synergids and egg cells, decreasing progressively to the lowest concentration in the antipodal cells (Pagnussat *et al.*, 2009). After fertilisation, auxin is strongly involved in the proper seed development, indeed mutants defective of auxin-related genes show dramatic embryo defects (Möller and Weijers, 2009). The increased auxin signalling in seeds has been observed using auxin reporter systems (Dorcey *et al.*, 2009). Moreover, the application of exogenous auxin in many species, including *Arabidopsis*, results in the production of parthenocarpic fruits (Vivian-Smith and Koltunow, 1999; Dorcey *et al.*, 2009; Pandolfini, 2009), suggesting that auxin, along with fertilisation, may be the trigger for seed and fruit development (Cao *et al*., 2020).

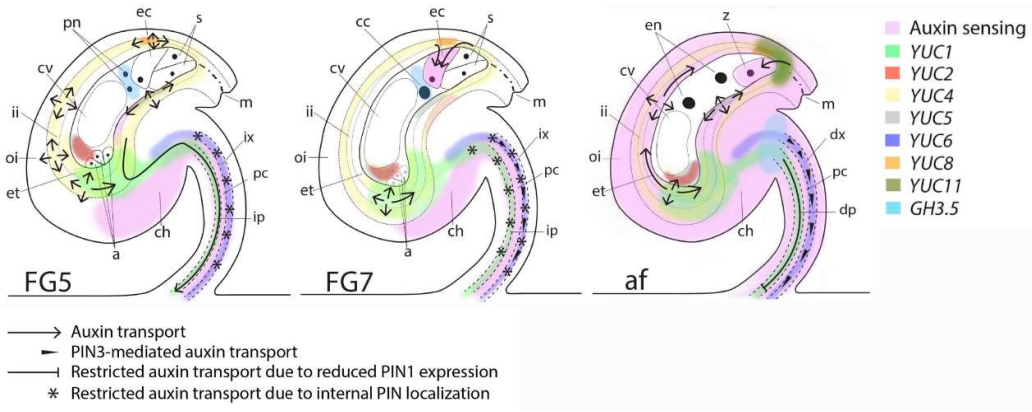

Fig. 1. Image modified from Larsson *et al.* (2017). Schematic model of auxin biosynthesis, transport and perception before anthesis (FG5), at anthesis (FG7) and shortly after fertilisation (af). In the first stage, auxin biosynthesis is highlighted by *YUC* expression in the inner integuments, in the FG and in the funicular provasculature. Transport (via PIN1, PIN3 and PIN6) occurs through the immature xylem (stars). In the second stage, the transport is directed to PIN1 in the immature phloem (stars) and to PIN3 in the immature xylem (arrowheads). At the final stage, all sporophytic tissues can sense auxin, whereas auxin biosynthesis (via *YUC5* and *YUC11*) is restricted to the micropylar pole of the integuments. Transport is reduced by low expression levels of PIN1 and PIN6 in the phloem and xylem, whereas PIN3 ensures auxin transport in the xylem to the integuments. a: antipodal cells; cc: central cell; ch: chalaza, cv: central vacuole; dp: differentiating phloem; dx: differentiating xylem; ec: egg cell; en: endosperm; et: endothelium; ii: inner integument; ip: immature phloem; ix: immature xylem; m: micropyle; oi: outer integument; pc: procambium; pn: polar nuclei; s: synergid cells; z: zygote.

CKs represent a class of phytohormones particularly involved in plant growth and development (Terceros *et al.*, 2020). They are commonly divided into two major groups based on their chemical structure: adenine and phenylurea derivatives (Mok and Mok, 2001). Indeed, in 1955, an unrelated compound identified as *N/N´*-diphenylurea (DPU) was discovered to have growth-promoting properties, followed by several other phenylurea compounds. However, their activity is generally lower compared to adenine-type CKs, usually identified as natural CKs (Mok and Mok, 1994). In particular, they are further classified in isoprenoid and aromatics based on their N^6-side chain (Mandal *et al.*, 2022). Isoprenoid CKs, which include derivatives of isopentenyladenine, *trans*-zeatin, *cis*-zeatin, and dihydrozeatin type, are more common in nature. In particular, isopentenyladenine and *trans*-zeatin are the most prevalent forms, together with their sugar conjugates, and show higher activity than *cis*-zeatin, although the species, tissue and stage of development should also be considered (Mok and Mok, 2001; Sakakibara, 2005). In recent years, the role of CKs in plant reproductive biology has been increasingly studied. Indeed, CKs are crucial in

ovule initiation and patterning, but also in seed formation (Bartrina *et al.*, 2011; Barro-Trastoy *et al.*, 2020). For example, reduced initiation of ovule primordia was observed in mutants in which cytokinins synthesis or perception is affected (Cucinotta *et al.*, 2020). In addition, the triple CK receptor mutant *ahk2-2 ahk3-3 cre1-12/ahk4* show impairment of integument initiation, arrest of gametogenesis or embryo sac with only one or two nuclei (Kinoshita-Tsujimura *et al.*, 2011; Bencivenga *et al.*, 2012; Cheng *et al.*, 2013; Zhang *et al*., 2022). Similarly to auxin, precisely in the embryo sac, CKs are essential in establishing cell identity. The balance between biosynthesis, degradation and signalling components is different and characterises the fate of each cell type. Genes involved in CKs biosynthesis and degradation, such as *ISOPENTENYLTRANSFERASE 1* (*IPT1*) and *CYTOKININ OXIDASE 7* (*CKX7*) are exclusive of cells belonging to the micropylar pole (synergid cells and egg cell). *CKX7* expression is regulated by transcription factors (TFs) such as *VERDANDI* (*VDD*), *VALKYRIE* (*VAL*) and *REPRODUCTIVEMERISTEM* (*REM*), which are expressed in synergid cells (Terceros *et al.*, 2020). Concerning signalling components, *ARABIDOPSIS THALIANA HISTIDINE PHOSPHOTRANSFER PROTEINS* (*AHPs*), such as *AHP2* and *AHP5*, were detected in all the gametophytic cells, while *AHP1* was expressed in synergids and central cell, and *AHP3* was located only in the central cell. In addition, the cytokinin-independent kinase CKI1 activity was confined in antipodals and central cells and interacts with AHPs (Terceros *et al.*, 2020).

Even in the sporophytic tissues of the ovule the expression of genes involved in CKs biosynthesis and degradation was detected. More in details, in *Arabidopsis LONELY GUY 3* (*LOG3*) was expressed in the funiculus, while *LOG4* in the integuments and in the chalaza. Lastly, the content of CKs is controlled by *ALTERED MERISTEM PROGRAM 1* (*AMP1*), whose expression was found in integuments, synergids and egg cell (Terceros *et al.*, 2020; **Fig. 2**).

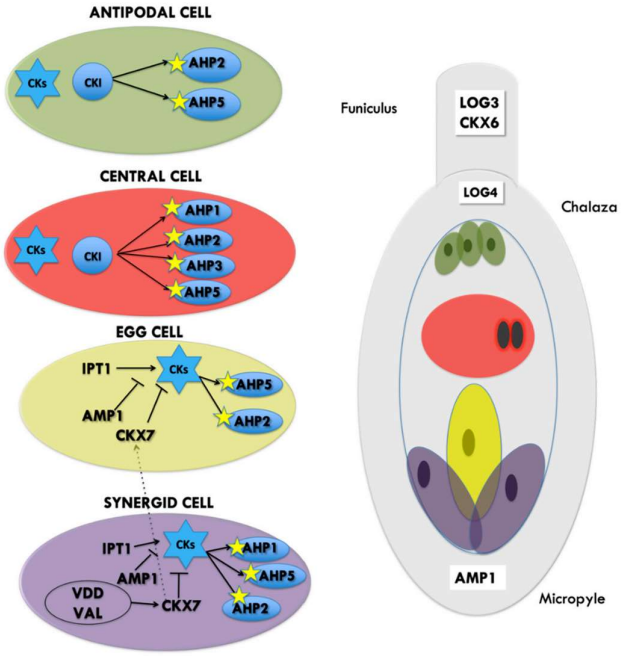

Fig. 2. Image from Terceros *et al.* (2020). Role of CKs in embryo sac development in *Arabidopsis*. Grey: sporophytic tissues; green: antipodal cells; red: central binucleated cell; yellow: egg cell; purple: synergid cells; yellow stars: phosporyl group.

Furthermore, CKs are known to be closely involved in cell cycle regulation. Indeed, they are implicated in the control of both G_1/S and G_2/M transitions (Schaller *et al.*, 2014). The G_1/S transition requires the interaction between the cyclin-dependent kinases A (CDKA) and D-type cyclins (CYCDs) to form the CDKA/CYCD complex (Schaller *et al.*, 2014), and three different *CYCD3* are induced by CKs activity. However, the main role of CKs seems to be related to the entry into M-phase, since in tobacco culture cells the G_2/M transition is inhibited by lovastatin, a substance which block CKs biosynthesis (Schaller *et al.*, 2014; Shimotohno *et al.*, 2021).

There also appears to be a link between the pollination event and the accumulation of CKs in the ovules, although this has not been fully investigated. Indeed, unpollinated maize ovules are not able to accumulate CKs, suggesting that the pollination process may be linked, in caryopsis, to *de novo* synthesis and/or CKs transfer from the maternal plant (Rijavec *et al.*, 2011).

However, all the information concern *Arabidopsis* and other model species, while these topics are still little studied in gymnosperms plants, particularly in *Ginkgo*.

Here, for the first time, we analysed the auxin and *trans*-zeatin distribution during the ovule development in a gymnosperm plant, providing evidence that pollen signal affects hormones tissue localization also in *Ginkgo*.

MATERIAL AND METHODS

Ovules collection

Pools of pollinated (PO) and unpollinated (UO) ovules, were collected during the pollination timeframe (March and April 2023). PO were collected from ten female plants at the Botanical Garden of the University of Calabria, Rende (CS), Italy, while UO were collected from female and isolated plants, located in Montalto Uffugo (CS), Italy. Fifty ovules were collected at each selected stage: 1 (UO_1, PO_1), 6 (UO_6, PO_6), and 8 days (UO_8, PO_8) after the end of the pollination drop emission, respectively.

Indol-3-acetic acid immunolocalisation

Twenty ovules at different stages of development were fixed in a 3% (w/v) paraformaldehyde and 0.5% (v/v) glutaraldehyde mixture in PBS buffer (135 mM NaCl, 2.7 mM KCl, 1.5 mM KH_2PO_4, 8mM K_2HPO_4, pH 7.3) for 3 h at 4°C, as described in Chiappetta *et al.* (2009). Sections of 30-50 µm were cut by a vibratome (Leica VT1000E, Germany) and incubated overnight at 4°C with anti-auxin mouse monoclonal primary antibody (clone 1E11-C11, Sigma-Aldrich, Milan, Italy) diluted 1:250 in PBS/BSA solution (10 mM phosphate solution, 0.8% bovine serum albumin). Subsequently, sections were washed three times for 10 minutes with 1XPBS and then incubated with the secondary antibody (anti-mouse IgG alkaline phosphatase conjugate; Promega Italia, Milan, Italy) diluted 1:150 in 1XPBS solution for 3 h at room temperature. After washing, sections were developed with NBT (4-Nitro blue tetrazolium chloride) and BCIP (5-bromo-4-chloro-3-indolylphosphate) mix for 10 min, rinsed with blocking buffer (100 mM Tris-HCl, pH 8.0; 1 mM EDTA), mounted on slides and immediately observed and photographed. To verify the efficiency of the experiment, some sections were processed with the omission of the primary anti-auxin

antibody (CTRL samples). Histological sections were observed by Leica DRMB microscope and images were taken with the digital camera Leica DFC 320 (Leica, Milan, Italy).

trans-zeatin immunolocalisation

Twenty ovules at different stages of development were treated as reported above. Sections were incubated overnight at 4°C with anti-rabbit polyclonal primary antibody *trans*-zeatin riboside (AGRIAS09429, Agrisera, Sweden), diluted 1:150 in PBS/BSA solution. Notably, the antibody presents cross-reactivity only with the free riboside form of zeatin. Subsequently, sections were incubated with the secondary antibody (anti-rabbit IgG alkaline phosphatase conjugate; Promega Italia, Milan, Italy) diluted 1:100 in 1XPBS solution for 3 h at room temperature.

Multiple immunolocalisation of auxin and trans-zeatin

Ten ovules at PO_6 and UO_6 stage were firstly collected, fixed and treated as reported above. Sections were incubated overnight at 4°C with a mixture of anti-auxin and *trans*-zeatin riboside primary antibodies diluted 1:250 and 1:150 in PBS/BSA solution respectively. The next day, sections were washed three times for 10 minutes in 1XPBT (1X PBS and 0.1% (v/v) Tween-20) and incubated with a mixture of the secondary antibodies (Donkey anti-Mouse IgG (H+L) Highly Cross-Adsorbed Secondary Antibody, Alexa Fluor™ 488, Invitrogen; Donkey anti-Rabbit IgG (H+L) Highly Cross-Adsorbed Secondary Antibody, Alexa Fluor™ 647, Invitrogen) diluted both 1:100 in 1XPBT solution for 3 h at room temperature in the dark. Then, the sections were washed three times for 10 minutes in 1XPBT, mounted on slides and observed by a confocal scanning laser microscope (Leica TCS SP8 inverted). As negative control, some sections were not incubated with primary antibodies mix.

RESULTS AND DISCUSSION

Auxin distribution pattern is affected by pollination failure

Several process, such as the switch from ovule to seed or from gynoecium to fruit, require a tight communication between male and female reproductive organs but also between sporophytic and gametophytic tissues. In this context, auxin represent an essential molecule, widely studied in *Arabidopsis* and different species (Larsson *et al.*, 2017), but the spatio-temporal details of its localisation in gymnosperms reproductive structures are still elusive. Here, for the first time, we proposed a time course of auxin in three different developmental stage of *Ginkgo* ovules collected under pollination and non-pollination conditions.

At both PO_1 and UO_1 stages, the auxin distribution were comparable in all tissues, suggesting that the possible presence of pollen has not affected the pattern of auxin distribution at this stage (**Figure 3**). A widespread signal was found in the integument of both samples, in particular in the layers that will differ in *endotesta* (**Figure 3A, E**). At the micropyle level, the signal mainly affected the most apical area and the pollen chamber, where it was concentrated in the innermost row of cells (**Figure 3B, D, H**). At the pollination time, the pollen chamber has reached its maximum volume and the signal is concentrated mainly in highly vacuolated isodiametric cells resulting from division and elongation of the distal micropylar parietal tissue cells (Douglas *et al.*, 2007). In the nucellus, the signal was concentrated in the most central part, particularly in the distal micropylar tissue, whose cells elongate and divide to increase the volume of the pollen chamber (Douglas *et al.*, 2007; **Figure 3A, E-F**). In addition, a precise cluster of labelled cells was found around the female gametophyte, which is in a coenocytic stage and undergoing free nuclear divisions (Douglas *et al.*, 2007; **Figure 3C, G**). In the *tapetum*, however, there was a progressive reduction in the number of labelled cells (**Figure 3C, G**).

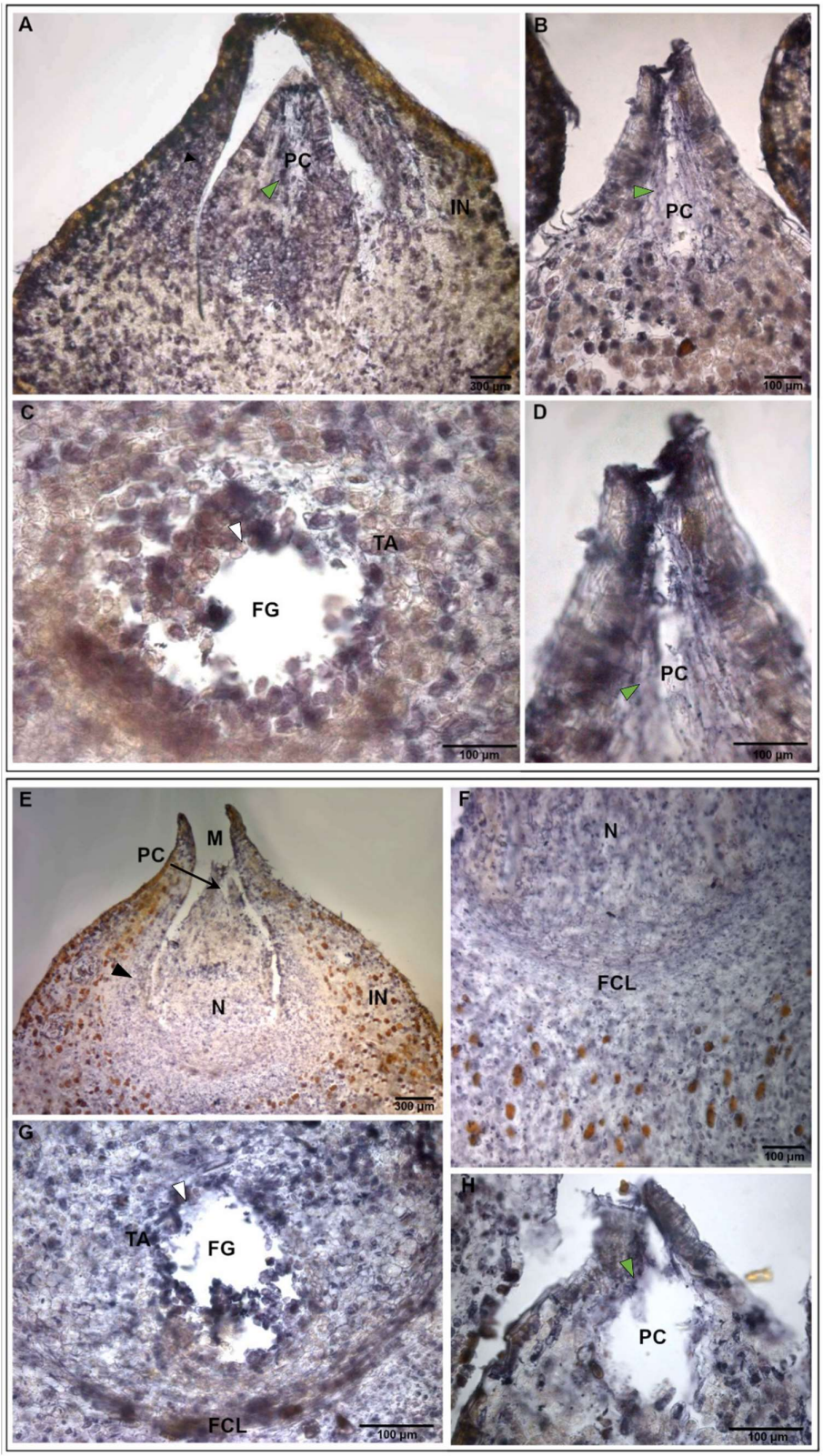

Figure 3. Spatio-temporal distribution of free Indole-3-acetic acid (IAA) 1 day after the end of drop emission in pollinated and unpollinated *Ginkgo biloba* ovules. Immunoreaction is evidenced as purple-violet staining. The signal was detected in longitudinal histological sections of pollinated (PO) **(A-D)** and unpollinated ovules (UO) **(E-H)** at stage 1. Magnifications of pollinated **(B-D)** and unpollinated **(F-H)** ovules. FCL, flattened-cells layer; FG, female gametophyte; IN, integument; M, micropyle; N, nucellus; PC, pollen chamber. White arrow heads indicate the signal in female gametophyte and *tapetum*; black arrow heads indicate the signal in the innermost layer of integument, green arrow heads indicate the signal in the pollen chamber. **(A, E)** Scale bars: 300 µm; **(B-D, F-H)** Scale bars: 100 µm.

However, there were notable differences at later stages. Indeed, 6 days after the end of drop emission in pollinated ovules, PO_6 stage, the signal was evident in the integument, especially in the layer that will differ in the *endotesta*. In the layers that will differ in *sarcotesta* and *sclerotesta*, the signal did not present specific domains, but appeared as spots of marked cells (**Figure 4A**). In addition, the signal was observed also in the most apical part of the micropyle (**Figure 4B**), and, in the nucellus, in the distal micropylar tissue (**Figure 4B-C**). In fact, after pollination, the cells of this tissue stop dividing and undergo to radial and asymmetric enlargement, probably causing, as a physical effect, the bending of the pollen chamber (Douglas *et al.*, 2007). Furthermore, a circumscribed signal was also found in the layers of flattened-cells (**Figure 4C**). The cells of this tissue are organised in two or three layers before pollination, but after pollination numerous divisions occur and at this stage the tissue is composed of twenty or more layers (Douglas *et al.*, 2007). The signal around the gametophyte was still clearly visible, strongly suggesting an auxin pulse in this area, probably due to the division of the gametophyte, which is increasing in size (**Figure 4B-C**). At this stage of development, the female gametophyte is multinucleate and still surrounded by the *tapetum*, which will begin a process of degeneration in the following stages. Finally, a signal was often visible in the flattened-cells layer and in the flap, representing the abscission area of the ovule, which could indicate the presence of a possible cross-talk with ethylene (**Figure 4A**).

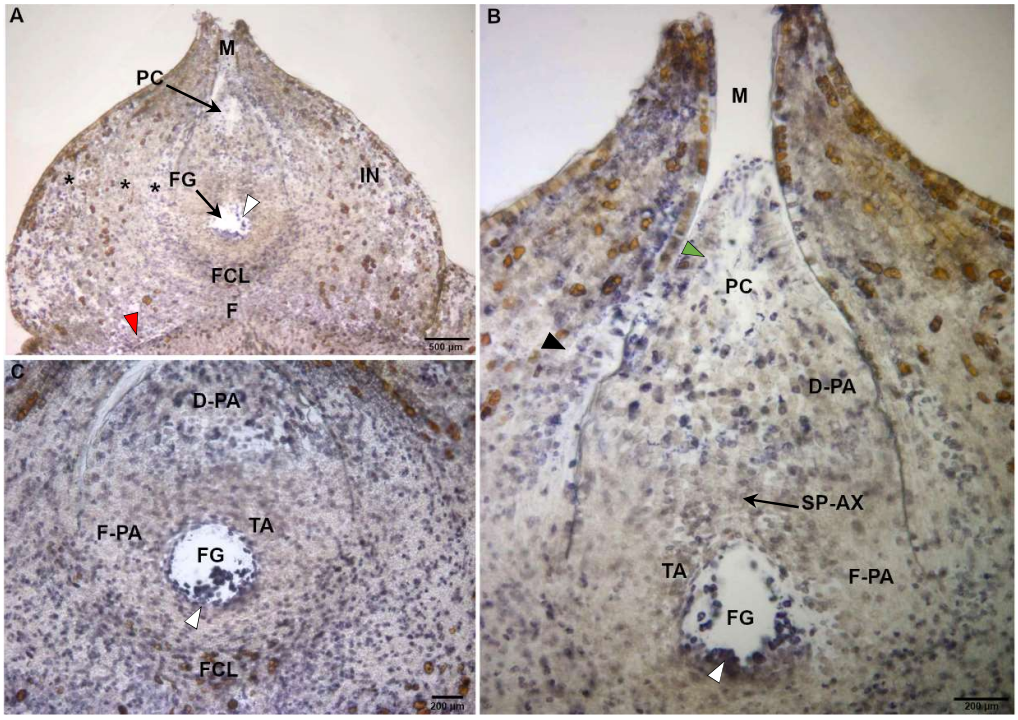

Figure 4. Spatio-temporal distribution of free Indole-3-acetic acid (IAA) 6 days after the end of drop emission in pollinated *Ginkgo biloba* ovules. Immunoreaction is evidenced as purple-violet staining. The signal was detected in longitudinal histological sections of pollinated ovules (PO) at stage 6. Magnifications of pollen chamber **(B)** female gametophyte **(C, D)** and nucellus **(E)**. D-PA: distal micropylar parietal tissue; FCL: flattened-cells layer; F-PA: flanking parietal tissue; FG: female gametophyte; IN: integument; M: micropyle; PC: pollen chamber; SP-AX: sporangial axial column of cells; TA: *tapetum*. Black stars indicate the three different integument layers; red arrow head indicates the signal in the flap; white arrow heads indicate the signal in female gametophyte and *tapetum*; black arrow head indicates the signal in the innermost layer of integument, green arrow head indicates the signal in the pollen chamber. **(A)** Scale bar: 500 µm; **(B-C)** Scale bar: 200 µm.

At the last stage (PO_8), 8 days after the end of drop emission in pollinated ovules, the results were almost comparable to those obtained for the previous stage at histological level (**Figure 5A**). However, a decrease in the signal was observed in the cells of the micropylar canal (**Figure 5D**). In fact, although the histological area was unchanged, the number of labelled cells was reduced. Furthermore, the pollen chamber was almost completely collapsed and the signal was observed in the innermost part (**Figure 5B**). In the distal micropylar tissue, the signal appeared unchanged, indicating that the cells are probably continuing the process of radial enlargement (**Figure 5D**). The immunoreaction was still observed around the gametophyte, highlighting the key role of auxin in its development (**Figure 5E**).

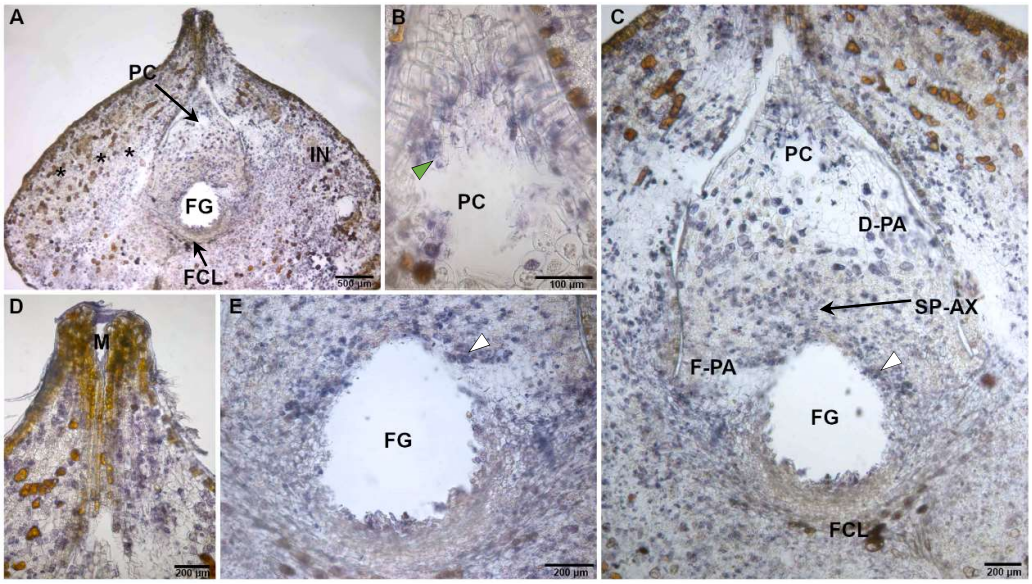

Figure 5. Spatio-temporal distribution of free Indole-3-acetic acid (IAA) 8 days after the end of drop emission in pollinated *Ginkgo biloba* ovules. Immunoreaction is evidenced as purple-violet staining. The signal was detected in longitudinal histological sections of pollinated ovules (PO) at stage 8. Magnifications of pollen chamber **(B)**, micropyle **(C)**, female gametophyte **(D)** and nucellus **(E)**. D-PA: distal micropylar parietal tissue; FCL: flattened-cells layer; F-PA: flanking parietal tissue; FG: female gametophyte; IN: integument; M: micropyle; PC: pollen chamber; SP-AX: sporangial axial column of cells. Black stars indicate the three different integument layers; green arrow head indicates the signal in the pollen chamber, white arrow heads indicate the signal in female gametophyte and *tapetum*. **(A)** Scale bar: 500 µm; **(C-E)** Scale bars: 200 µm; **(B)** Scale bar: 100 µm.

A different pattern was observed in UO. In this case, the pattern of auxin distribution appeared more widespread than in pollinated ovules. In particular, 6 days after the end of drop emission in unpollinated ovules, UO_6 stage (**Figure 6**), a laceration was clearly visible at the base of the nucellus, in the flattened-cells layers, which appeared to be marked along all its borders (**Figure 6A, D**). The *tapetum* was strongly stained, but a cluster of marked cells around the gametophyte was not visible if compared to PO_6 (**Figure 6B**). The integument was extensively stained, unlike PO_6 (**Figure 6A, C, E**), although the layer most affected by the immunoreaction was the innermost one. In addition, a large presence of phenols characterises the integument, compared to PO_6 (**Figure 6A**).

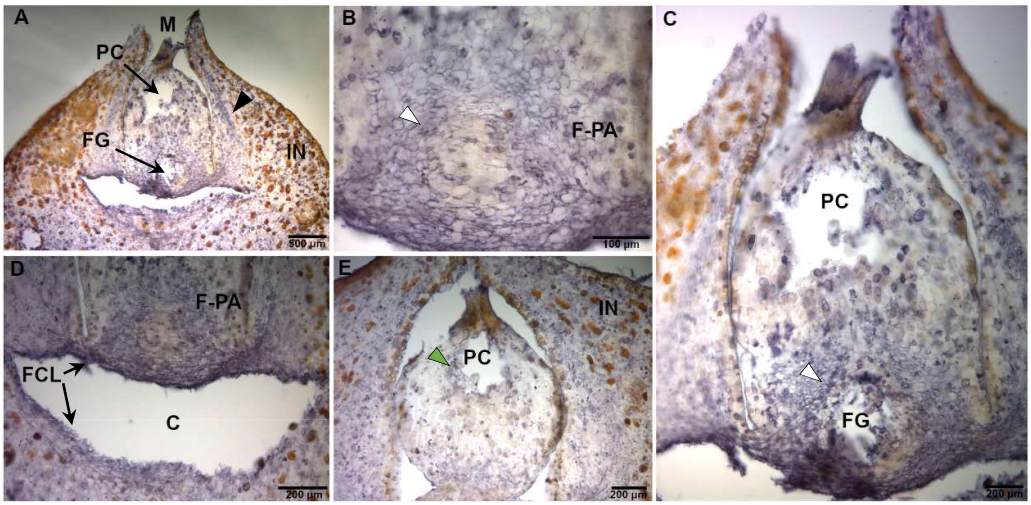

Figure 6. Spatio-temporal distribution of free Indole-3-acetic acid (IAA) 6 days after the end of drop emission in unpollinated *Ginkgo biloba* ovules. Immunoreaction is evidenced as purple-violet staining. The signal was detected in longitudinal histological sections of unpollinated ovules (UO) at stage 6. Magnifications of female gametophyte **(B),** nucellus **(C),** cavity **(D)** and pollen chamber **(E)**. C: cavity; F-PA: flanking parietal tissue; FG: female gametophyte; IN: integument; M: micropyle; PC: pollen chamber. White arrow heads indicate the signal in female gametophyte and *tapetum*; black arrow heads indicate the signal in the innermost layer of integument, green arrow heads indicate the signal in the pollen chamber. **(A)** Scale bar: 500 µm; **(C-E)** Scale bars: 200 µm; **(B)** Scale bar: 100 µm.

At stage UO_8 (**Figure 7**), the chalazal tissue was collapsed and the cells delimiting the nucellus showed an unusual shape and are marked in the walls (**Figure 7A, B**). Indeed, the morphological changes of both the chalazal tissue and the *tapetum* prevented their distinction and consequently the identification of the specific signal domain (**Figure 7B**). However, the integument appeared completely marked, in particular the *endotesta* cells were elongated and flattened (**Figure 7A, C**). The micropyle, the pollen chamber and the flattened-cells layer were also labelled, indicating a massive presence of auxin in the ovule structure (**Figure 7C**). Again, the cavity at the base of the nucellus was found to be marked (**Figure 7D**) and an increase in phenols content was observed in the integument (**Figure 7A)**.

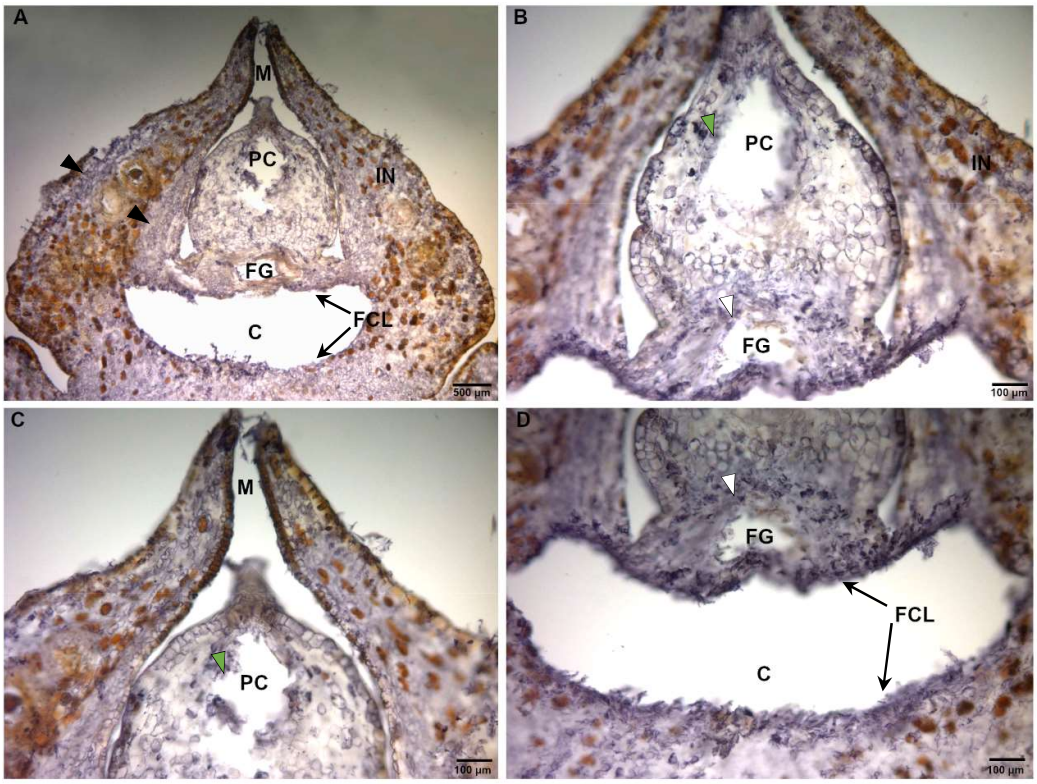

Figure 7. Spatio-temporal distribution of free Indole-3-acetic acid (IAA) 8 days after the end of drop emission in unpollinated *Ginkgo biloba* ovules. Immunoreaction is evidenced as purple-violet staining. The signal was detected in longitudinal histological sections of unpollinated ovules (UO) at stage 8. Magnifications of nucellus **(B),** pollen chamber and micropyle **(C)** and cavity **(D)**. C: cavity; FG: female gametophyte; IN: integument; M: micropyle; PC: pollen chamber. White arrow heads indicate the signal in female gametophyte and *tapetum*; black arrow heads indicate the signal in the integument, green arrow heads indicate the signal in the pollen chamber. **(A)** Scale bar: 500 µm; **(B-D)** Scale bars: 100 µm.

No immunoreaction was observed in ovules processed without primary antibody (CTRL; **Figure 8A-C**).

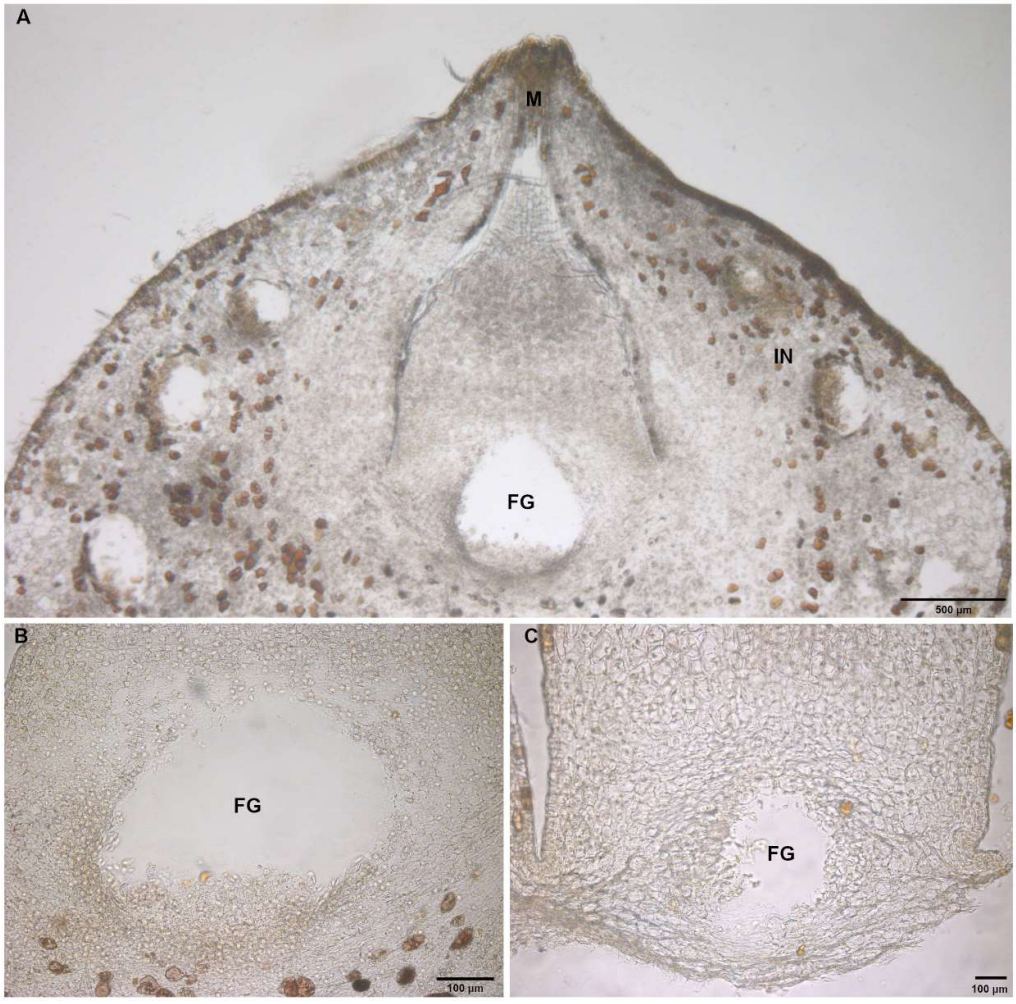

Figure 8. Longitudinal histological sections of *Ginkgo biloba* ovules collected 6 days after the end of drop emission. Sections were processed with the omission of IAA primary antibody as negative control of pollinated **(A, B)** and unpollinated **(C)** ovules. **(B, C)** Magnifications of female gametophyte of pollinated **(B)** and unpollinated **(C)** ovules. FG, female gametophyte; IN, integument; M, micropyle. **(A)** Scale bar: 500 µm; **(B, C)** Scale bars 100 µm.

Taken together, the results suggest a dynamic and ordered distribution of auxin in the nucellus after pollination event whilst a disorder in the pattern of distribution of auxin, in unpollinated ovules. Indeed, Li and collaborators (2007) reported that in rice, many genes involved in auxin metabolism are highly expressed in the stigma at the time of pollination and pollen germination. In *Nicotiana tabacum*, auxin also appears to be present in the stigma and style during pollen tube production (Chen and Zhao 2008; Sundberg and Østergaard; 2009). Our results seem to be in agreement with the literature; indeed, the pollen chamber, where pollen capture and germination take

place, was always labelled in all the development stages of PO, indicating the presence of auxin. Furthermore, as reported above, correct influx and efflux of maternal auxin deputed to PIN transporters are crucial for the correct expansion of FG (Wang *et al.*, 2021). Concerning the results obtained in UO, it should be noted that auxin could be involved in the induction of PCD. High concentrations of auxin have been shown to induce cell death in plant tissues (Kacprzyk *et al.*, 2022). Excess auxin can lead to the production of Reactive Oxygen Species (ROS) within cells and the accumulation of ROS, in turn, could trigger PCD pathways (Kacprzyk *et al.*, 2022). On the other hand, a cross-talk between auxin and other signalling pathways is crucial, as auxin signalling pathways are interconnected with other signalling pathways in plants. For example, auxin and other hormones such as ethylene and jasmonic acid often interact to regulate plant responses to various stresses. Often, stress responses involve programmed cell death mechanisms, and auxin signalling could, indirectly, influence these processes (Mazzoni-Putman *et al.*, 2021).

Unpollinated ovules show a decrease in CKs accumulation

CKs are a class of plant hormones that play essential roles in various physiological processes, including cell division, shoot and root development, and differentiation. Among these, CKs also have significant effects in female reproductive organs and seed development (Bencivenga *et al.*, 2012; Cucinotta *et al.*, 2020; Terceros *et al.*, 2020).

In the first stage analysed of *Ginkgo* ovules development, no differences of *trans*-zeatin distribution were observed by comparing PO and UO (**Figure 9**). The results suggest that the possible arrival of pollen has not yet affected the metabolism of CKs. More specifically, in both PO_1 and UO_1, signal was widespread throughout the integument (**Figure 9A, E**). However, of the three layers of the integument, a strong immunoreaction was observed in the outermost layer, which will differentiate into *sarcotesta*, characterised by thin-walled cells and numerous mucilaginous ducts (Douglas *et al.*, 2007) (**Figure 9A, E**). In addition, in the integument, a gradient of signal intensity progressively increased in the micropylar region, similar to the distribution pattern of auxin at the same stage of development (**Figure 9G**).

Interestingly, as far as the pollen chamber was concerned, the signal affected the inner regions more than the isodiametric cells that delimit it (**Figure 9B**). As mentioned above, at this developmental stage the pollen chamber has reached its maximum volume to accommodate the pollen grains (D'Apice *et al.*, 2021). Immediately below the pollen chamber is the distal micropylar parietal tissue, clearly marked. The cells that make up this tissue undergo cell expansion processes to exert a mechanical stress that causes the more apical parts of the pollen chamber to collapse and finally trap the pollen (Douglas *et al.*, 2007).

Concerning the basal region of the nucellus, the signal was more intense. In particular, the flanking parietal tissue surrounding the sporogenous tissue was intensely labelled (**Figure 9C, F**). This is a critical area of high proliferative activity that ensures the progressive increase in size of the nucellus through a precise pattern of cell division. The cells closest to the sporogenous tissue divide transversely and then elongate, while the outer cells divide longitudinally (Douglas *et al.*, 2007). Again, the main target seemed to affect the gametophyte. An intense signal outlined the *tapetum* and circumscribed the gametophyte (**Figure 9D**) more pronounced than in auxin immunolocalisation. As mentioned earlier, at this stage of development the gametophyte is in a coenocytic stage and will undergo intense proliferative activity, probably requiring the activity of CKs. The ovule collar also showed immunostaining (**Figure 9A, E**). The origin of this structure, typical of Ginkgophytes, has long been debated but remains elusive (see Eichler, 1873; Schaffner, 1927; Coulter and Chamberlain, 1910; Florin, 1949; Foster and Gifford, 1974; Douglas *et al.*, 2007). It results from the activity of undifferentiated or meristematic cells at the base of the ovule and includes cells that divide periclinally and anticlinally both before and after pollination to ensure its increase in size.

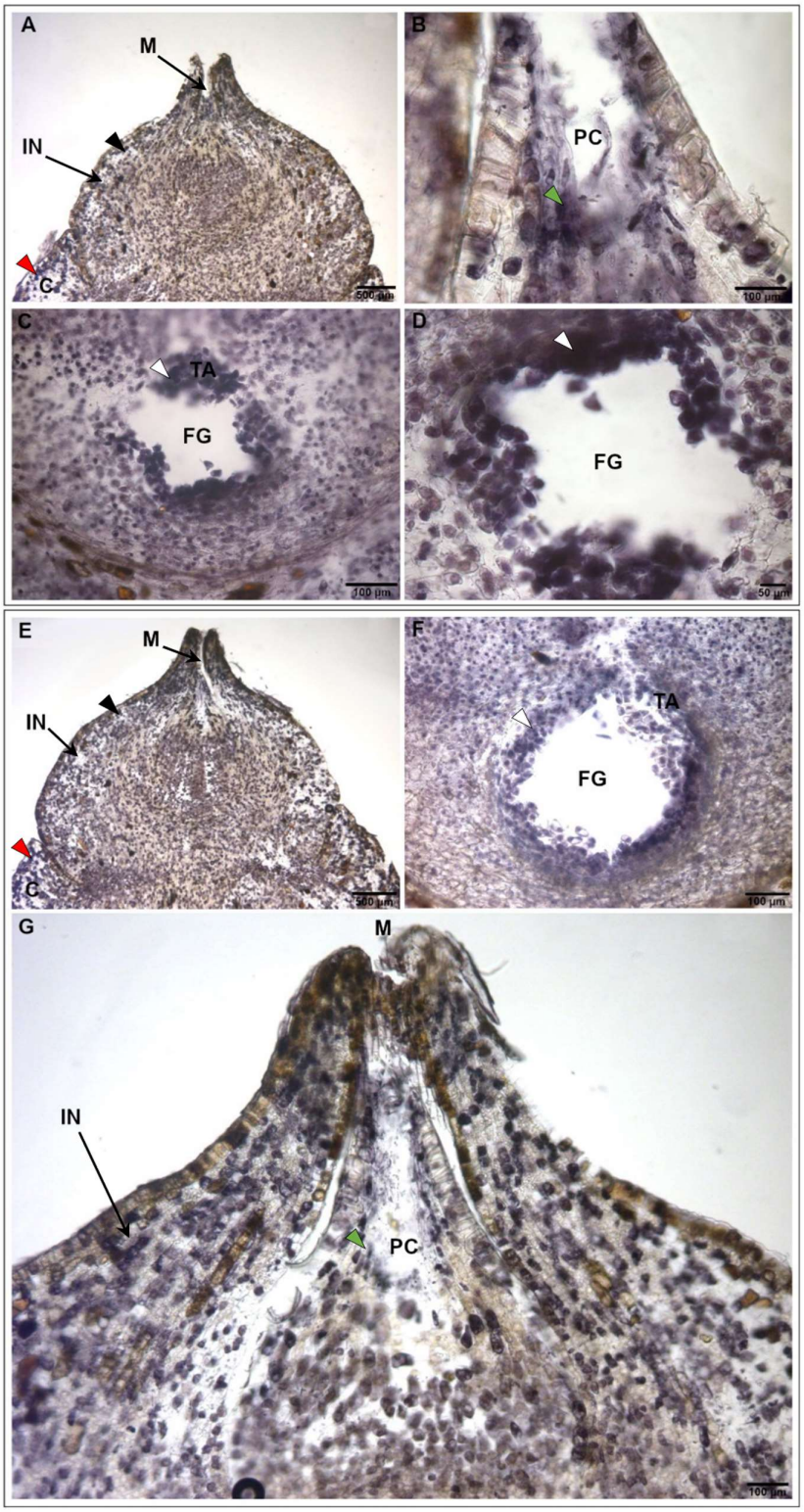

Figure 9. Spatio-temporal distribution of *trans*-zeatin 1 day after the end of drop emission in pollinated and unpollinated *Ginkgo biloba* ovules. Immunoreaction is evidenced as purple-violet staining. The signal was detected in longitudinal histological sections of pollinated (PO) **(A-D)** and unpollinated ovules (UO) **(E-G)** at stage 1. Magnifications of pollinated **(B-D)** and unpollinated **(F-G)** ovules. C, collar; FG: female gametophyte; IN: integument; M: micropyle; PC: pollen chamber. Red arrow heads indicate the signal in the collar; white arrow heads indicate the signal in female gametophyte and *tapetum*; black arrow heads indicate the signal in the integument, green arrow heads indicate the signal in the pollen chamber. **(A, E)** Scale bars: 500 µm; **(B, C, F, G)** Scale bars: 100 µm; **(D)** Scale bar: 50 µm.

Significant differences were observed in the last two stages. For PO, similar to the previous experiment, the signal in integument was less pronounced in PO_6 compared to the first stage **(Figure 10A)**. In addition, the most intensely stained layer was the one that will differentiate into the *endotesta*, while the less stained layer was the intermediate layer (future *sclerotesta*), where the immunoreaction was only visible in a few clusters **(Figure 10A)**. Within the nucellus, the signal was more precisely localised. In fact, the distal micropylar tissue was labelled, especially close to the pollen chamber **(Figure 10B)**, while in the basal regions of the nucellus it was observed as a gradient. The *tapetum* and the cells closest to the gametophyte were intensely labelled, in the flanking parietal tissue the signal was visible but progressively less intense as one moved away from the gametophyte **(Figure 10C)**. An intense signal was also found in the flattened-cells layers, a concave, multilayered tissue at the base of the nucellus, which is responsible for delimiting the sporogenous tissue. It is of particular interest because it has only previously been observed in some Cycadophytes, such as *Strangeria* (Lang, 1900) and *Zamia* (Smith, 1910). Other Gnetophytes, such as *Ephedra* (Takaso, 1985) and *Gnetum* (Takaso and Bouman 1986), show a few flattened-cells (two to five) in the hypodermal layer adjacent to the nucellar tissue, but only at later stages of development. Conifers also have flattened-cells, not to define the boundaries of the nucellus, but further down (Buchholz 1941; Kemp 1959; Tomlinson *et al.* 1989; Takaso and Tomlinson 1991). In *Ginkgo*, however, this layer is formed by cells that continue to divide actively after pollination, forming a multilayered tissue characterised by thick-walled and highly vacuolated cells. Close to fertilisation, this tissue is partially incorporated into the *sarcotesta* and partially into the *sclerotesta* (Douglas *et al.*, 2007). The presence of such tissue in *Ginkgo* is probably justified by the early development of the nucellus compared to other species, as these cells are of archesporial origin.

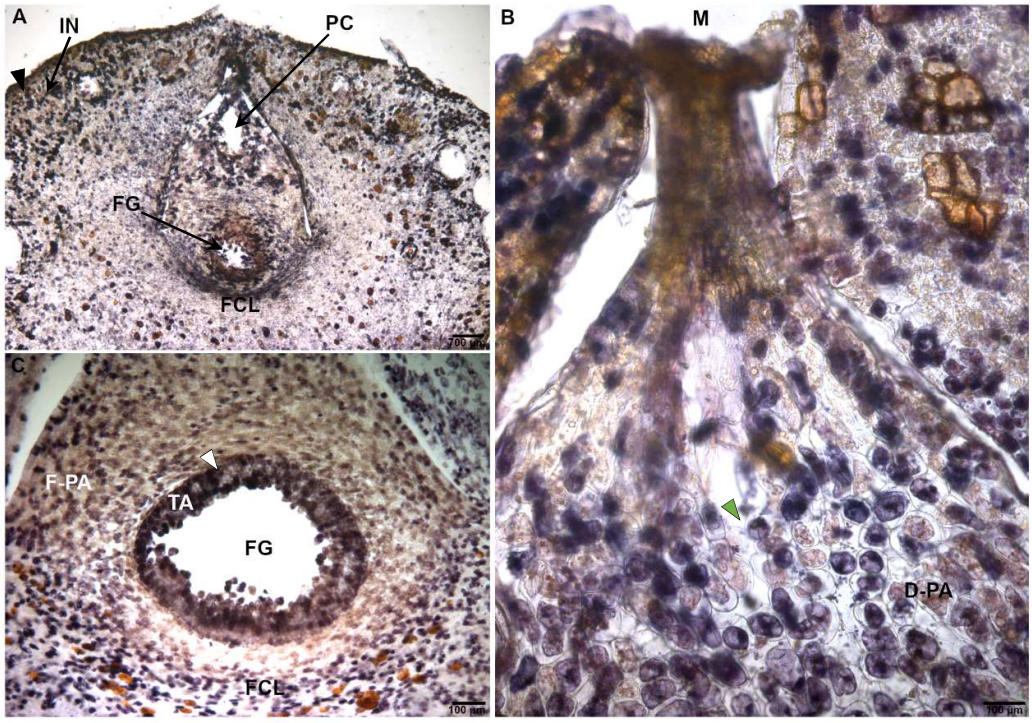

Figure 10. Spatio-temporal distribution of *trans*-zeatin 6 days after the end of drop emission in pollinated *Ginkgo biloba* ovules. Immunoreaction is evidenced as purple-violet staining. The signal was detected in longitudinal histological sections of pollinated ovules (PO) at stage 6. Magnifications of pollen chamber **(B)** and female gametophyte **(C)**. D-PA: distal micropylar parietal tissue; FCL: flattened-cells layer; F-PA: flanking parietal tissue; FG: female gametophyte; IN: integument; PC: pollen chamber; TA: *tapetum*. Black arrow head indicates the signal in the integument; green arrow head indicates the signal in the pollen chamber; white arrow head indicates the signal in female gametophyte and *tapetum*. **(A)** Scale bar: 700 µm; **(B-C)** Scale bars: 100 µm.

A similar distribution of *trans*-zeatin was observed in PO_8 **(Figure 11)**. Indeed, the same pattern was observed in the integument **(Figure 11A)**, in the micropyle **(Figure 11B)** and globally also in the nucellus **(Figure 11A)**, although the signal seemed to be more intense in the basal regions, such as the flanking parietal tissue **(Figure 11C)**. The gametophyte remained the main target for the localisation of *trans*-zeatin at this stage **(Figure 11C)**.

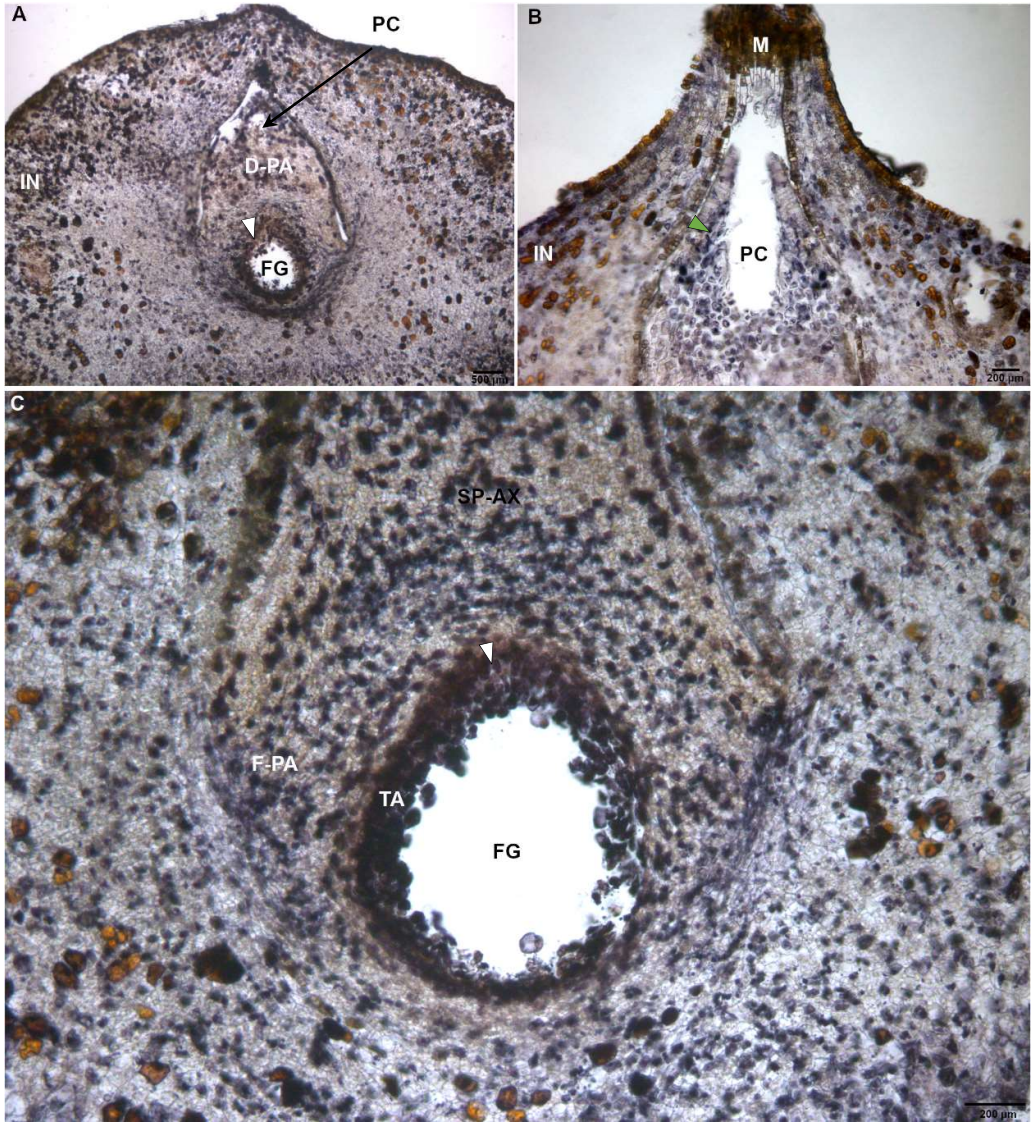

Figure 11. Spatio-temporal distribution of *trans*-zeatin 8 days after the end of drop emission in *Ginkgo biloba* pollinated ovules. Immunoreaction is evidenced as purple-violet staining. The signal was detected in longitudinal histological sections in pollinated ovules (PO) at stage 8. Magnifications of micropyle **(B)** and female gametophyte **(C)**. D-PA: distal micropylar parietal tissue; FCL: flattened-cells layer; F-PA: flanking parietal tissue; FG: female gametophyte; IN: integument; M: micropyle; PC: pollen chamber; SP-AX: sporangial axial column of cells; TA: *tapetum*. White arrow heads indicate the signal in female gametophyte and *tapetum*; green arrow head indicates the signal in the pollen chamber. **(A)** Scale bar: 500 µm; **(B-C)** Scale bars: 200 µm.

On the contrary, a progressive switching off of the signal was observed in UO **(Figure 12)**, indicating the absence of *trans*-zeatin activity, probably together with other CKs, in the case of unsuccessful pollination. In particular, in UO_6, slight labelling was observed in the flap **(Figure 12A)**, while in the nucellus a few labelled cells were observed near the pollen chamber and in the micropylar tissue **(Figure 12C)**. The *tapetum* was weakly marked **(Figure 12C)**. Finally, in UO_8, the signal was almost completely absent, with very few marked cells observed around the pollen chamber and in the lower parts of the nucellus **(Figure 12B, D)**.

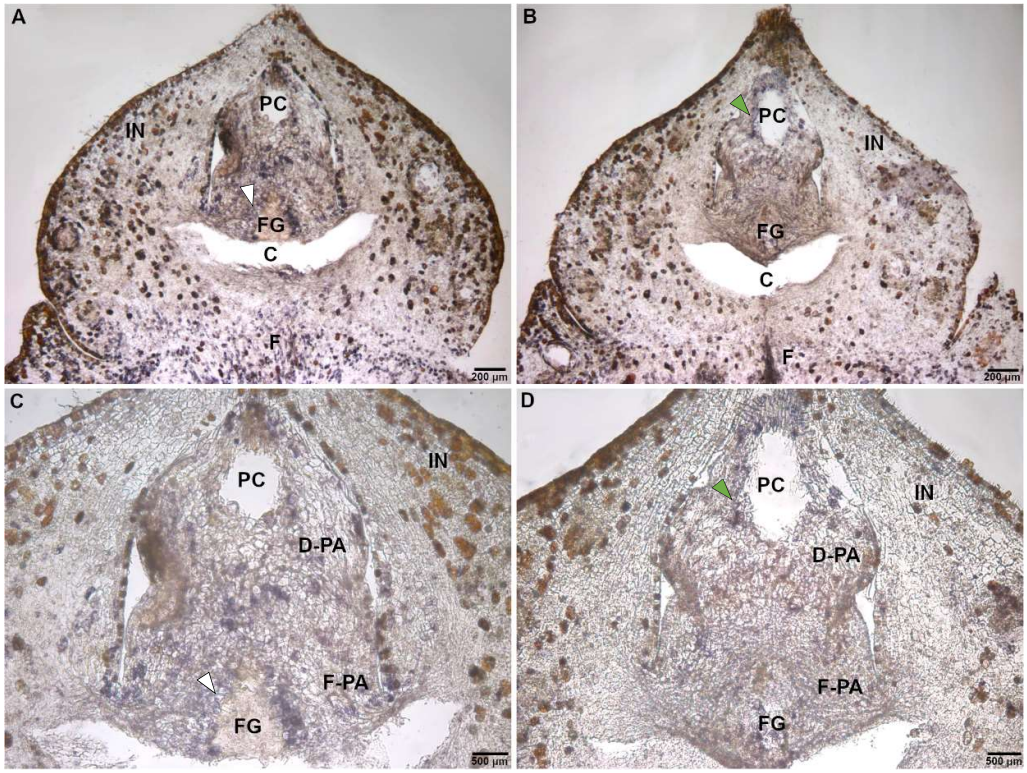

Figure 12. Spatio-temporal distribution of *trans*-zeatin 6 and 8 days after the end of drop emission in pollinated *Ginkgo biloba* ovules. Immunoreaction is evidenced as purple-violet staining. The signal was detected in longitudinal histological sections in unpollinated ovules (UO) at stages 6 **(A, C)** and 8 **(B, D)**. Magnifications of nucellus **(C-D)**. C: cavity; FG: female gametophyte; IN: integument; PC: pollen chamber. White arrow heads indicate the signal in female gametophyte and *tapetum*; green arrow heads indicate the signal in the pollen chamber. **(C-D)** Scale bars: 500 µm; **(A-B)** Scale bars: 200 µm.

There was no detectable immunoreaction in ovules processed without the primary antibody (CTRL) (**Figure 13**).

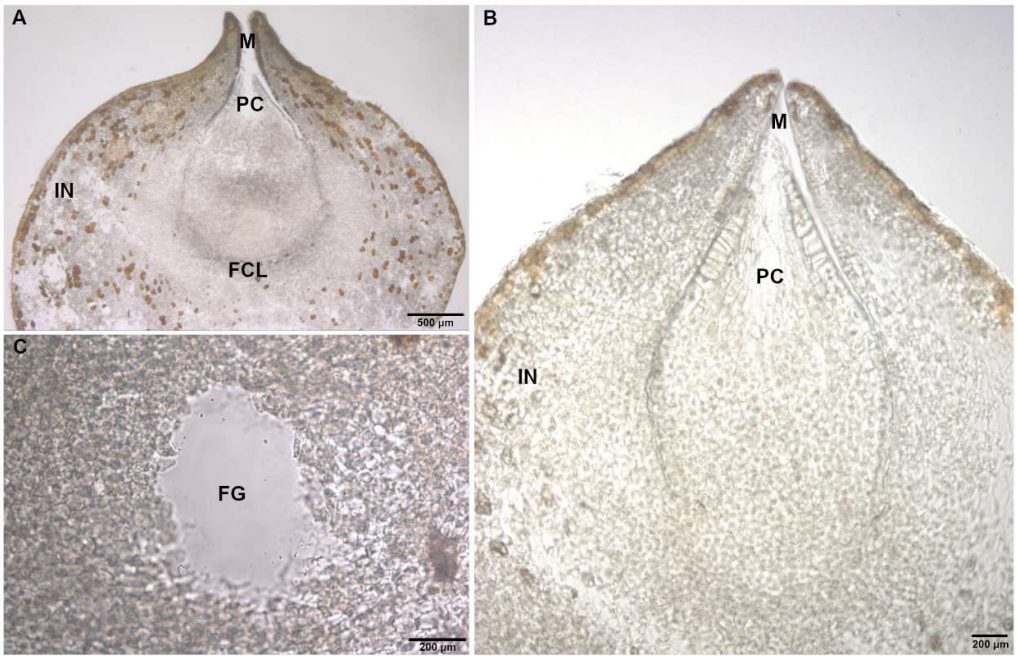

Figure 13. Longitudinal histological sections of *Ginkgo biloba* ovules collected 6 days after the end of drop emission. Sections were processed with the omission of *trans*-zeatin primary antibody as negative control of pollinated **(A, C)** and unpollinated **(B)** ovules. (B) Magnification of female gametophyte of pollinated ovules. FCL, flattened-cells layers; FG, female gametophyte; IN, integument; M, micropyle, PC, pollen chamber. **(A)** Scale bar: 500 µm; **(B, C)** Scale bar: 200 µm.

Taken together, our results show a partial overlap of the histological domains of auxin and *trans*-zeatin localisation, especially in PO. To further investigate this aspect, a multiple immunolocalisation of the two hormones was performed at the six-day post-pollination stage, which has often proved to be of particular interest **(Figure 14)**. The results of multiple immunolocalisation performed at PO_6, confirm the presence of both auxin and *trans*-zeatin in nucellus **(Figure 14A)**; a massive presence of *trans*-zeatin (red) and auxin (green) was observed throughout the lower part of the nucellus, and in the cells surrounding the gametophyte **(Figure 14D)**. At the micropyle level, the presence of both hormones was confirmed, although the auxin signal appeared to be predominant **(Figure 14B)**. In UO_6, on the other hand, the *trans*-zeatin signal was almost absent, while the auxin signal was noticeable **(Figure 14C, E)**.

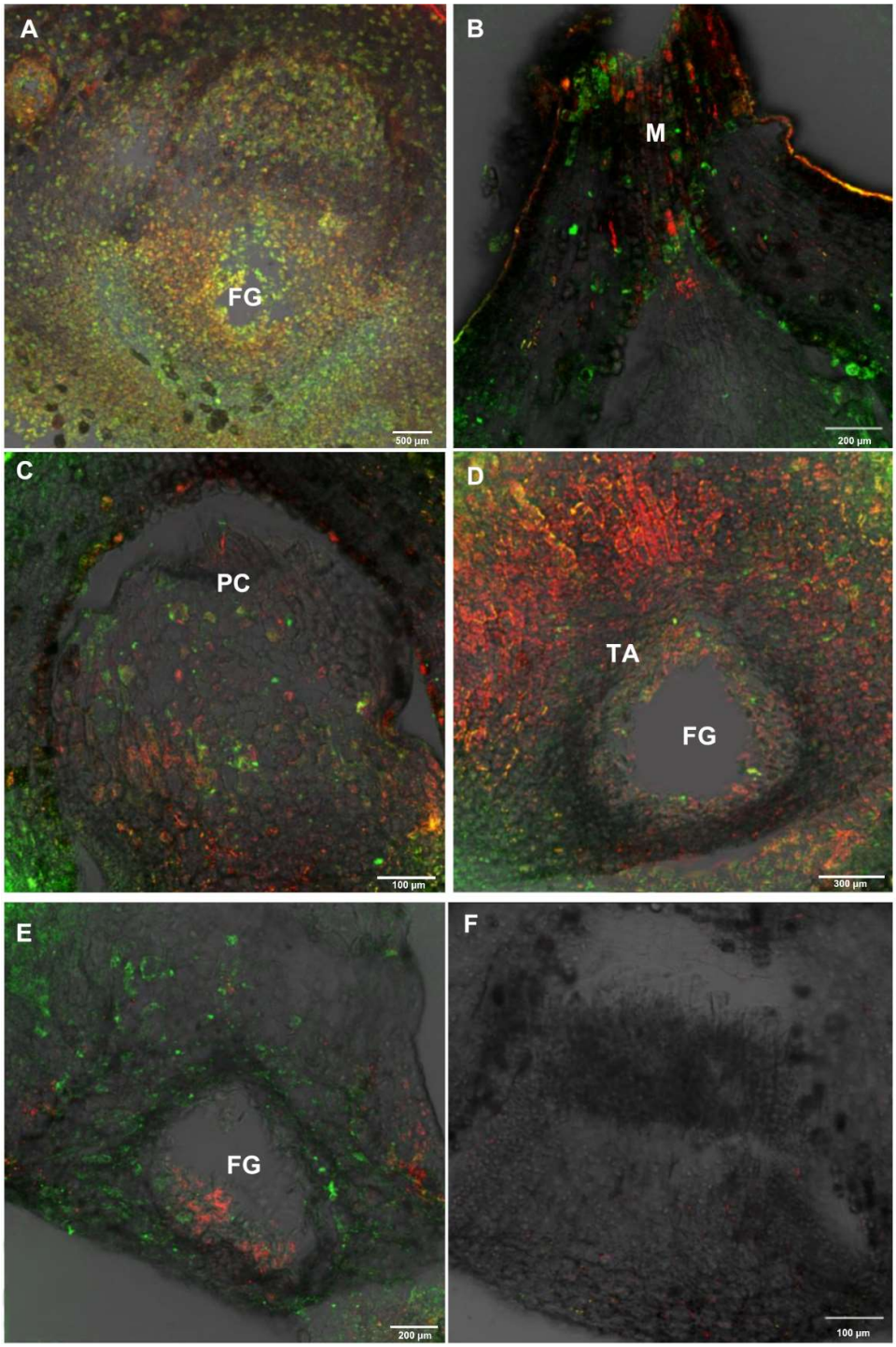

Figure 14. Spatio-temporal distribution of free Indole-3-acetic acid (IAA) and *trans*-zeatin 6 days after the end of drop emission in pollinated and unpollinated *Ginkgo biloba* ovules. Immunoreaction is evidenced as red and green fluorescence. The signal was detected in longitudinal histological sections of pollinated (PO) **(A-B, D)** and unpollinated (UO) **(C, E)** ovules at stage 6. **(F)** section treated with the omission of primary antibodies. Green signal indicates the presence of auxin (channel 1), red signal indicates the presence of *trans*-zeatin (channel 2). Yellow spots indicate the overlapping between the two signals. The images are the results of the merged of channel 1, 2 and transmission. M, micropyle; PC, pollen chamber; FG, female gametophyte; TA, *tapetum*. **(A)** Scale bar: 500 µm; **(D)** Scale bar: 300 µm; **(B, E)** Scale bars: 200 µm **(C, F)** Scale bars: 200 µm.

Taken together, these results suggest that the arrival of pollen is crucial for the proper metabolism of CK hormones. In PO, the ovule undergoes a correct increase in size in both sporophytic and gametophytic tissues, which are under intense proliferative activity through free nuclear divisions. In contrast, UO undergoing abortion showed a strong decrease in CK signal, corresponding to the global down-regulation of genes involved in cell cycle regulation, as reported in Chapter III. Indeed, our previous results have shown an upregulation in PO compared to UO of genes related to cell cycle regulation and DNA replication and damage repair, particularly at the 6-day stage. In particular, *CDKB1* (*Gb_38629*) was downregulated in UO, indicating a slowing of the cell cycle transitions when pollination does not occur. Given the crucial role that CKs play in controlling these processes, it is reasonable to assume that their defective metabolism in this context is closely linked to the cell cycle abnormalities observed.

Based on these evidences we can conclude that in *Ginkgo* there is an auxin signal that surrounds the FG, where it meets the activity of CKs. However, the ovules can have two different fates. In pollinated ovules the synergistic action of auxin and cytokinin cause the correct development. Instead, in unpollinated ovules the progressive decrease in CK activity and the alteration of auxin distribution pattern, are involved in the ovule abortion, showing the key role that the pollination event has in regulating the distribution of these two phytohormones.

REFERENCES

Barro-Trastoy, D., Dolores Gomez, M., Tornero, P., and Perez-Amador, M. A. (2020). On the way to ovules: the hormonal regulation of ovule development. *Critical Reviews in Plant Sciences*, *39*(5), 431-456.

Bartrina, I., Otto, E., Strnad, M., Werner, T., and Schmülling, T. (2011). Cytokinin regulates the activity of reproductive meristems, flower organ size, ovule formation, and thus seed yield in *Arabidopsis thaliana*. *The Plant Cell*, *23*(1), 69-80.

Bencivenga, S., Colombo, L., and Masiero, S. (2011). Cross talk between the sporophyte and the megagametophyte during ovule development. *Sexual plant reproduction*, *24*, 113-121.

Bencivenga, S., Simonini, S., Benková, E., and Colombo, L. (2012). The transcription factors BEL1 and SPL are required for cytokinin and auxin signaling during ovule development in *Arabidopsis*. *The Plant Cell*, *24*(7), 2886-2897.

Buchholz, J. T. (1941). Embryogeny of the Podocarpaceae. *Botanical gazette*, *103*(1), 1-37.

Cao, J., Li, G., Qu, D., Li, X., and Wang, Y. (2020). Into the seed: auxin controls seed development and grain yield. *International Journal of Molecular Sciences*, *21*(5), 1662.

Ceccato, L., Masiero, S., Roy, D. S., Bencivenga, S., Roig-Villanova, I., Ditengou, F. A., Palme, K., Simon, R., and Colombo, L. (2013). Maternal control of PIN1 is required for female gametophyte development in *Arabidopsis*. *PloS one*, *8*, e66148.

Chen, D., and Zhao, J. (2008). Free IAA in stigmas and styles during pollen germination and pollen tube growth of *Nicotiana tabacum*. *Physiologia Plantarum*, *134*(1), 202-215.

Cheng, C. Y., Mathews, D. E., Eric Schaller, G., and Kieber, J. J. (2013). Cytokinin-dependent specification of the functional megaspore in the *Arabidopsis* female gametophyte. *The Plant Journal*, *73*(6), 929-940.

Chiappetta, A., Fambrini, M., Petrarulo, M., Rapparini, F., Michelotti, V., Bruno, L., Greco, M., Baraldi, R., Salvini, M., Pugliesi, C., and Bitonti, M. B. (2009). Ectopic expression of *LEAFY COTYLEDON1-LIKE* gene and localized auxin accumulation mark embryogenic competence in epiphyllous plants of *Helianthus annuus* × *H. tuberosus*. *Annals of Botany*, *103*(5), 735-747.

Coulter, J. M., Chamberlain, C. J. (1910) *Morphology of gymnosperms*. University of Chicago Press.

Cucinotta, M., Di Marzo, M., Guazzotti, A., de Folter, S., Kater, M. M., and Colombo, L. (2020). Gynoecium size and ovule number are interconnected traits that impact seed yield. *Journal of Experimental Botany*, *71*(9), 2479-2489.

D'Apice, G., Moschin, S., Araniti, F., Nigris, S., Di Marzo, M., Muto, A., Banfi, C., Bruno, L., Colombo, L., and Baldan, B. (2021). The role of pollination in controlling *Ginkgo biloba* ovule development. *New Phytologist*, *232*(6), 2353-2368.

Dorcey, E., Urbez, C., Blázquez, M. A., Carbonell, J., and Perez-Amador, M. A. (2009). Fertilization-dependent auxin response in ovules triggers fruit development through the modulation of gibberellin metabolism in Arabidopsis. *The Plant Journal*, *58*(2), 318-332.

Douglas, A. W., Stevenson, D. W., and Little, D. P. (2007). Ovule development in *Ginkgo biloba* L., with emphasis on the collar and nucellus. *International Journal of Plant Sciences*, *168*(9), 1207-1236.

Eichler, A.W. (1873). Sind die Coniferen Gymnospermen oder nicht? *Flora 56*, 241–272.

Florin, R. (1949). *The Morphology of Trichopitys Heteromorpha Saporta, a Seed-plant of Palaeozoic Age, and the Evolution of the Female Flowers in the Ginkgionae*. Almqvist & Wiksell.

Foster, A. S., and Gifford, E. M. (1959). Comparative morphology of vascular plants. *Comparative morphology of vascular plants.*

Kacprzyk, J., Burke, R., Schwarze, J., and McCabe, P. F. (2022). Plant programmed cell death meets auxin signalling. *The FEBS Journal*, *289*(7), 1731-1745.

Kemp, M. (1959). Morphological and ontogenetic studies on *Torreya californica*. II. Development of the megasporangiate shoot prior to pollination. *American Journal of Botany*, *46*(4), 249-261.

Kinoshita-Tsujimura, K., and Kakimoto, T. (2011). Cytokinin receptors in sporophytes are essential for male and female functions in *Arabidopsis thaliana*. *Plant signaling & behavior*, *6*(1), 66-71.

Lang, W. H. (1900). Studies in the development and morphology of cycadean sporangia: II. The ovule of *Stangeria paradoxa*. *Annals of Botany*, *14*(54), 281-306.

Larsson, E., Vivian-Smith, A., Offringa, R., and Sundberg, E. (2017). Auxin homeostasis in *Arabidopsis* ovules is anther-dependent at maturation and changes dynamically upon fertilization. *Frontiers in Plant Science*, *8*, 1735.

Li, M., Xu, W., Yang, W., Kong, Z., and Xue, Y. (2007). Genome-wide gene expression profiling reveals conserved and novel molecular functions of the stigma in rice. *Plant Physiology*, *144*(4), 1797-1812.

Mandal, S., Ghorai, M., Anand, U., Roy, D., Kant, N., Mishra, T., Mane, A. B., Jha, N. K., Lal, M. K., Tiwari, R. K., Kumar, M., Radha Ghosh, A., Bhattacharjee, R., Proćków, J., and Dey, A. (2022). Cytokinins: a genetic target for increasing yield potential in the CRISPR era. *Frontiers in Genetics*, *13*, 883930.

Mazzoni-Putman, S. M., Brumos, J., Zhao, C., Alonso, J. M., and Stepanova, A. N. (2021). Auxin interactions with other hormones in plant development. *Cold Spring Harbor Perspectives in Biology*, *13*(10), a039990.

Mok, D. W., and Mok, M. C. (1994). *Cytokininschemistry, activity, and function*. CRC press.

Mok, D. W., and Mok, M. C. (2001). Cytokinin metabolism and action. *Annual review of plant biology*, *52*(1), 89-118.

Möller, B., and Weijers, D. (2009). Auxin control of embryo patterning. *Cold Spring Harbor perspectives in biology*, *1*(5), a001545.

Nole-Wilson, S., Azhakanandam, S., and Franks, R. G. (2010). Polar auxin transport together with *AINTEGUMENTA* and *REVOLUTA* coordinate early *Arabidopsis* gynoecium development. *Developmental biology*, *346*(2), 181-195.

Pagnussat, G. C., Alandete-Saez, M., Bowman, J. L., and Sundaresan, V. (2009). Auxin-dependent patterning and gamete specification in the *Arabidopsis* female gametophyte. *Science*, *324*(5935), 1684-1689.

Pandolfini, T. (2009). Seedless fruit production by hormonal regulation of fruit set. *Nutrients*, *1*(2), 168-177.

Paque, S., and Weijers, D. (2016). Q&A: Auxin: the plant molecule that influences almost anything. *BMC biology*, *14*(1), 1-5.

Rijavec, T., Jain, M., Dermastia, M., and Chourey, P. S. (2011). Spatial and temporal profiles of cytokinin biosynthesis and accumulation in developing caryopses of maize. *Annals of Botany*, *107*(7), 1235-1245.

Sakakibara, H. (2005). Cytokinin biosynthesis and regulation. *Vitamins and Hormones*, *72*, 271-287.

Schaffner, J. H. (1927). *Ginkgo* a flowerless seed plant. *American Journal of Botany*, *14*(3), 126-128.

Schaller, G. E., Street, I. H., and Kieber, J. J. (2014). Cytokinin and the cell cycle. *Current opinion in plant biology*, *21*, 7-15.

Serbes, I. E., Palovaara, J., and Groß-Hardt, R. (2019). Development and function of the flowering plant female gametophyte. *Current Topics in Developmental Biology*, *131*, 401-434.

Shimotohno, A., Aki, S. S., Takahashi, N., and Umeda, M. (2021). Regulation of the plant cell cycle in response to hormones and the environment. *Annual review of plant biology*, *72*, 273-296.

Smith, F. G. (1910). Development of the ovulate strobilus and young ovule of *Zamia floridana*. *Botanical Gazette*, *50*(2), 128-141.

Sundberg, E., and Østergaard, L. (2009). Distinct and dynamic auxin activities during reproductive development. *Cold Spring Harbor perspectives in biology*, *1*(6), a001628.

Takaso, T. (1985). A developmental study of the integument in gymnosperms 3. *Ephedra distachya* L. and *E. equisetina* Bge. *Acta botanica neerlandica*, *34*(1), 33-48.

Takaso, T., and Bouman, F. (1986). Ovule and seed ontogeny in Gnetum gnemon L. *The botanical magazine*, *99*, 241-266.

Takaso, T., and Tomlinson, P. B. (1991). Cone and ovule development in *Sciadopitys* (Taxodiaceae-Coniferales). *American Journal of Botany*, *78*(3), 417-428.

Terceros, G. C., Resentini, F., Cucinotta, M., Manrique, S., Colombo, L., and Mendes, M. A. (2020). The importance of cytokinins during reproductive development in *Arabidopsis* and beyond. *International Journal of Molecular Sciences*, *21*(21), 8161.

Tomlinson, P. B., Takaso, T., and Rattenbury, J. A. (1989). Cone and ovule ontogeny in *Phyllocladus* (Podocarpaceae). *Botanical Journal of the Linnean Society*, *99*(3), 209-221.

Vivian-Smith, A., and Koltunow, A. M. (1999). Genetic analysis of growth-regulator-induced parthenocarpy in *Arabidopsis*. *Plant Physiology*, *121*(2), 437-452.

Wang, J., Guo, X., Xiao, Q., Zhu, J., Cheung, A. Y., Yuan, L., Vierling, E., and Xu, S. (2021). Auxin efflux controls orderly nucellar degeneration and expansion of the female gametophyte in *Arabidopsis*. *New Phytologist*, *230*(6), 2261-2274.

Zhang, J., Pai, Q., Yue, L., Wu, X., Liu, H., and Wang, W. (2022). Cytokinin regulates female gametophyte development by cell cycle modulation in *Arabidopsis thaliana*. *Plant Science*, *324*, 111419.

CHAPTER V

Conclusions and future perspectives

During my Ph. D. project, I focused my attention on processes that are specific to developmental biology, while combining an *evo-devo* approach. Indeed, to date there is a vast amount of knowledge about the morphology of reproductive structures and the molecular networks underlying their development in model organisms and, more generally, in angiosperms. In contrast, although the anatomy is well described, little is known about the corresponding processes in gymnosperms. More recently, there has been an increased focus on non-model plants and additional contributions to improve knowledge in this regard. Indeed, it is still often difficult to work with non-model systems because the results are often putative and predictive due to the almost complete lack of appropriate tools. Therefore, the starting point of my research was a thorough study of the literature in this field, using *Arabidopsis thaliana* as a reference model, which is still the model organism par excellence in all fields of plant biology.

In fact, the easy genetic manipulation means that a very large number of mutants are available, enabling the study of all the processes involved in the plant's life cycle and the characterisation of the genes involved in each of them. However, one of the few limitations of *Arabidopsis* is the close temporal proximity of fundamental processes such as pollination and fertilisation. Indeed, to date, most of the mechanisms underlying the ovule-to-seed switch are well understood and the molecular signalling that triggers this switch is attributed to fertilisation. This proximity in time between pollination and fertilisation is related to an evolutionary process that took thousands and thousands of years. Indeed, in much more ancient plants, such as gymnosperms and, in particular, *Ginkgo*, pollination and fertilisation are separated by a long interval (i.e. four/five months).

This characteristic has allowed us to study the crucial role of the single pollination event in determining the developmental progression of the ovule, the differentiation of the female gametophyte and the transformation of the ovule integument into the seed coat long before fertilisation occurs. Interestingly, the unique integument of the ovule, after pollination but before fertilisation, differentiates into

three layers and the outermost, named *sarcotesta*, takes on a fleshy consistency, remembering the fleshy fruits, although they cannot be identified as such because gymnosperms lack an ovary.

Based on these premises, my research was focused on the molecular network triggered by pollination event in a gymnosperm as *Ginkgo biloba*. Firstly, I contributed to the identification of some PRC2 target genes before and after pollination that are putatively involved in seed coat differentiation in *Ginkgo*. Interestingly, the results reported here suggest that the mechanism of action of PRC2 involving H3K27me3 is conserved. Indeed, the chromatin immunoprecipitation experiment using an antibody specific for H3K27me3 was not only technically successful, but also revealed the presence of some target genes already known in *Arabidopsis*, such as some *MADS-box* genes. In addition, also *GbPIN1* presented trimethylation peaks after pollination. Interestingly, the orthologous *AtPIN1* it's known to be the main player which determines the influx of maternal auxin in the nucellus, driving the female gametophyte expansion.

Subsequently, given the increasingly important role that pollination has been shown to play to ensure proper ovule development, transcriptomic profiles of pollinated and unpollinated ovules collected at the end of the pollination drop emission period were analysed. The results have provided a better understanding of the role of pollen arrival, which appears to be crucial in activating pathways such as DNA replication and damage repair, as well as cell cycle regulation and mitosis. Conversely, it inhibits genes involved in senescence and apoptosis. Indeed, cyto-histological analysis immediately revealed that unpollinated ovules undergo early disorganisation of the tissues that characterise the nucellus, further emphasising the role of pollination in preventing early PCD processes. Concerning hormone metabolism, the same *GbPIN1* previously identified as target of PRC2 after pollination, showed an upregulation and its transcript different localisation in unpollinated ovules, suggesting that its expression depends on the pollination event and is regulated by epigenetic mechanisms.

Based on these evidences, the cyto-histological localisation domains of auxin and cytokinin was investigated. Indeed, they are extensively studied in plant biology

because of their involvement in all the processes that occur during the life cycle of a plant. A large amount of information is available in the literature on their activity during ovule and seed development. In *Arabidopsis*, the availability of numerous marker lines makes it relatively easy to identify the localisation domains of each phytohormone. This is not possible in *Ginkgo*, so the localisation of auxin and *trans*-zeatin, the two most important hormones involved in these processes, was studied using immunocytochemical approaches. Once again, the pollination event appeared to be crucial for the presence/absence of the two hormones in specific tissues at different stages of development. In pollinated ovules, an organised localisation of auxin and cytokinin in specific structures, such as the female gametophyte, was observed. In contrast, unpollinated ovules showed a disorganised distribution of auxin and an almost complete absence of *trans*-zeatin.

Altogether, the results I obtained during my research project contribute in a small way to adding piece in a fascinating but poorly understood topic, and to providing a comprehensive view of the evolutionary processes that have led to the biodiversity we see on Earth today, and which humanity has a moral duty to protect.

APPENDIX

Some of the results presented in this thesis, together with additional data contributed by research groups from the Universities of Milan and Padua coordinated by Professor Colombo and Professor Baldan respectively, have been discussed in a research paper pubblished in the Journal of Experimental Botany (Manuscript n. 1).

1. Muto, A., **Talarico, E.**, D'Apice, G., Di Marzo, M., Moschin, S., Nigris, S., Babolin, N., Greco, E., Araniti, F., Chiappetta, A., Colombo, L., Baldan, B., Bruno, L., Development of pollinated and unpollinated ovules in *Ginkgo biloba*: shedding light on pollen arrival's role in determining the ovule tissue maturation. *Journal of Experimental Botany, erae102.*

Here, we deeply investigated the pathways activated/deactivated by pollen arrival and in relation to auxin localisation by comparing the transcriptomic profiles of pollinated and unpollinated ovules of *Ginkgo biloba*. Selected genes involved in auxin transport, cell cycle regulation and encoding transcription factors were used to localise transcripts by an *in situ* hybridisation approach.

However, in these three years of research activity I also had the opportunity to explore other research topics already underway in my laboratory. Hence, the obtained results contributed to the preparation of other research papers, listed below.

One of the topics of my research group is the effects of the heavy metal cadmium (Cd) on the organisation of both Shoot and Root Apical Meristem (SAM and RAM respectively) and also in the Root System (RS) (Manuscripts 2, 3 and 4).

2. Araniti, F.*, **Talarico, E.***, Madeo, M. L., Greco, E., Minervino, M., Álvarez-Rodríguez, S., Muto, A., Ferrari, M., Chiappetta, A., Bruno, L. 2023. Short-term exposition to acute cadmium toxicity induces the loss of root gravitropic stimuli perception through PIN2-mediated auxin redistribution in *Arabidopsis thaliana* (L.) Heynh. *Plant Science*, *332*, 111726.
    a. *Equally contributed

3. Bruno, L., **Talarico, E.**, Madeo, M. L., Muto, A., Minervino, M., Araniti, F., Bitonti, M. B., Chiappetta, A., 2021. Cadmium affects cell niches maintenance in *Arabidopsis thaliana* post-embryonic shoot and root apical meristem by altering the expression of *WUS/WOX* homolog genes and cytokinin accumulation. *Plant physiology and biochemistry 167, 785–794.*

4. Pacenza, M., Muto, A., Chiappetta, A., Mariotti, L., **Talarico, E.**, Picciarelli, P., Picardi, E., Bruno, L., Bitonti, M.B., 2021. In *Arabidopsis thaliana* Cd differentially impacts on hormone genetic pathways in the methylation defective *ddc* mutant compared to wild type. *Scientific reports, 11, 1-17.*

Cd is one of the most studied heavy metals, due to its high toxicity and high solubility in water. Its long biological half-life (almost 30 years) makes it a cumulative contaminant and becomes a risk for all living species. In plant species, Cd is absorbed, transported and accumulated in all plant organs, inducing complex changes at genetic, biochemical and physiological levels.

It is well known that plants are sessile organisms, unable to escape stress conditions. Moreover, they undergo recurrent ontogenesis, and their indeterminate growth is coordinated and ensured by the activity of SAM and RAM located at the apices of the shoot and root, respectively. In fact, these two regions are characterized by perfect synchrony between two opposing events: the continuous self-renewal of stem cells and the differentiation of derivatives to form future organs. Specifically, in the SAM, the maintenance of the indeterminate state is ensured by the gene activity of *WUSCHEL/ CLAVATA* and *SHOOT MERISTEMLESS* (*STM*), while in the RAM, it is maintained by *WOX5* and *PLETHORA* genes activity.

In Manuscript n. 2 (Araniti *et al*., 2023) *Arabidopsis thaliana* seedlings were grown on control medium and then transferred (5 days after germination) on fresh control medium and on medium enriched with Cd 100 µM and Cd 150 µM for different times. Seedlings were used for several approaches. Indeed, morpho-histological, molecular, pharmacological and metabolomics experiments were carried out. Thanks also to the use of numerous marker lines containing chimeric constructs of interest fused with GFP, the results show that short-term acute Cd treatment induces early cell

differentiation, evidenced by both a lowering of the transition zone and an high Reactive Oxygen Species (ROS) production, such as hydrogen peroxide (H_2O_2). The latter one interferes with both microtubule orientation pattern, by affecting transition zone cell expansion, and auxin distribution, by altering the PINFORMED family, particularly PIN2. The loss of activity of PIN2, associated with an abnormal modulation of statoliths content and sucrose metabolism, reduced root gravitropic response.

My contribution to this paper was molecular and confocal microscopy analysis, statistical analysis and I participated in the drafting together with Prof. Bruno and Dr. Araniti.

In Manuscript n. 3 (Bruno *et al.*, 2021), we focused our attention on the effect of short-term acute Cd treatments on both SAM and RAM. Here, 5-day-old seedlings exposed or not to Cd 100 μM and Cd 150 μM were used for morpho-histological and molecular experiments. Again, both wild type and specific marker lines were used to observe the expression patterns of WUS/CLV3 and WOX5. These genes play a crucial role in establishing and maintaining the stem cell niche and in controlling the size of the meristem. In addition *TCSn::GFP* cytokinin-sensitive sensor was used to evaluate the presence of the hormone, known to be involved in the control of shoot and root growth. The results showed that Cd impacts both shoot and root meristems in size and shape, by inducing misexpression of *WOX* paralogous genes and cytokinins accumulation.

During this research activity, I contributed to in vitro culture and I performed histological staining and data analysis.

In Manuscript n. 4 (Pacenza *et al.*, 2021), we investigated the plant epigenetic response to abiotic stress. Indeed, DNA methylation modulates plant growth plasticity under stress condition, although the mechanisms underlying it are still poorly understood. Here, was used *drm1 drm2 cmt3* (*ddc*) mutant of *Arabidopsis thaliana*, defective in DNA methylation, to evaluate the epigenetic modulation of hormone pathways under Cd treatment. Transcriptomic profiles of *ddc* and wild type after long-term exposition (21 days) to Cd (25 μM and 50 μM) were compared and DEGs involved in hormone pathways were identified. The results showed an increase of both level and signalling of growth-sustaining hormones (auxins, CKs, GAs) and a decrease

of stress-related hormones (JA, ABA, SA), probably to mitigate the potential side effects associated with their prolonged activation. These responses were more efficiencies in *ddc* with respect to wild type, accordingly with its better growth performance. Probably, the hypomethylated DNA status of *ddc* plants confers greater genomic plasticity than wild type plants, providing the basis for its rapid response to modulate genetic pathways and hormone-related activities to ensure flexible growth.
My contribution was related to the root growth kinetics under Cd and 5-azacytidine treatments.

In other two manuscript we evaluated the effects of different phytotoxic molecules, such as coumarin and *trans*-cinnamic acid on root development in *Arabidopsis thaliana* and *Zea mays* respectively.

5. Bruno, L., **Talarico, E.**, Cabeiras-Freijanes, L., Madeo, M. L., Muto, A., Minervino, M., Lucini, L., Miras-Moreno, B., Sofo, A., Araniti, F., 2021. Coumarin interferes with polar auxin transport altering microtubule cortical array organization in *Arabidopsis thaliana* (L.) Heynh. Root Apical Meristem. *International Journal of Molecular Sciences, 22,14, 7305.*

6. López-González, D., Bruno, L., Díaz-Tielas, C., Lupini, A., Aci, M.M., **Talarico, E.**, Madeo, M.L., Muto, A., Sánchez-Moreiras, A.M., Araniti, F. 2023. Short-term effects of *trans*-cinnamic acid on the metabolism of *Zea mays* L. Roots. *Plants, 12, 189.*

In Manuscript n. 5 (Bruno *et al.*, 2021) we investigated the effect of coumarin on RAM organisation and polar auxin transport. *PINs::GFP* marker lines, immunolabelling experiments and metabolomics GC-MS analysis to estimate auxin content were used. The obtained results showed that short-term exposition (48 hours) to coumarin (100 μM) alters the RAM morphology by affecting the organisation of cortical microtubules and the biosynthesis and transport of auxin, especially in the acropetal. This leads to an accumulation of auxin in the pericycle cells, promoting the formation of lateral roots.
In this paper, I contributed to perform experiments related to confocal microscopy analysis.

In Manuscript n. 6, the phenolic compound *trans*-cinnamic acid was added to the hydroponic culture of maize to assess the effect on vascular bundle elements and metabolism

in maize roots. After a short exposure of *trans*-cinnamic acid (6 to 24 hours) at a high concentration (103 μM), a reduction in the content of several amino acids was observed, probably due to altered nitrogen uptake. After 48 hours of exposure, *trans*-cinnamic acid seemed to induce a change in lignin and galactose metabolism. In fact, plants could convert the compound into lignin to detoxify it by activating phenylalanine metabolism.
I focused my attention on the in vitro culture and on the histological analysis carried out on sections cut by vibratome and observed by confocal microscopy.

Lastly, other research activity carried on in my research group is related to the use of fertilising mixed compost in agriculture and its effects on crop quality (Manuscript n. 7).

7. Rizzo, S., Minervino, M., Muto, A., **Talarico, E.**, Muzzalupo, I., Araniti, F., Chiappetta, A., Bruno, L., 2022. Impact of municipal solid waste compost amendment and mineral fertilisation on soil properties and *Cucumis melo* L. subsp. *melo* var. *cantalupensis* crop quality. *Agrochimica, 66, 3-20*.

The study assessed the effects of compost amendment and mineral fertiliser on soil properties and in plants of *Cucumis melo* L. subsp. *melo* var. *cantalupensis*. The purpose was to compare the effects of traditional NPK mineral fertiliser and compost on soil properties and plants, including qualitative and sensory analysis parameters. The obtained results suggest that the application of compost in agricultural fields leads to an enhancement of biological parameters, resulting in a more active soil microbial community.
Here, I contributed to perform chemical and biochemical analyses.

In addition, I had the chance to have oral communications at two congresses, as reported below:

- Greco, E., **Talarico E.**, Madeo, M.L., Minervino, M., Muto, A., Ferrari, M., Chiappetta, A.A., Bruno, L. "Short term exposition to acute cadmium toxicity induces the loss of root gravitropic stimuli perception through PIN2 polar auxin transport in *Arabidopsis thaliana*". 118° Congresso della Società Botanica Italiana (SBI) - IX International Plant Science Conference (IPSC), Pisa, Settembre 2023;

- **Talarico, E.**, Muto, A., Moschin, S., Di Marzo, M., Nigris, S., Chiappetta, A.A., Colombo, L., Baldan, B., Bruno, L. “Pollination event affects auxin and cytokinin accumulation and distribution in *Ginkgo biloba* ovule”. Riunione Annuale dei gruppi di lavoro SBI, Biologia Cellulare e Molecolare - Biotecnologie e differenziamento, Ancona, Giugno 2023.

SOCIETY FOR EXPERIMENTAL BIOLOGY

Journal of Experimental Botany
https://doi.org/10.1093/jxb/erae102 Advance Access Publication 9 March 2024

RESEARCH PAPER

Development of pollinated and unpollinated ovules in *Ginkgo biloba*: unravelling the role of pollen in ovule tissue maturation

Antonella Muto[1], Emanuela Talarico[1], Greta D'Apice[2,3], Maurizio Di Marzo[4], Silvia Moschin[2,3], Sebastiano Nigris[2,3], Nicola Babolin[4], Eleonora Greco[1], Fabrizio Araniti[5], Adriana Chiappetta[1], Lucia Colombo[4], Barbara Baldan[2,3], and Leonardo Bruno[1,*]

[1] Department of Biology, Ecology and Earth Sciences (DiBEST), University of Calabria, 87036 Arcavacata of Rende (Cosenza), Italy
[2] Botanical Garden, University of Padova, 25123 Padova, Italy
[3] Department of Biology, University of Padova, 35121 Padova, Italy
[4] Department of Biosciences, University of Milano, 20133 Milano, Italy
[5] Department of Agricultural and Environmental Sciences - Production, Landscape, Agroenergy (Di.S.A.A.), University of Milano, 20133 Milano, Italy

* Correspondence: leonardo.bruno@unical.it

Received 22 January 2024; Editorial decision 28 February 2024; Accepted 6 March 2024

Editor: Zoe Wilson, University of Nottingham, UK

Abstract

In gymnosperms such as *Ginkgo biloba*, the arrival of pollen plays a key role in ovule development, before fertilization occurs. Accordingly, *G. biloba* female plants geographically isolated from male plants abort all their ovules after the pollination drop emission, which is the event that allows the ovule to capture pollen grains. To decipher the mechanism induced by pollination required to avoid ovule senescence and then abortion, we compared the transcriptomes of pollinated and unpollinated ovules at three time points after the end of the emission of pollination drop. Transcriptomic and *in situ* expression analyses revealed that several key genes involved in programmed cell death such as senescence and apoptosis, DNA replication, and cell cycle regulation were differentially expressed in unpollinated ovules compared to pollinated ovules. We provide evidence that the pollen captured by the pollination drop affects auxin local accumulation and might cause deregulation of key genes required for the ovule's programmed cell death, activating both the cell cycle regulation and DNA replication genes.

Keywords: Auxin, female gametophyte, gymnosperm, ovule, pollen, senescence, transcriptome, transcription factors.

Introduction

Ovule development is a complex process conserved in angiosperms and gymnosperms, from sporangium formation to functional megaspore (FM) differentiation (Yadegari and Drews, 2004). Ovule structure is composed of a megasporangium (nucellus) protected by one or more sterile outer integuments. Integuments are initiated as annular outgrowths and ultimately extend upwards around the nucellus to delimit the micropyle. This apical opening allows the male

Abbreviations: DAD, days after drop; DEG, differentially expressed gene; FCL, flattened-cells layer, FG, female gametophyte; FM, functional megaspore; FNMM, free nuclear mitosis of the megagametophyte; GO, Gene Ontology; ISH, *in situ* hybridization, KEGG, Kyoto Encyclopaedia of Genes and Genomes; MMC, megaspore mother cell; PCD, programmed cell death; PCW, pollination condition by WGCNA; PD, pollination drop; PO, pollinated ovules; TF, transcription factor; UO, unpollinated ovules; WGCNA, weighted gene correlation network analysis.

gametophyte to deliver one or more male gametes inside the female gametophyte (FG) (Rudall, 2021). The FG is formed by a multistep process consisting of two phases: megasporogenesis and megagametogenesis (Yadegari and Drews, 2004). Megasporogenesis initiates with the differentiation of a single cell near the nucellus named the megaspore mother cell (MMC), which, through a meiotic division, will form a tetrad of spores. Only the most basal spore of the tetrad persists and forms the FG through free nuclear mitosis of megagametophyte (FNMM) (Douglas *et al.*, 2007). Then, in several gymnosperms, cellularization generates a FG that differentiates two archegonia, each bearing one egg cell (Zhang and Zheng, 2016). Overall, ovules are formed by sporophytic tissues such as the integument(s) and the FG, each performing a specific function controlled by complex genetic and molecular networks controlling cell proliferation, specific cell commitment and differentiation, as well as programmed cell death (PCD) during different developmental stages.

To date, the genetic networks and molecular mechanisms controlling ovule development have been extensively investigated in angiosperms, using model species such as *Arabidopsis thaliana* (Drews and Koltunow, 2011; Cucinotta *et al.*, 2014, 2020). Although relevant contributions have been added recently, ovule development in gymnosperms is still largely unexplored (Shigyo *et al.*, 2006;Yamada *et al.*, 2008; Chen *et al.*, 2017; Zumajo-Cardona *et al.*, 2021). Recent works have investigated in particular the genetic and molecular pathways during ovule development in *Ginkgo biloba* through an integrated approach encompassing morphological, transcriptomic, metabolomic (D'Apice *et al.*, 2021), and *in situ* hybridization (ISH) analyses (Zumajo-Cardona *et al.*, 2021; D'Apice *et al.*, 2022).

In Arabidopsis, as in several angiosperms, double fertilization, which is temporally close to the pollination event, is required for further differentiation of ovule integuments into seed coats (Figueiredo *et al.*, 2016; Figueiredo and Köhler, 2018). Events occur differently in *Ginkgo*, where pollination is separated from fertilization by a long period of time (i.e. 4/5 months), the signal for further ovule development and FG differentiation is provided by the arrival of pollen in the pollination chamber, which triggers the differentiation of three distinguishable layers in the ovule integument, driving its transformation into the seed coats long before fertilization takes place (D'Apice *et al.*, 2021, 2022). In line with these observations, *Ginkgo* female plants geographically isolated from male plants abort all their ovules after pollination drop (PD) emission, which in this species allows the identification of the ovule receptive phase to pollination (Friedman, 1987). In Arabidopsis, it has been demonstrated that the PCD process occurs in the tissue of the unpollinated stigmas. In particular, transcriptional profiling revealed that the NAC transcription factors (TFs) *ORESARA1* (*ORE1*) and *KIRA1* (*KIR1*) activated the senescence programme in unpollinated pistils (Gao *et al.*, 2018).

In this work, we aimed to study the pollen-induced molecular pathway in *G. biloba*, which promotes ovule development into a seed, repressing a senescence programme.

To this aim, we performed a transcriptomic analysis on ovules collected immediately after the pollination time from both female plants that received pollen and from plants geographically isolated and unable to receive pollen.

The pollination time was easily identified due to *Ginkgo*'s characteristic, common to many gymnosperms, of secreting a drop from the ovule sporophytic tissue through the micropylar canal.This drop captures the pollen and drags it inside the ovule, where it will germinate (Prior *et al.*, 2019).

The expression analysis we performed on selected genes sheds light on some molecular mechanisms that regulate FG development in this gymnosperm. Our data also supported the hypothesis that local auxin accumulation plays a fundamental role in ovule development, affecting both nucellus degeneration and FG development, even in gymnosperms. Interestingly, we have identified several key pathways related to ovule development, such as hormone signalling, senescence and apoptosis, cell cycle regulation, DNA replication, and damage repair, as well as the down-regulation of ATP synthesis-related proteins that are differentially regulated in pollinated and unpollinated ovules (PO and UO respectively). Our results suggest that the pollen triggers the initiation of ovule enlargement and further differentiation inhibiting PCD, specifically targeting key genes associated with the senescence and apoptosis pathway, while simultaneously activating genes involved in hormone signalling, DNA replication, and cell cycle regulation.

Materials and methods

Plant material

Pools of PO and UO were collected during the pollination timeframe (March and April 2021). PO were collected from 10 female plants at the Botanical Garden of the University of Calabria, Cosenza, Italy (39° 17′ 43″ N, 16° 15′ 13″ E) while UO were collected from 10 female, isolated plants located in the Coretto Garden (Cosenza) Calabria (39° 41′ 49″ N, 16° 25′ 43″ E). Ovules were collected at stages 6, 7 (stages before the pollination event), stage 8.1 (drop emission stage), and three stages after the end of the drop emission (days after drop, DAD), respectively 1 (UO_1, PO_1), 6 (UO_6, PO_6), and 8 d (UO_8, PO_8), as described in D'Apice *et al.* (2021).

For the molecular analyses, 30 ovules for each stage were pooled from 10 plants during the growing season for both conditions. Samples were immediately frozen into liquid nitrogen and stored at −80 °C.

Morphometric analyses

A total of 30 PO and UO from each stage analysed, respectively UO_1, UO_6, UO_8, PO_1, PO_6, and PO_8, which were randomly collected from different trees and used for size measurement. Ovules were measured considering the diameter at the broadest part, using the software ImageJ (Schneider *et al.*, 2012). Statistical analyses were performed on diameter values, first testing the homogeneity (Leven Median test) and then analysed by ANOVA and Tukey's rank test (P<0.05).

Paraffin embedding and sample section observations

For each stage analysed, at least 25 ovules randomly collected from different trees were processed, as reported by D'Apice *et al.* (2021). Ovules were fixed in 4% (w/v) paraformaldehyde in phosphate buffer saline (PBS) (10×PBS: 1.3M NaCl, 70 mM Na_2HPO_4, 30mM NaH_2PO_4; pH 7.4) with vacuum infiltration and then left overnight in fixative at 4 °C. The next day, samples were dehydrated in an ethanol series (30%, 50%, 70%, 85%, 95% in distilled sterile water for 1 h each step) and subsequently ethanol was replaced using a xylene series (25%, 50%, 75%, and 100% for 1 h each step). Lastly, xylene was gradually replaced by Paraplast Plus (Fisher Scientific), with changes every day. Embedded ovules were maintained at 4 °C until they were processed, and sections of 10 µm were cut with a Leica RM2125RT microtome. Slides were deparaffinized and rehydrated to be stained with 0.05% (w/v) toluidine blue. Histological sections were analysed with a Leica DRMB microscope to determine their developmental stage, and images were acquired with a Leica DFC 320 digital camera (Leica, Milan, Italy).

RNA isolation and RNA sequencing library synthesis

Total RNA extraction was performed separately for each of the 18 samples (three biological replicates of a pool of ovules were used for each of the three stages analysed for PO and UO) using 100 mg of ground ovule according to the manufacturer's recommendations in the Agilent Total RNA Isolation mini kit (Agilent Technologies, Santa Clara, CA, USA). cDNAs were then processed for library preparation by NOVOGENE Services and sequencing with an Illumina HiSeq 2500 RNA-seq. (50M, 15G) platform (Illumina, San Diego, CA) to generate paired-end reads of 150 bp for each fragment. Statistics of RNA-seq alignment for each of the 18 libraries obtained is reported in Supplementary Table S1. Raw data are deposited in the National Center for Biotechnology Information (NCBI) with the code Bioproject PRJNA700482 (https://www.ncbi.nlm.nih.gov/bioproject?term=PRJNA700482&cmd=DetailsSearch). Strand-specific libraries were constructed from mRNA of both UO and PO collected 1, 6, and 8 DAD. DESeq2 was then used to identify significant pollination-associated gene expression changes in ovule samples. Differentially expressed genes (DEGs), with a *P*-adjusted <0.05 and |log2 (ratio)| >1.5, as the thresholds to determine the significance of DEGs, were identified after pairwise comparisons between libraries of the same time points (UO_1/PO_1; UO_6/PO_6; UO_8/PO_8).

Weighted gene co-expression network analysis (WGCNA)

Co-expressed DEGs were identified by a scale-free WGCNA (Pearson's correlation coefficient ≥0.65 and $P \leq 0.05$), and a soft threshold value, power of 16, was used to transform the adjacency matrix to meet the scale-free topology criteria for optimal clustering (Langfelder and Horvath, 2008). Module-trait relationship figures were created in the R environment. A matrix of 14 914 relatively highly expressed genes (fragments per kilobase million, FPKM >10 in any sample) was filtered and applied to WGCNA. Modules were designated by colour and consisted of genes with similar expression patterns when referring to the 'pollination condition' trait. Genes belonging to the same module showed highly correlated expression patterns (Hollender *et al.*, 2014). 'Pollination condition' trait data were used for correlation network analyses with gene expression trends.

Real-time quantitative PCR (RT–qPCR) analysis

To validate the expression of selected genes, identified based on Illumina RNA-seq results, quantitative real-time PCR experiments were performed according to D'Apice *et al.* (2021). Primer sequences are reported in Supplementary Table S2. As RNA-seq (FPKM) and RT–qPCR produce relative gene expression measures, the Pearson correlation coefficient calculation was used for each pair of genes selected to evaluate concordance in gene expression.

In situ hybridization

Chemical fixation and tissue processing for RNA *in situ* hybridization were performed as described by D'Apice *et al.* (2022), considering at least 30 PO and UO from each stage analysed. The sequences of the probes are listed in Supplementary Table S2. Target sequences were amplified with primers containing the T7 sequence at the 5' of the forward primer (sense) and the 5' of the reverse primer (antisense) sites from cDNA obtained from total RNA retrotranscribed using the Invitrogen SuperScript III kit (Invitrogen, Waltham, Massachusetts, USA). The PCR products were then used for *in vitro* transcription using DIG-11-UTP, using the DIG RNA Labelling Kit (Roche Diagnostics GmbH, Mannheim, Germany) and stored at −20 °C before hybridization. Tissue treatments, pre-hybridization, post-hybridization washes, and antibody treatment were performed according to the protocol described by Ambrose *et al.* (2000). Probes were hybridized overnight at 55 °C in a 50% formamide humidified box. The anti-DIG-AP Fab fragments antibody (Roche Diagnostics GmbH) was diluted 1:700 and incubated for 2 h at room temperature. Detection was then developed overnight using the NBT/BCIP detection solution (Roche Diagnostics GmbH). Slides were then washed in stop buffer (100 mM Tris-HCl, pH 8.0; 1 mM EDTA), dehydrated, and mounted with Canada balsam (CARLO ERBA Reagents). Images were captured using a Leica DFC 320 digital camera (Leica).

Immunohistochemical localization of indole-3-acetic acid (IAA)

A total of 30 PO and UO from each stage analysed were randomly collected from different trees after the end of emission of the pollination drop. Immunolocalization was performed as described in Chiappetta *et al.* (2009). Ovules were collected and fixed in a 3% (w/v) paraformaldehyde and 0.5% (v/v) glutaraldehyde mixture in 1×PBS buffer (10×PBS: 135 mM NaCl, 2.7 mM KCl, 1.5 mM KH_2PO_4, 8 mM K_2HPO_4, pH 7.3). Longitudinal sections of 50 µm thickness were cut with a vibratome (Leica VT1000E, Germany) and incubated with anti-IAA monoclonal primary antibody (Sigma-Aldrich) diluted 1:250 in phosphate buffered saline/bovine serum albumin (PBS/BSA) solution (10 mM phosphate solution, 0.8% bovine serum albumin) overnight at 4 °C. The next day, sections were washed (3 × 10 min) and incubated with the secondary antibody (anti-mouse IgG alkaline phosphatase conjugate; Promega Italia, Milan, Italy) diluted 1:150 in 1×PBS solution for 3 h at room temperature. Detection was performed with a 4-nitro blue tetrazolium chloride (NBT) and 5-bromo-4-chloro-3-indolylphosphate (BCIP) mix, then rinsed with blocking buffer (100 mM Tris-HCl, pH 8.0; 1 mM EDTA). Control samples were processed without the primary IAA antibody. Images were taken with a Leica DRMB microscope equipped with a Leica DFC 320 camera.

In situ detection of DNA fragmentation (TUNEL assay)

Fifteen *Ginkgo* ovules for each analysed stage, respectively UO_1−8, PO_1−8, were fixed in 4% (w/v) paraformaldehyde in 1× PBS overnight at 4 °C. Next day, the samples were dehydrated through an ethanol series, as described above, and embedded in Paraplast Plus (Sigma-Aldrich).

Sections of 10 µm were cut and stretched on poly-L-lysine coated slides. Sections were then dewaxed in a xylene series and re-hydrated. According to the manufacturer's instructions, a terminal deoxynucleotidyl transferase dUTP nick end labeling (TUNEL) assay was performed using 'Click-iTTM Plus TUNEL assay' (Thermo Fisher Scientific).

The labelling reaction was performed in the dark for 1 h in a humidified chamber at 37 °C. A negative control was obtained by excluding terminal deoxynucleotidyl transferase (TdT) from the reaction mixture. As a positive control, some sections were incubated with DNase I (1 U ml^{-1}) for 30 min at room temperature before the TUNEL assay.

Confocal images of median longitudinal sections were obtained using a Leica inverted TCS SP8 confocal scanning laser microscope.

The detection of green fluorescence of incorporated EdUTP- Alexa FluorTM 488 (excitation peak centred at 495 nm, emission peak wavelength of 519 nm) and DAPI staining (1 g ml^{-1}) (excitation peak centred at 358 nm, emission peak wavelength of 461 nm) were performed by combining the settings indicated in the sequential scanning microscope facility.

Results

Lack of pollination event induces dramatic changes in ovule size and morphology

To unravel the role of pollination in ovule development, we elaborated the growth kinetics by measuring the diameter of the PO and the UO starting from the opening of the buds (Stage 6) to 10 d after the end of PD emission. Although the emission of PD occurred in the middle of April at both sites (see 'Material and methods'), the isolated female plants exhibited a significant extension of this stage. It lasted ~1 week in plants in which pollination occurred and ~2 weeks in isolated unpollinated female plants (Fig. 1A). Concerning the ovules growth kinetic, no significant differences were observed between PO and UO until the emission of the PD (stage 8.1). After PD emission, the size of the PO grew rapidly. At the same time, the UO decreased in size and initiated a senescence process leading to ovules dropping in the middle of May (Fig. 1A). We performed histological analysis on ovules collected at the following stages: PO_1, PO_6, PO_8, UO_1, UO_6, UO_8. At PO_1 and UO_1, cyto-histological differences were observed. In particular, at UO_1, a slight loss of tissue integrity and organization was observed in the most basal regions of the nucellus, similar to a laceration initiation (Fig. 1E). However, the integument was formed, the micropyle presented the characteristic teardrop shape, and the FG was in a coenocytic stage (Fig. 1B, E). In PO_6, the cells surrounding the pollen chamber collapsed inwards, reducing its narrow opening. In this stage, the FG presented multiple nuclei enclosed in a single cell, typically resulting from nuclear divisions uncoupled from cytokinesis (Fig. 1C). Indeed, at the centre of the FG was located a large vacuole surrounded by several dozen free nuclei. Until the final stage, an increase in the number of free nuclei was observed exclusively in the FG of the PO (Fig. 1C–D). In contrast, in UO_6 the FG were empty of free nuclei, resulting in a bigger vacuole size. Moreover, in UO_6, a tissue laceration was observed in the flattened-cells layer (FCL) in all ovules analysed (Fig. 1F). At the last stage, in PO_8, the FG was growing, the tapetum was degenerating, and the three layers of the integument were completely distinguishable (Fig. 1D). Conversely, in the UO_8 stage, the morphology of the ovule was completely altered, the nucellus appeared disorganized and the tissue laceration in the FCL was more extended when compared to UO_6 (Fig. 1G). Based on our observations, we concluded that pollination prevents the ovule cyto-histological disorganization and allows ovule development progression.

Pollination causes dramatic changes in the ovule transcriptome

To investigate the genetic and molecular networks controlling ovule response to pollination in *Ginkgo*, we performed a transcriptomic analysis on ovules collected from both plants that received pollen and unpollinated plants. A total of 6394 DEGs linked to pollination were identified from these pairwise comparisons (Fig. 2A). In particular, the UO_1/PO_1 list contained 1274 DEGs (651 up-regulated and 623 down-regulated), UO_6/PO_6 had 4471 DEGs (2383 up-regulated and 2088 down-regulated), and UO_8/PO_8 had 3400 DEGs (1177 up-regulated and 2223 down-regulated) (Fig. 2A). In addition, we further investigated conserved and stage-specific DEGs between subsequent developmental stages using a Venn diagram (Fig. 2B). As expected, the highest number of stage-specific DEGs (2139, 33.5% of total) were found in the comparison of UO_6/PO_6, followed by UO_8/PO_8 (with 1276, 20% of total), whereas the lowest number of stage-specific DEGs (530, 8.3% of total) was found in the comparison at 1 DAD. These data suggested that several biological processes dramatically changed from 1 DAD to 6 DAD in the ovules after the pollination event. We also identified 300 (4.7% of total) conserved DEGs in all three comparisons analysed (Fig. 2B). Gene Ontology (GO) enrichment analysis, performed for DEGs in each of the comparisons for both the UO and the PO, showed that most of the DEGs were enriched in response regulation pathways, such as several abiotic and biotic stress response categories including defence response to fungi or defence response to bacteria and wounding (Supplementary Fig. S1A–C). Also GO terms involved in stimuli and hormones, particularly ethylene and auxin-activated signalling pathways, regulation of transcription DNA-templated, methylation, and lipid catabolic process were also significantly impacted (Supplementary Fig. S1A–C). Kyoto Encyclopaedia of Genes and Genomes (KEGG) enrichment analysis showed that the most impacted pathways were those for phenylpropanoid biosynthesis, flavonoid biosynthesis, mismatch repair, DNA replication, homologous recombination, cutin, suberin and wax biosynthesis, and plant hormone signal transduction (Supplementary Fig. S2A–C).

Pollination-specific modules were then identified using WGCNA. The WGCNA, considering the 14 914 genes with FPKM >10, resulted in 60 distinct modules (Supplementary Table S3, Fig. S3A, B). Indeed, 7906 genes (Supplementary Table S3), grouped in 19 modules, were found to be correlated significantly and specifically with the 'pollination condition' trait (Supplementary Fig. S3A, B; Supplementary Tables S3, S4). We overlapped the DEGs UO/PO list and the 'pollination condition by WGCNA' (PCW). The frequency of the module with the DEGs UO/PO listing is shown in Supplementary Fig. S4. The integration of these two bioinformatic analyses led to the identification of genes associated with specific pathways, including hormone metabolism,

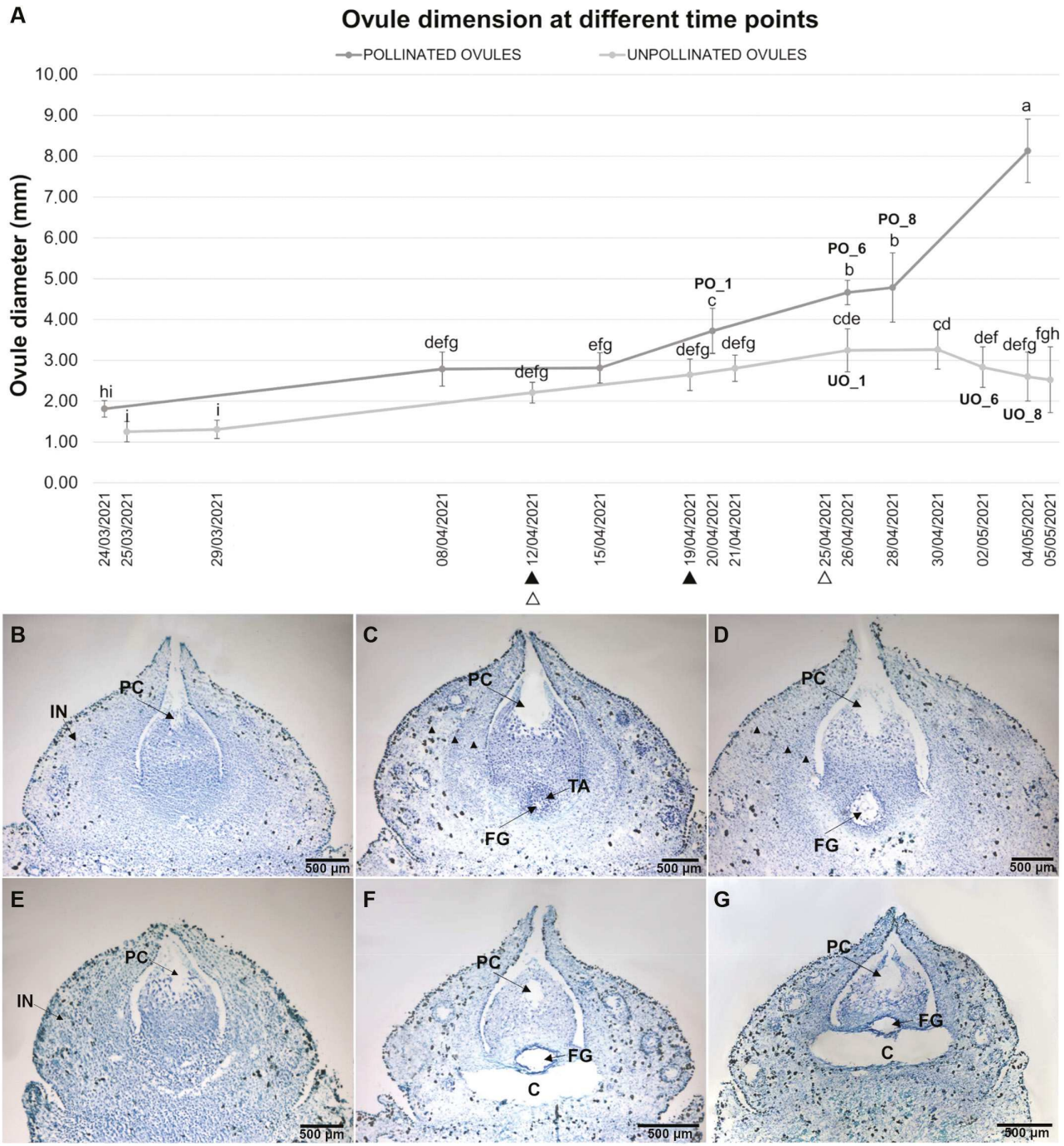

Fig. 1. Morphologic and microscopic observations of the *G. biloba* ovules over time (from April to May). (A) Growth kinetics of pollinated (PO) and unpollinated ovules (UO), considering the diameter of the ovule. Mean ±SD are represented as bars. The arrowheads, black for the PO and white for the UO, indicates the range of drop time emission. Statistical significant differences among values is indicated with different letters ($P<0.05$, ANOVA). (B–G) Cytological observations during the three developmental stages analysed, 1 (B, E), 6 (C, F), and 8 (D, G) DAD in both PO (B–D) and UO (E–G) ovules. The histological sections were stained with toluidine blue. C, cavity; FG, female gametophyte; IN, integument; PC, pollen chamber; TA, tapetum.

programmed cell death (senescence and apoptosis), cell cycle regulation and mitosis, DNA replication and damage repair (Fig. 2C), that were significantly affected by the pollination signal (Supplementary Tables S5, S6, S7). All the RT–qPCR results support the reliability of the RNA-seq analysis (Supplementary Fig. S5).

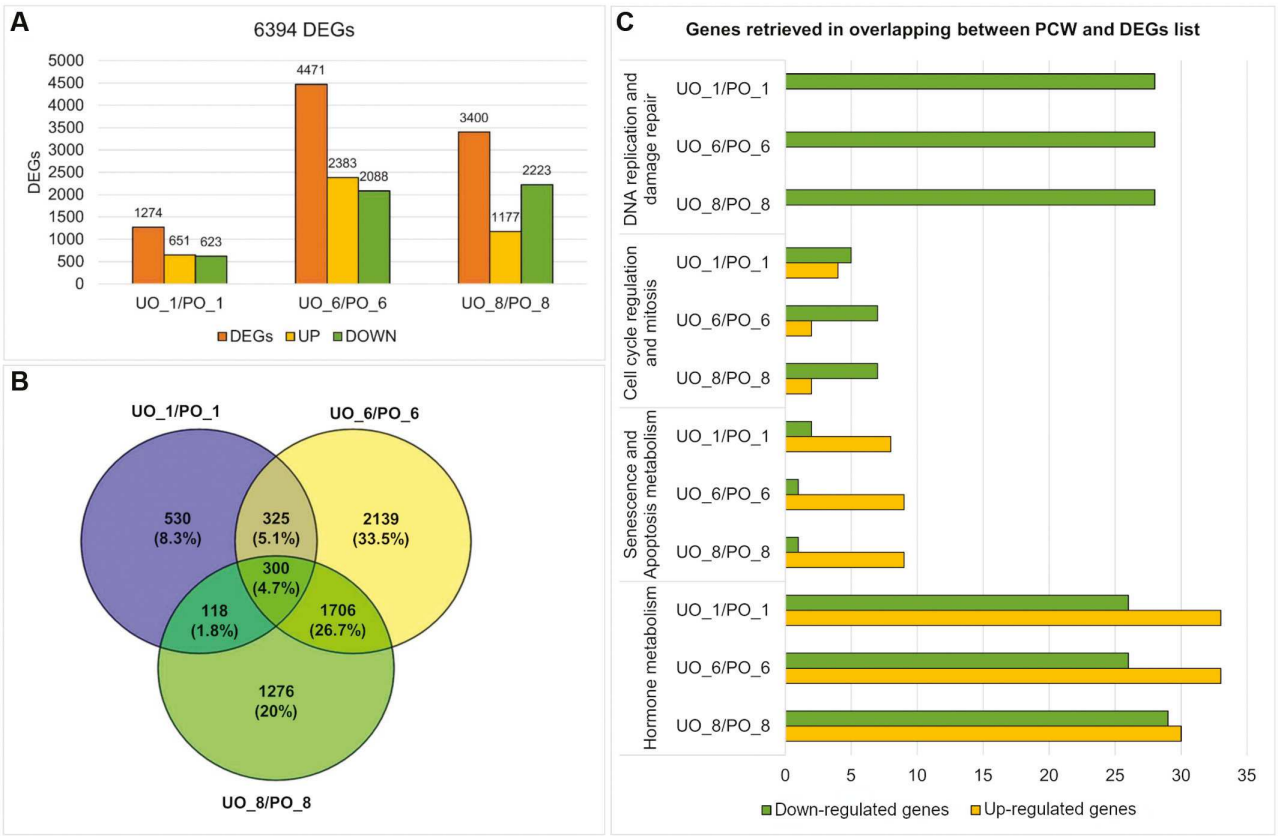

Fig. 2. Transcriptomic analysis changes considering libraries at all time points of pollinated and unpollinated libraries (UO/PO) at 1, 6, and 8 DAD. (A) Differentially expressed genes (DEGs) considering the comparison between unpollinated/pollinated ovules and among three time points (UO_1/PO_1, UO_6/PO_6, and UO_8/PO_8, respectively). Gene expression level values were normalized with the DESEQ2 software (*P* value corrected <0.05 and log2FC |1.5|). (B) Venn diagram describing the overlapping of DEGs sets from pairwise comparisons of pollinated and unpollinated ovules (UO_1 versus PO_1, UO_6 versus PO_6, UO_8 versus PO_8). (C) Diagram of the DEGs UO/PO list and 'pollination condition by WGCNA' (PCW) related to the main pathways impacted.

Auxin homeostasis is differentially regulated depending on the pollination event

Most DEGs were related to hormones biosynthesis and signalling (Supplementary Fig. S6), so we decided to focus on auxin because its role in ovule development in other species is well characterized (Barro-Trastoy *et al.*, 2020; Cucinotta *et al.*, 2021). Concerning the auxin pathway, 27 genes were included in both the DEGs and PCW lists (Supplementary Table S5). A heat map with this fraction involved in the auxin pathway was created to summarize the gene expressions in both conditions in the three time points analysed (Supplementary Fig. S7). The PO showed a higher expression of auxin-related genes, especially in the UO_6/PO_6 comparison. Notably, auxin efflux carriers (PINs) play a key role in ovule auxin accumulation. In this work, we investigated the *Ginkgo* orthologue of *AtPIN1* (*Gb_06199*) by ISH, given its known importance in ovule initiation and development (Ceccato *et al.*, 2013). In PO_1, the *Gb_06199* mRNA signal was widespread, but more intense in the flap zone (Fig. 3A), whereas in PO_6 it was localized in the nucellus, integument, and flap zone (Fig. 3B). Instead, in PO_8 the signal was restricted to the FG and the flap zone (Fig. 3C). Regarding the UO, in the first stage, *Gb_06199* transcripts were detected in the flap zone and in the nucellus (Fig. 3E), whereas in UO_6 and UO_8 they appeared widespread and not specifically localized, except for a cluster of marked cells around the FG (Fig. 3F, G).

In this context, the endogenous levels of free IAA were also estimated in the PO and the UO (Fig. 4). In PO_1, the IAA signal was intense and distributed throughout all ovule tissues (Fig. 4A). In PO_6, the signal was more restricted to the chalaza zone (Fig. 4D), the pollen chamber, and the integuments at the micropylar level (Fig. 4B). In PO_8 ovules the signal was weak and spread over the ovule tissues (Fig. 4G). Clusters of marked cells around the gametophyte of the PO in all the stages were observed (Fig. 4D, E, H). Regarding the UO, in both UO_6 and UO_8, auxin accumulation was quite comparable. Indeed, the integuments and tapetum were strongly stained, but no clusters of marked cells around the gametophyte were evident (Fig. 4C, F, I).

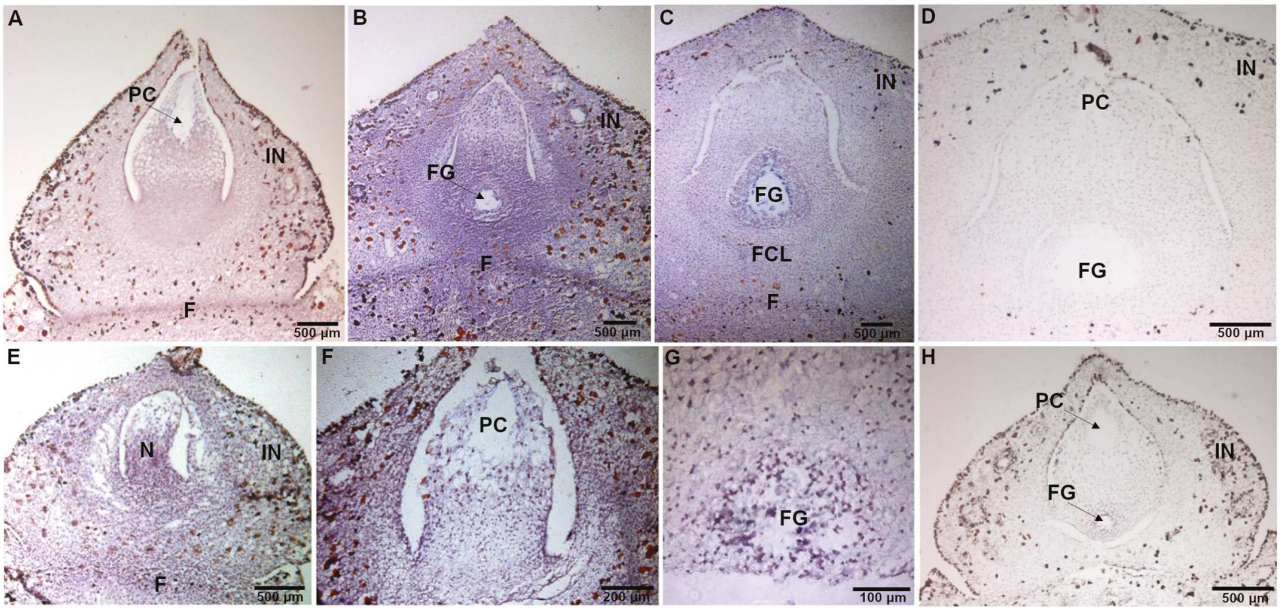

Fig. 3. Localization of *PIN1* (*Gb_06199*) transcripts by *in situ* hybridization with dig-labelled antisense probes (A–C, E–G). Longitudinal sections of pollinated (PO) (A–C) and unpollinated ovules (UO) (E–G) at stages 1 (A, E), 6 (B, F), and 8 (C, G). Signal is evidenced by purple staining (A–C, E–G). Longitudinal sections of PO and UO hybridized with the *PIN1* sense probe (D, H). F, flap; FCL, flattened-cells layer; FG, female gametophyte; IN, integument; N, nucellus; PC, pollen chamber.

The findings indicate an organized auxin distribution pattern within the nucellus of the PO. Conversely, in the absence of pollination, this distribution appears disorganized in the ovule.

NAC and *MYB* genes are differentially expressed upon pollination

Among the DEGs between the PO and the UO, 96 TFs, represented by 37 different families, were found in common between the DEGs and PCW lists (Supplementary Table S8). The heat map displays the expression patterns of 96 TFs genes identified through transcriptome analysis in both UO and PO at the analysed stages (Supplementary Fig. S8).

Considering the involvement of *MYB* and *NAC* genes in ovule development (Schubert *et al.*, 2019; Zhang *et al.*, 2021), we analysed the expression domains of selected MYB and NAC encoding genes. ISH was performed comparing stages UO_6 and PO_6, as this comparison showed the most significant differences in gene expression changes based on RNA-seq results. *MYB Gb_15607* was localized in the degenerated FG of the UO (Fig. 5B). A weaker expression of the gene was also visible in the FG of the PO at the same stage (Fig. 5A). *R2R3MYB5* (*Gb_02997*) was only and weakly expressed in the tapetum of the PO (Fig. 5C), whereas no expression was localized in the UO (Fig. 5D). *R2R3MYB25* (*Gb_39852*) was expressed in the degenerating nucellus and the innermost part of the UO integument (Fig. 5F), whereas in the PO the localization was slightly visible in the tapetum (Fig. 5E). *NAC Gb_05670* was expressed in the degenerating nucellus of the UO and in the flanking integument (Fig. 5J). Instead, the signal of *Gb_05670* in the PO was slightly visible in the FG (Fig. 5I). In addition, *NAC Gb_13930* was strongly expressed in the FG of the UO (Fig. 5L), whereas it was weakly visible in the FG of the PO (Fig. 5K). Interestingly, *NAC Gb_35309* and *Gb_18916* showed patterns of expression similar to *Gb_05670*. Indeed, they were expressed in the degenerated nucellus and in the integument of the UO (Fig. 5N, P). In the PO, their expression was weak but widespread through the nucellus and in the inner part of the integument (Fig. 5M, O). Longitudinal sections of PO and UO hybridized with sense probe for each gene are shown in Supplementary Fig. S9.

Genes related to programmed cell death, cell cycle regulation, DNA replication, and damage repair exhibit different expression in pollinated compared to unpollinated ovules

Through bioinformatic analysis we selected 27 senescence-related genes (Supplementary Table S6), nine of which were in common between the DEGs and PCW lists: one cysteine proteinase (*CYSP*), three metacaspase (*MCA*), one KDEL-tailed cysteine endopeptidase (*CEP1*), two ribonuclease 1 (*RNS1*), two autophagy-related protein (*ATG*). Considering apoptosis metabolism, among the 36 genes found (Supplementary Table S6), only a proteasome subunit beta (*PSB3*, *Gb_09326*) gene was in common between the two lists.

The common genes analysed (10) displayed higher expression levels in the UO_6 and UO_8 compared to the PO stages,

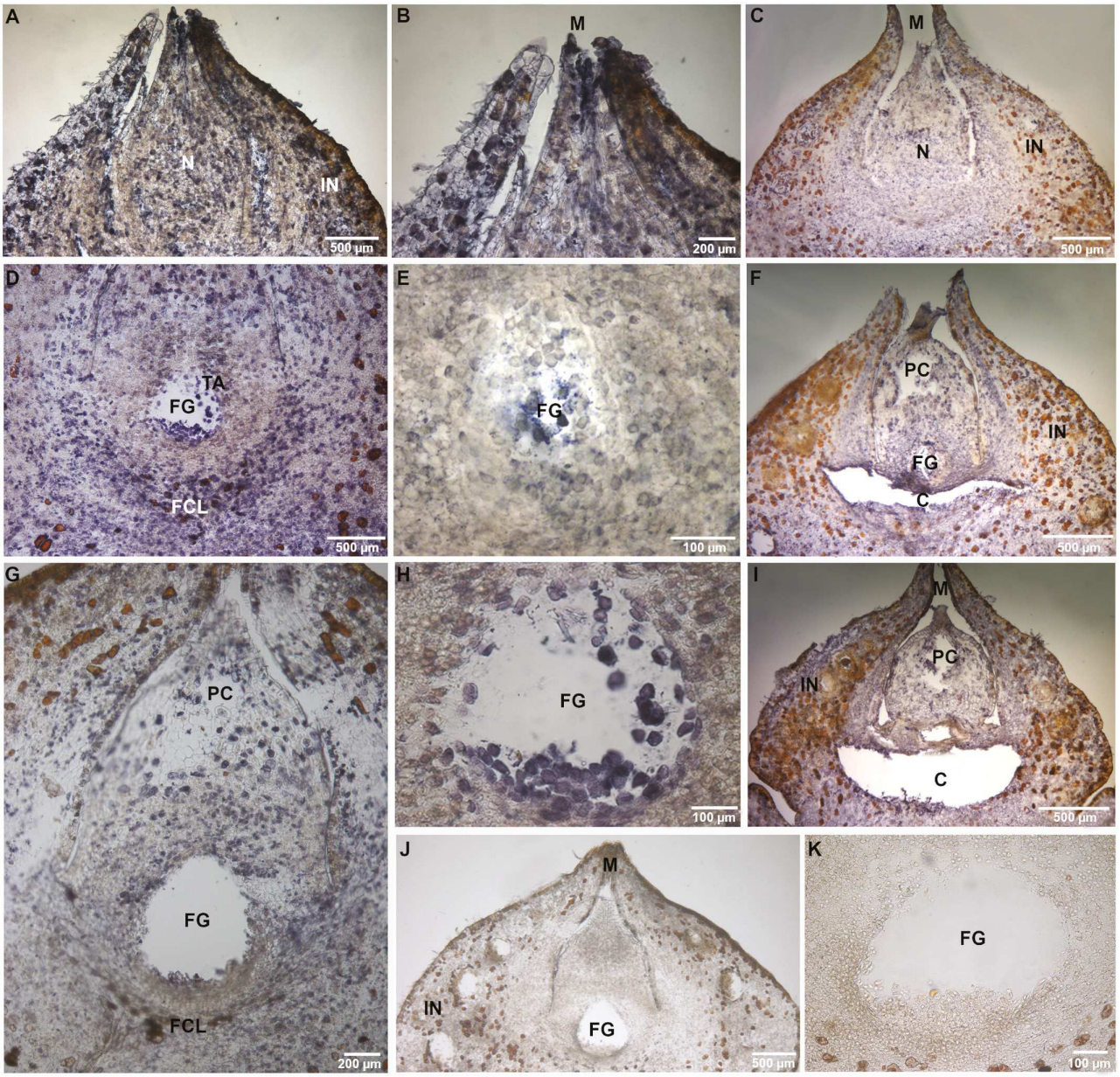

Fig. 4. Spatio-temporal distribution of free indole-3-acetic acid (IAA) across ovule development stages. Immuno-reaction is evidenced as purple-violet staining. The signal was detected in longitudinal section in pollinated (PO) (A, B, D, E, G, H) and unpollinated ovules (UO) (C, F, I) at stages 1, (A–C, E) 6 (D, F, H) and 8 (G, I). Details of FG (D, E, H) and pollen chamber (B) of pollinated ovules, showing the massive IAA accumulation. (J–K) Longitudinal sections of ovules processed without primary antibody (negative control). C, cavity; FCL, flattened-cells layer; FG, female gametophyte; IN, integument; M, micropyle; N, nucellus; PC, pollen chamber; TA, tapetum.

except for the *PSB3 Gb_09326*, which exhibited an opposite trend (Supplementary Fig. S10). In plants, most of the enzymes acting in PCD belong to the cysteine protease (CYSP) family (van Doorn and Woltering, 2008). Consequently, we analysed *CYSP1 Gb_13610* expression pattern in ovules by ISH. In PO_1 and PO_6, *CYSP1* expression was localized in all tissues of the ovules with a higher signal in the nucellus as well as in the flap zone (Fig. 6A, B). In PO_8, *CYSP1* expression was confined in the nucellus and around the FG (Fig. 6C). Concerning UO_1, no differences were observed when compared to the PO_1 (Fig. 6A, E). In both UO_6 and UO_8, *CYSP1* was expressed in all ovule tissues, with a strong localization around the FG (Fig. 6F, G).

The histological analysis showed an abnormal FG development in UO samples, suggesting defects in karyokinesis that might indicate cell cycle misregulation. RNA-seq data analysis supported this observation. Indeed, considering both the DEGs and the PCW lists, we selected nine

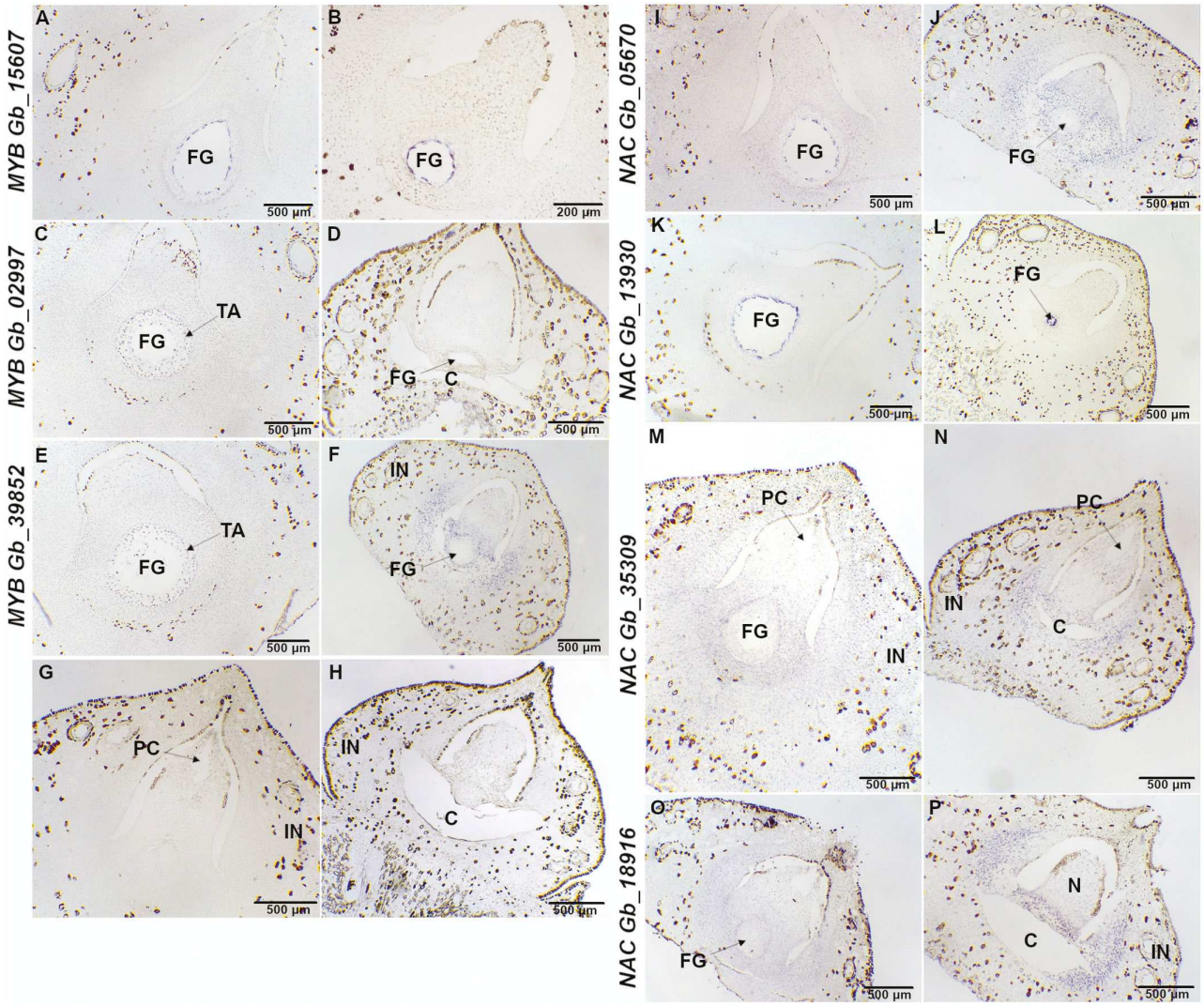

Fig. 5. Localization of selected *MYB* and *NAC* transcripts by *in situ* hybridization in longitudinal sections of pollinated (PO) and unpollinated (UO) ovules with dig-labelled antisense probes (A–N). *In situ* hybridizations of *G. biloba MYB Gb_15607* transcript in stage PO_6 (A) and UO_6 (B), *MYB Gb_02997* transcript in stage PO_6 (C) and UO_6 (D) and *MYB Gb_39852* transcript in stage PO_6 (E) and UO_6 ovules (F). (G–H) Longitudinal sections of PO and UO hybridized with *MYB Gb_39852* sense probe. *In situ* hybridizations of *G. biloba NAC Gb_05670* transcript in stage PO_6 (I) and UO_6 (J), *NAC Gb_13930* transcript in stage PO_6 (K) and UO_6 (L), *NAC Gb_35309* transcript in stage PO_6 (M) and UO_6 (N), and *NAC Gb_18916* transcript in the stage PO_6 (O) and UO_6 (P). Signal is evidenced by purple staining (A–F; I–P). C, cavity; FG, female gametophyte; IN, integument; N, nucellus; PC, pollen chamber; TA, tapetum.

key common genes encoding regulators of the cell cycle and mitosis (Supplementary Table S7), whose expression is shown in the heat map (Supplementary Fig. S11). Among these nine genes, we analysed *Cyclin-dependent kinase B1-1* (*CDKB1*) *Gb_38629* localization (Fig. 7), given its known role in the regulation of cell cycle progression (Umeda *et al.*, 1999; Porceddu *et al.*, 2001). *CDKB1* (*Gb_38629*) was down-regulated in the UO with respect to the PO and its expression was detected in all PO stages in the FG, nucellus, and FCL (Fig. 7A–C). The same localization was found in the UO at the same stages, with a gradual decrease in the signal (Fig. 7E–G).

Considering genes related to DNA replication and damage repair, 28 were in common among the two lists (Supplementary Table S7). The expression trend of the 28 genes is illustrated in Supplementary Fig. S12. All the genes showed a higher expression in the PO compared to the UO in all developmental stages analysed, although the most significant difference was found at 6 DAD (Supplementary Fig. S12).

Programmed cell death detection of aborted ovules

TUNEL assay was applied to longitudinal sections of UO and PO to determine how early cell degeneration starts in the UO

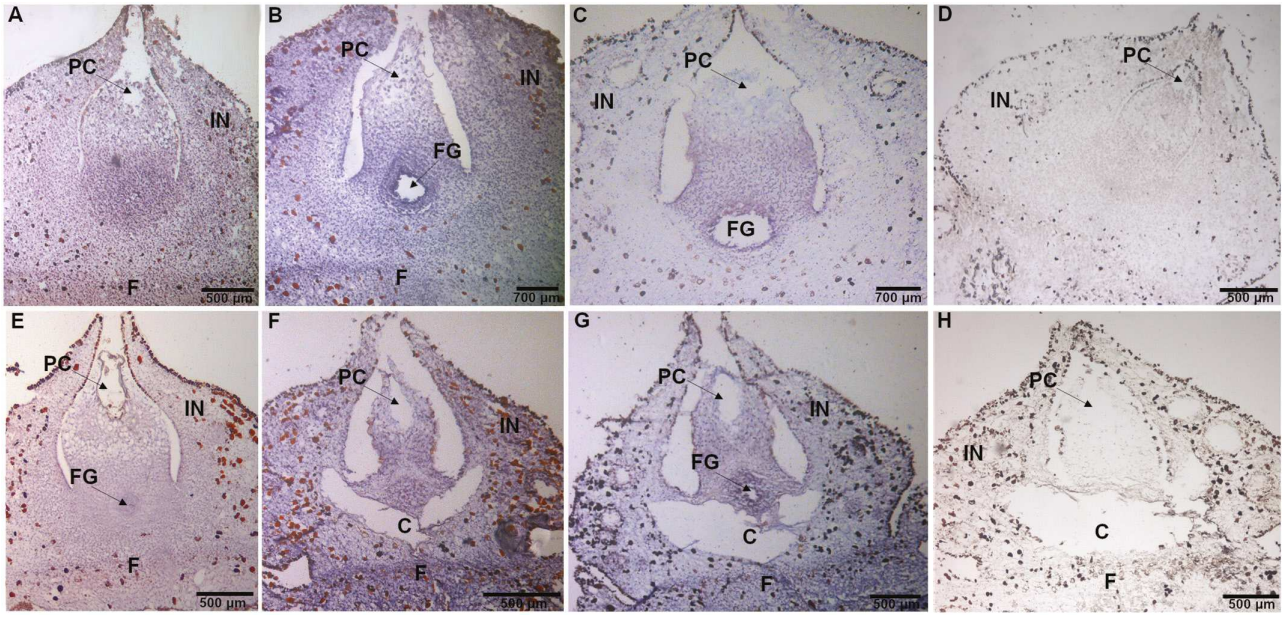

Fig. 6. Localization of *CYSP1* (*Gb_13610*) transcripts by *in situ* hybridization with dig-labelled antisense probe (A–C, E–G). Longitudinal sections of pollinated (PO) (A–D) and unpollinated ovules (UO) (E–H) at stages 1 (A, E), 6 (B, F) and 8 (C, G). Signal is evidenced by purple staining (A–C, E–G). Longitudinal sections of PO and UO hybridized with *CYSP1* sense probe (D, H). C, cavity; F, flap; FG, female gametophyte; IN, integument; PC, pollen chamber.

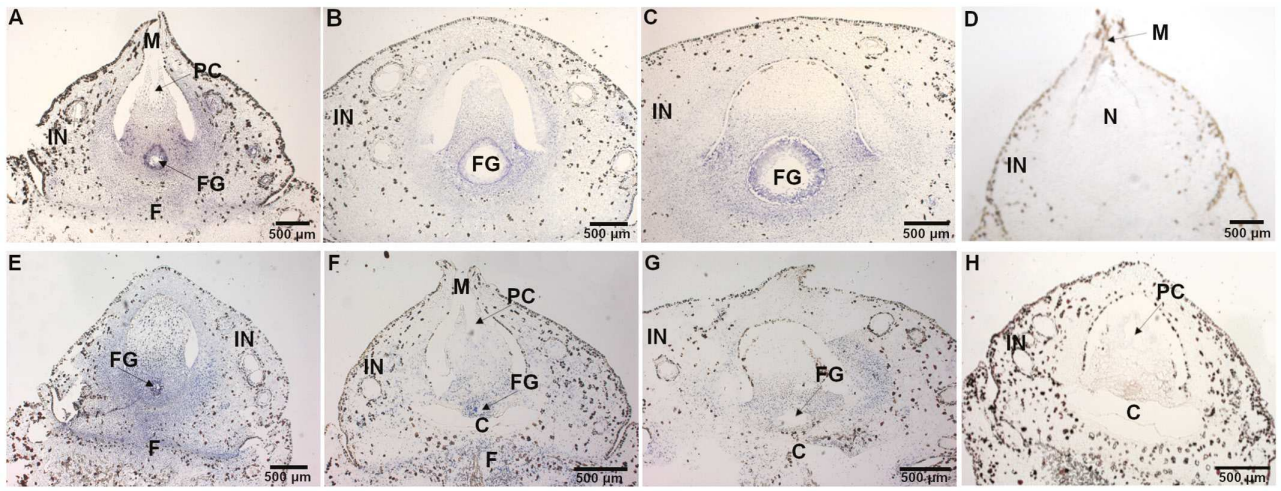

Fig. 7. Localization of *CDKB1* (*Gb_38629*) transcripts by *in situ* hybridization with dig-labelled antisense probe (A–F). Longitudinal sections of pollinated (PO) (A–C) and unpollinated ovules (UO) (D–F) at stages 1 (A, D), 6 (B, E), and 8 (C, F). Signal is evidenced by purple staining (A–F). Longitudinal sections of PO and UO hybridized with *CDKB1* sense probe (G, H). C, cavity; F, flap; FG, female gametophyte; IN, integument; M, micropyle; N, nucellus; PC, pollen chamber.

based on cytological features and the transcriptomic dataset (Fig. 8; Supplementary Fig. S13). Specifically, at UO_1, DNA fragmentation was observed exclusively in the basal zone of the nucellus, where, according to cyto-histological analysis, tissue degeneration and cavity will be evident in later stages (Fig. 8D). In the last stages, UO_6 (Fig. 8E) and UO_8 (Fig. 8F), several nuclei were TUNEL positive differently from the PO, where a sporadic signal is localized in the integument (Fig. 8A–C). This experiment confirms our hypothesis that in the UO, a PCD programme immediately starts in the absence of pollination, and we concluded that pollination inhibits PCD program in the PO.

Discussion

Microstructure of pollinated and abortive ovules

Based on morphological observations, we have hypothesized that pollination could be the signal for further ovule

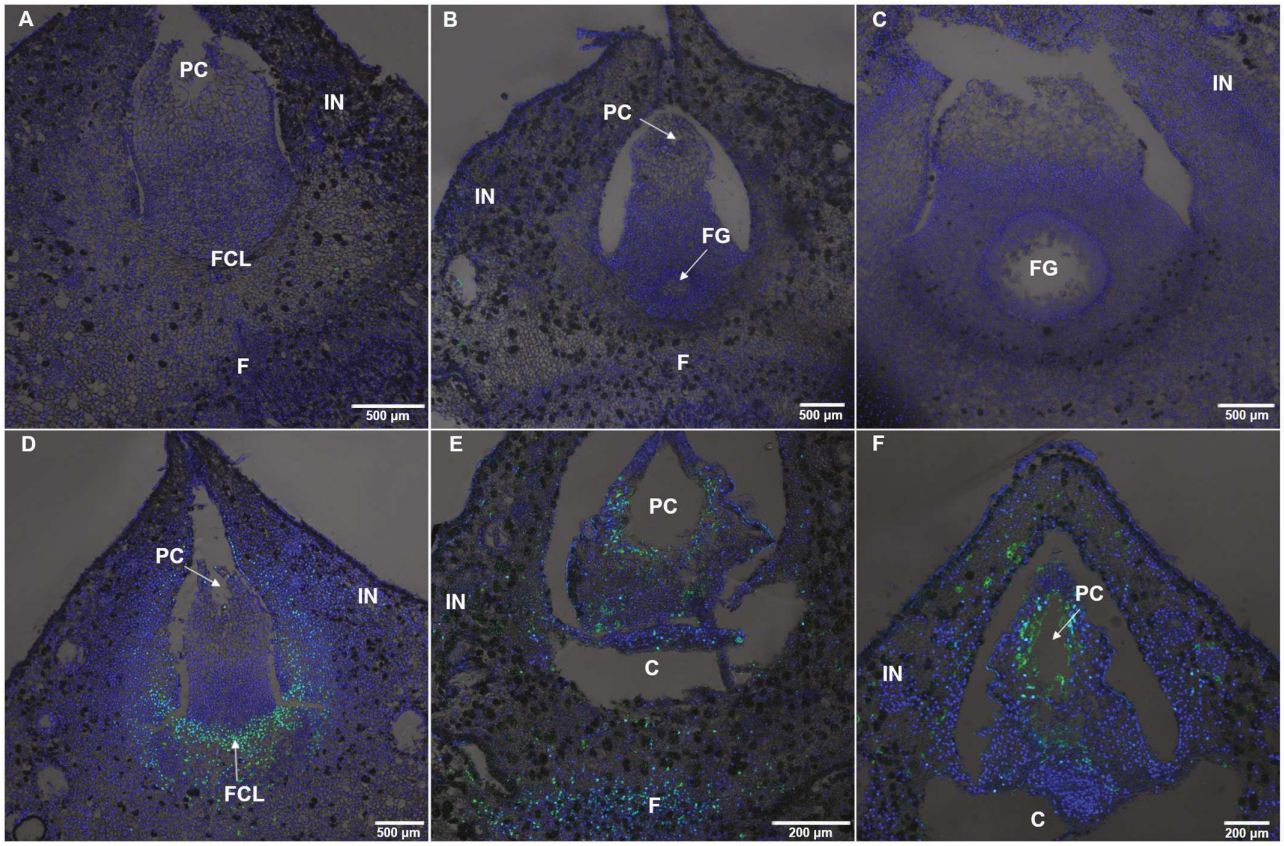

Fig. 8. DNA degradation in nuclei from pollinated and unpollinated ovules. Nuclear DNA fragmentation was visualized *in situ* using TUNEL staining on longitudinal paraffin sections in pollinated (PO) (A–C) and unpollinated (UO) (D–F) ovules at stages 1 (A, D), 6 (B, E), and 8 (C, F). Green colour indicates nuclear DNA fragmentation. Nuclei were counterstained with DAPI (blue colour). C, cavity; F, flap; FCL, flattened-cells layer; FG, female gametophyte; IN, integument; M, micropyle; PC, pollen chamber.

development and FG differentiation, leading to the formation of three distinguishable layers in the ovule integument, driving its transformation into the seed coats long before fertilization takes place (D'Apice *et al.*, 2021, 2022). In gymnosperms, molecular evidence suggesting that the pollination process stimulates the gene expression changes required for ovule developmental progression have not been described. This is due to the difficulty of investigating pollen signalling in the field, and to the scarcity of ovule mutants in these species (Lu *et al.*, 2016). In addition, in *Ginkgo*, which possess orthotrope ovules, pollination drops capture pollen from the environment, and transport it inside the nucellus (Jin *et al.*, 2012). During this process, pollen grains are hydrated on the surface of the PD and enter into the nucellus with the chance of fertilizing the egg cell (Jin *et al.*, 2012). It has been demonstrated that viable pollen sank faster than unviable pollen, suggesting an effective screening mechanism for *Ginkgo* (Jin *et al.*, 2012; Lu *et al.*, 2016).

Pollen arrival is crucial for ovule development progression. Female *Ginkgo* plants isolated from male plants aborted all of their ovules after the pollination drop (Friedman, 1987). Starting from this observation, this study aimed to explore the possible mechanism associated with ovule abortion in unpollinated *Ginkgo* ovules by combining anatomical observations and a transcriptomic approach. The relation between ovule development and successful pollination suggests a strict communication between the ovule integument, the FG, and the male gametophyte. Indeed, in our studies, the PD in *Ginkgo* pollinated plants lasted for approximately 7 d, whereas unpollinated plants showed a prolonged period of PD production. According to Jin *et al.* (2012), these results suggested that plants invest energy to persistently secrete abundant PDs during the pollination period, counterbalancing the evaporation effect of wind and sunlight. In addition, the inner structures of the pollinated and abortive ovules were considerably different. Indeed, the presence of a cavity in the basal portion of the nucellus in the UO is in line with results obtained in other species, such as *Punica granatum* (Wetzstein *et al.*, 2013), *Cucumis sativus* (Li *et al.*, 2014), and *Camellia oleifera* (Gao *et al.*, 2017). Moreover, in *Prunus mume* the absence of reproductive events induces anomalies in embryo sac development and differentiation (Sun *et al.*, 2016).

Differential expression of some ovule-related genes might affect the growth of the *G. biloba* ovule

The RNA-seq approach was used to investigate the genetic pathways involved in ovule abortion in the absence of

a pollination event. Thus, the differences in gene expression between the UO and the PO at three developmental stages were analysed. The data revealed that most of the DEGs were found at 6 DAD, suggesting that the responses to the pollination occurred about 1 week after pollen arrival. Interestingly, this stage coincides with the germination of the male gametophyte (Friedman, 1987). It is therefore possible to assume that this process also plays a crucial role in determining the large number of DEGs at 6 DAD. Accordingly, Yao *et al.* (2018) revealed extensive changes in the transcriptome of the gymnosperm *Pinus tabuliformis* during the FNMM between the fertile line (FL) and the sterile line (SL). In this study, 7174 DEGs were found at three developmental stages, named FNM1, 2, and 3. The highest number of DEGs was found at FNM2, suggesting the evident differences in the transcriptional level at FNM2.

Our functional GO annotation revealed that the most of the significant DEGs fell into the biological process categories of hormones, senescence, cell cycle regulation, and stress and defence response genes. In accordance, Gong *et al.* (2021) performed a similar study, investigating the transcriptomic data of natural ovule abortion mutants (female sterile line, STE) and the wild type (female fertile line, FER) of *Pinus tabuliformis*. Upon comparing our GO analysis with that conducted by Gong and colleagues, we found a nearly complete overlap of the GO terms. This indicates that in gymnosperms, the lack of pollination leads to abnormal mitosis and apoptosis.

Both auxin signalling and programmed cell death are essential for ovule developmental progression in *G. biloba*

Auxin has been studied due to its important role in ovule development (Larsson *et al.*, 2017), and its interesting modulation after the pollination event.

In different species, pollination and subsequent fertilization induced the rapid accumulation of several hormones, including auxin and gibberellins, which play key roles in the induction of fruit set (Dorcey *et al.*, 2009; McAtee *et al.*, 2013). Moreover, recent studies indicate that cellular preparation for PCD is coordinated primarily by transcriptional regulation of hormone signalling (Li *et al.*, 2022; Ni *et al.*, 2022; Guo *et al.*, 2023). In particular, auxin signalling and PCD regulation seem to be often connected (Kacprzyk *et al.*, 2022).

Thus, in this work, we mainly focused on the crosstalk between auxin and PCD during *Ginkgo* ovule development, focusing on its impact on degeneration of the nucellus. In the ovule, the nucellus is a short-lived tissue that, as it degenerates, allows the expansion of the FG (Domínguez *et al.*, 2001), in both gymnosperms and angiosperms (Daneva *et al.*, 2016).

Although a set of DEGs involved in hormone signalling and nucellar cell death were identified (Li *et al.*, 2019), the molecular network controlling the nucellar PCD in *Ginkgo* ovules has not been well understood.

In a previous study, we showed that during stage 9, the micropyle opening is narrower, and nucellus cells adjacent to the pollen chamber collapse inwards, gradually reducing its dimension until closing it (D'Apice *et al.*, 2021). Then, the haustorial pollen tube consumes the nucellar tissue, which is also thinning because of the expansion of the coenocytic FG. This generally forms more than 1000 free nuclei before cellularization begins (Lee, 1955).

In Arabidopsis, one part of the nucellus degenerates before fertilization, whereas the other part persists until after fertilization (Xu *et al.*, 2016). Recently, it was reported that nucellar degeneration after pollination and before fertilization starts in the cells adjacent to the developing FG, and it is controlled by auxin (Wang *et al.*, 2021). Indeed, our IAA immunolocalization data suggest a dynamic and ordered influx and efflux of auxin in the nucellus after pollination and a disordered distribution of auxin in the UO. This might cause the failure of the nucellar and FG normal development, with the consequent abortion of the UO. Auxin efflux under control of PIN proteins is essential to achieve appropriate auxin maxima and for normal auxin signalling in a wide range of developmental processes, as demonstrated in Arabidopsis and maize (McSteen and Hake, 2001; Carraro *et al.*, 2006; Gallavotti *et al.*, 2008; Křeček *et al.*, 2009; Forestan *et al.*, 2012). Data analysis performed in this work has shown that four *PIN* genes, identified as *PIN3 Gb_03217*, *Gb_29191*, *Gb_02144*, and *PIN4 Gb_23207*, presenting up-regulation in the PO across the different time-points. Interestingly, only the expression of *PIN1 Gb_06199* showed a strong reduction as soon as the pollen was received, suggesting a possible post-pollination regulation mechanism. Moreover, ISH on *PIN1 Gb_06199* transcripts revealed different cyto-histological expression domains between the PO and the UO. Our results are in line with the current literature, which reports that auxin efflux carrier PIN1 transports auxin into the nucellus, while PIN3, PIN4, and PIN7 deliver auxin to degenerating nucellar cells and concomitantly control FG central vacuole expansion (Wang *et al.*, 2021). In Arabidopsis, the *pin1* mutant displays inhibited nucellar cells degeneration, whereas the *pin3/4/7* triple mutant shows accelerated nucellar cell death but with reduced vacuolation, suggesting that auxin accumulation in the nucellus may promote PCD (Wang *et al.*, 2021). The evidence demonstrates the effect of auxin on PCD induced during plant development or by environmental factors (reviewed by Kacprzyk *et al.*, 2022).

Our results suggest that the hormonal regulatory pathways in *Ginkgo* ovules are similar to those found in angiosperms. Thus, we can hypothesize a conserved mechanism underlying this developmental process.

Transcription Factors as bridges linking pollen signalling and programmed cell death control

Transcription factors may act as bridges linking phytohormone signalling with PCD regulation (Li *et al.*, 2019).

Several homologues of the TFs associated with PCD have been identified as DEGs, including MYB and NAC TFs.

Homologues of MYB (Plackett *et al.*, 2011) and bHLH (Ko *et al.*, 2014) have been known to promote tapetum PCD. MADS-box TFs were found to induce nucellar PCD during rice seed development (Yin *et al.*, 2012). Additionally, it was found that some NAC proteins function downstream of the ethylene signalling pathway to modulate the cascade of leaf senescence-associated PCD (Matallana-Ramírez, 2012).

Our results also suggest the involvement of *Ginkgo* NAC TFs in the degeneration process of the nucellus and the FG in the UO. The analysed *NAC* expression was mainly concentrated in the nucellus, which starts to degenerate approximately 1 week/10 d after the non-arrival of pollen. Among them, NAC *Gb_13930* seems to be mainly involved in FG degeneration because a strong signal was concentrated in that region. After all, the other studied NAC genes might be involved in the death process of the entire nucellus because of their more widespread expression in this tissue. This was supported by recent discovery in Arabidopsis ovules, in which the combined triple mutation of *NAC-LIKE ACTIVATED BY AP3/PI* (*NAP/ANAC029*), *SPEEDY HYPONASTIC GROWTH* (*SHYG*), and *ORESARA1* (*ORE1*) genes, which are the most expressed NAC at 4 d after emasculation, caused a delay in ovule senescence and an extension of the fertility interval (Van Durme *et al.*, 2023). The expression of *Ginkgo* NAC in these tissues may indicate their involvement in the complete degradation and lignification of the nucellus and FG. However, the process of lignification could only be observed after the final stage (UO_8) examined in this study. This hypothesis is supported by the demonstrated requirement of NAM, CUC2, VND1-7, NST1, and NST2 in regulating the lignification process during xylem differentiation (Kubo *et al.*, 2005; Mitsuda *et al.*, 2005; Nakano *et al.*, 2015). Nevertheless, some of these transcripts were also observable in the PO, especially in the contact region between the tapetum and the FG. This might be explainable because during the FG enlargement, at stage 9 of ovule development, the tapetum surrounding the FG goes through PCD and degeneration (Douglas *et al.*, 2007; D'Apice *et al.*, 2021). The expression of senescence/PCD genes in the nucellus of PO is not surprising because at this stage, the nucellus rapidly degenerates due to FG enlargement and male gametophyte growth (D'Apice *et al.*, 2021). Regarding *MYB* genes, the most expressed gene was *Gb_39852*, which seems to be directly correlated with the degeneration of the nucellus and the adjacent portion of the integument in the UO. Patzlaff *et al.* (2003) described that the R2R3-MYB gene of *Pinus taeda* (*PtMYB4*) was expressed only in cells which were destined to lignify suggesting that the selected MYB TFs seem to be associated with the lignification process.

Ovule abortion occurs due to a different reprogramming of programmed cell death, cell cycle regulation and DNA replication induced by pollen

PCD is the genetic regulation of cell suicide, playing an essential role in multicellular organism development, homeostasis, and integrity (Ameisen, 2002).

In plants, three main types of PCD are reported: apoptotic-like cell death (AL-PCD), senescence-associated death, and vacuole-mediated cell death, which resembles autophagy (Mondal *et al.*, 2021). In this work, most of the PCD-associated genes were categorized in the senescence pathway, which is a highly regulated process that requires the expression of many regulatory genes and involves the interaction of many signalling pathways (Buchanan-Wollaston, 2008).

Several genes involved in senescence were identified, and they were often referred to as SAGs or senescence-up-regulated genes. Some of the identified senescence-induced genes encode proteases, protease regulators, RNases, Gln synthetase, metallothioneins, glutathione *S*-transferase, catalase, ACC oxidase, lipases, glyoxylate cycle enzymes, endoxyloglucan transferase, pathogenesis-related proteins, ATP sulfurylase, Cyt P450, and polyubiquitin (Buchanan-Wollaston, 1997; Weaver *et al.*, 1997).

Here, the transcriptomic approach has shown the presence of two senescence key genes, *Gb_13610* and *Gb_10444*, strongly up-regulated in the UO, codifying for cysteine proteinase and KDEL- cysteine endopeptidase (KDEL CysEP), respectively, which are known to be involved in PCD (Beers *et al.*, 2000, 2004; Schaller, 2004). We focused on the *Gb_13610* cysteine proteinase, whose transcript was essentially revealed in the flap zone in both the PO and the UO. Unsurprisingly, *CYSP1* was found in tissues undergoing PCD, especially in cells that eventually collapse. Similar results were obtained in the unpollinated ovaries of *Pisum sativum* (Cercós *et al.*, 1999), in the outer integument developing into the seed coat of *Phalaenopsis* (Nadeau *et al.*, 1996), and in the megagametophyte cells after germination of *Picea glauca* seeds (He and Kermode, 2003). In *Brassica napus*, *BnCysp1* is associated with PCD of the inner integument of the ovule (Wan *et al.*, 2002).

On the other hand, because the whole FNMM process corresponds to continuous karyokinesis (Yao *et al.*, 2018; Zhang *et al.*, 2020), the abnormal FG development observed in the UO suggested an anomaly in the cell cycle and its regulation, that alone or in concomitance with other mechanisms, leads to ovule abortion. Thus, *CDKB*, known for its function in regulating the cell cycle, was investigated. The decreasing expression in the UO detected for the *CDKB1* is in line with the general role of these proteins. Indeed, the DNA damage signals are transmitted via several proteins, suppressing the activity of cyclin-dependent kinase to arrest the cell cycle.

At last, in *Ginkgo* ovules, one senescence-associated event was the reduction in dimension after PD emission. Indeed, before abortion, the UO already showed a reduced size, with respect to the PO, which exhibited exponential growth after PD emission. In addition, the UO showed a large cavity between the nucellus and the flap zone, suggesting the presence of several apoptotic cells in this portion. During PCD, the earliest sign of cellular disruption is DNA fragmentation (Kuthanova *et al.*, 2008). Indeed, through the TUNEL assay, we showed that DNA fragmentation started immediately at the UO_1 stage,

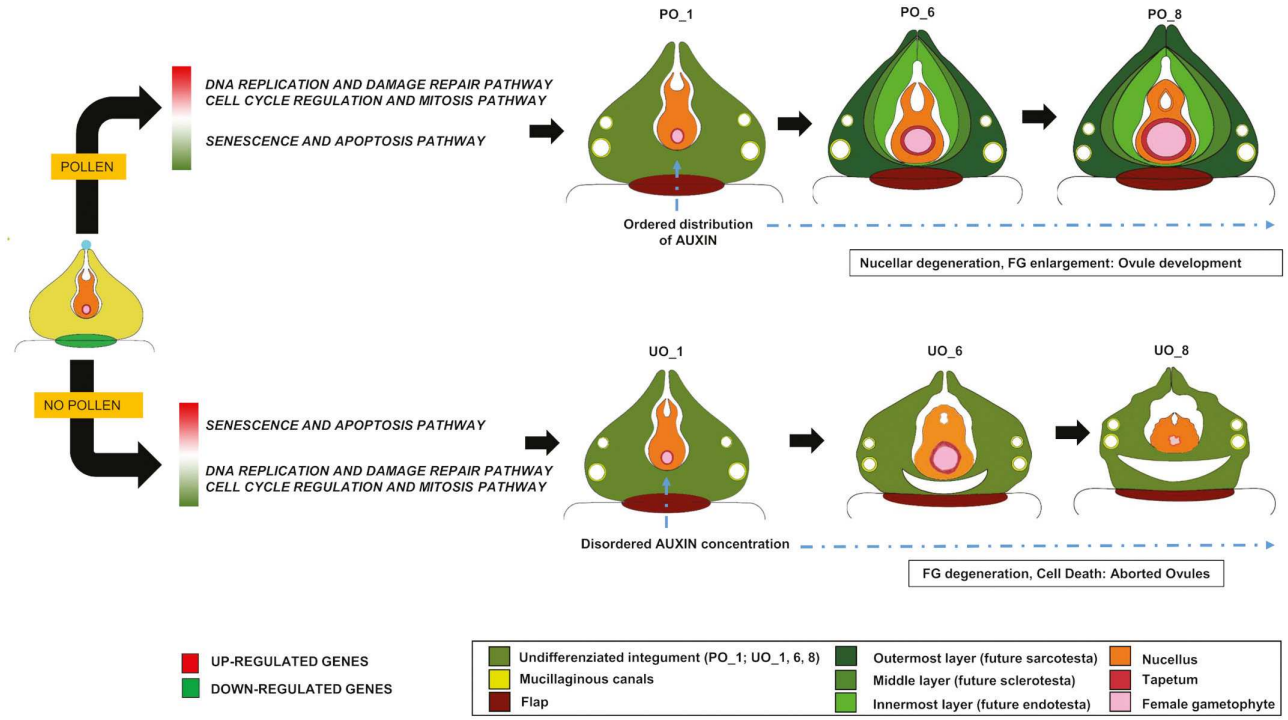

Fig. 9. Simplified scheme representing how the pollination event is crucial for ovule development in *G. biloba*. Pollen captured by the pollination drop blocks the cyto-histological disorganization of the ovule and allows ovule development progression. On the contrary, ovules from female *G. biloba* plants that were geographically isolated and did not receive pollen gradually aborted all their ovules after the emission of the pollination drop due to cyto-histological disorganization. In pollinated ovules (PO), ordered auxin distribution and up-regulation of key genes involved in cell cycle regulation and mitosis, DNA replication and damage repair were observed. In addition, genes associated with PCD and senescence were down-regulated. Overall, this genetic network is likely to be involved in gametophyte expansion and nucellar degeneration. The opposite trend in gene expression was observed in unpollinated ovules (UO), which showed gametophyte degeneration, cytohistological alterations and finally abortion.

with the signal accumulating at the base of the nucellus before the cavity became visible, confirming our hypothesis. In the last stages, DNA fragmentation affects other structures, including nucellar tissues and integuments, highlighting the massive presence of cells undergoing PCD.

Overall, the results confirmed our initial hypothesis that pollination inhibits the earliest PCD programme in the PO, leading to their proper development.

Given the complex network of molecular players described in this work, we have reported a scheme that shows how the pollination event is crucial for ovule development in *Ginkgo* and the cause of abortion in the unpollinated ovules (Fig. 9), with the aim of integrating all the results discussed here, and providing a useful reference for stimulating and establishing new studies of these processes in non-model plants.

Supplementary data

The following supplementary data are available at *JXB* online.

Fig. S1. GO enrichment analysis and comparison of all DEGs in UO_1 versus PO_1, UO_6 versus PO_6, and UO_8 versus PO_8.

Fig. S2. Pathway enrichment analysis and comparison of all DEGs in UO_1 versus PO_1, UO_6 versus PO_6, and UO_8 versus PO_8.

Fig. S3. Module-Day trait association identified by WGCNA in the PO and the UO in all three stages analysed.

Fig. S4. The frequency of overlapping between DEGs identified by DESeq2 and WGCNA.

Fig. S5. Comparison between RNA-seq expression levels (green bars) and RT–qPCR expression levels (orange lines) of the most affected pathways.

Fig. S6. Diagram of the DEGs UO/PO list and 'pollination condition by WGCNA' (PCW) related to the metabolism of the hormones.

Fig. S7. Auxin pathway modulation.

Fig. S8. Heat maps illustrate the variations in expression of 96 genes encoding TFs.

Fig. S9. *MYB* and *NAC* sense probe control.

Fig. S10. Senescence pathway modulation.

Fig. S11. Cell cycle regulation and mitosis pathway modulation.

Fig. S12. DNA replication and damage repair pathway modulation.

Fig. S13. TUNEL assay in the PO and the UO.

Table S1. Statistics of RNA-seq alignment for all the 18 libraries obtained.

Table S2. Primers used in the present work.

Table S3. Output obtained by Weighted Gene Correlation Network Analysis (WGCNA) by using a matrix of 14 914 genes (FPKM >10 in any sample) showing both correlation and annotation of genes.

Table S4. Summary of the significant modules used in this work correlated with the 'Pollination trait' obtained by WGCNA.

Table S5. Bioinformatic RNA-seq elaboration concerning hormone metabolism.

Table S6. Bioinformatic RNA-seq elaboration concerning senescence and apoptosis pathways.

Table S7. Bioinformatic RNA-seq elaboration concerning cell cycle regulation, mitosis, DNA replication, and damage repair.

Table S8. TF families involved in ovule development in pollinated and unpollinated conditions.

Acknowledgements

We are grateful to Maria Beatrice Bitonti for revising the manuscript. We thank Coretto Garden (Montalto Uffugo, Cosenza, Italy) for providing us with the ovules of isolated female plants of *G. biloba*.

Author contributions

LB, BB, LC, and FA planned and designed the study; AM, EG, ET, GD, SM, MDM, SN, and NB performed the experiments and analysed the data; AM and ET analysed sequencing data; AM wrote the first draft; and LB, BB, LC, AM, AC, SN, SM, MDM, ET, NB, and FA provided critical editing of the manuscript.

Conflict of interest

The authors declare no conflict of interest.

Funding

This work was funded by MIUR (Ministry of Education, University and Research) PRIN (Progetto di Ricerca di Interesse Nazionale) Project titled 'Evolution of Molecular Networks Controlling Seed Coat Differentiation,' with grant number 20175R447S, CUP H24I17000290001. The post-doctoral fellowship for AM was funded by the MIUR PRIN Project with grant number 20175R447S. ET is a recipient of a PhD fellowship granted by the University of Calabria, Italy. This project has received funding from the European Union's Horizon 2020 RISE programme (Marie Skłodowska-Curie grant agreement number 101007738).

Data availability

The datasets generated for this study can be found in the Sequence Read Archive (SRA) database at NCBI (SRA BioProject PRJNA700482; https://www.ncbi.nlm.nih.gov/bioproject?term=PRJNA700482&cmd=DetailsSearch) and within its supplementary data published online. Correspondence and requests for materials should be addressed to the corresponding author.

References

Ambrose BA, Lerner DR, Ciceri P, Padilla CM, Yanofsky MF, Schmidt RJ. 2000. Molecular and genetic analyses of the *silky1* gene reveal conservation in floral organ specification between eudicots and monocots. Molecular Cell **5**, 569–579.

Ameisen JC. 2002. On the origin, evolution, and nature of programmed cell death: a timeline of four billion years. Cell Death & Differentiation **9**, 367–393.

Barro-Trastoy D, Dolores Gomez M, Tornero P, Perez-Amador MA. 2020. On the way to ovules: the hormonal regulation of ovule development. Critical Reviews in Plant Sciences **39**, 431–456.

Beers EP, Jones AM, Dickerman AW. 2004. The S8 serine, C1A cysteine and A1 aspartic protease families in *Arabidopsis*. Phytochemistry **65**, 43–58.

Beers EP, Woffenden BJ, Zhao C. 2000. Plant proteolytic enzymes: possible roles during programmed cell death. Plant Molecular Biology **44**, 399–415.

Buchanan-Wollaston V. 1997. The molecular biology of leaf senescence. Journal of Experimental Botany **48**, 181–199.

Buchanan-Wollaston V. 2008. Senescence processes in plants. Annual Plant Reviews, Volume 26. Annals of Botany **101**, 197.

Carraro N, Forestan C, Canova S, Traas J, Varotto S. 2006. *ZmPIN1a* and *ZmPIN1b* encode two novel putative candidates for polar auxin transport and plant architecture determination of maize. Plant Physiology **142**, 254–264.

Ceccato L, Masiero S, Sinha Roy D, Bencivenga S, Roig-Villanova I, Ditengou FA, Palme K, Simon R, Colombo L. 2013. Maternal control of PIN1 is required for female gametophyte development in *Arabidopsis*. PLoS One **8**, e66148.

Cercós M, Santamaría S, Carbonell J. 1999. Cloning and characterization of *TPE4A*, a thiol-protease gene induced during ovary senescence and seed germination in pea. Plant Physiology **119**, 1341–1348.

Chen F, Zhang X, Liu X, Zhang L. 2017. Evolutionary analysis of MIKCc-Type MADS-Box genes in gymnosperms and angiosperms. Frontiers in Plant Science **8**, 895.

Chiappetta A, Fambrini M, Petrarulo M, *et al*. 2009. Ectopic expression of *LEAFY COTYLEDON1-LIKE* gene and localised auxin accumulation mark embryogenic competence in epiphyllous plants of *Helianthus annuus* x *H. tuberosus*. Annals of Botany **103**, 735–747.

Cucinotta M, Cavalleri A, Chandler JW, Colombo L. 2021. Auxin and flower development: a blossoming field. Cold Spring Harbor Perspectives in Biology **13**, a039974.

Cucinotta M, Colombo L, Roig-Villanova I. 2014. Ovule development, a new model for lateral organ formation. Frontiers in Plant Science **5**, 117.

Cucinotta M, Di Marzo M, Guazzotti A, de Folter S, Kater MM, Colombo L. 2020. Gynoecium size and ovule number are interconnected traits that impact seed yield. Journal of Experimental Botany **71**, 2479–2489.

Daneva A, Gao Z, Van Durme M, Nowack MK. 2016. Functions and regulation of programmed cell death in plant development. Annual Review of Cell and Developmental Biology **32**, 441–468.

D'Apice G, Moschin S, Araniti F, Nigris S, Di Marzo M, Muto A, Banfi C, Bruno L, Colombo L, Baldan B. 2021. The role of pollination in controlling *Ginkgo biloba* ovule development. The New Phytologist **232**, 2353–2368.

D'Apice G, Moschin S, Nigris S, Ciarle R, Muto A, Bruno L, Baldan B. 2022. Identification of key regulatory genes involved in the sporophyte and gametophyte development in *Ginkgo biloba* ovules revealed by in situ expression analyses. American Journal of Botany **109**, 887–898.

Domínguez F, Moreno J, Cejudo FJ. 2001. The nucellus degenerates by a process of programmed cell death during the early stages of wheat grain development. Planta **213**, 352–360.

Dorcey E, Urbez C, Blázquez MA, Carbonell J, Perez-Amador MA. 2009. Fertilization-dependent auxin response in ovules triggers fruit development through the modulation of gibberellin metabolism in *Arabidopsis*. The Plant Journal **58**, 318–332.

Douglas AW, Stevenson DW, Little DP. 2007. Ovule development in *Ginkgo biloba* L., with emphasis on the collar and nucellus. International Journal of Plant Sciences **168**, 1207–1236.

Drews GN, Koltunow AMG. 2011. The female gametophyte. The Arabidopsis Book **9**, e0155.

Figueiredo DD, Batista RA, Roszak PJ, Hennig L, Köhler C. 2016. Auxin production in the endosperm drives seed coat development in *Arabidopsis*. eLife **5**, e20542.

Figueiredo DD, Köhler C. 2018. Auxin: a molecular trigger of seed development. Genes & Development **32**, 479–490.

Forestan C, Farinati S, Varotto S. 2012. The maize PIN gene family of auxin transporters. Frontiers in Plant Science **3**, 16.

Friedman WE. 1987. Growth and development of the male gametophyte of *Ginkgo biloba* within the ovule (*in vivo*). American Journal of Botany **74**, 1797–1815.

Gallavotti A, Yang Y, Schmidt RJ, Jackson D. 2008. The relationship between auxin transport and maize branching. Plant Physiology **147**, 1913–1923.

Gao C, Yang R, Yuan D. 2017. Characteristics of developmental differences between fertile and aborted ovules in *Camellia oleifera*. Journal of the American Society for Horticultural Science **142**, 330–336.

Gao Z, Daneva A, Salanenka Y, *et al*. 2018. KIRA1 and ORESARA1 terminate flower receptivity by promoting cell death in the stigma of *Arabidopsis*. Nature Plants **4**, 365–375.

Gong Z, Han R, Xu L, Hu H, Zhang M, Yang Q, Zeng M, Zhao Y, Zheng C. 2021. Combined transcriptome analysis reveals the ovule abortion regulatory mechanisms in the female sterile line of *Pinus tabuliformis* Carr. International Journal of Molecular Sciences **22**, 3138.

Guo Y, Zhang S, Li Y, Zhang X, Liu H, Liu S, Liu J, Wang G. 2023. A transcriptomic evaluation of the mechanism of programmed cell death of the replaceable bud in Chinese chestnut. Open Life Sciences **18**, 20220635.

He X, Kermode AR. 2003. Proteases associated with programmed cell death of megagametophyte cells after germination of white spruce (*Picea glauca*) seeds. Plant Molecular Biology **52**, 729–744.

Hollender CA, Kang C, Darwish O, Geretz A, Matthews BF, Slovin J, Alkharouf N, Liu Z. 2014. Floral transcriptomes in woodland strawberry uncover developing receptacle and anther gene networks. Plant Physiology **165**, 1062–1075.

Jin B, Wang D, Lu Y, Jiang XX, Zhang M, Zhang L, Wang L. 2012. Female short shoot and ovule development in *Ginkgo biloba* L. with emphasis on structures associated with wind pollination. International Scholarly Research Notices **2012**, e230685.

Kacprzyk J, Burke R, Schwarze J, McCabe PF. 2022. Plant programmed cell death meets auxin signalling. The FEBS Journal **289**, 1731–1745.

Ko SS, Li MJ, Sun-Ben Ku M, *et al*. 2014. The bHLH142 transcription factor coordinates with TDR1 to modulate the expression of EAT1 and regulate pollen development in rice. The Plant Cell **26**, 2486–2504.

Křeček P, Skůpa P, Libus J, Naramoto S, Tejos R, Friml J, Zažímalová E. 2009. The PIN-FORMED (PIN) protein family of auxin transporters. Genome Biology **10**, 249.

Kubo M, Udagawa M, Nishikubo N, Horiguchi G, Yamaguchi M, Ito J, Mimura T, Fukuda H, Demura T. 2005. Transcription switches for protoxylem and metaxylem vessel formation. Genes & Development **19**, 1855–1860.

Kuthanova A, Opatrny Z, Fischer L. 2008. Is internucleosomal DNA fragmentation an indicator of programmed death in plant cells? Journal of Experimental Botany **59**, 2233–2240.

Langfelder P, Horvath S. 2008. WGCNA: an R package for weighted correlation network analysis. BMC Bioinformatics **9**, 559.

Larsson E, Vivian-Smith A, Offringa R, Sundberg E. 2017. Auxin homeostasis in *Arabidopsis* ovules is anther-dependent at maturation and changes dynamically upon fertilization. Frontiers in Plant Science **8**, 1735.

Lee CL. 1955. Fertilization in *Ginkgo biloba*. Botanical Gazette **117**, 79–100.

Li D, Wu D, Li S, Guo N, Gao J, Sun X, Cai Y. 2019. Transcriptomic profiling identifies differentially expressed genes associated with programmed cell death of nucellar cells in *Ginkgo biloba* L. BMC Plant Biology **19**, 1–17.

Li J, Wu Z, Cui L, *et al*. 2014. Transcriptome comparison of global distinctive features between pollination and parthenocarpic fruit set reveals transcriptional phytohormone cross-talk in cucumber (*Cucumis sativus* L.). Plant and Cell Physiology **55**, 1325–1342.

Li W, Li Q, Lyu M, *et al*. 2022. Lack of ethylene does not affect reproductive success and synergid cell death in *Arabidopsis*. Molecular Plant **15**, 354–362.

Lu Y, Zhang L, Cheng F, Zhao J, Cui J, Li W, Li W, Jin B. 2016. The morphology, ultrastructure, element distribution and motion behaviour in pollen of *Ginkgo biloba* L. Trees **30**, 2189–2201.

Matallana-Ramírez LP. 2012. Unraveling the ORE1 regulon in *Arabidopsis thaliana*: molecular and functional characterization of up-and down-stream components. Doctoral dissertation, Universität Potsdam.

McAtee P, Karim S, Schaffer R, David K. 2013. A dynamic interplay between phytohormones is required for fruit development, maturation, and ripening. Frontiers in Plant Science **4**, 79.

McSteen P, Hake S. 2001. barren inflorescence2 regulates axillary meristem development in the maize inflorescence. Development **128**, 2881–2891.

Mitsuda N, Seki M, Shinozaki K, Ohme-Takagi M. 2005. The NAC transcription factors NST1 and NST2 of *Arabidopsis* regulate secondary wall thickenings and are required for anther dehiscence. The Plant Cell **17**, 2993–3006.

Mondal R, Antony S, Roy S, Chattopadhyay SK. 2021. Programmed cell death (PCD) in plant: molecular mechanism, regulation, and cellular dysfunction in response to development and stress. Regulation and Dysfunction of Apoptosis **2**, 1–20.

Nadeau JA, Zhang XS, Li J, O'Neill SD. 1996. Ovule development: identification of stage-specific and tissue-specific cDNAs. The Plant Cell **8**, 213–239.

Nakano Y, Yamaguchi M, Endo H, Rejab NA, Ohtani M. 2015. NAC-MYB-based transcriptional regulation of secondary cell wall biosynthesis in land plants. Frontiers in Plant Science **6**, 288.

Ni X-L, Hou H, Xie Q, Zhang H, Yan P, Lv Y. 2022. Caspase 3-like protease is involved in ethylene-induced programmed cell death during aerenchyma formation in *Helianthus annuus* stem. Microscopy Research and Technique **85**, 3707–3715.

Patzlaff A, McInnis S, Courtenay A, *et al*. 2003. Characterisation of a pine MYB that regulates lignification. The Plant Journal **36**, 743–754.

Plackett AR, Thomas SG, Wilson ZA, Hedden P. 2011. Gibberellin control of stamen development: a fertile field. Trends in Plant Science **16**, 568–578.

Porceddu A, Stals H, Reichheld J-P, Segers G, Veylder LD, Barrôco R de P, Casteels P, Montagu MV, Inzé D, Mironov V. 2001. A plant-specific cyclin-dependent kinase is involved in the control of G2/M progression in plants. Journal of Biological Chemistry **276**, 36354–36360.

Prior N, Little SA, Boyes I, Griffith P, Husby C, Pirone-Davies C, Stevenson DW, Tomlinson PB, von Aderkas P. 2019. Complex reproductive secretions occur in all extant gymnosperm lineages: a proteomic survey of gymnosperm pollination drops. Plant Reproduction **32**, 153–166.

Rudall PJ. 2021. Evolution and patterning of the ovule in seed plants. Biological Reviews of the Cambridge Philosophical Society **96**, 943–960.

Schaller A. 2004. A cut above the rest: the regulatory function of plant proteases. Planta **220**, 183–197.

Schneider CA, Rasband WS, Eliceiri KW. 2012. NIH Image to ImageJ: 25 years of image analysis. Nature Methods **9**, 671–675.

Schubert R, Dobritzsch S, Gruber C, *et al*. 2019. Tomato MYB21 acts in ovules to mediate jasmonate-regulated fertility. The Plant Cell **31**, 1043–1062.

Shigyo M, Hasebe M, Ito M. 2006. Molecular evolution of the AP2 subfamily. Gene **366**, 256–265.

Sun H, Shi T, Song J, Xu Y, Gao Z, Song X, Ni Z, Cai B. 2016. Pistil abortion in Japanese apricot (*Prunus mume* Sieb. et Zucc.): isolation and functional analysis of PmCCoAOMT gene. Acta Physiologiae Plantarum **38**, 114.

Umeda M, Umeda-Hara C, Yamaguchi M, Hashimoto J, Uchimiya H. 1999. Differential expression of genes for cyclin-dependent protein kinases in rice plants. Plant Physiology **119**, 31–40.

van Doorn WG, Woltering EJ. 2008. Physiology and molecular biology of petal senescence. Journal of Experimental Botany **59**, 453–480.

Van Durme M, Olvera-Carrillo Y, Pfeiffer ML, Doll NM, De Winter F, Lin Z, Nowack MK. 2023. Fertility loss in senescing *Arabidopsis* ovules is controlled by the maternal sporophyte via a NAC transcription factor triad. Proceedings of the National Academy of Sciences of the United States of America **120**, e2219868120.

Wan L, Xia Q, Qiu X, Selvaraj G. 2002. Early stages of seed development in *Brassica napus*: a seed coat-specific cysteine proteinase associated with programmed cell death of the inner integument. The Plant Journal **30**, 1–10.

Wang J, Guo X, Xiao Q, Zhu J, Cheung AY, Yuan L, Vierling E, Xu S. 2021. Auxin efflux controls orderly nucellar degeneration and expansion of the female gametophyte in *Arabidopsis*. The New Phytologist **230**, 2261–2274.

Weaver LM, Himelblau E, Amasino RM. 1997. Leaf senescence: gene expression and regulation. Genetic Engineering: Principles and Methods **19**, 215–234.

Wetzstein HY, Yi W, Porter JA, Ravid N. 2013. Flower position and size impact ovule number per flower, fruitset, and fruit size in pomegranate. Journal of the American Society for Horticultural Science **138**, 159–166.

Xu W, Fiume E, Coen O, Pechoux C, Lepiniec L, Magnani E. 2016. Endosperm and nucellus develop antagonistically in *Arabidopsis* seeds. The Plant Cell **28**, 1343–1360.

Yadegari R, Drews GN. 2004. Female gametophyte development. The Plant Cell **16**, S133–S141.

Yamada T, Hirayama Y, Imaichi R, Kato M. 2008. *AINTEGUMENTA* homolog expression in *Gnetum* (gymnosperms) and implications for the evolution of ovulate axes in seed plants. Evolution & Development **10**, 280–287.

Yao Y, Han R, Gong Z, Zheng C, Zhao Y. 2018. RNA-Seq analysis reveals gene expression profiling of female fertile and sterile ovules of *Pinus tabulaeformis* Carr. during free nuclear mitosis of the female gametophyte. International Journal of Molecular Sciences **19**, 2246.

Yin LL, Xue HW. 2012. The MADS29 transcription factor regulates the degradation of the nucellus and the nucellar projection during rice seed development. The Plant Cell **24**, 1049–1065.

Zhang M, Li W, Feng J, Gong Z, Yao Y, Zheng C. 2020. Integrative transcriptomics and proteomics analysis constructs a new molecular model for ovule abortion in the female-sterile line of *Pinus tabuliformis* Carr. Plant Science **294**, 110462.

Zhang M, Zheng C. 2016. Archegonium and fertilization in Coniferopsida. Trees **30**, 75–86.

Zhang S, Dong R, Wang Y, Li X, Ji M, Wang X. 2021. NAC domain gene VvNAC26 interacts with VvMADS9 and influences seed and fruit development. Plant Physiology and Biochemistry **164**, 63–72.

Zumajo-Cardona C, Little DP, Stevenson D, Ambrose BA. 2021. Expression analyses in *Ginkgo biloba* provide new insights into the evolution and development of the seed. Scientific Reports **11**, 21995.

Plant Science 332 (2023) 111726

Contents lists available at ScienceDirect

Plant Science

journal homepage: www.elsevier.com/locate/plantsci

Short-term exposition to acute cadmium toxicity induces the loss of root gravitropic stimuli perception through PIN2-mediated auxin redistribution in *Arabidopsis thaliana* (L.) Heynh

Fabrizio Araniti [a,1], Emanuela Talarico [b,1], Maria Letizia Madeo [b], Eleonora Greco [b], Marco Minervino [b], Sara Álvarez-Rodríguez [c], Antonella Muto [b], Michele Ferrari [b], Adriana Chiappetta [b], Leonardo Bruno [b,*]

[a] Department of Agricultural and Environmental Sciences, University of Milano, Milan 20133, Italy
[b] Department of Biology, Ecology and Earth Sciences (DiBEST), University of Calabria, Arcavacata of Rende, CS 87036, Italy
[c] Universidade de Vigo, Departamento de Bioloxía Vexetal e Ciencias do Solo, Facultade de Bioloxía, Campus Lagoas-Marcosende s/n, 36310 Vigo, Spain

ARTICLE INFO

Keywords:
Auxin transport
Heavy metals
Metabolomics
Oxidative stress
Root gravitropism
Starch and sucrose metabolism

ABSTRACT

Cadmium (Cd), one of the most widespread and water-soluble polluting heavy metals, has been widely studied on plants, even if the mechanisms underlying its phytotoxicity remain elusive. Indeed, most experiments are performed using extensive exposure time to the toxicants, not observing the primary targets affected. The present work studied Cd effects on *Arabidopsis thaliana* (L.) Heynh's root apical meristem (RAM) exposed for short periods (24 h and 48 h) to acute phytotoxic concentrations (100 and 150 μM). The effects were studied through integrated morpho-histological, molecular, pharmacological and metabolomic analyses, highlighting that Cd inhibited primary root elongation by affecting the meristem zone via altering cell expansion. Moreover, Cd altered Auxin accumulation in RAM and affected PINs polar transporters, particularly PIN2. In addition, we observed that high Cd concentration induced accumulation of reactive oxygen species (ROS) in roots, which resulted in an altered organization of cortical microtubules and the starch and sucrose metabolism, altering the statolith formation and, consequently, the gravitropic root response. Our results demonstrated that short Cd exposition (24 h) affected cell expansion preferentially, altering auxin distribution and inducing ROS accumulation, which resulted in an alteration of gravitropic response and microtubules orientation pattern.

1. Introduction

Cadmium (Cd), widely recognised as one of the most harmful contaminants affecting the environment, is an inhibitor of plant growth and development, affecting them from the subcellular to the ecosystem level (Qadir et al., 2014). The metabolic role of Cd in living organism is not known (Verma et al., 2008), but it has become a widespread pollutant because of its massive use in different branches of industry (Smith, 2009). One of the main problems related to Cd toxicity is its significantly long biological half-life (almost 30 years), making it a cumulative contaminant through the trophic levels of the food chain, becoming a risk for humans and animals (Bolan et al., 2013; Placek et al., 2016).

In plant species, Cd is easily absorbed, transported and accumulated in all plant organs, including roots, shoots and fruits (Verma et al., 2008). The primary visible toxicity symptoms are chlorosis, necrosis, stunted growth and leaf epinasty (Bolan et al., 2013). However, these symptoms are only visible when the phytotoxic effects are in an advanced state (Gill et al., 2012; Li et al., 2015), whereas alteration of physiological and biochemical parameters (photosynthesis, respiration, water relations, gas exchange, enzymatic activity, among others) could be detected earlier (Li et al., 2015).

Although the effects of Cd are visible throughout the plant, the root is

Abbreviations: DAB, 3,3′-diamino benzidine; Cd, Cadmium; CYCB1;1, Cyclin-dependent protein kinase; DAG, Days After Germination; EtOH, ethanol; GFP, Green Fluorescent Protein; H_2O_2, hydrogen peroxide; PIN, PINFORMED protein; KI, potassium iodide; QC, Quiescent Center; ROS, Reactive Oxygen Species; RAM, Root Apical Meristem; TZ, Transition Zone; TUB6, α-tubulin.

* Corresponding author.
E-mail address: leonardo.bruno@unical.it (L. Bruno).
[1] These authors contributed equally to this work.

https://doi.org/10.1016/j.plantsci.2023.111726
Received 17 January 2023; Received in revised form 31 March 2023; Accepted 2 May 2023
Available online 4 May 2023

the first organ that meets this heavy metal in soil, and consequently, it is the most likely organ that will experience damage and Cd toxicity (Cherif et al., 2011). The increased reactive oxygen species (ROS) production is the first set of active forms associated with stress. It has been demonstrated that the interaction between Cd cations and the cellular components starts in a matter of seconds with a vast number of metabolic responses that lead to the production of ROS burst and, as a consequence, alterations of plant growth, development and in extreme cases plant death (Lukačová et al., 2013; Choppala et al., 2014). In particular, it is known that exposure to Cd induces oxidative stress in *Arabidopsis thaliana* (L.) Heynh, due to superoxide anion ($O_2^{\bullet-}$) and hydrogen peroxide (H_2O_2) accumulation, which activate MPK3 and MPK6 (Cho and Seo, 2005; Liu et al., 2010).

Higher ROS accumulation was also observed in Cu-treated plants (Drążkiewicz et al., 2004). However, in contrast with other redox-active metals (Cu, Fe), Cd cannot induce the production of ROS through a Haber–Weiss/Fenton-like reaction because it cannot be an electron acceptor or donor under physiological conditions (Shahid et al., 2014).

Moreover, since heavy metals are present at various concentrations on the soil surface and upper soil layers and are concentrated locally or distributed evenly in a large soil volume, they could be in contact with specific regions of the root apparatus or the growing root tip as a whole.

The root is one of the most important and sensitive organs of plants, and apical root growth, as well as its morphology and architecture, is a result of interactive processes of cell division, elongation and differentiation, which balance is mediated by cross-talk between auxin and cytokinins (Lee and Benfey, 2007). Recently, to unravel the mode of action of heavy metals and their impact on plant growth and development, model species such as *A. thaliana*, *Oryza sativa* L. and its transgenic lines were largely employed (Satoh-Nagasawa et al., 2012; Bruno et al., 2017).

Bruno et al. (2021b), in a short-time experiment using Cd at high concentrations (to highlight the prompt response of the plants to Cd toxicity), reported that the phytotoxic effects induced by Cd on *Arabidopsis* root and shoot growth were strongly connected with alterations on the shoot and root meristems stem cell niche. They observed that Cd altered the expression of *WUS/WOX* homolog genes accompanied by an accumulation of cytokinin in both meristems. In addition, recent studies also focused on Cd effects on root meristem, highlighting that this heavy metal could affect root growth by altering the *SCARECROW* (*SCR*) expression and auxin-cytokinin cross-talk (Bruno et al., 2017).

In particular, the authors demonstrated that relatively low doses of cadmium (25 and 50 μM) supplied for 8 days could affect stem cell niche, leading to an alteration of root radial pattern and consequently to inhibition of primary root growth. These effects are mainly a consequence of an alteration of auxin/cytokinin homeostasis. Moreover, they related for the first time the Cd toxicity to misexpression of *SCR* transcription factors, which is known to be involved in the auxin/cytokinin cross-talk that finely modulates root apical meristem (RAM) maintenance and activity (Bruno et al., 2017).

These findings support the hypothesis that Cd could significantly affect the most critical anatomical regions responsible for plant growth and development.

Besides its role in root shaping, the root apex is also the organ in which the organelles responsible for perceiving the gravitropic stimulus reside, a physiological response also mediated by auxin and cytokinin balance and pivotal for plant survival (Aloni et al., 2006).

Auxin has been found to affect plant responses to abiotic stress such as phosphate starvation, salt stress and the excess of heavy metals (Cd, Al, Ni and Cu). Auxin homeostasis is crucial in root development and environmental responses by regulating its biosynthesis, distribution and transport.

In addition, several carriers mediate the polar auxin transport, and they are classically divided into AUXIN1/LIKE AUX1 (AUX/LAX) family, the influx carriers, and PINFORMED (PIN) family, the efflux carriers (Vieten et al., 2007; Křeček et al., 2009; Péret et al., 2012). It has been known that PINs play a specific role in the auxin transport: in particular, PIN2 is involved in the basipetal transport of auxin to the outer root cell layers (Marchant et al., 1999; Rashotte et al., 2000), while PIN1, PIN3 and PIN7, are usually localized at the basal end of the vascular cells, and they are involved in the acropetal auxin flow in the root stele (Blilou et al., 2005; Kleine-Vehn and Friml, 2008).

Auxin, and its polar transport, plays a role in stress-induced changes. It has been reported that heavy metals, such as Al and Ni, could inhibit the root length, affecting auxin redistribution through modulation of PIN2, while Cu showed as target PIN1 (Kollmeier et al., 2001; Sun et al., 2010).

Moreover, the decreased auxin levels are linked to a reduction of PIN1/3/7 protein accumulation under Cd stress, but not to a decrease of PIN1/3/7 transcript levels. In addition, auxin signaling is also repressed due to the Cd-mediated stabilization of AXR3/IAA17 protein (Yuan and Huang, 2016).

Yuan and Huang (2016) indicate that PIN2 is one of the primary targets, but the molecular mechanism of action remains elusive.

Therefore, the work aimed to evaluate the effects of short-time exposure to highly phytotoxic Cd concentrations on Arabidopsis RAM, through an integrated morpho-histological, molecular, pharmacological and metabolomic approach.

In particular, we reported that short exposure and high Cd concentration impact the primary root growth of *Arabidopsis* seedlings without affecting the meristematic cell division.

Our results highlighted that Cd inhibits the specific auxin transporters, particularly PIN2, disturbing auxin transport in RAM. Moreover, the impact of Cd on sucrose metabolism and loss of gravitropic root response have been described. We also raised the presence of ROS Cd-induced in root and the alteration of integrity and orientation of cortical microtubules in cells belonging to the elongation zone.

2. Material and methods

2.1. Plant materials and growth conditions

Seeds of *A. thaliana* (L.) Heynh ecotype Columbia (Col-0) and the seeds of transgenic lines of interest were sterilised as reported by Forgione et al. (2019).

5 Days After Germination (DAG), *Arabidopsis* seedlings were transferred on the agar control medium (CTRL) and in medium enriched with the concentration of $CdCl_2$ 100 μM (Cd 100 μM) and 150 μM (Cd 150 μM). The two different Cd concentrations and the exposition time were selected according to the effect induced in the seedlings, as described in Bruno et al. (2021b). More precisely, these concentrations can inhibit the growth of the primary root and induce morphological alterations to the entire plant. Three independent replicates were performed for each treatment, and a minimum of 50 seedlings per treatment and replicate were analysed.

2.2. Growth parameters analysed

Lateral root length was monitored in seedlings grown in-vitro in a vertical position every two days from the first day of transfer in Cd (seedlings 5 days old) to the eighth (seedlings 13 days old).

Measurements of lateral root length were performed through image analysis, using ImageJ software (https://imagej.nih.gov/ij/), scanning the plates.

Also, lateral root density was calculated every two days as described by Lešková et al. (2020). The length and width of the cells belonging to the transition zone (TZ) were calculated after 5 days of exposure to Cd.

2.3. Analysis of GFP localization via confocal laser microscopy

Seedlings of transgenic lines containing Green Fluorescent Protein (GFP) construct germinated on control agar medium (CTRL) and

transferred in a medium containing Cd (100–150 μM respectively), were used to monitor GFP expression as described below.

Concerning *PINs* (Benková et al., 2003; Nakamura et al., 2004; Blilou et al., 2005), the synthetic auxin reporter *DR5* (Ottenschläger et al., 2003) and *CYCB1;1::GFP* (Moreno-Romero et al., 2008) transgenic lines, GFP expression was monitored in seedlings grown in CTRL for 5 days and then exposed for 1, 3, and 24 h in Cd 150 μM, based on Lešková et al. (2020). Instead, seedlings of *p35S::GFP-TUB6* transgenic line were transferred at 5 DAG in Cd 150 μM for 24 h.

The images of GFP transgenic lines were also acquired before their transferring on the new agar medium (treated and untreated) to be sure that the transferring was not affecting the signal (Supplementary Fig. S1).

Confocal scanning laser microscope (Leica TCS SP8 inverted) equipped with 40x oil immersion objective was used to acquire the images of median longitudinal sections. Argon laser excitation wavelength at 488 nm and an emission window of 509 nm were used for capturing the GFP signal (Bruno et al., 2017). GFP signal intensities were measured on different root zones of transgenic lines based on pixel intensity measurements using ImageJ software (Schindelin et al., 2012).

Three independent replicates were performed, and a minimum of 50 seedlings were analysed for each sample.

2.4. Histochemical stainings and pharmacological treatments

To consider the architecture of meristematic cells in the primary root, *Arabidopsis* seedlings (Col-0), grown on CTRL medium and after 5 DAG exposed for five days to Cd, were used for mPS-PI staining as described in Truernit et al. (2008).

To evaluate starch grains accumulation, root tips were incubated in Lugol solution (Sigma, Germany) for 5 min, then rinsed in distilled water. The time-course analysis was performed on the roots of seedlings grown on CTRL medium, and roots of seedlings transferred after 5 DAG in Cd 100 μM and Cd 150 μM, monitored every day from the first day up to the fourth day of treatment.

As indicator of cell death Trypan blue (Bio Basic Inc., Markham, Ontario, Canada) was used. 5 days-old seedlings grown on CTRL medium and transferred in Cd 100 μM and Cd 150 μM from 1 to 6 days were stained with 0.5 % Trypan blue solution in dark for 5 min, as reported in Duan et al. (2010), and washed in distilled water.

To localise H_2O_2 production, we used the method described by Vanacker et al. (2000) in *Arabidopsis* seedlings, with some modifications. Seedlings grown on CTRL medium and exposed to Cd 100 μM and Cd 150 μM for 24 h were immersed in 3,3′-diamino benzidine (DAB) solution (at final concentration 1 mg/ml, pH 5.5) and infiltrated under vacuum for 3 min. Then samples were incubated at room temperature in darkness for 2 h and washed with EtOH 50 %.

All slides were mounted and analysed by Leica DRMB microscope, and images were taken with the digital camera Leica DFC320 (Leica, Milan, Italy).

To evaluate the interactions between the auxin transporter PIN2, microtubules organization and ROS we have planned a pharmacological approach following the protocol proposed by Zwiewka et al. (2019). In particular, 24 h after transplant the seedlings were treatead with Cd 150 μM, potassium iodide (KI) 1 mM, H_2O_2 2 mM and their combinations (KI+Cd, H_2O_2 + Cd).

2.5. RNA isolation and quantitative real-time PCR (qRT-PCR)

Roots of *A. thaliana* seedlings treated (Cd 150 μM) or not (CTRL) with Cd for 24 h and 48 h were used to isolate total RNA as described in Bruno et al. (2017). According to the manufacturer's instructions, 3 μg of RNA were retrotranscribed using SuperScript III Reverse Transcriptase (Invitrogen, Milan, Italy) from each sample.

Quantitative real-time PCR (qRT-PCR) was performed, as reported by Bruno et al. (2017) and primers used were reported by Araniti et al. (2017). As normalization control, the housekeeping gene AT2G28390 (*MONENSIN SENSITIVITY1, SAND*) was used (Remans et al., 2008). The obtained results were analysed according to the $2^{-\Delta\Delta Ct}$ method (Livak and Schmittgen, 2001). The mean values are represented (± standard error), and three independent biological replicates were performed. Statistical analysis was performed using Student's t-test (*P < 0.05; **P < 0.01; ***P < 0.001).

2.6. Root gravitropism analyses

The experiments to evaluate the root response to gravitropic stimulus have been carried out as previously described by Araniti et al. (2016). In particular, 5 days old *A. thaliana* seedlings, transferred to a new medium containing Cd (100 μM and 150 μM) or not (CTRL) and the vertically grown seedlings were rotated 90° to gravistimulate the roots, then root curvature was monitored after 3, 6, 12 and 24 h and the effects observed during root reorientation were scored using Image Pro Plus (Media Cybernetics, Inc, Rockville, USA).

2.7. Metabolomics analysis focused on starch and sucrose metabolism

Metabolomic analyses were carried out on *Arabidopsis* seedlings treated for 48 h with Cd (100 μM and 150 μM) or not (CTRL), using an Agilent gas chromatograph (GC 7890 A), equipped with a A 5MS column (30 m x 0.25 mm × 0.25 μm + 10 m pre-column), linked to a single quadrupole mass spectrometer (MS 5975 C INERT XL MSD) and a CTC ANALYTICS PAL autosampler.

Plants were treated as previously described, separated into shoots and roots using a razor blade, and shoots were discarded, whereas root samples were immediately snap-frozen in liquid nitrogen. An aliquot of root pools (1 pool of 100 seedlings per sample and replicate) was used for the experiments. Metabolome extraction, derivatisation and GC-MS analysis were carried out using the protocol proposed by Lisec et al. (2006) and modified as described by Misra et al. (2020).

Chromatogram alignment, deconvolution, peaks intensity extraction and annotation were carried out using the open-source software MS-DIAL, following the protocol previously described by Misra et al. (2020). Peaks annotation was done following the metabolomics standards initiative (MSI) guidelines for metabolite identification (Sansone et al., 2007). In particular, features were annotated using Level 2 [identification based on the spectral database (match factor > 80 %)] and Level 3 (only compound groups were known, e.g. specific ions and RT regions of metabolites).

2.8. Statistical analysis

For each sample were carried out three independent replicates, each comprising minimum 50 seedlings, and the results represent the mean value (± standard error).

Statistical analyses were performed, first testing the homogeneity (Leven Median test) and then analysed by ANOVA using the Tukey's rank test ($P \leq 0.05$) as post-hoc. Letters on graphs indicate significant differences.

Concerning the metabolomics analysis, the MS-DIAL extracted intensities of metabolites involved in starch and sucrose metabolism have been analysed through univariate analysis using the open-source software Metaboanalyst 5.0 (2021). In particular, data were normalised by the internal standard, Log_{10} transformed, and Pareto scaled. Successively, normalised data were further analysed through the one-way ANOVA using the Fisher's LSD test as post-hoc ($P \leq 0.05$) and the P value was further evaluated through the False Discovery Rate using $P \leq 0.05$ as a cutoff. Only the metabolites belonging to the starch and sucrose metabolism, highlighted by a KEGG-based enrichment analysis, were considered.

3. Results

3.1. Cadmium impacts primary root development by affecting apical root meristem and elongation boundary

To assess the effects of cadmium on the entire root system, we focused our attention on the length and density of lateral roots in response to Cd at selected concentrations. For this purpose, 5-day-old *Arabidopsis* seedlings were exposed to Cd 100 μM and Cd 150 μM. The length and density of lateral roots were evaluated every other day from the day of transfer in Cd until the eighth day of treatment (Fig. 1). The results pointed up that lateral root density increased in the treated plants, but a slowdown in their growth was observed, especially at the maximum concentration of Cd (Fig. 1 B, C). To further investigate the alteration of Cd at the cyto-histological level, we evaluated the meristem cells in root seedlings after 5 days of exposition to Cd 100 μM and Cd 150 μM (Fig. 2). In particular, we observed that prolonged exposure to Cd-induced cell deformations and the treated seedlings showed complete disorganization of the meristematic zone. Indeed, the root morphology is not tapered, and the cortical cells appeared deformed in size and shape (Fig. 2 B, C). We also examined the width and the length of cells at the TZ boundary and a significant decrease was found in length but not in width (Fig. 2 D, E). In particular, seedlings exposed to Cd presented more rounded cells than CTRL ones (Fig. 2 A-C, magnification).

To highlight if meristem size decrease was connected to an inhibition of the cell cycle progression, the mitotic activity was assayed using the transgenic line *CYCB1;1::GFP*. Meristems of Cd exposed roots were shorter than control, and the mitotic activity detected in these roots remained unaffected until 24 h at 100 and 150 μM of Cd exposition (Fig. 3).

The results demonstrated that short Cd exposition only for 24 h had a minor effect on the mitotic activity and preferentially target cell expansion. The results confirm that Cd promotes the cell's exit from the primary root meristem zone.

3.2. Cd alters auxin distribution by inhibiting mainly the auxin transporter PIN2

It has been demonstrated that Cd impacts the PIN polar auxin transport and, finally, the auxin accumulation in the root.

To identify which PIN is immediately affected by Cd, we investigated *pPINs::PINs-GFP* reporter families involved in polar auxin transport in a time-course experiment on seedlings exposed for 1, 3 and 24 h under 150 μM of Cd (Fig. 4 A-H).

In untreated roots, PIN proteins were characterised by a classical presence and distribution at the cellular level. We focused only on this Cd concentration because it showed the major effect on root system

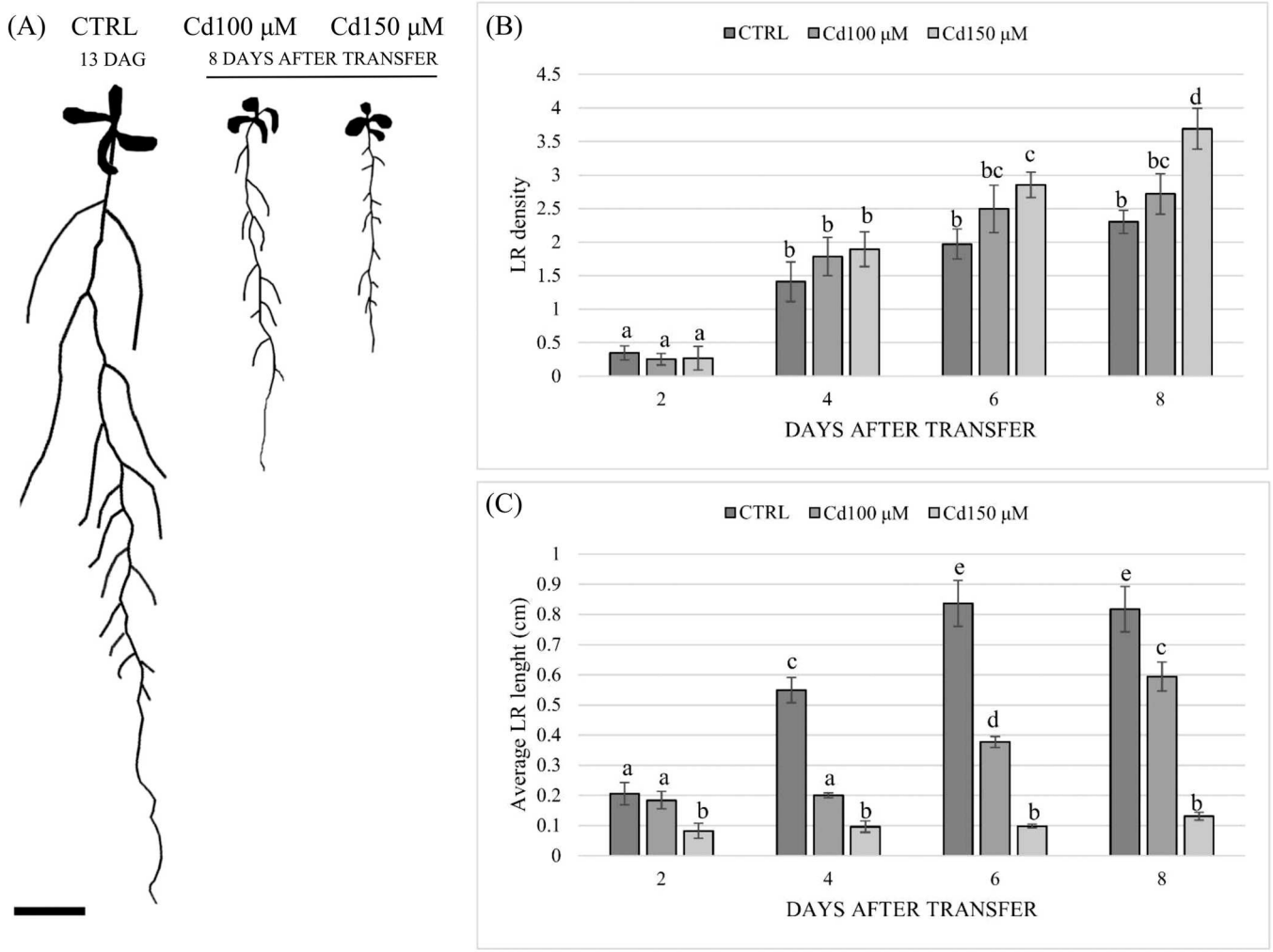

Fig. 1. Cd effects in root's length and density. (A) Picture of CTRL at 13 DAG and Cd-treated seedling after 8 days of treatment (13 DAG); scale bar 1 cm. (B) Lateral root density. (C) Average lateral root length. Statistical analysis was performed using ANOVA and Tukey's ranked test ($P < 0.05$) and different letters indicate significant differences. Data present the mean ± Standard Error (SE) of three independent experiments.

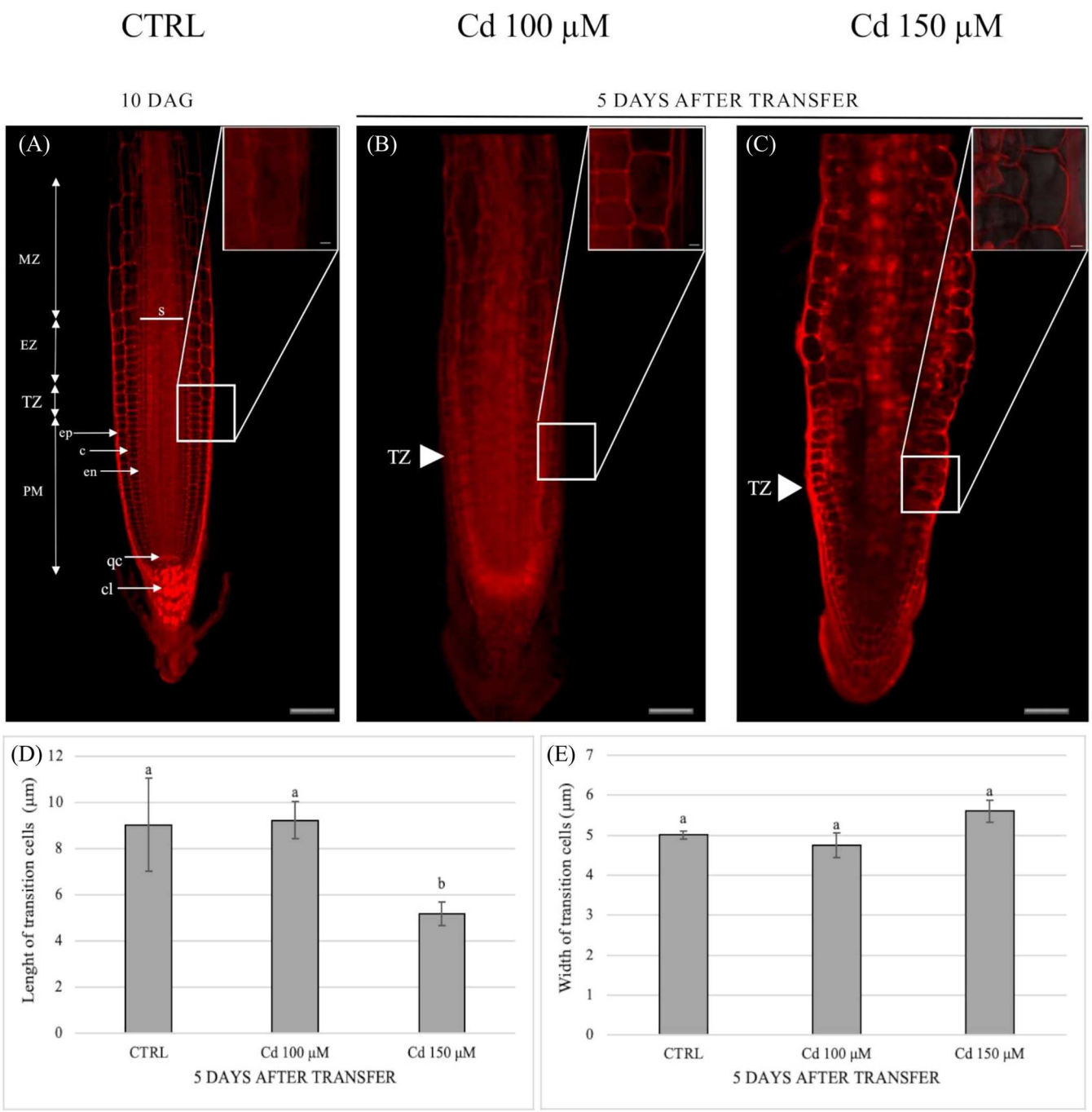

Fig. 2. Confocal laser images of primary root tip. Roots of *A. thaliana* seedlings first grown on control medium for 5 days and then transferred to (A) medium as control (CTRL) and on a medium added with (B) 100 µM and (C) 150 µM Cd for 5 days. (D, E) Length and width of meristematic cells of transition zone. Statistical analysis was performed using ANOVA and Tukey's ranked test ($P < 0.05$) and different letters indicate significant differences. Data present the mean ± Standard Error (SE) of three independent experiments. cl, columella; c, cortex; en, endodermis; ep, epidermis; PM, proximal meristem; qc, quiescent center; s, stele; TZ, transition zone; EZ, elongation zone; MZ, maturation zone. (A–C) Scale bars 50 µm.

architecture.

More in detail, no significant differences were observed in plants treated with Cd for PIN1 and PIN3 distribution along the RAM within 1 and 3 h at 150 µM Cd treatment (Fig. 4 A'', E''). However, concerning PIN7 distribution, we obtained a slight decrease of GFP signal already after 3 h of treatment (Fig. 4 G''). While, after 24 h of Cd exposition, we noticed a slight GFP signal decrease for PIN3 and PIN7, but not for PIN1 (Fig. 4 B, F, H). By contrast, the PIN2 signal was strongly repressed by Cd even after 24 h of exposure (Fig. 4 C''', D). In addition, after 48 h of treatment, GFP signal decrease was found for all PINs, associated with a general alteration of localization (Supplementary Fig. S2, A-D).

In line with the downregulation of the PIN protein expression after 24 h of treatment, the genes encoding these families were also found to be regulated. In particular, *PIN2* expression was the most downregulated at 150 µM of Cd (Fig. 5). This decrease of *PINs* expression was more pronounced after 48 h (Supplementary Fig. S2,E-H).

We also monitored the maximum auxin accumulation by using auxin-responsive reporter *pDR5::GFP* in a time-course experiment under Cd 150 µM treatment (Fig. 4 I-J).

Regarding *pDR5::GFP* distribution, in CTRL we observed in the root

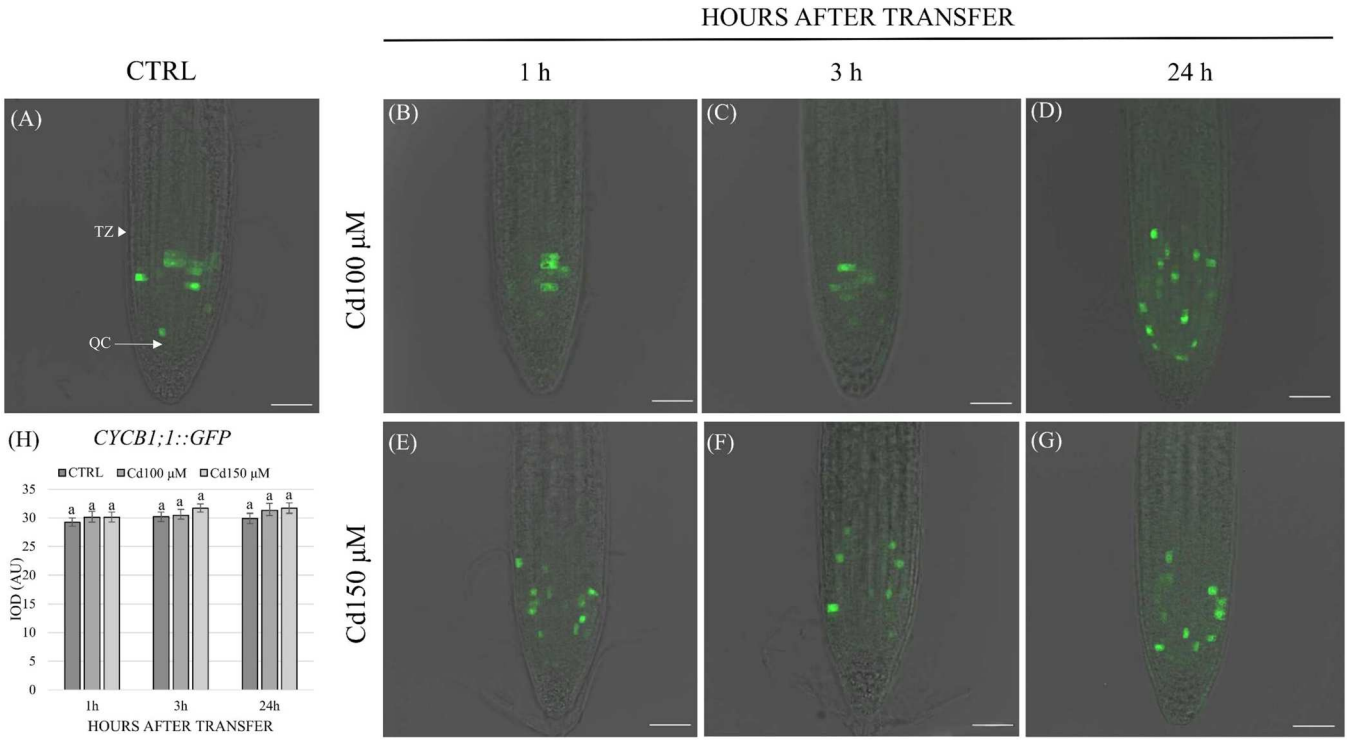

Fig. 3. Confocal laser images of primary root tip of *A. thaliana CYCB1;1::GFP* transgenic line. (A-G) Seedlings were first grown on control medium for 5 days and then transferred to medium as control (CTRL) and on a medium added with 100 µM and 150 µM Cd for 1, 3 and 24 h. (H) Integrated optical density (IOD) expressed as arbitrary units (AU) of fluorescence intensity. Statistical analysis was performed using ANOVA and Tukey's ranked test ($P < 0.05$) and different letters indicate significant differences. Data present the mean ± Standard Error (SE) of three independent experiments. Scale bars 50 µm.

tip the typical auxin maximum accumulation in QC, columella and procambium cells (Fig. 4 I). Instead, in roots exposed to Cd, a significant decrease was observed only after 24 h of treatment at Cd 150 µM (Fig. 4 J).

In conclusion, the results strongly support that the PIN2 protein is an important target of Cd stress, consequently impacting polar auxin distribution.

3.3. Cd induced alterations of the gravitropic root response

It is known that alterations in auxin distribution could interfere with the gravitropic response. Therefore, we evaluated *Arabidopsis* seedlings' response to gravitropic stimulation in plants treated with Cd (100 µM and 150 µM) until 24 h.

The results pointed out that treated root apexes, at both concentrations and in a dose-dependent manner, lost the ability to perceive gravity (Fig. 6). Notably, in CTRL seedlings gravitropic curvature of the root apex was already observable after 6 h of treatment, and a bending of ≃90° was achieved after only 12 h. On the contrary, although Cd-treated seedlings could perceive the gravitropic stimulus, their response was significantly slower and more marked, after 24 h, in 150 µM treated seedlings than in 100 µM (Fig. 6).

Based on this result, we hypothesized that the loss of gravitropism response might also be related to Cd-induced changes in columella cells' differentiation and starch accumulation (Fig. 7). To verify this thesis, a Lugol's staining of starch granules and a targeted metabolomic analysis focused on metabolites belonging to the starch and sucrose metabolism were performed. The results highlighted that the number of columella-stained layers in seedlings exposed to Cd 100 µM and 150 µM decreased after 3 d and 4 d respectively (Fig. 7 B''', C''). To investigate if the loss of statoliths was related to cell death, seedlings at 5 DAG were exposed to both Cd concentrations (100 µM and 150 µM) and monitored for 6 days. The results showed that cell death started in the proximal meristem of seedlings treated with Cd 100 µM and 150 µM after 4 and 5 days, respectively (Supplementary Fig. S3,E′, D′'). After 6 days of Cd exposure, cell death also occurred in the RAM (Supplementary Fig. S3, F', F′').

Since the strongest effects on statolith formation were significantly observable after 48 h we have focused the metabolomic analysis only on this time of exposure. The results confirmed that 48 h treatment of *Arabidopsis* roots strongly altered the starch and sucrose metabolism, and the effects were more marked on plants treated with Cd 150 µM (Fig. 7 D). In particular, the lower concentration (100 µM) induced an accumulation of fructose and trehalose, whereas slightly reduced glucose 6-phosphate, cellobiose and sucrose (Fig. 7 D). On the contrary, the highest concentration assayed induced a dropping down of all the annotated metabolites (Fig. 7 D). Globally, these results indicated that Cd has a strong negative impact on the number of mature columella cells and starch metabolism.

3.4. Cadmium interferes with cortical microtubule orientations and induces oxidative stress in roots

The inhibited cell expansion, and the strong inhibition of PIN2 accumulation under Cd treatment, suggest that cortical microtubule integrity and orientation in the elongation zone were affected.

To investigate how Cd impacts the integrity and orientation of cortical microtubules, seedlings of *p35S::GFP-TUB6* transgenic line of *Arabidopsis* at 5 DAG were exposed to Cd 150 µM for 1, 2, 3 and 4 days; at each time of exposure, root cortical microtubules in elongation zones were evaluated (Fig. 8).

The obtained results showed a strong impact of Cd on the arrangement and strand thickness of microtubules, which in treated roots lost symmetry and appeared reduced in density (Fig. 8 E-H). On the contrary, in CTRL roots, microtubules presented proper arrangement and density, and they appeared parallel to the transverse axis of the cells (Fig. 8 A-D).

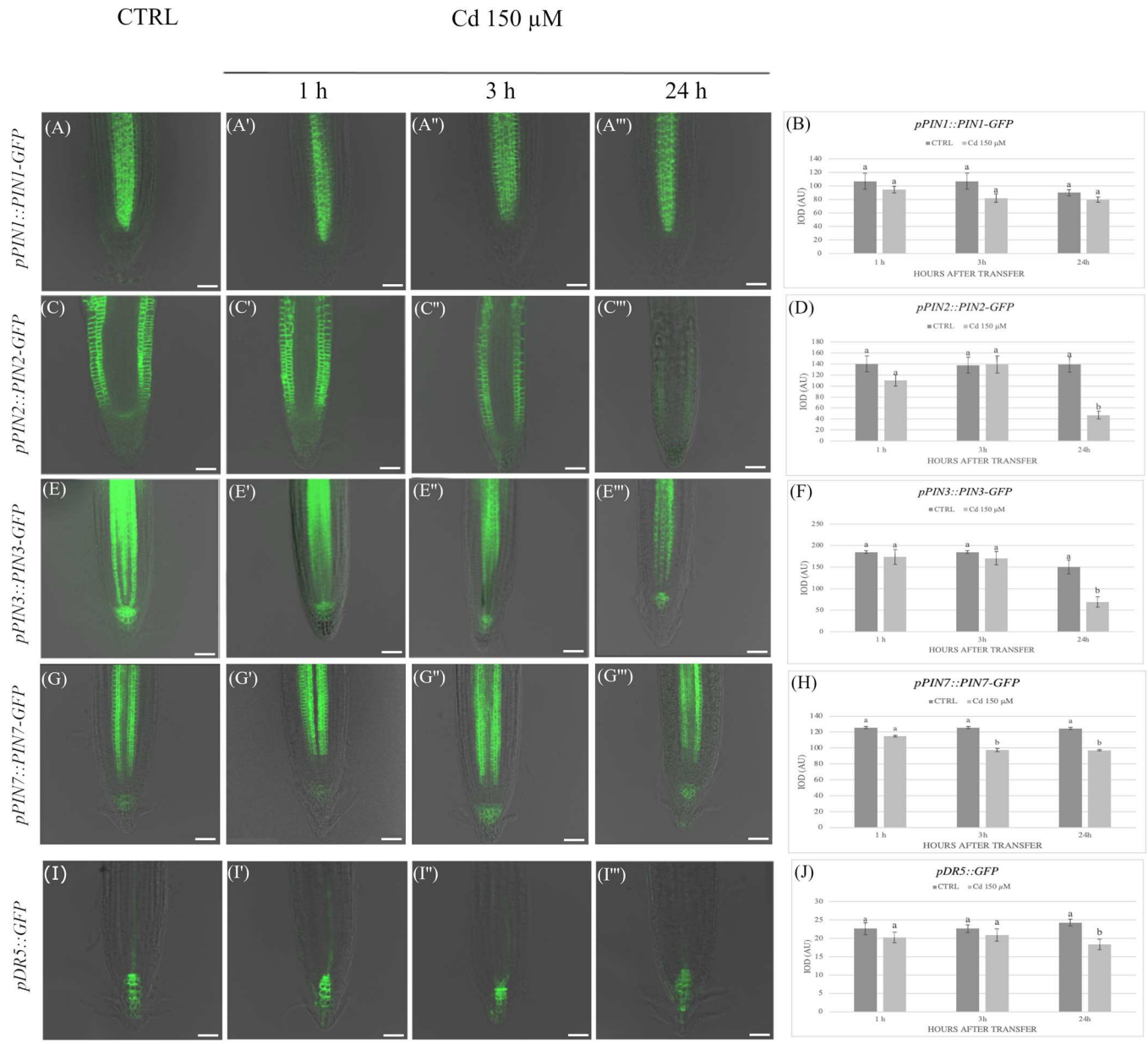

Fig. 4. Confocal laser images of primary root tip of *A. thaliana pPINs::PINs-GFP* (A, C, E, G) and *pDR5::GFP* (I). *pPIN1::PIN1-GFP, pPIN2::PIN2-GFP, pPIN3::PIN3-GFP, pPIN7::PIN7-GFP, pDR5::GFP* transgenic lines first grown on control medium for 5 days and then transferred to medium as control (CTRL) and on a medium added with 150 µM Cd for 1, 3 and 24 h. (B, D, F, H, J) Integrated optical density (IOD) expressed as arbitrary units (AU) of fluorescence intensity. Statistical analysis was performed using ANOVA and Tukey's ranked test ($P < 0.05$) and different letters indicate significant differences. Data present the mean ± Standard Error (SE) of three independent experiments. Scale bars 50 µm.

In particular, after 3 days of Cd exposition, we observed a reorientation of microtubules, most of which present oblique or random and longitudinal realignments (Fig. 8 I). In addition, Cd induced a gradual decrease in microtubule density, suggesting that Cd may induce their depolymerisation.

3.5. Increased ROS in Cd-treated seedlings contribute to Cd-regulated PIN2 accumulation

ROS are important secondary messengers, and their level is associated with many types of stress. In particular, Cd induces high ROS levels and inhibits root elongation.

In this context, ROS accumulation was assayed with DAB staining on seedlings of *Arabidopsis* exposed or not to Cd (100 and 150 µM) for 24 h. The microscopy analysis showed for DAB assay a staining increase in root exposed at 100 µM of Cd, which reached the maximum intensity when the seedlings were exposed at Cd 150 µM. More in detail, the Cd 100 µM signal was detected in the cortical and epidermal cells of the distal meristem (Fig. 9 B), while in roots exposed at Cd 150 µM, the signal was detected in all meristem (Fig. 9 C).

Therefore, the possible role of H_2O_2, the link with cortical microtubules, and PIN2 expression reduction were further investigated.

To assess the effects of H_2O_2 on the cortical microtubule integrity and orientation in the elongation zone, *p35S::GFP-TUB6* transgenic lines were exposed to 2 mM H_2O_2 for 24 h.

The results showed a reorientation of microtubules under Cd 150 µM and 2 mM H_2O_2 (Fig. 10 B, C). In particular, the treatment induced a more oblique and random orientation than the control.

H_2O_2 and Cd 150 µM added together in the medium increased the random and longitudinal orientation of cortical microtubules (Fig. 10 F).

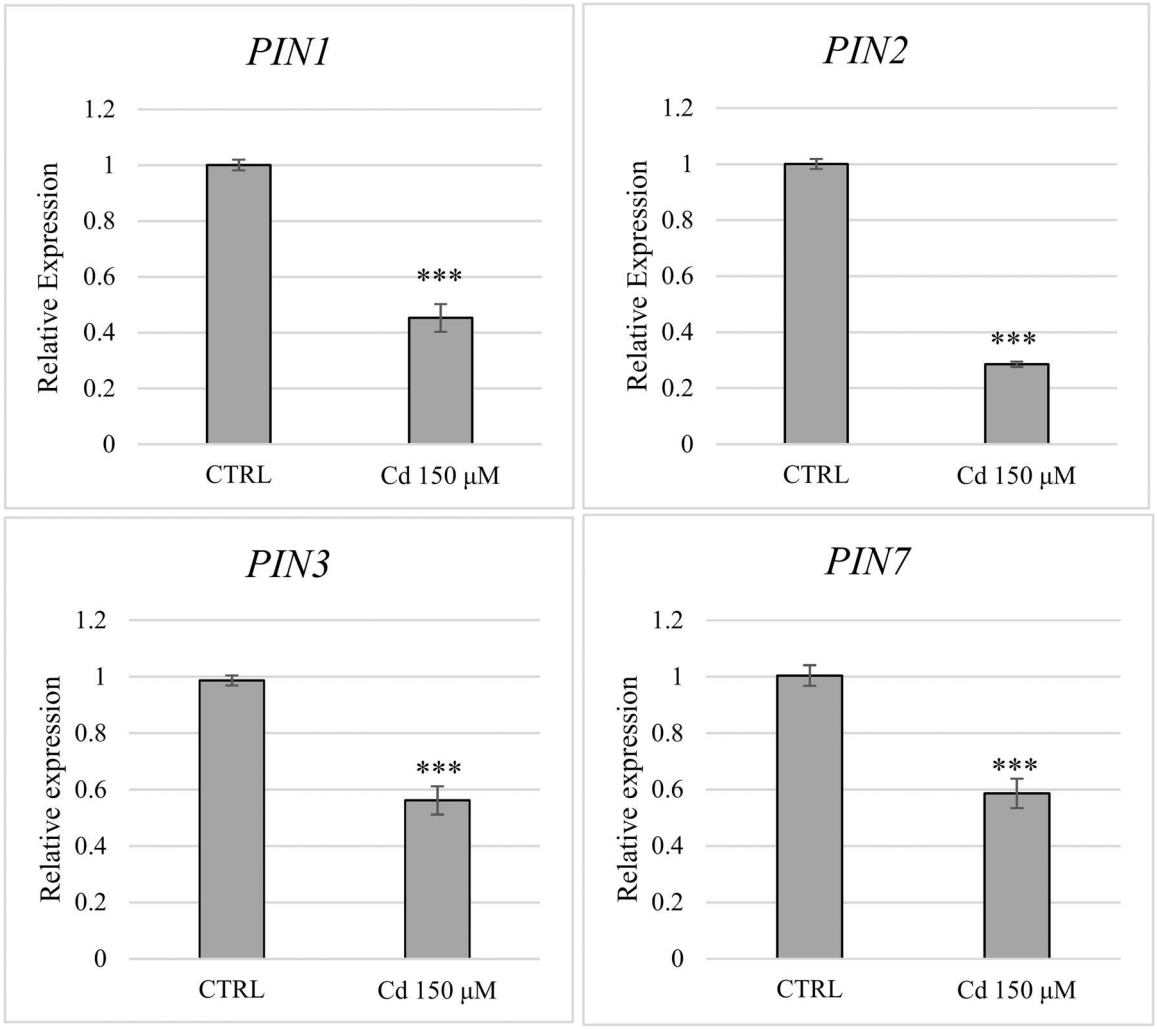

Fig. 5. Relative expression by qRT-PCR of *PIN1, PIN2, PIN3* and *PIN7* in primary roots of *A. thaliana.* Seedlings germinated on growth medium as control (CTRL) and transferred on medium added with 150 µM for 24 h. Mean expression levels were calculated from three biological replicates, obtained from three independent experiments. Results were analyzed using STEP One Software 2.0 (Applied Biosystems), using the $2^{-\Delta\Delta Ct}$ method (Livak and Schmittgen, 2001). The results represent the mean value (± standard error) of three independent biological replicates. Asterisks indicate significant pairwise differences using Student's t-test (*P < 0.05; **P < 0.01; ***P < 0.001).

The application to the transgenic line *p35S::GFP-TUB6* of KI, a known H_2O_2 scavenger, partially rescues the orientation of the microtubule pattern (Fig. 10 E). In particular, the microtubule orientation was comparable to the control lines (Fig. 10 D, E).

To evaluate the effects of H_2O_2 on the PIN2 protein levels in the root tip, *pPIN2::PIN2-GFP* transgenic lines were exposed to H_2O_2 (2 mM) for 24 h (Fig. 11).

Confocal analysis confirmed the PIN2 proteins signal decrease, and a more detailed analysis showed a strong accumulation in intracellular compartments (Fig. 11 H). Moreover, H_2O_2 treatment caused minor effects on PIN2 localization, but suppressed its intracellular trafficking (Fig. 9 C, I).

In addition, the PIN2 protein signal disappeared completely when *pPIN2::PIN2-GFP* transgenic seedlings were exposed to both H_2O_2 and 150 µM of Cd (Fig. 11 F).

KI application to the transgenic line *pPIN2::PIN2-GFP* exposed to Cd 150 partially rescued the inhibition signal of PIN2 protein (Fig. 11 E, J). Taken together, these results suggest a possible link between changes in ROS accumulation Cd-induced and the alteration in cortical microtubule orientation that finally affected PIN2 protein distribution.

4. Discussion

Short-time exposure to Cd significantly altered the entire root and root meristem morphology of *Arabidopsis* seedlings, inducing alterations in the main root subclasses (primary root length, lateral root density, etc.), cell anatomy, and its organisation at both assayed concentrations (100 µM and 150 µM). In particular, Cd reduced the primary root and lateral root length, whereas lateral root density increased, suggesting stimulation of their differentiation. In addition, a clear increase in root hair density and length was observed, which distribution was significantly closer to the root meristem. Similar effects were observed in *Arabidopsis* roots treated with natural compounds interacting with auxin distribution, particularly its polar transport (Hu et al., 2012; Lupini et al., 2014; Bruno et al., 2021a).

For example, as also observed by Bruno et al. (2021a) in coumarin-treated plants, *Arabidopsis* RAM treated with Cd was characterised by swollen protodermal cells mainly due to a more radial expansion of the cell than longitudinal. Moreover, as also observed in plants treated with natural products and heavy metals, the RAM of treated roots was shorter (composed of a lower number of cells) and larger than control, suggesting an advancement of transition and differentiation zones due to a premature cell cycle exit from the

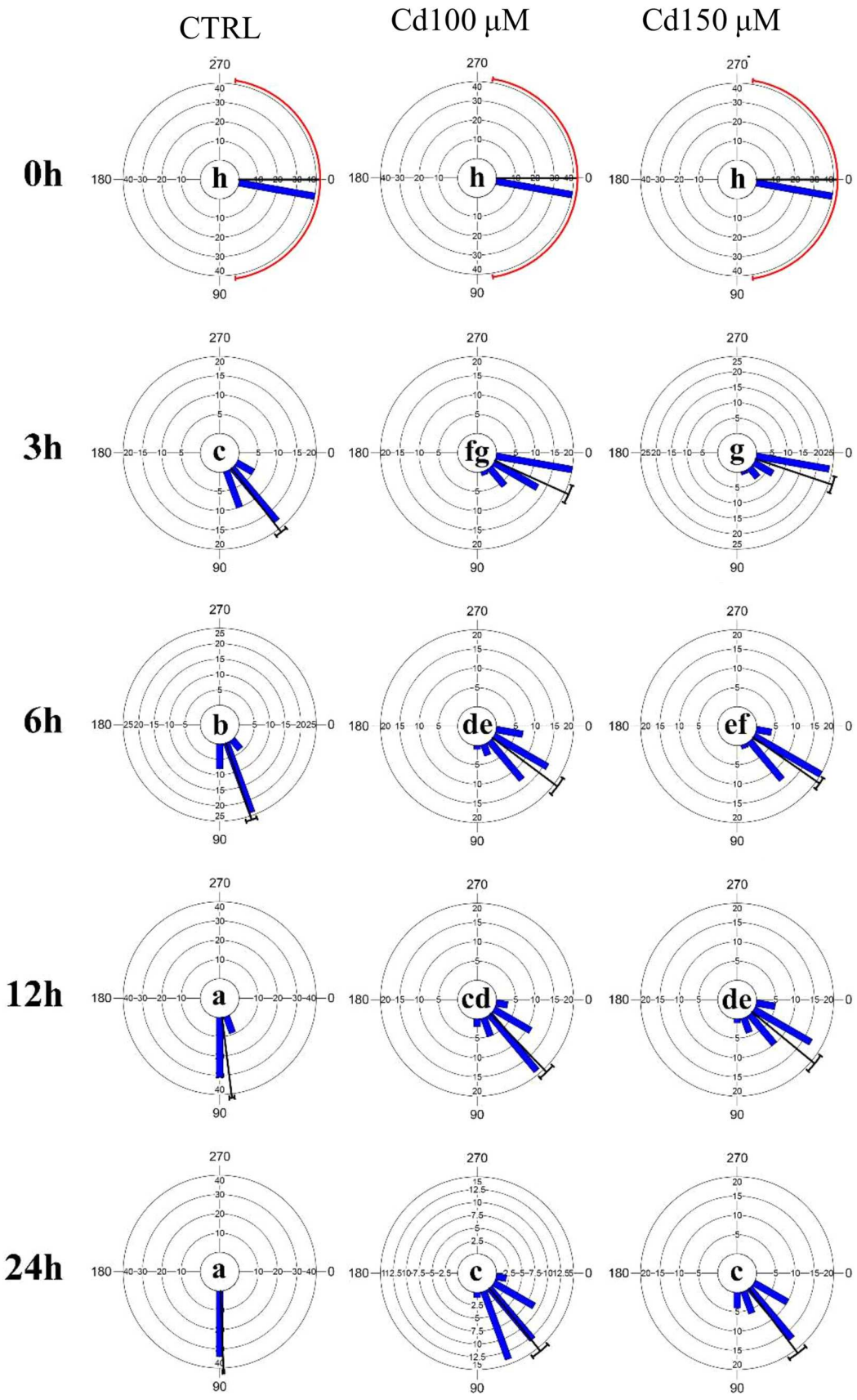

Fig. 6. Cd effect on the time-course gravitropic curvature of *Arabidopsis thaliana* primary roots after 90° rotation. Images were taken after 3, 6, 12 and 24 h. Data were analysed through ANOVA and a Tukey's rank test ($P < 0.05$). Letters on graphs indicate significant differences. $N = 10$.

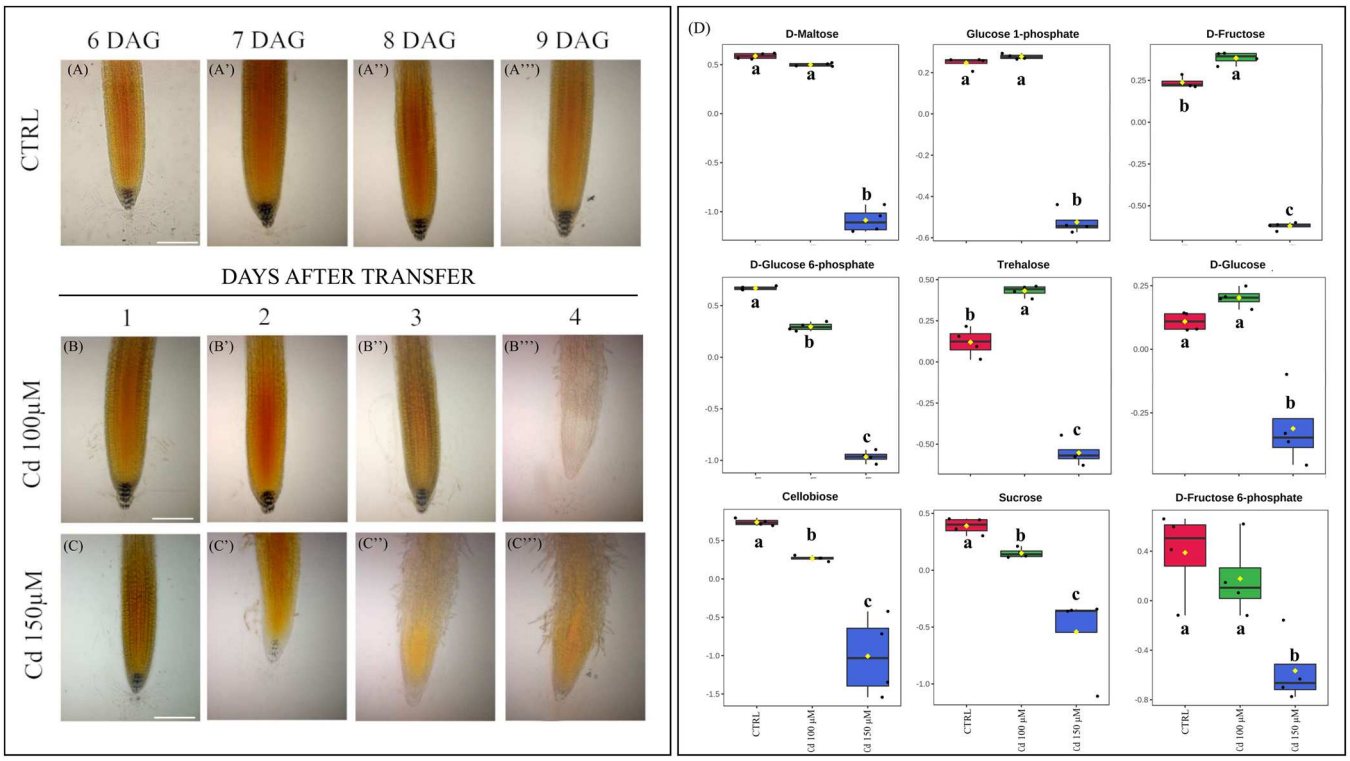

Fig. 7. Lugol's staining and GC-MS analysis. Accumulation patterns of starch granules in the columella root cap of *A. thaliana* seedlings first grown on control medium for 5 days and then transferred to medium as control (CTRL) (A) and on a medium added with 100 µM (B) and 150 µM (C) Cd for 5 days. Scale bars 50 µm. (D) Changes induced by 48 h Cd treatment (100 µM and 150 µM) in metabolites involved in starch and sucrose metabolism and CTRL. The GC-MS analysis allowed to identify and relatively quantify 9 out of 18 metabolites involved in these pathways. Here are reported all the metabolites involved in the pathway, highlighting in bold those identified during the analysis: Cellodextrin; Cellobiose; D-Fructose; Sucrose; beta-D-Glucoside; Uridine diphosphate glucose; Glucose 1-phosphate; Glucose 6-phosphate; D-Glucose; Amylose; Trehalose; Maltodextrin; Starch; D-Maltose; Dextrin; Isomaltose; Fructose 6-phosphate; Alpha-D-Glucose 1,6-bisphosphate. Data were analysed through one-way ANOVA using the Fisher's LSD test as post-hoc ($P \leq 0.05$) and the P value was further evaluated through the False Discovery Rate using $P \leq 0.05$ as cutoff. $N = 4$.

meristematic zone (Araniti et al., 2017; Bruno et al., 2017).

Furthermore, high Cd exposition inhibited primary root growth via repressing expansion in cells of elongation zone.

An anisotropic expansion defect was also observed in maize, rice and *Arabidopsis* plants treated to the Al and Cd metals, respectively (Blancaflor et al., 1998; Jones et al., 2006; Wu et al., 2014; Lešková et al., 2020). In particular, the authors found that in Al-stressed rice plants, the mechanical properties of root were correlated with increased cell rigidity and, consequently, reduced cell elasticity (Wu et al., 2014). However, the directionality of cell elongation depends on the orientation of the cortical microtubules (Baskin, 2005). Under Ni treatment, the microtubules' orientation in the elongation boundary cell was characterized by a transverse arrangement of cortical microtubules in relation to the elongation axis (Lešková et al., 2020). The same effect was found in our experiments, in which the rearrangement and disorganization of the microtubules were observed after two days of Cd exposition. However, in this scenario, we found that Cd exposition did not affect cell division and integrity at the meristematic zone, although the primary root was reduced. A similar effect was observed in the root exposed to Ni (Lešková et al., 2020). On the contrary, Cu treatment inhibited the mitotic activity in the apical root meristem and premature induced cell death (Lequeux et al., 2010; Yuan et al., 2013). Globally these results indicated that different metals interfere with the different developmental programs in the root.

Auxin plays a pivotal role in the different plant development processes, including root elongation and its polar distribution in the root also contributes to generating the gravitropic perception (Karampelias et al., 2016; Lešková et al., 2020). In general, it has been demonstrated that different types of metal significantly impact auxin accumulation and transport (Wang et al., 2015).

Interestingly, the activation of signaling and biosynthesis of auxin and other hormones under Cd treatment, are also modulated by DNA methylation. Indeed, it was reported that, under a long-lasting Cd treatment, the triple *A. thaliana drm1 drm2 cmt3* (*ddc*) methylation defective mutant exhibited a better growth performance than wild-type plants (Pacenza et al., 2021).

Notably, the PIN proteins are involved in cell elongation and root gravitropic stimuli. In this scenario, we observed in a time-course of Cd treatment (1, 3 and 24 h) that PIN1 protein, although if characterized by a reduction trend after 24 h, was not significantly affected by Cd within 24 h of treatment, while PIN2, PIN3 and PIN7 resulted inhibited at 24 h of Cd exposition. In particular, the PIN2 protein resulted in being the most impacted. Concerning the *PINs* gene expression, all the genes analysed were down-regulated. Moreover, after 48 h of treatments all the GFP PINs protein were strongly degraded. Therefore, we hypothesized that PIN1, PIN2, PIN3 and PIN7 were regulated at both transcriptional and post-transductional levels and PIN1 protein was more stable than the others PINs, suffering later the Cd effects.

In addition, previous studies demonstrated that during long exposition (8 days after germination) to low Cd doses (50 µM) selectively affected PIN1, 3 and 7 more than PIN2 (Bruno et al., 2017). A similar selectivity was also observed with other heavy metals such as Cu, which affected only PIN1, and Ni which mainly altered PIN2 (Yuan et al., 2013; Lešková et al., 2020).

Altogether, these results further support the concept that the differences in the modulation of *PIN* expression and PIN proteins levels under different metal stresses and concentrations could be a common mechanism which underlies response stress-mediated to remodel root growth

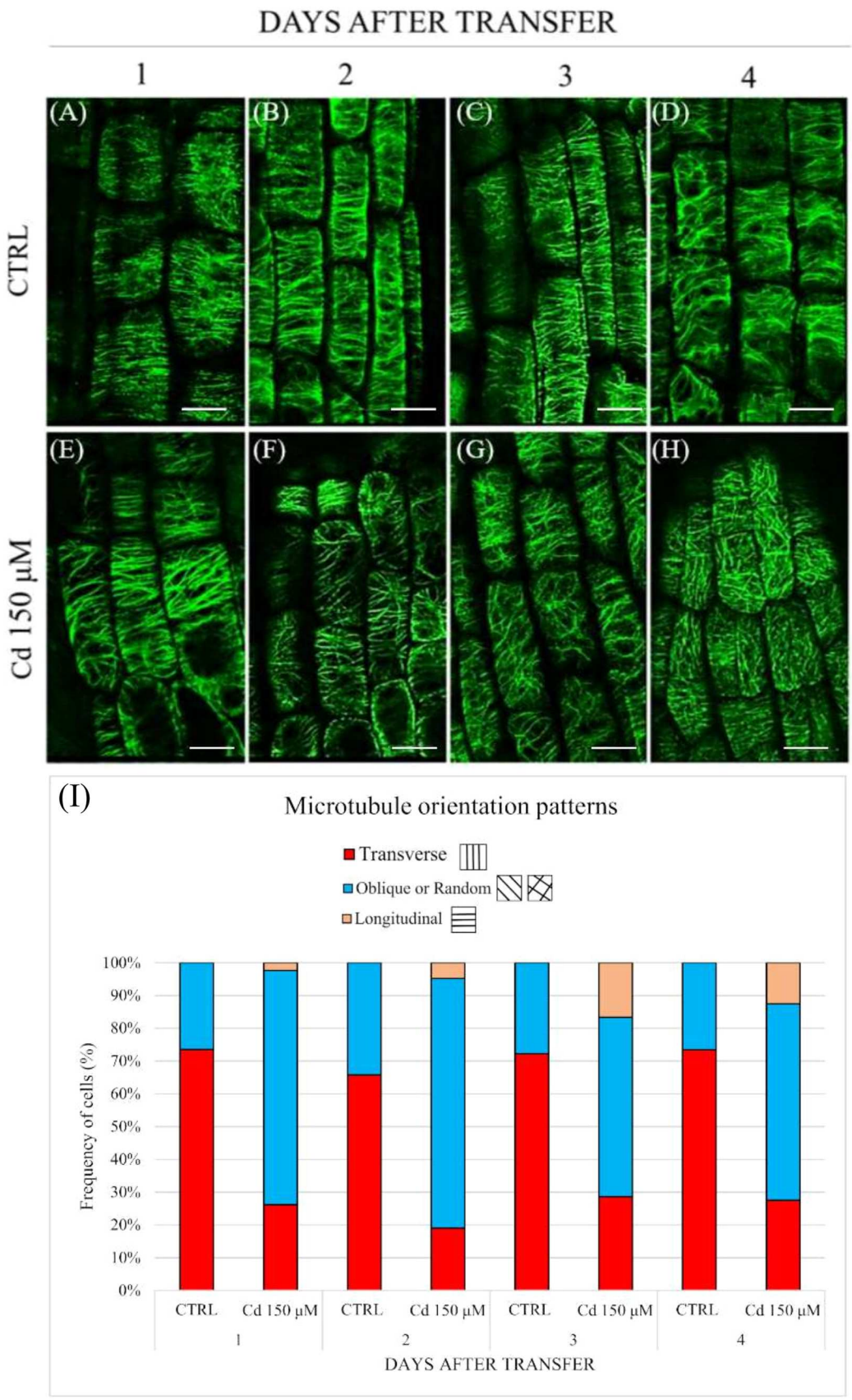

Fig. 8. Cd-induced changes in microtubules orientation in epidermal cells of transition zone assessed. (A - H) Confocal laser images of the microtubular marker line *p35S::GFP-TUB6* taken at the different time-points (1, 2, 3, 4 days) after transfer in medium added with Cd 150 µM or not (CTRL). Scale bars 10 µm. (I) Frequency of different microtubule orientation patterns in epidermal cells of the transition zone (n > 30 cells per condition and time-point).

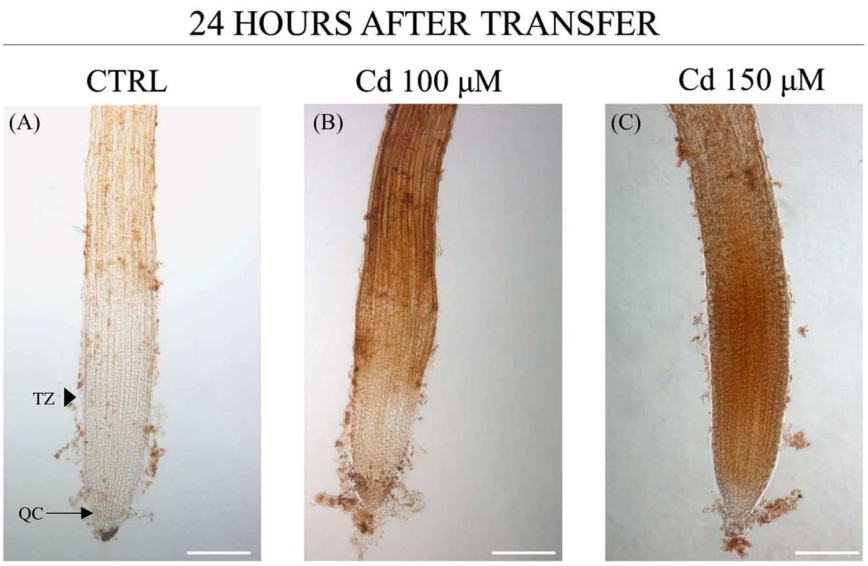

Fig. 9. DAB staining in primary root. H_2O_2 detected in primary root of *A. thaliana* seedlings after 24 h in CTRL (A) and exposed to 100 (B) and 150 (C) µM of Cd. TZ, transition zone; QC, quiescent center. Scale bars 50 µm.

and architecture, as well as gravitropic perception could be correlated with metal stress avoidance. It has been widely discussed that a plant's gravitropic response is a complex physiological process mediated by the interaction among statoliths, ROS signaling and auxin distribution, mediated by efflux transporters and microtubule organisation (Geisler et al., 2014; Su et al., 2017; Zhang et al., 2019).

Phenotypic analysis using *pin2* single and *pin3pin7* double mutant showed inhibition on cell elongation and gravitropic response (Kleine-Vehn et al., 2010; Zhou et al., 2022). Therefore, to understand how Cd treatment could mediate this alteration, we have tried to focus on these aspects using pharmacological and metabolomic approaches and GFP transgenic lines.

During the gravitropic assay, we observed that Cd-treated plants could still perceive the gravitropic stimuli, but their response was significantly slower than in the control plants. In addition, a significant reduction in statolith content was observed in plants treated with Cd, especially at the highest concentration. Statoliths are widely known for their involvement in root gravitropism, together with auxin gradient formation and microtubules organization (Aloni et al., 2006; Geisler et al., 2014; Zhang et al., 2019).

Similar effects were observed by Lešková et al. (2020) in nickel-treated roots. Moreover, either Hu et al. (2012) in plants treated with narciclasine, an alkaloid known to interact with auxin transport, or Hu et al. (2013), in plants treated with Cd, observed that starch granules were significantly reduced in treated plants following the auxin gradient (less auxin in the RAM resulted in a reduction of starch granules).

Further, the metabolomic analysis, carried out on 5-day-old seedlings treated for 48 h with Cd, showed a significant alteration of the starch and sucrose metabolism, pivotal for statolith starch granules formation (Abt and Zeeman, 2020). Similarly, Devi et al. (2007) previously reported the Cd-induced significant down-accumulation of several sugars belonging to this pathway and the reduction of starch production in roots.

The increase in RAM width and the reduction of RAM length were observed in plants treated with microtubule interferents such as taxol, oryzalin and colchicine (Baskin et al., 1994; Baskin et al., 2004).

Moreover, phenotypes similar to Cd-treated seedlings were also observed in *Arabidopsis* mutants characterised by a reduced expression of α-tubulin genes (TUA6/AS) (Bao et al., 2001).

The involvement of auxin transport alteration and microtubule organisation was also suggested by the alteration of the gravitropic response observed in Cd-treated seedlings.

Therefore, the altered gravitropic response observed in Cd-treated roots could be due to Cd-induced anatomical alterations mediated by microtubule arrangement and auxin distribution, as Ishida et al. (2007) suggested in experiments carried out on *A. thaliana*. Moreover, Araniti et al. (2016) reported that the loss of gravitropism in *Arabidopsis* seedlings treated with a phytotoxin was induced by microtubule malformations related to hormonal and ROS unbalance. According to the literature (Wang et al., 2004), a significant increase in $O_2^{\bullet-}$ and H_2O_2 was observed in Cd-treated plants, accompanied by an alteration of auxin distribution and microtubule organisation. Concerning auxin transport, the results highlighted a slightly significant change in GFP signal intensity in the root tip of seedlings exposed to Cd. On the contrary, severe effects were observed on its redistribution, particularly in *pPIN2::PIN2-GFP* was observed a strong alteration induced by Cd treatment. Zwiewka et al. (2019) reported that H_2O_2 accumulation selectively affected PIN2, and similar effects were observed in nickel-treated roots due to ROS bursts (Lešková et al., 2020).

Moreover, as also observed in our experiment, H_2O_2 inhibited PIN2 recycling, altering the delivery of PIN2-containing vesicles to their final destinations and inducing a formation of intracellular agglomerates in our transgenic line *pPIN2::PIN2-GFP*. Moreover, they also demonstrated the tight connection among H_2O_2 burst, cytoskeleton organisation and PIN2 trafficking, demonstrating that H_2O_2 accumulation affects the actin dynamics, thus modulating PIN2 trafficking. Since our results highlighted a Cd-mediated accumulation of H_2O_2 and significant alteration in microtubule organisation, it could be speculated that, in Cd-treated roots also, ROS burst could be involved with the changes observed in PIN2 distribution and agglomerates accumulation. This hypothesis was confirmed through pharmacological bioassays using H_2O_2 and KI, a known H_2O_2 scavenger, which partially restored microtubule organisation and PIN2 vesicle distribution.

5. Conclusions

Our results demonstrated that short acute Cd exposition only for 24 h had an effect preferentially on cell expansion, affecting the auxin distribution and inducing ROS accumulation, which resulted in an alteration of microtubules orientation pattern and sucrose metabolism.

Globally, our results confirm that short-term acute Cd treatment induced root architecture remodelling, which led to a reduced gravitropic response. These effects were mediated by an altered auxin distribution where PIN2 was the main actor involved. Further studies

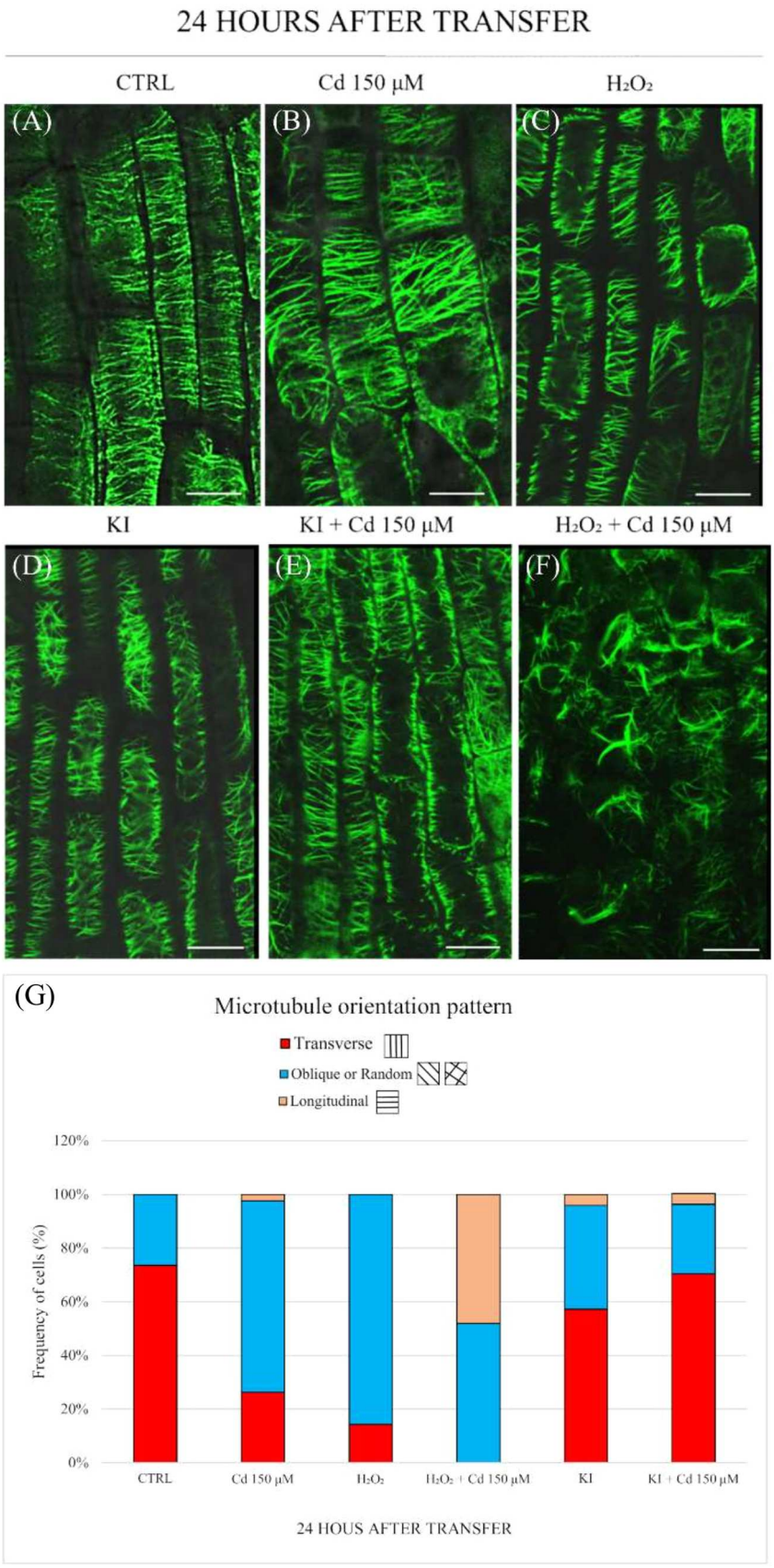

Fig. 10. Cd-, H_2O_2-, KI-induced changes in microtubules orientation in epidermal cells of transition zone. Confocal images were taken 24 h after transfer in medium as control (CTRL) (A) and in medium added with Cd 150 µM (B), H_2O_2 2 mM (C), H_2O_2 2 mM + Cd 150 µM (D), KI 1 mM (E) and KI 1 mM + Cd 150 µM (F). Scale bars 10 µm. (G) Frequency of different microtubule orientation patterns in epidermal cells of the transition zone (n > 30 cells per condition and time-point).

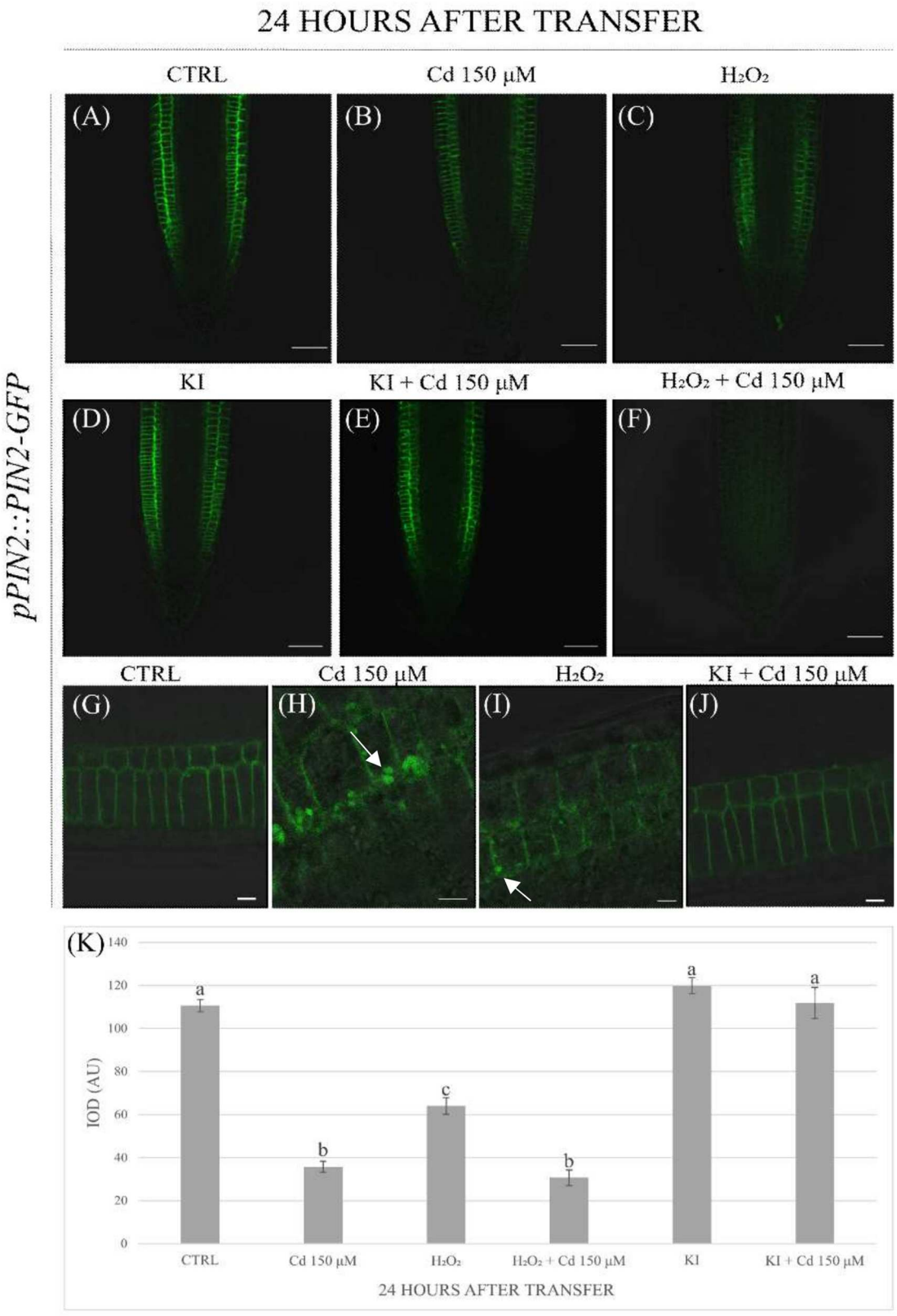

Fig. 11. Analysis of *pPIN2::PIN2-GFP* accumulation. Seedlings were monitored after 24 h from the transfer in medium as control (CTRL) (A) and in medium added with Cd 150 µM (B), H_2O_2 2 mM (C), H_2O_2 2 mM + Cd 150 µM (D), KI 1 mM (E) and KI 1 mM + Cd 150 µM (F). (G – J) Close-up view of PIN2 localization in cell membranes and in intracellular agglomerates. (A – F) Scale bars 50 µm. (G – J) Scale bars 10 µm. (K) Integrated optical density (IOD) expressed as arbitrary units (AU) of fluorescence intensity. Statistical analysis was performed using ANOVA and Tukey's ranked test ($P < 0.05$) and different letters indicate significant differences. Data present the mean ± Standard Error (SE) of three independent experiments.

should be focused on deeply studying the effects of short-term acute Cd expositions on ROS balance in RAM.

Funding

The work was supported by University of Calabria (ex 60%). The confocal microscope was supplied by PON Ricerca e Competitività 2007–2013, Sistema Integrato di Laboratori per L'Ambiente – (SILA) PONa3_00341, CM2–Centro di Microscopia e Microanalisi.

CRediT authorship contribution statement

F.A., E.T., A.C., L.B., designed research; **F.A., E.T., M.L.M., E.G., M.M. S.A.R., L.B.**, performed research; **F.A., E.T., M.L.M., E.G., A.M., M.F., A.C., L.B.** analysed data and discussed results; **F.A., A.C., L.B.**, supervised the research; **F.A., E.T. and L.B**. wrote the paper. All authors have read and agreed to the published version of the manuscript.

Declaration of Competing Interest

The authors declare that they have no known competing financial interests or personal relationships that could have appeared to influence the work reported in this paper.

Data availability

No data was used for the research described in the article.

Acknowledgement

We are grateful to Jiri Friml, Hyung-Taeg Cho, Ikram Blilou, and Marcus Heisler, who gently supplied the transgenic lines used in the experiments.

Appendix A. Supporting information

Supplementary data associated with this article can be found in the online version at doi:10.1016/j.plantsci.2023.111726.

References

M.R. Abt, S.C. Zeeman, Evolutionary innovations in starch metabolism, Curr. Opin. Plant Biol. 55 (2020) 109–117, https://doi.org/10.1016/j.pbi.2020.03.001.

R. Aloni, E. Aloni, M. Langhans, C.I. Ullrich, Role of cytokinin and auxin in shaping root architecture: regulating vascular differentiation, lateral root initiation, root apical dominance and root gravitropism, AoB Plants 97 (2006) 883–893, https://doi.org/10.1093/aob/mcl027.

F. Araniti, L. Bruno, F. Sunseri, M. Pacenza, I. Forgione, M.B. Bitonti, M.R. Abenavoli, The allelochemical farnesene affects *Arabidopsis thaliana* root meristem altering auxin distribution, Plant Physiol. Biochem. 121 (2017) 14–20, https://doi.org/10.1016/j.plaphy.2017.10.005.

F. Araniti, E. Graña, U. Krasuska, R. Bogatek, M.J. Reigosa, M.R. Abenavoli, A. M. Sanchez-Moreiras, Loss of gravitropism in farnesene-treated *Arabidopsis* is due to microtubule malformations related to hormonal and ROS unbalance, PLoS One 11 (2016), e0160202, https://doi.org/10.1371/journal.pone.0160202.

Y. Bao, B. Kost, N.H. Chua, Reduced expression of α-tubulin genes in *Arabidopsis thaliana* specifically affects root growth and morphology, root hair development and root gravitropism, Plant J. 28 (2001) 145–157, https://doi.org/10.1046/j.1365-313X.2001.01142.x.

T.I. Baskin, Anisotropic expansion of the plant cell wall, Annu. Rev. Cell Dev. Biol. 21 (2005) 203–222, https://doi.org/10.1146/annurev.cellbio.20.082503.103053.

T.I. Baskin, G.T. Beemster, J.E. Judy-March, F. Marga, Disorganization of cortical microtubules stimulates tangential expansion and reduces the uniformity of cellulose microfibril alignment among cells in the root of *Arabidopsis*, Plant Physiol. 135 (2004) 2279–2290, https://doi.org/10.1104/pp.104.040493.

T.I. Baskin, J.E. Wilson, A. Cork, R.E. Williamson, Morphology and microtubule organization in *Arabidopsis* roots exposed to oryzalin or taxol, Plant Cell Physiol. 35 (1994) 935–942, https://doi.org/10.1093/oxfordjournals.pcp.a078679.

E. Benková, M. Michniewicz, M. Sauer, T. Teichmann, D. Seifertová, G. Jürgens, J. Friml, Local, efflux-dependent auxin gradients as a common module for plant organ formation, Cell 115 (2003) 591–602, https://doi.org/10.1016/S0092-8674(03)00924-3.

E.B. Blancaflor, D.L. Jones, S. Gilroy, Alterations in the cytoskeleton accompany aluminum-induced growth inhibition and morphological changes in primary roots of maize, Plant Physiol. 118 (1998) 159–172, https://doi.org/10.1104/pp.118.1.159.

I. Blilou, J. Xu, M. Wildwater, V. Willemsen, I. Paponov, J. Friml, R. Heidstra, M. Aida, K. Palme, B. Scheres, The PIN auxin efflux facilitator network controls growth and patterning in *Arabidopsis* roots, Nature 433 (2005) 39–44, https://doi.org/10.1038/nature03184.

N.S. Bolan, T. Makino, A. Kunhikrishnan, P.J. Kim, S. Ishikawa, M. Murakami, R. Naidu, M.B. Kirkham, Cadmium contamination and its risk management in rice ecosystems, Adv. Agron. 119 (2013) 183–273, https://doi.org/10.1016/B978-0-12-407247-3.00004-4.

L. Bruno, M. Pacenza, I. Forgione, L.R. Lamerton, M. Greco, A. Chiappetta, M.B. Bitonti, In *Arabidopsis thaliana* cadmium impact on the growth of primary root by altering SCR expression and auxin-cytokinin cross-talk, Front. Plant. Sci. 8 (2017) 1323–1336, https://doi.org/10.3389/fpls.2017.01323.

L. Bruno, E. Talarico, L. Cabeiras-Freijanes, M.L. Madeo, A. Muto, M. Minervino, L. Lucini, B. Miras-Moreno, A. Sofo, F. Araniti, Coumarin interferes with polar auxin transport altering microtubule cortical array organization in *Arabidopsis thaliana* (L.) Heynh. root apical meristem, Int. J. Mol. Sci. 22 (2021a) 7305–7324, https://doi.org/10.3390/ijms22147305.

L. Bruno, E. Talarico, M.L. Madeo, A. Muto, M. Minervino, F. Araniti, M.B. Bitonti, A. Chiappetta, Cadmium affects cell niches maintenance in *Arabidopsis thaliana* post-embryonic shoot and root apical meristem by altering the expression of *WUS/WOX* homolog genes and cytokinin accumulation, Plant Physiol. Biochem. 167 (2021b) 785–794, https://doi.org/10.1016/j.plaphy.2021.09.014.

J. Cherif, C. Mediouni, W.B. Ammar, F. Jemal, Interactions of zinc and cadmium toxicity in their effects on growth and in antioxidative systems in tomato plants (*Solarium lycopersicum*), J. Environ. Sci. 23 (2011) 837–844, https://doi.org/10.1016/S1001-0742(10)60415-9.

U.H. Cho, N.H. Seo, Oxidative stress in *Arabidopsis thaliana* exposed to cadmium is due to hydrogen peroxide accumulation, Plant Sci. 168 (2005) 113–120, https://doi.org/10.1016/j.plantsci.2004.07.021.

G. Choppala, Saifullah, N. Bolan, S. Bibi, M. Iqbal, Z. Rengel, A. Kunhikrishnan, N. Ashwath, Y.S. Ok, Cellular mechanisms in higher plants governing tolerance to cadmium toxicity, CRC Crit. Rev. Plant Sci. 33 (2014) 374–391, https://doi.org/10.1080/07352689.2014.903747.

R. Devi, N. Munjral, A.K. Gupta, N. Kaur, Cadmium induced changes in carbohydrate status and enzymes of carbohydrate metabolism, glycolysis and pentose phosphate pathway in pea, Environ. Exp. Bot. 6 (2007) 167–174, https://doi.org/10.1016/j.envexpbot.2007.05.006.

M. Drążkiewicz, E. Skórzyńska-Polit, Z. Krupa, Copper-induced oxidative stress and antioxidant defence in *Arabidopsis thaliana*, Biometals 17 (2004) 379–387, https://doi.org/10.1023/B:BIOM.0000029417.18154.22.

Y. Duan, W. Zhang, B. Li, Y. Wang, K. Li, C. Han, Y. Zhang, X. Li, An endoplasmic reticulum response pathway mediates programmed cell death of root tip induced by water stress in Arabidopsis, New Phytol. 186 (2010) 681–695, https://doi.org/10.1111/j.1469-8137.2010.03207.x.

I. Forgione, M. Wołoszý nska, M. Pacenza, A. Chiappetta, M. Greco, F. Araniti, M. R. Abenavoli, M. Van Lijsebettens, M.B. Bitonti, L. Bruno, Hypomethylated drm1 drm2 cmt3 mutant phenotype of *Arabidopsis thaliana* is related to auxin pathway impairment, Plant Sci. 280 (2019) 383–396, https://doi.org/10.1016/j.plantsci.2018.12.029.

M. Geisler, B. Wang, J. Zhu, Auxin transport during root gravitropism: transporters and techniques, Plant Biol. 16 (2014) 50–57, https://doi.org/10.1111/plb.12030.

S.S. Gill, N.A. Khan, N. Tuteja, Cadmium at high dose perturbs growth, photosynthesis and nitrogen metabolism while at low dose it up regulates sulfur assimilation and antioxidant machinery in garden cress (*Lepidium sativum* L.), Plant Sci. 182 (2012) 112–120, https://doi.org/10.1016/j.plantsci.2011.04.018.

Y. Hu, L. Yang, X. Na, J. You, W. Hu, X. Liang, J. Liu, L. Mao, X. Wang, H. Wang, Y. Bi, Narciclasine inhibits the responses of *Arabidopsis* roots to auxin, Planta 236 (2012) 597–612, https://doi.org/10.1007/s00425-012-1632-z.

Y.F. Hu, G. Zhou, X.F. Na, L. Yang, W.B. Nan, X. Liu, Y.Q. Zhang, J.L. Li, Y.R. Bi, Cadmium interferes with maintenance of auxin homeostasis in *Arabidopsis* seedlings, J. Plant Physiol. 170 (2013) 965–975, https://doi.org/10.1016/j.jplph.2013.02.008.

T. Ishida, S. Thitamadee, T. Hashimoto, Twisted growth and organization of cortical microtubules, J. Plant Res. 120 (2007) 61–70, https://doi.org/10.1007/s10265-006-0039-y.

D.L. Jones, E.B. Blancaflor, L.V. Kochian, S. Gilroy, Spatial coordination of aluminium uptake, production of reactive oxygen species, callose production and wall rigidification in maize roots, Plant Cell Environ. 29 (2006) 1309–1318, https://doi.org/10.1111/j.1365-3040.2006.01509.x.

M. Karampelias, P. Neyt, S. De Groeve, S. Aesaert, G. Coussens, J. Rolčík, L. Bruno, N. De Winne, A. Van Minnebruggen, M. Van Montagu, M.R. Ponce, *ROTUNDA3* function in plant development by phosphatase 2A-mediated regulation of auxin transporter recycling, Proc. Natl. Acad. Sci. USA 113 (2016) 2768–2773.

J. Kleine-Vehn, Z. Ding, A.R. Jones, M. Tasaka, M.T. Morita, J. Friml, Gravity-induced PIN transcytosis for polarization of auxin fluxes in gravity-sensing root cells, Proc. Natl. Acad. Sci. USA 107 (2010) 22344–22349, https://doi.org/10.1073/pnas.1013145107.

J. Kleine-Vehn, J. Friml, Polar targeting and endocytic recycling in auxin-dependent plant development, Annu. Rev. Cell Dev. Biol. 24 (2008) 447–473, https://doi.org/10.1146/annurev.cellbio.24.110707.175254.

M. Kollmeier, P. Dietrich, C.S. Bauer, W.J. Horst, R. Hedrich, Aluminum activates a citrate-permeable anion channel in the aluminum-sensitive zone of the maize root apex. A comparison between an aluminum-sensitive and an aluminum-resistant cultivar, Plant Physiol. 126 (2001) 397–410, https://doi.org/10.1104/pp.126.1.397.

P. Křeček, P. Skůpa, J. Libus, S. Naramoto, R. Tejos, J. Friml, E. Zažímalová, The PIN-FORMED (PIN) protein family of auxin transporters, Genome Biol. 10 (2009) 1–11, https://doi.org/10.1186/gb-2009-10-12-249.

J.Y. Lee, P.N. Benfey, Root apical meristems, in: K. Roberts (Ed.), Handbook of Plant Science, 2 Volume Set, 1, John Wiley & Sons, 2007, pp. 47–53, https://doi.org/10.1002/9780470015902.a0020121.

H. Lequeux, C. Hermans, S. Lutts, N. Verbruggen, Response to copper excess in *Arabidopsis thaliana*: impact on the root system architecture, hormone distribution, lignin accumulation and mineral profile, Plant Physiol. Biochem. 48 (2010) 673–682, https://doi.org/10.1016/j.plaphy.2010.05.005.

A. Lešková, M. Zvarík, T. Araya, R.F. Giehl, Nickel toxicity targets cell wall-related processes and PIN2-mediated auxin transport to inhibit root elongation and gravitropic responses in *Arabidopsis*, Plant Cell Physiol. 61 (2020) 519–535, https://doi.org/10.1093/pcp/pcz217.

S. Li, W. Yang, T. Yang, Y. Chen, W. Ni, Effects of cadmium stress on leaf chlorophyll fluorescence and photosynthesis of *Elsholtzia argyi*—a cadmium accumulating plant. Int, J. Phytoremediat. 17 (2015) 85–92, https://doi.org/10.1080/15226514.2013.828020.

J. Lisec, N. Schauer, J. Kopka, L. Willmitzer, A.R. Fernie, Gas chromatography mass spectrometry–based metabolite profiling in plants, Nat. Protoc. 1 (2006) 387–396, https://doi.org/10.1038/nprot.2006.59.

X.M. Liu, K.E. Kim, K.C. Kim, X.C. Nguyen, H.J. Han, M.S. Jung, H.S. Kim, S.H. Kim, H. C. Park, D.J. Yun, W.S. Chung, Cadmium activates *Arabidopsis* MPK3 and MPK6 via accumulation of reactive oxygen species, Phytochemistry 71 (2010) 614–618, https://doi.org/10.1016/j.phytochem.2010.01.005.

K.J. Livak, T.D. Schmittgen, Analysis of relative gene expression data using real-time quantitative PCR and the 2− ΔΔCT method, Methods 25 (2001) 402–408, https://doi.org/10.1006/meth.2001.1262.

Z. Lukačová, R. Švubová, J. Kohanová, A. Lux, Silicon mitigates the Cd toxicity in maize in relation to cadmium translocation, cell distribution, antioxidant enzymes stimulation and enhanced endodermal apoplasmic barrier development, Plant Growth Regul. 70 (2013) 89–103, https://doi.org/10.1007/s10725-012-9781-4.

A. Lupini, F. Araniti, F. Sunseri, M.R. Abenavoli, Coumarin interacts with auxin polar transport to modify root system architecture in *Arabidopsis thaliana*, Plant Growth Regul. 74 (2014) 23–31, https://doi.org/10.1007/s10725-014-9893-0.

A. Marchant, J. Kargul, S.T. May, P. Muller, A. Delbarre, C. Perrot-Rechenmann, M. J. Bennett, AUX1 regulates root gravitropism in *Arabidopsis* by facilitating auxin uptake within root apical tissues, EMBO J. 18 (1999) 2066–2073, https://doi.org/10.1093/emboj/18.8.2066.

B.B. Misra, V. Das, M. Landi, M.R. Abenavoli, F. Araniti, Short-term effects of the allelochemical umbelliferone on *Triticum durum* L. metabolism through GC–MS based untargeted metabolomics, Plant Sci. 298–307 (2020), 110548, https://doi.org/10.1016/j.plantsci.2020.110548.

J. Moreno-Romero, M. Carme Espunya, M. Platara, J. Ariño, M. Carmen Martínez, A role for protein kinase CK2 in plant development: evidence obtained using a dominant-negative mutant, Plant J. 55 (2008) 118–130, https://doi.org/10.1016/j.plaphy.2021.09.014.

M. Nakamura, K. Naoi, T. Shoji, T. Hashimoto, Low concentrations of propyzamide and oryzalin alter microtubule dynamics in *Arabidopsis* epidermal cells, Plant Cell Physiol. 45 (2004) 1330–1334, https://doi.org/10.1093/pcp/pch300.

I. Ottenschläger, P. Wolff, C. Wolverton, R.P. Bhalerao, G. Sandberg, H. Ishikawa, M. Evans, K. Palme, Gravity-regulated differential auxin transport from columella to lateral root cap cells, Proc. Natl. Acad. Sci. USA 100 (2003) 2987–2991, https://doi.org/10.1073/pnas.0437936100.

M. Pacenza, A. Muto, A. Chiappetta, L. Mariotti, E. Talarico, P. Picciarelli, E. Picardi, L. Bruno, M.B. Bitonti, In *Arabidopsis thaliana* Cd differentially impacts on hormone genetic pathways in the methylation defective ddc mutant compared to wild type, Sci. Rep. 11 (2021) 1–17, https://doi.org/10.1038/s41598-021-90528-5.

B. Péret, K. Swarup, A. Ferguson, M. Seth, Y. Yang, S. Dhondt, N. James, I. Casimiro, P. Perry, A. Syed, H. Yang, AUX/LAX genes encode a family of auxin influx transporters that perform distinct functions during *Arabidopsis* development, Plant Cell 24 (2012) 2874–2885, https://doi.org/10.1105/tpc.112.097766.

A. Placek, A. Grobelak, M. Kacprzak, Improving the phytoremediation of heavy metals contaminated soil by use of sewage sludge, Int. J. Phytoremediat. 18 (2016) 605–618, https://doi.org/10.1080/15226514.2015.1086308.

S. Qadir, S. Jamshieed, S. Rasool, M. Ashraf, N.A. Akram, P. Ahmad, Modulation of plant growth and metabolism in cadmium-enriched environments, Rev. Environ. Contam. Toxicol. 229 (2014) 51–88, https://doi.org/10.1007/978-3-319-03777-6_4.

A.M. Rashotte, S.R. Brady, R.C. Reed, S.J. Ante, G.K. Muday, Basipetal auxin transport is required for gravitropism in roots of *Arabidopsis*, Plant Physiol. 122 (2000) 481–490, https://doi.org/10.1104/pp.122.2.481.

T. Remans, K. Smeets, K. Opdenakker, D. Mathijsen, J. Vangronsveld, A. Cuypers, Normalisation of real-time RT-PCR gene expression measurements in *Arabidopsis thaliana* exposed to increased metal concentrations, Planta 227 (2008) 1343–1349, https://doi.org/10.1007/s00425-008-0706-4.

S.A. Sansone, D. Schober, H.J. Atherton, O. Fiehn, H. Jenkins, P. Rocca-Serra, D. V. Rubtsov, I. Spasic, L. Soldatova, C. Taylor, A. Tseng, Metabolomics standards initiative: ontology working group work in progress, Metabolomics 3 (2007) 249–256, https://doi.org/10.1007/s11306-007-0069-z.

N. Satoh-Nagasawa, M. Mori, N. Nakazawa, T. Kawamoto, Y. Nagato, K. Sakurai, H. Takahashi, A. Watanabe, H. Akagi, Mutations in rice (*Oryza sativa*) heavy metal ATPase 2 (OsHMA2) restrict the translocation of zinc and cadmium, Plant Cell Physiol. 53 (2012) 213–224, https://doi.org/10.1093/pcp/pcr166.

J. Schindelin, I. Arganda-Carreras, E. Frise, V. Kaynig, M. Longair, T. Pietzsch, S. Preibisch, C. Rueden, S. Saalfeld, B. Schmid, J.Y. Tinevez, Fiji: an open-source platform for biological-image analysis, Nat. Methods 9 (2012) 676–682, https://doi.org/10.1038/nmeth.2019.

M. Shahid, B. Pourrut, C. Dumat, M. Nadeem, M. Aslam, E. Pinelli, Heavy-metal-induced reactive oxygen species: phytotoxicity and physicochemical changes in plants, Rev. Environ. Contam. Toxicol. 232 (2014) 1–44, https://doi.org/10.1007/978-3-319-06746-9_1.

S.R. Smith, A critical review of the bioavailability and impacts of heavy metals in municipal solid waste composts compared to sewage sludge, Environ. Int. 35 (2009) 142–156, https://doi.org/10.1016/j.envint.2008.06.009.

S.H. Su, N.M. Gibbs, A.L. Jancewicz, P.H. Masson, Molecular mechanisms of root gravitropism, Curr. Biol. 27 (2017) R964–R972, https://doi.org/10.1016/j.cub.2017.07.015.

P. Sun, Q.Y. Tian, J. Chen, W.H. Zhang, Aluminium-induced inhibition of root elongation in *Arabidopsis* is mediated by ethylene and auxin, J. Exp. Bot. 61 (2010) 347–356, https://doi.org/10.1093/jxb/erp306.

E. Truernit, H. Bauby, B. Dubreucq, O. Grandjean, J. Runions, J. Barthélémy, J. C. Palauqui, High-resolution whole-mount imaging of three-dimensional tissue organization and gene expression enables the study of phloem development and structure in *Arabidopsis*, Plant Cell 20 (2008) 1494–1503, https://doi.org/10.1105/tpc.107.056069.

H. Vanacker, T.L. Carver, C.H. Foyer, Early H2O2 accumulation in mesophyll cells leads to induction of glutathione during the hyper-sensitive response in the barley-powdery mildew interaction, Plant Physiol. 123 (2000) 1289–1300, https://doi.org/10.1104/pp.123.4.1289.

K. Verma, G.S. Shekhawat, A. Sharma, S.K. Mehta, V. Sharma, Cadmium induced oxidative stress and changes in soluble and ionically bound cell wall peroxidase activities in roots of seedling and 3–4 leaf stage plants of *Brassica juncea* (L.) czern, Plant Cell Rep. 27 (2008) 1261–1269, https://doi.org/10.1007/s00299-008-0552-7.

A. Vieten, M. Sauer, P.B. Brewer, J. Friml, Molecular and cellular aspects of auxin-transport-mediated development, Trends Plant Sci. 12 (2007) 160–168, https://doi.org/10.1016/j.tplants.2007.03.006.

R. Wang, J. Wang, L. Zhao, S. Yang, Y. Song, Impact of heavy metal stresses on the growth and auxin homeostasis of *Arabidopsis* seedlings, Biometals 28 (2015) 123–132, https://doi.org/10.1007/s10534-014-9808-6.

Y. Wang, J. Fang, S.S. Leonard, K.M.K. Rao, Cadmium inhibits the electron transfer chain and induces reactive oxygen species, Free Radic. Biol. Med. 36 (2004) 1434–1443, https://doi.org/10.1016/j.freeradbiomed.2004.03.010.

D. Wu, H. Shen, K. Yokawa, F. Baluška, Alleviation of aluminium-induced cell rigidity by overexpression of OsPIN2 in rice roots, J. Exp. Bot. 65 (2014) 5305–5315, https://doi.org/10.1093/jxb/eru292.

H.M. Yuan, X. Huang, Inhibition of root meristem growth by cadmium involves nitric oxide-mediated repression of auxin accumulation and signalling in *Arabidopsis*, Plant Cell Environ. 39 (2016) 120–135, https://doi.org/10.1111/pce.12597.

H.M. Yuan, H.H. Xu, W.C. Liu, Y.T. Lu, Copper regulates primary root elongation through PIN1-mediated auxin redistribution, Plant Cell Physiol. 54 (2013) 766–778, https://doi.org/10.1093/pcp/pct030.

Y. Zhang, P. He, X. Ma, Z. Yang, C. Pang, J. Yu, G. Wang, J. Friml, G. Xiao, Auxin-mediated statolith production for root gravitropism, New Phytol. 224 (2019) 761–774, https://doi.org/10.1111/nph.15932.

H. Zhou, H. Ge, J. Chen, X. Li, L. Yang, H. Zhang, Y. Wang, Salicylic acid regulates root gravitropic growth via clathrin-independent endocytic trafficking of PIN2 auxin transporter in *Arabidopsis thaliana*, Int. J. Mol. Sci. 23 (2022) 9379–9392, https://doi.org/10.3390/ijms23169379.

M. Zwiewka, A. Bielach, P. Tamizhselvan, S. Madhavan, E.E. Ryad, S. Tan, M. Hrtyan, P. Dobrev, R. Vanková, J. Friml, V.B. Tognetti, Root adaptation to H_2O_2-induced oxidative stress by ARF-GEF BEN1-and cytoskeleton-mediated PIN2 trafficking, Plant Cell Physiol. 60 (2019) 255–273, https://doi.org/10.1093/pcp/pcz001.

Plant Physiology and Biochemistry 167 (2021) 785–794

Contents lists available at ScienceDirect

Plant Physiology and Biochemistry

journal homepage: www.elsevier.com/locate/plaphy

Cadmium affects cell niches maintenance in *Arabidopsis thaliana* post-embryonic shoot and root apical meristem by altering the expression of WUS/WOX homolog genes and cytokinin accumulation

Bruno Leonardo [a,*], Talarico Emanuela [a], Madeo Maria Letizia [a], Muto Antonella [a], Minervino Marco [a], Araniti Fabrizio [b], Bitonti Maria Beatrice [a], Chiappetta Adriana [a]

[a] Dipartimento di Biologia, Ecologia e Scienza della Terra, Università della Calabria (DiBEST-UNICAL), Arcavacata di Rende, Italy
[b] Dipartimento di Scienze Agrarie e Ambientali - Produzione, Territorio, Agroenergia, Università Statale di Milano, Via Celoria n° 2, 20133, Milano, Italy

ARTICLE INFO

Keywords:
Cytokinin
Root growth
Shoot apex growth
Stem cell niches
WOX
WUS/CLV

ABSTRACT

Cadmium (Cd) is one of the most widespread polluting heavy metals in both terrestrial and aquatic environments and represents an extremely significant pollutant causing severe environmental and social problems due to its high toxicity and large solubility in water. In plants, the root is the first organ that get in contact with Cd. It is absorbed by the root system and translocated to the shoot and leaves through xylem loading, causing a variety of genetic, biochemical, and physiological damages. Cd inhibits both the root and shoot growth, but the mechanisms underlying this inhibition remain elusive. In this context in the present work we focused the attention on the effects of Cd on meristem size and organization of both shoot and root. To this aim morpho-histological and molecular analyses were carried out on 5 days old seedlings exposed or not to Cd (100 μM and 150 μM for 24) of wild type and transgenic lines expressing molecular markers with an important role in shoot and root pattern organization. More precisely, we monitored the expression pattern of WUS/CLV3 and WOX5 transcription factors involved in the establishment and maintenance of stem cell niche and the control of meristem size and of *TCSn::GFP* cytokinin-sensitive sensor as relevant components of hormone circuit controlling shoot and root growth. The results highlighted that the treatments with Cd impacts shoot and root size and shape by altering the paralogous WOX genes expression via cytokinin accumulation.

1. Introduction

Cadmium (Cd) is one the most widespread heavy metals in both terrestrial and marine environments and represents an extremely significant pollutant due to its high toxicity and large solubility in water causing severe environmental and social problems (Gallego et al., 2012; Song et al., 2017).

In plants, Cd is absorbed by the root system and translocated to the shoot and leaves through xylem loading, causing a variety of genetic, biochemical, and physiological damages (Jin et al., 2003; Herbette et al., 2006; Liu et al., 2011; Greco et al., 2012; Bruno et al., 2017; Pacenza et al., 2021). Globally, cadmium's effect leads to reduced plant growth and negatively impacts development and reproduction (Keunen et al., 2011; Huybrechts et al., 2019; Haider et al., 2021; Pacenza et al., 2021).

It is well known that in plants, the embryonic organization is rudimentary, and the developmental process occurs primarily after germination. In particular, the embryo's apical-basal axis is delineated by two meristematic poles, the shoot and root apical meristems (SAM and RAM), which determine the future growth direction of the plant. In contrast, the radial axis specifies the identity and arrangement of tissues in concentric layers.

During post-embryonic development, the SAM is essential for forming the vegetative plant body. As well-defined in *Arabidopsis* model plant, it is organized into three functional zones with different cell division rates and different functions (Medford et al., 1992). The central zone (CZ) consists of stem cells that maintain indeterminate growth and

Abbreviations: Ctrl, control; Cd, cadmium; DAG, days after germination; GFP, green fluorescent protein; MCN, meristematic cell number; MZL, meristematic zone length; MZW, meristematic zone width; NDC, number of dividing cells; OC, organization center; QC, quiescent center; SAM, Shoot apical meristem; RAM, root apical meristem; SCNs, stem cell niches.

* Corresponding author.
E-mail address: leonardo.bruno@unical.it (B. Leonardo).

https://doi.org/10.1016/j.plaphy.2021.09.014
Received 8 August 2021; Received in revised form 8 September 2021; Accepted 9 September 2021
Available online 11 September 2021

produce daughter cells for the neighbouring peripheral (PZ) and rib zones (RZ) (Steeves and Sussex, 1989; Schoof et al., 2000). From the PZ and RZ zones, lateral organs and the pith tissues are produced, respectively. Progenitor tissue layers L1, L2, L3 are radially organized in the *Arabidopsis* SAM, L1 cells give rise to the epidermis while L2 and L3 subepidermal layers form internal tissues.

It has been reported that the homeostasis between cell proliferation and differentiation is balanced by an intricated network in which transcription factors (TFs), hormones, and epigenetic mechanisms participate (Riou-Khamlichi et al., 1999; Perrot-Rechenmann, 2010; Zhang et al., 2010; Sanmartín et al., 2011; Heyman et al., 2013; Zhang et al., 2013; Dehghan Nayeri, 2014).

Within this network, the CLAVATA (CLV)/WUSHELL (WUS) signalling pathway represents the principal genetic network controlling the equilibrium between the three zones of the SAM. In particular, *WUS* encodes for a TF and it is required to specify stem cell fate. Its expression is restricted to few cells in the CZ underlying the L2 layer, which form the organizing centre (OC) of the SAM. The restriction of WUS expression is under the control of spatial negative-feedback loop in which WUS activates the expression of the CLV3 ligand-encoding gene in the stem cells and CLV3, in turn, restricts WUS expression to the OC (Laux et al., 1996; Mayer et al., 1998; Brand et al., 2000; Schoof et al., 2000; Groβ-Hardt and Laux, 2003).

Thus, when the number of the stem cells increases, more CLV3 ligand is produced, resulting in fewer cells expressing WUS, thereby attenuating stem cell promoting activity and, in turn, the expression of a ligand-encoding gene (Brand et al., 2000; Schoof et al., 2000). In such a way the homeostasis of stem cell niche (SCN) is assured.

At the opposite pole, the RAM produces the primary root, which is organized radially, with initial cells that produce daughter cell files in concentric layers (Dolan et al., 1993; Scheres et al., 1994; Van Lijsebettens and Van Montagu, 2005). These cells enter the elongation zone, in which they continue to divide and start expanding and differentiating, giving rise to the stele, the endodermis/cortex and root-cap/epidermis tissues. Furthermore, within the root meristem, a group of mitotically inactive cells, which form the quiescent center (QC), keeps the surrounding initials in an indeterminate state, and its presence is essential for the proper root development (Van den Berg et al., 1997; Perilli et al., 2012). Different genes are involved in the establishment and maintenance of RAM. The homeodomain transcription factor WOX5, a paralog of WUS, is required in the QC to maintain the undifferentiated state of the surrounding stem cells (Sarkar et al., 2007). While PLETHORA (PLT) and SCARECROW (SCR) transcription factors are involved in QC specification (Nawy et al., 2005; Sarkar et al., 2007).

According to the concept proposed by Mayer et al. (1998), the maintenance of the undifferentiated state of the stem cells in these two meristems is controlled by similar mechanisms. Therefore, it has been proposed that the QC in the RAM corresponds to the OC in the SAM.

Crosstalk between these master genes and hormone classes is also relevant in root and shoot patterning and development. In fact, the auxin in the RAM, promotes *PLT* genes expression and cell proliferation. Moreover it is involved in the specification of QC position through the generation and stabilization of an auxin maximum. Assured by auxin flux along the root tips generated by the action of the PIN protein family's auxin efflux carriers.

Through a feedback mechanism, auxin-induced *PLT* genes promote *PIN* expression, assuring a high steady-state level of auxin and maintaining the (SCN) (Aida et al., 2004; Blilou et al., 2005; Galinha et al., 2007).

In turn, cytokinins (CKs) act antagonistically to auxin in controlling root pattern and development. Namely, CKs induce cell division in the QC by repressing the WOX5 gene. Moreover, CKs promote cell differentiation at root transition zone (TZ) by modulating PIN expression and therefore auxin distribution while auxins promote cell division, suppressing cytokinin signalling (Dello Ioio et al., 2007, 2008; Růžička et al., 2009; Perilli and Sabatini, 2010; Perilli et al., 2010).

Also in the SAM stem cell fate is under auxin and CKs antagonistic control. Namely, CKs promotes *WUS* expression thus contributing to ensure the correct apical/basal placement and size of SCN by promoting *WUS* expression (Heidstra and Sabatini, 2014).Whereas auxin positively interacts with four closely related negative regulators of cytokinins signalling A-type ARABIDOPSIS RESPONSE REGULATOR (ARR) genes (To et al., 2004). On the other hand the specific localization of auxin is necessary for new organ primordium fate (Reinhardt et al., 2003). In particular new organ initiation is mediated by the AUXIN RESPONSE FACTOR5/MONOPTEROS (ARF5/MP) (Berleth and Jurgens, 1993; Hardtke and Berleth, 1998), and its direct target DORNROSCHEN (DRN) through the positive control of *CLV3* expression which results drastically reduced in *drn* mutants. Accordingly *drn* mutants develop an enlarged meristem in association with a higher accumulation of *WUS* transcript, supporting the importance of MP – DRN pathway in meristem regulation (Kirch et al., 2003; Luo et al., 2018).

In addition to the above-mentioned endogenous factors, plant development is greatly modulated by environmental factors (i.e., light, temperature, and water availability) that control both meristem activity (active *vs.* quiescent state) and commitment (vegetative *vs* reproductive/phase change), as well as organs growth and shape (Sarkar et al., 2007; Dello Ioio et al., 2008). Consequently, stressful conditions related to environmental factors negatively impact plant growth and development. Concerning specifically Cd pollution, its toxic effects on plant growth are well known and related to the induction of several changes at the genetic, biochemical and physiological level, phytohormone signalling, on transcript levels of cell cycle-related genes, alteration in transition from the vegetative to the reproductive phase (Maistri et al., 2011; Huybrechts et al., 2019).

Plant root system, as the first organ sensing soil heavy metals, is strongly affected by Cd which in *Arabidopsis* inhibits primary root growth, while lateral root formation is somehow stimulated (Xu et al., 2010; Yuan and Huang, 2016). There are that the inhibitory effect on primary root is linked to an impairment of auxin optimal accumulation at the root tip, which in turn reduces the size and activity of RAM (Blilou et al., 2005; Hu et al., 2013; Yuan and Huang, 2016; Bruno et al., 2017). In addition, in our previous work, we further demonstrated that a long-lasting Cd exposure of *Arabidopsis* seedlings inhibits primary root growth via affecting RAM stem cell niche and root radial patterning (Bruno et al., 2017).

To our knowledge, there are no data in the literature concerning how Cd alters the homeostasis of the SAM. The present study was addressed to compare Cd-induced effects on SAM and RAM homeostasis of *Arabidopsis thaliana* seedlings. Based on the literature data (Yuan and Huang, 2016), a short treatment was applied (24 h) using two different Cd concentrations (100 μM or 150 μM). GFP transgenic lines for different markers of meristem activity were used to verify putative alteration in their histological expression domains under Cd treatments.

2. Material and methods

2.1. Plant materials and growth conditions

Seeds of *A. thaliana* (L.) Heynh. ecotype Columbia (Col-0) and the transgenic lines *pWUS::GFP (N23897-* Jönsson et al. 2005*)*, *pCLV3::GFP-ER (N23895)*, *CYCB1;1::GFP* (Moreno-Romero et al., 2008Moreno-Romero et al., 2008*); TCSn::GFP* (Zürcher et al., 2013), *pWOX5::GFP* (Blilou et al., 2005), were used. Seeds were sterilized and grown as reported in Forgione et al. (2019). Briefly, the seeds were washed in absolute ethanol for 2 min, then in 1.75% hypochlorite solution (NaClO) for 12 min and three final 5 min washing steps using sterile distilled water.

The seeds were sown on Petri dishes and germinated on a 0.7% agar medium enriched with 1% sucrose and micro and macronutrients (1/2 Murashige & Skoog basal salt, Sigma Aldrich, Italia). Plated seeds were left at 4 °C for 48 h to sincronhyze the germination and then incubated

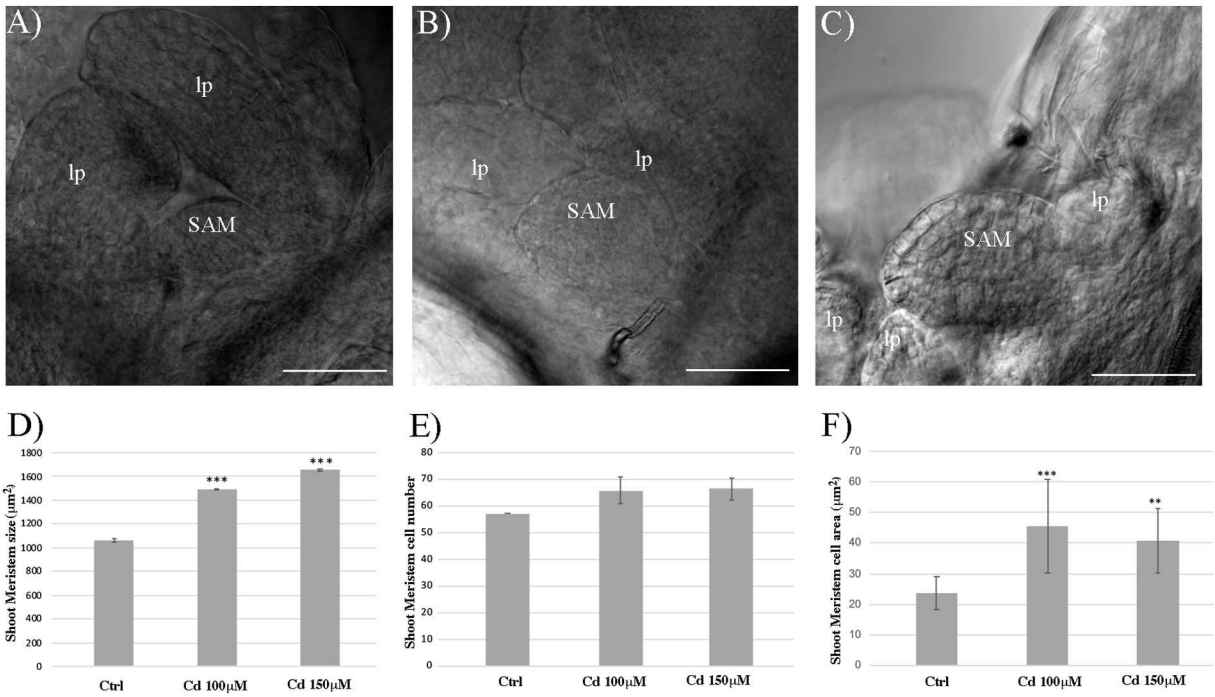

Fig. 1. Images of primary shoot apex of *A. thaliana* seedlings first cultivated on control medium for 5 days and then transferred to (A) on medium as control (Ctrl) and on medium added with (B) 100 and (C) 150 μM Cd exposed for 24 h. (D) Shoot meristem size (μm^2), (E) shoot meristem cell number, (F) shoot meristem cells area (μm^2). Data present the mean ± standard deviation (SD) of three independent experiments. Statistical analysis was performed by using Student's t-test and asterisks indicate significant pairwise differences (*P < 0.05; **P < 0.01; ***P < 0.001). SAM, shoot apex meristem; lp, leaf primordia. (A–C) scale bars 50 μm.

vertically in a growth chamber at 21 °C, under 16 h/8 h light/dark photoperiod (150 μmol m^{-2} s^{-1}) and 60% of relative humidity.

After germination, *Arabidopsis* seedlings (5 days old) were transferred for 24 h on the previously described agar control medium (Ctrl) enriched with concentrations of Cd ($CdCl_2$) 100 μM, or 150 μM.

The two different Cd concentrations and the time exposition were selected according to Yuan and Huang (2016). In particular, these two different concentrations inhibited the growth of primary root elongation and induced morphological modifications to the entire plant without killing it.

Three independent replicates were performed for each treatment, and a minimum of 70 seedlings per treatment and replicate were analyzed.

2.2. Shoot and root apical meristem size

Concerning the root meristem size, treated and untreated seedlings were stained with propidium iodide following the MPS-PI-staining protocol (Truernit et al., 2008).

The root meristem size was quantified as described in Bruno et al. (2017); in addition, the area of RAM meristematic cell area, root and stele amplitude, were all quantified. Image analysis was carried out using the software IMAGE J (www.imagej.net).

Concerning SAM analysis, before the observations shoot meristems were cleared in chloral hydrate solution (4 g chloral hydrate, 1 ml glycerol and 2 ml water) (Musielak et al., 2016). Succesively, shoot meristems were observed and analyzed to evaluate meristem size, number and area of its cells.

SAM and RAM observations were carried out using a DIC optic on a Leica inverted TCS SP8 confocal scanning laser microscope with a 40X oil immersion objective.

2.3. Confocal visualization and quantification of GFP expression

Green fluorescent protein expression was monitored in seedlings of the *A. thaliana* transgenic lines grown on control agar plates in a vertical position for 5 DAG, then transferred on medium containing Cd (100 μM and 150 μM) for 24 h.

Confocal images of median longitudinal sections were obtained using a Leica inverted TCS SP8 confocal scanning laser microscope, and excitation and emission wavelength were 488 and 509 nm, respectively (Bruno et al., 2017).

GFP signal intensity measurements were carried out on the shoot and root apex of transgenic lines *pWOX5::GFP*, *pWUS::GFP*, *pCLV3::GFP*, *CYCB1;1::GFP*, *TCSn::GFP*, in seedlings grown in Ctrl conditions and under both Cd treatment (100–150 μM). Measurements were performed in SAM and RAM with Leica Application Suite X software (LAS X). Three independent replicates were performed, and a minimum of 40 seedlings was analyzed for each sample.

2.4. Cell cycle progression by using cyclin B1;1::GFP transgenic line

In the shoot apex of transgenic line *CYCLIN B1;1::GFP*, the total number of cells in the G2-M phase of the cell cycle were counted. The cell division rate index was calculated from the data based on the formulas proposed by Burbano et al. (2011).

2.5. Statistical analysis

The experiments were settled in a completely randomized design with 3 replications. Data were first checked for deviations from normality (D'Agostino-Pearson test), tested for homogeneity (Leven Median test), and then the significance of differences between datasets was evaluated using the Student's test ($P \leq 0.05$). Results were then presented as mean value (±standard deviation). Asterisks indicate significant pairwise differences using Student's t-test (*P < 0.05; **P < 0.01; ***P < 0.001).

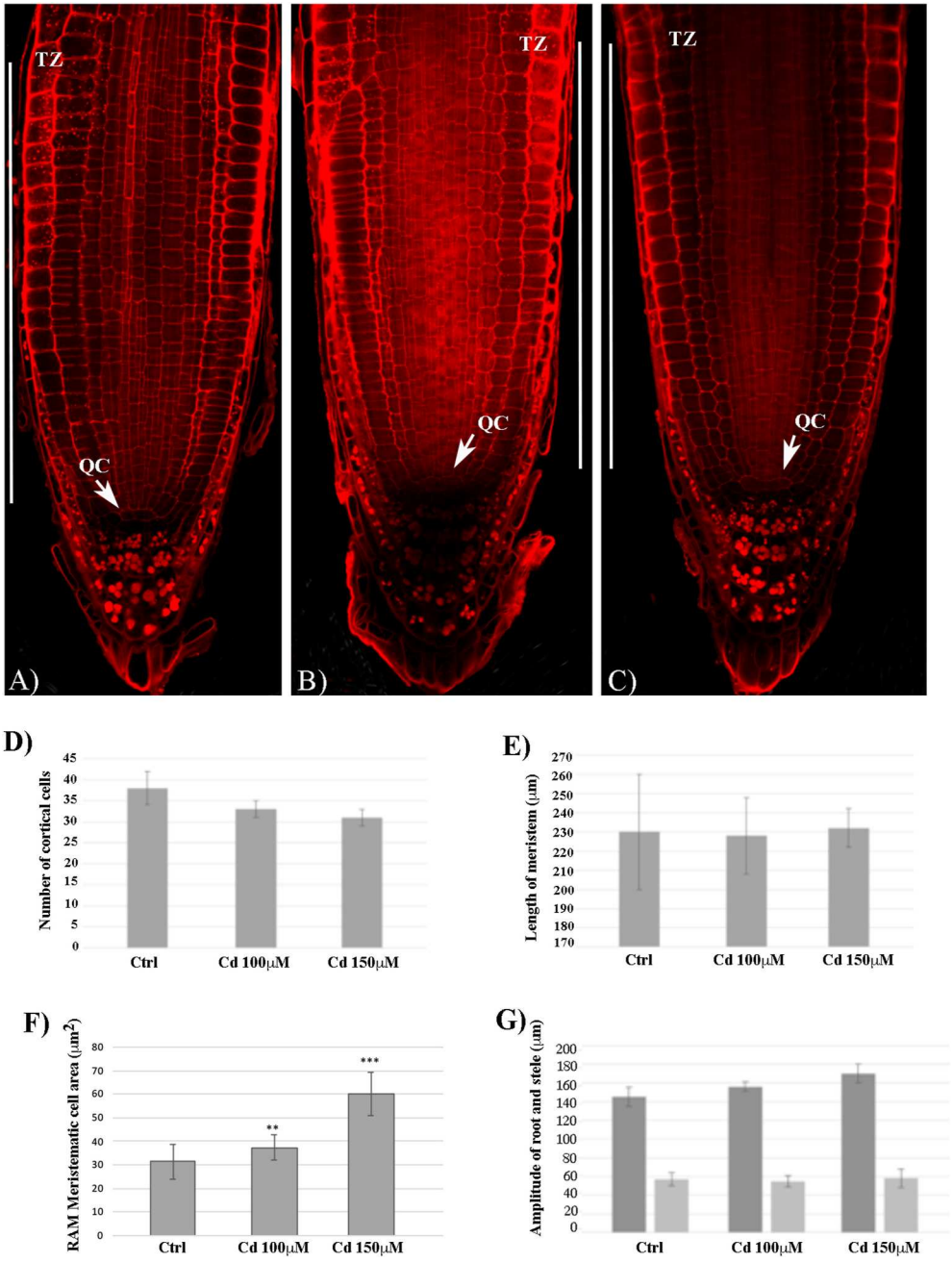

Fig. 2. Confocal laser images of primary root tip of *A. thaliana* seedlings first cultivated on control medium for 5 days and then transferred to (A) medium as control (Ctrl) and on medium added with (B) 100 and (C) 150 μM Cd exposed for 24 h. (D) Cortical cells number, (E) meristem length (μm), (F) RAM Meristematic cell area (μm^2), (G) root and stele amplitude (μm). Data present the mean ± standard deviation (SD) of three independent experiments. Statistical analysis was performed by using Student's t-test and asterisks indicate significant pairwise differences (*P < 0.05; **P < 0.01; ***P < 0.001). QC, quiescent center; TZ, transition zone. (A–C) scale bars 15 μm.

3. Results

3.1. Cadmium increases shoot apical meristem by increasing cell size

It has been reported that Cd is a widespread phytotoxic heavy metal that inhibits plant growth and development. To further explore how Cd stress modulates the shoot and root apical meristems, 5-day-old *Arabidopsis* seedlings were exposed to $CdCl_2$ 100 μM and 150 μM for 24 h.

To quantify the effects of these perturbations, we measured overall SAM size, the area of the single cells of cells on median sections (Fig. 1). The obtained results highlighted a significant increase (60%) of SAM size in seedlings exposed to cadmium than the Ctrl ones (Fig. 1A,B,C,D).

To identify the reason for the SAM enlargement after Cd exposition, we counted the cells number of the overall SAM in the Ctrl and 100–150 Cd treatments (Fig. 1A,B,C,E).

Concerning the parameter "cell number", no statistical differences were observed among control and Cd treatments (Fig. 1A,B,C,E).

Using the mitotic *CYCLIN B1;1::GFP* as a marker to visualize cells in the G2-M phase of the cell cycle, we tested whether the SAM enlargement in meristem size was caused by a higher division rate of meristematic cells (Supplemnetary Fig. 1A,A',B,B',C,C'). The marker genes expression domains were quantified by automated image analysis of individual SAM sections from Ctrl and Cd treatment (see Methods for details). Notably, the percentage of GFP marker cells in the SAM of Cd treated *CYCLIN B1;1::GFP* were similar to those of untreated seedlings (Supplemnetary Fig. 1D), implying that changes in the division potential of meristematic cells do not cause the increase of SAM size upon exposure to Cd.

Finally, we focused our attention on the area of the single cells in the SAM cells. In particular, after Cd treatment, an increment of this parameter was observed, suggesting that Cd exposition increases the SAM size by inducing an increase in single-cell area (Fig. 1F).

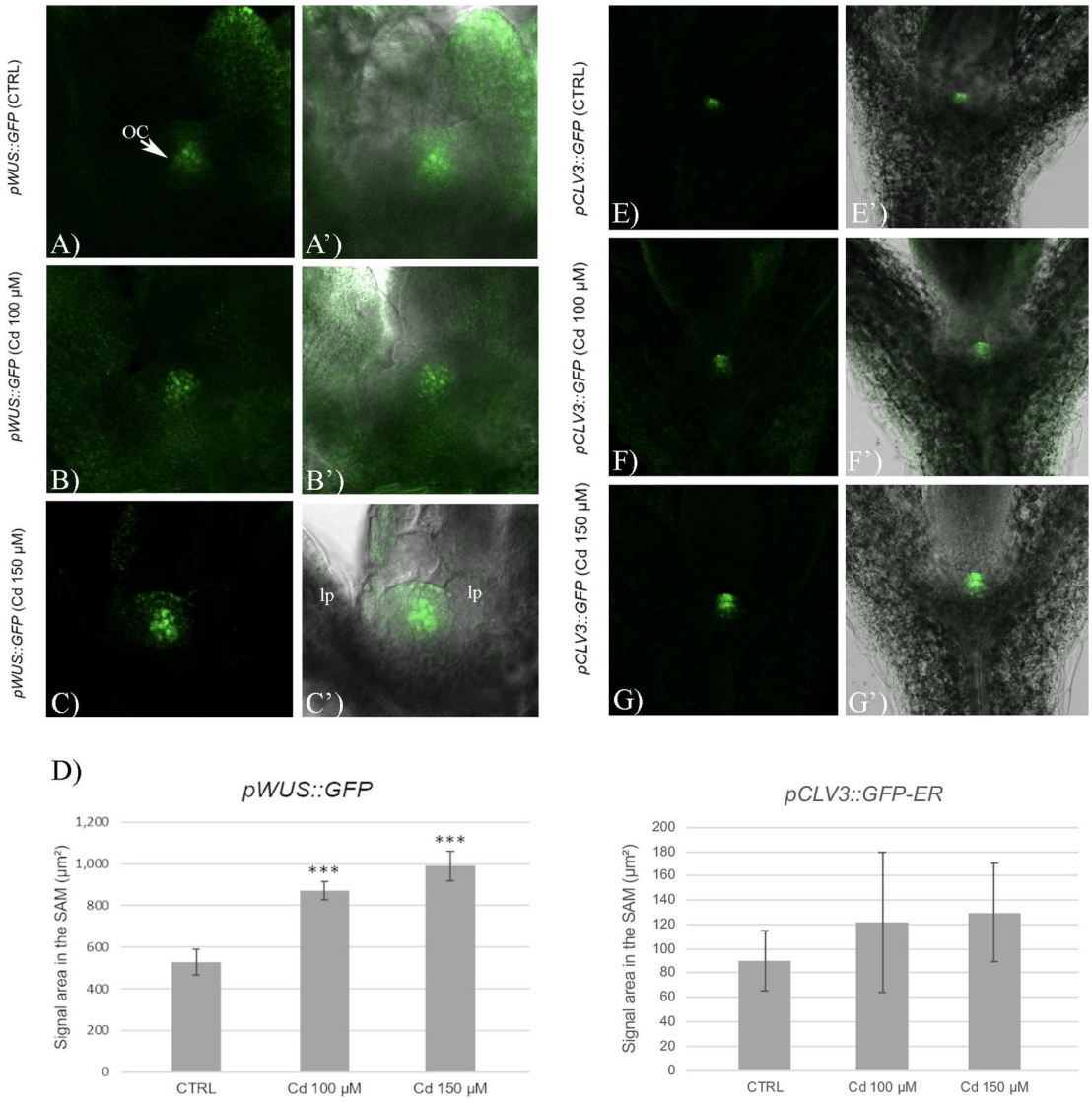

Fig. 3. Confocal laser images of shoot apex of *A. thaliana pWUS::GFP* and *pCLV3::GFP* transgenic lines first cultivated on control medium for 5 days and then transferred to (A,A′,E,E′) on control medium (Ctrl) and on medium added with (B,B'F,F′) 100 µM and (C,C′,G,G′) 150 µM Cd exposed for 24 h (A,B,C,E,F,G): confocal laser image; (A′,B′,C′,E′,F′,G′): merged image. (D) *pWUS::GFP* and (H) *pCLV3::GFP* relative signal area (μm^2). The results represent the mean value (±standard deviation) of three independent biological replicates. Asterisks indicate significant pairwise differences using Student's t-test (*P < 0.05; **P < 0.01; ***P < 0.001). OC, organizing centre; lp, leaf primordia. (A–C'; E–G′) scale bars 75 µm.

3.2. Cadmium increases the radial pattern of the primary root and the cortical cell area in the RAM

Our previous work demonstrated that the impact on root growth induced by long exposition to Cd is dose- and time-dependent, and its main effects are attributable to the effects induced on RAM stem cell niche (Bruno et al., 2017).

Based on these results, we evaluated root meristem organization after a short Cd exposition (24 h) (Fig. 2A,B,C). Concerning RAM length, we observed that the distance from QC to TZ was comparable in treated *vs.* Ctrl roots (Fig. 2E). However, at the Cd concentration (100 µM and 150 µM), the number of precortex cells was faintly reduced in Cd-exposed *vs.* Ctrl roots (Fig. 2D). In line with this result, meristematic cells area was larger in Cd-treated root tips (100 µM and 150 µM) than in Ctrl (Fig. 2F).

Concerning the radial pattern, root width was considered and evaluated as the cross diameter at TZ level. The results pointed out that the both Cd concentration didn't induce significant differences in root width compared to control (Fig. 2G).

3.3. Cd impact on WUSCHEL/CLAVATA 3 expression pattern

Considering the above results, we planned to investigate the effects of Cd on the WUS/CLV3 expression pattern in the SAM by using *pWUS::GFP* and *pCLV3::GFP-ER* transgenic lines exposed for 24 h to Cd (100 µM and 150 µM) (Fig. 3).

Concerning *WUS* expression in Ctrl shoots (Fig. 3A,A′), GFP signal resulted in being typically confined to the OC cells (layer L3) as already reported (Müller et al., 2006; Yadav et al., 2011), while in 100 µM and 150 µM Cd-exposed seedlings, we observed an enlarged signal around OC (Fig. 3B,B′,C,C′,D) and an ectopic expression in layer L1 (Fig. 3C,C′). Moreover, an interesting ectopic *pWUS::GFP* pattern was observed in the treatments 150 µM. In particular, the 5% of the seedling exposed to Cd exhibited a GFP localization in the two OC of the SAM (Fig. 4A,A').

It is well known that CLAVATA 3 (CLV3) expression in cellular layers L1, L2, and L3 (Fig. 3E,E′) rules expression pattern of WUS around only layer L3 (Müller et al., 2006). Under Cd treatment, we observed a slight increase of GFP signal compared to Ctrl (Fig. 3F,F',G,G',H).

The experimental results provided evidence of dynamic regulation of

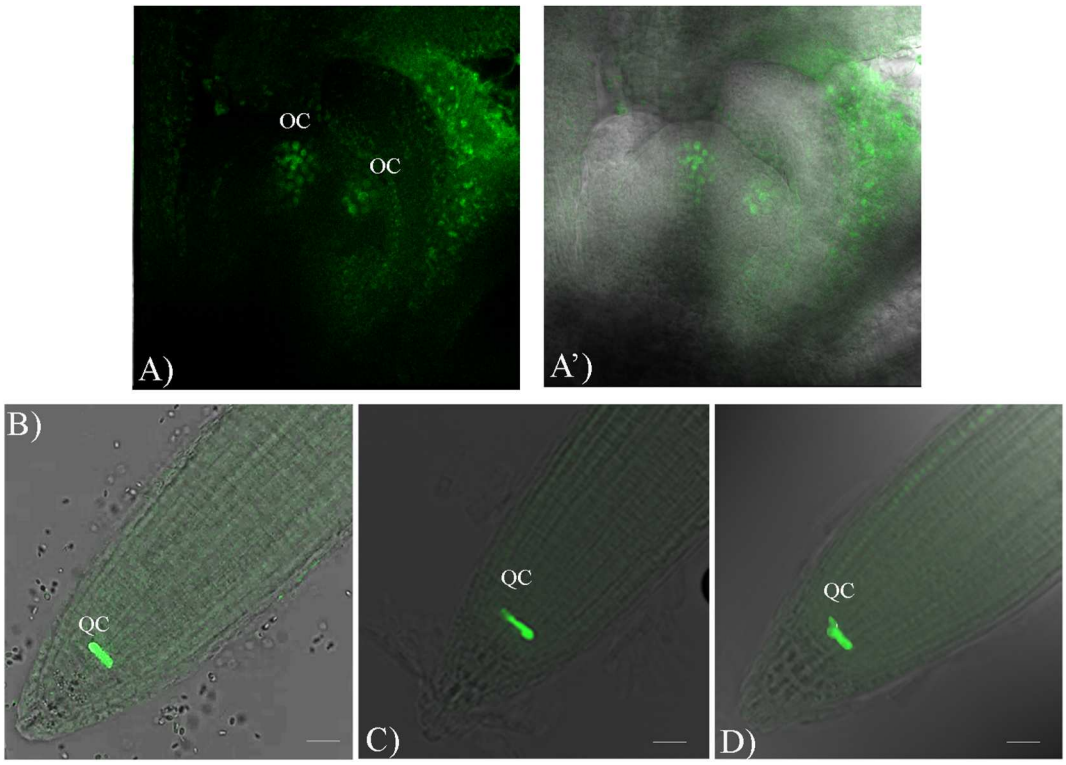

Fig. 4. Confocal laser image of shoot apex (A,A′) and primary root tip (B–D) of *A. thaliana*. (A,A′) *pWUS::GFP* transgenic line first cultivated on control medium for 5 days and then exposed to medium added with (A-A′) 150 μM Cd for 24 h. (A): confocal laser image (A′); merged. (B–D) Primary root tip of *A. thaliana* seedlings *pWOX5::GFP* transgenic line first cultivated on control medium for 5 days and then transferred to (B) on control medium (Ctrl) on medium added with (C) 100 μM and (D) 150 μM Cd exposed for 24 h. QC, quiescent center; OC, organizing centre. Scale bars 75 μm.

meristem domains, which is correlated with modulation in cell behaviour. Over the growth conditions examined, meristem size and the dimensions of the WUS domain were correlated with misexpression of WUS/CLV3.

3.4. Cd impact on WOX expression pattern in root

Concerning the RAM, attention was then paid to the QC. In particular, we used a *pWOX5::GFP* transgenic line of *A. thaliana* expressing a QC specific marker (Blilou et al., 2005), and we exposed the roots to Cd (100 μM and 150 μM) for 24 h. According to the literature, a canonical QC formed by 4 cells was detected in the untreated roots (Fig. 4B), while in the Cd-treated roots, we observed an ectopic signal of WOX5 (Fig. 4C and D). It is well known that the differentiation fate of the cells surrounding the QC is highly dependent on the QC itself (Van den Berg et al., 1997; Bitonti et al., 2006). Consistently, in Cd-treated roots, we observed a reduction of statolith accumulation (Fig. 2B and C). These results align with our previous work (Bruno et al., 2017) and confirm that short Cd exposition impacts QC cells and affects root growth.

3.5. Cd impact on SAM's and RAM's cytokinins signaling

It is well documented that plant development is largely controlled by interactions between auxin and cytokinins (Schaller et al., 2015). These interactions are of particular importance during the development of SAM and RAM.

In this context, due to cytokinins effect on the maintenance of totipotent status on meristematic cells, we analyzed some aspects of the cytokinins signalling pathway using the *TCSn::GFP* transgenic line of *A. thaliana* carrying a specific synthetic sensor (Fig. 5). GFP signal intensity was measured at the level of SAM (Fig. 5D) and RAM (Fig. 5H) on seedlings exposed to Cd, 100 μM and 150 μM for 24 h.

Concerning the SAM, GFP signal increased significantly in the seedlings exposed to Cd 100 μM reaching the highest signal intensity at Cd 150 μM (Fig. 5B,B′,C,C′). At histological level, in treated seedlings, the GFP signal was more intense in the provascular strand and in the SAM compared to control (Fig. 5C,C').

The obtained results suggest that in root the GFP signal is higher in treated than in control seedlings (Fig. 5H) and at the histological level the signal was present in the root cup (Fig. 5E,E′,F,F′,G,G′) and increased in root exposed at Cd 150 μM, mainly in the stele (Fig. 5G,G').

Globally the obtained results indicated that in treated seedlings, Cd treatment increased the GFP signal of *TCSn::GFP* sensor in SAM and RAM, suggesting an increase in CKs content.

4. Discussion

In the present work, using different marker lines of *Arabidopsis thaliana,* we reported for the first time the effects of short-lasting Cadmium treatment on SAM's and RAM's SNC, allowing us to elucidate the molecular mechanism underlying the concomitantly Cd-induced shoot and root inhibition.

As established in previous studies, plant growth is dependent on SAM and RAM maintenance, which is assured by a balance between the production of new meristematic cells and their displacement toward the differentiation (Beemster and Baskin, 1998; Ivanov, 2004; Reddy et al., 2004; Reddy and Meyerowitz, 2005).

SAM homeostasis appears to be a conserved mechanism in diverse monocot and dicot species. It is well known that in addition to the internal signal, several environmental cues affect the SAM homeostasis through hormone signalling and CLV/WUS loop.

Our results pointed out that 24 h Cd treatment (150 μM) induced an increase in the expression of WUS/CLV genes in transgenic lines and, consequently, an increase in SAM size. According to these results, Landrein et al. (2018) showed that the generation of active CKs in the SAM induced WUS expression during stem cell proliferation and

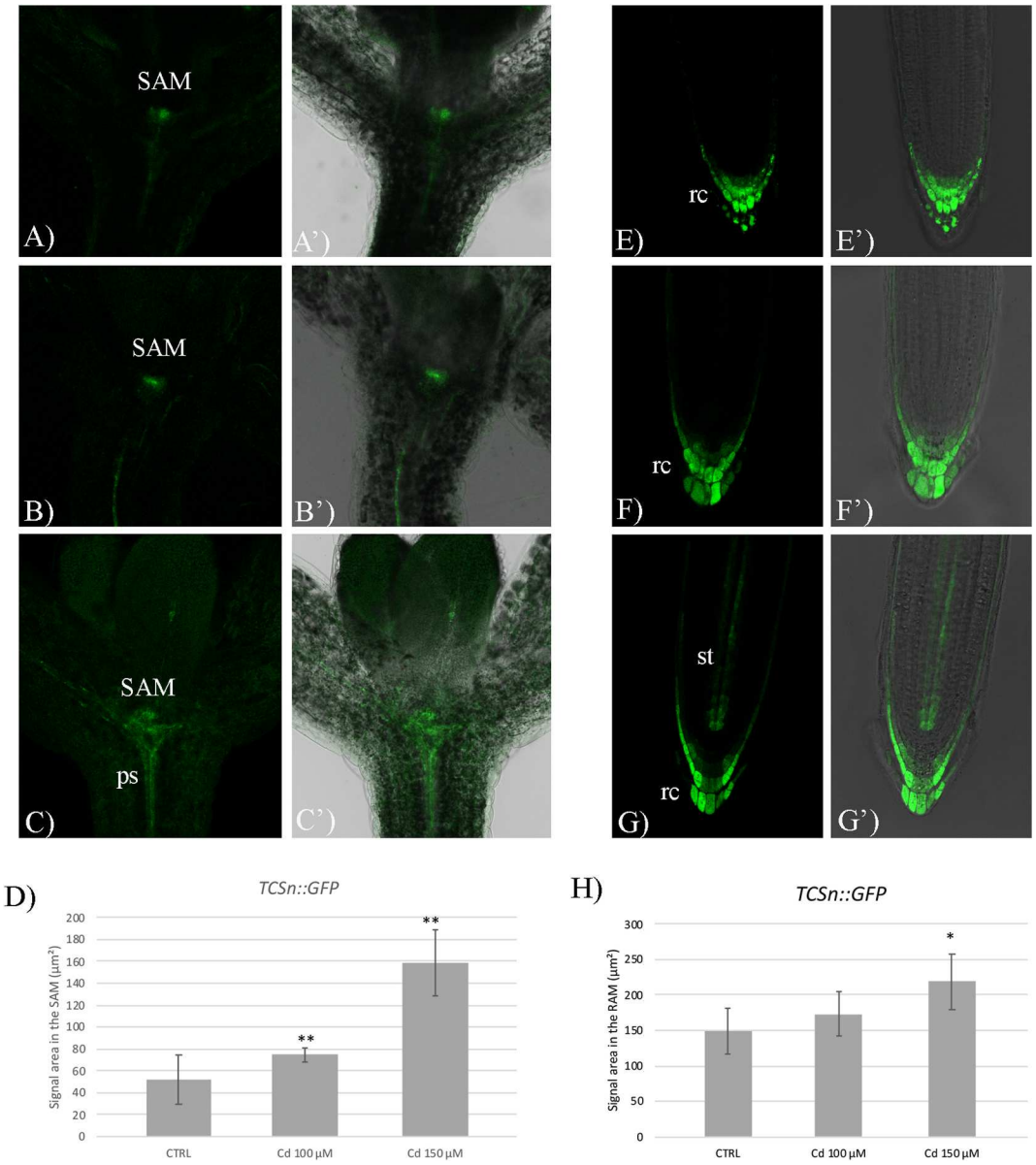

Fig. 5. Expression of TCSn cytokinin synthetic sensor in the shoot and root apex of seedlings of *A. thaliana*. *TCSn::GFP* transgenic line first cultivated on control medium for 5 days and then transferred to (A,A′,E,E′) on growth medium as control (Ctrl), on medium added with (B,B'F,F′) 100 µM and (C,C'G,G′) 150 µM Cd exposed for 24 h. (A-C, E-G) confocal laser image; (A′-C′, E′-G′) merged. *TCSn::GFP* relative signal area (µm^2), normalized to Ctrl (D) SAM and in (H) RAM. The results represent the mean value (±standard deviation) of three independent biological replicates. Asterisks indicate significant pairwise differences using Student's t-test (*P < 0.05; **P < 0.01; ***P < 0.001). SAM, shoot apical meristem; ps, procambium strand; st, stele; rc, root cup. (A–C'; E–G′) scale bars 75 µm.

increased meristem size and organ production rate. In addition, we observed an enhancement of cytokinins signalling in both shoot and root apex, which was consistent with the results reported by Sofo et al. (2013) for *Arabidopsis* Cd-treated plants, and with Piotrowska-Niczyporuk et al. (2012), which demonstrated that during Cd-induced stress, CKs are activated to reverse heavy metal-induced toxicity. More recently, we demonstrated that an epigenetic mutant of *Arabidopsis*, defective on both maintenance and *de novo* methylation (*ddc*), impacts CKs both at the transcriptomic and biochemical level downregulating cytokinin-oxidase expression after a prolonged exposure to this heavy-metal and within a specific threshold concentration (Pacenza et al., 2021).

Contrasting results have been reported in the literature about Cd treatment in *Arabidopsis* causing a downregulation of several G1/S marker genes such as *HISTONE H4* and *E2Fa* and G2/M marker genes, including *CYCB1;1* and *CYCB1;2* (Huybrechts et al., 2019).

However, based on our results, we support the hypothesis that an increase of CKs signal and the WUS/CLV pathway contribute to widening the SAM (increasing cells area) without interfering with the cell cycle progression.

Furthermore, it has been reported that short exposition to Cd treatment is insufficient to interfere with cell cycle progression. These results are in accordance with Yuan and Huang (2016), which demonstrated that Cd strongly inhibits primary root elongation, accelerating the root meristem elongation–differentiation rate of its cells without interfering with the cell cycle progression, since the percentages of GUS-stained cells in the root meristems of Cd-treated *CYCB1;1:GUS* were similar to those of untreated seedlings.

Also, the light is known to modulate the SAM activity by auxin and CKs and together with metabolic signals contributed to modulate WUS expression. In addition, the WUS expression at least partly, dependent on the activity of two CKs degrading enzymes from the CYTOKININ

OXIDASE (CKX) family. In this scenario, since the root is the first organ that makes contact with Cd in soil, we supposed that Cd's perception in the root leads to the over-production of CKs and their translocation to the shoot via xylem. Our results are in line with this hypothesis since, in Cd-treated seedlings, an increase of CKs signal is visible in the root stele and procambium strand of the SAM.

Interestingly, the widening of the SAM, observed in seedlings exposed to Cd treatment, overlap with the anatomical alterations observed in the *clv* mutants and the Clavata3 insensitive receptor kinase (*cik*), which are both characterized by alteration in stem cell activity.

Accordingly, in the present work, for the first time, we showed that WUS signal is detected one cell layer up and largely expanded in seedlings exposed to Cd compared to Ctrl. Besides, the Cd treatment induced in the SAM the formation of a new OC in which WUS was also detectable.

These results are in line with previous findings reporting that the *cik* mutant exhibited a significant enlarged SAM since the CIKs functions as co-receptor of CLV1, CLV2/CRN to mediate CLV3 signalling through phosphorylation.

Concomitantly, the CLV3 signal appeared to be increased under Cd exposition, suggesting that Cd could be impacted in the CLV pathway, inducing the loss of the restrict the stem cell domain in the SAM (Sánchez-Calderón et al., 2005).

Concerning roots, in a previous study we demonstrated that seedlings exposed to long-lasting Cd treatments were characterized by primary root growth inhibition mediated by the loss of RAM stem cell niche identity and root radial pattern alterations mediated by auxin-cytokinin crosstalk.

As reported in the results, the short-lasting Cd exposition significantly impacted the cortical cell area and the root meristem's radial pattern. In particular, Cd treatments induced an alteration of root meristem organization at the root apical level, which was characterized by a reduction in precortical cells number and by an increase in their size, suggesting an advancement of transition and differentiation zones and a consequent reduction of root growth, a phenomenon already observed in *Arabidopsis* roots treated with heavy metals and natural products (Araniti et al., 2017; Bruno et al., 2017).

In this context, it must be recalled that root patterning depends on the activity of the stem cell niches; we demonstrated that WOX5, a specific marker of the QC in the RAM, exhibited an ectopic expression. This result is in line with previous data, showing that in *A. thaliana* roots, a short Cd exposure (12 h) and long-lasting exposure, at comparable concentrations, caused a reduction of RAM size and an ectopic expression of WOX5 (Besson-Bard et al., 2009; Hu et al., 2013; Yuan and Huang, 2016; Bruno et al., 2017).

Similarly, both in the As hyperacumulator *Pteris vittate* and in *Vigna unguiculata*, the metalloid inhibits the proximal meristem by altering the root meristem via a loss of function of the stem cell niche and the QC (Forino et al., 2012; Kopittke et al., 2012). In addition, Fattorini et al. (2017) showed that in *Arabidopsis,* post-embryonic roots treated with Cd and Cd plus arsenic negatively affected QC identity and auxin localization.

As homolog of WUS, WOX5 is specifically expressed in the QC of the root and it is essential for stem cell maintenance in the RAM via a negative feedback signal provided by CLE40, which can reduce WOX5 expression (Zhang and Yu, 2014). WOX5 acts from the QC to maintain the distal stem cell population, and its function can replace WUS. Similarly, CLE40 can replace CLV3 if expressed in the shoot stem cell domain. Together, these results suggest that pathways controlling stem cells in shoot and root are at least partially conserved at the molecular level. A negative feedback loop between CLE40 and WOX5 and positive self-regulation of WOX5 likely occurs via the auxin signalling pathway.

Our results support the idea that Cd impacts the SNC of both SAM and RAM through similar mechanisms at the molecular level and it is possible that the plant, at least within defined limits of toxicity, quickly respond to Cd toxicity adjusting their architecture.

5. Conclusion

This study provides evidence that Cd-induced toxicity on the shoot and root growth is strongly dependent by the alterations induced on the SAM and RAM stem cell niche. For the first time we demonstrated that Cd-induced misexpression of both WUS/WOX5 related genes and in the cytokinins signalling, which play a pivotal role in the regulatory network underlying SAM and RAM maintenance and activity.

Altogether, the results answer the gap information, showing that the OC and QC, and consequently the primary meristem of *Arabidopsis* post-embryonic shoot and root, are the target of Cd. The Cd toxicity impacts cytokinin accumulation possibly leading to a different crosstalk with other hormones/stress-agents. This could justify the similar response observed on the two post-embryonic SNC shoot and root apical meristems.

Funding

This work was founded by grants from University of Calabria (MIUR – ex 60%).

Declaration of competing interest

The authors declare that they have no known competing financial interests or personal relationships that could have appeared to influence the work reported in this paper.

Acknowledgements

The confocal scanning laser microscope for this research were supplied by PON Ricerca e Competitività 2007–2013, Sistema Integrato di Laboratori per L'Ambiente – (SILA) PONa3_00341, CM2–Centro di Microscopia e Microanalisi.

Appendix A. Supplementary data

Supplementary data to this article can be found online at https://doi.org/10.1016/j.plaphy.2021.09.014.

Authors contribution

LB, AC, MBB, Planned the experiments. LB, ET, MML, MM, AM, performed the experiments. LB, AC, FA, MBB Analyzed the data and wrote the manuscript. All authors contributed to improve the paper and approved the final manuscript.

References

Aida, M., Beis, D., Heidstra, R., Willemsen, V., Blilou, I., Galinha, C., Nussaume, L., Noh, Y.S., Amasino, R., Scheres, B., 2004. The PLETHORA genes mediate patterning of the *Arabidopsis* root stem cell niche. Cell 119 (1), 109–120. https://doi.org/10.1016/j.cell.2004.09.018.

Araniti, F., Bruno, L., Sunseri, F., Pacenza, M., Forgione, I., Bitonti, M.B., Abenavoli, M. R., 2017. The allelochemical farnesene affects *Arabidopsis thaliana* root meristem altering auxin distribution. Plant Physiol. Biochem. 121, 14–20. https://doi.org/10.1016/j.plaphy.2017.10.005.

Beemster, G.T., Baskin, T.I., 1998. Analysis of cell division and elongation underlying the developmental acceleration of root growth in *Arabidopsis thaliana*. Plant Physiol. 116 (4), 1515–1526. https://doi.org/10.1104/pp.116.4.1515.

Berleth, T., Jurgens, G., 1993. The role of the monopteros gene in organising the basal body region of the *Arabidopsis* embryo. Development 118 (2), 575–587. https://doi.org/10.1242/dev.118.2.575.

Besson-Bard, A., Gravot, A., Richaud, P., Auroy, P., Duc, C., Gaymard, F., Taconnat, L., Renou, J.P., Pugin, A., Wendehenne, D., 2009. Nitric oxide contributes to cadmium toxicity in *Arabidopsis* by promoting cadmium accumulation in roots and by up-regulating genes related to iron uptake. Plant Physiol. 149 (3), 1302–1315. https://doi.org/10.1104/pp.108.133348.

Bitonti, M.B., Mazzuca, S., Ting, T., Innocenti, A.M., 2006. Magnetic field affects meristem activity and cell differentiation in *Zea* roots. Plant Biosyst. 140 (1), 87–93. https://doi.org/10.1080/11263500500511314.

Blilou, I., Xu, J., Wildwater, M., Qillemsen, V., Paponov, I., Friml, J., Heidstra, R., Aida, M., Palme, K., Scheres, B., 2005. The PIN auxin efflux facilitator network controls growth and patterning in *Arabidopsis* roots. Nature 433 (7021), 39–44. https://doi.org/10.1038/nature03184.

Brand, U., Fletcher, J.C., Hobe, M., Meyerowitz, E.M., Simon, R., 2000. Dependence of stem cell fate in *Arabidopsis* a feedback loop regulated by CLV3 activity. Science 289 (5479), 617–619. https://doi.org/10.1126/science.289.5479.617.

Bruno, L., Pacenza, M., Forgione, I., Lamerton, L.R., Greco, M., Chiappetta, A., Bitonti, M. B., 2017. In *Arabidopsis thaliana* cadmium impact on the growth of primary root by altering SCR expression and auxin-cytokinin cross-talk. Front. Plant Sci. 8, 1323. https://doi.org/10.3389/fpls.2017.01323.

Burbano, L., Fernandez, E., Cortes, E., 2011. Determination of time Mitotic of *Guadua angustifolia* var. *grandicaula* (family: gramineae) from roots meristem. Revista de investigaciones-universidad del quindio 22, 129–135.

Dehghan Nayeri, F., 2014. Identification of transcription factors linked to cell cycle regulation in *Arabidopsis*. Plant Signal. Behav. 9 (11), e972864 https://doi.org/10.4161/15592316.2014.972864.

Dello Ioio, R., Linhares, F.S., Scacchi, E., Casamitjana-Martinez, E., Heidstra, R., Costantino, P., Sabatini, S., 2007. Cytokinins determine *Arabidopsis* root-meristem size by controlling cell differentiation. Curr. Biol. 17 (8), 678–682. https://doi.org/10.1016/j.cub.2007.02.047.

Dello Ioio, R., Nakamura, K., Moubayidin, L., Perilli, S., Taniguchi, M., Morita, M.T., Aoyama, T., Costantino, P., Sabatini, S., 2008. A genetic framework for the control of cell division and differentiation in the root meristem. Science 322 (5906), 1380–1384. https://doi.org/10.1126/science.1164147.

Dolan, L., Janmaat, K., Willemsen, V., Linstead, P., Poethig, S., Roberts, K., Scheres, B., 1993. Cellular organisation of the *Arabidopsis thaliana* root. Development 119 (1), 71–84. https://doi.org/10.1242/dev.119.1.71.

Fattorini, L., Ronzan, M., Piacentini, D., Della Rovere, F., De Virgilio, C., Sofo, A., Altamura, M.M., Falasca, G., 2017. Cadmium and arsenic affect quiescent centre formation and maintenance in *Arabidopsis thaliana* post-embryonic roots disrupting auxin biosynthesis and transport. Environ. Exp. Bot. 144, 37–48. https://doi.org/10.1016/j.envexpbot.2017.10.005.

Forgione, I., Wołoszyńska, M., Pacenza, M., Chiappetta, A., Greco, M., Araniti, F., Abenavoli, M.R., Van Lijsebettens, M., Bitonti, M.B., Bruno, L., 2019. Hypomethylated drm1 drm2 cmt3 mutant phenotype of *Arabidopsis thaliana* is related to auxin pathway impairment. Plant Sci. 280, 383–396. https://doi.org/10.1016/j.plantsci.2018.12.029.

Forino, L.M.C., Castiglione, M.R., Bartoli, G., Balestri, M., Andreucci, A., Tagliasacchi, A. M., 2012. Arsenic-induced morphogenic response in roots of arsenic hyperaccumulator fern *Pteris vittata*. J. Hazard Mater. 235, 271–278. https://doi.org/10.1016/j.jhazmat.2012.07.051.

Galinha, C., Hofhuis, H., Luijten, M., Willemsen, V., Blilou, I., Heidstra, R., Scheress, B., 2007. PLETHORA proteins as dose-dependent master regulators of *Arabidopsis* root development. Nature 449 (7165), 1053–1057. https://doi.org/10.1038/nature06206.

Gallego, S.M., Pena, L.B., Barcia, R.A., Azpilicueta, C.E., Iannone, M.F., Rosales, E.P., Zawoznik, M.S., Groppa, M.D., Benavides, M.P., 2012. Unravelling cadmium toxicity and tolerance in plants: insight into regulatory mechanisms. Environ. Exp. Bot. 83, 33–46. https://doi.org/10.1016/j.envexpbot.2012.04.006.

Greco, M., Chiappetta, A., Bruno, L., Bitonti, M.B., 2012. In *Posidonia oceanica* cadmium induces changes in DNA methylation and chromatin patterning. J. Exp. Bot. 63 (2), 695–709. https://doi.org/10.1093/jxb/err313.

Groß-Hardt, R., Laux, T., 2003. Stem cell regulation in the shoot meristem. J. Cell Sci. 116 (9) https://doi.org/10.1242/jcs.00406, 1659-166.

Haider, F.U., Liqun, C., Coulter, J.A., Cheema, S.A., Wu, J., Zhang, R., Wenjun, M., Farooq, M., 2021. Cadmium toxicity in plants: impacts and remediation strategies. Ecotoxicol. Environ. Saf. 211, 111887 https://doi.org/10.1016/j.ecoenv.2020.111887.

Hardtke, C.S., Berleth, T., 1998. The *Arabidopsis* gene MONOPTEROS encodes a transcription factor mediating embryo axis formation and vascular development. EMBO J. 17 (5), 1405–1411. https://doi.org/10.1093/emboj/17.5.1405.

Heidstra, R., Sabatini, S., 2014. Plant and animal stem cells: similar yet different. Nat. Rev. Mol. Cell Biol. 15 (5), 301–312. https://doi.org/10.1038/nrm3790.

Herbette, S., Taconnat, L., Hugouvieux, V., Piette, L., Magniette, M.L., Cuine, S., Auroy, P., Richaud, P., Forestier, C., Bourguignon, J., Renou, J.-P., Vavasseur, A., Leonhardt, N., 2006. Genome-wide transcriptome profiling of the early cadmium response of *Arabidopsis* roots and shoots. Biochimie 88 (11), 1751–1765. https://doi.org/10.1016/j.biochi.2006.04.018.

Heyman, J., Cools, T., Vandenbussche, F., Heyndrickx, K.S., Van Leene, J., Vercauteren, I., Vanderauwera, S., Vandepoele, K., De Jaeger, G., Van Der Straeten, D., De Veylder, L., 2013. ERF115 controls root quiescent center cell division and stem cell replenishment. Science 342 (6160), 860–863. https://doi.org/10.1126/science.1240667.

Hu, Y.F., Zhou, G., Na, X.F., Yang, L., Nan, W.B., Liu, X., Zhang, Y.Q., Li, J.L., Bi, Y.R., 2013. Cadmium interferes with maintenance of auxin homeostasis in *Arabidopsis* seedlings. J. Plant Physiol. 170 (11), 965–975. https://doi.org/10.1016/j.jplph.2013.02.008.

Huybrechts, M., Cuypers, A., Deckers, J., Iven, V., Vandionant, S., Jozefczak, M., Hendrix, S., 2019. Cadmium and plant development: an agony from seed to seed. Int. J. Mol. Sci. 20 (16), 3971. https://doi.org/10.3390/ijms20163971.

Ivanov, V.B., 2004. Relationship between cell proliferation and transition to elongation in plant roots. Int. J. Dev. Biol. 41 (6), 907–915.

Jin, Y.H., Clark, A.B., Slebos, R.J., Al-Refai, H., Taylor, J.A., Kunkel, T.A., Resnick, M.A., Gordenin, D.A., 2003. Cadmium is a mutagen that acts by inhibiting mismatch repair. Nat. Genet. 34 (3), 326–329. https://doi.org/10.1038/ng1172.

Jönsson, H., Heisler, M., Reddy, G.V., Agrawal, V., Gor, V., Shapiro, B.E., Mjolsness, E., Meyerowitz, E.M., 2005. Modeling the organization of the WUSCHEL expression domain in the shoot apical meristem. Bioinformatics 21 (Suppl. l_1), i232–i240. https://doi.org/10.1093/bioinformatics/bti1036.

Keunen, E., Truyens, S., Bruckers, L., Remans, T., Vangronsveld, J., Cuypers, A., 2011. Survival of Cd-exposed *Arabidopsis thaliana*: are these plants reproductively challenged? Plant Physiol. Biochem. 49 (10), 1084–1091. https://doi.org/10.1016/j.plaphy.2011.07.013.

Kirch, T., Simon, R., Grünewald, M., Werr, W., 2003. The DORNROSCHEN/ENHANCER OF SHOOT REGENERATION1 gene of *Arabidopsis* acts in the control of meristem ccll fate and lateral organ development. Plant Cell 15 (3), 694–705. https://doi.org/10.1105/tpc.009480.

Kopittke, P.M., de Jonge, M.D., Menzies, N.W., Wang, P., Donner, E., McKenna, B.A., Paterson, D., Howard, D.L., Lombi, E., 2012. Examination of the distribution of arsenic in hydrated and fresh cowpea roots using two-and three-dimensional techniques. Plant Physiol. 159 (3), 1149–1158. https://doi.org/10.1104/pp.112.197277.

Landrein, B., Formosa-Jordan, P., Malivert, A., Schuster, C., Melnyk, C.W., Yang, W., Turnbull, C., Meyerowitz, E.M., Locke, J.C.W., Jonsson, H., 2018. Nitrate modulates stem cell dynamics in *Arabidopsis* shoot meristems through cytokinins. Proc. Natl. Acad. Sci. U.S.A. 115 (6), 1382–1387. https://doi.org/10.1073/pnas.1718670115.

Laux, T., Mayer, K.F., Berger, J., Jürgens, G., 1996. The WUSCHEL gene is required for shoot and floral meristem integrity in *Arabidopsis*. Development 122 (1), 87–96. https://doi.org/10.1242/dev.122.1.87.

Liu, Y.T., Chen, Z.S., Hong, C.Y., 2011. Cadmium-induced physiological response and antioxidant enzyme changes in the novel cadmium accumulator, *Tagetes patula*. J. Hazard Mater. 189 (3), 724–731. https://doi.org/10.1016/j.jhazmat.2011.03.032.

Luo, L., Zeng, J., Wu, H., Tian, Z., Zhao, Z., 2018. A molecular framework for auxin-controlled homeostasis of shoot stem cells in *Arabidopsis*. Mol. Plant 11 (7), 899–913. https://doi.org/10.1016/j.molp.2018.04.006.

Maistri, S., DalCorso, G., Vicentini, V., Furini, A., 2011. Cadmium affects the expression of ELF4, a circadian clock gene in *Arabidopsis*. Environ. Exp. Bot. 72 (2), 115–122. https://doi.org/10.1016/j.envexpbot.2011.02.010.

Mayer, K.H., Schoof, H., Haecker, A., Lenhard, M., Jurgens, G., Laux, T., 1998. Role of WUSCHEL in regulating stem cell fate in the *Arabidopsis* shoot meristem. Cell 95 (6), 805–815. https://doi.org/10.1016/s0092-8674(00)81703-1.

Medford, J.I., Behringer, F.J., Callos, J.D., Feldmann, K.A.F., 1992. Normal and abnormal development in the *Arabidopsis* vegetative shoot apex. Plant Cell 4 (6), 631–643. https://doi.org/10.1105/tpc.4.6.631.

Moreno-Romero, J., Carme Espunya, M., Platara, M., Ariño, J., Carmen Martínez, M.A., 2008. Role for protein kinase CK2 in plant development: evidence obtained using a dominant-negative mutant. Plant J. 55 (1), 118–130. https://doi.org/10.1111/j.1365-313X.2008.03494.x.

Müller, R., Borghi, L., Kwiatkowska, D., Laufs, P., Simon, R., 2006. Dynamic and compensatory responses of *Arabidopsis* shoot and floral meristems to CLV3 signaling. Plant Cell 18 (5), 1188–1198. https://doi.org/10.1105/tpc.105.040444.

Musielak, T.J., Slane, D., Liebig, C., Bayer, M., 2016. A versatile optical clearing protocol for deep tissue imaging of fluorescent proteins in *Arabidopsis thaliana*. PloS One 11 (8), e0161107. https://doi.org/10.1371/journal.pone.0161107.

Nawy, T., Lee, J.Y., Colinas, J., Wang, J.Y., Thongrod, S.C., Malamy, J.E., Birnbaum, K., Benfey, P.N., 2005. Transcriptional profile of the *Arabidopsis* root quiescent center. Plant Cell 17 (7), 1908–1925. https://doi.org/10.1105/tpc.105.031724.

Pacenza, M., Muto, A., Chiappetta, A., Mariotti, L., Talarico, E., Picciarelli, P., Picardi, E., Bruno, L., Bitonti, M.B., 2021. In *Arabidopsis thaliana* Cd differentially impacts on hormone genetic pathways in the methylation defective ddc mutant compared to wild type. Sci. Rep. 11 (1), 1–17. https://doi.org/10.1038/s41598-021-90528-5.

Perilli, S., Sabatini, S., 2010. Analysis of root meristem size development. Methods Mol. Biol. 655, 177–187. https://doi.org/10.1007/978-1-60761-765-5_12.

Perilli, S., Di Mambro, R., Sabatini, S., 2012. Growth and development of the root apical meristem. Curr. Opin. Plant Biol. 15 (1), 17–23. https://doi.org/10.1016/j.pbi.2011.10.006.

Perilli, S., Moubayidin, L., Sabatini, S., 2010. The molecular basis of cytokinin function. Curr. Opin. Plant Biol. 13 (1), 21–26. https://doi.org/10.1016/j.pbi.2009.09.018.

Perrot-Rechenmann, C., 2010. Cellular responses to auxin: division versus expansion. Cold Spring Harbor Perspect. Biol. 2 (5), a001446. https://doi.org/10.1101/cshperspect.a001446.

Piotrowska-Niczyporuk, A., Bajguz, A., Zambrzycka, E., Godlewska-Żyłkiewicz, B., 2012. Phytohormones as regulators of heavy metal biosorption and toxicity in green alga *Chlorella vulgaris* (Chlorophyceae). Plant Physiol. Biochem. 52, 52–65. https://doi.org/10.1016/j.plaphy.2011.11.009.

Reddy, G.V., Meyerowitz, E.M., 2005. Stem-cell homeostasis and growth dynamics can be uncoupled in the *Arabidopsis* shoot apex. Science 310 (5748), 663–667. https://doi.org/10.1126/science.1116261.

Reddy, G.V., Heisler, M.G., Ehrhardt, D.W., Meyerowitz, E.M., 2004. Real-time lineage analysis reveals oriented cell divisions associated with morphogenesis at the shoot apex of *Arabidopsis thaliana*. Development 131 (17), 4225–4237. https://doi.org/10.1242/dev.01261.

Reinhardt, D., Pesce, E.R., Stieger, P., Mandel, T., Baltensperger, K., Bennett, M., Traas, J., Friml, J., Kuhlemeier, C., 2003. Regulation of phyllotaxis by polar auxin transport. Nature 426 (6964), 255–260. https://doi.org/10.1038/nature02081.

Riou-Khamlichi, C., Huntley, R., Jacqmard, A., Murray, J.A., 1999. Cytokinin activation of *Arabidopsis* cell division through a D-type cyclin. Science 283 (5407), 1541–1544. https://doi.org/10.1126/science.283.5407.1541.

Růžička, K., Šimášková, M., Duclercq, J., Petrášek, J., Zažímalová, E., Simon, S., Friml, J., Van Montagu, M.C., Benková, E., 2009. Cytokinin regulates root meristem activity

via modulation of the polar auxin transport. Proc. Natl. Acad. Sci. U.S.A. 106 (11), 4284–4289. https://doi.org/10.1073/pnas.0900060106.

Sánchez-Calderón, L., López-Bucio, J., Chacón-López, A., Cruz-Ramírez, A., Nieto-Jacobo, F., Dubrovsky, J.G., Herrera-Estrella, L., 2005. Phosphate starvation induces a determinate developmental program in the roots of *Arabidopsis thaliana*. Plant Cell Physiol. 46 (1), 174–184. https://doi.org/10.1093/pcp/pci011.

Sanmartín, M., Sauer, M., Muñoz, A., Zouhar, J., Ordóñez, A., van de Ven, W.T., Caro, E., de la Paz Sánchez, M., Raikhel, N.V., Gutiérrez, C., Sánchez-Serrano, J.J., Rojo, E., 2011. A molecular switch for initiating cell differentiation in *Arabidopsis*. Curr. Biol. 21 (12), 999–1008. https://doi.org/10.1016/j.cub.2011.04.041.

Sarkar, A.K., Luijten, M., Miyashima, S., Lenhard, M., Hashimoto, T., Nakajima, K., Scheres, B., Heidstra, R., Laux, T., 2007. Conserved factors regulate signalling in *Arabidopsis thaliana* shoot and root stem cell organizers. Nature 446 (7137), 811–814. https://doi.org/10.1038/nature05703.

Schaller, G.E., Bishopp, A., Kieber, J.J., 2015. The yin-yang of hormones: cytokinin and auxin interactions in plant development. Plant Cell 27 (1), 44–63. https://doi.org/10.1105/tpc.114.133595.

Scheres, B., Wolkenfelt, H., Willemsen, V., Terlouw, M., Lawson, E., Dean, C., Weisbeek, P., 1994. Embryonic origin of the *Arabidopsis* primary root and root meristem initials. Development 120 (9), 2475–2487.

Schoof, H., Lenhard, M., Haecker, A., Mayer, K.F.X., Jürgens, G., Laux, T., 2000. The stem cell population of *Arabidopsis* shoot meristems is maintained by a regulatory loop between the CLAVATA and WUSCHEL genes. Cell 100 (6), 635–644. https://doi.org/10.1016/s0092-8674(00)80700-x.

Sofo, A., Vitti, A., Nuzzaci, M., Tataranni, G., Scopa, A., Vangronsveld, J., Remans, T., Falasca, G., Altamura, M.M., Degola, F., Sanità di Toppi, L., 2013. Correlation between hormonal homeostasis and morphogenic responses in *Arabidopsis thaliana* seedlings growing in a Cd/Cu/Zn multi- pollution context. Physiol. Plantarum 149 (4), 487–498. https://doi.org/10.1111/ppl.12050.

Song, Y., Jin, L., Wang, X., 2017. Cadmium absorption and transportation pathways in plants. Int. J. Phytoremediation 19 (2), 133–141. https://doi.org/10.1080/15226514.2016.1207598.

Steeves, T.A., Sussex, I.M., 1989. Patterns in Plant Development, second ed. Cambridge University Press, Cambridge. https://doi.org/10.1017/CBO9780511626227.

To, J.P., Haberer, G., Ferreira, F.J., Deruere, J., Mason, M.G., Schaller, G.E., Alonso, J.M., Ecker, J.R., Kieber, J.J., 2004. Type-A *Arabidopsis* response regulators are partially redundant negative regulators of cytokinin signaling. Plant Cell 16 (3), 658–671. https://doi.org/10.1105/tpc.018978.

Truernit, E., Bauby, H., Dubreucq, B., Grandjean, O., Runions, J., Barthélémy, J., Palauqui, J.C., 2008. High-resolution whole-mount imaging of three-dimensional tissue organization and gene expression enables the study of phloem development and structure in *Arabidopsis*. Plant Cell 20 (6), 1494–1503. https://doi.org/10.1105/tpc.107.056069.

Van den Berg, C., Willemsen, V., Hendriks, G., Weisbeek, P., Scheres, B., 1997. Short-range control of cell differentiation in the *Arabidopsis* root meristem. Nature 390 (6657), 287–289. https://doi.org/10.1038/36856.

Van Lijsebettens, M., Van Montagu, M., 2005. Historical perspectives on plant developmental biology. Int. J. Dev. Biol. 49 (5–6), 453–465. https://doi.org/10.1387/ijdb.041927ml.

Xu, J., Yin, H., Liu, X., Li, X., 2010. Salt affects plant Cd-stress responses by modulating growth and Cd accumulation. Planta 231 (2), 449–459. https://doi.org/10.1007/s00425-009-1070-8.

Yadav, R.K., Perales, M., Gruel, J., Girke, T., Jönsson, H., Reddy, G.V., 2011. WUSCHEL protein movement mediates stem cell homeostasis in the *Arabidopsis* shoot apex. Genes Dev. 25 (19), 2025–2030. https://doi.org/10.1101/gad.17258511.

Yuan, H.M., Huang, X., 2016. Inhibition of root meristem growth by cadmium involves nitric oxide-mediated repression of auxin accumulation and signalling in *Arabidopsis*. Plant Cell Environ. 39 (1), 120–135. https://doi.org/10.1111/pce.12597.

Zhang, H., Han, W., De Smet, I., Talboys, P., Loya, R., Hassan, A., Rong, H., Jürgens, G., Paul Knox, J., Wang, M.H., 2010. ABA promotes quiescence of the quiescent centre and suppresses stem cell differentiation in the *Arabidopsis* primary root meristem. Plant J. 64 (5), 764–774. https://doi.org/10.1111/j.1365-313X.2010.04367.x.

Zhang, W., Yu, R., 2014. Molecule mechanism of stem cells in *Arabidopsis thaliana*. Phcog. Rev. 8 (16), 105–112. https://doi.org/10.4103/0973-7847.134243.

Zhang, W., Swarup, R., Bennett, M., Schaller, G.E., Kieber, J.J., 2013. Cytokinin induces cell division in the quiescent center of the *Arabidopsis* root apical meristem. Curr. Biol. 23 (20), 1979–1989. https://doi.org/10.1016/j.cub.2013.08.008.

Zürcher, E., Tavor-Deslex, D., Lituiev, D., Enkerli, K., Tarr, P.T., Müller, B., 2013. A robust and sensitive synthetic sensor to monitor the transcriptional output of the cytokinin signaling network in planta. Plant Physiol. 161 (3), 1066–1075. https://doi.org/10.1104/pp.112.211763.

scientific reports

Check for updates

OPEN

In *Arabidopsis thaliana* Cd differentially impacts on hormone genetic pathways in the methylation defective *ddc* mutant compared to wild type

Marianna Pacenza[1], Antonella Muto[1], Adriana Chiappetta[1], Lorenzo Mariotti[2], Emanuela Talarico[1], Piero Picciarelli[2], Ernesto Picardi[3], Leonardo Bruno[1]✉ & Maria Beatrice Bitonti[1]

DNA methylation plays an important role in modulating plant growth plasticity in response to stress, but mechanisms involved in such control need further investigation. We used *drm1 drm2 cmt3* mutant of *Arabidopsis thaliana*, defective in DNA methylation, to explore metabolic pathways downstream epigenetic modulation under cadmium (Cd) stress. To this aim, a transcriptomic analysis was performed on *ddc* and WT plants exposed to a long-lasting (21 d) Cd treatment (25/50 µM), focusing on hormone genetic pathways. Growth parameters and hormones amount were also estimated. Transcriptomic data and hormone quantification showed that, under prolonged Cd treatment, level and signalling of growth-sustaining hormones (auxins, CKs, GAs) were enhanced and/or maintained, while a decrease was detected for stress-related hormones (JA, ABA, SA), likely as a strategy to avoid the side effects of their long-lasting activation. Such picture was more effective in *ddc* than WT, already at 25 µM Cd, in line with its better growth performance. A tight relationship between methylation status and the modulation of hormone genetic pathways under Cd stress was assessed. We propose that the higher genome plasticity conferred to *ddc* by DNA hypomethylated status underlies its prompt response to modulate hormones genetic pathways and activity and assure a flexible growth.

Plants, as sessile organisms, are under constant influence of environment, which modulates their growth and development through a multiplicity of signals. Therefore, plants evolved molecular mechanisms to sense and rapidly adapt to the wide range of environmental changes occurring at diurnal, seasonal and stochastic level, thus exhibiting high growth plasticity[1].

A role in such plasticity is paid by epigenetic mechanisms, including DNA methylation, which act on the chromatin status allowing a simultaneous and wide regulation of gene expression. Indeed, studies on both the model *Arabidopsis thaliana* and fruit crops demonstrated that methylome dynamic, beside playing a role at evolution level, is involved in the control of plant ontogenesis and modulate plant response to external cues, including multiple stresses[2]. In particular, either hypermethylation or hypomethylation were detected in plants under different stressors[3]. However, despite all this information, many aspects of the mechanisms that translate the information superimposed by DNA methylation into downstream regulation of gene expression remain still unclear.

A suitable tool to investigate these aspects is provided by *Arabidopsis thaliana* methylation-defective mutants, many of which exhibit phenotype pleiotropic alterations[4,5]. In plants, DNA cytosine methylation occurs in all sequence context and is driven by three enzyme families: the METHYLTRANSFERASES (MET), acting in maintaining methylation in the symmetric CG context, the DOMAINS REARRANGED METHYLTRANSFERASES

[1]Department of Biology, Ecology and Earth Science, University of Calabria, Arcavacata di Rende, CS, Italy. [2]Department of Agriculture, Food and Environment, University of Pisa, Pisa, PI, Italy. [3]Department of Biosciences, Biotechnology and Biopharmaceutics, University of Bari, Bari, BA, Italy. ✉email: leonardo.bruno@unical.it

(DRMs), acting as de novo methyltransferases in the asymmetric CHH context (H = A, C or T) and the plant specific CHROMOMETHYLASES (CMTs), acting primarily in the maintenance of CHG symmetric and CHH asymmetric methylation, but also playing a role in de novo DNA methylation[5,6]. DNA glycosylases contribute to the overall methylome pattern by removing methylated cytosines[5]. In this work, we used the triple *Arabidopsis thaliana drm1 drm2 cmt3* (*ddc*) mutant, combining mutations on *DRM1, DRM2*, and *CMT3* genes, defective in both maintenance and de novo DNA methylation[7]. The aim was to investigate molecular and cellular mechanisms that are modulated by DNA methylation in response to stressful factors, such as heavy metal presence.

Heavy metals are naturally present in soils and some of them are required at trace quantities as essential elements. However, at high levels they affect cell homeostasis and are harmful for all organisms[8]. In our study we selected Cd, one of the most harmful and not essential heavy metals, as a stressor due to its ubiquitous presence, long incubation period, ability to migrate and strong ecotoxicity[8]. Moreover, Cd in the soil is easily adsorbed by plants and at high concentration inhibits their growth and development by impacting on several metabolic processes through a wide range of structural and molecular changes, including epigenetic modifications[9].

On this basis, *Arabidopsis ddc* mutant and wild type (WT) lines were exposed, from germination to 21 d after germination (DAG), to 25 and 50 µM Cd concentrations, whose growth inhibitory effect was previously documented in WT[10]. Plant growth parameters were monitored, and a transcriptome approach was applied to compare how genetic networks and related pathways were affected by Cd in *ddc* mutant compared to WT. The obtained results clearly showed that methylation status is involved in modulating plant response to Cd stress.

Results

Plant growth. Primary root length and rosette size were estimated. Control root length, measured until 21 DAG, was lightly minor in *ddc vs* WT (Fig. 1A). Cd differentially inhibited root growth in the two samples: at 21 DAG, 25 and 50 µM Cd-treated roots were 1.2 and 2.2 fold shorter than control roots in *ddc,* while in the WT Cd-treated roots were 1.8 and 2.8 fold shorter than control ones (Fig. 1A). Consequently, at 21 DAG root of Cd-treated samples was longer in *ddc vs* WT, particularly at the lowest Cd concentration.

Rosette size was estimated at 21 DAG, corresponding to the period necessary for its full development[11], by evaluating leaf number and area. Control plants of both *ddc* and WT exhibited a complete leaf series, although most leaves resulted smaller in *ddc* (Fig. 1B,C). Cd affected rosette development reducing leaf number and area, less in *ddc* than WT, resulting into a higher leaf area and/or number in *ddc* under both Cd concentrations (Fig. 1B,C).

Gene expression profile. RNA-Seq analysis provided an overview of gene expression profile of Cd-treated and control plants of both *ddc* and WT. The following comparisons were performed**:** *ddc vs* WT under control (Ctrl) conditions (*ddc vs* WT-Ctrl) and 25 and 50 µM Cd treatment (*ddc vs* WT-25 µM Cd; *ddc vs* WT-50 µM Cd); 25/50 µM Cd-treated *vs* Ctrl in *ddc* (25 µM Cd *vs* Ctrl-*ddc*; 50 µM Cd *vs* Ctrl-*ddc*); 25/50 µM Cd-treated *vs* Ctrl in the WT (25 µM Cd *vs* Ctrl-WT; 50 µM Cd *vs* Ctrl-WT).

After DEGs identification (see Supplementary Fig. S1 online) 14 of them were analysed through qRT-PCR to validate transcriptomic analysis (see Supplementary Fig. S2 online). Results were fully consistent with RNA-seq data. Gene Enrichment analysis was also performed, evidencing that Cd strongly impacted on transcriptome in both *ddc* and WT, but in a largely different way (see Supplementary Figs. S3–S9 online). Notwithstanding, a common aspect was that in both *ddc* and WT the genetic pathways (GPs) more impacted by Cd dealt with photosynthesis, stress responses and hormone biosynthesis and signalling.

Expression pattern of genetic pathways related to hormones. In view of hormones pivotal role in plant development and stress response and considering the assessed epigenetic control on their action and signalling[12], in this work we analysed in depth how the expression pattern (EP) of hormone-related GPs was modulated in *ddc vs* WT under Cd stress. The most relevant differences are discussed.

Auxins. Under control conditions, GPs related to auxin biosynthesis showed comparable EP in *ddc* and WT and no DEGs were detected (Fig. 2A). 25 µM Cd induced significant changes only in *ddc* resulting into: i) *TAA1* and *YUC5* downregulation along indole-3-pyruvic acid (IPA) pathway; ii) *CYP71A13* and *NIT2* overexpression along indole-3-acetaldoxime (IAOX) auxiliary pathway, while *CYP79B3* was downexpressed (Fig. 2A). Differently, 50 µM Cd induced similar changes in *ddc* and WT consisting in: (i) a downexpression of *YUC2* along IPA pathway in both samples and *YUC5* and *YUC9* in *ddc* and WT, respectively; (ii) overexpression of *CYP71A12, CYP71A13, NIT2*, *NIT4* and downexpression of *CYP71A16* along IAOX pathway in *ddc* and WT (Fig. 2A).

Auxin level and homeostasis also depend on its oxidative degradation, conjugation and methylation[13]. Under control conditions, GPs related to auxin conjugation and methylation showed comparable EPs in *ddc* and WT and no DEGs were detected (Fig. 2B,C)**,** but were differentially impacted by Cd, mainly at 25 µM concentration. Namely, at 25 µM Cd several genes related to auxin conjugation (*GH3.3, GH3.17, YDK1*) and methylation (*MES7, MES17*) were downregulated in *ddc*, whereas in WT only *MES18,* involved in methyl-indole-3-acetate production, was downregulated (Fig. 2B,C). At 25 µM Cd most of the above genes were downregulated in *ddc vs* WT (Fig. 2B,C), while at 50 µM Cd only two genes, working in auxin methylation were differentially modulated in *ddc* and WT (Fig. 2B,C).

Under control conditions, GP related to auxin signalling exhibited similar EP in *ddc* and WT (Fig. 2D). Differences were induced by Cd. Namely, at 25 µM Cd, *AUX/IAA* family genes, which acts in signalling repression, were globally downregulated in *ddc,* while in WT the repressor *IAA34* was overexpressed (Fig. 2D). Differently, 50 µM Cd effects on *ddc* and WT were quite similar, dealing with *AUX/IAA* family genes downregulation (Fig. 2D). In *ddc vs* WT comparisons, at 25 µM Cd above genes were downregulated, while no differences were found at 50

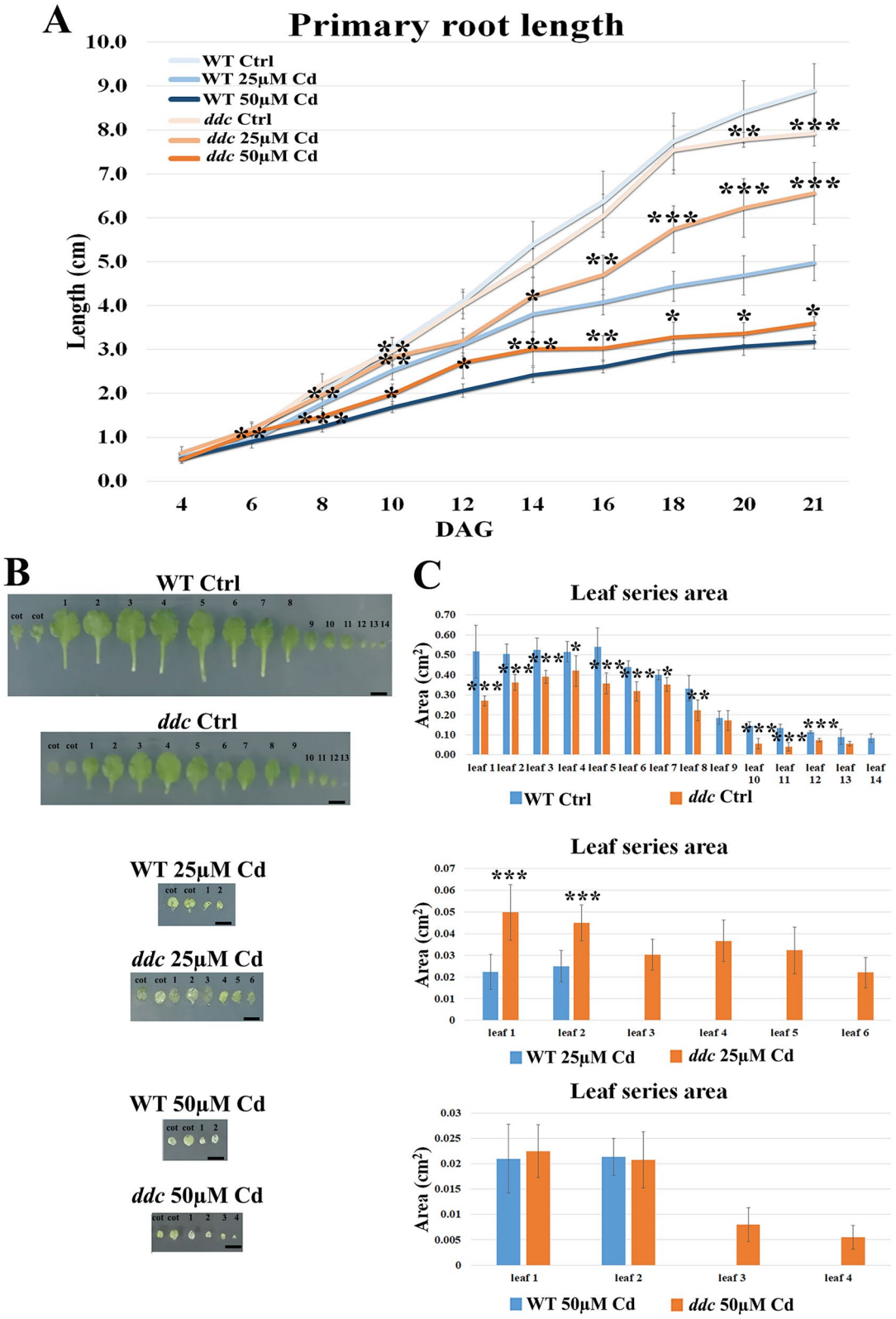

Figure 1. (**A**) Primary root length (**B**) Picture of rosette leaf series and (**C**) rosette leaf area (cm^2) of WT and *ddc* plants of *A. thaliana*, germinated and grown for 21 DAG in long day condition: (i) on growth medium added with 25 or 50 µM Cd; (ii) on growth medium without Cd as control (Ctrl). Root length was monitored up to 21 days after germination (DAG) every two days from germination. The results represent the mean value (± SD) of three independent biological replicates (n = 45). Asterisks indicate significant pairwise differences using Student's *t*-test *(*P ≤ 0.05; ** P ≤ 0.01; *** P ≤ 0.001)*, performed between *ddc vs* WT subjected to the same treatment. Bars, 0.5 cm.

A

IAA biosynthetic pathways

Gene	AGI	log$_2$ (Fold Change)						
		ddc vs WT - Ctrl	25 µM Cd *vs* Ctrl – *ddc*	25 µM Cd *vs* Ctrl – WT	*ddc vs* WT - 25 µM Cd	50 µM Cd *vs* Ctrl – *ddc*	50 µM Cd *vs* Ctrl – WT	*ddc vs* WT -50 µM Cd
CYP71A12	AT2G30750	-	-	-	-	2.929	3.037	-
CYP71A13	AT2G30770	-	2.617	-	-	4.520	4.322	-
CYP71A14	AT5G24960	-	-	-	-	-	-	-
CYP71A16	AT5G42590	-	-	-	-	-3.943	-4.295	-
CYP79B3	AT2G22330	-	-2.400	-	-	-	-	-
NIT2	AT3G44300	-	2.786	-	-	3.740	4.282	-
NIT4	AT5G22300	-	-	-	-	2.448	2.834	-
TAA1	AT1G70560	-	-2.697	-	-2.135	-	-	-
YUC2	AT4G13260	-	-	-	-	-2.900	-2.030	-
YUC5	AT5G43890	-	-4.381	-	-	-2.960	-	-
YUC9	AT1G04180	-	-	-	-	-	-3.030	-

B

Indole-3-acetyl-amino acid biosynthesis

Gene	AGI	log$_2$ (Fold Change)						
		ddc vs WT - Ctrl	25 µM Cd *vs* Ctrl – *ddc*	25 µM Cd *vs* Ctrl – WT	*ddc vs* WT - 25 µM Cd	50 µM Cd *vs* Ctrl – *ddc*	50 µM Cd *vs* Ctrl – WT	*ddc vs* WT -50 µM Cd
GH3.3	AT2G23170	-	-2.452	-	-2.753	-	-	-
GH3.17	AT1G28130	-	-2.365	-	-	-	-	-
YDK1	AT4G37390	-	-4.710	-	-2.995	-	-	-

C

Methyl-indole-3-acetate interconversion

Gene	AGI	log$_2$ (Fold Change)						
		ddc vs WT - Ctrl	25 µM Cd *vs* Ctrl – *ddc*	25 µM Cd *vs* Ctrl – WT	*ddc vs* WT - 25 µM Cd	50 µM Cd *vs* Ctrl – *ddc*	50 µM Cd *vs* Ctrl – WT	*ddc vs* WT -50 µM Cd
IAMT1	AT5G55250	-	-	-	-	-4.131	-2.920	-
MES7	AT2G23560	-	-2.245	-	-2.129	-	-	-
MES16	AT4G16690	-	2.164	-	-	2.207	2.123	-
MES17	AT3G10870	-	-3.367	-	-2.107	-	-	-
MES18	AT5G58310	-	-	-4.478	-	-	-	-

D

IAA signalling pathway

Gene	AGI	log$_2$ (Fold Change)						
		ddc vs WT - Ctrl	25 µM Cd *vs* Ctrl – *ddc*	25 µM Cd *vs* Ctrl – WT	*ddc vs* WT - 25 µM Cd	50 µM Cd *vs* Ctrl – *ddc*	50 µM Cd *vs* Ctrl – WT	*ddc vs* WT -50 µM Cd
AXR3	AT1G04250	-	-2.025	-	-	-	-2.010	-
IAA1	AT4G14560	-	-3.423	-	-4.774	-2.195	-	-
IAA3	AT1G04240	-	-	-	-2.863	-	-2.980	-
IAA5	AT1G15580	-	-	-	-	-4.808	-	-
IAA6	AT1G52830	-	-	-	-	-	-3.222	-
IAA14	AT4G14550	-	-	-	-4.359	-2.815	-	-
IAA19	AT3G15540	-	-	-	-	-3.913	-3.122	-
IAA27	AT4G29080	-	-3.612	-	-2.192	-2.558	-2.893	-
IAA30	AT3G62100	-	-	-	-	-3.513	-	-
IAA31	AT3G17600	-	-	-	-	-2.455	-	-
IAA34	AT1G15050	-	3.617	3.074	-	-	-	-
SAUR1	AT4G34770	-	-2.717	-	-3.146	-2.653	-	-
SAUR3	AT4G34790	-	-2.128	-	-3.175	-2.244	-	-
SAUR7	AT2G21200	-	-	-	-	-3.209	-	-
SAUR10	AT2G18010	3.407	-	3.439	-	-	-	-
SAUR12	AT2G21220	-	-	-	-	2.863	-	-
SAUR13	AT4G38825	-	-	-	-	-3.200	-3.111	-
SAUR14	AT4G38840	-	-	-	-	-2.077	-2.631	-
SAUR15	AT4G38850	-	-	-	-	-	-3.031	-
SAUR16	AT4G38860	-	-	-	-	-3.046	-3.364	-
SAUR20	AT5G18020	-	-4.208	-	-3.414	-	-	-
SAUR22	AT5G18050	-	-	-	-	-	-4.955	-
SAUR26	AT3G03850	-	-2.916	-	-2.393	-	-4.832	-
SAUR27	AT3G03840	-	-	-	-	-4.538	-4.157	-
SAUR28	AT3G03830	-	-2.736	-	-2.045	-4.253	-4.415	-
SAUR30	AT5G53590	-	-2.611	-	-2.079	-	-	-
SAUR33	AT3G61900	-2.983	-	-	-	3.897	-	-
SAUR36	AT2G45210	-	-	-	-	2.563	2.292	-
SAUR37	AT4G31320	-	-	-	-	-3.729	-3.331	-
SAUR40	AT1G79130	-	3.823	-	-	-	-	-
SAUR41	AT1G16510	-	-	-	-	2.196	-	-
SAUR48	AT3G09870	-	-	-	3.866	-	2.869	-
SAUR52	AT1G75590	-	-	-	-	-2.061	-	-
SAUR53	AT1G19840	-	-	-	-	-3.359	-	-
SAUR59	AT3G60690	-	2.498	-	-	2.690	-	-
SAUR71	AT1G56150	-	-	-	-	-	2.299	-
YKD1	AT4G37390	-	-4.710	-	-2.995	-	-	-

Figure 2. Genes differentially expressed (DEGs) along the pathway of (**A**) auxin biosynthesis, auxin conjugation, (**B**) indole-3-acetyl-amino acid biosynthesis, (**C**) methyl-indole-3-acetate interconversion and (**D**) auxin signalling in *ddc* and WT plants identified through a transcriptomic approach. For each comparison, the log$_2$(fold change) of the analysed DEGs was shown in orange and in blue for the upregulated and downregulated genes, respectively. Plants were grown for 21 DAG in long day condition: (i) on growth medium added with 25 or 50 µM Cd; (ii) on growth medium without Cd as control (Ctrl).

µM Cd (Fig. 2D). Moreover, and somehow unexpectedly, following 50 µM Cd it was observed in both *ddc* and WT a downregulation of several *SAUR*s members, belonging to a large family of auxin responsive genes, which in turn can also have an impact on auxin pathway[14] (Fig. 2D). Interestingly, such effect was more pronounced in *ddc* than WT. However, it must be mentioned that, although most of them are induced by auxin, several other hormones and co-factors acts upstream *SAUR* genes, regulating their activity in response to both endogenous stimuli and environmental cues[14].

In summary, in both *ddc* and WT, Cd induced: i) a downregulation of IPA pathway, which is the main auxin biosynthetic pathway[15] and a simultaneous upregulation of IAOX auxiliary biosynthetic pathway; ii) an enhancement of hormone signalling. However, in the WT such effects occurred only at 50 µM Cd. Moreover, in *ddc* Cd also induced a downregulation of GPs related to auxin conjugation.

Cytokinins. In all comparisons, GPs related to CKs biosynthesis showed similar EPs, unless for the downregulation in 50 µM Cd-treated WT *vs* Ctrl of *IPT5,* encoding rate-limiting enzyme along the pathway[16] (Fig. 3A).

Major differences were observed for GPs related to CKs catabolism and conjugation, occurring through cleavage by oxidation and glycosylation, respectively[16]. Under control conditions, these GPs also exhibited similar EPs in *ddc* and WT (Fig. 3B-D). At both 25 and 50 µM Cd a downregulation of *CKX5* and *CKX6,* encoding cytokinin-oxidases, occurred only in *ddc* (Fig. 3B). Differently, Cd impact on GPs related to CKs *N*-glycosylation was almost comparable in *ddc* and WT, resulting into the overexpression of two different genes working in N^7- and N^9-glycosylation pathways at 25 µM Cd, and one gene at the higher concentration (Fig. 3C).

Note that at 25 µM Cd the above genes were both overexpressed in *ddc vs* WT, while no differences were found at 50 µM Cd (Fig. 3C). Cd impact on GP related to cytokinin *O*-glycosylation was major, especially in *ddc*, involving at 25 µM Cd the overexpression of seven genes along this pathway compared to Ctrl (Fig. 3D), and one gene in WT 25 µM Cd *vs* Ctrl (Fig. 3D). By contrast, at 50 µM Cd the expression pattern along this pathway was similar in *ddc* and WT, being characterised by the upregulation of the same seven genes above mentioned and the downregulation of *AT5G38010* (Fig. 3D). Finally, at 25 µM Cd, five genes along these pathways resulted upregulated in *ddc vs* WT while a similar EP occurred in *ddc* and WT under 50 µM Cd treatment (Fig. 3D).

Concerning GP involved in CKs signalling, under control conditions *A-ARRs*, encoding negative regulators of CKs signalling[17], were downregulated and signalling was likely enhanced in *ddc vs* WT (Fig. 3E). 25 µM Cd induced a downregulation of *ARR11 A-type ARRs* and *B-ARR* family *ARR10* transcription factors, which control primary plant response to CKs, only in *ddc* (Fig. 3E). Whereas, at 50 µM Cd both *ddc* and WT showed *A-ARR* downregulation, supposedly leading to pathway upregulation (Fig. 3E). At 25 µM Cd *AHP1,* encoding positive regulators of CKs signalling[18], was downregulated in *ddc vs* WT, while *ARR17* was overexpressed, suggesting that signalling was downregulated also in *ddc vs* WT (Fig. 3E). No differences occurred between *ddc* and WT at 50 µM Cd (Fig. 3E).

In summary, transcriptomic analysis evidenced that GP related to the biosynthesis of *trans*-zeatin, the most relevant CK, was negatively affected by Cd only in the WT at 50 µM Cd. In response to Cd, GPs related to CKs inactivation were enhanced in both *ddc* and WT, but in *ddc* a downregulation of GP related to CKs cleavage also occurred. Finally, hormone signalling was differentially modulated by Cd in relation to both the sample (*ddc vs* WT) and heavy metal concentration, resulting into a downregulation at 25 µM Cd only in *ddc* and an enhancement in *ddc* and WT at 50 µM Cd.

Gibberellins. Under control conditions, GPs related GAs biosynthesis showed similar EPs in *ddc vs* WT (Fig. 4A). 25 µM Cd induced in *ddc*: i) a downregulation of *GA2* encoding the *ent*-kaurene synthase, a pivotal enzyme along the early GAs biosynthetic pathways to synthetize GA_{12}; ii) a downregulation of *GA4*, a key gene of GAs biosynthesis, along which bioactive GAs are synthetized[19] (Fig. 4A). No Cd-induced modulation was observed in the WT (Fig. 4A). On the contrary, at 50 µM Cd both *ddc* and WT showed a downregulation of *GA5* (Fig. 4A). Finally, in *ddc vs* WT the only difference dealt with *GA2* downregulation at 25 µM Cd (Fig. 4A).

GPs controlling GAs inactivation also showed a comparable transcriptional pattern in *ddc* and WT under control conditions, and no DEGs were detected (Fig. 4B). 25 µM Cd induced a downregulation of *DAO2* and *AOP1*, encoding GA2ox enzymes, only in *ddc* (Fig. 4B). Accordingly, in *ddc vs* WT these genes were downregulated only at the lowest Cd concentration (Fig. 4B).

Under control conditions, also GP related to GAs signalling was not differentially modulated in *ddc vs* WT (Fig. 4C). A downregulation of genes encoding DELLA proteins, which act as repressors[20], was induced only in *ddc* by 25 µM Cd (Fig. 4C) and in both *ddc* and WT at 50 µM Cd (Fig. 4C), suggesting an enhancement of hormone signalling. Consequently, DELLA-codifying genes resulted downregulated also in *ddc vs* WT only at the lowest Cd concentration (Fig. 4C).

In summary, in *ddc* the lowest Cd treatment negatively affected GPs related to GAs biosynthesis but, at the same time, hormone signalling resulted enhanced. In the WT similar effects were observed only at 50 µM Cd.

Jasmonic acid. Under control conditions, six genes along the GP related to JA biosynthesis were downregulated in *ddc vs* WT (Fig. 5A). 25 µM Cd induced in *ddc* a downregulation of this GP, except for *LOX4* upregulation (Fig. 5A) and a downregulation involving eight genes in WT (Fig. 5A). At 50 µM, Cd effects were limited to *LOX5* downregulation and *LOX4* and *OPR1* upregulation in *ddc* and *LOX5* and *AOS* downregulation in WT (Fig. 5A). No Cd–induced differences were found in *ddc vs* WT (Fig. 5A).

Concerning the JA signalling-related GP, in control conditions *JAZ5* gene, encoding a protein acting as repressor[21], was downregulated in *ddc vs* WT, highlighting a signalling enhancement (Fig. 5B). Interestingly, *JAZ10* and *JAZ9* were differentially impacted by 25 µM Cd in *ddc* and WT resulting upregulated and

A ***trans*-zeatin biosynthesis**

Gene	AGI	log$_2$ (Fold Change)						
		ddc vs WT - Ctrl	25 µM Cd *vs* Ctrl – *ddc*	25 µM Cd *vs* Ctrl – WT	*ddc vs* WT - 25 µM Cd	50 µM Cd *vs* Ctrl – *ddc*	50 µM Cd *vs* Ctrl – WT	*ddc vs* WT -50 µM Cd
IPT5	AT5G19040	-	-	-	-	-	-2.227	-

B **CKs degradation**

Gene	AGI	log$_2$ (Fold Change)						
		ddc vs WT - Ctrl	25 µM Cd *vs* Ctrl – *ddc*	25 µM Cd *vs* Ctrl – WT	*ddc vs* WT - 25 µM Cd	50 µM Cd *vs* Ctrl – *ddc*	50 µM Cd *vs* Ctrl – WT	*ddc vs* WT -50 µM Cd
CKX5	AT1G75450	-	-3.188	-	-2.120	-2.164	-	-
CKX6	AT3G63440	-	-2.519	-	-	-2.345	-	-

C **CKs N^7 and N^9 glycosilation**

Gene	AGI	log$_2$ (Fold Change)						
		ddc vs WT - Ctrl	25 µM Cd *vs* Ctrl – *ddc*	25 µM Cd *vs* Ctrl – WT	*ddc vs* WT - 25 µM Cd	50 µM Cd *vs* Ctrl – *ddc*	50 µM Cd *vs* Ctrl – WT	*ddc vs* WT -50 µM Cd
UGT73C1	AT2G36750	-	-	3.279	2.341	-	-	-
UGT73C5	AT2G36800	-	3.415	-	2.148	3.839	3.712	-

D **CKs *O*-glycosilation**

Gene	AGI	log$_2$ (Fold Change)						
		ddc vs WT - Ctrl	25 µM Cd *vs* Ctrl – *ddc*	25 µM Cd *vs* Ctrl – WT	*ddc vs* WT - 25 µM Cd	50 µM Cd *vs* Ctrl – *ddc*	50 µM Cd *vs* Ctrl – WT	*ddc vs* WT -50 µM Cd
UDP-glucosyl transferase family gene	AT5G38010	-	-	-	-	-2.649	-3.278	-
UDP-glucosyl transferase family gene	AT2G36770	-	2.562	-	2.230	3.035	3.845	-
UDP-glucosyl transferase family gene	AT2G36780	-	2.675	-	-	3.243	3.688	-
UGT73C1	AT2G36750	-	-	3.279	2.341	-	-	-
UGT73C5	AT2G36800	-	3.415	-	2.148	3.839	3.712	-
UGT73C6	AT2G36790	-	2.317	-	2.602	2.754	2.411	-
UGT76E12	AT3G46660	-	-	-	2.203	-	-	-
UGT73C7	AT3G53160	-	2.539	-	-	2.933	2.507	-
UGT85A1	AT1G22400	-	2.685	-	-	2.680	2.893	-
UGT87A2	AT2G30140	-	2.061	-	-	2.242	2.396	-

E **CKs signalling pathway**

Gene	AGI	log$_2$ (Fold Change)						
		ddc vs WT - Ctrl	25 µM Cd *vs* Ctrl – *ddc*	25 µM Cd *vs* Ctrl – WT	*ddc vs* WT - 25 µM Cd	50 µM Cd *vs* Ctrl – *ddc*	50 µM Cd *vs* Ctrl – WT	*ddc vs* WT -50 µM Cd
AHP1 B-type ARRs	AT3G21510	-	-	-	-2.191	-	-	-
ARR10 B-type ARRs	AT4G31920	-	-2.642	-	-	-	-	-
ARR3 A-type ARRs	AT1G59940	-	-	-	-	-2.007	-2.958	-
ARR5 A-type ARRs	AT3G48100	-2.018	-	-	-	-	-	-
ARR11 A-type ARRs	AT1G67710	-	-2.269	-	-	-	-	-
ARR15 A-type ARRs	AT1G74890	-2.577	-	-	-	-	-4.060	-
ARR16 A-type ARRs	AT2G40670	-	-	-	-	-	-3.088	-
ARR17 A-type ARRs	AT3G56380	-	-	-	2.555	-	-	-

Figure 3. Genes differentially expressed (DEGs) along the pathway of (**A**) *trans*-zeatin biosynthesis, (**B**) CKs degradation, (C) CKs N^7- and N^9-glucoside biosynthesis, (**D**) CKs *O*-glycosylation and (**E**) CKs signalling in *ddc* and WT plants identified through a transcriptomic approach. For each comparison, the log$_2$(fold change) of the analysed DEGs was shown in orange and in blue for the upregulated and downregulated genes, respectively. Plants were grown for 21 DAG in long day condition: (i) on growth medium added with 25 or 50 µM Cd; (ii) on growth medium without Cd as control (Ctrl).

downregulated, respectively. (Fig. 5B). At 50 µM Cd, *JAZ*s were overexpressed in both *ddc* and WT (Fig. 5B). No differences were detected in *ddc vs* WT exposed to Cd (Fig. 5B).

Globally, Cd negatively impacted on the GP related to JA biosynthesis especially in WT. Under Cd treatment hormone signalling was downregulated more in *ddc* than in WT, whatever concentration was applied.

A

GAs biosynthesis

Gene	AGI	log$_2$ (Fold Change)						
		ddc vs WT - Ctrl	25 µM Cd *vs* Ctrl – *ddc*	25 µM Cd *vs* Ctrl – WT	*ddc vs* WT - 25 µM Cd	50 µM Cd *vs* Ctrl – *ddc*	50 µM Cd *vs* Ctrl – WT	*ddc vs* WT -50 µM Cd
GA2	AT1G79460	-	-2.725	-	-3.359	-	-	-
GA4	AT1G15550	-	-2.599	-	-	-	-	-
GA5	AT4G25420	-	-	-	-	-2.653	-3.872	-

B

GAs inactivation

Gene	AGI	log$_2$ (Fold Change)						
		ddc vs WT - Ctrl	25 µM Cd *vs* Ctrl – *ddc*	25 µM Cd *vs* Ctrl – WT	*ddc vs* WT - 25 µM Cd	50 µM Cd *vs* Ctrl – *ddc*	50 µM Cd *vs* Ctrl – WT	*ddc vs* WT -50 µM Cd
AOP1	AT4G03070	-	-2.597	-	-2.790	-	-	-
DAO2	AT1G14120	-	-2.220	-	-2.050	-	-	-

C

GAs signalling pathway

Gene	AGI	log$_2$ (Fold Change)						
		ddc vs WT - Ctrl	25 µM Cd *vs* Ctrl – *ddc*	25 µM Cd *vs* Ctrl – WT	*ddc vs* WT - 25 µM Cd	50 µM Cd *vs* Ctrl – *ddc*	50 µM Cd *vs* Ctrl – WT	*ddc vs* WT -50 µM Cd
GAI (*DELLA* family gene)	AT1G14920	-	-2.830	-	-	-3.207	-2.114	-
RGL1 (*DELLA* family gene)	AT1G66350	-	-2.495	-	-2.161	-	-2.054	-

Figure 4. Genes differentially expressed (DEGs) along the pathway of (**A**) GAs biosynthesis, (**B**) GAs inactivation and (**C**) GAs signalling in *ddc* and WT plants identified through a transcriptomic approach. For each comparison, the log$_2$(fold change) of the analysed DEGs was shown in orange and in blue for the upregulated and downregulated genes, respectively. Plants were grown for 21 DAG in long day condition: (i) on growth medium added with 25 or 50 µM Cd; (ii) on growth medium without Cd as control (Ctrl).

Abscisic acid. Under control conditions, ABA biosynthesis-related GP showed comparable EP in *ddc* and WT, and no DEGs were detected (Fig. 5C). The only significant Cd effect dealt with *NCED3* downregulation both in *ddc* and WT, regardless of applied concentration (Fig. 5C). Under control conditions, also the GPs related to ABA catabolism showed a comparable EP in *ddc* and WT and no DEGs were detected (Fig. 5D), but Cd differentially impacted on *CYP* genes, involved in phaseic acid degradative production[22]. Namely, at 25 µM Cd, *CYP707A3* was downregulated only in *ddc* (Fig. 5D). Moreover, also *CYP707A2* appeared downregulated in *ddc vs* WT (Fig. 5D). At 50 µM Cd it was observed an upregulation of both *CYP707A2* and *CYP707A4* in *ddc,* and of only *CYP707A4* in WT (Fig. 5D).

Under control conditions, GP related to ABA inactivation through glucose conjugation showed similar EP in *ddc vs* WT (Fig. 5E). 25 µM Cd determined *AT4G15260* upregulation and *UGT71C3* downregulation only in *ddc* (Fig. 5E). At 50 µM, Cd equally impacted on *ddc* and WT, resulting into *UGT71C1* and *UGT2* downregulation, *AT5G49690, UGT71B5, UGT71B6* upregulation and, limited to WT, *AT4G15260* upregulation (Fig. 5E). No differences were highlighted in *ddc vs* WT exposed to Cd (Fig. 5E).

Under control conditions, the GP related to hormone signalling also presented a comparable EP in *ddc* and WT (Fig. 5F). In *ddc,* 25 µM Cd impact on this GP appeared rather complex, resulting in an upregulation of *PYL3*, encoding ABA receptor, and a downregulation of *PP2Cs (PP2CA* and *HAI1)* encoding negative regulators of ABA signalling[23]. Moreover, *ABI5*, codifying a key transcription factor in ABA signalling[24] belonging to AREBs/ABFs family, was upregulated. However, *SnRK2.7* gene, codifying a protein which activate the AREBs/ABFs transcription factors[24], was downregulated. Based on the prominent role of SnRK2s in plant response to ABA, it is likely that at 25 µM Cd ABA signalling was downregulated in *ddc* (Fig. 5F). Instead, 25 µM Cd determined in WT the upregulation of *PYL6* and the downregulation of *PP2Cs*, suggesting an enhancement of ABA signalling (Fig. 5F). At 50 µM Cd, *PYL6* was upregulated and *SnRK2.7* downregulated in both *ddc* and WT, while *HAI1* was downregulated only in *ddc* (Fig. 5F). When comparing *ddc vs* WT, at 25 µM Cd only *SnRK2.7* was downregulated, while no differences occurred at 50 µM Cd (Fig. 5F).

In summary, Cd determined a slight downregulation of GP related to ABA biosynthesis in both *ddc* and WT regardless of its concentration. ABA catabolic pathway was lightly downregulated in *ddc* at 25 µM Cd but upregulated in both samples at 50 µM Cd. At the transcriptomic level, ABA signalling featured as enhanced in WT and downregulated in *ddc* regardless of Cd concentration.

Ethylene. Along GP related to ethylene biosynthesis, under control conditions *ACS8* and *ACS11* were upregulated in *ddc vs* WT (Fig. 6A). 25 µM Cd determined *ACS8* and *ACO5* downregulation in *ddc* and *ACS4* upregulation in the WT (Fig. 6A). 50 µM Cd induced *ACS7* upregulation and *ACO5* downregulation in both *ddc* and WT and *ACS2* and *ACS11* overexpression only in WT (Fig. 6A). Finally, the only Cd-induced difference in *ddc vs* WT dealt with *ACO1* downregulation at 25 µM Cd (Fig. 6A).

A

JA biosynthesis

Gene	AGI	log$_2$ (Fold Change)						
		ddc vs WT - Ctrl	25 µM Cd *vs* Ctrl – *ddc*	25 µM Cd *vs* Ctrl – WT	*ddc vs* WT - 25 µM Cd	50 µM Cd *vs* Ctrl – *ddc*	50 µM Cd *vs* Ctrl – WT	*ddc vs* WT -50 µM Cd
AOC1	AT3G25760	-2.938	-	-2.931	-	-	-	-
AOC2	AT3G25770	-2.897	-	-2.782	-	-	-	-
AOS	AT5G42650	-	-2.887	-3.235	-	-	-2.342	-
KAT5	AT5G48880	-	-2.357	-2.336	-	-	-	-
LOX2	AT3G45140	-2.304	-	-2.261	-	-	-	-
LOX3	AT1G17420	-2.146	-2.756	-3.093	-	-	-	-
LOX4	AT1G72520	-3.032	2.036	-2.599	-	2.795	-	-
LOX5	AT3G22400	-	-3.355	-	-	-3.027	-2.024	-
OPR1	AT1G76680	-	-	-	-	2.226	-	-
OPR3	AT2G06050	-2.397	-	-2.383	-	-	-	-

B

JA signalling pathway

Gene	AGI	log$_2$ (Fold Change)						
		ddc vs WT - Ctrl	25 µM Cd *vs* Ctrl – *ddc*	25 µM Cd *vs* Ctrl – WT	*ddc vs* WT - 25 µM Cd	50 µM Cd *vs* Ctrl – *ddc*	50 µM Cd *vs* Ctrl – WT	*ddc vs* WT -50 µM Cd
JAZ1	AT1G19180	-	-	-	-	2.080	-	-
JAZ5	AT1G17380	-2.523	-	-	-	3.551	-	-
JAZ9	AT1G70700	-	-	-2.330	-	-	-	-
JAZ10	AT5G13220	-	2.338	-	-	2.727	2.230	-

C

ABA biosynthesis

Gene	AGI	log$_2$ (Fold Change)						
		ddc vs WT - Ctrl	25 µM Cd *vs* Ctrl – *ddc*	25 µM Cd *vs* Ctrl – WT	*ddc vs* WT - 25 µM Cd	50 µM Cd *vs* Ctrl – *ddc*	50 µM Cd *vs* Ctrl – WT	*ddc vs* WT -50 µM Cd
NCED3	AT3G14440	-	-4.516	-2.126	-	-4.189	-2.823	-

D

ABA degradation

Gene	AGI	log$_2$ (Fold Change)						
		ddc vs WT - Ctrl	25 µM Cd *vs* Ctrl – *ddc*	25 µM Cd *vs* Ctrl – WT	*ddc vs* WT - 25 µM Cd	50 µM Cd *vs* Ctrl – *ddc*	50 µM Cd *vs* Ctrl – WT	*ddc vs* WT -50 µM Cd
CYP707A2	AT2G29090	-	-	-	-2.639	2.170	-	-
CYP707A3	AT5G45340	-	-2.286	-	-	-	-	-
CYP707A4	AT3G19270	-	-	-	-	3.511	2.527	-

E

ABA glucose ester biosynthesis

Gene	AGI	log$_2$ (Fold Change)						
		ddc vs WT - Ctrl	25 µM Cd *vs* Ctrl – *ddc*	25 µM Cd *vs* Ctrl – WT	*ddc vs* WT - 25 µM Cd	50 µM Cd *vs* Ctrl – *ddc*	50 µM Cd *vs* Ctrl – WT	*ddc vs* WT -50 µM Cd
UDP-glucosyl transferase family gene	AT4G15260	-	2.092	-	-	-	2.189	-
UDP-glucosyl transferase family gene	AT5G49690	-	-	-	-	2.841	3.117	-
UGT2	AT1G05530	-	-	-	-	-3.652	-4.589	-
UGT71B5	AT4G15280	-	-	-	-	2.121	2.894	-
UGT71B6	AT3G21780	-	-	-	-	2.005	2.435	-
UGT71C1	AT2G29750	-	-	-	-	-4.401	-3.533	-
UGT71C3	AT1G07260	-	-2.210	-	-	-	-	-

F

ABA signalling pathway

Gene	AGI	log$_2$ (Fold Change)						
		ddc vs WT - Ctrl	25 µM Cd *vs* Ctrl – *ddc*	25 µM Cd *vs* Ctrl – WT	*ddc vs* WT - 25 µM Cd	50 µM Cd *vs* Ctrl – *ddc*	50 µM Cd *vs* Ctrl – WT	*ddc vs* WT -50 µM Cd
ABI5	AT2G36270	-	3.398	-	-	-	2.405	-
HAI1	AT5G59220	-	-2.594	-2.720	-	-2.479	-	-
PP2CA	AT3G11410	-	-2.439	-2.257	-	-	-	-
PYL3	AT1G73000	-	2.303	-	-	-	-	-
PYL6	AT2G40330	-	-	2.151	-	3.114	2.408	-
SNRK2.7	AT4G40010	-	-3.541	-	-2.161	-3.118	-3.418	-

Figure 5. Genes differentially expressed (DEGs) along the pathway of (**A**) JA biosynthesis, (**B**) JA signalling, (**C**) ABA biosynthesis, (**D**) ABA degradation, (**E**) ABA glucose ester biosynthesis and (**F**) ABA signalling in *ddc* and WT plants identified through a transcriptomic approach. For each comparison, the log$_2$(fold change) of the analysed DEGs was shown in orange and in blue for the upregulated and downregulated genes, respectively. Plants were grown for 21 DAG in long day condition: (i) on growth medium added with 25 or 50 µM Cd; (ii) on growth medium without Cd as control (Ctrl).

A

Ethylene biosynthesis

Gene	AGI	log$_2$ (Fold Change)						
		ddc vs WT - Ctrl	25 µM Cd *vs* Ctrl – *ddc*	25 µM Cd *vs* Ctrl – WT	*ddc vs* WT - 25 µM Cd	50 µM Cd *vs* Ctrl – *ddc*	50 µM Cd *vs* Ctrl – WT	*ddc vs* WT -50 µM Cd
ACO1	AT2G19590	-	-	-	-2.029	-	-	-
ACO5	AT1G77330	-	-2.043	-	-	-2.014	-2.092	-
ACS2	AT1G01480	-	-	-	-	-	2.157	-
ACS4	AT2G22810	-	-	2.067	-	-	-	-
ACS7	AT4G26200	-	-	-	-	2.844	3.696	-
ACS8	AT4G37770	2.339	-2.024	-	-	-	-	-
ACS11	AT4G08040	2.965	-	-	-	-	2.719	-

B

Ethylene signalling pathway

Gene	AGI	log$_2$ (Fold Change)						
		ddc vs WT - Ctrl	25 µM Cd *vs* Ctrl – *ddc*	25 µM Cd *vs* Ctrl – WT	*ddc vs* WT - 25 µM Cd	50 µM Cd *vs* Ctrl – *ddc*	50 µM Cd *vs* Ctrl – WT	*ddc vs* WT -50 µM Cd
ERF1	AT3G23240	-	-	-	-	3.229	3.604	-
ETR2	AT3G23150	-	-	2.233	-	2.287	3.100	-

C

SA signalling pathway

Gene	AGI	log$_2$ (Fold Change)						
		ddc vs WT - Ctrl	25 µM Cd *vs* Ctrl – *ddc*	25 µM Cd *vs* Ctrl – WT	*ddc vs* WT - 25 µM Cd	50 µM Cd *vs* Ctrl – *ddc*	50 µM Cd *vs* Ctrl – WT	*ddc vs* WT -50 µM Cd
CAPE3	AT4G33720	-	-	-	-2.459	-	-	-
PR1	AT2G14610	-3.343	-	-	-	-	2.482	-
PRB1	AT2G14580	-	-	-	-	-2.630	-3.195	-
TGA8	AT1G68640	-	-	-	-	-2.189	-	-
TGA10	AT5G06839	-	-2.992	-	-2.129	-	-	-

Figure 6. Genes differentially expressed (DEGs) along the pathway of (**A**) ethylene biosynthesis, (**B**) ethylene signalling and (**C**) SA signalling in *ddc* and WT plants identified through a transcriptomic approach. For each comparison, the log$_2$(fold change) of the analysed DEGs was shown in orange and in blue for the upregulated and downregulated genes, respectively. Plants were grown for 21 DAG in long day condition: (i) on growth medium added with 25 or 50 µM Cd; (ii) on growth medium without Cd as control (Ctrl).

GP related to ethylene signalling showed similar EP in *ddc* and WT both under control conditions (Fig. 6B) and at 25 µM Cd, except for the upregulation of *ETR2*, encoding ethylene receptor[25] in WT (Fig. 6B). At 50 µM Cd, both *ddc* and WT exhibited *ETR2* and *ERF1* overexpression suggesting an upregulation of ethylene signalling (Fig. 6B); no differences occurred in *ddc vs* WT (Fig. 6B).

In summary, in control conditions GP related to ethylene biosynthesis was upregulated in *ddc vs* WT. Cd determined a downregulation and upregulation of this GP in *ddc* and WT, respectively. Concerning hormone signalling, at the highest Cd concentration in both *ddc* and WT an upregulation of this GP occurred.

Salicylic acid. Regarding SA, only the GP related to signalling resulted differentially expressed. Under control conditions, the GP related to SA signalling showed similar EP in *ddc* and WT. However, *PR1*, a useful molecular marker for the systemic acquired resistance (SAR) in response to pathogens[26], was downregulated in *ddc vs* WT (Fig. 6C). 25 µM Cd induced a downregulation of genes codifying TGA10 transcription factor only in the *ddc* (Fig. 6C). Whereas, 50 µM Cd induced a downregulation of *PRB1* in both *ddc* and WT and of *TGA8* only in *ddc* (Fig. 6C). In *ddc vs* WT, differences were found only at 25 µM Cd, with the downregulation of *TGA10* and *CAPE3* (Fig. 6C).

Altogether, these results evidenced a Cd-induced downregulation of this GP, likely resulting in an impairment of hormone signalling in both WT and *ddc*, but in the latter this effect already occurred at the lowest Cd concentration.

Phytohormone level. Based on the major effects induced by 25 µM Cd treatment, hormone quantification was carried out on plants exposed to this concentration, compared to untreated control plants.

Under control conditions, IAA amount was higher in *ddc* than WT, although not significantly. After Cd treatment, a decreasing trend was observed only in WT, resulting into a significant lower level as compared to *ddc* (Fig. 7A).

Concerning CKs, both biological active (*tZ*) and inactive conjugate (*tZR, cZR, tZOG, cZOG*, iPR) forms were analysed (Fig. 7B–G). Under control conditions, all analysed CKs were present in *ddc*, but CKs conjugate forms and above all *O*-glycosylated exhibited the highest levels (Fig. 7B–G). By contrast, in WT *tZ* was not detectable and all the other CKs forms exhibited a lower level compared to the mutant, which appeared significant for *tZR*

and *cZOG* (Fig. 7B–G). Following Cd treatment, CKs levels increased in *ddc*, except for *tZ* decrease. In WT, the unique Cd effect dealt with *tZR* increase and *tZOG* decrease. Consequently, under Cd treatment the level of all CKs forms remained higher (from 0.25 to 3 times) in *ddc* than in WT (Fig. 7B–G).

Concerning GAs, precursors (GA_9, GA_{19}, GA_{20}), biologically active forms (GA_1, GA_3, GA_4, GA_7) and catabolites (GA_8, GA_{34}, GA_{29}, GA_{51}) were analysed (Fig. 7H–R). Under control conditions, GA_{19} amount was significantly higher in *ddc vs* WT, while the amount of GA_{20}, the other *in serie* precursor of hydroxylated forms, was comparable between the samples (Fig. 7H,I). Following Cd treatment, GA_{19} amount significantly increased in WT while a slight downtrend occurred in *ddc*, leading to comparable values in the two samples. The same trend was observed, but at less extent, for GA_{20} (Fig. 7H,I). Consistently, under control conditions also the amount of the active hydroxylated forms GA_1 and GA_3 was higher in WT than in *ddc* (Fig. 7J,K). Following Cd treatment, a decrease of their amount was detected only in WT, globally leading to a higher level of these GAs in *ddc* mutant compared to the WT (Fig. 7J,K). In addition, in *ddc* mutant also the related catabolites GA_8 and GA_{29} were globally lower than in WT, under both control conditions and Cd treatment (Fig. 7L,M).

Differences were observed also for GA_9, precursor of non-hydroxylated GAs: under Cd treatment its amount decreased in the WT and was instead induced in *ddc* mutant, resulting in a quite comparable value between the two samples (Fig. 7N). Consistently, the amount of active non-hydroxylated forms, GA_4 and GA_7, increased under Cd treatment only in *ddc* mutant; also in this case, at the end of heavy metal treatment, comparable values were detected in *ddc* and WT (Fig. 7O,P) In agreement with these results, following Cd treatment, the amount of catabolites GA_{51} and GA_{34} did not change in the WT, whereas in *ddc* it increased and decreased, respectively (Fig. 7Q,R).

As evident in Fig. 7S–V, differences were reported also for JA, ABA, SA and its predominant inactive conjugate, SA 2-*O*-β-D-glucoside (SAG). Under control conditions both JA and ABA amount was significantly lower in *ddc vs* WT and significantly decreased following Cd treatment only in the WT (Fig. 7S,T). Notwithstanding, under such condition the ABA amount remained lower in *ddc* than in WT while JA values were comparable in the two samples due its light, but not significant, increase in *ddc* (Fig. 7S,T). By contrast, under control conditions both SA and SAG amounts were significantly higher in *ddc* than in WT (Fig. 7U,V). Following Cd treatment, their amounts significantly decreased more in *ddc* than in WT, leading to an opposite condition (Fig. 7U,V).

Testing of the involvement of *SUPPRESSOR OF DRM1 DRM2 CMT3 (SDC)* gene in *ddc* response to Cd. Finally, we planned to inquire on the possible involvement of *SDC* gene in the response of *ddc* triple mutant to Cd exposure. Indeed, it has been reported that in *ddc* mutant the misexpression of such gene, which encodes a F-Box protein, is ultimately responsible of the developmental phenotypes of *ddc*, such as curled leaves and reduced growth, as evidenced by its reversion in the *drm1 drm2 cmt3 sdc* quadruple mutant[27]. Note that in the WT *SDC* is silenced, being methylated in all its sequence contexts because of the redundant action of DRM2 and CMT3 enzymes. By contrast, in *ddc*, where *DRM2* and *CMT3* expression is silenced, the loss of non-CG methylation in the promoter region of *SDC* F-box gene determines its overexpression[27].

According to the above mentioned data[27], we firstly verified that under control conditions *SDC* resulted silent in the WT and overexpressed in *ddc* also in our transcriptomic analysis (data not shown, complete raw transcriptomic data are available at NCBI SRA under the BioProject accessionPRJNA641242;https://www.ncbi.nlm.nih.gov/Traces/study/?acc=PRJNA641242). Moreover, our data also showed that at the transcriptomic level *SDC* is not modulated by Cd since its expression level did not significantly change in *ddc* nor in WT whatever heavy metal concentration was applied.

Thereafter, we tested the involvement of *SDC* in the growth response of *ddc* mutant under Cd exposure, by monitoring primary root length of *Arabidopsis thaliana* WT, *ddc* and *sdc* plants grown under the following conditions: (i) on growth medium without Cd as control (Ctrl) (ii) on a medium supplemented with 25/50 μM Cd; (iii) limited to the WT and *sdc* mutant plants, on a medium supplemented with 25/50 μM Cd plus 15 μM 5-Azacytidine (5-Aza), an inhibitor of DNA methylation applied in order to mimic the hypomethylated state of *ddc* mutant.

Under control conditions, all three samples showed a similar root length. However, at 21 DAG, root was lightly shorter in *ddc vs* WT, while *sdc* displayed an intermediate length (Fig. 8A). Under both Cd treatments, roots were averagely longer in *ddc* than in WT. Again, *sdc* roots exhibited an intermediate length, more similar to WT than *ddc* (Fig. 8 B,C). Interestingly, WT and *sdc* plants treated with Cd plus 5-Aza had longer roots than the plants treated only with Cd, and quite comparable to *ddc* roots exposed to Cd (Fig. 8 D,E).

Discussion

This study showed that, under a long-lasting Cd treatment, *A. thaliana ddc* mutant exhibited a better growth performance than WT plants especially at 25 μM Cd concentration, tightly related to a differential modulation of GPs highly relevant for plant growth.

Attention was mainly focused on GPs related to hormones, key molecules in the control of plant growth and stress response, whose action is regulated by interconnected epigenetic mechanisms[12,28]. Accordingly, all hormone-related GPs were differentially modulated in *ddc vs* WT under control conditions but mainly under Cd stress, although at different extent for each hormone class. That is consistent with literature data showing that many plant hormones and other signal molecules are involved in Cd sensing and downstream plant response[10,29]. However, the general picture is somehow controversial differing in relation to species, plant organ and age, concentration and duration of metal exposure[30].

In our work, for all hormone classes the major differences between *ddc* and WT occurred at the lowest Cd concentration (25 μM Cd). In particular, for auxin Cd impact was prominent on hormone conjugation rather than biosynthesis. Namely, the two GPs related to auxin biosynthesis were oppositely affected by Cd in both *ddc*

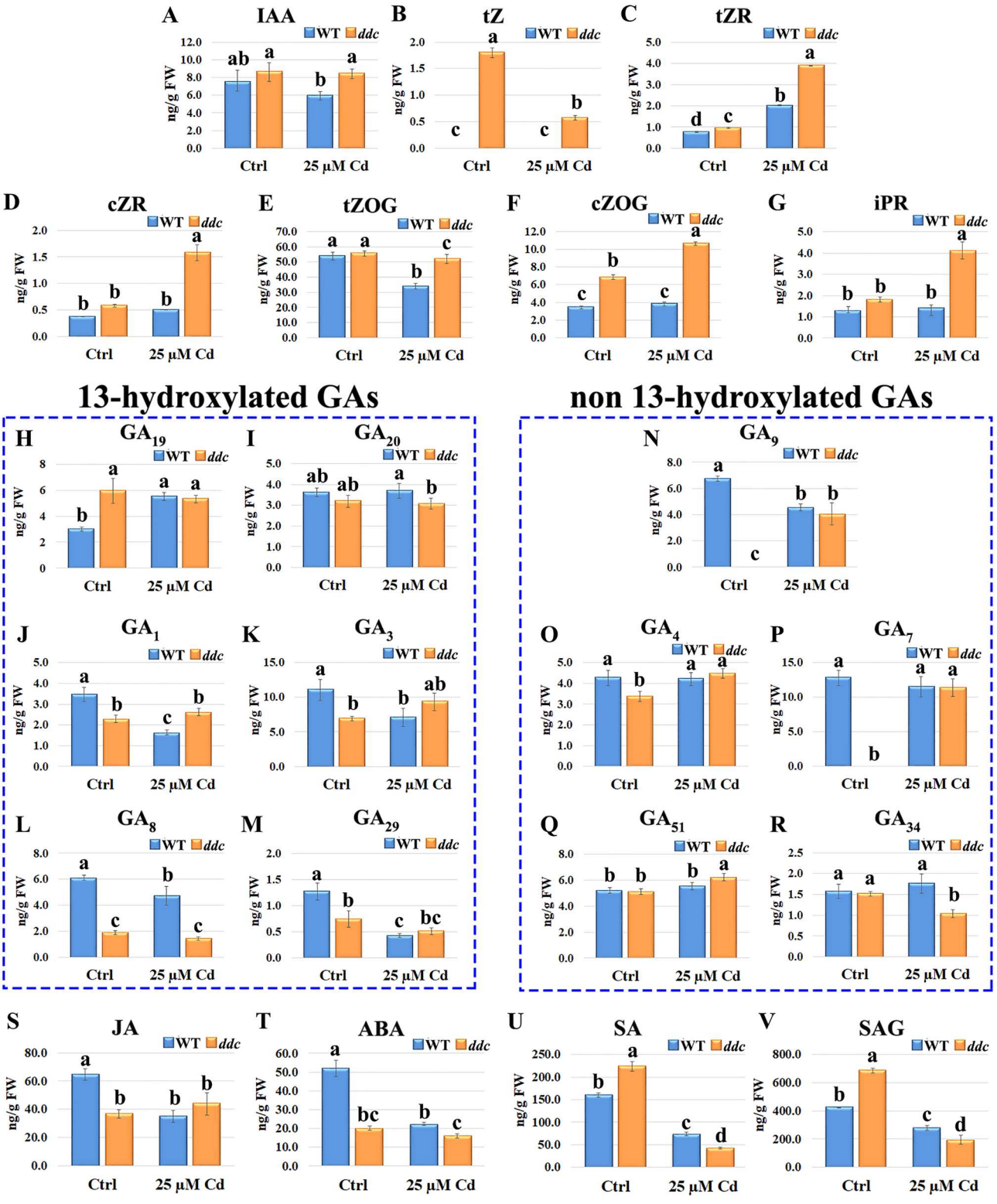

Figure 7. (**A**) IAA, (**B**–**G**) CKs, (**H**–**R**) GAs, (**S**) JA, (**T**) ABA, (**U**) SA and (**V**) SAG amount in *A. thaliana ddc* mutant and WT plants grown in Ctrl conditions and treated with 25 µM Cd estimated by GC–MS. The results represent the mean value (± SD) of three independent biological replicates. Statistical analysis was performed by using two-way ANOVA with Tukey post hoc test ($P \leq 0.05$) after Shapiro–Wilk normality test. Means with the same letter are not significantly different at $P \leq 0.05$.

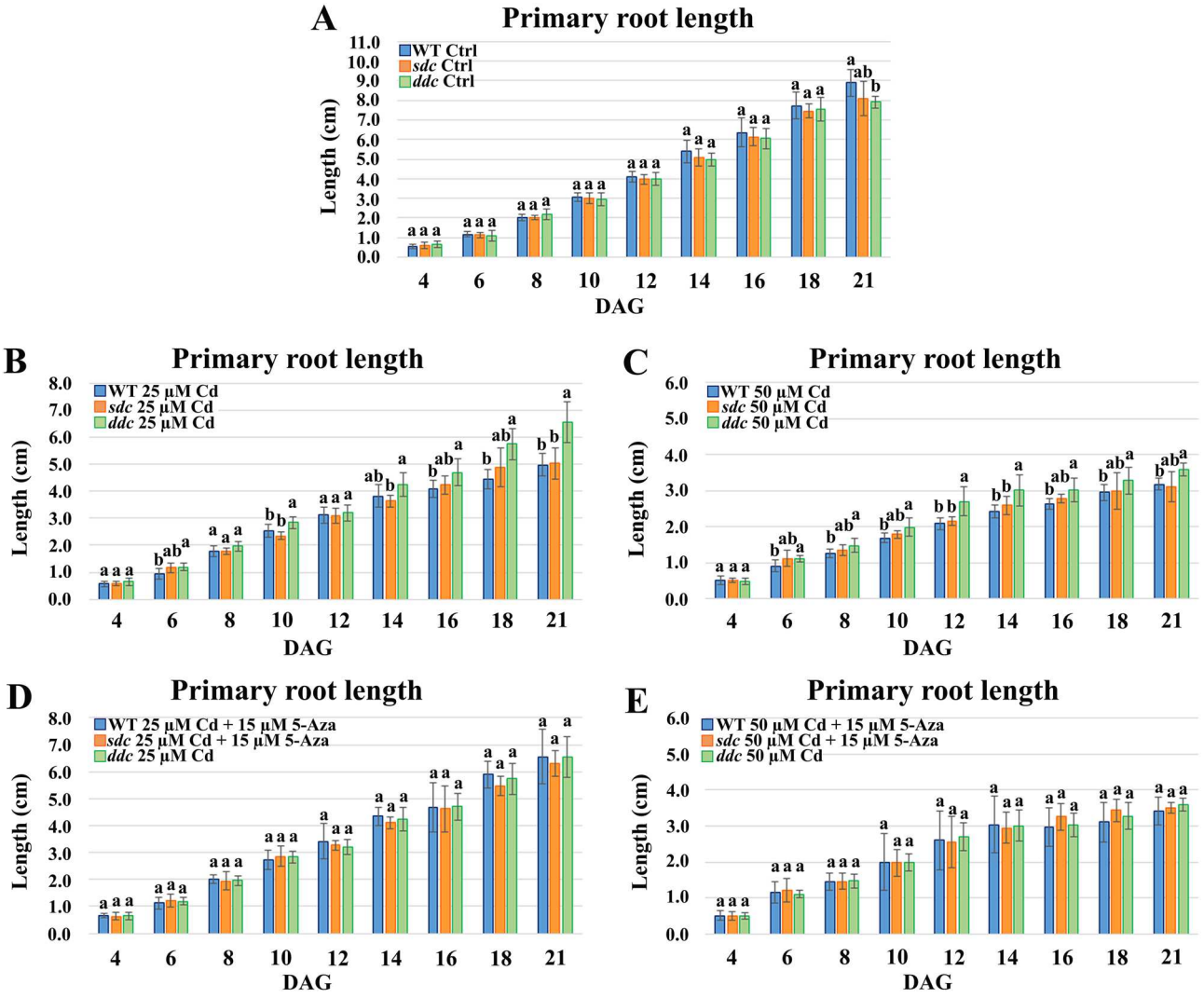

Figure 8. Primary root length of WT, *sdc* and *ddc* plants of *A. thaliana*, germinated and grown in long day condition (**A**) on growth medium without Cd as control (Ctrl), (**B**,**C**) on a medium supplemented with 25/50 µM Cd, (**D**,**E**) limited to WT and *sdc* plants, on a medium supplemented with 25/50 µM Cd plus 15 µM 5-Azacytidine (5-Aza). Root length was monitored up to 21 days after germination (DAG) every two days from germination. The results represent the mean value (± SD) of three independent biological replicates (n = 45). Statistical analysis was performed between samples at the same growth stage, by using two-way ANOVA with Tukey post hoc test ($P \leq 0.05$) after Shapiro–Wilk normality test. Means with the same letter are not significantly different at $P \leq 0.05$.

and WT, likely as a compensatory mechanism to maintain hormone level. However, at 25 µM Cd IAA amount, which is the most relevant auxin, was higher in *ddc* than WT, evidencing that maintenance of bioactive auxin level was more efficient in the mutant. The downregulation of genes involved in auxin conjugation detected in *ddc* under such treatment provides a suitable explanation for this behaviour.

Transcriptomic data also suggested an enhancement of auxin signalling in *ddc vs* WT at 25 µM Cd. Notably, in *Arabidopsis* a Cd-induced simultaneous decrease of IAA content and increase of IAA oxidase activity resulted into a downregulation of numerous auxin-responsive and growth-related genes[31]. Moreover, under Cd exposure high level of IAA were found to prevent growth inhibition and increase heavy metal tolerance[32]. Therefore, although at post-transcriptional level a different regulation can occur, the better growth performance of *ddc* under 25 µM Cd could be warranted by transcriptomic changes addressed to prevent hormone inactivation and enhance its signalling. Interestingly, in our previous work an organ-specific and opposite alterations of auxin translocation and homeostasis was detected in *ddc* root and leaf as compared to WT, tightly related to mutant phenotypic alterations[33]. Furthermore, such hormone pathway alterations were associated to organ-specific changes in the expression level of auxin-related genes, which in some cases were in turn associated to gene-specific defective methylation level[33]. Altogether, these results highlight that a relationship between methylation status and auxin metabolism and translocation play a relevant role in modulating growth and development of *ddc* under both control conditions and Cd stress.

CKs also resulted differentially impacted by Cd in *ddc vs* WT both at transcriptomic and biochemical level. As for all hormones, CKs homeostasis relies on the balance between biosynthesis, catabolism and/or inactivation[34]. Transcriptomic major differences dealt with GPs related to CKs catabolism and inactivation rather than biosynthesis, at least at the lowest Cd concentration. Literature data showed an increase of CKs catabolic oxidation in *Triticum durum* exposed to 0.04 mM Cd[35]. A more complex picture was detected in our samples under a long-lasting treatment at a lower concentration (25 µM Cd). Namely, a Cd-induced downregulation of cytokinin-oxidase genes was observed only in *ddc*. Simultaneously, GPs related to CKs inactivation through *N*-glycosylation were upregulated in both *ddc* and WT, while *O*-glycosylation was upregulated only in *ddc*. Accordingly, hormone quantification showed that CKs *O*-glycosylated forms increased in Cd-treated *ddc* and were more abundant than in WT. Notably, while *N*-glycosylation causes irreversible CKs inactivation, *O*-glycosylated CKs represent the hormone fraction available for storage and transport, that can be reconverted in active CKs by β-glucosidases[16]. Therefore, the genetic modulation implemented by *ddc* under 25 µM Cd concentration was addressed to preserve CKs pool. That is consistent with the high CKs level detected in *ddc vs* WT at 25 µM Cd, despite the GP related to hormone biosynthesis exhibited a comparable EP. Incidentally, CKs are essential for counteracting leaf senescence, protecting photosystems and enhancing photosynthesis[36]. Accordingly, under Cd treatment leaf number and area was higher in *ddc vs* WT, evidencing that leaf growth was less impaired in *ddc*. Therefore, the genetic modulation underway in *ddc* could represent an important strategy to assure resistance to Cd stress.

On the other hand, also GAs play a relevant role in leaf development[37]. A downregulation of pathways related to the biosynthesis of active GAs occurred in *ddc* at 25 µM Cd. Likely as a compensatory defence mechanism, a strong downregulation of the GPs related to GAs inactivation and an enhancement of hormone signalling also occurred in *ddc* at the lowest Cd concentration.

A rather complex picture emerged for JA, SA and ABA, which represent the most relevant hormones for the perception and downstream response of plants to stresses, including heavy metals[38]. Namely, under control conditions, at transcriptomic level JA biosynthesis was downregulated and a lower hormone amount was detected in *ddc vs* WT. Whereas, for SA and ABA a post-transcriptional regulation can be envisaged, as already demonstrated for ABA[39], since GPs related to their biosynthesis showed similar EP in *ddc vs* WT, despite of significantly higher and lower hormone level detected in *ddc,* respectively.

At 25 µM Cd, a downregulation of biosynthesis-related GPs and hormone level, was observed for all three hormones. However, for SA and ABA this effect was more pronounced in *ddc* than WT, while JA was more affected in WT than *ddc.* likely explaining the comparable JA level in Cd-treated *ddc* and WT. 25 µM Cd also induced a downregulation of GP related to ABA degradation only in *ddc vs* WT, probably as a compensatory mechanism for maintaining adequate hormone level. An opposite effect was observed for GP related to ABA signalling, which appeared upregulated in the WT and downregulated in *ddc* whatever concentration was used.

This scenario was unexpected, since it is largely documented that level and activity of these stress-related hormones, mainly of ABA, usually increase following abiotic stress, including heavy metal[40]. However, the exact mechanisms of hormone action and their crosstalk with the whole signalling network of plant under stress are yet to be fully clarified. In addition, hormone dynamic under stress largely depends on the species, the plant organ and growth stage, the stress intensity and duration[40]. For example, Cd treatment was found to induce a differential JA accumulation in several plant species, including *A. thaliana* which exhibited a biphasic model, with an early hormone accumulation, followed by cyclic decreases and increases[41]. Notably, low JA concentrations act as protectant against Cd stress, while higher concentrations induce toxic effects, such as ROS accumulation, root growth inhibition and lipid peroxidation[42]. Similar toxicity is displayed by high levels of SA, which has been proposed as the 'life or death switch' of cells[43]. Moreover, negative effects on plant growth can be exerted also by high levels of ABA, which acts as an antagonist of GAs action[39]. Therefore, it is likely that under the long-lasting Cd treatment that we applied, plant activity was directed to avoid toxic effects related to a prolonged activation of all these three hormone classes, by decreasing their level and/or downregulating their signalling. Interestingly, in *ddc* which exhibited the best growth performance, these adaptive responses were more pronounced.

In summary, our results clearly showed that, under a prolonged metal exposure and within a specific threshold concentration (i.e. 25 µM Cd), a differential transcriptional modulation of hormone pathways is a key mechanism for the capacity of *A. thaliana ddc* mutant, defective in methylation, to better counteract Cd toxicity compared to WT. Moreover, *ddc* prompt response at the lowest Cd concentration (i.e. 25 µM Cd) also evidenced that such aptitude was associated to its greater capacity to sense heavy metal stress and put in place an early modulation of gene expression. We propose that this behaviour is related to the higher genome plasticity conferred to *ddc* by DNA hypomethylated status.

In this context it is relevant to recall that the overexpression of the *SDC* F-box gene in *ddc*, due to the loss of non-CG methylation in its promoter region, is reported to be ultimately responsible of the developmental phenotypes of this mutant, such as curled leaves and reduced growth[27].

In line with this evidence, also our transcriptomic analysis evidenced that, under control conditions, *SDC* is silent in the WT and overexpressed in *ddc*. Furthermore, since *SDC* expression level did not significantly change in *ddc* nor in WT whatever Cd concentration was applied, our data also evidenced that, at the transcriptomic level, *SDC* expression is not modulated by Cd. Moreover and very interestingly, the analysis of root growth allowed us to verify that under Cd treatment the roots of WT and *sdc* plants where shorter than *ddc* ones whereas, following treatment with both Cd and the DNA methylation inhibitor 5-Aza, both displayed longer roots, quite comparable to *ddc* ones. Thus, under Cd exposure a root length comparable to *ddc* was reported only in 5-Aza-treated plants mimicking *ddc* global DNA hypomethylation status, independently by the activation or the silencing of *SDC* which occurs in *ddc* and *sdc*, respectively. These results pointed out two important evidences: (i) a global DNA hypomethylation is certainly involved in a better plant response to Cd stress; (ii) such response is independent by *SDC* gene.

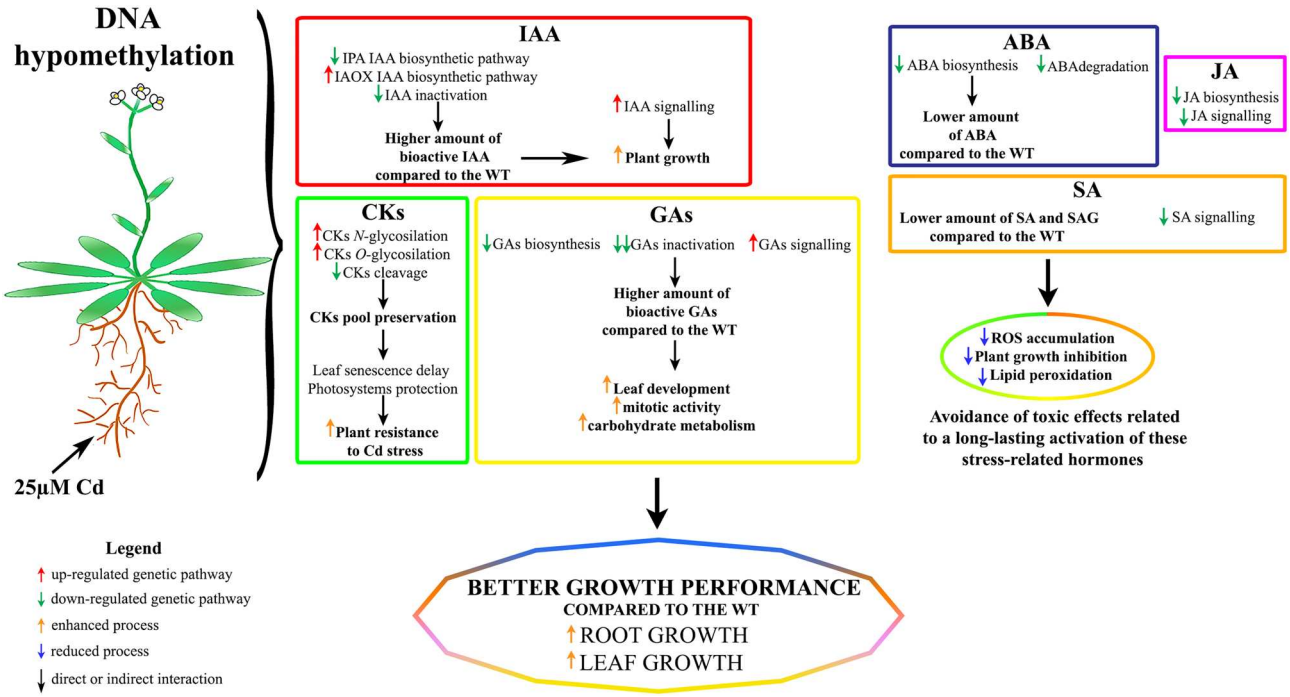

Figure 9. Scheme summarizing the modifications in hormone-related genetic pathways in *A. thaliana ddc* mutant plants under 25 μM Cd stress. The related effects of these modifications are also indicated.

Therefore, it appears that *SDC* activity is not directly related to the response to Cd. Future analysis of methylome status of *ddc* and WT under Cd treatment could give further insight into the different and interacting loci with a direct and or indirect role in the transduction pathways and response mechanisms to Cd stress of *ddc* mutant.

At present, on the basis of our results, the following scheme is proposed to link transcriptomic and hormonal differences to the major Cd tolerance exhibited by *ddc* (Fig. 9). The emerging picture is that plant activity is directed to enhance and/or maintain the level and signalling of hormones which are relevant in sustaining the growth, such as auxins, CKs and GAs more than those of hormones specifically related to stress response such as JA, ABA and SA. This could represent the plant strategy, more effective in *ddc* than in WT, to avoid the negative effects of long-lasting activity of stress-related hormones. In view of the emerging relationship between the phytohormone action and epigenetic mechanisms[12], this supposed role of methylation status in modulating plant strategy for 'life or death switch' under stress condition appears relevant at both theorical and applicative level.

Methods

Plant Lines and growth conditions. Plants of *Arabidopsis thaliana* (L.) Heynh ecotype Columbia-0 (Col-0), *drm1 drm2 cmt3.11 (ddc)* DNA methylation mutant and *suppressor of drm1 drm2 cmt3* (*sdc*) silencing mutant, both in Col-0 background, were used. *Arabidopsis thaliana* seeds and plants were handled according to[45] and by following the methods recommended by Arabidopsis Biological Resource Center (ABRC; https://abrc.osu.edu/) available at https://www.arabidopsis.org/download_files/Protocols/abrc_plant_growth.pdf.

Seeds were surface sterilized and sown on Petri dishes containing half-strength MS medium[45]. Regarding the different treatments, medium was supplemented with 25 μM and 50 μM Cd, as described by[10], and/or 15 μM 5-Azacytidine (5-Aza), according to[46]. Detailed information on plant lines and selected treatment conditions are reported in Supplementary Methods S1 online. We will refer to the different samples as follows: WT Ctrl, WT 25 μM Cd, WT 50 μM Cd, WT 25 μM Cd + 15 μM 5-Aza, WT 50 μM Cd + 15 μM 5-Aza, *ddc* Ctrl, *ddc* 25 μM Cd, *ddc* 50 μM Cd, *sdc* Ctrl, *sdc* 25 μM Cd, *sdc* 50 μM Cd, *sdc* 25 μM Cd + 15 μM 5-Aza, *sdc* 50 μM Cd + 15 μM 5-Aza.

Cd quantification. Cd quantification was performed according to[47] on samples collected at 21 DAG. Three independent replicates were carried out. For statistical analysis, two-way ANOVA with Tukey post hoc test ($P \leq 0.05$) was applied after Shapiro–Wilk normality test. The results of such analysis are provided in Supplementary Fig. S10 online.

Growth parameters analysis. Root length was monitored in plants grown in vitro in a vertical position every two days until 21 DAG. Rosette leaf number and area were evaluated in plants grown in round Petri dishes for 21 DAG. Leaf series was obtained as described by[48]. Measurements were performed by scanning the plates and analysing the resulting images by using ImageJ software (https://imagej.nih.gov/ij/). Three independent replicates were performed (n = 45). Statistical analysis was carried out by using Student's *t*-test (*, $P \leq 0.05$; **, $P \leq 0.01$; ***, $P \leq 0.001$) between *ddc vs* WT grown in the same conditions.

Total RNA extraction. Total RNA was isolated from 100 mg of plant tissue by using the RNeasy Plant Mini kit (Qiagen, Hilden, Germany) and DNA contamination was eliminated through on column DNase digestion (RQ1 RNase-Free Dnase, Cat. Nr. M6101). Extracted RNA was quantified by using the Qubit RNA BR (Broad-Range) Assay Kit, while its integrity was checked by using an Agilent 2100 Bioanalyzer (Agilent Technologies). Only RNA samples with an RNA integrity number ≥ 8 were subsequently used.

RNA-seq. cDNA libraries were constructed from 1 µg of total RNA, using the Illumina TruSeq Stranded Total RNA Sample Preparation Kit (Illumina, San Diego, CA, USA). Quality of the obtained libraries and the fragments length were verified on the Bioanalyzer 2100 by using an Agilent 2100 DNA 1000 Kit and quantified by fluorimetry using the Qubit dsDNA HS (High sensitivity) Assay kit (Q232854). The sequencing of the cDNA libraries was carried out on Illumina Genome Analyzer IIx (SCS v2.10) platform.

Preprocessing and analysis of RNA-seq data. RNA-Seq reads in FASTQ format were inspected using FASTQC program (http://www.bioinformatics.babraham.ac.uk/projects/fastqc/). Only reads with Phred quality score Q > 30 (Q30 Quality Score) were used (from 90 to 95%, for a total of 29.4 Giga reads of 50 bp paired-end reads). Reads were cleaned by using Trim Galore (http://www.bioinformatics.babraham.ac.uk/projects/trim_galore/) and matched to Arabidopsis TAIR10 gene sequences database, allowing for two mismatched bases. Only the alignments unique and concordant in SAM format were converted in binary BAM format by SAMtools. Basic statistics were calculated using Picard tools (CollectRnaSeq Metrics.jar) (http://picard.sourceforge.net/). Transcriptome quantification and RNA differential expression were performed using CuffDiff2 (http://cufflinks.cbcb.umd.edu/) software version 2.1.1, as described by[49].

Gene expression levels were determined by FPKM calculation, using the Cufflinks method[50]. Bioinformatic analysis was performed by multiple pairwise comparisons of gene expression levels. Differentially expressed genes (DEGs) were selected on the basis of fold change (FC) ($5 \geq |\log_2 FC| \geq 2$ and FDR < 0.05).

Gene enrichment analysis. A functional annotation analysis of DEGs was performed by using Gene Ontology (GO) annotations[51] (http://www.geneontology.org/). Gene Enrichment analysis, based on biological process ontology and KEGG database, was performed by selecting the over-represented GO terms through the ClueGO plug-in of the Cytoscape software[52,53]. The significance of each term and group was determined by the calculation of a Bonferroni-corrected *P*-value using the hypergeometric distribution. Only the GO terms with $P \leq 0.05$ were selected.

Analysis of hormone-related pathways. The analysis of hormone-related pathways was performed by using the KEGG Mapper tool[54] (https://www.genome.jp/kegg/mapper.html) for hormones signalling pathways and the online tool PlantMetGenMAP[55] (http://bioinfo.bti.cornell.edu/cgibin/MetGenMAP/home.cgi), which allows a large-scale exploration of gene expression data-set and the identification of the significantly altered biochemical pathways and biological processes through robust statistical tests.

Libraries results validation through quantitative Real-Time PCR (qRT-PCR). Transcriptomic analysis was validated by estimating the expression level of 14 hormone-related key genes. Primers sequences and additional information regarding the selected genes are shown in Supplementary Table S1 online. Detailed information is reported on Supplementary Methods S1 online.

Hormone level quantification. Hormone level quantification was performed on WT and *ddc* mutant plants grown in control conditions and under 25 µM Cd treatment, collected at 21 DAG. Detailed information on hormone level quantification methods is reported on Supplementary Methods S1 online.

Data availability

Raw transcriptomic data generated during and/or analysed during the current study are available at NCBI SRA under the BioProject accession PRJNA641242 (https://www.ncbi.nlm.nih.gov/Traces/study/?acc=PRJNA641242).

Received: 21 April 2020; Accepted: 12 May 2021
Published online: 26 May 2021

References

1. Chiappetta, A. *et al.* A dehydrin gene isolated from feral olive enhances drought tolerance in Arabidopsis transgenic plants. *Front. Plant Sci.* **6**, 392 (2015).
2. Bitonti, M. B. *et al.* Distinct nuclear organization, DNA methylation pattern and cytokinin distribution mark juvenile, juvenile-like and adult vegetative apical meristems in peach (*Prunus persica* (L.) Batsch). *J. Exp. Bot.* **53**, 1047–1054 (2002).
3. Pecinka, A. & Mittelsten Scheid, O. Stress-induced chromatin changes: A critical view on their heritability. *Plant Cell Physiol.* **53**, 801–808 (2012).
4. Finnegan, E. J., Peacock, W. J. & Dennis, E. S. Reduced DNA methylation in *Arabidopsis thaliana* results in abnormal plant development. *Proc. Natl. Acad. Sci. U. S. A.* **93**, 8449–8454 (1996).
5. Zhang, H., Lang, Z. & Zhu, J.-K. Dynamics and function of DNA methylation in plants. *Nat. Rev. Mol. Cell Biol.* **19**, 489–506 (2018).
6. Wendte, J. M. *et al.* Epimutations are associated with CHROMOMETHYLASE 3-induced *de novo* DNA methylation. *Elife* **8**, e47891 (2019).
7. Cao, X. & Jacobsen, S. E. Locus-specific control of asymmetric and CpNpG methylation by the DRM and CMT3 methyltransferase genes. *Proc. Natl. Acad. Sci. U. S. A.* **99**, 16491–16498 (2002).

8. Pinto, A. P. *et al.* Influence of organic matter on the uptake of cadmium, zinc, copper and iron by sorghum plants. *Sci. Total Environ.* **326**, 239–247 (2004).
9. Greco, M., Chiappetta, A., Bruno, L. & Bitonti, M. B. In *Posidonia oceanica* cadmium induces changes in DNA methylation and chromatin patterning. *J. Exp. Bot.* **63**, 695–709 (2012).
10. Bruno, L. *et al.* In *Arabidopsis thaliana* cadmium impact on the growth of primary root by altering SCR expression and auxin-cytokinin cross-talk. *Front. Plant Sci.* **8**, 1323 (2017).
11. Boyes, D. C. *et al.* Growth stage-based phenotypic analysis of Arabidopsis: A model for high throughput functional genomics in plants. *Plant Cell* **13**, 1499–1510 (2001).
12. Yamamuro, C., Zhu, J.-K. & Yang, Z. Epigenetic modifications and plant hormone action. *Mol. Plant* **9**, 57–70 (2016).
13. Jiang, Z., Li, J. & Qu, L.J. Auxins in *Hormone Metabolism and Signaling in Plants* (eds. Li, J., Li, C., Smith, S.M.) 39–76 (Academic Press, 2017). https://doi.org/10.1016/B978-0-12-811562-6.00002-5.
14. Ren, H. & Gray, W. M. M. SAUR proteins as effectors of hormonal and environmental signals in plant growth. *Mol. Plant* **8**, 1153–1164 (2015).
15. Brumos, J., Alonso, J. M. & Stepanova, A. N. Genetic aspects of auxin biosynthesis and its regulation. *Physiol. Plant.* **151**, 3–12 (2013).
16. Feng, J., Shi, Y., Yang, S. & Zuo, J. Cytokinins in *Hormone Metabolism and Signaling in Plants* (eds. Li, J., Li, C., Smith, S.M.) 77–106 (Academic Press, 2017). https://doi.org/10.1016/B978-0-12-811562-6.00003-7.
17. Hwang, I. & Sheen, J. Two-component circuitry in Arabidopsis cytokinin signal transduction. *Nature* **413**, 383 (2001).
18. Imamura, A., Yoshino, Y. & Mizuno, T. Cellular localization of the signaling components of Arabidopsis His-to-Asp phosphorelay. *Biosci. Biotechnol. Biochem.* **65**, 2113–2117 (2001).
19. Gao, X., Zhang, Y., He, Z. & Fu, X. Gibberellins in *Hormone Metabolism and Signaling in Plants* (eds. Li, J., Li, C., Smith, S.M.) 107–160 (Academic Press, 2017). https://doi.org/10.1016/B978-0-12-811562-6.00004-9.
20. Yoshida, H. & Ueguchi-Tanaka, M. DELLA and SCL3 balance gibberellin feedback regulation by utilizing INDETERMINATE DOMAIN proteins as transcriptional scaffolds. *Plant Signal. Behav.* **9**, e29726 (2014).
21. Chini, A. *et al.* The JAZ family of repressors is the missing link in jasmonate signalling. *Nature* **448**, 666 (2007).
22. Kushiro, T. *et al.* The Arabidopsis cytochrome P450 CYP707A encodes ABA 8′-hydroxylases: Key enzymes in ABA catabolism. *EMBO J.* **23**, 1647–1656 (2004).
23. Park, S.-Y. *et al.* Abscisic acid inhibits type 2C protein phosphatases via the PYR/PYL family of START proteins. *Science (80-.)* **324**, 1068–1071 (2009).
24. Brocard, I. M., Lynch, T. J. & Finkelstein, R. R. Regulation and role of the Arabidopsis abscisic acid-insensitive 5 gene in abscisic acid, sugar, and stress response. *Plant Physiol.* **129**, 1533–1543 (2002).
25. Hua, J. & Meyerowitz, E. M. Ethylene responses are negatively regulated by a receptor gene family in *Arabidopsis thaliana*. *Cell* **94**, 261–271 (1998).
26. Chern, M., Canlas, P. E. & Ronald, P. C. Strong suppression of systemic acquired resistance in Arabidopsis by NRR is dependent on its ability to interact with NPR1and its putative repression domain. *Mol. Plant* **1**, 552–559 (2008).
27. Henderson, I. R. & Jacobsen, S. E. Tandem repeats upstream of the Arabidopsis endogene *SDC* recruit non-CG DNA methylation and initiate siRNA spreading. *Genes Dev.* **22**, 1597–1606 (2008).
28. Davies, P. J. *Plant Hormones: Biosynthesis, Signal Transduction, Action!* (Kluwer Academic, New York, 2004).
29. Fattorini, L. *et al.* Cadmium and arsenic affect quiescent centre formation and maintenance in *Arabidopsis thaliana* post-embryonic roots disrupting auxin biosynthesis and transport. *Environ. Exp. Bot.* **144**, 37–48 (2017).
30. Chmielowska-Bąk, J., Lefèvre, I., Lutts, S. & Deckert, J. Short term signaling responses in roots of young soybean seedlings exposed to cadmium stress. *J. Plant Physiol.* **170**, 1585–1594 (2013).
31. Hu, Y. F. *et al.* Cadmium interferes with maintenance of auxin homeostasis in Arabidopsis seedlings. *J. Plant Physiol.* **170**, 965–975 (2013).
32. Srivastava, R. K., Pandey, P., Rajpoot, R., Rani, A. & Dubey, R. S. Cadmium and lead interactive effects on oxidative stress and antioxidative responses in rice seedlings. *Protoplasma* **251**, 1047–1065 (2014).
33. Forgione, I. *et al.* Hypomethylated drm1 drm2 cmt3 mutant phenotype of *Arabidopsis thaliana* is related to auxin pathway impairment. *Plant Sci.* **280**, 383–396 (2018).
34. Wang, J., Ma, X.-M., Kojima, M., Sakakibara, H. & Hou, B.-K. Glucosyltransferase UGT76C1 finely modulates cytokinin responses via cytokinin N-glucosylation in *Arabidopsis thaliana*. *Plant Physiol. Biochem.* **65**, 9–16 (2013).
35. Veselov, D., Veselov, D., Kudoyarova, G., Symonyan, M. & Veselov, S. Effect of cadmium on ion uptake, transpiration and cytokinin content in wheat seedlings. *Bulg. J. Plant Physiol.* **29**, 353–359 (2003) (**Special Issue**).
36. Piotrowska-Niczyporuk, A., Bajguz, A., Zambrzycka, E. & Godlewska-Żyłkiewicz, B. Phytohormones as regulators of heavy metal biosorption and toxicity in green alga *Chlorella vulgaris* (Chlorophyceae). *Plant Physiol. Biochem.* **52**, 52–65 (2012).
37. Mansour, M. & Kamel, A.-R. Interactive effect of heavy metals and gibberellic acid on mitotic activity and some metabolic changes of *Vicia faba* L. plants. *Cytol. Int. J. Cytol.* **70**, 275–282 (2005).
38. Verma, V., Ravindran, P. & Kumar, P. P. Plant hormone-mediated regulation of stress responses. *BMC Plant Biol.* **16**, 86 (2016).
39. Shu, K., Zhou, W., Chen, F., Luo, X. & Yang, W. Abscisic acid and gibberellins antagonistically mediate plant development and abiotic stress responses. *Front. Plant Sci.* **9**, 416 (2018).
40. Asgher, M., Khan, M. I. R., Anjum, N. A. & Khan, N. A. Minimising toxicity of cadmium in plants-role of plant growth regulators. *Protoplasma* **252**, 399–413 (2015).
41. Maksymiec, W., Wójcik, M. & Krupa, Z. Variation in oxidative stress and photochemical activity in *Arabidopsis thaliana* leaves subjected to cadmium and excess copper in the presence or absence of jasmonate and ascorbate. *Chemosphere* **66**, 421–427 (2007).
42. Soares, A. M. D. S., Souza, T. F. D., Jacinto, T. & Machado, O. L. T. Effect of Methyl Jasmonate on antioxidative enzyme activities and on the contents of ROS and H_2O_2 in *Ricinus communis* leaves. *Braz. J. Plant Physiol.* **22**, 151–158 (2010).
43. Gust, A. A. & Nürnberger, T. A life or death switch. *Nature* **486**, 198 (2012).
44. Rivero, L. *et al.* Handling Arabidopsis plants: Growth, preservation of seeds, transformation, and genetic crosses. *Methods Mol Biol.* **1062**, 3–25 (2014).
45. Murashige, T. & Skoog, F. A revised medium for rapid growth and bio assays with tobacco tissue cultures. *Physiol. Plant.* **15**, 473–497 (1962).
46. Zhao, Q. *et al.* 5-Azacytidine promotes shoot regeneration during Agrobacterium-mediated soybean transformation. *Plant Physiol. Biochem.* **141**, 40–50 (2019).
47. Liu, K. *et al.* Major factors influencing cadmium uptake from the soil into wheat plants. *Ecotoxicol. Environ. Saf.* **113**, 207–213 (2015).
48. Cookson, S. J., Turc, O., Massonnet, C. & Granier, C. Phenotyping the Development of Leaf Area in *Arabidopsis thaliana*. In *Plant Developmental Biology. Methods in Molecular Biology (Methods and Protocols)* Vol. 655 (eds Hennig, L. & Köhler, C.) 89–103 (Humana Press, Totowa, NJ, 2010).
49. Annese, A. *et al.* Whole transcriptome profiling of Late-Onset Alzheimer's Disease patients provides insights into the molecular changes involved in the disease. *Sci. Rep.* **8**, 4282 (2018).
50. Roberts, A., Pimentel, H., Trapnell, C. & Pachter, L. Identification of novel transcripts in annotated genomes using RNA-Seq. *Bioinformatics* **27**, 2325–2329 (2011).

51. Ashburner, *et al.* Gene Ontology: Tool for the unification of biology. *Nat. Genet.* **25**, 25–29 (2000).
52. Shannon, P. *et al.* Cytoscape: A software environment for integrated models of biomolecular interaction networks. *Genome Res.* **13**, 2498–2504 (2003).
53. Bindea, G. *et al.* ClueGO: A Cytoscape plug-in to decipher functionally grouped gene ontology and pathway annotation networks. *Bioinformatics* **25**, 1091–1093 (2009).
54. Kanehisa, M. & Goto, S. KEGG: Kyoto encyclopedia of genes and genomes. *Nucleic Acids Res.* **28**, 27–30 (2000).
55. Joung, J.-G. *et al.* Plant MetGenMAP: An integrative analysis system for plant systems biology. *Plant Physiol.* **151**, 1758–1768 (2009).

Acknowledgements

We acknowledge Maria Greco (Francis Crick Institute, London UK) for her pioneer work on *ddc* response to Cd. This work was supported by grants from the University of Calabria-Italy (ex 60%). Illumina Genome Analyzer IIx (SCS v2.10) platform for this research was supplied by PON Ricerca e Competitività 2007–2013, Sistema Integrato di Laboratori per L'Ambiente – (SILA) PONa300341, Piattaforma Omica.

Author contributions

M.P., L.B., A.C., M.B.B. designed research; M.P., A.M., L.B., L.M., E.T. performed research; M.P., E.P. performed bioinformatic analysis; M.P., A.M., L.B., A.C., L.M., P.P., M.B.B. analysed data and discussed results; L.B., M.B.B. supervised the research; M.P. and M.B.B. wrote the paper. All authors contributed to improving the paper and approved the final manuscript.

Competing interests

The authors declare no competing interests.

Additional information

Supplementary Information The online version contains supplementary material available at https://doi.org/10.1038/s41598-021-90528-5.

Correspondence and requests for materials should be addressed to L.B.

Reprints and permissions information is available at www.nature.com/reprints.

Publisher's note Springer Nature remains neutral with regard to jurisdictional claims in published maps and institutional affiliations.

International Journal of
Molecular Sciences

MDPI

Article

Coumarin Interferes with Polar Auxin Transport Altering Microtubule Cortical Array Organization in *Arabidopsis thaliana* (L.) Heynh. Root Apical Meristem

Leonardo Bruno [1,*], Emanuela Talarico [1], Luz Cabeiras-Freijanes [2,3], Maria Letizia Madeo [1], Antonella Muto [1], Marco Minervino [1], Luigi Lucini [4], Begoña Miras-Moreno [4], Adriano Sofo [5] and Fabrizio Araniti [6,*]

1 Dipartimento di Biologia, Ecologia e Scienza della Terra, Università della Calabria (DiBEST-UNICAL), 87036 Arcavacata di Rende, Italy; emanuela.talarico@unical.it (E.T.); marialetizia.madeo@unical.it (M.L.M.); antonella.muto@unical.it (A.M.); marco.minervino@unical.it (M.M.)
2 Department of Plant Biology and Soil Science, Campus Lagoas-Marcosende, University of Vigo, 36310 Vigo, Spain; lcabeiras@uvigo.es
3 CITACA, Agri-Food Research and Transfer Cluster, Campus da Auga, University of Vigo, 32004 Ourense, Spain
4 Department for Sustainable Food Process, Università Cattolica del Sacro Cuore, Via Emilia Parmense 84, 29122 Piacenza, Italy; luigi.lucini@unicatt.it (L.L.); mariabegona.mirasmoreno@unicatt.it (B.M.-M.)
5 Department of European and Mediterranean Cultures: Architecture, Environment, and Cultural Heritage (DICEM), University of Basilicata, 75100 Matera, Italy; adriano.sofo@unibas.it
6 Dipartimento di Scienze Agrarie e Ambientali—Produzione, Territorio, Agroenergia, Università Statale di Milano, Via Celoria n°2, 20133 Milano, Italy
* Correspondence: leonardo.bruno@unical.it (L.B.); fabrizio.araniti@unimi.it (F.A.)

Abstract: Coumarin is a phytotoxic natural compound able to affect plant growth and development. Previous studies have demonstrated that this molecule at low concentrations (100 µM) can reduce primary root growth and stimulate lateral root formation, suggesting an auxin-like activity. In the present study, we evaluated coumarin's effects (used at lateral root-stimulating concentrations) on the root apical meristem and polar auxin transport to identify its potential mode of action through a confocal microscopy approach. To achieve this goal, we used several *Arabidopsis thaliana* GFP transgenic lines (for polar auxin transport evaluation), immunolabeling techniques (for imaging cortical microtubules), and GC-MS analysis (for auxin quantification). The results highlighted that coumarin induced cyclin B accumulation, which altered the microtubule cortical array organization and, consequently, the root apical meristem architecture. Such alterations reduced the basipetal transport of auxin to the apical root apical meristem, inducing its accumulation in the maturation zone and stimulating lateral root formation.

Keywords: specialized metabolite; phytotoxic; lateral roots; root apical meristem; root swelling; cortical microtubules

check for updates

Citation: Bruno, L.; Talarico, E.; Cabeiras-Freijanes, L.; Madeo, M.L.; Muto, A.; Minervino, M.; Lucini, L.; Miras-Moreno, B.; Sofo, A.; Araniti, F. Coumarin Interferes with Polar Auxin Transport Altering Microtubule Cortical Array Organization in *Arabidopsis thaliana* (L.) Heynh. Root Apical Meristem. *Int. J. Mol. Sci.* **2021**, *22*, 7305. https://doi.org/10.3390/ijms22147305

Academic Editor: Toshio Morikawa

Received: 13 June 2021
Accepted: 5 July 2021
Published: 7 July 2021

Publisher's Note: MDPI stays neutral with regard to jurisdictional claims in published maps and institutional affiliations.

1. Introduction

Because of sessile conditions, plants have evolved marked metabolic plasticity to increase their defense and competitive abilities. They have developed different biochemical pathways involved in the biosynthesis of a plethora of specialized metabolites to counteract the challenges arising during their growth and development [1]. These small molecules, characterized by an overwhelming structural diversity, a robust taxonomic restriction, and specificity within species, play a pivotal role in plant survival and adaptation to the environment. Plants could use them for a wide range of functions such as communication, reproductive purposes, nutrient acquisition, and trophic interactions [2,3]. For most known secondary metabolites, their specific ecological role, their involvement in physiological processes, and their mode of action have not yet been established [4].

The plant–plant interaction mediated by specialized metabolites is known as allelobiosis (positive interaction) and allelopathy (negative interaction), and the molecules at the basis of these interactions are known as allelochemicals. This ecological phenomenon plays an essential role in plant adaptation and competitive ability in the ecosystem, allowing plants to positively or negatively affect neighbouring species' growth and development [5].

Some allelochemicals used by plants as a chemical weapon to increase their competitive abilities could represent promising alternatives for producing new potential ecofriendly herbicides [6]. Moreover, they could positively/negatively affect the growth and development of sensitive species interfering with several biochemical and physiological aspects shaping their morphology [7].

Coumarins constitute a widely studied class of allelochemicals produced through the phenylpropanoid pathway via o-hydroxycinnamic acid lactonization [8,9]. They are present in almost all higher plants and microorganisms and are actively released into the environment through root exudation or dead plant tissue decay [10,11]. These specialized metabolites are involved in several ecological roles, such as the modulation of dynamical processes of species coexistence in plant communities [12], Fe acquisition and assimilation through root hair exudation and re-absorption [13–16], and the shaping of root microbiome composition [17].

The simplest compound belonging to this chemical class is 1,2-benzopyrone, also known as coumarin, mostly known for its phytotoxicity and potential hormone-like activity [18,19]. One of the first hypotheses suggesting an auxin-like effect of coumarin was proposed by Neumann [20]. He demonstrated that this specialized metabolite stimulated the elongation of *Helianthus* hypocotyls' excised segments, suggesting that its action was comparable to auxin. This hypothesis was further supported by Jansson and Svensson [21], who observed that coumarin alone causes an increase in fresh weight mainly by stimulating large numbers of roots and increasing soybean biomass. Abenavoli et al. [19], studying the effects of coumarin on the root morphology of *Arabidopsis thaliana*, observed that low concentrations ($\simeq$100 µM) of this molecule reduced primary root growth and stimulated the lateral root number parameter. Those findings strongly supported the hypothesis that coumarin could exert an auxin-like activity or interact with auxin distribution within the root. Successively, Lupini et al. [22], using several transgenic lines of *Arabidopsis thaliana* (defective in influx and efflux carriers), demonstrated that the efflux carrier PIN2 and the influx carrier AUX1 could be involved in coumarin-induced root branching, suggesting that auxin redistribution might be directly or indirectly affected by this molecule.

However, the exact mechanism of coumarin on root growth has not been clarified yet. A complex molecular signalling network probably governs coumarin's morpho-physiological responses, where auxin transport and/or biosynthesis could play an important role. In fact, auxin is considered the leading candidate in controlling the stress-induced morphogenic response inducing the inhibition of root elongation, enhancing lateral roots formation and stimulating the production of adventitious roots under stressful environmental conditions [23,24]. Its polar transport plays a central role in organ development and elongation, in shoot/root branching and plastic growth responses [25], in lateral root initiation [26,27], in lateral root primordial formation [28], and in emergence [29]. Transported via influx and efflux proteins in a polarized stream, auxin action depends on its differential distribution along with tissues [28,30], and it is known that its fluxes are driven by an interplay between cell wall structure and the dynamics of microtubule and actin filaments [31]. Moreover, it has been demonstrated that intact microtubules are required for polar auxin trafficking [32].

Recently, it has been demonstrated that several natural compounds exert their biological activity interfering with auxin distribution along the root and its biosynthesis [33–40]. Moreover, it has been proven that compounds such as citral, farnesene, norharmane, weisiensin B, and narciclasine strongly affect the microtubule organization, altering the root ultrastructure of the *Arabidosis* root, as well as its isotropic growth [33,36,37,41,42]. As two of the main effects exerted by coumarin are lateral roots formation and root tip

swelling (a phenomenon observed with several microtubule interferents) [43], and the maintenance of auxin fluxes is known to depend on the interaction between cytoskeleton and PINs proteins [31], we hypothesized that the main coumarin effects could be related to microtubule alteration, followed by an alteration in PIN distribution. Therefore, using sub-lethal doses of coumarin, we decided to investigate coumarin's effects on the primary root tip anatomy, microtubule organization, and polar auxin transport, trying to deepen our knowledge on the potential mode of action of this specialized metabolite.

2. Results

2.1. Effects of Coumarin on RAM

Seven days of coumarin treatment significantly altered the RAM of *Arabidosis* (Figures 1 and 2). In particular, coumarin-treated roots were characterized by a reduction in MCN (46% lower than that in control) (Figure 2a), accompanied by a decrease in MZL (44%) (Figure 2b) and an increase in MZW (1.2-fold higher than that in control) (Figure 2c). In coumarin-treated seedlings, these data suggest the advancement of the transition zone and a premature exit of cells from the meristematic area (Figures 1 and 2).

The advancement of the transition zone in coumarin-treated roots was accompanied by an abnormal shape and asymmetric organization of protodermis and precortex cells characterized by a swollen and abnormal shape (Figure 1a–d). Therefore, we decided to quantify these alterations by measuring protodermis, precortex, proendodermis, and procambium cells at the first elongated precortex cell level.

In coumarin-treated seedlings, the protodermis, precortex, and proendodermis cells' length and width were significantly increased by the treatment (Figures 1 and 2d,e). On the contrary, the length (34%) and width (16%) of procambium cells were significantly reduced and increased, respectively (Figure 2d,e). On the contrary, the number of cell files forming the procambium was significantly higher (40%) than that in control (Figure 2h). Besides, a substantial alteration at the columella level was also observed. The columella of the *Arabidosis*-treated roots was characterized, compared to the control, by a reduction in CL (28%) and an increase in CW (18%) (Figure 2f). In addition, the number of statoliths was significantly reduced by the treatment (60% lower than that of the control) (Figure 2g), but no changes in columella stem cell layers were observed (data not shown). Other significant alterations in treated roots, such as incomplete cell division, fused lateral roots, high production of root hairs close to the meristem, and a high production of adventitious root primordia, were observed (Figure S1a–d).

Concerning cortical microtubule immunolabeling, in control roots, microtubules were well-defined and typically arranged, parallel to the transverse axis of the cells, and uniform in density (Figure 3a,c). On the contrary, in treated roots, they were erratically arranged with evident loss of symmetry, reduced density, and microtubule strands thicker than those of the control (Figure 3b,d).

Finally, the alterations observed on colchicine-treated roots are similar to those of seedlings treated with coumarin, confirming its potential effect as a microtubule effector (Figure S2).

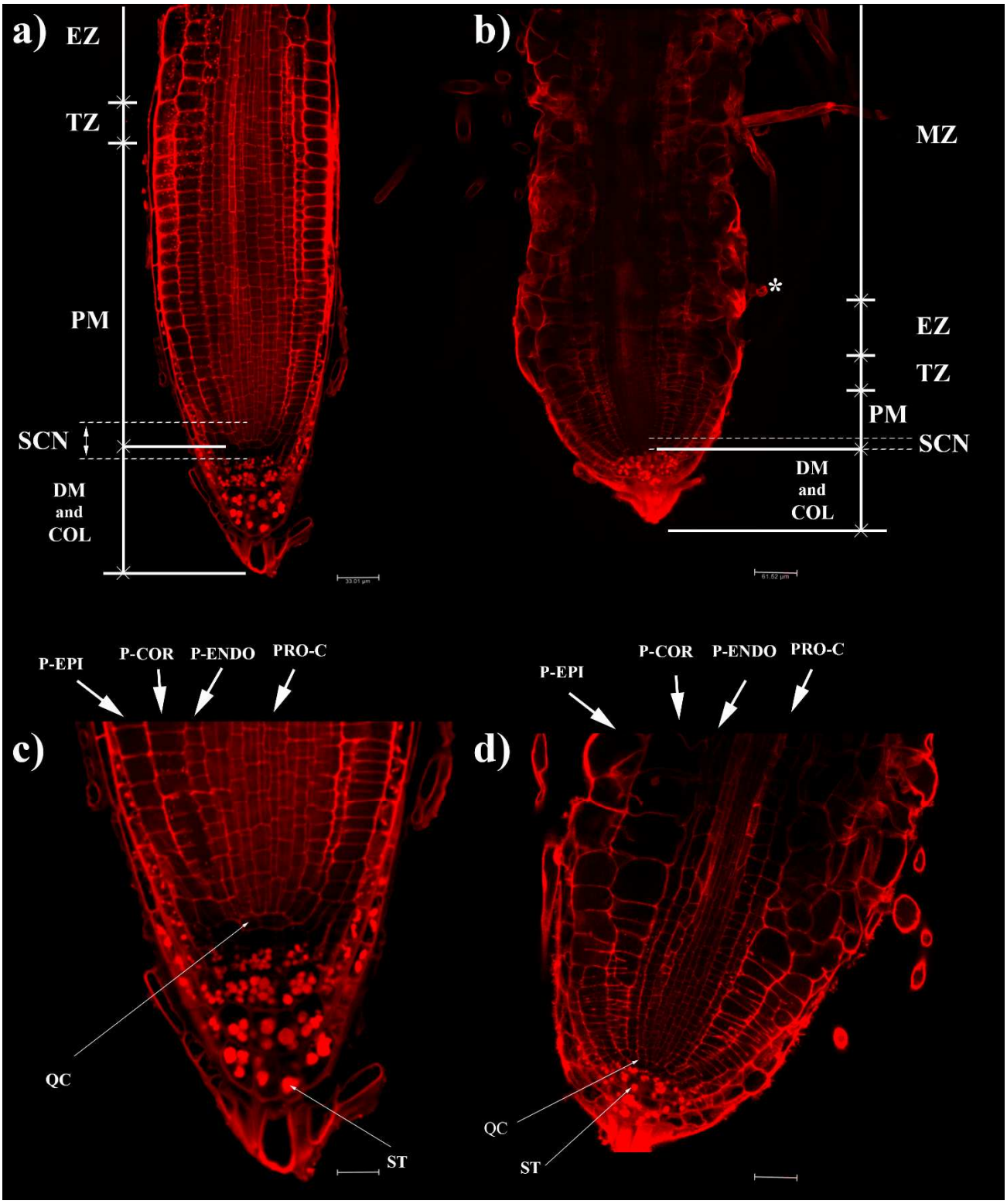

Figure 1. (**a**–**d**) Confocal laser microscope images of primary root tip, stained with propidium iodide, in 4 days old seedlings of *A. thaliana* treated for 7 days with coumarin 0 (**a**,**c**) and 100 µM (**b**,**d**). (**c**,**d**) Higher magnification of (**a**,**b**), respectively. *Arabidosis* RAM developmental zones: meristematic zone (MZ), the transition zone (TZ), and the elongation zone (EZ). The meristematic zone is divided into the distal meristem (DM) and the proximal meristem (PM). Moreover, in RAM, the stem cell niche (SCN) could be observed, as well as the quiescent center (QC), statoliths (ST), protodermis (P-EPI), precortex (P-COR), proendodermis (P-ENDO), and procambium (PRO-C); * first visible root hair. Scale bars: (**a**) 33.01; (**b**) 61.52; (**c**) 66.02; (**d**) 123.04 µm. N = 20.

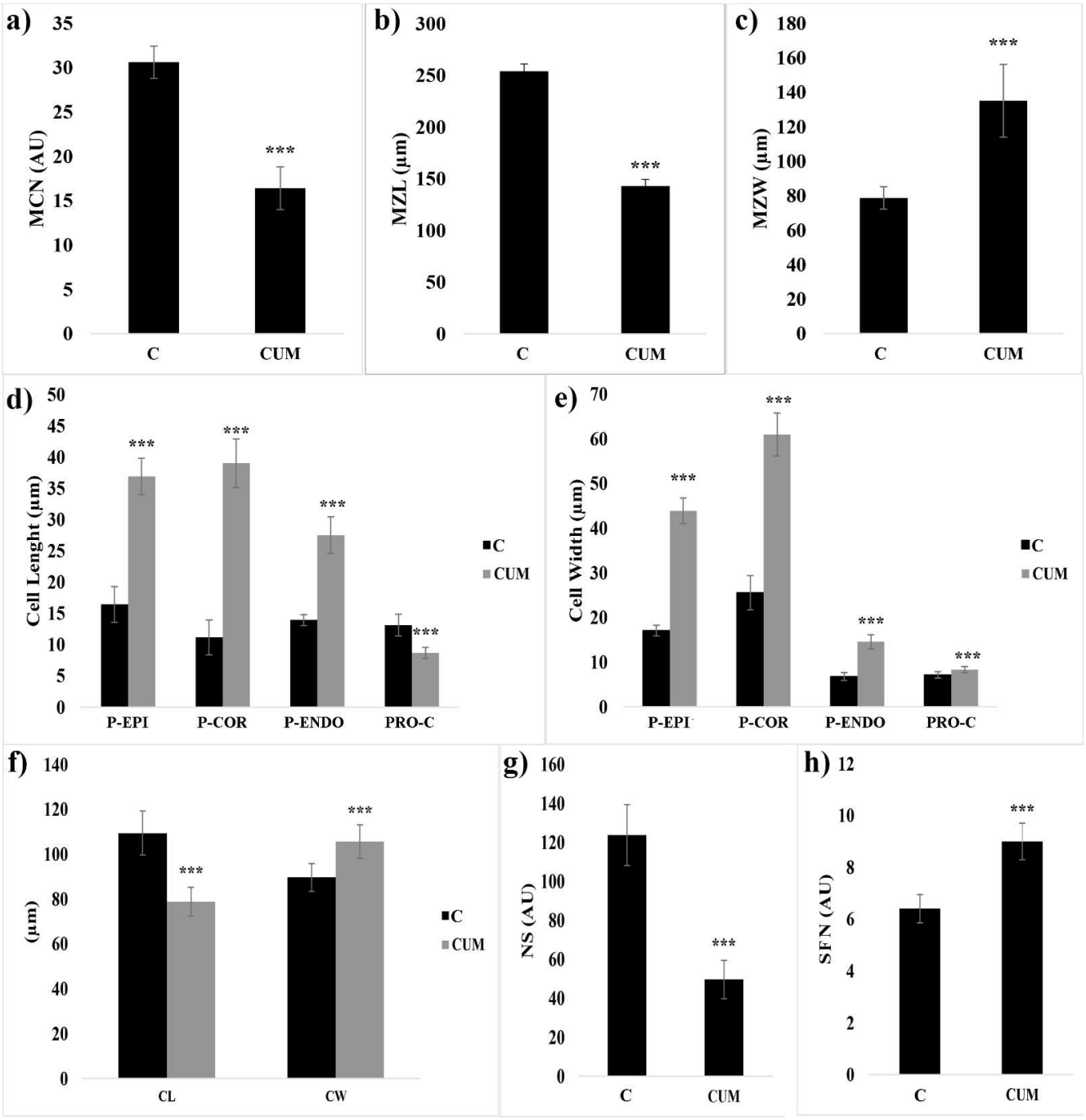

Figure 2. RAM morphology of 4 days old *Arabidosis* seedlings treated for 7 days with coumarin 0 (C) or 100 (CUM) µM. (**a**) MCM—meristem cell number; (**b**) MZL—meristem zone length; (**c**) MZW—meristem zone width; (**d**) cell length; (**e**) cell width; (**f**) CL—columella length; CW—columella width; (**g**) NS—number of statoliths; (**h**) SFN—procambium files number. Protodermis (P-EPI); precortex (P-COR); proendodermis (P-ENDO); procambium (PRO-C). Data are presented as mean ± standard deviation (SD). Statistical analysis was performed using the Student's *t*-test with *** $p \leq 0.001$. N = 20.

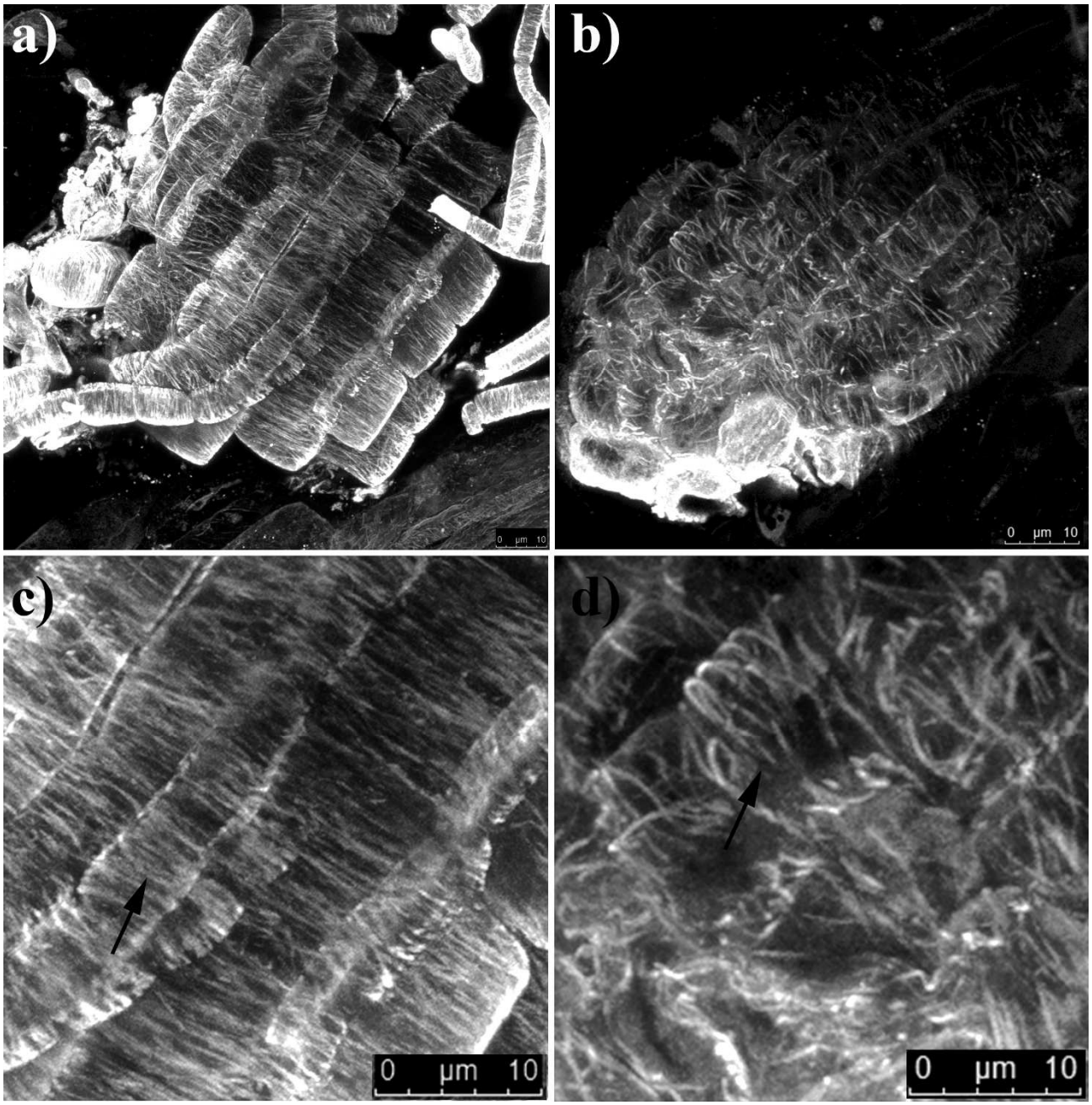

Figure 3. Microtubule immunostaining of 4 days old *Arabidopsis* roots treated for 7 days with coumarin. (**a**) Control cells (0 µM); (**b**) coumarin-treated cells (100 µM); (**c**,**d**) zoomed-in view of a specific area of the images of (**a**,**b**), respectively, to make coumarin-induced microtubule alterations clearly visible. Black arrows (in (**c**,**d**)) indicate parallel, dense, and well-organized microtubules in the control cells and disorganized and lax microtubules in coumarin-treated cells. Scale bars (images **a**,**b**): 10 µm. N = 20.

2.2. Effects of Coumarin on Cell Division

Given that root-meristem size is determined by both the rate of cell differentiation and cell division rate [44–46], to assess whether a reduction in cell division could also cause the decline in RAM size, we analyzed either the mitotic index or cyclin B's turnover, which is an essential protein expressed during the G2 phase of the cell cycle, which is degraded during mitosis [47,48].

The results reported highlighted a substantial reduction in dividing cells (55% lower than that of the control) (Figure 4a). The confocal microscopic analysis revealed that

untreated *Arabidosis* seedlings showed a GFP-fusion cyclin B1;1 signal in some RAM cells (Figure 4b). In contrast, both the percentage of GFP-labeled cells and the relative intensity of the fluorescent signal slightly increased in roots treated with 100 µM of coumarin (Figure 4c). Those results suggest a disturbance in cyclin B's degradation, resulting in abnormal mitosis in the RAM.

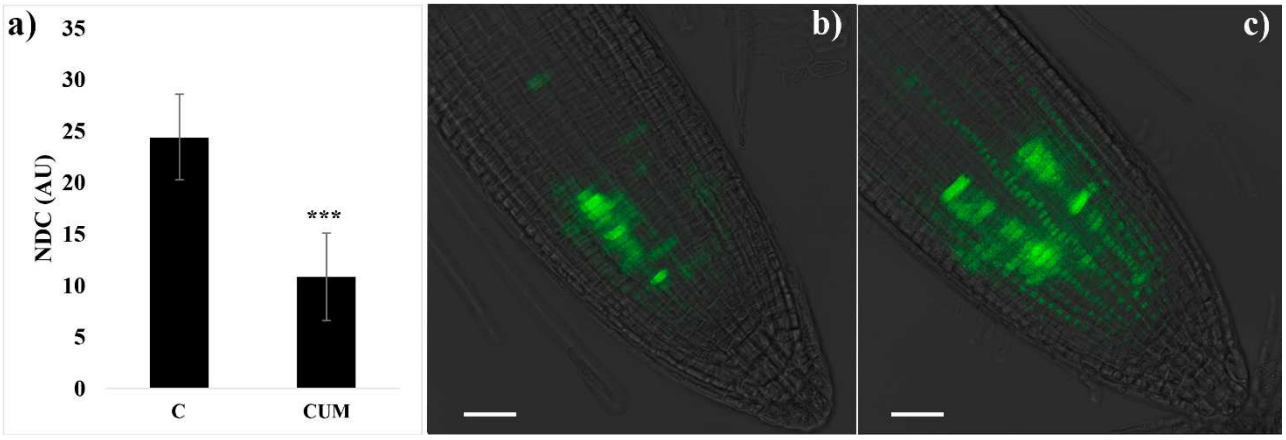

Figure 4. Effects of coumarin 0 (C) or 100 (CUM) µM on cell division in 4 days old *Arabidopsis thaliana* RAM. (**a**) Mitotic index expressed as the number of dividing cells (NDC). Data are presented as mean ± standard deviation (SD). Statistical analysis was performed using the Student's *t*-test with *** $p \leq 0.001$. N = 20. (**b**,**c**) Confocal microscopy imaging of *Arabidosis* transgenic line *cyclin B1;1::GFP* in control (**b**) and treated (**c**) RAM. Scalebar 50 µm.

2.3. Effects of Coumarin on Auxin Content and Polar Transport

Previous research has suggested that the alterations observed on the root morphology of coumarin-treated (100 µM) roots could be mediated by an alteration in the polar auxin transport [22]. Therefore, we decided to quantify the auxin content in the roots of seedlings exposed to coumarin for 48 h and monitor its effects on the principal auxin transporting proteins.

Auxin distribution and quantification were carried out on the full seedlings roots using the auxin-responsive reporter *pDR5::GFP* and through a GC/MS approach. In contrast, coumarin's effects on auxin transporting proteins were evaluated using the previously described GFP transgenic lines (see Materials and Methods).

The monitoring of the auxin-responsive reporter *pDR5::GFP* revealed that the 48 h coumarin treatment impaired auxin distribution. Indeed, in control roots, the *pDR5*-dependent GFP distribution reflected the typical auxin maximum distribution in the root tip (i.e., QC, initial and mature columella cells) and procambium cells (Figure 5). In coumarin-treated roots, a significant weak decrease (7%) in GFP signal intensity was observed in the root tip (Figure 5a,b,e). On the contrary, in the procambium at the MZ level, an increase in GFP intensity (73% higher than that in the control) was observed (Figure 5c–e). Besides, an accumulation of GFP fluorescence (higher than that in control roots (Figure 5c) was observed locally in the elongation zone and along the entire root until the root and stem boundary, suggesting auxin accumulation (Figure 5d).

To verify the effects of long coumarin exposure on DR5 signal, we also carried out experiments on plants treated for 7 days, which confirmed a substantial impairment in GFP signal intensity (Figure S3a,b). In the columella of the coumarin-treated root, the GFP was widespread, whereas in the procambium we observed a signal higher than that in control, confirming what was observed after 48 h of treatment (Figure S3b).

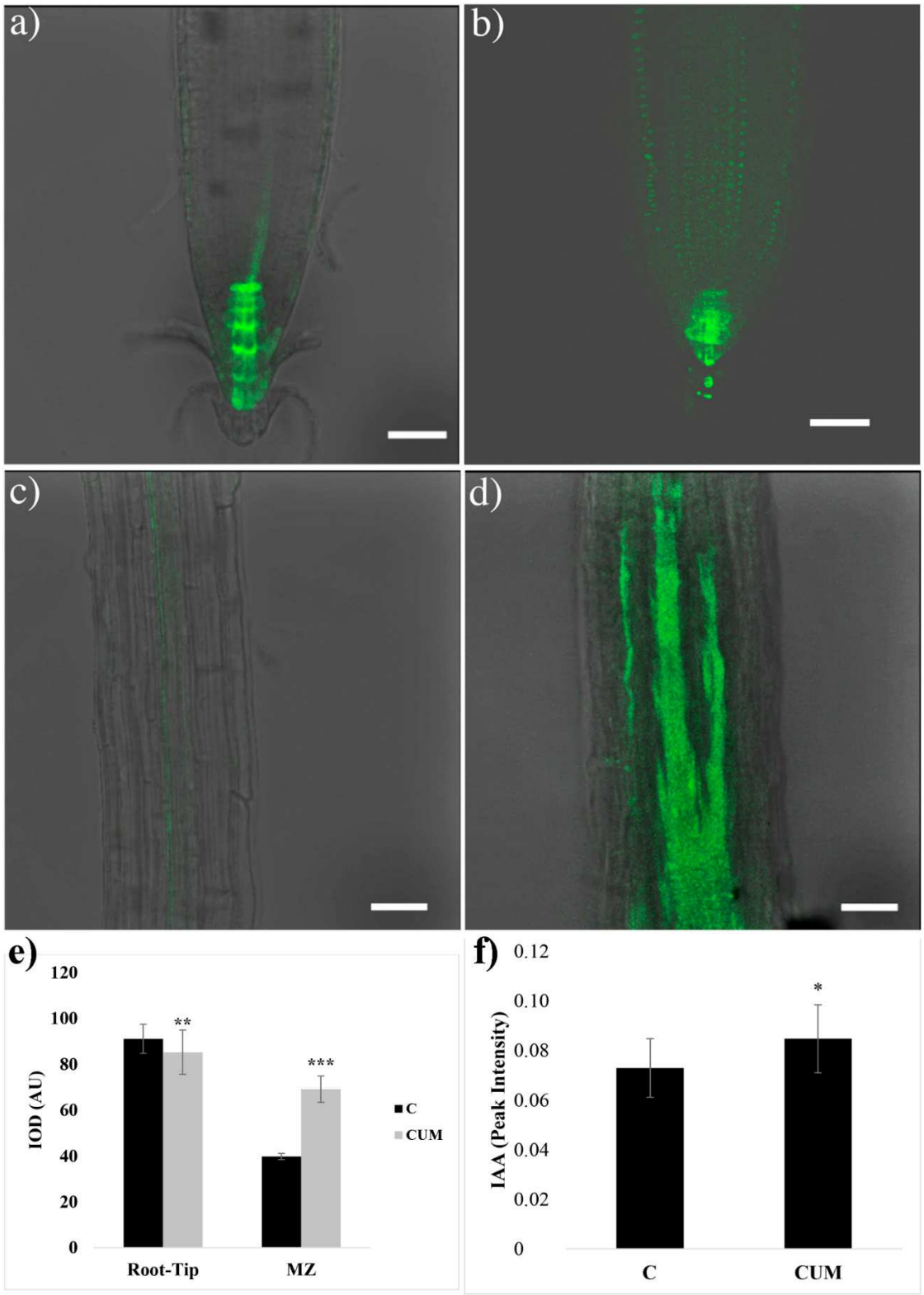

Figure 5. Fluorescence detection in 4 days old *A. thaliana pDR5::GFP* transgenic line (auxin responsive reporter) grown for 48 h in untreated agar medium ((**a**) (RAM) and (**c**) (elongation zone)) or 100 µM of coumarin enriched agar medium ((**b**) (RAM) and (**d**) (elongation zone)). Scale bars 34 µm. N = 20. (**e**) Integrated optical density (IOD) expressed as arbitrary units (AU) of fluorescence intensity measured in the root tip and the MZ (maturation zone) of *Arabidosis* treated for 48 h with 0 or 100 µM of coumarin (N = 10); (**f**) auxin content in *Arabidosis* roots treated for 48 h with coumarin 0 (C) or 100 (CUM) µM. Data are presented as mean ± standard deviation (SD). Statistical analysis was performed using the Student's *t*-test with * $p \leq 0.05$, ** $p \leq 0.01$, *** $p \leq 0.001$. N = 4.

Finally, the GC/MS auxin quantification pointed out, in 48 h coumarin-treated roots, an auxin accumulation (16%) higher than that in control (Figure 5f).

Based on these observations, *PINs::PINs-GFP* (auxin efflux carriers) transgenic lines were used to monitor the location of the auxin transporters in coumarin-treated and untreated root tips (Figure 6a–j). Interestingly, the distribution pattern of three PIN proteins appeared strongly affected by coumarin treatment, showing an altered distribution, as well as a reduction in their presence.

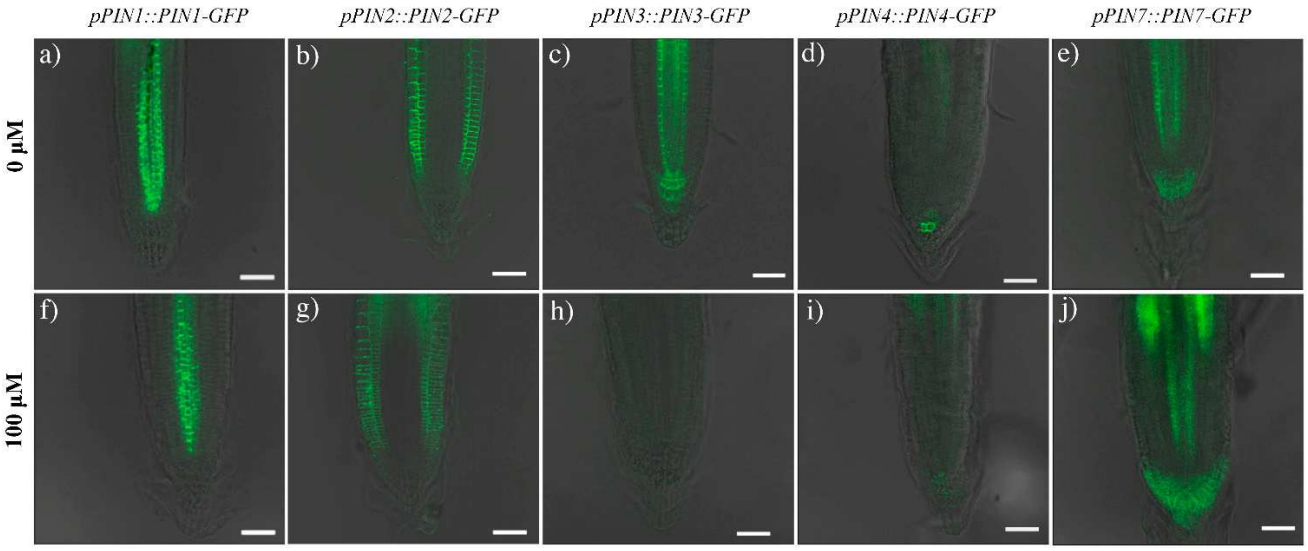

Figure 6. Images of the RAM in 4 days old seedlings of *A. thaliana* transgenic lines (*pPIN1::PIN1-GFP* (**a**,**f**), *pPIN2::PIN2-GFP* (**b**,**g**), *pPIN3::PIN3-GFP* (**c**,**h**), *pPIN4::PIN4-GFP* (**d**,**i**), *pPIN7::PIN7-GFP* (**e**,**j**)) treated for 48 h with coumarin 0 (**a**–**e**) or 100 µM (**f**–**j**). Scale bars 30 µm. N = 20.

In untreated roots, PINs proteins were characterized by a classical presence and distribution. As detailed in the bibliography [28], PIN1 is mainly situated at the basal end of provascular stelar and proendodermal cells (Figure 6a). PIN2 is localized basally in the procambium cells, the protodermal cells' apical side, and the lateral root cap (Figure 6b). PIN3 is expressed in the columella, at the basal side of vasculature cells, and at the lateral side of the pericycle cells of the elongation zone (Figure 6c). PIN4 is localized in the stem cell niche and basally in provascular cells (Figure 6d). Finally, PIN7 resides at the lateral and basal membranes of provascular cells in the meristem and elongation zone (Figure 6e). In contrast, in columella' cells, it coincides with the PIN3 domain [49] (Figure 6c,e). In plants treated with coumarin, no significant differences were observed in the PIN1 and PIN2 distribution along the RAM after 48 h of coumarin treatment. The GFP intensity was reduced by 16% and 32%, respectively (Figures 6a,b,f,g and 7). The GFP fluorescence in PIN3 (IOD 81% lower than that in control) and PIN4 (IOD 72% lower than that in control) was absent (Figures 6c,d,h,i and 7), whereas in PIN7, the GFP signal was highly intense in the basal side of the procambium cells and widespread in columella's cells (Figure 6e,j), pointing out an increase in IOD that was 23% higher than that in control (Figure 7).

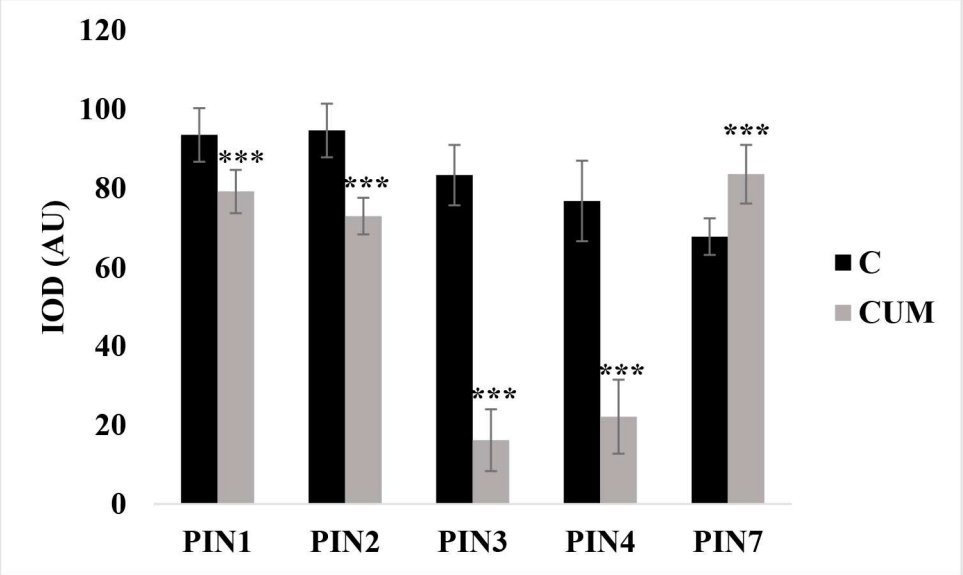

Figure 7. Integrated optical density (IOD) of PINs proteins expressed as arbitrary units (AU) of fluorescence intensity measured on the entire RAM of *Arabidosis* treated for 48 h with coumarin 0 (C) or 100 (CUM) µM. Data are presented as mean ± standard deviation (SD). Statistical analysis was performed using the Student's *t*-test with *** $p \leq 0.001$. N = 10.

3. Discussion

In recent years, to reveal the effects of natural compounds on phytohormone pathways and their interference on plant growth and development, the model plant *A. thaliana* and its various mutants and transgenic lines have been widely employed.

In the present study, we evaluated coumarin's effects on auxin biosynthesis and distribution by testing its effects on the root development of WT *Arabidosis* seedlings. Moreover, we assessed this molecule's possible interaction with microtubule organization and its potential impact on auxin transport.

Coumarin's phytotoxicity and its ability to alter both root anatomy and morphology have been primarily documented [12,50]. Previous studies have demonstrated that this molecule is a potent inhibitor of germination and seedling growth and development [51,52]. On the contrary, at relatively low concentrations (100 µM), it significantly stimulates lateral root and root hair production, whereas the total root length is significantly reduced [22]. Similar effects (reduction in primary root growth, increase in lateral root number, and root hair density) have generally been observed on *Arabidosis* seedlings treated with exogenous auxins such as IAA, 2,4-D, and NAA [53]. Due to that, it has been widely speculated that coumarin at low concentrations could exert an auxin-like effect [18,20], and recent studies have reported that coumarin's effects are probably due to an alteration in the polar auxin transport [22]. In particular, Lupini et al. [22], using several auxin influxes and efflux mutants (*aux1-22*, *lax3*, *pin1*, *eir1-4*, and *pin3-5*), hypothesized that coumarin treatment (100 µM) could modulate root development interacting with the polar auxin transport. However, no further studies have been carried out to explore this potential mode of action in depth.

In this study, we demonstrated that coumarin's effect is anything but an effect similar to auxin. The alterations induced by this molecule are, according to our data, a substantial alteration in the root tips cortical microtubule organization accompanied by an alteration in cell division and auxin transport, synthesis, and its *PINs*-mediated distribution.

Coumarin treatments induced a reduction in cell division and alteration in RAM organization. The RAM of treated plants was characterized by swollen protodermal and procambium cells, which expanded radially more than longitudinally. Moreover, a reduction in the RAM (formed by a lower number of cells than that in control) and an increase in its width were observed, suggesting an advancement of transition and

differentiation zones. The reduction in meristem size is commonly observed in plants treated with natural products, heavy metals, and xenobiotics [40,54]. For example, a reduction in RAM size was observed in *Arabidosis* seedlings treated with brassinolide, farnesene, and narciclasine [40,44,55]. Besides, in plants treated with cadmium, early differentiation of meristematic cells was induced by a premature cell cycle exit from the meristematic zone [50].

In coumarin-treated seedlings, the reduction in meristem size was accompanied by an accumulation of CYCLIN B1;1, suggesting that coumarin could have affected the meristematic activity, resulting in the loss of cell division potential in the root. Previous studies have demonstrated that coumarin negatively affects mitosis in almost all phases, inducing chromosomal aberrations, binucleated cells, incomplete phragmoplasts, and DNA damages [56,57]. Culligan et al. [58] reported that DNA damaging agents could induce, as also observed in our experiments, the accumulation of CYCLIN B1;1, as well as root swelling. Moreover, Wu et al. [59], using the *Arabidosis* mutant *radially swollen 4* (*RSW4*) (a mutant with swollen root due to microtubule disorganization), suggested that CYCLIN B1;1 accumulates in response to DNA damages [60] or DNA damaging agents [58,61]. Besides, they observed that the superabundant cyclin is associated with altered root histology and root swelling mediated by microtubule disorganization. The hypothesis that CYCLIN B1;1 accumulation could induce an alteration in the microtubule cortical array organization was further confirmed by Weingartner et al. [62] in transgenic tobacco expressing a nondegradable version of CYCLIN B1;1 and by Serralbo et al. [63] using the *hobbit* mutant of *A. thaliana* characterized by a reduced function of the complex responsible for CYCLIN B1;1 degradation. Both mutant and transgenic lines were characterized by microtubule disorganization and swollen cell shape, supporting the idea that CYCLIN B1;1 accumulation disrupts cortical microtubules. Despite the evidence that CYCLIN B1;1 accumulation could alter microtubule organization, the possibility that these effects are directly induced by coumarin and not a consequence of pleiotropic effects at the moment is just speculation, which should be explored in depth.

The swelling phenomenon, generally accompanied by a reduction in RAM length, has mainly been observed in plants treated with microtubule interferents (stabilizers and destabilizers) such as colchicine, taxol, and oryzalin [64,65]. In particular, colchicine interferes with microtubule dynamics, blocking polymerization at the end of the mitotic spindle, leading to metaphase arrest [66]. In contrast, oryzalin binds to plant tubulin, preventing its polymerization and making extant microtubules more likely to depolymerize [64,67,68]. The effects of both molecules on root tip anatomy are similar to the effects induced by coumarin. The images of *Arabidosis* root tips presented by Baskin et al. [65] perfectly overlap with the effects observed in coumarin-treated plants. Those results suggest that coumarin might interact with the organization of microtubule arrays. The hypothesis was further confirmed by the immunolabeling bioassay, where microtubules of treated plants appeared fragmented and erratically arranged.

As the reduction in cell division and primary root growth, the increment in lateral root number, and the increase in root hair length and density are typical effects of plants treated with auxin and auxinic herbicides [69–71], we decided to investigate the effects of coumarin on both auxin content and transport. Moreover, Li et al. [72], using the hydroxycoumarin 4-methyl-umbelliferone, observed an auxin accumulation in *Arabidosis*-treated root that mediated F-actin disruption and, as a consequence, malformation of the RAM. Furthermore, it is known that auxin plays a pivotal role in the maintenance of root distal stem cell identity, and alterations in its balance could result in the loss of the QC identity, as well as an alteration in the cellular organization of the RAM in *Arabidosis* [73]. The GC-MS-driven relative quantification of auxin content pointed out a slight increase in this plant hormone in treated roots. This increase could justify the previously reported coumarin-induced stimulation of peroxidase and IAA-oxidase activity (enzymes involved in IAA catabolism) [74]. As well as coumarin, scopoletin (a natural coumarin with auxin-like activity and a chemical structure remarkably similar to the simple coumarin [7] at low concentrations inhibited

auxin's catabolism, causing its accumulation [75]. Simultaneously, as coumarin, it has been proven that the same molecule stimulated IAA oxidase activity [75]. Both molecules probably promote auxin accumulation, which activates IAA-oxidase activity to restore its concentration to physiological levels.

The auxin gene reporter *DR5::GFP* further suggested that coumarin also induced an alteration in its distribution as, in treated plants, a high *GFP* signal was observed in the elongation and maturation zone, as well as a weak reduction in the RAM. Casimiro et al. [76] demonstrated that auxin accumulation in the maturation zone is pivotal for lateral root production. They showed that the acropetal polar transport inhibitor NPA (N-1-naphthylphthalamic acid) induced IAA accumulation in the root apex and its reduction in basal tissues critical for lateral root initiation. They concluded that both root and shoot and root acropetal and basipetal auxin transport activities are required during the initiation and emergence phases of lateral root development. In addition, De Rybel et al. [77], using the synthetic non-auxin probe naxillin, a molecule that stimulates lateral root formation, reported (as also observed in our experiments) that 24 h of treatment with this molecule induced both the synthetic auxin-responsive marker *pDR5::GUS* locally in the maturation zone (specifically in xylem pole cells adjacent to the pericycle) and CYCLIN B1;1. They also demonstrated that the naxillin-auxin accumulation in roots was due to the naxillin-induced conversion of the auxin precursor indole-3-butyric acid into the active auxin indole-3-acetic acid. Besides, it has also been demonstrated that the induction of CYCLIN B1;1 expression coincides with the formation of a new lateral root primordium and, thus, lateral root development [78,79]. These results suggest that coumarin could alter auxin's polar transport and synthesis by inducing auxin accumulation in the elongation and maturation zone of the root, activating the physiological and biochemical mechanisms involved in lateral roots production.

Previous studies focusing on the effects of microtubule de-polymerizing agents demonstrated that these molecules could interfere with auxin polar efflux transporters. In particular, oryzalin visibly interfered with PIN1 (in the procambium) and PIN2 (in young cortex cells), resulting in reduced auxin's polar distribution. These findings indicated that intact microtubules are pivotal for proper auxin polar trafficking in plant cells [32]. In contrast to what was observed with oryzalin, coumarin did not affect the distribution of PIN1 and PIN2, but significantly reduced the protein abundance. On the contrary, it completely suppressed PIN3 and PIN4 protein abundance. Those results suggest that coumarin specifically inhibited the acropetal auxin flux in the procambium, in the columella cells (PIN3), and from the central RAM toward the quiescent center (PIN4). Therefore, auxin procurement to the RAM was only guarded by PIN1 and PIN7, which justifies the presence (even if lower than that in the control) of auxin in the root tip. The alteration in auxin balance observed at the quiescent center level could confirm our hypothesis that coumarin could induce the loss of the root distal stem cell identity and could justify the lack of columella cell expansion, resulting in a reduced columella area in treated roots. Moreover, the alteration in the local auxin maximum/gradient within the RAM, which is generated by the PIN directional auxin transporters, could be the reason for the reduction in statolith observed in coumarin-treated roots. In fact, Zhang et al. [80] demonstrated that auxin regulates the expression of three key starch granule synthesis genes involved in statolith production. Finally, the diffuse GFP signal observed in PIN7 in the elongation zone, as confirmed by the DR5 auxin reporter, suggests auxin accumulation in the elongation zone and particularly in the maturation zone of the root, where lateral root initiation occurs. It is known that auxin regulates root system architecture by promoting the acquisition of founder cell identity in pericycle cells [81,82] and by stimulating LR development [76,83].

4. Materials and Methods

4.1. Reagents Used

All the reagents used in the following experiments (EtOH, NaCLO, MES, Triton X-100, plant agar, propidium iodide, Schiff reagent, among others) were purchased from Sigma Aldrich S.r.l. (Via Monte Rosa, Milano, Italy).

4.2. Plant Material and Growth Conditions

Seeds of *Arabidopsis thaliana* (L.) Heynh. Ecotype Columbia (Col-0) and *pDR5::GFP* [28], *pPIN1::PIN1-GFP* [84], *pPIN2::PIN2-GFP* [49], *pPIN3::PIN3-GFP* [49], *pPIN4::PIN4-GFP* [49], *pPIN7::PIN7-GFP* [49], and *cyclin B1;1::GFP* [85] transgenic lines were used for the experiments. Seed sterilizations, growth conditions, and treatments were carried out as previously described by Lupini et al. [22], with some modifications.

Seeds were surface-sterilized for 3 min in 50% EtOH, and they were then washed for 3 min in a NaOCl solution (0.5%) enriched with Triton X-100 at 0.01%. Finally, sterilized seeds were washed three times in sterilized Milli-Q water and, to break dormancy and synchronize germination, were then maintained in a 0.1% agar solution at 4 °C for 48 h. Twenty-four seeds were then placed in square Petri dishes (100 × 150 mm) containing agarised (0.8% *w*/*v*) basal medium enriched with micro and macronutrients, plus sucrose (0.5% (*w*/*v*)), MES (1 g L^{-1}), pH 5.75 [22].

Petri dishes were placed vertically in a growth chamber at 22 °C, 65% relative humidity, 16 (light)/8 (dark) h photoperiod, and 300 µmol photon flux density m^{-2} s^{-1}. Five 4 days old seedlings (per treatment and replicate), chosen by uniformity were then transplanted for seven days (long-term experiment) or 48 h (short-term experiment) in the agar medium previously described enriched with coumarin 0 (control) and 100 µM of coumarin (treatment).

4.3. Long-Term Experiments

To highlight drastic changes induced by coumarin on the *Arabidosis* root apical meristem (RAM) and cortical microtubule organization, otherwise not visible during short-treatments, 4 days old *Arabidosis* seedlings were treated with coumarin for 7 days.

4.3.1. Root Anatomy: Meristem Size Analysis

For the analysis of the RAM, *A. thaliana* (Col-0) seedlings, for each treatment (coumarin 0 or 100 µM) and replication (N = 20), were fixed, stained with propidium iodide, and imaged by confocal microscopy according to Gonzàlez-Garcìa et al. [86].

At the end of the experiment, the following parameters were evaluated: (i) the number of cells composing the RAM (MCN), calculated counting the number of precortex cells extending from the quiescent center (QC) to the first elongated cortex cell; (ii) Meristem length (MZL), expressed as the distance (µm) from the QC to the first elongated cortex cell; (iii) RAM width (MZW), considered the distance between the two lines of cortex cells; (iv) the length and width of protodermal, precortical, and proendodermal cells; (v) the length (CL) (measured from the QC to the bottom of the columella) and width (CW) (measured at the QC level) of the columella; (vi) the columella (CA) area, considered as the total area of cells presenting statoliths.

A parallel experiment using colchicine (200 µM) was carried out to compare the effects of coumarin with a known microtubule polymerizing agent.

4.3.2. Microtubules Immunolabeling

According to the method of Holzinger et al. [87], the microtubule immunolabeling was carried out with some modifications. After coumarin treatment (0 or 100 µM), *A. thaliana* root tips were excised and fixed at room temperature for 45 min in PEM buffer (50 mM of PIPES, 2 mM of EGTA, 2 mM of $MnSO_4$; pH 7.2) containing 0.5% glutaraldehyde, 1.5% formaldehyde, and 0.1% Triton X-100.

Roots were successively washed for 20 min in the same buffer and then again in PEM buffer. Fixed roots were chopped into small pieces and digested, at room temperature for 30 min, with cellulase and pectolyase Y-23 (1%) solubilized in PEM buffer (pH 5.5). After the digestion step, samples were washed in PEM buffer (pH 7.2) and incubated for 10 min at −20 °C in methanol. The samples were successfully washed with phosphate buffer saline (PBS) (pH 7.4) and incubated for 20 min with 1 mg mL^{-1} of sodium borate in PBS. Samples were then further washed with PBS and incubated with 1% bovine serum albumin and 50 mM of glycine in PBS. After a final washing in PBS, the samples were incubated overnight with the primary antibody (anti-α tubulin B 5-1-2, Sigma-Aldrich, 1:1000 in PBS) at 4 °C, which was removed by three consecutive washes in PBS. The samples were then incubated with the secondary antibody (Alexa 488-conjugated goat anti-mouse IgG, Sigma-Aldrich, 1:200 in PBS) at 37 °C for 3 h. Besides, negative controls were performed alternately using the primary and secondary antibodies alone (data not shown).

Finally, immunolabelled roots were mounted in the Citifluor AF1 antifade agent to avoid fluorescence degradation. Visualization of the microtubules was performed using a Leica TCS SP5 confocal microscope (Wetzlar, Germany) with a 63X oil immersion objective and a 496 nm excitation wavelength (argon laser); and they were photographed with a LAS-AF software. The experiments were carried out with 20 replicates.

4.4. Short-Term Experiments

To avoid biased interpretation, due to cascade effects connected to prolonged exposure to the molecule, the experiments on cellular division, *PINs* proteins, and auxin quantification were carried out using a short exposure (48 h) of the seedlings to coumarin.

4.4.1. Mitotic Indices and Cyclin B1;1::GFP Localization

Cell division was observed by confocal microscopy (see the method described below in § localization of GFP signal in *Arabidopsis*'s primary roots) on the *cyclin B1;1::GFP* transgenic line treated for 48 h on the previously described agarized medium enriched with coumarin 0 or 100 μM.

The evaluation of mitotic indices in *A. thaliana* RAMs treated for 48 h with coumarin 0 or 100 μM was carried out as previously described by Cools et al. [88] with some modifications. In particular, the synchronization of root cell division was obtained by incubating the seedlings for 24 h in a hydroxyurea solution (2 mM, pH 6.0). After incubation, *Arabidosis* seedlings were washed in deionized water and transferred in a continuously aerated coumarin solution (0 or 100 μM) for 48 h. Seedlings were then collected, and RAMs were cut with a razor blade and then fixed in a solution composed of acetic acid, ethanol, and chloroform (6:1:3) with iron traces.

Samples were immediately stored at −20 °C for 24 h. After that, the fixing solution was renewed (no iron traces were added this time), and the samples were stored at −20 °C for four days. After fixing, to allow cells and chromosomes dispersion, samples were hydrolyzed at 60 °C for 20 min in HCl 1N. Then, to stain the chromosomes, RAM samples were immersed in Schiff reagent and placed under dark conditions for 2 h at room temperature. Finally, the reaction was stopped with a few drops of acetic acid, and the samples were mounted on a microscope slide and fixed, passing the mounted slide on a flame for 3 s. A total of 1000 cells were counted in between 30 and 40 meristems per treatment. Samples were observed using an Olympus BX41 optical microscope (100 × objective).

4.4.2. Localization of GFP Signal in Arabidosis's Primary Roots

The experiments on *pDR5::GFP*, *pPINs::GFP* were carried out on 4 days old seedlings transplanted for 48 h on agar medium enriched with coumarin (short-term experiment). Treated and untreated *A. thaliana* (Col-0) seedlings were collected, fixed, and mounted as previously described [40].

Confocal images of median longitudinal sections were obtained using a Leica inverted TCS SP8 confocal scanning laser microscope equipped with a 40× oil immersion objective.

The detection of green fluorescent protein (GFP) (excitation peak centered at about 488 nm and the emission peak wavelength of 509 nm) was performed by combining the microscope's sequential scanning facility's settings. More than 40 seedlings were analyzed per treatment, and five independent experiments were carried out. Channel settings for GFP and laser power were kept identical during the analysis of all samples to make the results comparable.

To evaluate auxin and PIN protein abundance, the GFP signal intensity was measured by quantifying the integrated optical density (IOD) parameter on the root tip and maturation zone, using the software ImagePro Plus (Media Cybernetics, Inc. 1700 Rockville Pike, Suite 240 Rockville, Rockville, MD, USA). The measurements have been obtained using the "Count/Size" tool. First, all the green signals in the area of interest have been manually selected using the tool "Intensity Range Selection." Successively, the IOD of the entire green selected area has been measured on the root tip and maturation zone for the *pDR5::GFP* transgenic line and on the entire root apex for the *PINs*.

4.4.3. Auxin Quantification

Auxin quantification was carried out on *Arabidosis* seedlings treated with coumarin (0 or 100 μM) for 48 h. The entire root of control or treated seedlings was excised, immediately snap-frozen in liquid nitrogen (to quench the metabolism), and powdered. One hundred milligrams of plant material was used for sample extraction and derivatization. Samples were derivatized and analyzed using a GC-MS apparatus following the protocol described by Rawlinson et al. [89] with some modifications.

To the powdered samples, a 20 μL solution of 3-indolepropionic acid (IPA 20 mg/mL) was added as the internal standard for relative quantification and normalization purposes. Successively, 147 μL of methanol (MeOH), 34 μL of pyridine, and 200 μL of NaOH (1% w/v) were added, and the samples were shaken for 40 s. After extraction, samples were derivatized using 20 μL of methyl chloroformate and shaking for 30 s (this step was repeated two times). To the derivatized samples, 400 μL of chloroform and 400 μL of a $NaHCO_3$ solution (50 mM of stock) were added, and the samples were shaken again for 1 min and centrifuged at 14,000 rpm per 1 min. An aliquot (100 μL) of the organic lower phase was collected and used for gas chromatography-mass spectrometry (GC-MS) analysis. A parallel experiment was carried out using, as an external standard, pure IAA for the assignment of the retention time.

GC-MS analysis was carried out using a Thermo Fisher gas chromatograph apparatus (Trace 1310) equipped with a single quadrupole mass spectrometer (ISQ LT) (Thermo Fisher Scientific, Str. Rivoltana, Km 4, 20090 Rodano, Milan, Italy). The capillary column (MEGA-5MS 30 m × 0.25 mm × 0.25 μm + 10 m pre-column) and the carrier gas was helium with a flow rate of 1 mL/min. The injector and transfer line were set at 250 °C and 270 °C, respectively. Samples (3 μL) were injected with a 35 psi pressure pulse, which was held for 1 min. The following GC temperature program was used: Isocratic for 1 min at 40 °C, from 40 °C to 320 °C at a rate of 20 °C min^{-1}, and then held isocratic for 2 min at 320 °C. The ion source was set to 200 °C, and the solvent delay was 4.5 min. Mass spectra were recorded in electronic ionization (EI) mode at 70 eV, scanning at a 50–400 m/z range to select appropriate EI mass fragments for each analyte. Then, the MS was run in selected ion monitoring (SIM) using one quantifier (m/z) and two qualifiers (m/z) ions. In particular, for IAA-methyl ester, the ions 189, 103, and 77 were selected for quantification. IAA identification and quantification were performed by comparing the RT with the IAA external standard and the mass spectra in the National Institute Standard and Technology (NIST 2011) spectral library. The relative IAA quantification was carried out by normalizing the IAA peak intensity with the intensity of the internal standard.

4.5. Statistical Analysis

A completely random design with 20 replications (4 for IAA quantification and 10 for the measurement of the GFP signal intensity) was adopted. Data were first checked for

deviations from normality (D'Agostino-Pearson test) and tested for homogeneity (Leven Median test). The significance of differences between data sets was evaluated by the Student's test ($p \leq 0.05$).

All anatomical measurements were carried out using the open-source software ImageJ.

5. Conclusions

The results suggest that coumarin strongly affects the RAM morphology of *Arabidopsis thaliana*, altering the microtubule cortical array organization, and unbiasing auxin biosynthesis and distribution. Coumarin, as also reported for other microtubule de-polymerizing drugs (e.g., oryzalin), through the alteration in IAA efflux carriers distribution, altered the normal acropetal transport of auxin from the maturation zone to the apical RAM, which was guaranteed only by PIN1 and PIN7. Consequently, it resulted in an auxin accumulation in the maturation zone's pericycle cell, inducing lateral root formation.

Further studies will focus on understanding whether coumarin acts as a microtubule polymerizing or depolymerizing agent, as well as on studying the signaling involved in response to coumarin using mutants characterized by cyclin and microtubule alterations. Moreover, we will study coumarin's effects through combined-*omics* approaches.

Supplementary Materials: The following are available online at https://www.mdpi.com/article/10.3390/ijms22147305/s1.

Author Contributions: Conceptualization, F.A. and L.B.; methodology, F.A. and L.B.; software, F.A. and L.B.; validation, A.M., B.M.-M., L.C.-F., M.L.M., M.M. and E.T.; formal analysis, A.M., B.M.-M., L.C.-F., M.M., M.L.M. and E.T.; investigation, F.A., L.B., L.L. and A.S.; resources, F.A. and L.B.; data curation, F.A., L.B., L.L. and A.S.; writing and original draft preparation, F.A., L.B., L.L. and A.S.; writing—review and editing, A.M., B.M.-M., L.C.-F., M.L.M. and E.T.; visualization, A.M., B.M.-M., L.C.-F., M.L.M. and E.T.; supervision, F.A. and L.B.; project administration, F.A. and L.B.; funding responsible, F.A. All authors have read and agreed to the published version of the manuscript.

Funding: This research was supported by the Ministerio de Ciencia, Innovaciòn y Universidades RTI2018-094716-B-100.

Institutional Review Board Statement: Not applicable.

Informed Consent Statement: Not applicable.

Data Availability Statement: Not applicable.

Acknowledgments: We would like to thank Jiri Friml, Hyung-Taeg Cho, Ikram Blilou, and Marcus Heisler, who gently provided the mutated lines used in the experiments.

Conflicts of Interest: All authors have read and agreed to the published version of the manuscript. The authors declare that the research was conducted in the absence of any commercial or financial relationships that could be construed as a potential conflict of interest.

References

1. Delgoda, R.; Murray, J. Evolutionary perspectives on the role of plant secondary metabolites. In *Pharmacognosy*; Elsevier: Amsterdam, The Netherlands, 2017; pp. 93–100.
2. Theis, N.; Lerdau, M. The evolution of function in plant secondary metabolites. *Int. J. Plant Sci.* **2003**, *164*, S93–S102. [CrossRef]
3. Kessler, A.; Kalske, A. Plant secondary metabolite diversity and species interactions. *Annu. Rev. Ecol. Evol. System.* **2018**, *49*, 115–138. [CrossRef]
4. Duke, S.O.; Pan, Z.; Bajsa-Hirschel, J. Proving the mode of action of phytotoxic phytochemicals. *Plants* **2020**, *9*, 1756. [CrossRef]
5. Duke, S.O. Ecophysiological aspects of allelopathy. *Planta* **2003**, *217*, 529–539.
6. Dayan, F.E.; Duke, S.O. Natural compounds as next-generation herbicides. *Plant Physiol.* **2014**, *166*, 1090–1105. [CrossRef]
7. Graña, E.; Costas-Gil, A.; Longueira, S.; Celeiro, M.; Teijeira, M.; Reigosa, M.J.; Sánchez-Moreiras, A.M. Auxin-like effects of the natural coumarin scopoletin on Arabidopsis cell structure and morphology. *J. Plant Physiol.* **2017**, *218*, 45–55. [CrossRef]
8. Bourgaud, F.; Hehn, A.; Larbat, R.; Doerper, S.; Gontier, E.; Kellner, S.; Matern, U. Biosynthesis of coumarins in plants: A major pathway still to be unravelled for cytochrome P450 enzymes. *Phytochem. Rev.* **2006**, *5*, 293–308. [CrossRef]
9. Razavi, S.M. Plant Counnarins as Allelopathic Agents. *Int. J. Biol. Chem.* **2011**, *5*, 86–90. [CrossRef]
10. Matos, M.J.; Santana, L.; Uriarte, E.; Abreu, O.A.; Molina, E.; Yordi, E.G. Coumarins—An important class of phytochemicals. *Phytochem. Isol. Characterisation Role Hum. Health* **2015**, *25*, 533–538.

11. Costa, T.M.; Tavares, L.B.B.; de Oliveira, D. Fungi as a source of natural coumarins production. *Appl. Microbiol. Biotech.* **2016**, *100*, 6571–6584. [CrossRef] [PubMed]
12. Niro, E.; Marzaioli, R.; De Crescenzo, S.; D'Abrosca, B.; Castaldi, S.; Esposito, A.; Fiorentino, A.; Rutigliano, F. Effects of the allelochemical coumarin on plants and soil microbial community. *Soil Biol. Biochem.* **2016**, *95*, 30–39. [CrossRef]
13. Robe, K.; Conejero, G.; Gao, F.; Lefebvre-Legendre, L.; Sylvestre-Gonon, E.; Rofidal, V.; Hem, S.; Rouhier, N.; Barberon, M.; Hecker, A. Coumarin accumulation and trafficking in *Arabidopsis thaliana*: A complex and dynamic process. *New Phytol.* **2021**, *229*, 2062–2079. [CrossRef] [PubMed]
14. Clemens, S.; Weber, M. The essential role of coumarin secretion for Fe acquisition from alkaline soil. *Plant Signal. Behav.* **2016**, *11*, e1114197. [CrossRef]
15. Tsai, H.H.; Schmidt, W. Mobilization of iron by plant-borne coumarins. *Trends Plant Sci.* **2017**, *22*, 538–548. [CrossRef] [PubMed]
16. Robe, K.; Izquierdo, E.; Vignols, F.; Rouached, H.; Dubos, C. The coumarins: Secondary metabolites playing a primary role in plant nutrition and health. *Trends Plant Sci.* **2020**, *26*, 248–259. [CrossRef]
17. Lundberg, D.S.; Teixeira, P.J. Root-exuded coumarin shapes the root microbiome. *Proc. Natl. Acad. Sci. USA* **2018**, *115*, 5629–5631. [CrossRef]
18. Lupini, A.; Sorgonà, A.; Miller, A.J.; Abenavoli, M.R. Short-term effects of coumarin along the maize primary root axis. *Plant Signal. Behav.* **2010**, *5*, 1395–1400. [CrossRef]
19. Abenavoli, M.; Nicolò, A.; Lupini, A.; Oliva, S.; Sorgonà, A. Effects of different allelochemicals on root morphology of *Arabidopsis thaliana*. *Allelopath. J.* **2008**, *22*, 245–252.
20. Neumann, J. An auxin-like action of coumarin. *Science* **1959**, *129*, 1675–1676. [CrossRef]
21. Jansson, E.; Svensson, S.-B. Coumarin effects on *Glycine max* hypocotyl explants. *Physiol. Plant* **1980**, *48*, 486–490. [CrossRef]
22. Lupini, A.; Araniti, F.; Sunseri, F.; Abenavoli, M.R. Coumarin interacts with auxin polar transport to modify root system architecture in *Arabidopsis thaliana*. *Plant Growth Regul.* **2014**, *74*, 23–31. [CrossRef]
23. Pop, T.I.; Pamfil, D.; Bellini, C. Auxin control in the formation of adventitious roots. *Not. Bot. Horti Agrobot. Cluj Napoca* **2011**, *39*, 307–316. [CrossRef]
24. Potters, G.; Pasternak, T.P.; Guisez, Y.; Palme, K.J.; Jansen, M.A. Stress-induced morphogenic responses: Growing out of trouble? *Trends Plant Sci.* **2007**, *12*, 98–105. [CrossRef]
25. Zažímalová, E.; Murphy, A.S.; Yang, H.; Hoyerová, K.; Hošek, P. Auxin transporters—Why so many? *Cold Spring Harb. Perspect. Biol.* **2010**, *2*, a001552. [CrossRef] [PubMed]
26. Casimiro, I.; Beeckman, T.; Graham, N.; Bhalerao, R.; Zhang, H.; Casero, P.; Sandberg, G.; Bennett, M.J. Dissecting Arabidopsis lateral root development. *Trends Plant Sci.* **2003**, *8*, 165–171. [CrossRef]
27. Singh, S.; Yadav, S.; Singh, A.; Mahima, M.; Singh, A.; Gautam, V.; Sarkar, A.K. Auxin signaling modulates LATERAL ROOT PRIMORDIUM 1 (LRP 1) expression during lateral root development in Arabidopsis. *Plant J.* **2020**, *101*, 87–100. [CrossRef] [PubMed]
28. Benková, E.; Michniewicz, M.; Sauer, M.; Teichmann, T.; Seifertová, D.; Jürgens, G.; Friml, J. Local, efflux-dependent auxin gradients as a common module for plant organ formation. *Cell* **2003**, *115*, 591–602. [CrossRef]
29. Laskowski, M.; Biller, S.; Stanley, K.; Kajstura, T.; Prusty, R. Expression profiling of auxin-treated Arabidopsis roots: Toward a molecular analysis of lateral root emergence. *Plant Cell Physiol.* **2006**, *47*, 788–792. [CrossRef]
30. Dubrovsky, J.G.; Napsucialy-Mendivil, S.; Duclercq, J.; Cheng, Y.; Shishkova, S.; Ivanchenko, M.G.; Friml, J.; Murphy, A.S.; Benková, E. Auxin minimum defines a developmental window for lateral root initiation. *New Phytol.* **2011**, *191*, 970–983. [CrossRef]
31. Lehman, T.A.; Smertenko, A.; Sanguinet, K.A. Auxin, microtubules, and vesicle trafficking: Conspirators behind the cell wall. *J. Exp. Bot.* **2017**, *68*, 3321–3329. [CrossRef]
32. Kleine-Vehn, J.; Łangowski, Ł.; Wiśniewska, J.; Dhonukshe, P.; Brewer, P.B.; Friml, J. Cellular and molecular requirements for polar PIN targeting and transcytosis in plants. *Mol. Plant* **2008**, *1*, 1056–1066. [CrossRef]
33. Na, X.; Hu, Y.; Yue, K.; Lu, H.; Jia, P.; Wang, H.; Wang, X.; Bi, Y. Narciclasine modulates polar auxin transport in Arabidopsis roots. *J. Plant Physiol.* **2011**, *168*, 1149–1156. [CrossRef]
34. Hu, Y.; Yang, L.; Na, X.; You, J.; Hu, W.; Liang, X.; Liu, J.; Mao, L.; Wang, X.; Wang, H. Narciclasine inhibits the responses of Arabidopsis roots to auxin. *Planta* **2012**, *236*, 597–612. [CrossRef] [PubMed]
35. Graña, E.; Sotelo, T.; Díaz-Tielas, C.; Araniti, F.; Krasuska, U.; Bogatek, R.; Reigosa, M.J.; Sánchez-Moreiras, A.M. Citral induces auxin and ethylene-mediated malformations and arrests cell division in *Arabidopsis thaliana* roots. *J. Chem. Ecol.* **2013**, *39*, 271–282. [CrossRef] [PubMed]
36. Hu, Y.; Na, X.; Li, J.; Yang, L.; You, J.; Liang, X.; Wang, J.; Peng, L.; Bi, Y. Narciclasine, a potential allelochemical, affects subcellular trafficking of auxin transporter proteins and actin cytoskeleton dynamics in Arabidopsis roots. *Planta* **2015**, *242*, 1349–1360. [CrossRef]
37. Araniti, F.; Grana, E.; Krasuska, U.; Bogatek, R.; Reigosa, M.J.; Abenavoli, M.R.; Sanchez-Moreiras, A.M. Loss of gravitropism in farnesene-treated arabidopsis is due to microtubule malformations related to hormonal and ROS unbalance. *PLoS ONE* **2016**, *11*, e0160202. [CrossRef] [PubMed]
38. Li, P.; Ding, L.; Zhang, L.; He, J.; Huan, Z. Weisiensin B inhibits primary and lateral root development by interfering with polar auxin transport in *Arabidopsis thaliana*. *Plant Physiol. Biochem.* **2019**, *139*, 738–745. [CrossRef] [PubMed]

39. López-González, D.; Costas-Gil, A.; Reigosa, M.J.; Araniti, F.; Sánchez-Moreiras, A.M. A natural indole alkaloid, norharmane, affects PIN expression patterns and compromises root growth in *Arabidopsis thaliana*. *Plant Physiol. Biochem.* **2020**, *151*, 378–390. [CrossRef]
40. Araniti, F.; Bruno, L.; Sunseri, F.; Pacenza, M.; Forgione, I.; Bitonti, M.B.; Abenavoli, M.R. The allelochemical farnesene affects *Arabidopsis thaliana* root meristem altering auxin distribution. *Plant Physiol. Biochem.* **2017**, *121*, 14–20. [CrossRef] [PubMed]
41. Chaimovitsh, D.; Abu-Abied, M.; Belausov, E.; Rubin, B.; Dudai, N.; Sadot, E. Microtubules are an intracellular target of the plant terpene citral. *Plant J.* **2010**, *61*, 399–408. [CrossRef]
42. Graña, E.; Díaz-Tielas, C.; López-González, D.; Martínez-Peñalver, A.; Reigosa, M.; Sánchez-Moreiras, A. The plant secondary metabolite citral alters water status and prevents seed formation in *Arabidopsis thaliana*. *Plant Biol.* **2016**, *18*, 423–432. [CrossRef]
43. Svensson, S.B. The effect of coumarin on root growth and root histology. *Physiol. Plant* **1971**, *24*, 446–470. [CrossRef]
44. Mizukami, Y. A matter of size: Developmental control of organ size in plants. *Curr. Opin. Plant Biol.* **2001**, *4*, 533–539. [CrossRef]
45. Ioio, R.D.; Linhares, F.S.; Scacchi, E.; Casamitjana-Martinez, E.; Heidstra, R.; Costantino, P.; Sabatini, S. Cytokinins determine Arabidopsis root-meristem size by controlling cell differentiation. *Curr. Biol.* **2007**, *17*, 678–682. [CrossRef] [PubMed]
46. Ioio, R.D.; Nakamura, K.; Moubayidin, L.; Perilli, S.; Taniguchi, M.; Morita, M.T.; Aoyama, T.; Costantino, P.; Sabatini, S. A genetic framework for the control of cell division and differentiation in the root meristem. *Science* **2008**, *322*, 1380–1384. [CrossRef]
47. Doerner, P.; Jørgensen, J.-E.; You, R.; Steppuhn, J.; Lamb, C. Control of root growth and development by cyclin expression. *Nature* **1996**, *380*, 520–523. [CrossRef]
48. Criqui, M.C.; Parmentier, Y.; Derevier, A.; Shen, W.H.; Dong, A.; Genschik, P. Cell cycle-dependent proteolysis and ectopic overexpression of cyclin B1 in tobacco BY2 cells. *Plant J.* **2000**, *24*, 763–773. [CrossRef]
49. Blilou, I.; Xu, J.; Wildwater, M.; Willemsen, V.; Paponov, I.; Friml, J.; Heidstra, R.; Aida, M.; Palme, K.; Scheres, B. The PIN auxin efflux facilitator network controls growth and patterning in Arabidopsis roots. *Nature* **2005**, *433*, 39–44. [CrossRef] [PubMed]
50. Abenavoli, M.R.; Sorgonà, A.; Albano, S.; Cacco, G. Coumarin differentially affects the morphology of different root types of maize seedlings. *J. Chem. Ecol.* **2004**, *30*, 1871–1883. [CrossRef] [PubMed]
51. Jingyi, W.; Dandan, Y.; Jun, X.; Cai-xia, W.; Guo-qi, Z.; Chen-lan, H. Effect of coumarin on *Soughum sudanense* seed germination and seedling growth. *Pratac. Sci.* **2017**, *34*, 2279–2288.
52. Chen, B.-X.; Peng, Y.-X.; Gao, J.-D.; Zhang, Q.; Liu, Q.-J.; Fu, H.; Liu, J. Coumarin-induced delay of rice seed germination is mediated by suppression of abscisic acid catabolism and reactive oxygen species production. *Front. Plant Sci.* **2019**, *10*, 828. [CrossRef] [PubMed]
53. Laplaze, L.; Benkova, E.; Casimiro, I.; Maes, L.; Vanneste, S.; Swarup, R.; Weijers, D.; Calvo, V.; Parizot, B.; Herrera-Rodriguez, M.B. Cytokinins act directly on lateral root founder cells to inhibit root initiation. *Plant Cell* **2007**, *19*, 3889–3900. [CrossRef] [PubMed]
54. Bruno, L.; Pacenza, M.; Forgione, I.; Lamerton, L.R.; Greco, M.; Chiappetta, A.; Bitonti, M.B. In *Arabidopsis thaliana* cadmium impact on the growth of primary root by altering SCR expression and auxin-cytokinin cross-talk. *Front. Plant Sci.* **2017**, *8*, 1323. [CrossRef] [PubMed]
55. Na, X.; Hu, Y.; Yue, K.; Lu, H.; Jia, P.; Wang, H.; Wang, X.; Bi, Y. Concentration-dependent effects of narciclasine on cell cycle progression in Arabidopsis root tips. *BMC Plant Biol.* **2011**, *11*, 1–13. [CrossRef] [PubMed]
56. Cornman, I. The responses of onion and lily mitosis to coumarin and parasorbic acid. *J. Exp. Biol.* **1947**, *23*, 292–297. [CrossRef] [PubMed]
57. Yuksel, B.; Aksoy, O. Cytological effects of coumarin on the mitosis of *Lens culinaris* Medik. *Fresenius Environ. Bull.* **2017**, *26*, 6400–6407.
58. Culligan, K.; Tissier, A.; Britt, A. ATR regulates a G2-phase cell-cycle checkpoint in *Arabidopsis thaliana*. *Plant Cell* **2004**, *16*, 1091–1104. [CrossRef]
59. Wu, S.; Scheible, W.-R.; Schindelasch, D.; Van Den Daele, H.; De Veylder, L.; Baskin, T.I. A conditional mutation in *Arabidopsis thaliana* separase induces chromosome non-disjunction, aberrant morphogenesis and cyclin B1; 1 stability. *Development* **2010**, *137*, 953–961. [CrossRef]
60. De Schutter, K.; Joubès, J.; Cools, T.; Verkest, A.; Corellou, F.; Babiychuk, E.; Van Der Schueren, E.; Beeckman, T.; Kushnir, S.; Inze, D. Arabidopsis WEE1 kinase controls cell cycle arrest in response to activation of the DNA integrity checkpoint. *Plant Cell* **2007**, *19*, 211–225. [CrossRef]
61. Hefner, E.; Huefner, N.; Britt, A.B. Tissue-specific regulation of cell-cycle responses to DNA damage in Arabidopsis seedlings. *DNA Repair* **2006**, *5*, 102–110. [CrossRef]
62. Weingartner, M.; Criqui, M.-C.; Mészáros, T.; Binarova, P.; Schmit, A.-C.; Helfer, A.; Derevier, A.; Erhardt, M.; Bögre, L.; Genschik, P. Expression of a nondegradable cyclin B1 affects plant development and leads to endomitosis by inhibiting the formation of a phragmoplast. *Plant Cell* **2004**, *16*, 643–657. [CrossRef]
63. Serralbo, O.; Pérez-Pérez, J.M.; Heidstra, R.; Scheres, B. Non-cell-autonomous rescue of anaphase-promoting complex function revealed by mosaic analysis of HOBBIT, an Arabidopsis CDC27 homolog. *Proc. Natl. Acad. Sci. USA* **2006**, *103*, 13250–13255. [CrossRef]
64. Baskin, T.I.; Wilson, J.E.; Cork, A.; Williamson, R.E. Morphology and microtubule organization in Arabidopsis roots exposed to oryzalin or taxol. *Plant Cell Physiol.* **1994**, *35*, 935–942. [PubMed]

65. Baskin, T.I.; Beemster, G.T.; Judy-March, J.E.; Marga, F. Disorganization of cortical microtubules stimulates tangential expansion and reduces the uniformity of cellulose microfibril alignment among cells in the root of Arabidopsis. *Plant Physiol.* **2004**, *135*, 2279–2290. [CrossRef]
66. Fanale, D.; Bronte, G.; Passiglia, F.; Calò, V.; Castiglia, M.; Di Piazza, F.; Barraco, N.; Cangemi, A.; Catarella, M.T.; Insalaco, L. Stabilizing versus destabilizing the microtubules: A double-edge sword for an effective cancer treatment option? *Anal. Cell. Pathol.* **2015**, *2015*, 1–19. [CrossRef] [PubMed]
67. Morejohn, L.C.; Fosket, D.E. The biochemistry of compounds with anti-microtubule activity in plant cells. *Pharmacol. Ther.* **1991**, *51*, 217–230. [CrossRef]
68. Hugdahl, J.D.; Morejohn, L.C. Rapid and reversible high-affinity binding of the dinitroaniline herbicide oryzalin to tubulin from *Zea mays* L. *Plant Physiol.* **1993**, *102*, 725–740. [CrossRef] [PubMed]
69. Pitts, R.J.; Cernac, A.; Estelle, M. Auxin and ethylene promote root hair elongation in Arabidopsis. *Plant J.* **1998**, *16*, 553–560. [CrossRef] [PubMed]
70. Rahman, A.; Hosokawa, S.; Oono, Y.; Amakawa, T.; Goto, N.; Tsurumi, S. Auxin and ethylene response interactions during Arabidopsis root hair development dissected by auxin influx modulators. *Plant Physiol.* **2002**, *130*, 1908–1917. [CrossRef]
71. Campanoni, P.; Nick, P. Auxin-dependent cell division and cell elongation. 1-Naphthaleneacetic acid and 2, 4-dichlorophenoxyacetic acid activate different pathways. *Plant Physiol.* **2005**, *137*, 939–948. [CrossRef]
72. Li, X.; Gruber, M.Y.; Hegedus, D.D.; Lydiate, D.J.; Gao, M.-J. Effects of a coumarin derivative, 4-methylumbelliferone, on seed germination and seedling establishment in Arabidopsis. *J. Chem. Ecol.* **2011**, *37*, 880–890. [CrossRef]
73. Tian, H.; Niu, T.; Yu, Q.; Quan, T.; Ding, Z. Auxin gradient is crucial for the maintenance of root distal stem cell identity in Arabidopsis. *Plant Sign. Behav.* **2013**, *8*, e26429. [CrossRef]
74. Goren, R.; Tomer, E. Effects of seselin and coumarin on growth, indoleacetic acid oxidase, and peroxidase, with special reference to cucumber (*Cucumis sativa* L.) radicles. *Plant Physiol.* **1971**, *47*, 312–316. [CrossRef] [PubMed]
75. Andreae, W. Effect of scopoletin on indoleacetic acid metabolism. *Nature* **1952**, *170*, 83–84. [CrossRef]
76. Casimiro, I.; Marchant, A.; Bhalerao, R.P.; Beeckman, T.; Dhooge, S.; Swarup, R.; Graham, N.; Inzé, D.; Sandberg, G.; Casero, P.J. Auxin transport promotes Arabidopsis lateral root initiation. *Plant Cell* **2001**, *13*, 843–852. [CrossRef] [PubMed]
77. De Rybel, B.; Audenaert, D.; Xuan, W.; Overvoorde, P.; Strader, L.C.; Kepinski, S.; Hoye, R.; Brisbois, R.; Parizot, B.; Vanneste, S. A role for the root cap in root branching revealed by the non-auxin probe naxillin. *Nat. Chem. Biol.* **2012**, *8*, 798–805. [CrossRef] [PubMed]
78. Himanen, K.; Boucheron, E.; Vanneste, S.; de Almeida Engler, J.; Inzé, D.; Beeckman, T. Auxin-mediated cell cycle activation during early lateral root initiation. *Plant Cell* **2002**, *14*, 2339–2351. [CrossRef]
79. Vanneste, S.; De Rybel, B.; Beemster, G.T.; Ljung, K.; De Smet, I.; Van Isterdael, G.; Naudts, M.; Iida, R.; Gruissem, W.; Tasaka, M. Cell cycle progression in the pericycle is not sufficient for SOLITARY ROOT/IAA14-mediated lateral root initiation in *Arabidopsis thaliana*. *Plant Cell* **2005**, *17*, 3035–3050. [CrossRef]
80. Zhang, Y.; He, P.; Ma, X.; Yang, Z.; Pang, C.; Yu, J.; Wang, G.; Friml, J.; Xiao, G. Auxin-mediated statolith production for root gravitropism. *New Phytol.* **2019**, *224*, 761–774. [CrossRef]
81. Dubrovsky, J.G.; Sauer, M.; Napsucialy-Mendivil, S.; Ivanchenko, M.G.; Friml, J.; Shishkova, S.; Celenza, J.; Benková, E. Auxin acts as a local morphogenetic trigger to specify lateral root founder cells. *Proc. Nat. Acad. Sci. USA* **2008**, *105*, 8790–8794. [CrossRef] [PubMed]
82. Alarcón, M.; Salguero, J.; Lloret, P.G. Auxin modulated initiation of lateral roots is linked to pericycle cell length in maize. *Front. Plant Sci.* **2019**, *10*, 11. [CrossRef] [PubMed]
83. Laskowski, M.J.; Williams, M.E.; Nusbaum, H.C.; Sussex, I.M. Formation of lateral root meristems is a two-stage process. *Development* **1995**, *121*, 3303–3310. [CrossRef] [PubMed]
84. Ottenschläger, I.; Wolff, P.; Wolverton, C.; Bhalerao, R.P.; Sandberg, G.; Ishikawa, H.; Evans, M.; Palme, K. Gravity-regulated differential auxin transport from columella to lateral root cap cells. *Proc. Natl. Acad. Sci. USA* **2003**, *100*, 2987–2991. [CrossRef] [PubMed]
85. Moreno-Romero, J.; Carme Espunya, M.; Platara, M.; Ariño, J.; Carmen Martínez, M. A role for protein kinase CK2 in plant development: Evidence obtained using a dominant-negative mutant. *Plant J.* **2008**, *55*, 118–130. [CrossRef] [PubMed]
86. González-García, M.-P.; Vilarrasa-Blasi, J.; Zhiponova, M.; Divol, F.; Mora-García, S.; Russinova, E.; Caño-Delgado, A.I. Brassinosteroids control meristem size by promoting cell cycle progression in Arabidopsis roots. *Development* **2011**, *138*, 849–859. [CrossRef] [PubMed]
87. Holzinger, A.; Kawamura, E.; Wasteneys, G.O. Strategies for imaging microtubules in plant cells. In *Cytoskeleton Methods and Protocols*; Springer: Berlin/Heidelberg, Germany, 2009; pp. 243–262.
88. Cools, T.; Iantcheva, A.; Maes, S.; Van den Daele, H.; De Veylder, L. A replication stress-induced synchronization method for *Arabidopsis thaliana* root meristems. *Plant J.* **2010**, *64*, 705–714. [CrossRef]
89. Rawlinson, C.; Kamphuis, L.G.; Gummer, J.P.; Singh, K.B.; Trengove, R.D. A rapid method for profiling of volatile and semi-volatile phytohormones using methyl chloroformate derivatisation and GC–MS. *Metabolomics* **2015**, *11*, 1922–1933. [CrossRef]

plants

MDPI

Article

Short-Term Effects of *Trans*-Cinnamic Acid on the Metabolism of *Zea mays* L. Roots

David López-González [1], Leonardo Bruno [2], Carla Díaz-Tielas [1], Antonio Lupini [3], Meriem Miyassa Aci [3], Emanuela Talarico [2], Maria Letizia Madeo [2], Antonella Muto [2], Adela M. Sánchez-Moreiras [1] and Fabrizio Araniti [4,*]

1 Departmento de Bioloxía Vexetal e Ciencia do Solo, Facultade de Bioloxía, Universidade de Vigo, Campus Lagoas-Marcosende s/n, 36310 Vigo, Spain
2 Dipartimento di Biologia, Ecologia e Scienza della Terra, Università della Calabria (DiBEST-UNICAL), 87036 Arcavacata di Rende, Italy
3 Dipartimento Agraria, Università Mediterranea di Reggio Calabria, 89124 Reggio Calabria, Italy
4 Dipartimento di Scienze Agrarie e Ambientali—Produzione, Territorio, Agroenergia, Università Statale di Milano, Via Celoria n°2, 20133 Milano, Italy
* Correspondence: fabrizio.araniti@unimi.it

Abstract: *trans*-Cinnamic acid is a phenolic compound widely studied in plant metabolism due to its importance in regulating different plant processes. Previous studies on maize plants showed that this compound could affect plant growth and causes metabolic changes in the leaves when applied. However, its effects on root metabolism are not well known. This study analyses the short-term effect of *trans*-cinnamic acid on the morphology of vascular bundle elements and metabolism in maize roots. At short times (between 6 and 12 h), there is a reduction in the content of many amino acids which may be associated with the altered nitrogen uptake observed in earlier work. In addition, the compound caused an alteration of the vascular bundles at 48 h and seemed to have changed the metabolism in roots to favor lignin and galactose synthesis. The results obtained complement those previously carried out on maize plants, demonstrating that in the short term *trans*-cinnamic acid can trigger stress-coping processes in the treated plants.

Keywords: lignin; maize; metabolomics; root; stress; *trans*-cinnamic acid

Citation: López-González, D.; Bruno, L.; Díaz-Tielas, C.; Lupini, A.; Aci, M.M.; Talarico, E.; Madeo, M.L.; Muto, A.; Sánchez-Moreiras, A.M.; Araniti, F. Short-Term Effects of *Trans*-Cinnamic Acid on the Metabolism of *Zea mays* L. Roots. *Plants* **2023**, *12*, 189. https://doi.org/10.3390/plants12010189

Academic Editor: Ain Raal

Received: 22 November 2022
Revised: 21 December 2022
Accepted: 22 December 2022
Published: 2 January 2023

1. Introduction

Allelopathy is a phenomenon whereby specialized metabolites produced by living organisms (bacteria, fungi, viruses or plants) can positively or negatively affect the development of biological or agricultural systems [1]. Those characteristics make this ecological phenomenon a potential tool for the development of new botanical herbicides employable in sustainable weed management [2]. There is a wide variety of specialized metabolites, which can be grouped into three main groups: terpenoids, nitrogen compounds and phenolics [3]. Given the problems with the limited number of modes of action (MOAs) of current herbicides, numerous studies are focusing on the search for new MOAs using these specialized metabolites, which are characterized by a high structural diversity [4]. This high structural diversity makes possible that specialized metabolites of the same class might have different effects on plant metabolism. On the other side, compounds from different classes may have similar effects.

Harmaline, for example, is an indole alkaloid that alters the balance between the phytohormones auxin, cytokinin and ethylene, altering the development of *Arabidopsis thaliana* (L.), Heynh. seedlings [5]. Another indole alkaloid such as norharmane can decrease the growth of *A. thaliana* seedlings by altering the distribution of auxin transporter proteins (PINs) [6], and of adult *A. thaliana* plants by generating water stress when applied by irrigation, while inhibiting the germination and growth of some weed species [7]. Another

compound capable of generating water stress in *A. thaliana* adult plants is the monoterpene citral, which also inhibited the development of different weed species [8]. At the same time, farnesene, another terpenoid, was able to alter the distribution of the phytohormone auxin, which led to alterations in the meristem and caused a "left-handedness" phenotype [9].

Phenolic compounds have been studied for many years for their physiological and biochemical effects on plants as they actively participate in the response of plants to abiotic and biotic stress [10,11], particularly for their antioxidant properties [12,13]. Phenolic compounds are important not only for their effects on plants but also for their numerous antimicrobial [14,15], pharmacological [16,17] and industrial [18,19] properties. It is also important to highlight their role in the food industry because of their impact on so-called functional foods, which, in addition to their nutritional value, contain biologically active components with beneficial impact on health, reducing the risk of contracting certain diseases [20,21].

Cinnamic acids are a class of phenolic compounds studied for many years. Whitehead [22] observed how these acids accumulate in the soil after the decomposition of organic matter. These compounds can be presented as *cis*- or *trans*-isomers, and their activity depends on the type of isomer [23]. In particular, *cis*-form is more active than *trans*-form [24]. They are important for plant growth and development as they have protective functions and are key compounds in regulating the phenylpropanoid pathway [25]. However, high concentrations of these acids can trigger plant damage, such as alterations in membrane permeability [26], phytohormonal activity [27], or generation of oxidative stress [28], among others.

Lupini et al. [29] found that exogenous application of *trans*-cinnamic acid to maize plants inhibited plasma membrane H^+-ATPase activity, which reduced nitrate uptake and caused a reduction in root growth as well. In addition, Araniti et al. [30] showed that the application of *trans*-cinnamic acid to maize leaves causes stress to the plants, but they can cope with this stress by redirecting metabolism towards the production of protective metabolites such as galactose or ascorbic acid. Regarding the effects on roots, Salvador et al. [31] showed that different concentrations of *trans*-cinnamic acid (from 0.1 to 1 mM) increased indole-3-acetic acid (IAA) oxidase and cinnamate 4-hydroxylase (C4H) activities after 24 h of treatment. The increase in C4H activity led to an increase in lignin content which, together with the rise in IAA oxidase activity, led to a decrease in *Glycine max* L. Merr. root growth.

However, no metabolomic studies and short-term effects of *trans*-cinnamic acid have been studied up to now on treated roots, which could give light on the primary effects of *trans*-cinnamic acid on root metabolism.

Metabolomics is a handy tool used to observe changes in the metabolome of plants treated with phytotoxic compounds or to study metabolite changes under stress [32–34].

For this reason, a metabolomics approach accompanied by measurements of vascular bundle components was performed to observe the short-term changes that *trans*-cinnamic acid ED_{50} produced on *Zea mays* L. roots.

2. Results

2.1. Xylem Measurements

Treatment with the ED_{50} of *trans*-cinnamic caused alterations in the treated roots' measured parameters (Figure 1c,d). The compound caused a significant increase of 7% compared to control in the diameter of the vascular cylinder (Figure 1a), although the area of the xylem vessels was significantly reduced by 9% compared to control in the treated roots (Figure 1b).

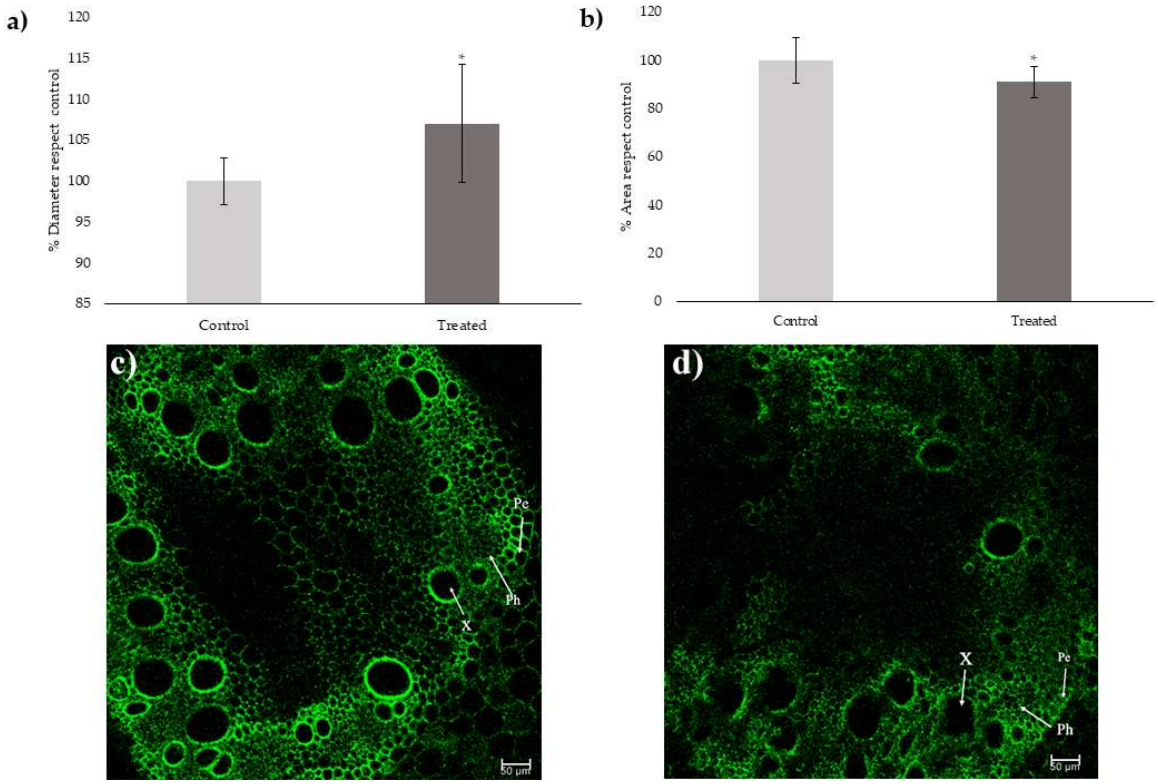

Figure 1. (**a**) Diameter of the vascular bundle after 48 h of treatment with *trans*-cinnamic acid expressed as a percentage with respect to the control. (**b**) Xylematic area after 48 h of treatment with *trans*-cinnamic acid expressed as percentage respect to the control. (**c**) Cross section of a maize control root. (**d**) Cross section of a maize *trans*-cinnamic treated root. (X), xylem; (Ph), phloem; (Pc); pericycle. (*) Indicates significant differences compared to the control (* $p \leq 0.05$, ** $p \leq 0.01$, *** $p \leq 0.001$). Scales bars = 50 µm. Data were analysed with a *t*-test at $p \leq 0.05$.

2.2. Untargeted Metabolomic Analysis

GC-MS-driven untargeted-metabolomic analysis was carried out to get more insights into the metabolic changes produced by the *trans*-cinnamic on maize seedlings at different treatment times, from 6 to 48 h.

A total of 651 compounds were identified using the MS-DIAL software; of these, 360 were unknown, whereas 291 were putatively annotated following the metabolomic society initiative (Supplementary Table S1). After manual feature annotation and discarding false annotated metabolites, a total of 134 primary and specialized metabolites were identified.

Data were analysed through unsupervised multivariate analysis to reduce the dimensionality of the data and visualize how they were grouped. The PCA's score plot, built by virtue of the two components PC1 vs. PC2, described the 48.3% of the total variability (Figure 1a). PC1 explained the highest variance (27.8%), while PC2 explained the 20.5% of the total variance. The PCA revealed discrimination between the groups, but this separation was unclear.

Then, the supervised PLS-DA showed the separation between control and treatments at different times (Figure 2b). The model was characterized by a R^2, Q^2 and accuracy higher than 0.8 (Supplementary Table S1), indicating good predictivity and high fitting of this model. The separation was achieved by virtue of the first two principal components (PC1 vs. PC2), which explained a total variance of 40.7%. Component 1 explained the highest variance (24.1%), while component 2 explained 16.6% of the total variance. The *trans*-cinnamic treatments, at times 1, 2 and 3, were closer to the control at T3 than their respective controls (T1 and T2). This may indicate a strong short-term acceleration of metabolism by the compound, which is maintained over time. After a long time (T4), there

was a clear separation between treatment and control, mainly due to PC2, indicating a significant difference between the metabolomes of control and treated plants.

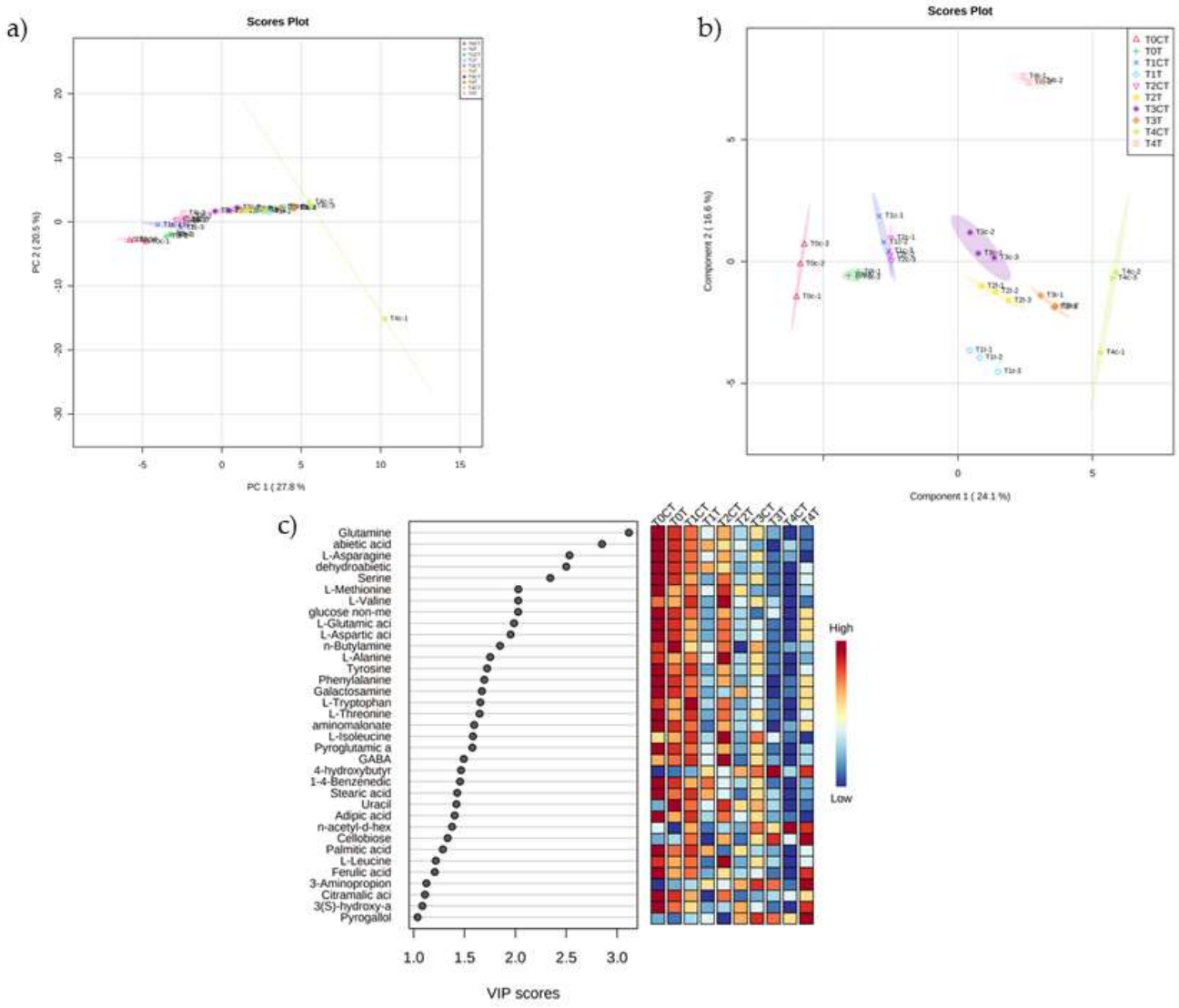

Figure 2. (**a**) Unsupervised PCA of the metabolomic changes on maize roots after 48 h treatment with 103 µM of *trans*−cinnamic acid. (**b**) Multivariate (PLS−DA) analysis of the metabolomic changes on maize roots after 48 h treatment with 103 µM of *trans*−cinnamic acid. (**c**) Important features identified by PLS−DA. The coloured boxes on the right indicate the relative concentrations of the corresponding metabolite in each group under study Times (T0 = 0 h; T1 = 6 h; T2 = 12 h; T3 = 24 h; T4 = 48 h). The treatments used were 0 µM (control, CT), and (treatment, T). N = 3.

PLS-DA derived variable importance of projection (VIP) scores (built on the metabolites with a VIP score higher than 1.4) (Figure 2c) revealed that glutamine, abietic acid, L-asparagine, dehydroabietic acid, serine, L-methionine, L-valine, glucose, L-glutamic acid, L-aspartic acid, n-butylamine, L-alanine, tyrosine, phenylalanine, galactosamine, L-tryptophan, L-threonine, aminomalonate, L-isoleucine, pyroglutamic acid, gamma-aminobutyric acid (GABA), 4-hydroxybutyric acid, 1-4-benzenedicarboxylic acid, stearic acid, uracil, and adipic acid were the metabolites that were mainly contributing to groups discrimination (Figure 3).

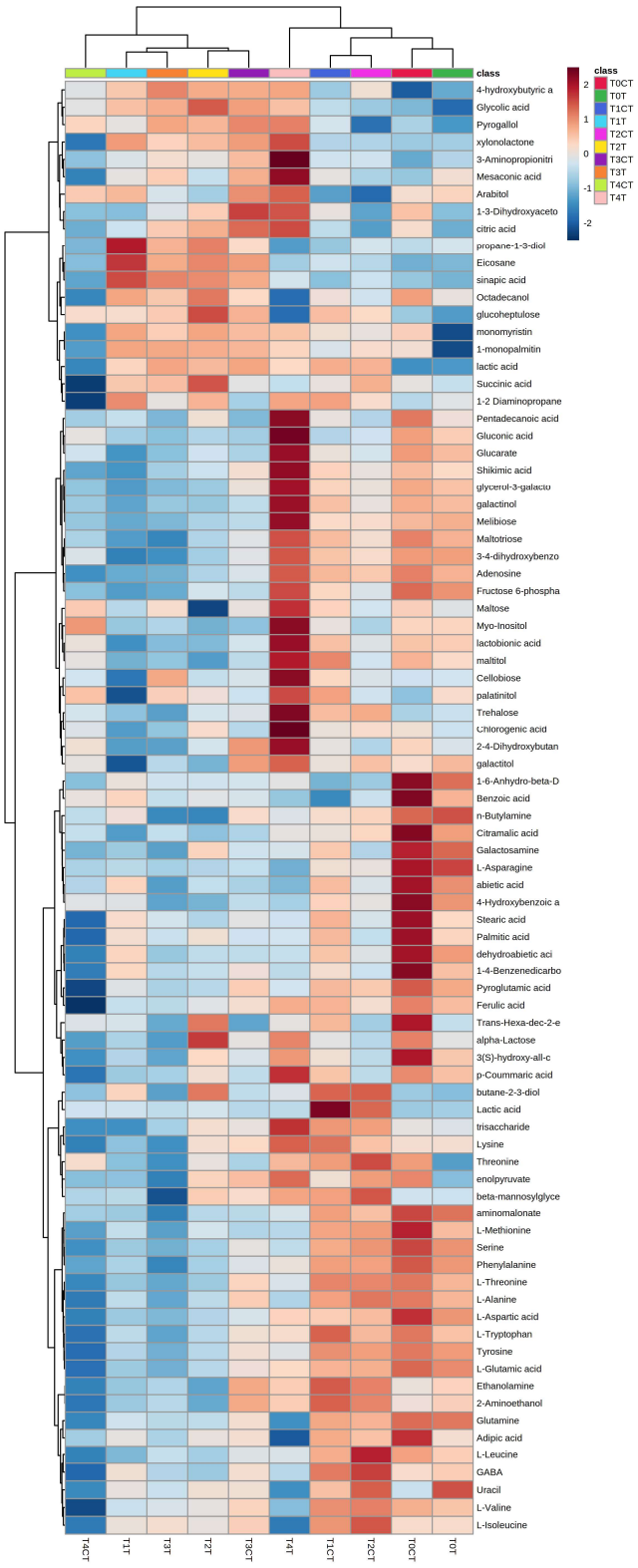

Figure 3. Clustering result shown as heatmap (distance measure using Euclidean, and clustering algorithm using Ward method) of all the metabolites identified in seedlings exposed to trans-cinnamic acid compared to control. Each square represents the effect of *trans*−cinnamic acid on the amount of each metabolite using a false−colour scale. Red or blue regions indicate increased or decreased metabolite content, respectively. Times (T0 = 0 h; T1 = 6 h; T2 = 12 h; T3 = 24 h; T4 = 48 h). The treatments used were 0 µM (control, CT), and 103 µM (treatment, T) N = 3.

A univariate ANOVA was performed to find which metabolites were significantly altered among treatments. The analysis revealed that 84 out of the 134 compounds identified were significantly altered (Supplementary Table S1). Those metabolites were presented on a heatmap showing how each metabolite varied according to time and treatment (Figure 3). The trend observed in the heat map showed the same dynamics as discussed in the PLS-DA. At T1, T2 and T3, there was a general decrease in the accumulation of several amino acids, such as glutamine, glutamic acid, alanine, aspartate, tyrosine, tryptophan, serine, etc., in the roots treated with *trans*-cinnamic acid compared to their controls. While at T4 it could be observed that the *trans*-cinnamic treatment resulted in the accumulation of many of the identified metabolites compared to the control, such as citric acid, lactic acid, shikimic acid, galactinol, melibiose, maltose, myo-inositol, cellobiose, trehalose, phenylalanine, chlorogenic acid, galactitol, ferulic acid, α-lactose, *p*-coumaric acid, or adipic acid among others.

A detailed analysis of the pathways and networks affected by trans-cinnamic treatment was performed using the "MetPa" module of Metaboanalyst. The analysis revealed that 39 routes were significantly affected; 14 had an impact score higher than 0.20 (Supplementary Table S1 and Table 1). In particular, the main pathways affected were: (i) biosynthesis of secondary metabolites—unclassified; (ii) alanine, aspartate and glutamate metabolism; (iii) isoquinoline alkaloid biosynthesis; (iv) phenylalanine metabolism; (v) cyanoamino acid metabolism; (vi) glycine, serine and threonine metabolism; (vii) beta-alanine metabolism; (viii) starch and sucrose metabolism; (ix) tyrosine metabolism; (x) galactose metabolism; (xi) arginine biosynthesis; (xii) cutin, suberine and wax biosynthesis; (xiii) glyoxylate and dicarboxylate metabolism; and (xiv) citrate cycle (TCA cycle).

Table 1. Results from ingenuity pathway analysis with MetPa carried out on *Zea mays* roots treated with 103 µM *trans*-cinnamic acid after exposure to various times with the compound.

Pathway	Total Cmpd	Hits	Impact	Raw *p*	FDR
Biosynthesis of secondary metabolites—unclassified	5	1	1	0.00076429	0.0014331
Alanine, aspartate and glutamate metabolism	22	9	0.77698	2.88×10^{-5}	0.00045239
Isoquinoline alkaloid biosynthesis	6	2	0.64705	0.00052097	0.0010779
Phenylalanine metabolism	12	1	0.42308	0.0035621	0.0048574
Cyanoamino acid metabolism	26	4	0.375	0.0013535	0.0021949
Glycine, serine and threonine metabolism	33	6	0.3547	0.00048176	0.0010323
beta-Alanine metabolism	18	4	0.3254	1.20×10^{-5}	0.00045239
Starch and sucrose metabolism	22	5	0.32054	0.0016991	0.0025486
Tyrosine metabolism	18	4	0.27568	0.0014806	0.0023377
Galactose metabolism	27	8	0.26927	0.0009734	0.0016687
Arginine biosynthesis	18	6	0.25243	0.00011212	0.00051746
Cutin, suberine and wax biosynthesis	14	2	0.25	0.00071144	0.001377
Glyoxylate and dicarboxylate metabolism	29	7	0.23322	6.03×10^{-5}	0.00045239
Citrate cycle (TCA cycle)	20	5	0.23269	0.019317	0.022726

Total Cmpd: the total number of compounds in the pathway; Hits: is the matched number from the uploaded data; Impact: is the pathway impact value calculated from pathway topology analysis; Raw *p*: is the original *p* value calculated from the enrichment analysis; FDR: false discovery rate; N = 3.

3. Discussion

In previous works with *trans*-cinnamic acid, Lupini et al. [29] showed that this compound had a strong phytotoxic effect on maize seedlings roots after 2 days of treatment, which varied according to the root type (primary, seminal, nodal and laterals). The growth inhibition observed in this study was related to the inhibition of the plasma membrane H^+-ATPase activity that would negatively alter nitrate uptake and acidification, thereby reducing cell wall loosening. Later, Araniti et al. [30] observed that after 5 days of treatment with *trans*-cinnamic acid on maize leaves, the compound caused stress, reducing leaf growth and seedling development. However, the plants could cope with this stress

by producing stress response-related metabolites such as salicylic acid. Moreover, treated plants were redirecting the metabolism to galactose production, leading to an increase in ascorbic acid content, an important compound in plant protection during oxidative stress. In this study, we focused on the short-term (6 to 48 h treatment) effects of *trans*-cinnamic acid on maize seedling roots, focusing on its effect on xylem vessels and how metabolism varied over time.

In cross-sections of maize roots after 48 h of treatment with ED_{50} of *trans*-cinnamic acid, it could be observed how the compound caused an increase in the diameter of the vascular cylinder and a reduction in the xylem vessels' area. An increase in the diameter of the vascular cylinder could be observed in situations of metal stress, such as cadmium in *Glycine max* L. [35] or under moderate salinity stress in soybean [36]. This alteration under salt stress was also observed in plants growing in arid areas, such as *Tamarix ramosissima* Ledeb. [37]. The increase in the diameter of the vascular cylinder after treatment with *trans*-cinnamic acid might indicate that the plants started to be stressed. Reduced xylem diameter observed after treatment may also be a symptom of stress. Lovisolo and Schubert [38] observed that *Vitis vinifera* L. plants subjected to water stress had a smaller xylem vessel area. Other species of commercial interest, such as tomato (*Solanum lycopersicum* L.) [39] and soybean [40], also saw their xylem area reduced when subjected to water stress. This alteration was also observed in pearl millet (*Pennisetum glaucum* [L.] R. Br.), a cereal species adapted to semi-arid environments [41]. Therefore, the alterations observed in *trans*-cinnamic acid-treated roots, joined to those observed by Lupini et al. [29], suggest that plants are experiencing stress and that their growth and development are compromised. Salvador et al. [31] also demonstrated that hosoybean roots' growth was altered after cinnamic acid treatment due to increased lignification and auxin alteration after 24 h treatment. However, no studies were previously done at very short times (under 24 h) to understand the primary mechanism of action of *trans*-cinnamic acid. Therefore, metabolomic measurements at different times for 48 h were taken to observe the changes that occurred in the metabolome over time (from 6 to 48 h).

In the PLS-DA, a clear separation between control and treatment was observed at tested times, reflected in the heatmap built using the significantly altered compounds resulting from the ANOVA analysis. It could be observed how the treatment with *trans*-cinnamic acid had already altered the metabolism after 6 h exposure to the compound, and that the variation in the metabolites was similarly maintained up to 24 h of treatment. This early variation was characterized by a decrease in the content of most amino acids as determined by GC-MS. This alteration in the levels of many amino acids could also be observed in the analysis of metabolic pathways, where up to six pathways related to amino acid metabolism were altered (alanine, aspartate and glutamate metabolism; phenylalanine metabolism; glycine, serine and threonine metabolism; beta-alanine metabolism; tyrosine metabolism; and arginine biosynthesis). The plant can take amino acids directly from the medium, but these are generally synthesised from the ammonium or nitrate that the plants absorb from the soil circulating solution [42]. The main site of formation is in the leaves, but amino acid is also synthesized in the roots [43]. Glutamine synthetase and glutamate synthase are the first enzymes involved in the amino acid synthesis, originating from glutamine and glutamate, from which most of the remaining amino acids are produced [44]. Therefore, low levels of these amino acids, such as those observed in the early times (T1, T2 and T3) of treatment with *trans*-cinnamic acid, can cause a drop in the content of the other amino acids. Lupini et al. [29] demonstrated how *trans*-cinnamic acid causes inhibition of nitrogen uptake in maize roots after 24 h of treatment. Several studies have also shown that plants growing on nitrogen-poor media show a low amino acid content [45,46]. Therefore, the inhibition of nitrogen uptake caused by *trans*-cinnamic acid could be the cause behind the decrease in amino acids observed in this study at very short treatment times, which could be considered the primary mechanism of action of the compound. This decrease in amino acids over time would also induce a reduction in protein synthesis, as observed by Araniti et al. [30] in their experiment with *trans*-cinnamic acid.

On the contrary, at 48 h of treatment the variation in metabolites was very different from the rest of the times and the control. As shown in the heatmap, it could be observed that after 48 h treatment many of the metabolites related to lignin syntheses, such as phenylalanine, ferulic acid or p-coumaric acid, were increased compared to the control [47].

Lignin biosynthesis begins with the transformation of phenylalanine into cinnamic acid, which is then transformed into p-coumaric acid [48]. These transformations are the first step in lignin and flavonoid synthesis [49]. The increase in phenylalanine and *p*-coumaric acid suggests an alteration in the phenylpropanoid pathway, confirmed by metabolic pathway analysis, where one of the affected pathways was phenylalanine metabolism. The addition of the compound could trigger metabolic pathways (such as lignin biosynthesis) to reduce the excess of *trans*-cinnamic acid and detoxify it from the cells. D'Apice et al. [50] observed that alterations in phenylalanine metabolism led to increased lignin synthesis and changes in many metabolites involved in this process.

Lignin is a biopolymer normally made up of three basic units of natural lignin polymers: p–hydroxyphenyl (H), guaiacyl (G), and syringyl (S), which are generated from three monolignols, p–coumaryl alcohols, coniferyl alcohols, and sinapyl alcohols, respectively [49]. A metabolite also involved in lignin synthesis, specifically in S-subunits, is sinapic acid [49]. Although this metabolite was decreased after 48 h of treatment, its levels were elevated until 24 h of treatment with *trans*-cinnamic acid, as seen in the heat map, suggesting that this compound was consumed over time to increase the synthesis of S-subunits.

Other compounds that accumulated in the roots after 48 h of treatment with the compound were shikimic acid and chlorogenic acid, which also influence lignin biosynthesis [51] and trehalose. Trehalose is synthesised from glucose-6-phosphate and uracil (another accumulated metabolite) and can activate lignin biosynthesis [52].

Increased lignin synthesis can improve resistance to lodging [53] or to biotic or abiotic stress [49], but it can also lead to growth inhibition, as observed by Deng et al. [54] after treating tomato plants with the natural growth regulator laxogenin C. The reduction in root growth in maize plants observed by Lupini et al. [29] after treatment with *trans*-cinnamic acid could be a consequence of an increase in lignification caused by an alteration in phenylalanine metabolism.

Finally, Araniti et al. [30] observed how galactose metabolism was affected in maize leaves in response to *trans*-cinnamic acid stress after 5 days. The accumulation of melibiose, galactinol, maltose, myo-inositol and α-lactose suggests that galactose metabolism may be affected, confirmed by analysis of metabolic pathways. Therefore, the mechanisms against the stress generated by *trans*-cinnamic early on amino acids after 6 h of treatment evolve to lignin production at about 48 h of treatment.

4. Conclusions

The results obtained in this study support those obtained by Lupini et al. [29] and Araniti et al. [30] in previous works with *trans*-cinnamic acid, in addition to providing new information on changes in the metabolome of maize roots treated with the compound. At very short times (from 6 to 24 h), the compound causes a decrease in many amino acids and alteration of many related metabolic pathways, confirming that inhibition of nitrogen uptake would be a primary mechanism of action of *trans*-cinnamic acid. In the last tested time (48 h), treatment with *trans*-cinnamic acid caused alterations in both root morphology (changes in the vascular cylinder) and metabolism. In an attempt to detoxify the excess of *trans*-cinnamic acid, the plant appears to convert it into lignin by activating phenylalanine metabolism. The compound also seems to increase galactose synthesis to cope with the stress generated by *trans*-cinnamic acid. Finally, it will be interesting and meaningful to investigate by molecular approaches based on NGS (RNA sequencing or ChipSeq) to provide useful information regarding the molecular mechanisms involved in plant response to *trans*-cinnamic acid.

5. Materials and Methods

5.1. Plant Material, Growth Conditions and Treatment

Seeds of maize (*Zea mays* L.) were primed and germinated according to [29]. After germination, plants with uniform size were transferred in hydroponic systems with a one-fourth strength Hoagland solution [29]. Seedlings were maintained in this solution for 48 h under the conditions described by [30]. Then seedlings were transferred for 2 days to the same medium with 103 µM *trans*-cinnamic acid. This value is the ED_{50} reported by [29] in previous studies. For the metabolomic assay, plants were harvested at different times (T0 = 0 h; T1 = 6 h; T2 = 12 h; T3 = 24 h; T4 = 48 h). The treatment and solution were renewed daily to maintain nutrients and trans-cinnamic concentrations constant and to avoid the compound's possible transformation and/or degradation.

5.2. Measurement of Xylem Area

After 48 h of treatment treated and untreated seedlings were collected and immediately processed. Roots' cross sections, thick 50 µm, were cut by a vibrotome (Leica VT1000E, Leica Biosystems 21440 W. Lake Cook Road Floor 5 Deer Park, IL 60010 United States) and subsequently mounted on microscope slides and observed under Leica inverted TCS SP8 confocal scanning laser microscope equipped with 20× and 40×/oil immersion objectives. Argon laser excitation wavelength at 488 nm and an emission window of 509 nm were used. The diameter of the vascular bundle and the area of the xylem were evaluated through the image processing and analysis program ImageJ (http://imagej.nih.gov/ij/docs/index.html; accessed on 1 September 2022). Both parameters were calculated as % compared to the control.

5.3. Untargeted Metabolomic Analysis

The effect of *trans*-cinnamic acid on the metabolism of *Zea mays* plants was evaluated at different treatment times (T0 = 0 h; T1 = 6 h; T2 = 12 h; T3 = 24 h; T4 = 48 h). The treatments used were 0 µM (control, CT), and 103 µM (treatment, T) of *trans*-cinnamic acid. Roots were collected at different times and frozen in liquid nitrogen to stop metabolism. Subsequently, samples were ground and 100 mg of plant material per replicate were weighed and placed in 2 mL vials.

For the extraction, 1400 µL of methanol (−20 °C) were added to the plant material and shaken for 10 s. As a quantitative internal standard, 60 µL of ribitol (0.2 mg mL^{-1} stock in ultrapure H_2O) were added. Samples were placed in a thermomixer at 70 °C under agitation for 10 min (950 rpm) and then centrifuged for 10 min at 11,000× *g*. The supernatant obtained was transferred to glass vials where 750 µL $CHCl_3$ (−20 °C) and 1500 µL ultrapure H_2O (4 °C) were sequentially added to carry out the separation of metabolites by their polarity. Vials were vortexed for 10 s and then centrifuged for 15 min at 2200 g. After centrifugation, 150 µL of the upper phase (polar phase) were taken and placed in 2 mL vials to be completely dried in a vacuum concentrator without heating. The samples' derivatisation was carried out in two steps. The first step was the metoximation of the samples, which was achieved by adding 40 µL of methoxyamine hydrochloride (20 mg mL^{-1} in pyridine) to the dried samples and incubating them for 2 h in a thermomixer at 37 °C (950 rpm). The second step of the derivatization consisted of the silylation of the samples, achieved by adding 70 µL of MSTFA to the aliquots. Samples were then shaken in a thermomixer at 37 °C (950 rpm) per 30 min. Finally, 110 µL of the derivatised samples were transferred into glass vials for GC-MS analysis.

5.4. GC-Quadrupole/MS Analysis

The derivatised extracts were injected into a MEGA-5MS capillary column (30 m × 0.25 mm × 0.25 µm equipped with 10 m of pre-column) using a gas chromatograph apparatus (Agilent 7890A GC, Cernusco sul Naviglio, Milan, Italy) equipped with a single quadrupole mass spectrometer (Agilent 5975C, Cernusco sul Naviglio, Milan, Italy). The injector temperature was set at 250 °C, and the source temperature was set at 260 °C. One µL of the sample was injected in

splitless mode with helium as a gas carrier (flow of 1 mL min^{-1}) using the following programmed temperature: isothermal 5 min at 70 °C followed by a 5 °C/min ramp to 350 °C and a final 5 min heating at 330 °C. Mass spectra were recorded in electronic impact (EI) mode at 70 eV, scanning at 40–600 m/z range, scan time 0.2 sec. Mass spectrometric solvent delay was settled as 9 min. Blank solvents (pyridine), n-alkane standards and pooled samples that served as quality control (QCs), were injected at scheduled intervals for instrumental performance, tentative identification, and monitoring of shifts in retention indices (RI). Solvent blanks were run between samples, and each mass was checked against the blank run to exclude possible contamination sources.

5.5. Analysis of GS-MS Data by MS-DIAL

The MS-DIAL software, with an open-source publicly available EI spectra library, was used for raw peaks extraction, data baseline filtering and calibration of the baseline, peak alignment, deconvolution analysis, integration of the peak height and peak annotation. The average peak width of 20 scans and a minimum peak height of 1000 amplitudes was applied for peak detection, and the sigma window value of 0.5, EI spectra cut-off of 10 amplitudes was implemented for deconvolution. For peaks identification, the retention time tolerance was settled at 0.5 min, the m/z tolerance was 0.5 Da, the EI similarity cut-off was 70%, and the identification score cut-off was 70%. The alignment parameters setting process and the retention time tolerance was 0.075 min.

We used publicly available libraries for compound annotation based on the mass spectral pattern as compared to EI spectral libraries such as the MSRI spectral libraries from Golm Metabolome Database [55] available from Max-Planck-Institute for Plant Physiology (Golm, Germany) and MassBank [56], MoNA (Mass Bank of North America).

Once the compounds and features were identified and annotated, the shared metabolites were only reported as quantified and confidently identified. For metabolite annotation and assignment of the EI-MS spectra, we followed the metabolomics standards initiative (MSI) guidelines for metabolite identification [57]. In particular, samples were annotated at: (i) Level 2: identification was based on the spectral database (match factor >70%); and (ii) Level 3: only compound groups were known, e.g., specific ions and RT regions of metabolites.

5.6. Statistical Analysis

GC-MS-driven untargeted metabolomics were carried out using a randomised design with three replications (n = 3).

Metabolomic data were normalised using the internal standard and analysed using Metaboanalyst 5.0 [58]. The missing values of the Lowess normalised dataset were replaced with a half of the minimum value found in the data set. Successively, data were Log_{10} transformed, and Pareto scaled. Data were then classified through Principal Component Analysis (PCA). PLS-DA was also employed to identify the differential metabolites by calculating the corresponding variable importance in the projection (VIP value). Finally, data were also analysed through the univariate analysis one-way ANOVA using the LSD test as post-hoc ($p \leq 0.05$). A false discovery rate was applied to the nominal p-value as a control for false-positive findings. Metabolites significantly affected by the treatments in the ANOVA test were presented as a heatmap and clustered using the Euclidean distance measurement and the Ward method for groups clusterisation.

Pathways analysis was carried out using the Metaboanalyst 5.0 tools and setting *Oryza sativa* L. as a metabolome reference database.

Supplementary Materials: The following supporting information can be downloaded at: https://www.mdpi.com/article/10.3390/plants12010189/s1, Table S1: untargeted metabolomics raw and statistical data.

Author Contributions: Conceptualization, F.A., A.L. and A.M.S.-M.; methodology, F.A., A.L., A.M.S.-M. and L.B.; software, D.L.-G., C.D.-T. and M.M.A.; validation, D.L.-G., C.D.-T., E.T., M.L.M., A.M. and M.M.A.; formal analysis, D.L.-G., C.D.-T., E.T., M.L.M., A.M. and M.M.A.; investigation, D.L.-

G., L.B., C.D.-T., A.L., M.M.A., E.T., M.L.M., A.M., A.M.S.-M. and F.A.; resources, A.M.S.-M. and F.A.; data curation, D.L.-G., C.D.-T., F.A. and A.M.S.; writing—original draft preparation, D.L.-G.; writing—review and editing, F.A., A.M.S.-M., A.L., M.M.A. and L.B.; visualisation, F.A., A.M.S.-M., A.L., M.M.A. and L.B.; supervision, F.A. and A.M.S.; project administration, A.M.S.-M. and F.A.; funding acquisition, A.M.S.-M. and F.A. All authors have read and agreed to the published version of the manuscript.

Funding: The MS was partially funded by the "Ministerio de Ciencia, Innovación y Universidades" [grant code RTI2018-094716-B-100].

Data Availability Statement: The datasets generated during and/or analysed during the current study are available from the corresponding author on reasonable request.

Conflicts of Interest: On behalf of the authors, I declare that none of the materials in this manuscript have been published or are concurrently submitted elsewhere. Moreover, the authors have no competing interests to declare.

References

1. Farooq, M.; Jabran, K.; Cheema, Z.A.; Wahid, A.; Siddique, K.H. The role of allelopathy in agricultural pest management. *Pest. Manag. Sci.* **2011**, *67*, 493–506. [CrossRef]
2. Shirgapure, K.H.; Ghosh, P. Allelopathy a tool for sustainable weed management. *Arch. Curr. Res. Int.* **2020**, *20*, 17–25. [CrossRef]
3. Wink, M. Modes of action of herbal medicines and plant secondary metabolites. *Medicines* **2015**, *2*, 251–286. [CrossRef] [PubMed]
4. Duke, S.O. Why have no new herbicide modes of action appeared in recent years? *Pest. Manag. Sci.* **2012**, *68*, 505–512. [CrossRef] [PubMed]
5. Álvarez-Rodríguez, S.; López-González, D.; Reigosa, M.J.; Araniti, F.; Sánchez-Moreiras, A.M. Ultrastructural and hormonal changes related to harmaline-induced treatment in *Arabidopsis thaliana* (L.) Heynh. root meristem. *Plant Physiol. Biochem.* **2022**, *179*, 78–89. [CrossRef] [PubMed]
6. López-González, D.; Costas-Gil, A.; Reigosa, M.J.; Araniti, F.; Sánchez-Moreiras, A.M. A natural indole alkaloid, norharmane, affects PIN expression patterns and compromises root growth in arabidopsis thaliana. *Plant Physiol. Biochem.* **2020**, *151*, 378–390. [CrossRef]
7. López-González, D.; Ledo, D.; Cabeiras-Freijanes, L.; Verdeguer, M.; Reigosa, M.J.; Sánchez-Moreiras, A.M. Phytotoxic activity of the natural compound norharmane on crops, weeds and model plants. *Plants* **2020**, *9*, 1328. [CrossRef]
8. Graña, E.; Sotelo, T.; Díaz-Tielas, C.; Reigosa, M.J.; Sánchez-Moreiras, A.M. The phytotoxic potential of the terpenoid citral on seedlings and adult plants. *Weed Sci.* **2013**, *61*, 469–481. [CrossRef]
9. Araniti, F.; Bruno, L.; Sunseri, F.; Pacenza, M.; Forgione, I.; Bitonti, M.B.; Abenavoli, M.R. The allelochemical farnesene affects arabidopsis thaliana root meristem altering auxin distribution. *Plant Physiol. Biochem.* **2017**, *121*, 14–20. [CrossRef]
10. Gelsomino, A.; Araniti, F.; Lupini, A.; Princi, G.; Petrovičová, B.; Abenavoli, M.R. Phenolic acids in plant-soil interactions: A microcosm experiment. *J. Allelochem. Inter.* **2015**, *1*, 25–38.
11. Kumar, S.; Abedin, M.M.; Singh, A.K.; Das, S. Role of phenolic compounds in plant-defensive mechanisms. In *Plant Phenolics in Sustainable Agriculture*; Lone, R., Shuab, R., Kamili, A.N., Eds.; Springer: Singapore, 2020; Volume 1, pp. 517–532.
12. Arvaniti, O.S.; Samaras, Y.; Gatidou, G.; Thomaidis, N.S.; Stasinakis, A.S. Review on fresh and dried figs: Chemical analysis and occurrence of phytochemical compounds, antioxidant capacity and health effects. *Food Res. J.* **2019**, *119*, 244–267. [CrossRef] [PubMed]
13. Kähkönen, M.P.; Hopia, A.I.; Vuorela, H.J.; Rauha, J.P.; Pihlaja, K.; Kujala, T.S.; Heinonen, M. Antioxidant activity of plant extracts containing phenolic compounds. *J. Agric. Food Chem.* **1999**, *47*, 3954–3962. [CrossRef] [PubMed]
14. Silva, V.; Igrejas, G.; Falco, V.; Santos, T.P.; Torres, C.; Oliveira, A.M.P.; Pereira, J.E.; Amaral, J.S.; Poeta, P. Chemical composition, antioxidant and antimicrobial activity of phenolic compounds extracted from wine industry by-products. *Food Control* **2018**, *92*, 516–522. [CrossRef]
15. Silva, V.; Falco, V.; Dias, M.I.; Barros, L.; Silva, A.; Capita, R.; Alonso-Calleja, C.; Amaral, J.S.; Igrejas, G.; Ferreira, I.C.F.R.; et al. Evaluation of the phenolic profile of castanea sativa mill. By-products and their antioxidant and antimicrobial activity against multiresistant bacteria. *Antioxidants* **2020**, *9*, 87. [CrossRef]
16. Lin, H.Y.; Chang, T.C.; Chang, S.T. A review of antioxidant and pharmacological properties of phenolic compounds in acacia confusa. *J. Tradit. Complement. Med.* **2018**, *8*, 443–450. [CrossRef] [PubMed]
17. Beserra, F.P.; Gushiken, L.F.S.; Hussni, M.F.; Ribeiro, V.P.; Bonamin, F.; Jackson, C.J.; Pellizzon, C.H.; Bastos, J.K. Artepillin C as an outstanding phenolic compound of brazilian green propolis for disease treatment: A review on pharmacological aspects. *Phytother. Res.* **2021**, *35*, 2274–2286. [CrossRef]
18. Albuquerque, B.R.; Heleno, S.A.; Oliveira, M.B.P.P.; Barros, L.; Ferreira, I.C.F.R. Phenolic compounds: Current industrial applications, limitations and future challenges. *Food Funct.* **2021**, *12*, 14–29. [CrossRef]

19. Macias-Garbett, R.; Serna-Hernández, S.O.; Sosa-Hernández, J.E.; Parra-Saldívar, R. Phenolic compounds from brewer's spent grains: Toward green recovery methods and applications in the cosmetic industry. *Front. Sustain. Food Syst.* **2021**, *5*, 681684. [CrossRef]
20. Caporaso, N.; Formisano, D.; Genovese, A. Use of phenolic compounds from olive mill wastewater as valuable ingredients for functional foods. *Crit. Rev. Food Sci. Nutr.* **2018**, *58*, 2829–2841. [CrossRef]
21. Mark, R.; Lyu, X.; Lee, J.J.L.; Parra-Saldívar, R.; Chen, W.N. Sustainable production of natural phenolics for functional food applications. *J. Funct. Foods* **2019**, *57*, 233–254. [CrossRef]
22. Whitehead, D.C. Identification of P-hydroxybenzoic, vanillic, p-coumaric and ferulic acids in soils. *Nature* **1964**, *202*, 418. [CrossRef] [PubMed]
23. Yin, Z.; Wong, W.; Ye, W.; Li, N. Biologically active cis-cinnamic acid occurs naturally in brassica parachinensis. *Chin. Sci. Bull.* **2003**, *48*, 555. [CrossRef]
24. Steenackers, W.; Klíma, P.; Quareshy, M.; Cesarino, I.; Kumpf, R.P.; Corneillie, S.; Araújo, P.; Viaene, T.; Goeminne, G.; Nowack, M.K.; et al. Cis-cinnamic acid is a novel, natural auxin efflux inhibitor that promotes lateral root formation. *Plant Physiol.* **2017**, *173*, 552–565. [CrossRef]
25. Salum, M.L.; Erra-Balsells, R. High purity cis-cinnamic acid preparation for studying physiological of trans-cinnamic and cis-cinnamic acids in higher plants. *Environ. Control Biol.* **2013**, *52*, 1–10. [CrossRef]
26. Baziramakenga, R.; Leroux, I.G.D.; Simard, R.R. Effects of benzoic and cinnamic acids on membrane permeability of soybean roots. *J. Chem. Ecol.* **1995**, *21*, 1271–1285. [CrossRef]
27. Lupini, A.; Araniti, F.; Sunseri, F.; Abenavoli, M.R. Coumarin interacts with auxin polar transport to modify root system architecture in arabidopsis thaliana. *Plant Growth Regul.* **2014**, *74*, 23–31. [CrossRef]
28. Ye, S.F.; Zhou, Y.H.; Sun, Y.; Zou, L.Y.; Yu, J.Q. Cinnamic acid causes oxidative stress in cucumber roots, and promotes incidence of fusarium wilt. *Environ. Exp. Bot.* **2006**, *56*, 255–262. [CrossRef]
29. Lupini, A.; Sorgonà, A.; Princi, M.P.; Sunseri, F.; Abenavoli, M.R. Morphological and physiological effects of trans-cinnamic acid and its hydroxylated derivatives on maize root types. *Plant Growth Regul.* **2016**, *78*, 263–273. [CrossRef]
30. Araniti, F.; Lupini, A.; Mauceri, A.; Zumbo, A.; Sunseri, F.; Abenavoli, M.R. The allelochemical trans-cinnamic acid stimulates salicylic acid production and galactose pathway in maize leaves: A potential mechanism of stress tolerance. *Plant Physiol. Biochem.* **2018**, *128*, 32–40. [CrossRef]
31. Salvador, V.H.; Lima, R.B.; Dos Santos, W.D.; Soares, A.R.; Böhm, P.A.F.; Marchiosi, R.; Ferrarese, M.D.L.L.; Ferrarese-Filho, O. Cinnamic acid increases lignin production and inhibits soybean root growth. *PLoS ONE* **2013**, *8*, e69105. [CrossRef]
32. Wang, Y.; Xu, L.; Shen, H.; Wang, J.; Liu, W.; Zhu, X.; Wang, R.; Sun, X.; Liu, L. Metabolomic analysis with Gc-Ms to reveal potential metabolites and biological pathways involved in pb &cd stress response of radish roots. *Sci. Rep.* **2015**, *5*, 18296. [CrossRef] [PubMed]
33. Van Dam, N.M.; Bouwmeester, H.J. Metabolomics in the Rhizosphere: Tapping into belowground chemical communication. *Trends Plant Sci.* **2016**, *21*, 256–265. [CrossRef]
34. Landi, M.; Misra, B.B.; Muto, A.; Bruno, L.; Araniti, F. Phytotoxicity, morphological, and metabolic effects of the sesquiterpenoid nerolidol on arabidopsis thaliana seedling roots. *Plants* **2020**, *9*, 1347. [CrossRef] [PubMed]
35. Pérez Chaca, M.V.; Vigliocco, A.; Reinoso, H.; Molina, A.; Abdala, G.; Zirulnik, F.; Pedranzani, H. Effects of cadmium stress on growth, anatomy and hormone contents in *glycine max* (L.) Merr. *Acta Physiol. Plant.* **2014**, *36*, 2815–2826. [CrossRef]
36. Silva, B.R.S.; Batista, B.L.; Lobato, A.K.S. Anatomical changes in stem and root of soybean plants submitted to salt stress. *Plant Biol.* **2021**, *23*, 57–65. [CrossRef]
37. Zhang, R.; Ma, X.; Wang, M.; Lv, H.; Zhu, C. Effects of salinity and water stress on the physiological and ecological processes and plasticity of tamarix ramosissima seedlings. *Acta Ecol. Sin.* **2016**, *36*, 433–441. [CrossRef]
38. Lovisolo, C.; Schubert, A. Effects of water stress on vessel size and xylem hydraulic conductivity in *Vitis vinifera* L. *J. Exp. Bot.* **1998**, *49*, 693–700. [CrossRef]
39. Hernandez-Espinoza, L.H.; Barrios-Masias, F.H. Physiological and anatomical changes in tomato roots in response to low water stress. *Sci. Hortic.* **2020**, *265*, 109208. [CrossRef]
40. Prince, S.J.; Murphy, M.; Mutava, R.N.; Durnell, L.A.; Valliyodan, B.; Grover Shannon, J.; Nguyen, H.T. Root xylem plasticity to improve water use and yield in water-stressed soybean. *J. Exp. Bot.* **2017**, *68*, 2027–2036. [CrossRef]
41. Purushothaman, R.; Zaman-Allah, M.; Mallikarjuna, N.; Pannirselvam, R.; Krishnamurthy, L.; Lakkegowda, C.; Gowda, L. Root anatomical traits and their possible contribution to drought tolerance in grain legumes. *Plant Prod. Sci.* **2013**, *16*, 1–8. [CrossRef]
42. Moran-Zuloaga, D.; Dippold, M.; Glaser, B.; Kuzyakov, Y. Organic nitrogen uptake by plants: Reevaluation by position-specific labeling of amino acids: Reevaluation of organic n uptake by plants by position-specific labeling. *Biogeochemistry* **2015**, *125*, 359–374. [CrossRef]
43. Novoa, R.; Loomis, R.S. Nitrogen and plant production. *Plant Soil* **1981**, *58*, 177–204. [CrossRef]
44. Lea, P.J.; Azevedo, R.A. Nitrogen use efficiency. 2. Amino acid metabolism. *Ann. Appl. Biol.* **2007**, *151*, 269–275. [CrossRef]
45. Perchlik, M.; Tegeder, M. Improving plant nitrogen use efficiency through alteration of amino acid transport processes. *Plant Physiol.* **2017**, *175*, 235–247. [CrossRef] [PubMed]

46. Xin, W.; Zhang, L.; Zhang, W.; Gao, J.; Yi, J.; Zhen, X.; Li, Z.; Zhao, Y.; Peng, C.; Zhao, C. An integrated analysis of the rice transcriptome and metabolome reveals differential regulation of carbon and nitrogen metabolism in response to nitrogen availability. *Int. J. Mol. Sci.* **2019**, *20*, 2349. [CrossRef] [PubMed]
47. Barros, J.; Serk, H.; Granlund, I.; Pesquet, E. The cell biology of lignification in higher plants. *Ann. Bot.* **2015**, *115*, 1053–1074. [CrossRef]
48. Vanholme, R.; De Meester, B.; Ralph, J.; Boerjan, W. Lignin biosynthesis and its integration into metabolism. *Curr. Opin. Biotechnol.* **2019**, *56*, 230–239. [CrossRef]
49. Dong, N.Q.; Lin, H.X. Contribution of phenylpropanoid metabolism to plant development and plant–environment interactions. *J. Integr. Plant Biol.* **2021**, *63*, 180–209. [CrossRef]
50. D'Apice, G.; Moschin, S.; Araniti, F.; Nigris, S.; Di Marzo, M.; Muto, A.; Banfi, C.; Bruno, L.; Colombo, L.; Baldan, B. The role of pollination in controlling ginkgo biloba ovule development. *New Phytol.* **2021**, *232*, 2353–2368. [CrossRef]
51. Silva, N.; Mazzafera, P.; Cesarino, I. Should I stay or should I go: Are chlorogenic acids mobilized towards lignin biosynthesis? *Phytochemistry* **2019**, *166*, 112063. [CrossRef]
52. Luo, Y.; Wang, Y.; Xie, Y.; Gao, Y.; Li, W.; Lang, S. Transcriptomic and metabolomic analyses of the effects of exogenous trehalose on heat tolerance in wheat. *Int. J. Mol. Sci.* **2022**, *23*, 5194. [CrossRef] [PubMed]
53. Yu, M.; Wang, M.; Gyalpo, T.; Basang, Y. Stem lodging resistance in hulless barley: Transcriptome and metabolome analysis of lignin biosynthesis pathways in contrasting genotypes. *Genomics* **2021**, *113*, 935–943. [CrossRef] [PubMed]
54. Deng, Y.; Wang, J.; Zhang, A.; Zhu, Z.; Ren, S.; Zhang, C.; Zhang, Q. Metabolomics mechanism and lignin response to laxogenin c, a natural regulator of plants growth. *Int. J. Mol. Sci.* **2022**, *23*, 2990. [CrossRef] [PubMed]
55. Kopka, J.; Schauer, N.; Krueger, S.; Birkemeyer, C.; Usadel, B.; Bergmüller, E.; Dörmann, P.; Weckwerth, W.; Gibon, Y.; Stitt, M.; et al. GMD@ CSB. DB: The golm metabolome database. *Bioinformatics* **2005**, *21*, 1635–1638. [CrossRef]
56. Horai, H.; Arita, M.; Kanaya, S.; Nihei, Y.; Ikeda, T.; Suwa, K.; Ojima, Y.; Tanaka, K.; Tanaka, S.; Aoshima, K.; et al. MassBank: A public repository for sharing mass spectral data for life sciences. *J. Mass Spectrom.* **2010**, *45*, 703–714. [CrossRef]
57. Fiehn, O.; Robertson, D.; Griffin, J.; Vab Der Werf, M.; Nikolau, B.; Morrison, N.; Sumner, L.W.; Goodacre, R.; Hardy, N.W.; Taylor, C.; et al. The metabolomics standards initiative (MSI). *Metabolomics* **2007**, *3*, 175–178. [CrossRef]
58. Pang, Z.; Chong, J.; Zhou, G.; De Lima Morais, D.A.; Chang, L.; Barrette, M.; Gauthier, C.; Jacques, P.É.; Li, S.; Xia, J. MetaboAnalyst 5.0: Narrowing the gap between raw spectra and functional insights. *Nucleic Acids Res.* **2021**, *49*, W388–W396. [CrossRef] [PubMed]

AGROCHIMICA

**International Journal of Plant Chemistry,
Soil Science and Plant Nutrition
of the University of Pisa**

Vol. 66 - No. 2-3 - April-September 2022

PISA
UNIVERSITY
PRESS

Agrochimica, Vol. 66 - No. 2-3 April-September 2022

Impact of municipal solid waste compost amendment and mineral fertilization on soil properties and *Cucumis melo* L. subsp. *melo* var. *cantalupensis* crop quality

Santina Rizzo[1], Marco Minervino[1], Antonella Muto[1], Emanuela Talarico[1], Innocenzo Muzzalupo[2], Fabrizio Araniti[3], Adriana Chiappetta[1], Leonardo Bruno[1,*]

[1] Dipartimento di Biologia, Ecologia e Scienze della Terra, Università della Calabria, 87036 Arcavacata di Rende, Cosenza, Italy

[2] Centro di Ricerca Olivicoltura, Frutticoltura e Agrumicoltura, Consiglio per la Ricerca in Agricoltura e l'Analisi dell'Economia Agraria, 87036 Rende, Cosenza, Italy

[3] Dipartimento di Scienze Agrarie e Ambientali - Produzione, Territorio, Agroenergia, Università degli Studi di Milano, 20133 Milano, Italy

Keywords: Compost, heavy metals, mineral fertilizer, melon, soil quality

Abstract: Composting is considered a sustainable method to handle and reprocess the organic fraction of Municipal Solid Waste (MSW). It has been largely demonstrated that compost has positive effects on agricultural soil fertility improving its physical, chemical and biological properties. This work aims to compare the MSW compost and NPK mineral fertilizer effects on both soil properties and crops including qualitative and sensorial analysis parameter. As experimental species, *Cucumis melo* L. subsp. *melo* var. *cantalupensis* was selected. Vegetative growth of plants has been assisted until these were harvested and then analysed to assess dimensions, quality and flavour. Additional analyses about nutrient elements and heavy metals content were carried out. Soil fertility was also estimated through chemical and biochemical analysis, carried out before soil fertilization and at the end of the crop cycle. Globally we observed that compost increased microbial activity and organic matter content in the soil, as compared to mineral fertilization. However, melon fruits produced with different soil fertilizations exhibited comparable dimensions and quality. Lastly, analyses about heavy metals content did not show any significant difference. In conclusion, the application of compost to agricultural land determines an improvement of biological parameters that results in a more active soil microbial community.

* Corresponding author: leonardo.bruno@unical.it
Received 5 May 2022; received in revised form 28 June 2022; accepted 6 July 2022.

DOI 10.12871/000218572022231

Introduction

Due to increasing population pressure and the ever-increasing loads of waste production, it has become difficult to cope with the challenge of handling the enormous quantities of waste. Among the techniques used for waste management, composting is considered to be a clean and sustainable method to handle and reprocess at least the organic fraction of Municipal Solid Waste (MSW) (Lim et al., 2016). Composting not only increases the capacity of waste recycling, but also it improves the side effect of waste disposal on environment giving a second life to waste, allowing to reduce the usage of chemical fertilizers (Lim et al., 2016). Moreover, it has been largely demonstrated that compost has positive effects on agricultural soil fertility improving its physical, chemical and biological properties (Watteau and Villemin, 2011)increasing soil OM is very important. On the other hand, the eutrophication of surface water caused by continuous use of phosphorus (P. Loss of soil fertility, mainly due to the excessive use of mineral fertilizers and the reduced intake of organic matter, is a widespread problem either in regions where geographical characteristics make agriculture difficult or in areas where intensive agriculture is practiced. Moreover, the use of compost as a fertilizer is a technique increasingly appreciated in agricultural land for food production, in the management of urban green areas as well as in the restoration of degraded and polluted areas. In addition, encouraging the use of MSW compost could both improve soil quality and reduce the use of non-renewable sources and waste management proble.Moreover, recent studies demonstrated that compost addition in soil could induce a long-term improvement (up to 9 years) of soil fertility and water retention (Nautiyal et al., 2010)in some cases, metals and excess nutrients can move through the soil profile into groundwater. Municipal solid waste compost has also been reported to have high salt concentrations, which can inhibit plant growth and negatively affect soil structure. A review of relevant agricultural studies is presented as well as recommendations for improving MSW compost quality. Its safe use in agriculture can be ensured with source separation (or triage of MSW to be composted. Because of that, the use of high quality compost is largely appreciated in organic farming and in semi-arid regions, which tend to desertification due to climate changes. In the last case, the scarce and irregular rainfalls, along with high rates of evapotranspiration, lead to poor biomass production and, therefore, to a limited input of plant residues in the soil which must be yearly integrated in order to avoid soil erosion and reduction of soil fertility. In Italy, among the horticultural species of economic

importance, *Cucumis melo* L. (netted melon) is one of the most widespread. This species is a highly diversified eudicot diploid species (2n = 2x = 24) originated in Asia, including several varieties. In particular, the varieties (vars.) *cantalupensis* (cantaloupe) and *inodorus* (honeydew) belong to the subsp. *melo*, whereas the vars. *momordica*, *conomon*, *dudaim*, and *chito* to the subsp. *agrestis* (Decker-Walters et al., 2002). Moreover, the 68% of the total national production is produced in the South of Italy since cantaloupes (*Cucumis melo* L. subsp. *melo* var. *cantalupensis*), the most appreciated variety, are warm climate crops and are cold and frost sensitive (Lim, 2012). Moreover, it has been largely used as bioindicator of heavy metals in soils, which are a common problem during MSW compost production (Othman and Asharuddin, 2013). In this context, the aim of the present study was to evaluate the effects of compost obtained from the organic fraction of MSW on both soil properties and melon crops, in comparison with conventional mineral fertilization NPK. A cantaloupe cultivar was used as a plant system. Soil samples were analyzed before the fertilization and after the crop cycle in order to search for any changes concerning the soil chemical and biological parameters and the qualitative characteristics of the fruit following the use of compost with respect to mineral fertilizer.

Materials and Methods

Site information and experimental setup

The field experiment was carried on soil previously used for agricultural activity, located in southern of Italy, Calabria region, locality San Marco Argentano (39°, 37' lat. N; 16°, 13' long. E; 99 m a.s.l.). The experimental field, about 0.08 ha, was divided into two portions of 400 square meters: one portion was fertilized with 11-22-16 NPK (NO_3^- 3.5%; NH_4^+ 7.5%; P_2O_5 22%; K_2O 16%) fertilizer from YaraMila® at 500 kg ha^{-1}. The other portion, supplementary divided into two plots, was manured with compost obtained from the organic fraction of MSW (supplied by Calabra Maceri e Servizi Ltd), and incorporated at the dose of 8 and 16 Mg ha^{-1} (Fig. 1). Doses of compost were decided considering data present in literature, showing that doses within the range 10-30 Mg ha^{-1} better suit in agricultural fields (Cicatelli et al., 2014).

Soil sampling

Soil samples, from 10 cm deep layer, were collected before fertilization (T0) and at the end of the crop cycle (T1). Sampling was carried

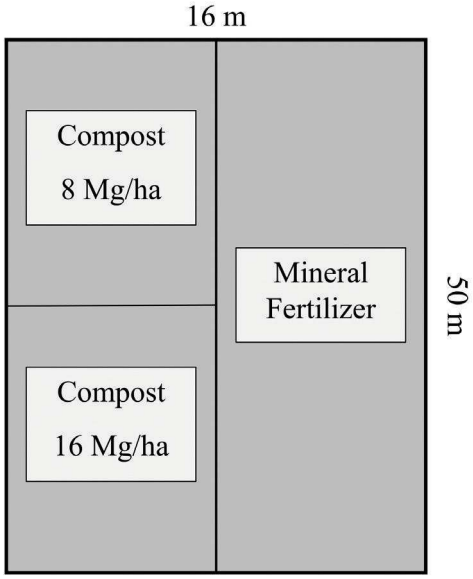

Fig. 1. Schematic representation of the experimental work field.

out using the quarting method described in "The Official Methods of Chemical Analysis of the Soil" (Ministero per le Politiche Agricole e Forestali, 1999); soil samples were sieved (2.0 mm mesh) and stored at 4°C.

Soil chemical analysis

For pH determination, 10 g of soil was mixed with 25 ml of distilled water, shaken for 2 h and then pH was measured using a laboratory pH meter; a ratio of 1:2 was instead used for the determination of electrical conductivity (EC) (Ministero per le Politiche Agricole e Forestali, 1999). Organic carbon (C) and organic matter (C × 1.724) were measured following the methods described by Springer and Klee (Springer and Klee, 1954) respectively, whereas total nitrogen in the soil was determined by Kjeldahl distillation method (Kjeldahl, 1883). Total calcium carbonate content measurement was performed using the De Astis calcimeter, while active carbonate content was estimated through Druineau method (Drouineau, 1942). In addition, to estimate the Cation Exchange Capacity (CEC) the Barium chloride–triethanolamine method was employed (Ministero per le Politiche Agricole e Forestali, 1999).

Finally, metals concentration in soil were determined through inductively coupled plasma optical emission spectroscopy (ICP-OES).

Soil biochemical analysis

Soil biochemical analysis were carried out according to "The Official Methods of Biochemical Analysis of the Soil" (Ministero per le Politiche Agricole e Forestali 2004). Soil microbial biomass was determined by fumigation-incubation method, whereas soil respiration was assessed by titrimetric method, measuring the CO_2 evolved into the soil in a hermetically closed system during a 3-day incubation period (25°C, in darkness). Fluorescein diacetate hydrolysis was measured using 3,6-diacetyl fluorescein as substrate and measuring the absorbance (CECIL CE1010, Cecil Instrumentation Services Ltd) of released fluorescein at 490 nm (as described in Ministero per le Politiche Agricole e Forestali, 2004). Acid and alkaline phosphatase activities were assayed by the hydrolysis rate of p-nitrophenylphosphate (disodium salt) supplied as substrate and then measuring the absorbance of released p-nitrophenol at 400 nm in a buffered solution at pH 6.5 and 11.0, respectively.

Selected plant species

Seedlings of cantaloupe variety were transplanted in rows at the beginning of March 2018 using an inter-row distance of 1.0 m, and a distance among plants in the row of 0.40-0.60 m. Plant growth was assisted, through irrigation as well as weeds and pests management, until fruit production.

Fruit sampling, qualitative and chemical analysis

At the end of the crop cycle, when melon fruits were at the right degree of commercial ripening, from each differentially fertilized parcel, 30 plants were randomly selected and melon fruits were collected. The physical quality parameters were then determined: weight (kg); longitudinal (section from calix to apex) and equatorial caliber (maximum cross-section) expressed in cm; peel thickness (mm); percentage between weight of seeds and placental tissues; pulp yield (mesocarp or edible portion, expressed as a percentage of fresh weight). Then, fruit shape index was calculated according to the equation proposed by Artés et al. (1993): fruit shape index = equatorial calibre/longitudinal calibre (Artés et al., 1993). Furthermore, quality factors such as pH, titratable activity and total soluble solids content in juice (°Brix), evaluated through refractometric analyses, have been estimated as previously described (Muto

et al., 2020; Artés et al., 1993). The titratable activity was estimated by titrating 1 ml of juice with 0.1 N NaOH, data were expressed as the percentage of citric acid. A representative sample of about 30 melons from each experimental condition was analysed through inductively coupled plasma-mass spectrometry (ICP-MS) to evaluate nutrients (nitrite, nitrate, Na, Mg, K, Ca, P, Fe, Zn) and heavy metals concentrations (Cr, Mn, Ni, Cu, B, Hg, Pb).

Sensorial analysis

Fruits was evaluated twice in two different sessions, June 5th and July 9th, by a trained group of 10 participants recruited from CibusLab association, Cosenza, Italy. The sensory evaluation area was equipped with ten booths, air conditioned at 20 ± 2°C and with 50 ± 5% relative humidity, and lit with a white light at 850 lux. The panelists were presented with a single melon fruit for each sample belonging to the three soil treatments, identified only by a randomly chosen 3-digit code. A quantitative–qualitative sensorial analysis was performed. Melon slices were separately placed on plates and presented to the tasters, which individually evaluated flavour intensity, crunchiness, consistence, sweetness, acidity, juiciness, bitterness, astringency and harmony. The assessors were instructed to sniff the samples to score the aroma attributes, and then taste (and swallow) the samples to score the overall taste/flavour attributes and the mouthfeel attributes. There was a 45 seconds pause after the end of the mouthfeel attributes and the assessors then scored the after-effects which included both taste and mouthfeel effects. At each sample and at each of the nine descriptors a score between 0 and 10 was assigned. 0 denoted a low evaluation for the descriptor, whereas 10 a high appreciation. Between samples, panelists cleansed their palate with cracker and water. The software Smart Sensory box premium (Smart Sensory Solutions s.r.l., Sassari, Italy) was used to acquire and process the data. The sensorial analysis was carried out on fifty melons collected from each soil parcel.

Element concentration in soil and fruits

For heavy metals concentration, soil granulometric fraction (2.0 sieved) was selected from each soil sample and analysed according to Lindsay and Norvell (1978). The nutrients and the heavy metal content were analyzed in the edible part of the melon, on a representative sample of

30 melons per treatment. Samples were trated as described in Cicatelli et al. (2014) and then analysed through ICP-OES (Cicatelli et al., 2014).

Statistics

The experiments were carried out in a completely randomized design with 3 replications. Data were first checked for normality through the Kolmogorov-Smirnov test and then tested for homogeneity of variances with the Levene's test. Data were then analysed through one way ANOVA ($P \leq 0.05$) as post hoc. Statistical analyses were performed using the software Microsoft Excel XLStat®.

Results

Chemical analysis of soil and heavy metals content

Before soil fertilization (T0), soil pH was around 8, classifying itself as a sub-alkaline soil. As a result of mineral fertilization, pH value decreased by about 1 unit, settling around a neutral value. No significant changes in soil pH were observed in soil amended with compost (Table 1). Both total limestone content (calcium carbonate), active carbonate and total N were not influenced by the treatments. Similarly, the organic C was reduced in soil minerally fertilized, whereas in soil treated with the highest amount of compost (16 Mg ha^{-1}) a stimulation was observed. Concerning the C/N ratio no significant differences were observed among treatments (Table 1). Differences in electrical conductivity (EC) were significant only among control and both amended soils. In particular, a ≈ 1 fold increase in EC was observed in both treatments (Table 1). On the contrary, as a result of both organic and mineral fertilization, no significant differences were found in the soils CEC (Table 1). It is well known that compost could contains traces of heavy metals. Therefore their content was evaluated through ICP mass (Table 2). The obtained results highlighted no significant differences among control and both minerally fertilized and amended soils. Globally, the obtained results pointed out that soils treated with organic amendments where characterized by an increase in organic C and electrical conductivity, while no differences in heavy metals content were observed. We concluded that the organic amendment improves the chemical proprieties of the soil.

Soil biochemical analysis

In order to assess the degree of microbiological activity of the soil, various biochemical analyses were performed. Results pointed out that whereas the microbial biomass was not influenced by the treatments, the

Table 1. Chemical characteristics of the soil at the beginning of the experiment (T0) and at the end of the crop cycle, after 94 days from seedlings transplant (T1).

	T0	T1		
	Pre fertilization	**Mineral**	**Compost 8 Mg ha^{-1}**	**Compost 16 Mg ha^{-1}**
pH (H_2O, 1:2.5)	8.07 ± 0.01 **a**	7.00 ± 0.01 **b**	7.98 ± 0.01 **a**	7.80 ± 0.01 **a**
Total $CaCO_3$ (% DW)	< 1.0	< 1.0	< 1.0	< 1.0
Active $CaCO_3$ (% DW)	0.049 ± 0.01 **a**	0.076 ± 0.02 **a**	0.083 ± 0.02 **a**	0.070 ± 0.01 **a**
Total N (% DW)	0.08 ± 0.02	0.09 ± 0.01	0.09 ± 0.02	0.12 ± 0.04
Organic C (% DW)	0.41 ± 0.01 **a**	0.26 ± 0.05 **b**	0.36 ± 0.01 **ab**	0.52 ± 0.04 **c**
C/N	5.47	3.25	4.50	5.67
EC 25°C (dS m^{-1})	0.29 ± 0.10 **a**	0.34 ± 0.10 **a**	0.54 ± 0.10 **b**	0.61 ± 0.10 **b**
CEC ($cmol_{(+)}kg^{-1}$)	11.89 ± 3.33	10.41 ± 0.75	10.07 ± 1.04	11.69 ± 0.85

Means ± standard error. Different letters indicate significant differences ($p \leq 0.05$). n = 10.

Table 2. Soil total metal concentrations at the beginning of the experiment (T0) and at the end of the crop cycle, after 94 days from seedlings transplant (T1).Means ± standard error.

	T0	T1		
	Pre fertilization	**Mineral**	**Compost 8 Mg/ha**	**Compost 16 Mg/ha**
Cu (mg kg^{-1})	7.20 ± 2.52	8.37 ± 1.96	9.90 ± 3.00	8.30 ± 1.40
Zn (mg kg^{-1})	28.60 ± 13.27	39.23 ± 15.91	35.70 ± 11.70	30.73 ± 4.10
Mn (mg kg^{-1})	319.00 ± 92.96	487.67 ± 118.16	398.00 ± 50.00	409.33 ± 68.42
Fe (mg kg^{-1})	8393 ± 3582	11804 ± 2833	11502 ± 3000	11944 ± 2266
B (mg kg^{-1})	8.53 ± 2.81	16.93 ± 5.75	27.40 ± 12.00	21.60 ± 10.87
Cd (mg kg^{-1})	0.17 ± 0.12	<0.002	0.30 ± 0.10	<0.002
Cr (mg kg^{-1})	12.23 ± 5.17	18.82 ± 2.51	22.63 ± 11.94	16.48 ± 1.33
Hg (mg kg^{-1})	0.75 ± 0.07	0.86 ± 0.17	0.87 ± 0.38	0.88 ± 0.25
Ni (mg kg^{-1})	8.77 ± 3.55	11.15 ± 4.10	14.72 ± 3.00	10.58 ± 2.03
Pb (mg kg^{-1})	3.27 ± 1.66	8.64 ± 1.85	6.8 ± 1.0	7.29 ± 1.67

Means ± standard error.

microbial respiration was significantly stimulated by both mineral fertilization and amendments (Figs. 2a, b). In particular, the amount of CO_2 ($mg \cdot g^{-1} \cdot s.s.\ h^{-1}$) produced by microbial respiration increased of almost three times in fertilized soil (Fig. 2b). The FDA hydrolysis activity was improved in compost-amended plots (Fig. 3a). The fluorescein emitted values ranged from 56.10 ($\mu g \cdot g^{-1}$) of mineral plot to 144.38 ($\mu g \cdot g^{-1}$) of the compost 16 Mg ha^{-1} fertilized plot. The analysis of phosphatase activity, both acidic and alkaline (Figs. 3b, c), showed no significant differences between mineral and compost fertilization.

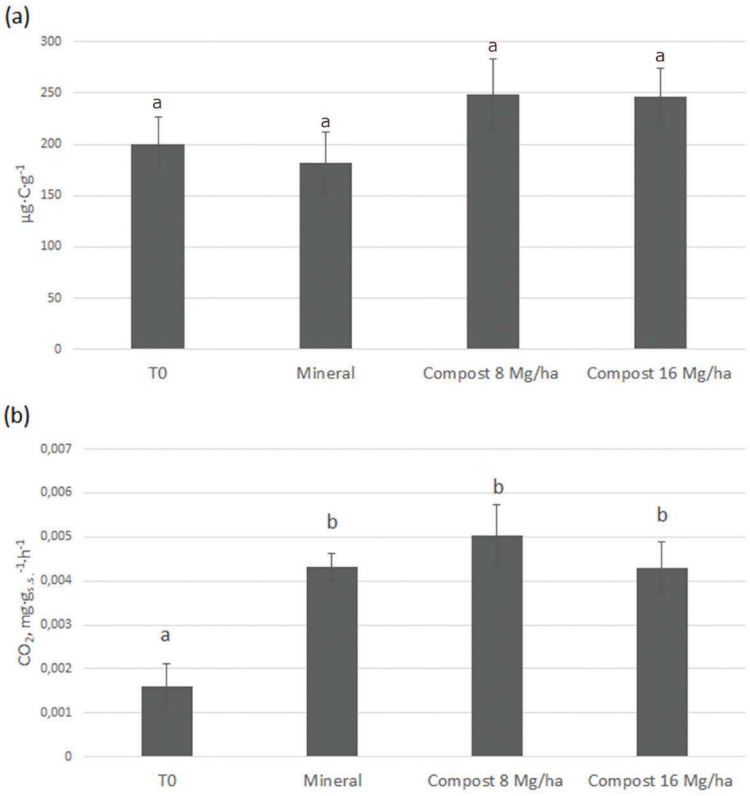

Fig. 2. (a) Microbic biomass and (b) respiration of soil before (T0) and after mineral and compost fertilization (T1). The results represent the mean value (± SD) of three independent biological replicates. Different letters indicate significant differences ($p \leq 0.05$).

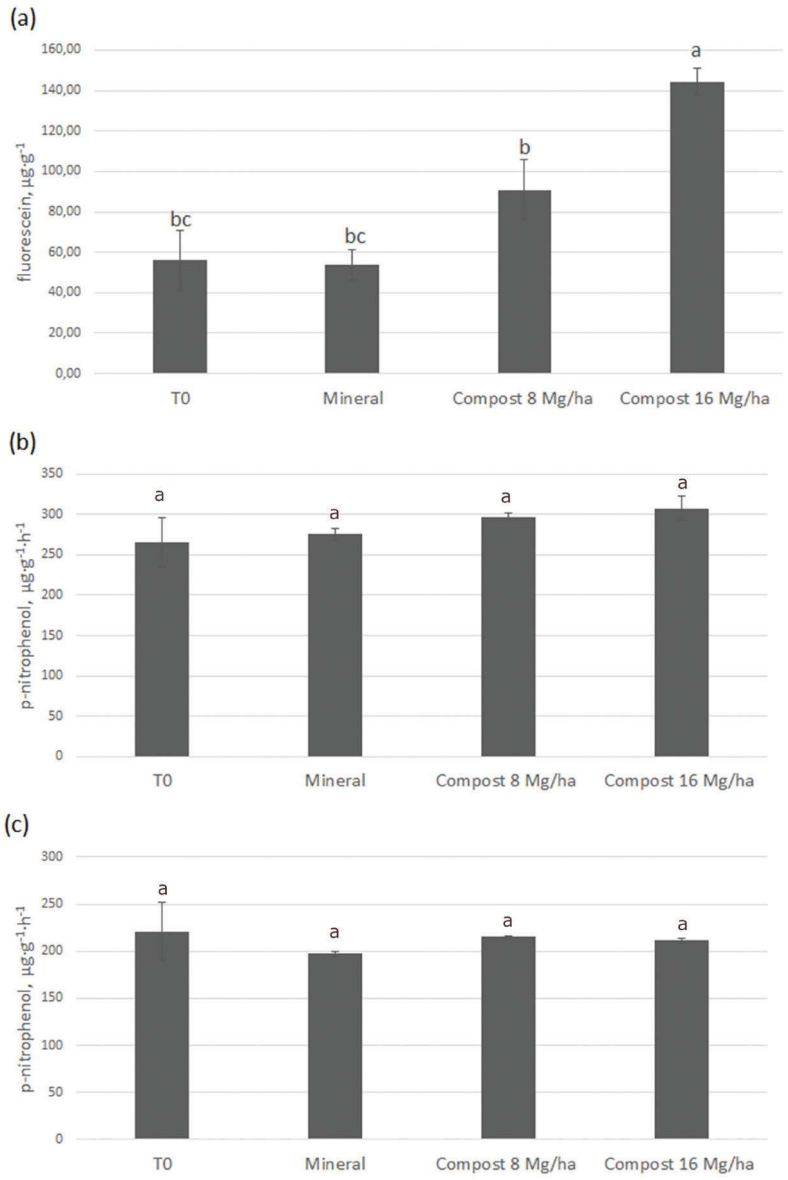

Fig. 3. Biochemical analysis of soil before (T0) and after mineral and compost fertilization (T1. (a) Fluorescein diacetate hydrolysis activity (b) acid and (c) alkaline phosphatase activity. The results represent the mean value (± SD) of three independent biological replicates. Different letters indicate significant differences ($p \leq 0.05$).

Qualitative analysis of fruits

Data analysis carried out on melon productivity and quality underlined that no differences in product yield were observed among treated plots. Moreover, no significant differences were observed in fruit dimensions, fresh weight, fruit shape and total fresh weight.

From the liquid extract obtained liquefying the mesocarp of each fruit, total soluble solids content in juice (°Brix), pH and titratable activity, were determined and no significant differences were found. Excepted for nitrite content, which significantly increased in fruits of plants grown in compost amended soil, the content in nutrient elements as well in heavy metals was not affected by treatments (Tables 3 and 4). Altogether, the obtained results clearly indicate that not differences in quality were observed in fruits collected from both mineral an organic amendment plots.

Sensorial analysis

Sensorial analysis of a first sampling of melons, carried out on June, showed better results for fruits cultivated under mineral fertilization

Table 3. Nutritional elements in melon fruits (mg kg^{-1}) measured after compost and mineral fertilization.

	Nitrite	**Nitrate**	**Na**	**Mg**	**K**	**Ca**	**P**
Mineral	1.25 ± 0.71 **a**	11.76 ± 9.98	980.36 ± 234.56	302.97 ± 78.36	1450.83 ± 348.49	498.67 ± 274.86	146.38 ± 47.05
Compost 8 Mg ha^{-1}	4.04 ± 0.99 **b**	29.56 ± 15.09	1172.50 ± 129.50	324.06 ± 31.65	2043.75 ± 415.64	787.75 ± 385.52	162.05 ± 34.94
Compost 16 Mg ha^{-1}	4.37 ± 0.85 **b**	33.77 ± 15.29	912.83 ± 187.19	285.22 ± 57.66	1991.00 ± 415.71	415.00 ± 2.79	155.70 ± 12.43

Means ± standard error. Different letters indicate significant differences ($p \leq 0.05$). n = 30.

Table 4. Heavy metals content in melon fruits (mg kg^{-1}) measured after compost and mineral fertilization.

	Cr	**Mn**	**Fe**	**Ni**	**Cu**	**Zn**	**B**	**Hg**	**Pb**
Mineral	< 3.1	0.63 ± 0.43	17.68 ± 11.38	3.76 ± 3.50	19.02 ± 15.00	3.87 ± 2.34	3.91 ± 0.70	6.22 ± 0.47	1.99 ± 1.50
Compost 8 Mg ha-1	< 3.1	0.63 ± 0.27	20.78 ± 8.96	3.18 ± 1.97	1.93 ± 0.70	3.83 ± 1.94	4.62 ± 3.54	5.66 ± 4.56	3.25 ± 2.88
Compost 16 Mg ha-1	< 3.1	0.55 ± 0.18	14.49 ± 5.36	4.07 ± 3.35	2.23 ± 0.55	3.93 ± 2.79	2.28 ± 1.39	3.84 ± 3.00	2.86 ± 2.00

Means ± standard error. Different letters indicate significant differences ($p \leq 0.05$). n = 30.

(Fig. 4a). In term of harmony and flavor intensity, the fruits cultivated under organic fertilization (8 and 16 Mg ha^{-1} MSW compost) had significantly lower score ($p>0.05$) compared to the fruits cultivated under mineral fertilization. While crunchiness and consistence of the fruits cultivated under organic fertilization with 16 Mg ha^{-1} MSW compost had significantly high score ($p>0.05$). On the contrary, the sensorial analysis carried on fruits collected on July did not point out any significant difference among fruits coming from the three differently fertilized soils with the exception of the crunchiness and consistence of the fruits (Fig. 4b).

Discussion

In the present study, the effects of organic fertilization, using a quality MSW compost, and the conventional NPK mineral fertilization on soil and melon fruits quality have been compared. Many chemical and biological parameters of both soils (physical and biochemical properties) and crop (productivity, quality and sensorial) have been investigated.

Soil chemical analysis

Among the parameters evaluated, mineral fertilization induced a pH reduction in the soil, whereas soil compost amendment didn't induce any significant variation. Such reduction could be due to the chemical characteristic of the mineral fertilizer rich in ammonium and sulfuric anhydride, which are known for their acidifying characteristics (Wallace, 1994). On the contrary, parameters such as limestone (total carbonates) and active calcium carbonate appear to be not affected by all treatments. Based on results reported in scientific literature (Crecchio et al., 2001), the significant increase in organic C, observed in soil treated with the highest compost fertilization, suggests a potential increase of organic matter in soil. The loss of organic matter in agricultural land, caused by intensive agricultural practices, excessive tillage and mineral fertilization is one of the main causes of soil fertility reduction (Crecchio et al., 2001). At the same time, the documented adverse effects on the environment and human health, the loss of efficacy by the most commonly commercialized synthetic pesticides, fungicides and insecticides, due to an indiscriminate use, has increased the need to provide new natural products as an alternative to hazardous chemicals (Commisso et al., 2021). In this regard, reintegrating the share of organic matter in the soil through fertilizers with a high organic C content, like compost, turns out to be one of the most effective solutions to fertility loss problems.

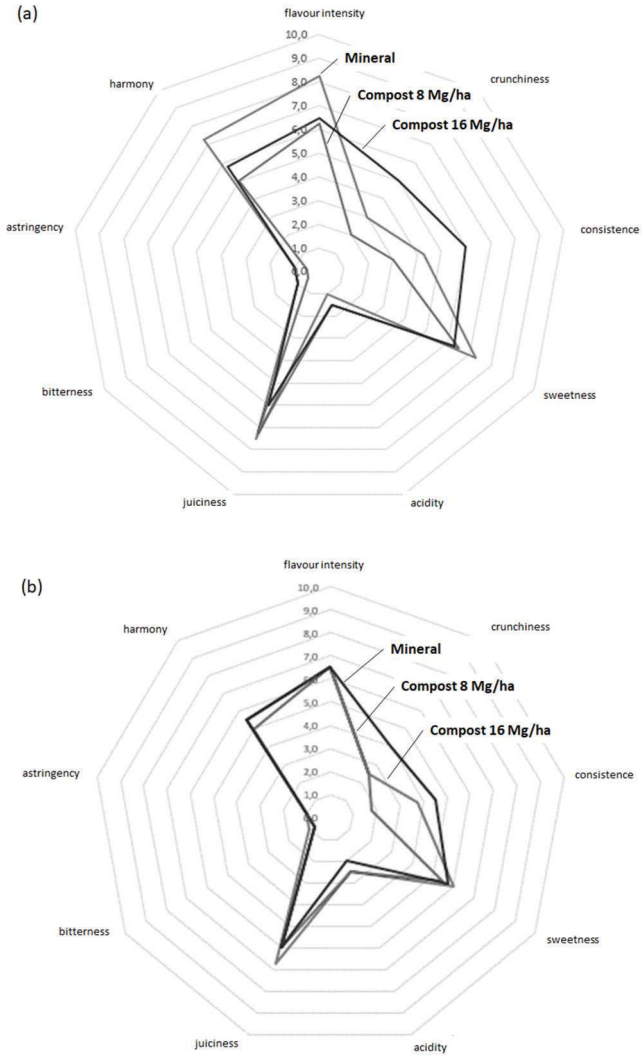

Fig. 4. Radar chart of the sensory analysis of (a) first sampling of melon fruits, carried out on 5th June 2018, and (b) second sampling of melon fruits, carried out on 9th July 2018.

The soluble salts present in the soil, whether derived from the soil itself or from fertilizations, are essential for plant nutrition, but their concentration must be contained within certain values. High concentrations can induce nutritional imbalances, with plant toxicity effects, damage to soil structure and, in some cases, changes in pH values. Although in our experiment compost amended soils were characterized by a higher EC, salts levels were maintained below the danger threshold for crops (ARPAV, 1990) and crop production and quality were not affected by this parameter, which represents one of the most important mechanisms by which the soil retains both macro- and micro-nutrients. Generally, soil amendment with organic matter, such as compost, significantly improve this chemical characteristic of the soil (Yüksel and Kavdır, 2020) whereas in our experimental conditions, no significant differences were found in the CEC at the end of crop cycle. Yüksel and Kavdır (2020) observed a two-fold increase in CEC parameters in soil amended with 40 Mg of MSW compost (Yüksel and Kavdır, 2020), while in our experiments the highest doses of compost employed was 16 Mg. Probably, the lack of CEC variation observed could be due to the lower doses of compost employed, to an excessive compost dilution in soil mainly due to the deep soil lavorations (40 cm) as well as to a rapid mineralization of the organic matter.

Heavy metals analysis

Because of the high variability of its composition, one of the main problems related to the use of MSW compost is the high presence of heavy metals and several techniques have been employed, where needed, to reduce their content. Interestingly, the analyses of heavy metals content in soil amended with both compost and chemical fertilization did not show any significant increases of these chemicals. Similar results were observed by Businelli et al. (2009), which found, during 10 years of experimentation, that the concentration of metals in the soil, following MSW compost fertilization, did not exceed the background concentrations, suggesting a potential loss of metals from the soil system (Businelli et al., 2009).

Biochemical analysis

In order to assess the effects of MSW compost amendment and classical mineral fertilization on soil microbiological activity, various biochemical analyses have been evaluated. The results obtained at the end of the crop cycle highlighted, that in both organic and mineral amended

soil microbial respiration weakly increased. Microbial biomass was not significantly affected, but tends to increase with compost amendment. The higher soil respiration values indicated a positive effect of the compost amendment on the biological quality of the soil (Cicatelli et al., 2014). The possible increase in microbial biomass could be due to two different factors: i) external contribution of microbial biomass contained in the compost matrix and, ii) development of the indigenous microbiota due to the increase of carbon substrates in the soil (Ros et al., 2006). The FDA hydrolysis activity was improved in the compost amended parcels, as already described by several authors (Cicatelli et al., 2014). The enzymes responsible for FDA hydrolysis are abundant in soil environment. Esterases, proteases and lipases, which have been shown to hydrolyse the FDA, are involved in many types of tissue decomposition. The ability to hydrolyse the FDA seems widespread, refined among the main decomposers, in bacteria and fungi (Schnürer and Rosswall, 1982). Generally, more than 90% of the energy flow in a soil system passes through microbial decomposers, so an assay that measures microbial decomposition activity will provide a good estimation of the total microbial activity. The analysis of acidic and alkaline phosphatase, which plays a fundamental role in the mineralization of organic P under low P conditions (Nannipieri et al., 1979), showed no significant differences between mineral and compost fertilization. These results are not in agreement with bibliography where MSW compost generally increase these parameters (Meena et al., 2016). In fact, Meena et al. (2016) reported that phosphatase activity was significantly increasing its activity in soils amended with 16 Mg ha^{-1} MSW compost (Meena et al., 2016). Anyway, as largely reported, alkaline phosphatase is synthesized by microorganisms only (not from plant residues) (Rastogi et al., 2019). Therefore, the lack of increment in phosphatase activity was connected with weak increment on microbial biomass observed in compost amended soil.

Qualitative analysis of fruits

Starting from data obtained, no significant differences were found in the quality of melon fruits produced in the experimentation, but rather, the melons produced did not deviate from the characteristic traits of the species (Artés et al., 1993), confirming that compost can effectively substitute mineral fertilizers in agronomic practices without altering fruit characteristics. Chemical analyses of nutrient elements content in melon fruits cultivated with the three different soil fertilizations showed

no significant differences, with the exception of the nitrite content that appeared to increase in melons grown with compost. The increase in nitrite content in fruits is a negative aspect in fruit and vegetables since high concentrations of this anion can create problems to human health. Anyway, the nitrite and nitrates content in melons grown in amended soil was below the threshold permitted by the law (Alexander et al., 2008). *Cucumis melo* is largely known to be a heavy metals accumulator (Othman and Asharuddin, 2013). As observed in our experiment, heavy metals content was particularly low in both amended soil and fruits cropped on it. This suggests, as already observed by Businelli et al. (2009), that heavy metals in soil were not translocated and accumulated in compost fertilized fruits maintaining a safety quality of the production.

Sensorial analysis

Sensorial analysis aims to test the organoleptic quality of the fruits (Senesi et al., 2002). Results of sensorial analysis showed no significant differences between fruits coming from the three differently fertilized soils. This outcome suggests that as chemical characteristics also the organoleptic quality was not affected by the different fertilizations.

Conclusions

The use of compost did not show great differences in productivity and quality of cultivated plants, compared to the more usual mineral fertilizers. Taking in account the size of fruits and content of nutritional elements, no significant differences were noted. No translocation of heavy metals from the soil to the edible parts of the plants has been detected, guaranteeing complete product safety. As for the organoleptic characteristics, no significant differences were found between the melon fruits cultivated on plots subjected to different fertilization strategies. Furthermore, an increase in the biological fertility of soil has been highlighted, confirming that the use of compost could be a fundamental tool to counteract the phenomenon of desertification and soil fertility loss. Lastly, microbiological activity of soil seems to be stimulated by organic fertilization, with an improvement of soil decomposition and mineralization activities. Our findings, associated with the ecological and economic benefits of using compost in agriculture, should promote this practice among farmers as well as reassure and persuade consumers to use food obtained from compost-amended soils.

Acknowledgements
This work was supported by Calabra Maceri e Servizi Ltd. SR is indebted to contract from the Calabra Maceri e Servizi Ltd. We give thanks to Dr. Adolfo Le Pera, Dr. Miriam Sellaro for scientific technical support, Mr. Cristian Rodolfo Altimari and Mr. Alberto Mazzei for the crop field assistances. Finally, we thank the panel group for sensorial analysis: Mr. Cristian Rodolfo Altimari, Dr. Tiziana Belfiore, Dr. Fabrizio Carbone, Dr. Anna Corapi, Dr. Francesca Iaquinta, Dr. Giovanni Misasi, Dr. Mario Reda, Dr. Chiara Rocca, Dr. Amelia Salimonti, Dr. Veronica Vizzarri.

REFERENCES

Alexander J., Benford D., Cockburn A., Cravedi J.P., Dogliotti E., Di Domenico A. et al. (2008). Nitrate in vegetables. Opinion of the scientific panel on contaminants in the food chain on a request from the European Commission to perform a scientific risk assessment on nitrate in vegetables. EFSA J. 689, 1-79.

ARPAV (1990). L'interpretazione delle analisi del terreno. Strumento per la sostenibilità ambientale. Veneto Agricoltura - Azienda Regionale per i settori Agricolo, Forestale e Agro-Alimentare.

Artés F., Escriche A.J., Martínez J.A., Marin J.G. (1993). Quality factors in four varieties of melon (*Cucumis melo* L.). J. Food. Qual. 16, 91-100.

Businelli D., Massaccesi L., Said-Pullicino D., Gigliotti G. (2009). Long-term distribution, mobility and plant availability of compost-derived heavy metals in a landfill covering soil. Sci. Total Environ. 407,1426-1435.

Cicatelli A., Baldantoni D., Iovieno P., Carotenuto M., Alfani A., De Feis I. et al. (2014). Genetically biodiverse potato cultivars grown on a suitable agricultural soil under compost amendment or mineral fertilization: Yield, quality, genetic and epigenetic variations, soil properties. Sci. Total Environ. 493,1025-1035.

Commisso M., Guarino F., Marchi L., Muto A., Piro A., Degola F. (2021). Bryoactivities: a review on how bryophytes are contributing to the arsenal of natural bioactive compounds against fungi. Plants 10, 203.

Crecchio C., Curci M., Mininni R., Ricciuti P., Ruggiero P. (2001). Short-term effects of municipal solid waste compost amendments on soil carbon and nitrogen content, some enzyme activities and genetic diversity. Biol. Fertil. Soils 34, 311-318.

Decker-Walters D.S., Chung S.M., Staub J.E., Quemada, H.D., López-Sesé A.I. (2002). The origin and genetic affinities of wild populations of melon (*Cucumis melo*, Cucurbitaceae) in North America. Plant Syst. Evol. 233, 183-197.

Drouineau G. (1942). Dosage rapide du calcaire actif du sol: Nouvelles données sur la separation et la nature des fractions calcaires. Ann. Agron. 12, 441-450.

Kjeldahl J. (1883). Neue Methode zur Bestimmung des Stickstoffs in organischen Körpern. Fresenius' Zeitschrift für Anal Chemie 22, 366-382.

Lim S.L., Lee L.H., Wu T.Y. (2016). Sustainability of using composting and vermicomposting technologies for organic solid waste biotransformation: recent overview, greenhouse gases emissions and economic analysis. J. Clean Prod. 111, 262-278.

Lim T.K. (2012). *Cucumis melo* L. (Cantalupensis Group) 'Charentais.' In: *Edible Medicinal and Non-Medicinal Plants*. Springer Netherlands, Dordrecht, pp. 201-203.

Lindsay E.L., Norvell W.A. (1978). Development of a DTPA soil test for zinc, iron, manganese, and copper. Soil Sci. Soc. Am. J. 42, 421-428.

Meena M.D., Joshi P.K., Narjary B., Sheoran P., Jat H.S., Chinchmalatpure A.R. et al. (2016). Effects of municipal solid waste compost, rice-straw compost and mineral fertilisers on biological and chemical properties of a saline soil and yields in a mustard–pearl millet cropping system. Soil Res. 54, 958.

Ministero per le Politiche Agricole e Forestali (1999). Approvazione dei "Metodi ufficiali di analisi chimica del suolo." Gazz. Uff. Rep. Ital. 248 - 21.10.1999.

Ministero per le Politiche Agricole e Forestali (2004). Approvazione dei "Metodi ufficiali di analisi biochimica del suolo". Gazz. Uff. Rep. Ital. 61 (13.03.2004).

Muto A., Müller C.T., Bruno L., McGregor L., Ferrante A., Chiappetta A.A.C. et al. (2020). Fruit volatilome profiling through GC×GC-ToF-MS and gene expression analyses reveal differences amongst peach cultivars in their response to cold storage. Sci. Rep. 27, 18333.

Nannipieri P., Pedrazzini F., Aarcara P.G., Piovanelli C. (1979). Changes in amino acids, enzyme activities, and biomasses during soil microbial growth. Soil Sci. 127, 26-34.

Nautiyal C.S., Chauhan P.S., Bhatia C.R. (2010). Changes in soil physico-chemical properties and microbial functional diversity due to 14 years of conversion of grassland to organic agriculture in semi-arid agroecosystem. Soil Tillage Res. 109, 55-60.

Othman N., Asharuddin S.M. (2013). *Cucumis melo* Rind as biosorbent to remove Fe(II) and Mn(II) from synthetic groundwater solution. Adv. Mater. Res. 795, 266-271.

Rastogi M., Nandal M., Nain L. (2019). Seasonal variation induced stability of municipal solid waste compost: an enzyme kinetics study. SN Appl. Sci. 1, 849.

Ros M., Pascual J.A., Garcia C., Hernandez M.T., Insam H. (2006). Hydrolase activities, microbial biomass and bacterial community in a soil after long-term amendment with different composts. Soil. Biol. Biochem. 38, 3443-3452.

Schnürer J., Rosswall T. (1982). Fluorescein diacetate hydrolysis as a measure of total microbial activity in soil and litter. Appl. Environ. Microbiol. 43, 1256-1261.

Senesi E., Scalzo R.L, Prinzivalli C., Testoni A. (2002). Relationships between volatile composition and sensory evaluation in eight varieties of netted muskmelon (*Cucumis melo* L. var reticulatus Naud). J. Sci. Food Agric. 82, 655-662.

Springer U., Klee J. (1954). Prüfung der Leistungsfähigkeit von einigen wichtigeren Verfahren zur Bestimmung des Kohlenstoffs mittels Chromschwefelsäure sowie Vorschlag einer neuen Schnellmethode. Zeitschrift für Pflanzenernährung, Düngung, Bodenkd 64, 1-26.

Wallace A. (1994). Soil acidification from use of too much fertilizer. Commun. Soil Sci. Plant Anal. 25, 87-92.

Watteau F., Villemin G. (2011). Characterization of organic matter microstructure dynamics during co-composting of sewage sludge, barks and green waste. Bioresour. Technol. 102, 9313-9317.

Yüksel O., Kavdır Y. (2020). Improvement of soil quality parameters by municipal solid waste compost application in clay-loam soil. Turkish J. Agric. - Food Sci. Technol 8, 603.